AFML-TR-65-2
PART V

TERNARY PHASE EQUILIBRIA IN TRANSITION METAL-BORON-CARBON-SILICON SYSTEMS

PART V. COMPENDIUM OF PHASE DIAGRAM DATA

E. RUDY

Aerojet-General Corporation

TECHNICAL REPORT AFML-TR-65-2, PART V

MAY 1969

AIR FORCE MATERIALS LABORATORY
AIR FORCE SYSTEMS COMMAND
WRIGHT-PATTERSON AIR FORCE BASE, OHIO

NOTICES

When Government drawings, specifications, or other data are used for any purpose other than in connection with a definitely related Government procurement operation, the United States Government thereby incurs no responsibility nor any obligation whatsoever; and the fact that the Government may have formulated, furnished, or in any way supplied the said drawings, specifications, or other data, is not to be regarded by implication or otherwise as in any manner licensing the holder or any other person or corporation, or conveying any rights or permission to manufacture, use or sell any patented invention that may in any way be related thereto.

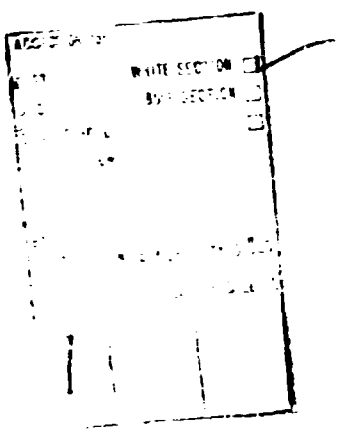

This document has been approved for public release and sale; its distribution is unlimited.

Copies of this report should not be returned, unless return is required by security considerations, contractual obligations, or notice on a specific document.

1000 - June 1969 - CO455 - 81-1798

TERNARY PHASE EQUILIBRIA IN TRANSITION METAL-BORON-CARBON-SILICON SYSTEMS

PART V. COMPENDIUM OF PHASE DIAGRAM DATA

E. RUDY

FOREWORD

The present report summarizes the phase diagram investigations carried out over a four-year period under USAF Contract No. AF 33(615)-1249. The program was initiated under Project No. 7350, Task No. 735001, on 1 January 1964 and continued under a two-year extension effort through 1967. Also contained in this compilation are phase diagram data gathered under two other Air Force programs, AF 33(615)-67-C-1513 and IITRI Subcontract P.O. No. 37942, over the time period from April 1967 through April 1969.

All experimental investigations were carried out at the Materials Research Laboratory, Aerojet-General Corporation, Sacramento, while part of the final data reduction and evaluation was performed by the author at the Oregon Graduate Center in Portland, Oregon. The contract was administered under the direction of the Air Force Materials Laboratory, Wright-Patterson Air Force Base. The project engineers were Capt. R.A. Peterson (1964) and Capt. P.J. Marchiando (MAMC) (1965 to 1968). Dr. E. Rudy, Aerojet-General Corporation (now at the Oregon Graduate Center, Portland, Oregon), served as principal investigator, and Prof. Dr. H. Nowotny, University of Vienna, as consultant on the first project.

Personnel who contributed in full, or in part, to the program included: E. Rudy (principal investigator), C.E. Brukl, St. Windisch, D.P. Harmon, J.R. Hoffman, Y.A. Chang, T.E. Eckert, J. Pomodoro, R. Cobb, and R. Taylor.

A total of 44 Technical Reports, covering in detail the phase diagram work, as well as the thermochemical calculations performed on the individual systems, were issued in the course of the programs. Additional studies on binary transition metal systems during the same time period were only of peripheral interest to the overall scope of the program and were, therefore, not reported formally. It was decided, however, to include these phase diagram data in this Summary Report.

The titles of the documentary reports which have been published previously, or are presently in print, are listed below.

Reports issued under U.S. Air Force Contract AF 33(615)-1249.

Part I. Related Binaries

Volume I	Mo-C System
Volume II	Ti-C and Zr-C Systems
Volume III	Systems Mo-B and W-B

Volume IV	Hf-C System
Volume V	Ta-C System. Partial Investigations in the Systems V-C and Nb-C
Volume VI	W-C System. Supplemental Information on the Mo-C System
Volume VII	Ti-B System
Volume VIII	Zr-B System
Volume IX	Hf-B System
Volume X	V-B, Nb-B and Ta-B Systems
Volume XI	Final Report on the Mo-C System
Volume XII	Revision of the Vanadium-Carbon and Niobium-Carbon Systems
Volume XIII	The Zirconium-Silicon and Hafnium-Silicon Systems
Volume XIV	Constitution of the Hafnium-Vanadium and Hafnium-Chromium Systems

Part II. Ternary Systems

Volume I	Ta-Hf-C System
Volume II	Ti-Ta-C System
Volume III	Zr-Ta-C System
Volume IV	Ti-Zr-C, Ti-Hf-C, and Zr-Hf-C Systems
Volume V	Ti-Hf-B System
Volume VI	Zr-Hf-B System
Volume VII	Systems Ti-Si-C, Nb-Si-C, and W-Si-C
Volume VIII	Ta-W-C System
Volume IX	Zr-W-B System. Pseudo-Binary System TaB_2-HfB_2
Volume X	Systems Zr-Si-C, Hf-Si-C, Zr-Si-B, and Hf-Si-B
Volume XII	Ti-Zr-B System
Volume XIII	Phase Diagrams of the Systems Ti-B-C, Zr-B-C, and Hf-B-C
Volume XIV	The Hafnium-Iridium-Boron System
Volume XV	Constitution of Niobium-Molybdenum-Carbon Alloys
Volume XVI	The Vanadium-Niobium-Carbon System
Volume XVII	Constitution of Ternary Ta-Mo-C Alloys
Volume XVIII	Constitution of Ternary Nb-W-C Alloys

Part III. Special Experimental Techniques

Volume I.	High Temperature Differential Thermal Analysis
Volume II	A Pirani-Furnace for the Precision Determination of the Melting Temperatures of Refractory Metallic Substances

Part IV. Thermochemical Calculations

Volume I	Thermodynamic Properties of Group IV, V, and VI Binary Transition Metal Carbides

Volume II	Thermodynamic Interpretation of Ternary Phase Diagrams
Volume III	Computational Approaches to the Calculation of Ternary Phase Diagrams.

Reports issued under U.S. Air Force Contract AF 33(615)-67-C-1513

Volume I.	The Phase Diagrams Ti-Nb-C, Ti-Ta-C, and Ti-Mo-C
Volume II.	Effect of Rhenium and Aluminum Additions on the Metal-Rich Equilibria in the Systems Ti-Mo-C and Ti-Nb-C
Volume III	Phase Studies in the Systems V-Ta-C and Nb-Ta-C
Volume IV	Effect of Molybdenum and Tungsten on the Subcarbide Solutions in the Systems Ta-V-C and Ta-Nb-C.
Volume V	The Phase Diagram W-B-C
Volume VI	Phase Equilibria in the Metal-Rich Region of the System Hf-Ta-N
Volume VII	The Phase Diagram Ti-V-C

This Compendium has been reviewed and is approved.

W. G. RAMKE
Chief, Ceramics and Graphite Branch
Metals and Ceramics Division
Air Force Materials Laboratory

ABSTRACT

This report contains a summary o. the phase diagram work conducted under U.S. Air Force Contracts AF 33(615)-1249 and AF 33(615)-67-C-1513 over the time period from 1 January 1964 through April 1969. Systems studied include binary transition metal systems, binary and ternary systems of refractory transition metals with carbon, boron, silicon, and nitrogen, and selected concentration-temperature sections of higher order systems involving the same elements.

TABLE OF CONTENTS

TABLE OF CONTENTS (Continued)

TABLE OF CONTENTS (Continued)

TABLE OF CONTENTS (Continued)

LIST OF ILLUSTRATIONS

LIST OF ILLUSTRATIONS (Cont'd)

LIST OF ILLUSTRATIONS (Cont'd)

LIST OF ILLUSTRATIONS (Cont'd)

LIST OF ILLUSTRATIONS (Cont'd)

LIST OF ILLUSTRATIONS (Cont'd)

LIST OF ILLUSTRATIONS (Cont'd)

LIST OF ILLUSTRATIONS (Cont'd)

LIST OF ILLUSTRATIONS (Cont'd)

LIST OF ILLUSTRATIONS (Cont'd)

LIST OF ILLUSTRATIONS (Cont'd)

LIST OF ILLUSTRATIONS (Cont'd)

LIST OF ILLUSTRATIONS (Cont'd)

LIST OF ILLUSTRATIONS (Cont'd)

LIST OF ILLUSTRATIONS (Cont'd)

LIST OF ILLUSTRATIONS (Cont'd)

LIST OF ILLUSTRATIONS (Cont'd)

LIST OF ILLUSTRATIONS (Cont'd)

LIST OF ILLUSTRATIONS (Cont'd)

LIST OF ILLUSTRATIONS (Cont'd)

LIST OF ILLUSTRATIONS (Cont'd)

LIST OF ILLUSTRATIONS (Cont'd)

LIST OF ILLUSTRATIONS (Cont'd)

LIST OF ILLUSTRATIONS (Cont'd)

LIST OF ILLUSTRATIONS (Cont'd)

LIST OF ILLUSTRATIONS (Cont'd)

LIST OF ILLUSTRATIONS (Cont'd)

I. INTRODUCTION AND REPORT ORGANIZATION

Introduction

The phase diagram data presented in this report contain the essential results of a five year effort on alloy constitution studies at the Materials Research Laboratory of Aerojet-General Corporation in Sacramento, California.

From the wealth of available experimental data it became evident towards the end of the project, that much of the essential information might become lost in the details of the documentary reports published on the individual systems; furthermore, the distribution of these documentary reports was limited and thus the information was available only to a fairly small number of individuals. After several meetings with Air Force technical personnel monitoring the research effort, notably Messrs. J. Krochmal, W. Ramke, and Capt. P.J. Marchiando of the Ceramics and Graphite Branch at Wright-Patterson Air Force Base, it was decided to extract the salient data from the individual system reports and combine them in a single volume compendium.

Although the temporary value of a mere data collection was realized, it was felt that such a summary volume might provide a convenient source of high temperature phase equilibrium data in this technically important class of systems, especially since most of the data are new and unpublished. It is planned to have this report followed by a more comprenensive and detailed publication at some later date.

Report Organization

The wealth of detailed phase equilibrium data has forced us to make compromises in respect to amount and detail of the material presented. Thus, to keep the size of the volume within reasonable limits, only the most important references were included and short discussions were limited to those

systems on which no previously published documentary reports are available for further reference. Brief remarks were also added in the reference section in instances where recent findings have superseded some of the earlier data.

The phase diagrams of the various systems are grouped in the report in the order shown below (Me, Me_1, Me_2 = refractory transition metal):

1. Binary Systems Me_1-Me_2
2. Binary Systems Me-C
3. Binary Systems Me-B
4. Binary Systems Me-Si
5. Ternary Systems Me_1-Me_2-C
6. Ternary Systems Me-Si-C
7. Ternary Systems Me-Si-B
8. Ternary Systems Me_1-Me_2-B
9. Ternary Systems Me-B-C
10. Ternary Systems Me_1-Me_2-N

The general order in which the individual systems from a given alloy group are presented follows the group number of the component metals in the periodic system and proceeding from the lighter to the heavier elements. Thus, for example, the ternary systems Me_1-Me_2-C begin with Ti-Zr-C

and continue through Ti-W-C. Next, all zirconium-containing systems, beginning with Zr-Hf-C, are listed, then all hafnium systems, and so forth.

The part of the report containing the phase diagram data collection is preceded by a compilation of the most important references and, in some instances, also a short description of the results leading to the finally accepted phase diagram.

II. NOTES AND REFERENCES TO THE PHASE DIAGRAM COLLECTION CONTAINED IN THIS COMPENDIUM

A. BINARY TRANSITION METAL SYSTEMS

The work on the transition metal binaries was conducted over the time period from May through August 1967. While of only peripheral interest in the overall scope of the program, the investigation of these systems has not been covered in separate documentary reports; a brief description of some of the systems is therefore given in sections preceding the references.

Section III.A.1. Ti-Zr-System

The finally adopted phase diagram, Figure 1, is based mainly on the work by E.T. Hayes et al.[1]. Early melting point data[1,2] are supplemented by measurements carried out in this laboratory (Figure 2). The reported α-β-transformation temperatures reported are compiled in Figure 3, preference being given to the data by E.T. Hayes et al.[1] and by P.A. Farrar and S.A. Adler[3]. Lattice parameter data are shown in Figure 4. Further references may be found in the handbooks listed under (4), (5), and (6).

Major References:

(1) E.T. Hayes, A.H. Roberson, and O.G. Paasche: USBM Report No. 4826, Nov. 1951.

(2) J.D. Fast: Rec. Trav. Chim. 58 (1939), 973.

(3) P.A. Farrar and S.A. Adler: Trans. AIME 236 (1966), 1061.

(4) M. Hansen: Constitution of Binary Alloys (McGraw-Hill, New York, 1958).

(5) R.P. Elliott: Constitution of Binary Alloys, First Supplement (McGraw-Hill, New York, 1965).

(6) W.B. Pearson: Handbook of Lattice Spacings and Structures of Metals and Alloys (Pergamon Press, New York, 1958); Volume 2 (Pergamon Press, New York, 1967).

Section III.A.2. Ti-Hf-System

Major References:

(1) E.T. Hayes and D.K. Deardorff: USBM-U-345 (1957).

(2) Y.A. Chang: USAF Tech. Rept. AFML-TR-65-2, Part II, Vol.V (May 1966).

(3) M. Hansen: Constitution of Binary Alloys (McGraw-Hill, New York, 1958).

(4) R.P. Elliott: Constitution of Binary Alloys, First Supplement (McGraw-Hill, New York, 1965).

(5) W.B. Pearson: Handbook of Lattice Spacings and Structures of Metals and Alloys (Pergamon Press, New York, 1958); Volume 2 (Pergamon Press, New York, 1967).

Section III.A.3. Ti-V System

Major References:

(1) H.K. Adenstedt, J.R. Peguinot and J.M. Rayner: Trans. ASM 44 (1952), 990.

(2) P. Pietrokowsky and P. Duwez: Trans. AIME 194 (1952), 627.

(3) F. Ermains, P.A. Farrar and H. Margolin: Trans. AIME 221 (1961), 904.

(4) M. Hansen, Constitution of Binary Alloys (McGraw-Hill, New York 1958).

(5) R.P. Elliott: Constitution of Binary Alloys, First Supplement (McGraw-Hill, New York, 1965).

(6) W.B. Pearson: Handbook of Lattice Spacings and Structures of Metals and Alloys (Pergamon Press, New York, 1958), Volume 2 (Pergamon Press, New York, 1967).

Section III.A.4. Ti-Nb System

Major References:

(1) M. Hansen, E.L. Kamen, H.D. Kessler and D.J. McPherson: Trans. AIME 191 (1951), 881.

(2) M. Hansen: Constitution of Binary Alloys (McGraw-Hill, New York 1958).

(3) R.P. Elliott: Constitution of Binary Alloys, First Supplement (McGraw-Hill, New York, 1965).

(4) W.B. Pearson: Handbook of Lattice Spacings and Structures of Metals and Alloys (Pergamon Press, New York, 1958); Volume 2 (Pergamon Press, New York, 1967).

Section III.A.5. Ti-Ta System

Major References:

(1) D. Summers-Smith: J. Inst. Met. 81 (1952/1953), 73.

(2) D.J. Maykuth, H.R. Ogden, and R.I. Jaffee: Trans. AIME 197 (1953), 231.

(3) P.B. Budberg and K.J. Shakova: Izvest. Akad. Nauk. SSSR., Neorg. Mat. 3 (1967). 656.

(4) M. Hansen: Constitution of Binary Alloys (McGraw-Hill, New York, 1958).

(5) R.P. Elliott: Constitution of Binary Alloys, First Supplement (McGraw-Hill, New York, 1965).

(6) W.B. Pearson: Handbook of Lattice Spacings and Structures of Metals and Alloys (Pergamon Press, New York, 1958); Volume 2 (Pergamon Press, New York, 1967).

Section III.A.6. Ti-Cr System

Major References:

(1) R.J. VanThyne, H.D. Kessler, and M. Hansen: Trans. ASM 44 (1952), 974.

(2) P.A. Farrar and H. Margolin: Trans. AIME 227 (1963), 1342.

(3) M.K. McQuillan: J. Inst. Met. 79 (1951), 379.

(4) F. Ermains, P.A. Farrar, and H. Margolin: Trans. AIME 221 (1961), 904.

(5) F.B. Cuff, N.J. Grant, and C.F. Floe: Trans. AIME 194 (1952), 848.

(6) W.S. Micheev: Trud. Inst. Met. Baikova No.2, Izd. Akad. Nauk SSSR (Moskan 1957), 154.

(7) M. Hansen: Constitution of Binary Alloys (McGraw-Hill, New York, 1958).

(8) R.P. Elliott: Constitution of Binary Alloys, First Supplement (McGraw-Hill, New York, 1965).

(9) W.B. Pearson: Handbook of Lattice Spacings and Structures of Metals and Alloys (Pergamon Press, New York, 1958); Volume 2 (Pergamon Press, New York, 1967).

Section III.A.7. Ti-Mo System

Major References:

(1) M. Hansen, E.L. Kamen, H.D. Kessler, and D.J. McPherson: Trans. AIME 191 (1951), 881.

(2) M. Hansen: Constitution of Binary Alloys (McGraw-Hill, New York, 1958).

(3) R.P. Elliott: Constitution of Binary Alloys, First Supplement (McGraw-Hill, New York, 1965).

(4) W.B. Pearson: Handbook of Lattice Spacings and Structures of Metals and Alloys (Pergamon Press, New York, 1958); Volume 2 (Pergamon Press, New York, 1967).

Section III.A.8. Ti-W System

Major References:

(1) D.J. Maykuth, H.R. Ogden, and R.I. Jaffee: Trans. AIME 197 (1953), 231.

(2) M. Hansen: Constitution of Binary Alloys (McGraw-Hill, New York, 1958).

(3) R.P. Elliott: Constitution of Binary Alloys, First Supplement (McGraw-Hill, New York, 1965).

(4) W.B. Pearson: "Handbook of Lattice Spacings and Structures of Metals and Alloys (Pergamon Press, New York, 1958); Volume 2 (Pergamon Press, New York, 1967).

Section III.A.9. Zr-Hf System

Major References:

(1) J.D. Fast: J. Appl. Phys. 23, No. 3 (1952), 350.

(2) E.T. Hayes and D.K. Deardorff: USBM-U-345 (1957).

(3) R.F. Domagala: J. Less-Comm. Met. 11 (1966), 70-72.

(4) D.P. Harmon: USAF Tech. Rept. AFML-TR-65-2, Part II, Vol. VI (Aug. 1966).

(5) M. Hansen: Constitution of Binary Alloys (McGraw-Hill, New York, 1958).

(6) R.P. Elliott: Constitution of Binary Alloys, First Supplement (McGraw-Hill, New York, 1965).

(7) W.B. Pearson: Handbook of Lattice Spacings and Structures of Metals and Alloys (Pergamon Press, New York, 1958); Volume 2 (Pergamon Press, New York, 1967).

Section III.A.10 Zr-V System

Major References:

(1) J.T. Williams: Trans. AIME 203 (1955), 345.

(2) M. Hansen: Constitution of Binary Alloys (McGraw-Hill, New York, 1958).

(3) R.P. Elliott: Constitution of Binary Alloys, First Supplement (McGraw-Hill, New York, 1965).

(4) W.B. Pearson: Handbook of Lattice Spacings and Structures of Metals and Alloys (Pergamon Press, New York, 1958); Volume 2 (Pergamon Press, New York, 1967).

Section III.A.11 Zr-Nb System

Major References:

(1) B.A. Rogers and D.F. Atkins: Trans. AIME.

(2) C.E. Lundin and R.H. Cox: US Atomic Energy Comm. TID-12369 (1960).

(3) A.G. Knapton: J. Less Comm. Met. 2 (1960), 119.

(4) Y.F. Bychkov, A.N. Rozanov, D.M. Skorov: Soviet. J. At. Energy 2 (1957), 165.

(5) C.W. Berghout: Phys. Lett. I (1962), 292.

(6) M. Hansen: Constitution of Binary Alloys (McGraw-Hill, New York, 1958).

(7) R.P. Elliott: Constitution of Binary Alloys, First Supplement (McGraw-Hill, New York, 1965).

(8) W.B. Pearson: Handbook of Lattice Spacings and Structures of Metals and Alloys (Pergamon Press, New York, 1958); Volume 2 (Pergamon Press, New York, 1967).

Section III.A.12.1 Zr-Ta System

Major References:

(1) D.E. Williams, R.J. Jackson, and W.L. Larsen: Trans. AIME 224 (1962), 751.

(2) L.F. Pease and J.H. Brophy: Trans. AIME 227 (1963), 1245.

(3) V.S. Emelyanov, YuG. Godin, and A.I. Evstyukhin: Soviet J. Atom. Energ. 2 (1957), 43.

(4) D.P. Harmon and C.E. Brukl: USAF Report AFML-TR-65-2, Part II, Vol. III (Jan. 1966).

(5) M. Hansen; Constitution of Binary Alloys (McGraw-Hill, New York, 1958).

(6) R.P. Elliott: Constitution of Binary Alloys, First Supplement (McGraw-Hill, New York, 1965).

(7) W.B. Pearson: Handbook of Lattice Spacings and Structures of Metals and Alloys (Pergamon Press, New York, 1958); Volume 2 (Pergamon Press, New York, 1967).

Section III.A.13 Zr-Cr System

The constitution diagram established by us in general confirms previous work by E.T. Hayes et al.[1], and R.F. Domagala et al.[2]. The allotropy of the $ZrCr_2$[3, 4] also was confirmed. Quenching studies conclusively showed the C14-type modification to be the high temperature polymorph, whereas the C15-type laves phase forms the stable modification below approximately 1600°C (a = 7.197 Å to a = 7.219 Å). These findings are in accord with those of C.G. Jordan and P. Duwez[4].

Major References:

(1) E.T. Hayes, A.H. Roberson, and M.H. Davies: Trans. AIME 194 (1952), 304.

(2) R.F. Domagala, D.J. McPherson, and M. Hansen: Trans. AIME 197 (1953), 279.

(3) W. Rostoker: Trans. AIME 197 (1953), 304

(4) C.G. Jordan and P. Duwez: Jet Propul. Lab., Calif. Inst. Tech., Prog. Rept. 20-196 (1953). Work quoted in (6).

(5) M. Hansen: Constitution of Binary Alloys (McGraw-Hill, New York, 1958).

(6) R.P. Elliott: Constitution of Binary Alloys, First Supplement (McGraw-Hill, New York, 1965).

(7) W.B. Pearson: Handbook of Lattice Spacings and Structures of Metals and Alloys (Pergamon Press, New York, 1958); Volume 2 (Pergamon Press, New York, 1967).

Section III.A.14 Zr-Mo System

In the revised phase diagram, Figure III.A.14.1, a minimum in the β-Zr solid solution and a peritectic reaction isotherm $L + \beta\text{-Zr} + ZrMo_2$ replaces the eutectic reaction at 1520°C proposed by R.F. Domagala et al.[1]. The new results are based on careful melting point determinations, Figure III.A.14.2, lattice parameter measurements, Figures IV.A.14.3 and IV.A.14.4, but especially on metallographic studies on heat-treated and quenched alloys. The supersaturated β-(Zr, Mo) solid solution containing more than ~20 At% Mo disproportionates very rapidly upon cooling and the resulting precipitation structures very closely resemble (compare the micrographic series shown below) eutectic structures; this may explain the previous finding of an eutectic by R.F. Domagala et al.[1].

The homogeneity range of the only intermediate phase, $ZrMo_2$, must be very small, because no variation of the lattice parameter with the composition could be detected. In the average, $a = 7.600 \pm 0.001$ Å were measured for the cubic, C15-type phase; this parameter agrees well with data reported in the literature[2, 4].

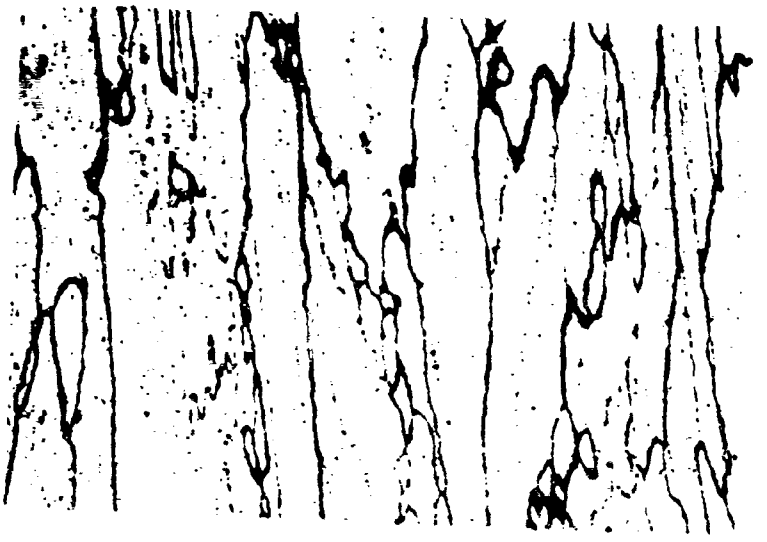

Figure (a): Zr-Mo (70-30 At%). Melted, Re-equilibrated for 2 Minutes at 1590°C and Cooled at ~120°C per Second. X120

β-(Zr, Mo) Solid Solution Showing Inter- and Intragranular Nucleation Centers for the Precipitation of $ZrMo_2$.

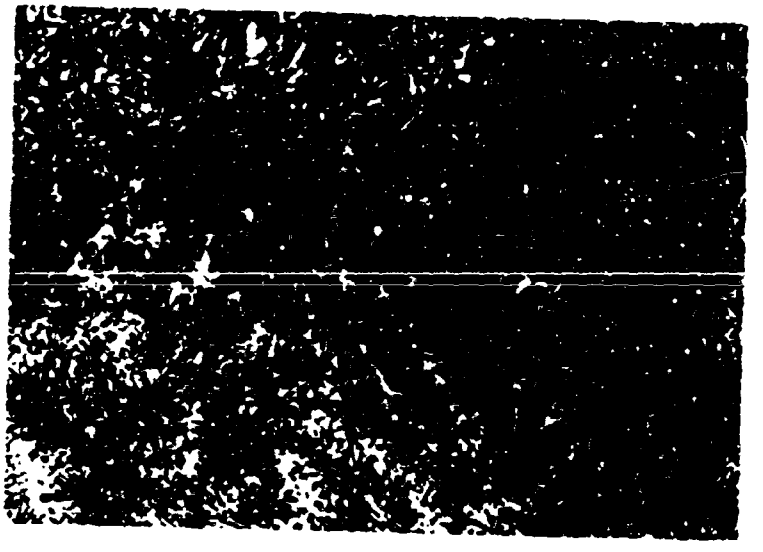

Figure (b): Same Alloy as in Figure (a), but Cooled at ~10°C per Second from 1590°C. X400

Partially Composed β-Zr Solid Solution.

X-Ray Analysis: β-(Zr, Mo)-ss Containing Approximately 20 At% Mo (a ≈ 3.50 Å) and $ZrMo_2$ (a = 7.600 Å).

Figure (c): Zr-Mo (66-34 At%) Melted, Reequilibrated at 1590°C and Cooled at ~100°C per Second. X250

Note Beginning Decomposition of the β-Phase.

X-Ray: Mostly A2, a = 3.435 Å.

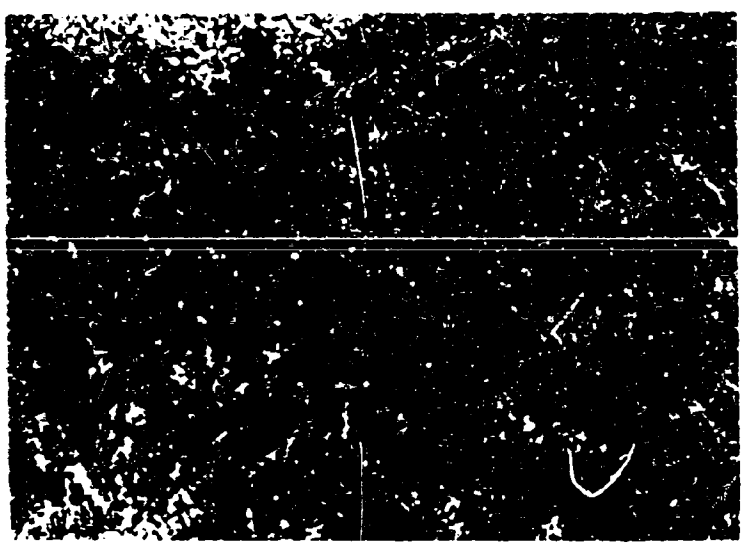

Figure (d): Same Alloy as (c), but Cooled at Less Than 20°C per Second from 1590°C. X425

Note the Close Resemblance of the Disproportionation Structure to a Eutectic or Eutectoid Structure.

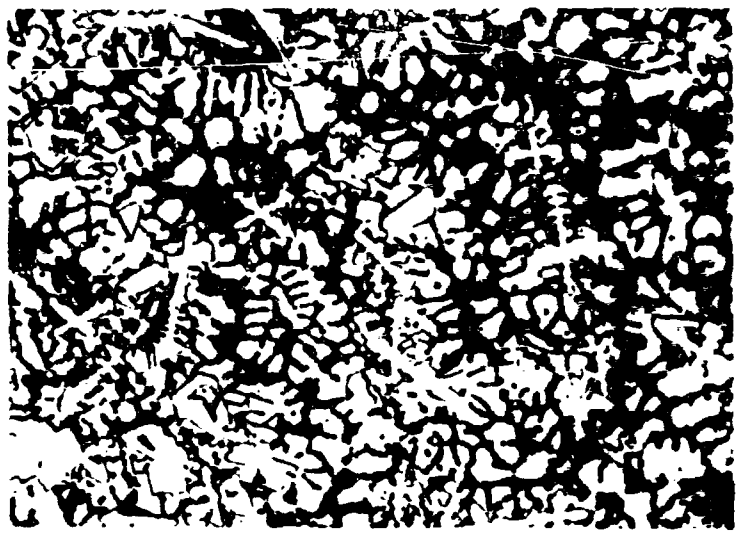

Figure (e): Zr-Mo (66-34 At%), Melted and Quenched. X375
Peritectic Reaction Structure

Major References:

(1) R.F. Domagala, I.J. McPherson, and M. Hansen: Trans AIME 197 (1953), 73.

(2) M. Hansen: Constitution of Binary Alloys (McGraw-Hill, New York, 1958).

(3) R.P. Elliott: Constitution of Binary Alloys, First Supplement (McGraw-Hill, New York, 1965).

(4) W.B. Pearson: Handbook of Lattice Spacings and Structures of Metals and Alloys (Pergamon Press, New York, 1958); Volume 2 (Pergamon Press, New York, 1967).

Section III.A.15 Zr-W System

The phase relationships in the zirconium-tungsten system were recently reexamined in this laboratory by Y.A. Chang[1]. The general features of the resulting diagram, Figure 1, correspond to those originally established by R.F. Domagala et al.[2]. For the β-Zr + ZrW_2 eutectic temperature, our data confirm the measurements by G.A. Geach et al.[3], being somewhat at variance with the values given in (2).

Major References:

(1) Y.A. Chang: Unpublished work under USAF Contract 33(615)-1249 (1967).

(2) R.F. Domagala, D.J. McPherson, and M. Hansen: Trans. AIME 197, 73.

(3) G.A. Geach and F. Slattery: Trans. AIME 197 (1953), 743.

(4) M. Hansen: Constitution of Binary Alloys (McGraw-Hill, New York, 1958).

(5) R.P. Elliott: Constitution of Binary Alloys, First Supplement (McGraw-Hill, New York, 1965).

Section III.A.16.1 Hf-V System

Previous investigations of the system by S. Komjathy[1] are considerably at variance with more recent work done at the U.S. Bureau of Mines[2]. With the exception of a peritectic isotherm L + V $\rightleftharpoons$ HfV_2 at 1480° proposed in the latter work, the redetermination of the phase relationships in this laboratory[3] is in good agreement with the investigation at the U.S. Bureau of Mines. Lattice parameters of a = 7.398 Å (Hf-rich) to a = 7.386 Å (V-rich) for the cubic, C15-type, HfV_2 phase (3) fall into the range of values reported earlier in the literature[4-6].

Major References:

(1) S. Komjathy: J. Less Common Met. 3 (1961), 468.

(2) D.K. Deardorff, M.I. Copeland, L.L. Oden, and H. Kato: U.S. Bur. Mines Rept. of Invest. No. 6594, 1965.

(3) E. Rudy and St. Windisch: J. Less Common Met. 15 (1968), 13.

(4) M. Hansen: Constitution of Binary Alloys (McGraw-Hill, New York, 1958).

(5) R.P. Elliott: Constitution of Binary Alloys, First Supplement (McGraw-Hill, New York, 1965).

(6) W.B. Pearson: Handbook of Lattice Spacings and Structures of Metals and Alloys (Pergamon Press, New York, 1958); Volume 2 (Pergamon Press, New York, 1967).

Section III.A.17 Hf-Nb System

The melting temperatures of Hf-Nb alloys determined in this laboratory support the occurrence of a melting point minimum such as proposed by M.A. Tylkina et al.[2]

The metallographic and X-ray diffraction evidence also supports this finding, since alloys located at, or in the vicinity of, the position of the suspected melting point minimum proved to be uncored after quenching from liquidus temperatures.

Major References:

(1) A. Taylor and N.J. Doyle: J. Less Comm. Met. 7 (1964), 37.

(2) M.A. Tylkina, I.A. Tsyganova, and Ye.M. Savitskii: Zhur. Nerog. Chim. 9, No. 7 (1964), 1650.

(3) P. Duwez: J. Appl. Phys. 22 (1951), 1174.

(4) A.E. Dwight: Columbium Metallurgy (Interscience, New York, 1961), 383

(5) M. Hansen: Constitution of Binary Alloys (McGraw-Hill, New York, 1958).

(6) R.P. Elliott: Constitution of Binary Alloys, First Supplement (McGraw-Hill, New York, 1965).

(7) W.B. Pearson: Handbook of Lattice Spacings and Structures of Metals and Alloys (Pergamon Press, New York, 1958); Volume 2 (Pergamon Press, New York, 1967).

Section III.A.18 Hf-Ta System

Major References.

(1) L.L. Oden, D.K. Deardorff, M.I. Copeland, and H.Kato: U.S. Bur. Mines Rept. of Invest. 6521 (1964).

(2) M. Hansen: Constitution of Binary Alloys (McGraw-Hill, New York, 1958).

(3) R.P. Elliott: Constitution of Binary Alloys, First Supplement (McGraw-Hill, New York, 1965).

Section III.A.19 Hf-Cr System

The only previously available information concerned existence and structure of the intermediate phase $HfCr_2$[1,2]. $HfCr_2$ is dimorphic, having a hexagonal, C14 ($MgZn_2$) type of structure (a = 5.067 Å, c = 8.237 Å) up to 1000°C, and a cubic, C15-type structure (a = 7.15 Å) above 1200°C[3]. The polymorphy of $HfCr_2$ was confirmed by S.P. Alisova et al.[2], but the $MgZn_2$-type attributed to the high temperature polymorph, whereas the C15-type (a ~ 4.26 Å) was said to be stable below approximately 1100°C. Our experiments (4) ascertained the C14-modification to be the stable form at high temperatures; the phase has a noticeable homogeneity range at elevated temperatures, extending from approximately 64 At.% Cr (a = 5.090 Å, c = 8.25 Å) to 67 At.% Cr (a = 5.056 Å, c = 8.21 Å) at 1500°C.

Major References:

(1) R.P. Elliott: USAF Contract AF 18(600)-642, Tech. Rept. No. 1, 1954.

(2) S.P. Alisova, P.B. Budberg, and K.I. Shakova: Kristallographiya 9 (1963), 106.

(3) R.P. Elliott: Trans. ASM 53 (1961), 321

(4) E. Rudy and St. Windisch: J.Less Comm.Metals 15 (1968), 13.

(5) M. Hansen: Constitution of Binary Alloys (McGraw-Hill, New York, 1958).

(6) R.P. Elliott: Constitution of Binary Alloys, First Supplement (McGraw-Hill, New York, 1965).

(7) W.B. Pearson: Handbook of Lattice Spacings and Structures of Metals and Alloys (Pergamon Press, New York, 1958); Volume 2 (Pergamon Press, New York, 1967).

Section III.A.20 Hf-Mo System

Except for some details concerning the phase equilibria in the hafnium-rich region of the system, our work confirms the previous investigations by A. Taylor et al.[1]. The solidus liquidus temperatures in hafnium-rich alloys are separated by only a very small temperature interval, as evidenced by the melting behavior as well as by the fact that practically no coring could be observed metallographically and by X-rays in alloys quenched from the liquid state. While there appears little question concerning the polymorphous nature of $HfMo_2$[1,2], experiments conducted under the present program indicate the occurrence of the different modifications to be more affected by the stoichiometry of the alloys than indicated in the work by (1). Since the transformation behavior of $HfMo_2$ does not appear to be sufficiently delineated, it is not shown in the diagram depicted in Figure 1.

Major References

(1) A. Taylor, N.J. Doyle, and J.Kagle: J.Less Comm.Met. 3 (1961), 265.

(2) R.P. Elliott: Trans ASM 53 (1961), 321

(3) M. Hansen: Constitution of Binary Alloys (McGraw-Hill, New York, 1958).

(4) R.P. Elliott: Constitution of Binary Alloys, First Supplement (McGraw-Hill, New York, 1965).

(5) W.B. Pearson: Handbook of Lattice Spacings and Structures of Metals and Alloys (Pergamon Press, New York, 1958); Volume 2 (Pergamon Press, New York, 1967).

Section III.A.21 Hf-W System

The melting isotherms determined in this work agree within the error limits with earlier measurements by H. Braun and E.Rudy[1]; however, the composition of the nonvariant melts as well as the eutectoid, as determined in this work, clearly are in favor of the data reported by B.C. Giessen et al.[2].

Major References:

(1) H. Braun and E. Rudy: Z. Metallkde 51 (1960), 360.

(2) B.C. Giessen, I. Rump, and N.J. Grant: Trans AIME 224 (1962), 60.

(3) M. Hansen: Constitution of Binary Alloys, (McGraw-Hill, New York, 1958).

(4) R.P. Elliott: Constitution of Binary Alloys, First Supplement. (McGraw-Hill, New York, 1965).

(5) W.B. Pearson: Handbook of Lattice Spacings and Structures of Metals and Alloys, (Pergamon Press, New York, 1958); Volume 2 (Pergamon Press, New York, 1967).

Section III.A.22 V-Nb System

Major References:

(1) H.A. Wilhelm, O.N. Carlson, and J.M. Dickinson: Trans. AIME 200 (1954), 915.

(2) M. Hansen: Constitution of Binary Alloys (McGraw-Hill, New York, 1958.

(3) W.B. Pearson: Handbook of Lattice Spacings and Structures of Metals and Alloys, (Pergamon Press, New York, 1958); Volume 2 (Pergamon Press, New York, 1967).

Section III.A.23 V-Ta System

Major References:

(1) O.N. Carlson, D.T. Eash, and A.L. Eustice in: "Reactive Metals" (Interscience, New York, 1959), 277.

(2) W.N. Eremko, L.A. Tretyatsenko, and R.I. Yakhimovits: Zhur. Neorg. Chim. 5 (1960), 2290.

(3) A.P. Nefedov, E.M. Sokolovskaya, A.T. Grigrortev, W.I. Tsetsernikov, I.G. Sokolova, and L.S. Gusei: Vestn. Moskan Univ. Chim., 1965, No. 5 (1965), 42 (data not includes - publication received after evaluation).

(4) M. Hansen: Constitution of Binary Alloys (McGraw-Hill, New York, 1958).

(5) R.P. Elliott: Constitution of Binary Alloys, First Supplement (McGraw-Hill, New York, 1965).

(6) W.B. Pearson: Handbook of Lattice Spacings and Structures of Metals and Alloys (Pergamon Press, New York, 1958); Volume 2 (Pergamon Press, New York, 1967).

Section III.A.24 V-Cr System

Major References:

(1) O.N. Carlson, D.T. Eash, and A.L. Eustice in: "Reactive Metals" (Interscience, New York, 1959), 277.

(2) E.M. Savitskii, W.W. Baron, and Yu.W. Efimov: Trudy Inst. Met. Im. A.A. Baikova Akad. Nauk. SSK 1960, 230.

(3) V.N. Svetsnikov, Y.A. Kochertsinkii, V.M. Pan, E.E. Emaistrenko, and A.K. Shurin: Izled. Zharopr. Splav., Akad. Nauk SSSR, Inst. Met. 4 (1959), 248.

(4) M. Hansen: Constitution of Binary Alloys (McGraw-Hill New York, 1958).

(5) R.P. Elliott: Constitution of Binary Alloys, First Supplement (McGraw-Hill, New York, 1965).

(6) W.B. Pearson: Handbook of Lattice Spacings and Structures of Metals and Alloys (Pergamon Press, New York, 1958), Volume 2 (Pergamon Press, New York, 1967).

Section III.A.25 V-Mo System

Major References:

(1) W.W. Baron, Yu.V. Efimov, and E.M. Savitskii: Izvest. Akad. Nauk SSSR, Otd. Tekhn. Nauk, 1958 (4), 36-40.

(2) M. Hansen: Constitution of Binary Alloys: (McGraw-Hill, New York, 1958).

(3) R.P. Elliott: Constitution of Binary Alloys, First Supplement (McGraw-Hill, New York, 1965).

(4) W.B. Pearson: Handbook of Lattice Spacings and Structures of Metals and Alloys (Pergamon Press, New York, 1958); Volume 2 (Pergamon Press, New York, 1967).

Section III.A.26 V-W System

Major References:

(1) R. Kieffer, K. Sedlatschek, and H. Braun: J.Less Comn .Met. 1 (1959), 19; Z.Metallkde 50 (1959), 18.

(2) W.W. Baron, Yu.V. Efimov, and E.M. Savitskii: Izvest. Akad. Nauk SSSR, Otd. Tekhn. Nauk, Met i Toplivo 1960, 70.

(3) M. Hansen: Constitution of Binary Alloys (McGraw-Hill, New York, 1958).

(4) R.P. Elliott: Constitution of Binary Alloys, First Supplement (McGraw-Hill, New York, 1965).

(5) W.B. Pearson: Handbook of Lattice Spacings and Structures of Metals and Alloys, (Pergamon Press, New York, 1958); Volume 2 (Pergamon Press, New York, 1967).

Section III.A.27. Nb-Ta System

Major References:

(1) D.E. Williams and W.H. Pechin: Trans ASM 50 (1958), 1081.

(2) H. Buckle: Z. Metallkde 37 (1946), 53.

(3) M. Hansen: Constitution of Binary Alloys (McGraw-Hill, New York, 1958).

(4) R.P. Elliott: Constitution of Binary Alloys, First Supplement (McGraw-Hill, New York, 1965).

(5) W.B. Pearson: Handbook of Lattice Spacings and Structures of Metals and Alloys (Pergamon Press, New York, 1958); Volume 2 (Pergamon Press, New York, 1967).

Section III.A.28. Nb-Cr System

Major References:

(1) W.P. Elyutin and W.F. Funke: Izvest. Akad. Nauk SSSR, Otd. Tekhn. Nauk No. 3 (1956), 68.

(2) W.N. Eremenko, G.W. Zudilova, and L.A. Gayevskaya: Metalloved. i. Obr. Metal. No. 1 (1958), 11.

(3) W.M. Pan: Fiz. Metall. Metalloved. 12 (1961), 455.

(4) G. Petzow and A. Junker: J. Less Comm. Met. 5 (1963), 462.

(5) M. Hansen: Constitution of Binary Alloys (McGraw-Hill, New York, 1958).

(6) R.P. Elliott: Constitution of Binary Alloys, First Supplement (McGraw-Hill, New York, 1965).

(7) W.B. Pearson: Handbook of Lattice Spacings and Structures of Metals and Alloys (Pergamon Press, New York, 1958); Volume 2 (Pergamon Press, New York, 1967).

Section III.A.29 Nb-Mo System

Major References:

(1) I.I. Kornilov and R.S. Polyakova: Trudy Institut. Metall. im. A.A. Baikov Akad. Nauk SSSR No.2 (1957), 149.

(2) H. Bückle: Z. Metallkde 37 (1946), 53.

(3) E. Rudy, C.E. Brukl, and St. Windisch: Trans AIME 239 (1967), 1796.

(4) M. Hansen: Constitution of Binary Alloys (McGraw-Hill, New York, 1958).

(5) R.P. Elliott: Constitution of Binary Alloys, First Supplement (McGraw-Hill, New York, 1965).

(6) W.B. Pearson: Handbook of Lattice Spacings and Structures of Metals and Alloys (Pergamon Press, New York, 1958); Volume 2 (Pergamon Press, New York, 1967).

Section III.A.30 Nb-W System

Major References:

(1) V.S. Micheev and D.M. Pevtsvov: Zh. Neorg. Chim. 3 (1958), 861.

(2) B.I. Krimer and Yu.E. Matveev: Proizv i Obrab. Stali i Splav., Moscow Steel Inst. 38 (1958), 420.

(3) H. Bückle: Z. Metallkde 37 (1946), 53.

(4) M. Hansen: Constitution of Binary Alloys (McGraw-Hill, New York, 1958).

(5) R.P. Elliott: Constitution of Binary Alloys, First Supplement (McGraw-Hill, New York, 1965).

(6) W.B. Pearson: Handbook of Lattice Spacings and Structures of Metals and Alloys (Pergamon Press, New York, 1958); Volume 2 (Pergamon Press, New York, 1967).

Section III.A.31 Ta-Cr System

In addition to the lattice parameter measurements on the hexagonal (C14-type) high temperature modification of $TaCr_2$, Figure III.A.31.5, metallographic as well as X-ray analysis indicated also a sizeable homogeneity range for the cubic (C15-type) low temperature modification. In the average, $a = 7.02$ Å were found for excess tantalum ($X_{cr} < 0.64$), and $a = 6.97_5$ Å for excess chromium-containing alloys ($X_{cr} > 0.67$) in alloys which were equilibrated at 1400°C.

Major References:

(1) O. Kubaschewski and H. Speidel: J. Inst. Met. 75 (1948), 410.

(2) A.T. Grigoreev, V.V. Kuprina, and N.A. Nedumov: Zh. Neorg. Chim. 4 (1959).

(3) M. Hansen: Constitution of Binary Alloys (McGraw-Hill, New York, 1958).

(4) R.P. Elliott: Constitution of Binary Alloys, First Supplement (McGraw-Hill, New York, 1965).

(5) W.B. Pearson: Handbook of Lattice Spacings and Structures of Metals and Alloys (Pergamon Press, New York, 1958); Volume 2 (Pergamon Press, New York, 1967).

Section III.A.32 Ta-Mo System

Major References:

(1) G.A. Geach and D. Summers-Smith: J.Inst. Met. 80 (1951), 143.

(2) M. Hansen: Constitution of Binary Alloys (McGraw-Hill, New York, 1958).

(3) R.P. Elliott: Constitution of Binary Alloys, First Supplement (McGraw-Hill, New York, 1965).

(4) W.B. Pearson: Handbook of Lattice Spacings and Structures of Metals and Alloys (Pergamon Press, New York, 1958); Volume 2 (Pergamon Press, New York, 1967).

Section III.A.33 Ta-W System

Major References:

(1) H. Buckle: Z. Metallkde 37 (1946), 53.

(2) E. Rudy: US Air Force Tech. Doc. Report AFML-TR-65-2, Part II, Volume VIII (March 1966).

(3) M. Hansen: Constitution of Binary Alloys (McGraw-Hill, New York, 1958).

(4) R.P. Elliott: Constitution of Binary Alloys, First Supplement (McGraw-Hill, New York, 1965).

(5) W. B. Pearson: Handbook of Lattice Spacings and Structures of Metals and Alloys (Pergamon Press, New York, 1958); Volume 2 (Pergamon Press, New York, 1967).

Section III.A.34 Cr-Mo System

Major References:

(1) W. Trzebiatowski and H. Ploszek: Nat. Wiss. 26 (1938), 462.

(2) O. Kubaschewski and A. Schneider: Z. Elektrochem. 48 (1942), 671.

(3) J.W. Putman, R.D. Potter, and N.J. Grant: Trans ASM 43 (1951), 824.

(4) D.S. Bloom and N.J. Grant: Trans. AIME 200 (1954), 261.

(5) M. Hansen: Constitution of Binary Alloys (McGraw-Hill, New York, 1958).

(6) R.P. Elliott: Constitution of Binary Alloys, First Supplement (McGfaw-Hill, New York, 1965).

(7) W.B. Pearson: Handbook of Lattice Spacings and Structures of Metals and Alloys (Pergamon Press, New York, 1958); Volume 2 (Pergamon Press, New York, 1967).

Section III.A.35 Cr-W System

Major References:

(1) H T. Greenaway: J. I· t. Met. 80 (1951) - 589

(2) W. Trzebiatowski, H. Ploszek, and J. Lobzowski: Anal.Chem. 19 (1947), 93.

(3) O. Kubaschewski and A. Schneider: Z. Elektrochem. 48 (1942), 671.

(4) M. Hansen: Constitution of Binary Alloys (McGraw-Hill, New York, 1958).

(5) R.P. Elliott: Constitution of Binary Alloys, First Supplement (McGraw-Hill, New York, 1965).

(6) W.B. Pearson: Handbook of Lattice Spacings and Structures of Metals and Alloys (Pergamon Press, New York, 1958); Volume 2 (Pergamon Press, New York, 1967).

Section III.A.36 Mo-W System

Major References:

(1) F.A. Fahrenwald: Trans. AIME 54 (1917), 570.

(2) Z. Jeffries: Trans. AIME 56 (1917), 600.

(3) M. Hansen: Constitution of Binary Alloys (McGraw-Hill, New York, 1965).

(4) R.P. Elliott: Constitution of Binary Alloys, First Supplement (McGraw-Hill, New York, 1965).

(5) W.B. Pearson: Handbook of Lattice Spacings and Structures of Metals and Alloys (Pergamon Press, New York, 1958); Volume 2 (Pergamon Press, New York, 1967).

Section III.A.37 Hf-Ir Alloys

Major References:

(1) J.H. Schwartz and M.V. Nevitt: Trans AIME 212 1958, 700.

(2) A.E. Dwight: Trans AIME 215 (1959), 283.

(3) A.E. Dwight and P.A. Beck: Trans AIME 215 (1959), 976.

(4) C.E. Brukl and E. Rudy: US Air Force Tech. Doc. Report AFML-TR-65-2, Part II, Vol. XIV (July 1967).

(5) R.P. Elliott: Constitution of Binary Alloys, First Supplement (McGraw-Hill, New York, 1965).

(6) W.B. Pearson: Handbook of Lattice Spacings and Structures of Metals and Alloys (Pergamon Press, New York, 1958); Volume 2 (Pergamon Press, New York, 1967).

B. BINARY TRANSITION METAL CARBON SYSTEMS

Section III.B.1 Ti-C System

Major References:

(1) M. Hansen: Constitution of Binary Alloys (McGraw-Hill, New York, 1958).

(2) R.P. Elliott: Constitution of Binary Alloys, First Supplement (McGraw-Hill, New York, 1965).

(3) W.B. Pearson: Handbook of Lattice Spacings and Structures of Metals and Alloys (Pergamon Press, New York, 1958); Volume 2 (Pergamon Press, New York, 1967).

(4) E.K. Storms, Refractory Carbides (Academic Press, 1967).

(5) E. Rudy, D.P. Harmon, and C.E. Brukl: US Air Force Tech. Doc. Report AFML-TR-65-2, Part I, Vol. II (August 1965).

Section III.B.2 Zr-C System

Major References:

(1) M. Hansen: Constitution of Binary Alloys (McGraw Hill, New York, 1958).

(2) R.P. Elliott: Constitution of Binary Alloys, First Supplement (McGraw-Hill, New York, 1965).

(3) W.B. Pearson: Handbook of Lattice Spacings and Structures of Metals and Alloys (Pergamon Press, New York, 1958); Volume 2 (Pergamon Press, New York, 1967).

(4) E.K. Storms: Refractory Carbides (Academic Press, 1967).

(5) E. Rudy, D.P. Harmon, and C.E. Brukl: US Air Force Tech. Doc. Report AFML-TR-65-2, Part I, Vol. II (August 1965)

Section III.B.3 Hf-C System

Major References:

(1) M. Hansen: Constitution of Binary Alloys (McGraw-Hill, New York, 1958).

(2) R.P. Elliott: Constitution of Binary Alloys, First Supplement (McGraw-Hill, New York, 1965).

(3) W.B. Pearson: Handbook of Lattice Spacings and Structures of Metals and Alloys (Pergamon Press, New York, 1958); Volume 2 (Pergamon Press, New York, 1967).

(4) E.K. Storms: Refractory Carbides (Academic Press, 1967)

(5) D.K. Deardorff, M.I. Copeland, and R.P. Adams: US Bureau Mines Rept. of Invest. No. 6983 (July 1967).

(6) E. Rudy: US Air Force Doc. Report AFML-TR-65-2, Part I, Vol.IV (October 1965).

Section III.B.4 V-C System

Major References:

(1) M. Hansen: Constitution of Binary Alloys: (McGraw-Hill, New York 1958).

(2) R.P. Elliott: Constitution of Binary Alloys, First Supplement (McGraw-Hill, New York, 1965).

(3) W.B. Pearson: Handbook of Lattice Spacings and Structures of Metals and Alloys (Pergamon Press, New York, 1958); Volume 2 (Pergamon Press, New York, 1967).

(4) E.K. Storms: Refractory Carbides (Academic Press, 1967).

(5) E. Rudy, St. Windisch, and C.E. Brukl: US Air Force Tech. Doc. Report AFML-TR-65-2, Part I, Vol. XII (Sept. 1967); Planseeber. Pulvermet. 1968, in print.

Section III.B.5 Nb-C System

Major References:

(1) M. Hansen: Constitution of Binary Alloys (McGraw-Hill, New York, 1958).

(2) R.P. Elliott: Constitution of Binary Alloys, First Supplement (McGraw-Hill, New York, 1965).

(3) W.B. Pearson: Handbook of Lattice Spacings and Structures of Metals and Alloys (Pergamon Press, New York, 1958); Volume 2 (Pergamon Press, New York, 1967).

(4) E.K Storms: Refractory Carbides (Academic Press 1967).

(5) E. Rudy, St. Windisch, and C.E. Brukl: US Air Force Tech. Doc. Report AFML-TR-65-2, Part I, Vol. XII (Sept. 1967). Planseeber. Pulvermet. 1968, in print.

Section III.B.6 Ta-C System

Since the time of publication of the documentary report, additional work on the α-β-Ta_2C transition led to the assumption of a transformation behavior as shown in Figure 1.

Major References:

(1) E. Rudy and D.P. Harmon: US Air Force Tech. Doc. Report AFML-TR-65-2, Part I, Vol. V (Dec. 1965).

(2) M. Hansen: Constitution of Binary Alloys (McGraw-Hill, New York, 1958).

(3) R.P. Elliott: Constitution of Binary Alloys, First Supplement (McGraw-Hill, New York, 1965).

(4) W.B. Pearson: Handbook of Lattice Spacings and Structures of Metals and Alloys (Pergamon Press, New York, 1958); Volume 2 (Pergamon Press, New York, 1967).

(5) E.K. Storms: Refractory Carbides (Academic Press, 1967).

Section III.B.7 Cr-C System

Major References:

(1) M. Hansen: Constitution of Binary Alloys (McGraw-Hill, New York, 1958).

(2) R.P. Elliott: Constitution of Binary Alloys, First Supplement (McGraw-Hill, New York, 1965).

(3) W.B. Pearson: Handbook of Lattice Spacings and Structures of Metals and Alloys (Pergamon Press, New York, 1958); Volume 2 (Pergamon Press, New York, 1967).

(4) E.K. Storms: Refractory Carbides (Academic Press 1967).

Section III.B.8 Mo-C System

Major References:

(1) M. Hansen: Constitution of Binary Alloys (McGraw-Hill, New York, 1958).

(2) R.P. Elliott: Constitution of Binary Alloys, First Supplement (McGraw-Hill, New York, 1965).

(3) W.B. Pearson: Handbook of Lattice Spacings and Structures of Metals and Alloys (Pergamon Press, New York, 1958); Volume 2 (Pergamon Press, New York, 1967).

(4) E.K. Storms: Refractory Carbides (Academic Press, 1967).

(5) E. Rudy, St. Windisch, A.J. Stosick, and J.R. Hoffman: US Air Force Tech. Report AFML-TR-65-2, Part I, Vol. XI (April 1967). Trans. AIME 239 (1967), 1247.

Section III.B.9 W-C System

Major References:

(1) M. Hansen: Constitution of Binary Alloys (McGraw-Hill, New York, 1958).

(2) R.P. Elliott: Constitution of Binary Alloys, First Supplement (McGraw-Hill, New York, 1965).

(3) W.B. Pearson: Handbook of Lattice Spacings and Structures of Metals and Alloys (Pergamon Press, New York, 1958); Volume 2 (Pergamon Press, New York, 1967).

(4) E.K. Storms: Refractory Carbides (Academic Press, 1967).

(5) E. Rudy, St. Windisch, and J.R. Hoffman: US Air Force Tech. Doc. Report AFML-TR-65-2, Part I, Vol. VI (Jan 1966).

(6) E. Rudy and J.R. Hoffman: Planseeber. Pulvermet. 15 (1967). 174.

C. BINARY TRANSITION METAL-BORON AND METAL-SILICON SYSTEMS

Section III.C. Metal-Boron Systems

Section III.D. Metal-Silicon Systems

For these system groups, the following, general references, as well as the report references listed under the individual systems may be consulted for a detailed compilation and evaluation of earlier investigations.

General References to Sections III.C. and III.D.:

(1) M. Hansen: Constitution of Binary Alloys (McGraw-Hill, New York, 1958).

(2) R.P. Elliott: Constitution of Binary Alloys, First Supplement (McGraw-Hill, New York, 1965).

(3) W.B. Pearson: Handbook of Lattice Spacings and Structures of Metals and Alloys (Pergamon Press, New York, 1958); Volume 2 (Pergamon Press, New York, 1967).

Section III.C.1. Ti-B System

Report Reference:

(1) E. Rudy and St. Windisch: US Air Force Tech. Doc. Report AFML-TR-65-2, Part I, Vol. VII (Jan 1966).

Section III.C.2. Zr-B System

Report Reference:

(1) E. Rudy and St. Windisch: US Air Force Tech. Doc. Report AFML-TR-65-2, Part I, Vol. VIII (Jan 1966).

Section III.C.3 Hf-B System

Report Reference:

(1) E. Rudy and St. Windisch: US Air Force Tech. Doc. Report AFML-TR-65-2, Part I, Vol. IX (Feb. 1966).

Section III.C.4 V-B System

Report Reference:

(1) E. Rudy and St. Windisch: US Air Force Tech. Doc. Report AFML-TR-65-2, Part I, Vol. X (May 1966).

Section III.C.5 Nb-B System

Report Reference:

(1) E. Rudy and St. Windisch: US Air Force Tech. Doc. Report AFML-TR-65-2, Part I, Vol. X (May 1966).

Section III.C.6 Ta-B System

Report Reference:

(1) E. Rudy and St. Windisch: US Air Force Tech. Doc. Report AFML-TR-65-2, Part I, Vol. X (May 1966).

Section III.C.7 Mo-B System

Report Reference:

(1) E. Rudy and St. Windisch: US Air Force Tech. Doc. Report AFML-TR-65-2, Part I, Vol. III (Sept. 1965).

Section III.C.8 W-B System

Report Reference

(1) E. Rudy and St. Windisch: US Air Force Tech. Doc. Report AFML-TR-65-2, Part I, Vol. III (Sept. 1965).

Section III.D.1 Zr-Si System

Report Reference:

(1) C.E. Brukl: US Air Force Tech. Doc. Rreport AFML-TR-65-2 Part I, Vol. XIII (Nov. 1967).

Section III.D.2 Hf-Si System

Report Reference:

(1) C.E. Brukl: US Air Force Tech. Doc. Report AFML-TR-65-2, Part I, Vol. XIII (Nov. 1967).

D. TERNARY SYSTEMS Me_1-Me_2-C, Me-Si-C, Me-Si-B, Me_1-Me_2-B, Me-B-C, and Me-B-N

Section III.E. Ternary Metal-Carbon Systems

Section III.F. Quaternary Metal-Carbon Systems

Section III.G. Metal-Silicon-Carbon Systems

Section III.H. Metal-Silicon-Boron Systems

Section III.I. Ternary Metal-Boron Systems

Section III.K. Metal-Boron-Carbon System

Section III.L. Ternary Metal-Nitrogen Systems

The following, general, references may be consulted for a comprehensive compilation of earlier work on these ternary system classes:

(1) R. Kieffer and F. Benesovsky: Hartstoffe (Springer, Wien, 1963).

(2) W.B. Pearson: Handbook of Lattice Spacings and Structures of Metals and Alloys (Pergamon Press, New York, 1958); Volume 2 (Pergamon Press, New York, 1967).

Section III.E.1 Ti-Zr-C System

References:

(1) C.E. Brukl and D.P. Harmon: US Air Force Tech. Doc. Report AFML-TR-65-2, Part II, Vol. IV (Feb. 1966).

(2) Yu.V. Voroshilov, L.V. Gorshkova, N.M. Popova, and T.F. Fedorov: Poroshk. Metallurgiya No.5 (1967), 81.

Section III.E.2 Ti-Hf-C System

References:

(1) C.E. Brukl and D.P. Harmon: US Air Force Tech. Doc. Rept. AFML-TR-65-2, Part II, Vol. IV (Feb. 1966).

(2) Yu.V. Voroshilov, L.V. Gorshkova, N.M. Popova, and T.F. Fedorov: Poroshk. Metallurgiya No.5 (1967), 81.

Section III.E.3 Ti-V-C System

References:

(1) W.N. Eremenko and L.A. Tretyatsenko: Poroshk. Metallurgiya 6 (1964), 27.

(2) T.F. Fedorov, L.V. Gorshkova, and E.I. Gladyshevskiy: Russian Metallurgy (Eng. Transl.), 4 (1966), 60.

(3) L.A. Tretyatsenko and V.N. Eremenko: Poroshk. Metallurgiya, 7 (1966), 581.

(4) L.A. Tretyatsenko and V.N. Eremenko: Poroshk. Metallurgiya, 8 (1966), 33.

(5) E. Rudy: US Air Force Tech. Doc. Report AFML-TR-69-117, Part VII, "The Phase Diagram Ti-V-C" (May 1969).

Section III.E.4 Ti-Nb-C System

References:

(1) P. Stecher, F. Benesovsky, A. Neckel, and H. Nowotny: Monatsh. Chem. 95, 1636.

(2) T.F. Fedorov, N.M. Popova, and E.I. Gladyshevskiy: Izvest.Akad Nauk SSSR Metall. 3 (1965), 158.

(3) E. Rudy: US Air Force Tech. Doc. Report AFML-TR-69-117, Part I, "The Phase Diagrams Ti-Nb-C, Ti-Ta-C, and Ti-Mo-C" (May 1969).

Section III.E.5 Ti-Ta C System

References:

(1) J.G. McMullin and J.T. Norton: J.Met. 5 (1953), 1205.

(2) C.E. Brukl and D.P. Harmon: U.S. Air Force Tech. Doc. Report AFML-TR-65-2, Part II, Vol. II (July 1965).

(3) E. Rudy: US Air Force Technical Documentary Report AFML-TR-69-117, Part I, "The Phase Diagrams Ti-Nb-C, Ti-Ta-C, and Ti-Mo-C" (May 1969).

Section III.E.6 Ti-Mo-C System

References:

(1) H.J. Albert and J.T. Norton: Planseeber. Pulvermet. 4 (1956), 2.

(2) E. Rudy: U.S. Air Force Tech. Doc. Report AFML-TR-69-117, Part I, "The Phase Diagrams Ti-Nb-C, Ti-Ta-C, and Ti-Mo-C" (May 1969).

Section III.E.7 Zr-Hf-C System

References:

(1) C.E. Brukl and D.P. Harmon: U.S. Air Force Tech. Doc. Report AFML-TR-65-2, Part II, Vol. IV (Feb. 1966).

Section III.E.8 Zr-Ta-C System

Recent findings resulted in the assumption of a different mode of transformation of the Ta_2C-phase (see Section III.B.6). Although the gross features of the Zr-Ta-C system, as presented herein, will remain

unaffected by these changes in the Ta-C system, certain details of the ternary phase equilibria near the Ta_2C-phase will have to be modified.

References:

(1) D.P. Harmon and C.E. Brukl: US Air Force Tech. Doc. Rept. AFML-TR-65-2, Part II, Vol. III (Aug. 1965).

(2) A.I. Avgustinik and S.S. Ordanyan: Zhur. Prikl. Chim. 39 (1966), 318.

Section III.E.9 Ta-Hf-C System

The changes introduced by the different mode of transformation assumed for the Ta_2C-phase in more recent work (Section III.B.6) are being investigated at the present time.

References:

(1) E. Rudy and H. Nowotny: Mh.Chem. 94 (1963), 507.

(2) E. Rudy: US Air Force Tech. Doc. Report AFML-TR-65-2, Part II, Vol. I (June 1965).

(3) D.L. Deadmore and I. Zaplatynsky: NASA Rept. TN D-2768 (April 1965).

Section III.E.10. V-Nb-C System

References:

(1) Y.A. Chang: US Air Force Tech. Doc. Report AFML-TR-65-2, Part II, Vol. XVI (Dec. 1967).

Section III.E.11 Nb-Ta-C System

References:

(1) E. Rudy and P. Booker: U.S. Air Force Tech. Doc. Report AFML-TR-69-117, Part III, "Phase Studies in the Systems V-Ta-C and Nb-Ta-C" (May 1969).

Section III.E.12 Nb-Mo-C System

References:

(1) E. Rudy, F. Benesovsky, and K. Sedlatschek: Mh.Chem. 92 (1961), 841.

(2) E. Rudy, C.E. Brukl, and St. Windisch: U.S. Air Force Tech. Doc. Report AFML-TR-65-2, Part II, Vol. XV. Trans. AIME 239 (1967), 1795.

Section III.E.13 Nb-W-C System

References:

(1) E. Rudy and Y.A. Chang: Plansee Proc. 1964, 786.

(2) E. Rudy: U.S. Air Force Tech. Doc. Rept. AFML-TR-65-2, Part II, Vol. XVIII (March 1968).

Section III.E.14 Ta-Mo-C System

References:

(1) E. Rudy and Y.A. Chang: Plansee Proc., 1964, 786.

(2) E. Rudy, St. Windisch, and C.E. Brukl: U.S. Air Force Tech. Doc. Rept. AFML-TR-65-2, Part II, Vol. XVII (Dec. 1967). J. Amer. Ceram. Soc. 51 (1968), 239.

Section III.E.15 Ta-W-C System

The illustrations contained in this report represent an updated version of the system published in (2).

References:

(1) E. Rudy, El. Rudy, and F. Benesovsky: Mh.Chem. 93 (1962), 1176.

(2) E. Rudy: U.S. Air Force Tech. Doc. Rept. AFML-TR-65-2, Part II, Vol. VIII (March 1966).

Section III.F.1 Ta_2C-V_2C-Mo_2C System

References:

(1) C.E. Brukl: U.S. Air Force Tech. Doc. Report AFML-TR-69-117, Part IV, "Effect of Molybdenum and Tungsten on the Subcarbide Solutions in the Systems Ta-V-C and Ta-Nb-C" (May 1969).

Section III.F.2 Ta_2C-V_2C-W_2C System

References:

(1) C.E. Brukl: U.S. Air Force Tech. Doc. Report AFML-TR-69-117, Part IV, "Effect of Molybdenum and Tungsten on the Subcarbide Solutions in the Systems Ta-V-C and Ta-Nb-C" (May 1969).

Section III.F.3 Ta_2C-Nb_2C-Mo_2C System

References:

(1) C.E. Brukl: U.S. Air Force Tech. Doc. Report AFML-TR-69-117, Part IV, "Effect of Molybdenum and Tungsten on the Subcarbide Solutions in the Systems Ta-V-C and Ta-Nb-C" (May 1969)

Section III.F.4 Ta_2C-Nb_2C-W_2C System

References:

(1) C.E. Brukl: U.S. Air Force Tech. Doc. Report AFML-TR-69-117, Part IV, "Effect of Molybdenum and Tungsten on the Subcarbide Solutions in the Systems Ta-V-C and Ta-Nb-C" (May 1969).

Section III.G.1 Ti-Si-C System

References:

(1) L. Brewer and O. Krikorian: U.S. AEC Public. UCRL-2544 (1954). (tentative).

(2) C.E. Brukl: U.S. Air Force Tech. Doc. Rept. AFML-TR-65-2, Part II, Vol. VII (May 1966).

Section III.G.2 Zr-Si-C System

References:

(1) C.E. Brukl: U.S. Air Force Tech. Doc. Report AFML-TR-65-2, Part II, Vol.X (Sept. 1966).

Section III.G.3 Hf-Si-C System

References:

(1) C.E. Brukl: U.S. Air Force Tech. Doc. Report AFML-TR-65-2, Part II, Vol. X (Sept 1966).

Section III.G.4 Nb-Si-C System

References:

(1) L. Brewer and O. Krikorian: U.S. AEC Public. UCRL-2544 (1954). (tentative investigation).

(2) C.E. Brukl: U.S. Air Force Tech. Doc. Report AFML-TR-65-2, Part II, Vol. VII (May 1966).

Section III.G.5 W-Si-C System

References:

(1) L. Brewer and O. Krikorian: U.S. AEC Public. UCRL-2544 (1954) (tentative investigation).

(2) C.E. Brukl: U.S. Air Force Tech. Doc. Report AFML-TR-65-2, Part II, Vol. VII (May 1966).

Section III.G.1 Hf-Si-B System

References:

(1) C.E. Brukl: U.S. Air Force Tech. Doc. Rept. AFML-TR-65-2, Part II, Vol. X (Sept. 1966).

Section III.I.1 Ti-Zr-B System

References:

(1) T.E. Eckert: U.S. Air Force Tech. Doc. Report AFML-TR-65-2, Part II, Vol. XII (Jan 1967).

Section III.I.2 Ti-Hf-B System

References:

(1) Y.A. Chang: U.S. Air Force Tech. Doc. Report AFML-TR-65-2 Part II, Vol.V (May 1966).

Section III.I.3 Zr-Hf-B System

References:

(1) D.P. Harmon: U.S. Air Force Tech. Doc. Report AFML-TR-65-2, Part II, Vol. VI (Nov. 1965).

Section III.I.4 Zr-W-B System

References:

(1) Y.A. Chang: U.S. Air Force Tech. Doc. Report AFML-TR-65-2, Part II, Vol. IX (Oct. 1966).

Section III.I.5 Hf-Mo-B System

References:

(1) D.P. Harmon: U.S. Air Force Tech. Doc. Report AFML-TR-65-2, Part II, Vol. XI (Sept. 1966).

Section III.I.6 Hf-W-B System

References:

(1) D.P. Harmon: U.S. Air Force Tech. Doc. Report AFML-TR-65-2, Part II, Vol. XI (Sept. 1966).

Sections III.I.7; III.I.8; III.I.9; III.I.10: Investigations of Pseudobinaries Systems $Me_{(1)}B_2$-$Me_{(2)}B_2$ in the Systems Zr-Nb-B, Zr-Ta-B, Hf-Nb-B, and Hf-Ta-B.

References:

(1) T.E. Eckert: U.S. Air Force Tech. Doc. Report AFML-TR-65-2, Part II, Vol. XII (Jan 1967).

(2) Y.A. Chang: U.S. Air Force Tech. Doc. Report AFML-TR-65-2, Part II, Vol. IX (Oct. 1966).

Section III.K.1 Ti-B-C System

Major References:

(1) H. Nowotny, F. Benesovsky, C.E. Brukl, and O. Schob: Mh. Chem. 92 (1961), 403.

(2) E. Rudy and St. Windisch: U.S. Air Force Tech. Doc. Report AFML-TR-65-2, Part II, Vol. XIII (Dec.1966).

Section III.K.2 Zr-B-C System

References:

(1) L. Brewer and H. Haroldsen: J.Electrochem.Soc. 102 (1953), 399.

(2) H. Nowotny, E. Rudy, and F. Benesovsky: Mh.Chem. 92 (1961), 393.

(3) E. Rudy and St. Windisch: U.S. Air Force Tech. Doc. Report AFML-TR-65-2, Part II, Vol. XIII (Dec. 1966).

Section III.K.3 Hf-B-C System

References:

(1) H. Nowotny, E. Rudy, and F. Benesovsky: Mh.Chem. 92 (1961), 393.

(2) E. Rudy and St. Windisch: U.S. Air Force Tech. Doc. Report AFML-TR-65-2, Part II, Vol. XIII (Dec. 1966).

Section III.K.4 W-B-C System

References:

(1) L. Brewer and H. Haroldsen: J. Electrochem. Soc. 102 (1955), 399.

(2) E. Rudy, F. Benesovsky, and L. Toth: Z.Metallkde. 54 (1963), 345.

(3) E. Rudy: U.S. Air Force Tech. Doc. Report AFML-TR-69-117, Part V, "The Phase Diagram W-B-C" (May 1969).

Section III.L.1 Hf-Ta-N System

References:

(1) E. Rudy: Dissert. Techn. Hochschule Wien, 1960.

(2) P. Booker and C.E. Brukl: U.S. Air Force Tech. Doc. Report AFML-TR-65-2, Part VI, "Phase Equilibria in the Metal-Rich Region of the System Hf-Ta-N" (May 1969).

III. COLLECTION OF PHASE DIAGRAM DATA

A. BINARY TRANSITION METAL SYSTEMS

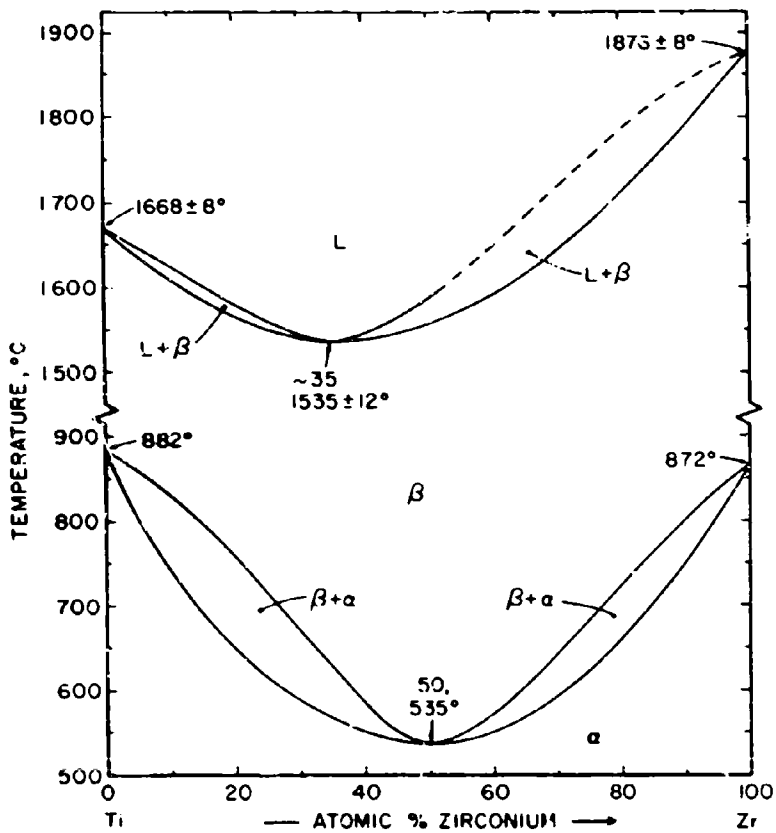

Figure III.A.1.1: Constitution Diagram Titanium-Zirconium.

(Temperature Error Figures Based on Estimated Overall Uncertainty).

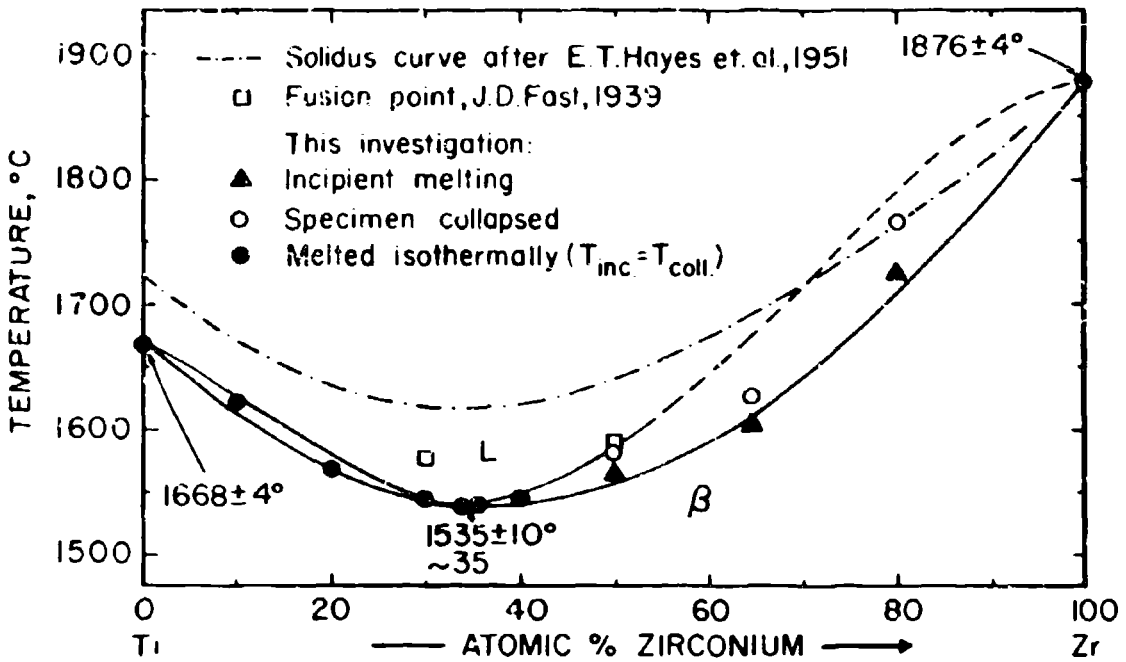

Figure III.A.1.2: Melting Temperatures of Ti-Zr Alloys.

(Temperature Error Figures Based on Reproducibility)

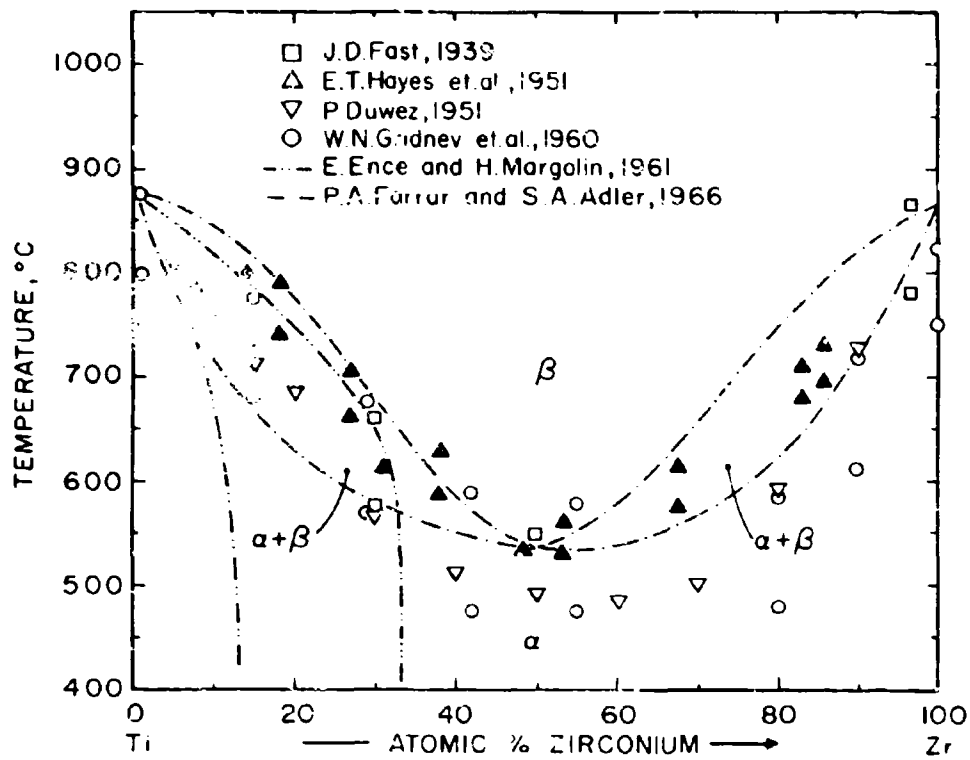

Figure III.A.1.3: α-β-Transformation in Ti-Zr Alloys.

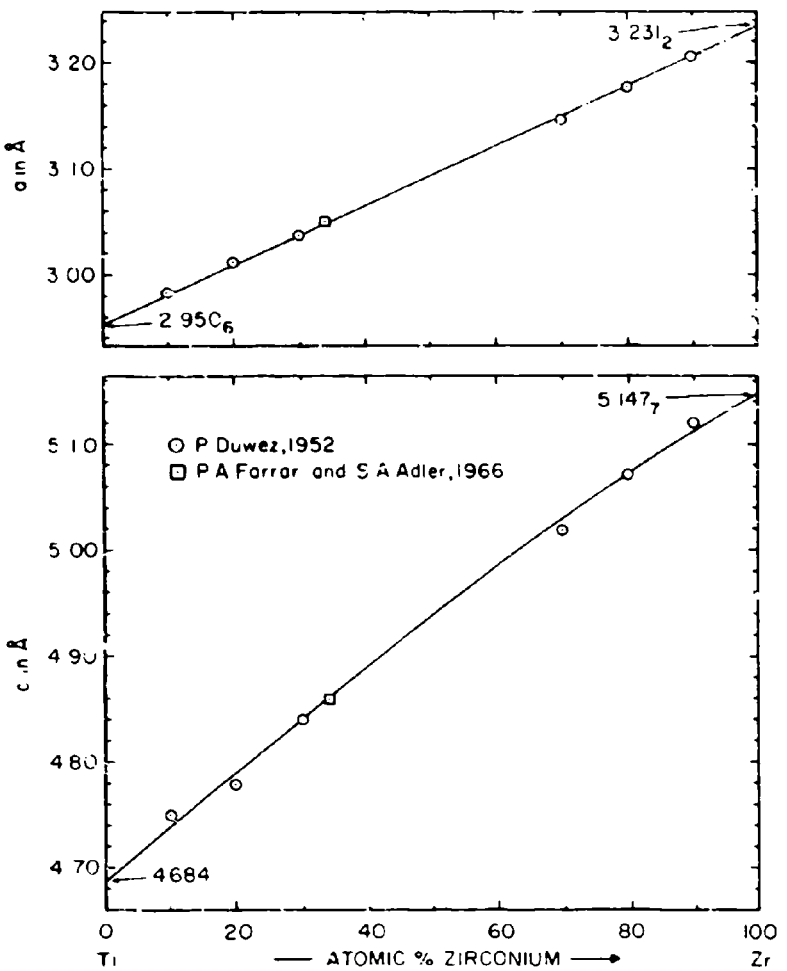

Figure III.A.1.4: Lattice Parameters of the α-(Ti, Zr) Solid Solution.

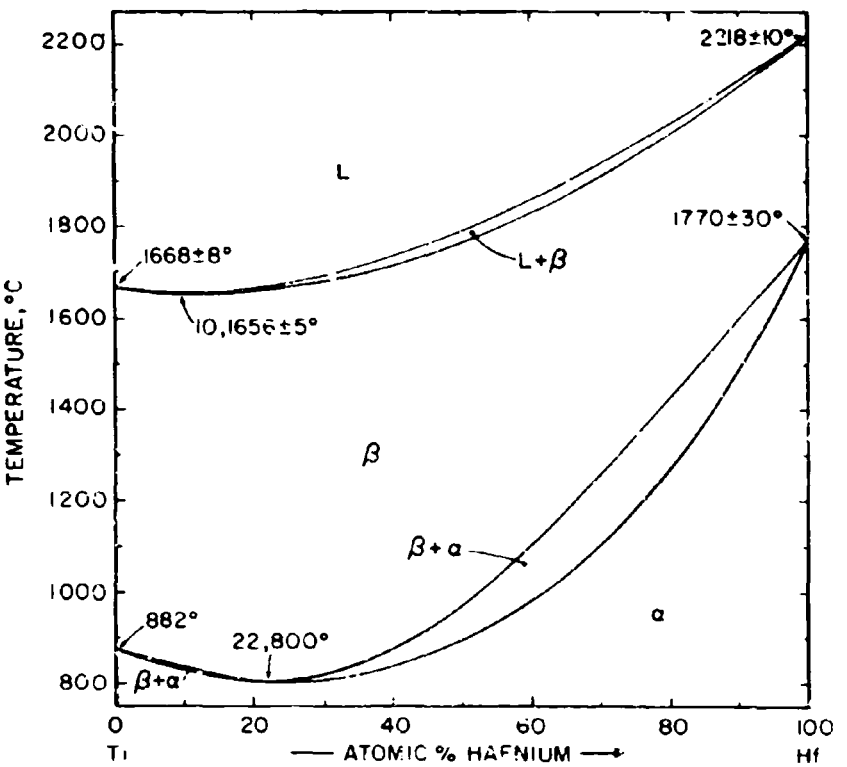

Figure III.A.2.1: Constitution Diagram Ti-Hf.

(Temperature Error Figures Based on Estimated Overall Uncertainty).

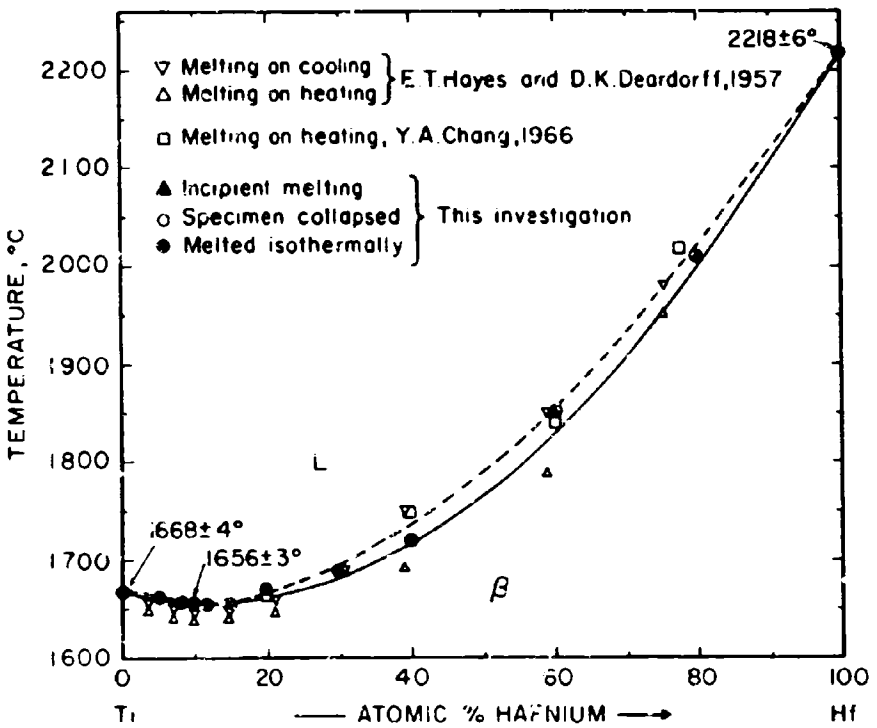

Figure III.A.2.7: Melting Temperatures of Ti-Hf Alloys.

(Temperature Error Figures Based on Reproducibility).

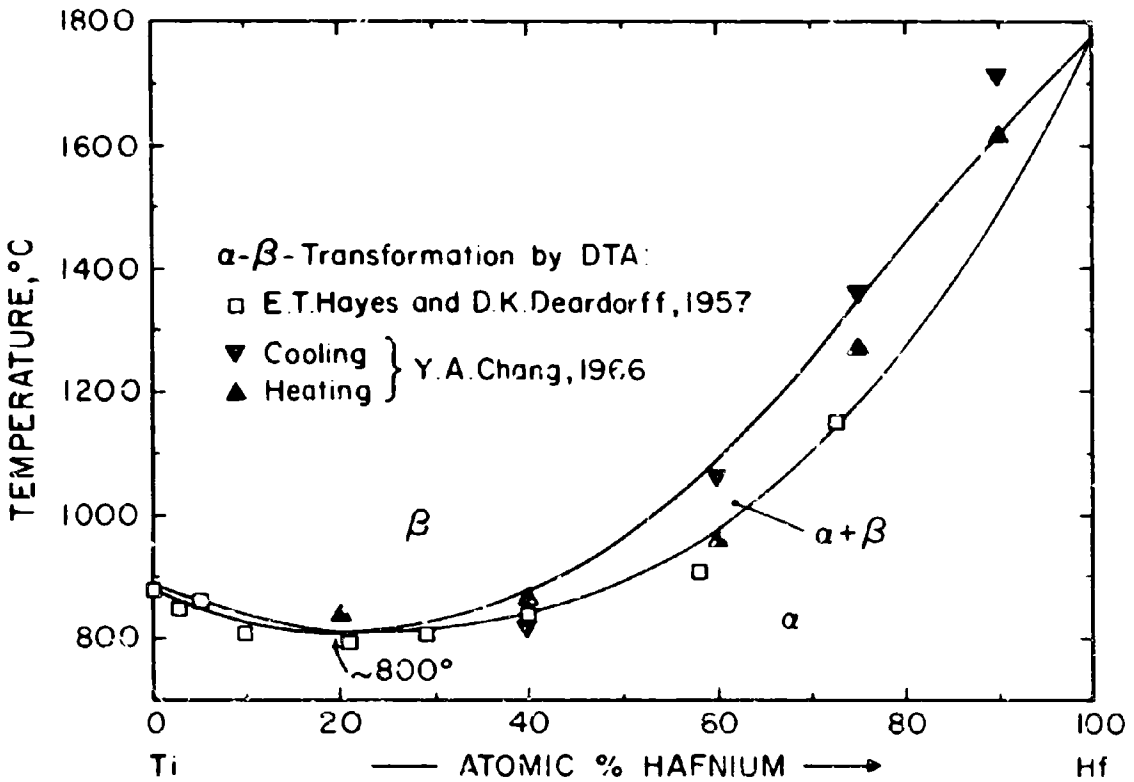

Figure III.A.2.3: α-β-Transformation in Binary Ti-Hf Alloys.

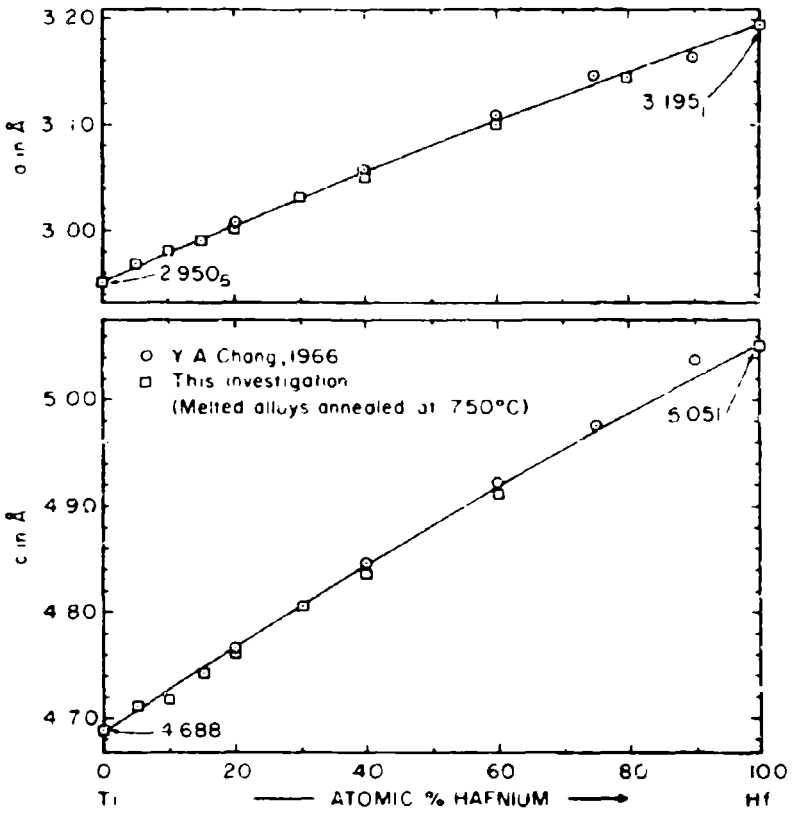

Figure III.A.2.4: Lattice Parameters of the α-(Ti,Hf) Solid Solution

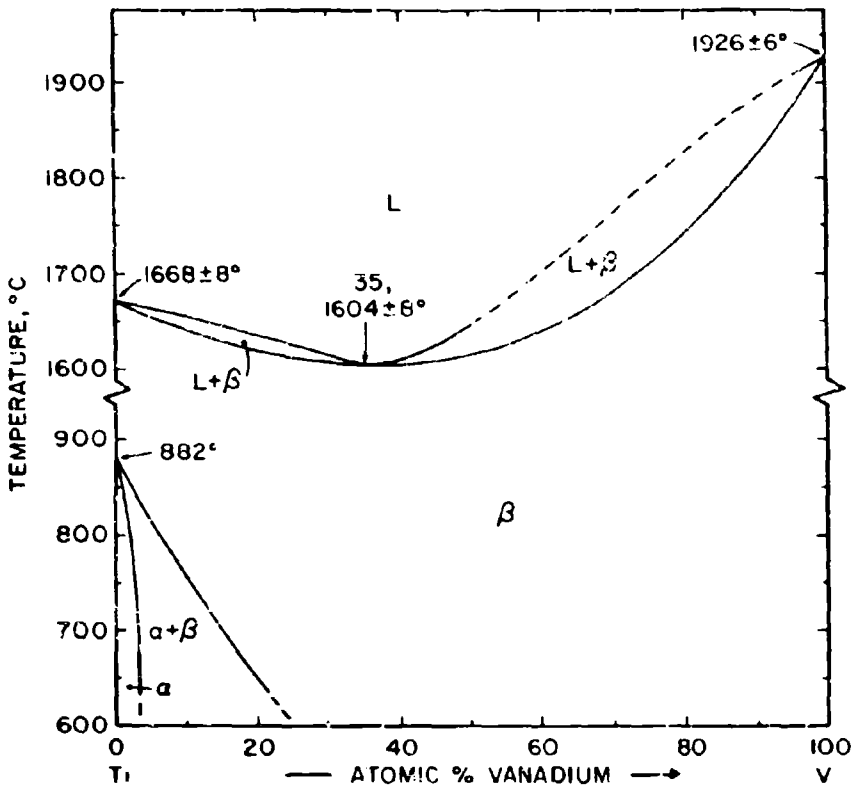

Figure III.A.3.1: Constitution Diagram Ti-V.

(Temperature Error Figures Based on Estimated Overall Uncertainty).

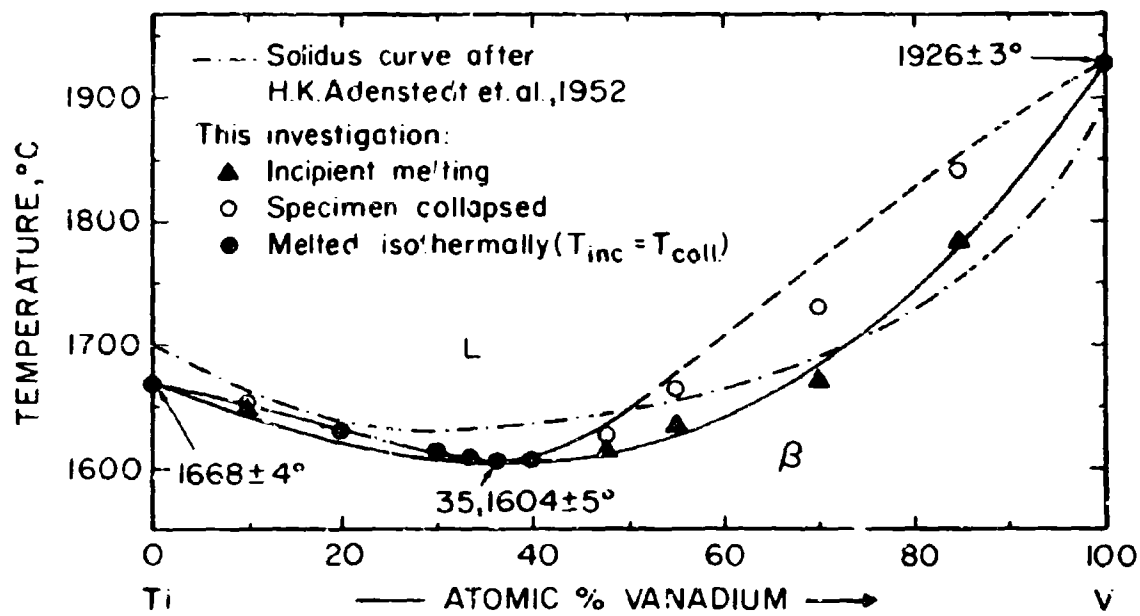

Figure III.A.3.2: Melting Temperatures of Ti-V Alloys.

(Temperature Error Figures Based on Reproducibility).

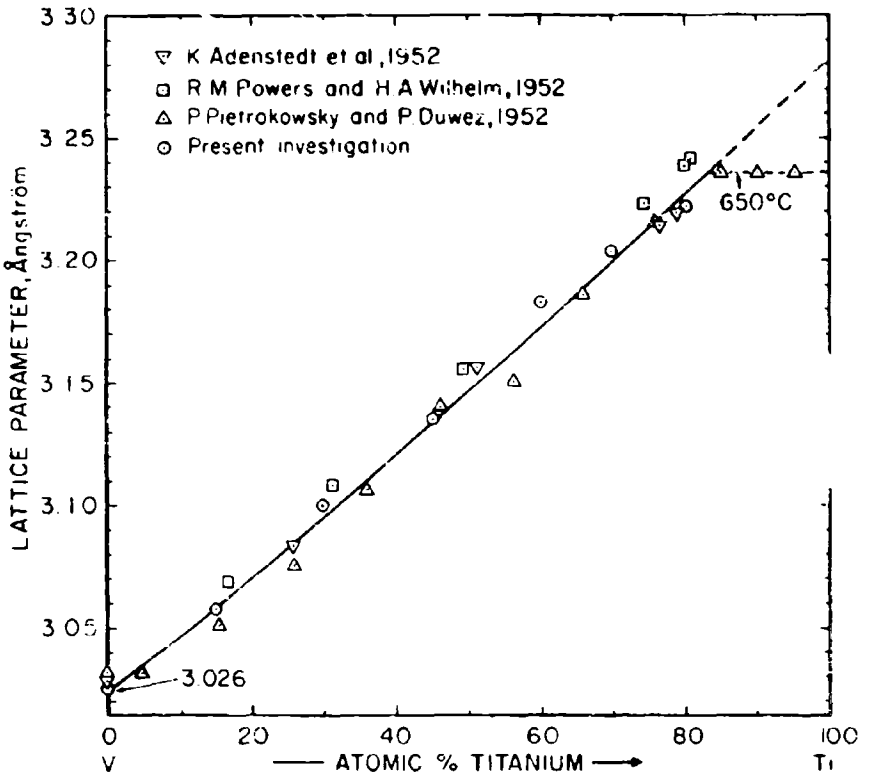

Figure III.A.3.3: Lattice Parameters of the β-(Ti, V) Solid Solution.

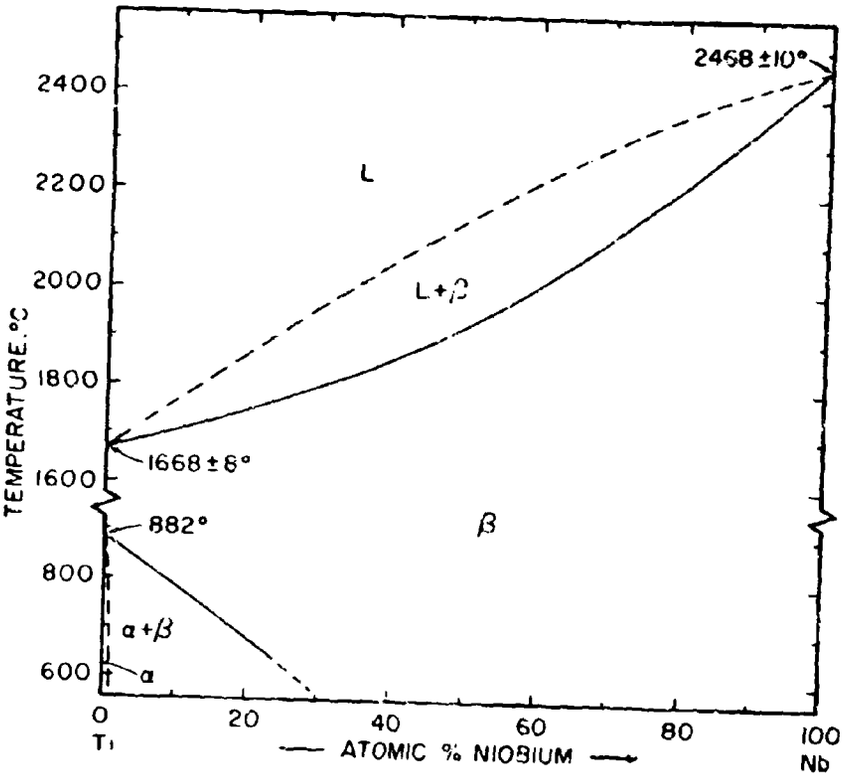

Figure III.A.4.1: Constitution Diagram Ti-Nb.

(Temperature Error Figures Based on Estimated Overall Uncertainty).

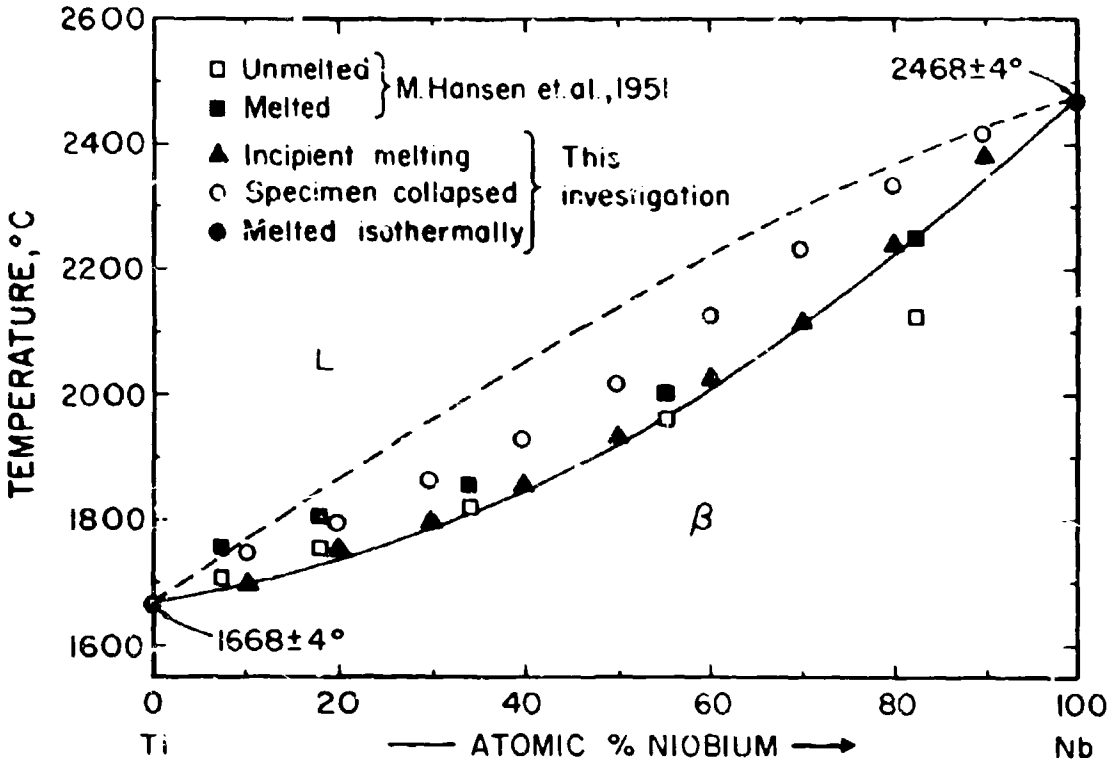

Figure III.A.4.2: Melting Temperatures of Ti-Nb Alloys.

(Temperature Error Figures Based on Reproducibility).

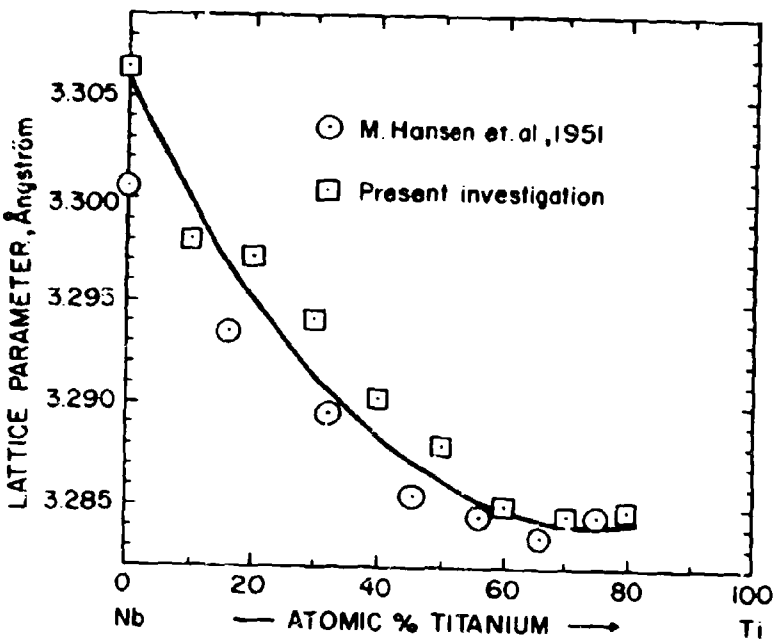

Figure III.A.4.3: Lattice Parameters of the β-(Ti, Nb) Solid Solution.

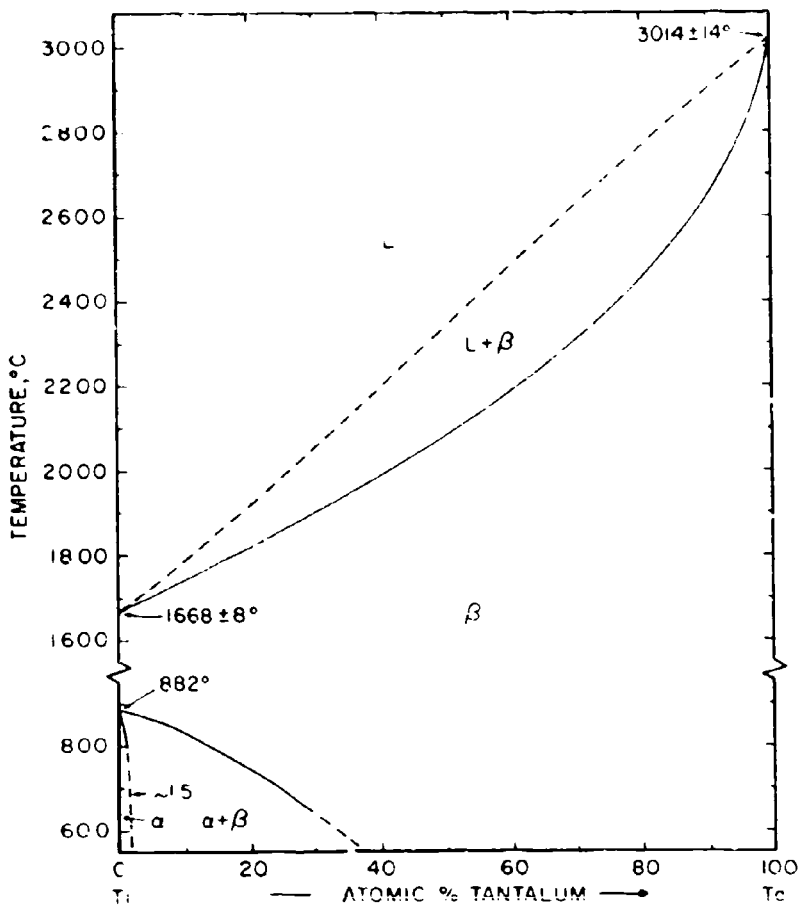

Figure III.A.5.1: Constitution Diagram Ti-Ta.

(Temperature Error Figures Based on Estimated Overall Uncertainty).

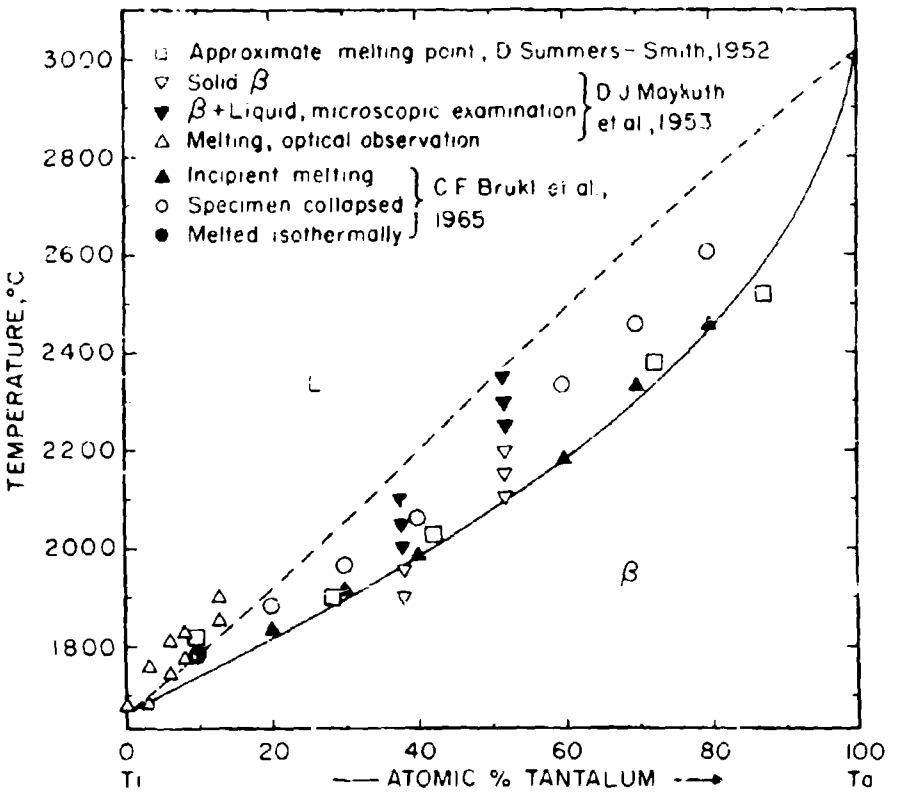

Figure III.A.5.2: Melting Temperatures of Ti-Ta Alloys.

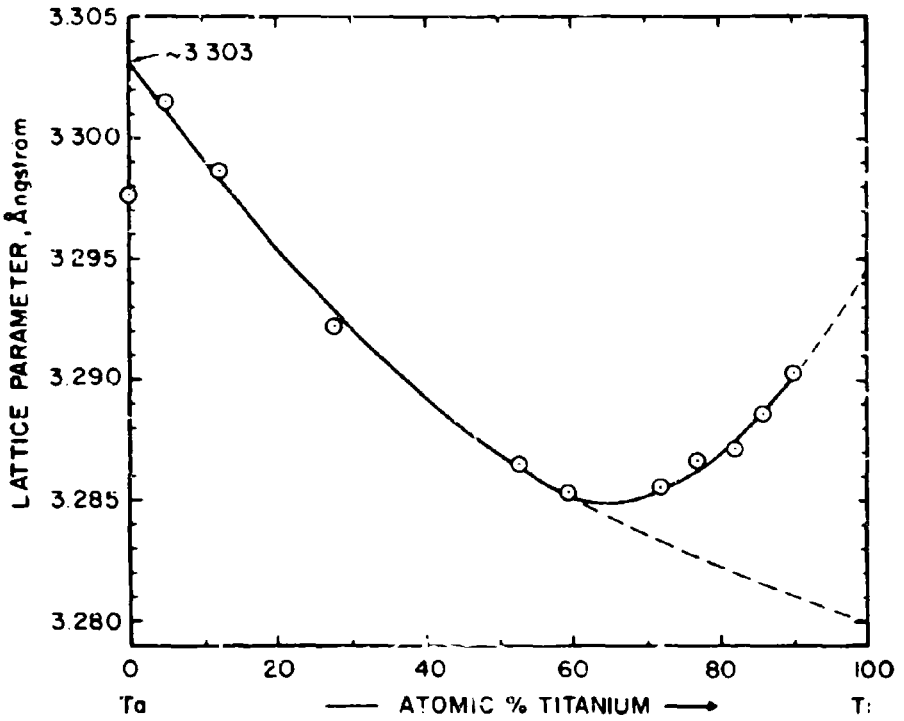

Figure III.A.5.3: Lattice Parameters of the β-(Ti, Ta) Solid Solution.

(After D. Summers-Smith, 1952. Alloys Quenched from 800° and 650°C, Respectively).

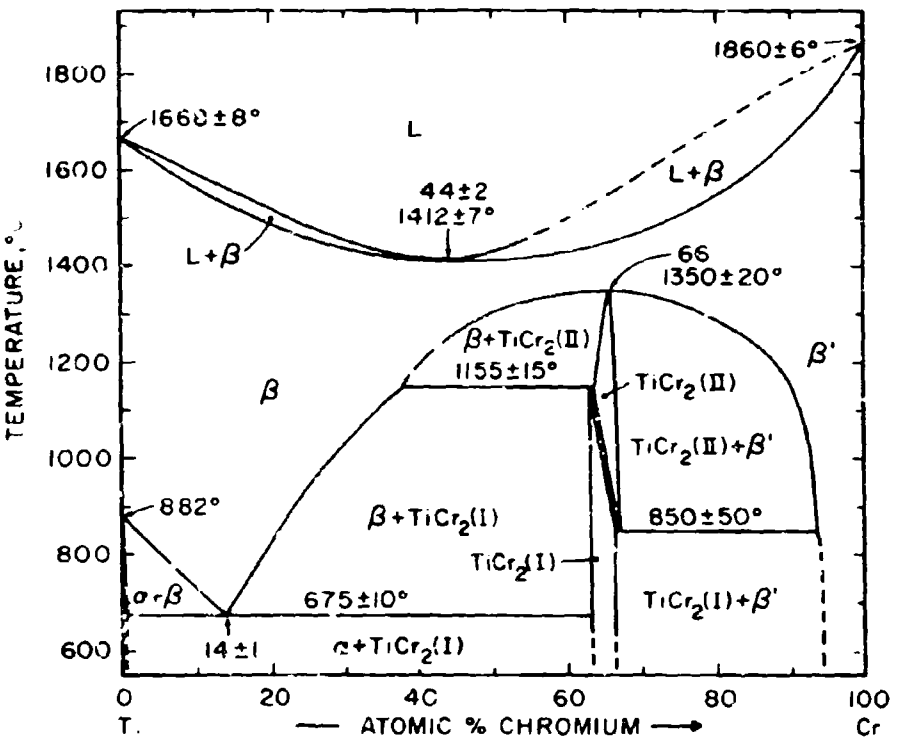

Figure III A.6.1: Constitution Diagram Ti-Cr.

(Temperature Error Figures Based on Estimated Overall Uncertainty).

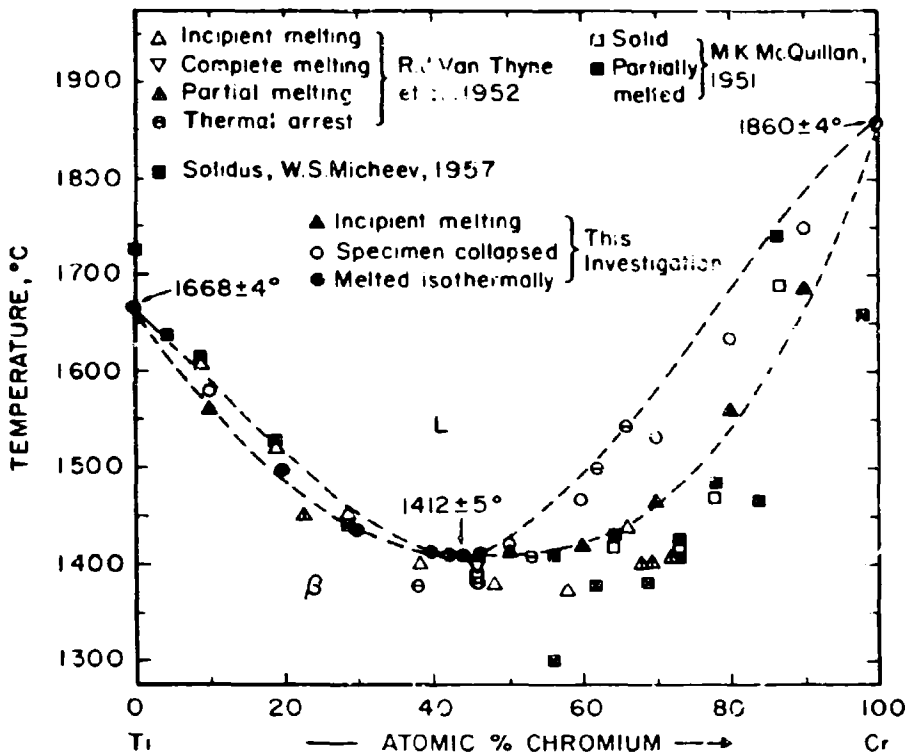

Figure III.A.6.2. Melting Temperatures of Ti-Cr Alloys.

(Temperature Error Figures Based on Reproducibility).

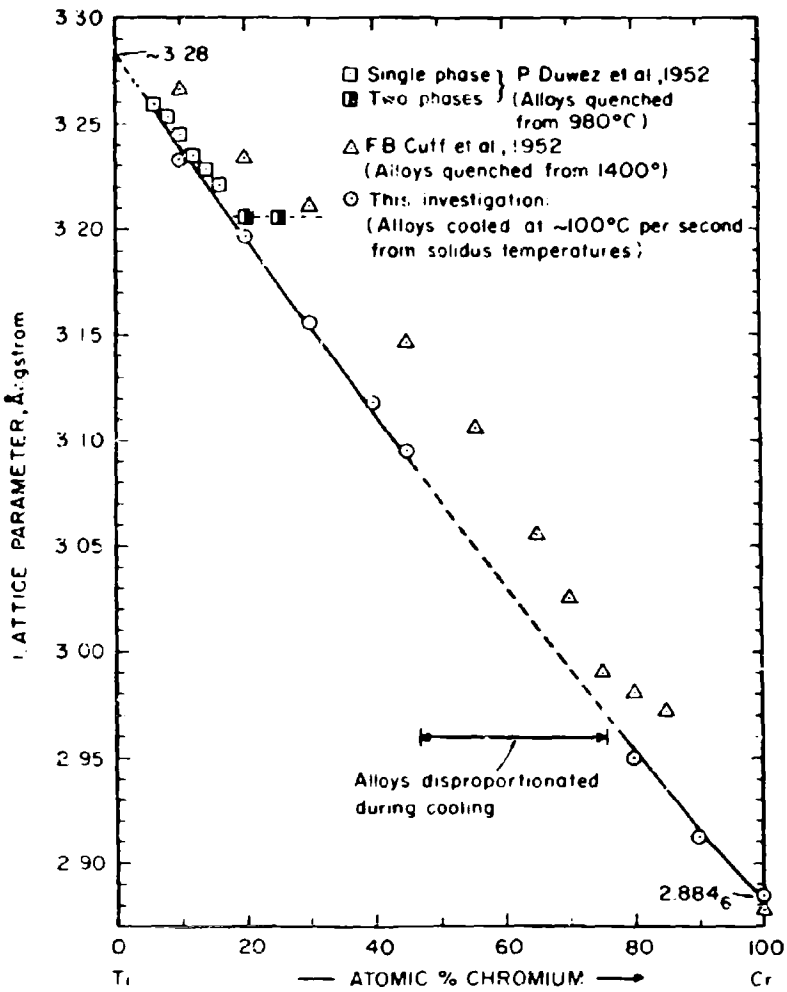

Figure III.A.6.3: Lattice Parameters of the β-(Ti, Cr) Solid Solution.

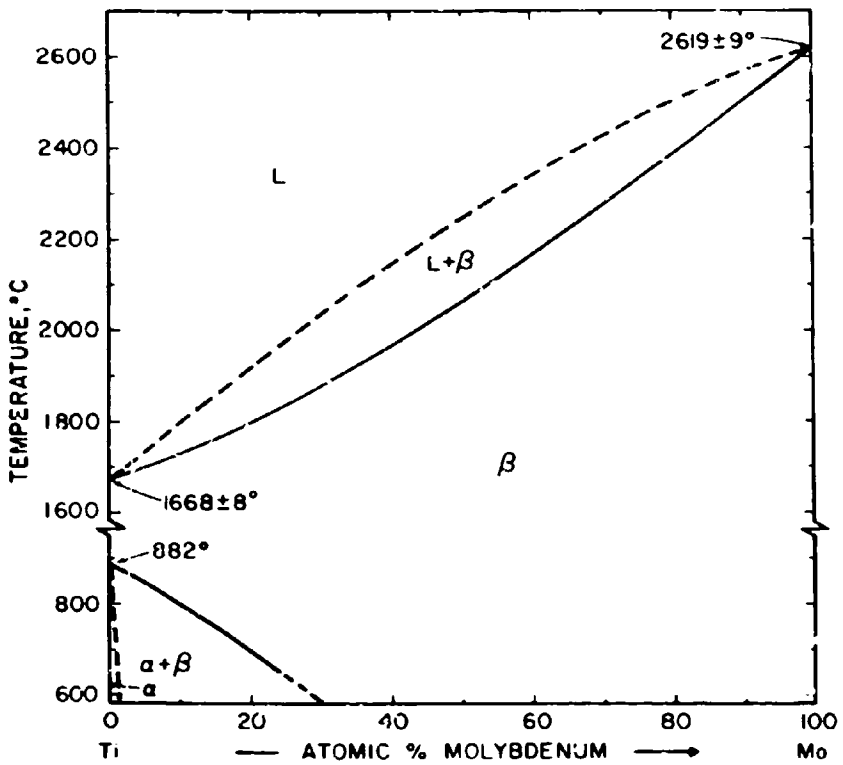

Figure III.A.7.1: Constitution Diagram Ti-Mo.

(Temperature Error Figures Based on Estimated Overall Uncertainty).

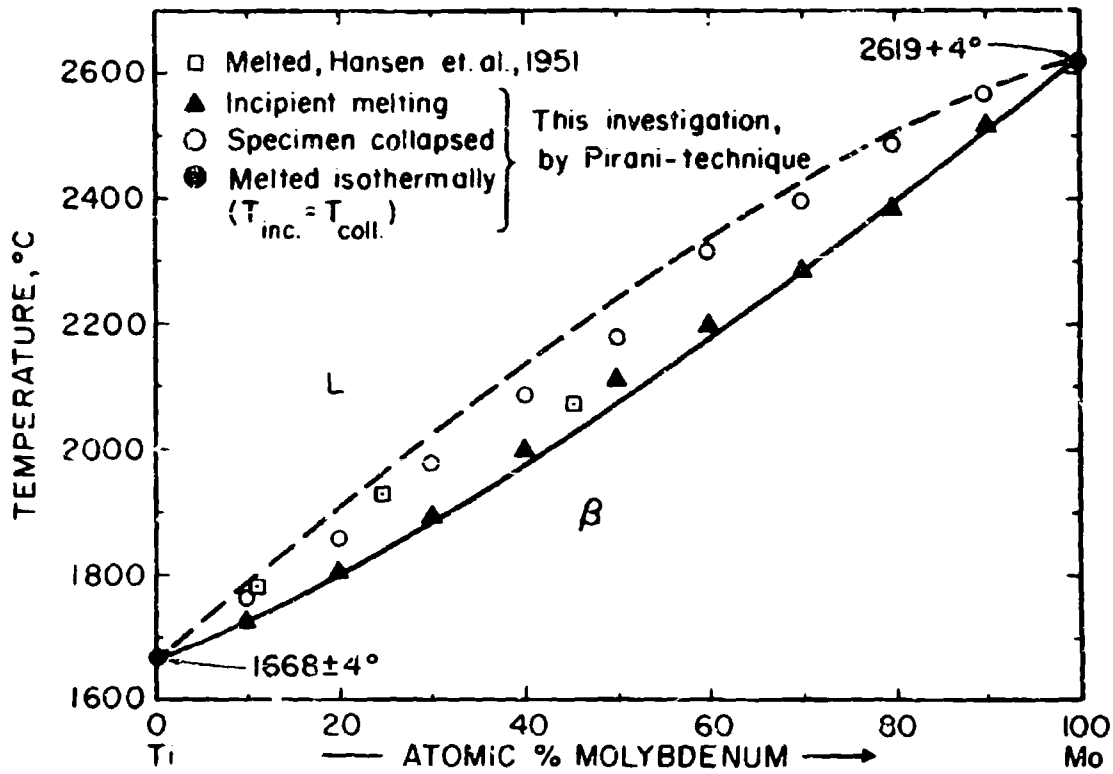

Figure III.A.7.2: Melting Temperatures of Ti-Mo Alloys.

(Temperature Error Figures Based on Reproducibility.

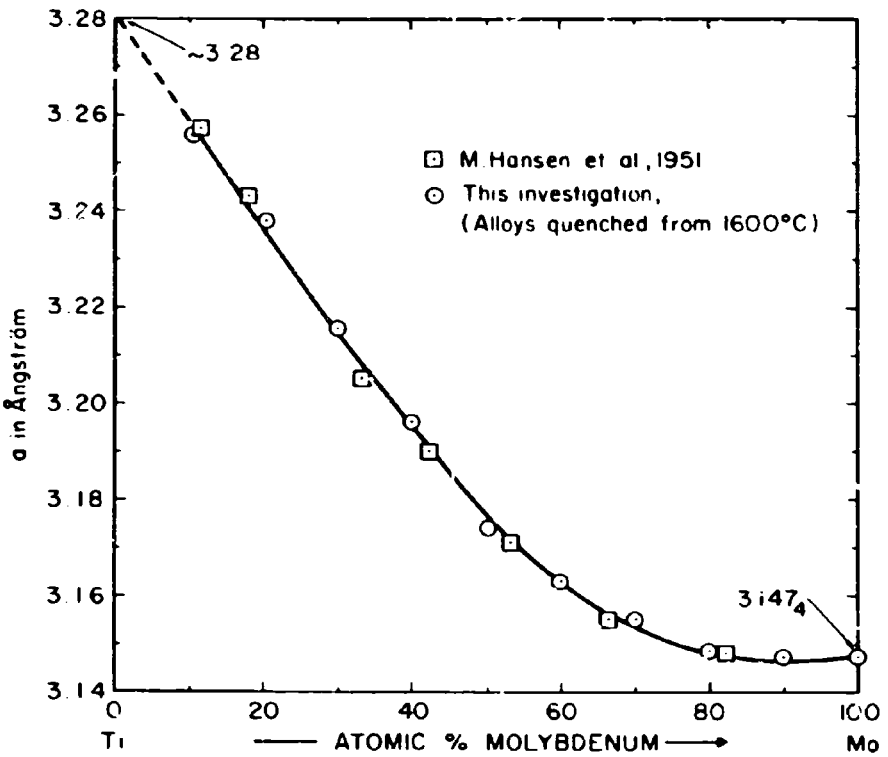

Figure III.A.7.3: Lattice Parameters of the β-(Ti, Mo) Solid Solution.

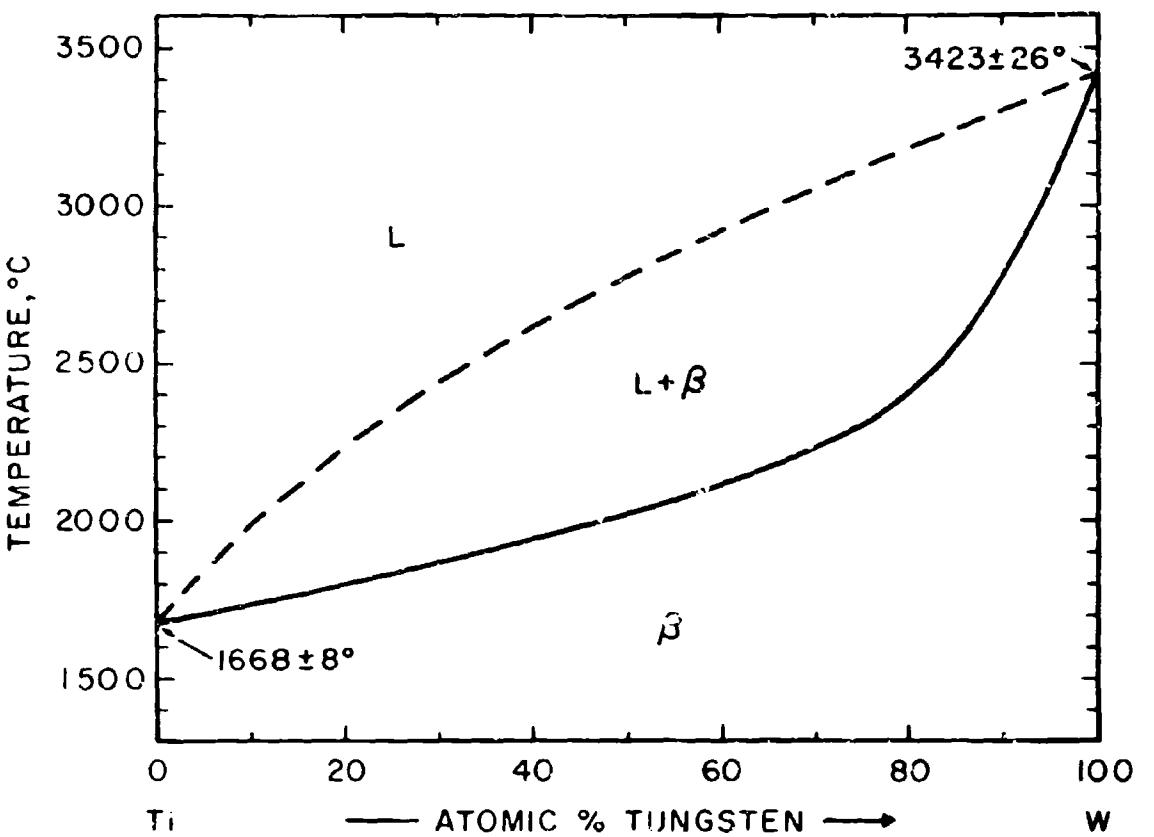

Figure III.A.8.1: Constitution Diagram Ti-W.

(Temperature Error Figures Based on Estimated Overall Uncertainty).

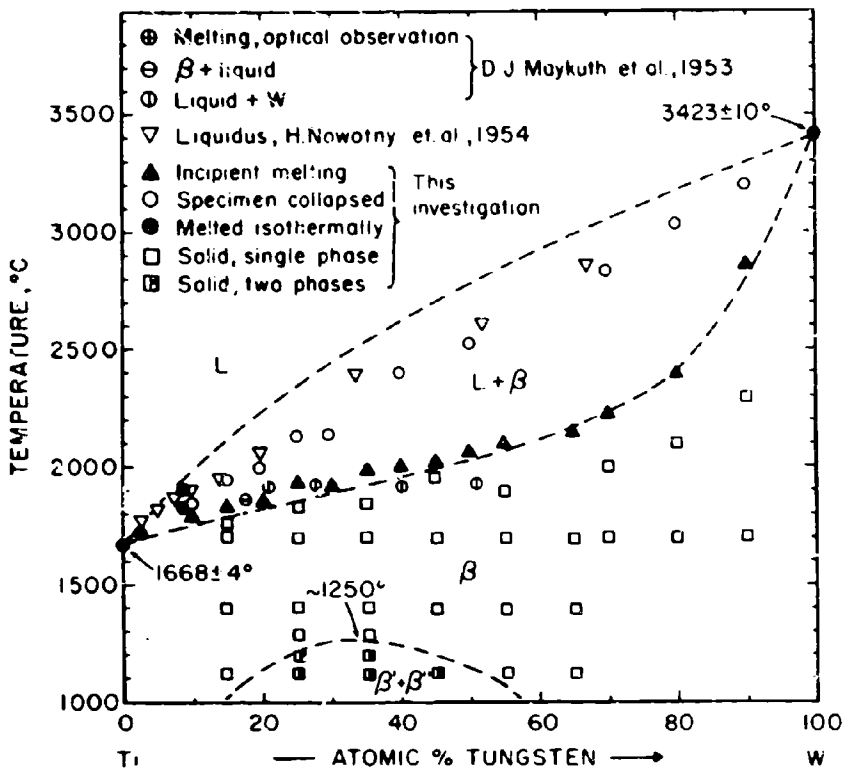

Figure III.A.8.2: Melting Temperatures and Qualitative Phase Evaluation of Solid-State Equilibrated Alloys.

(Temperature Error Figures Based on Reproducibility).

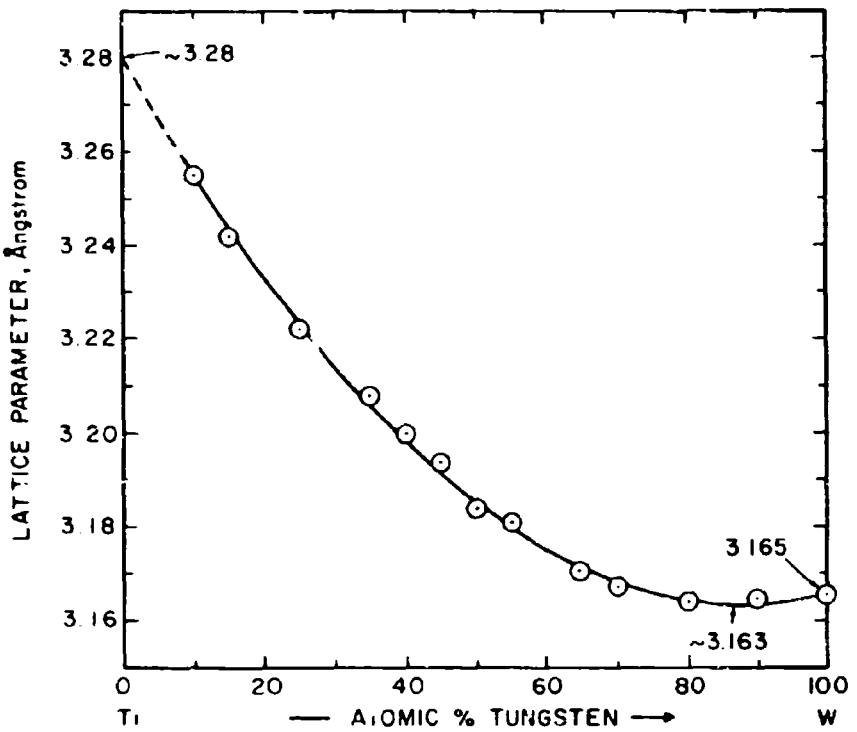

Figure III.A.8.3: Lattice Parameters of Ti-W Alloys.

(Alloys Equilibrated above 1300°C, this Investigation).

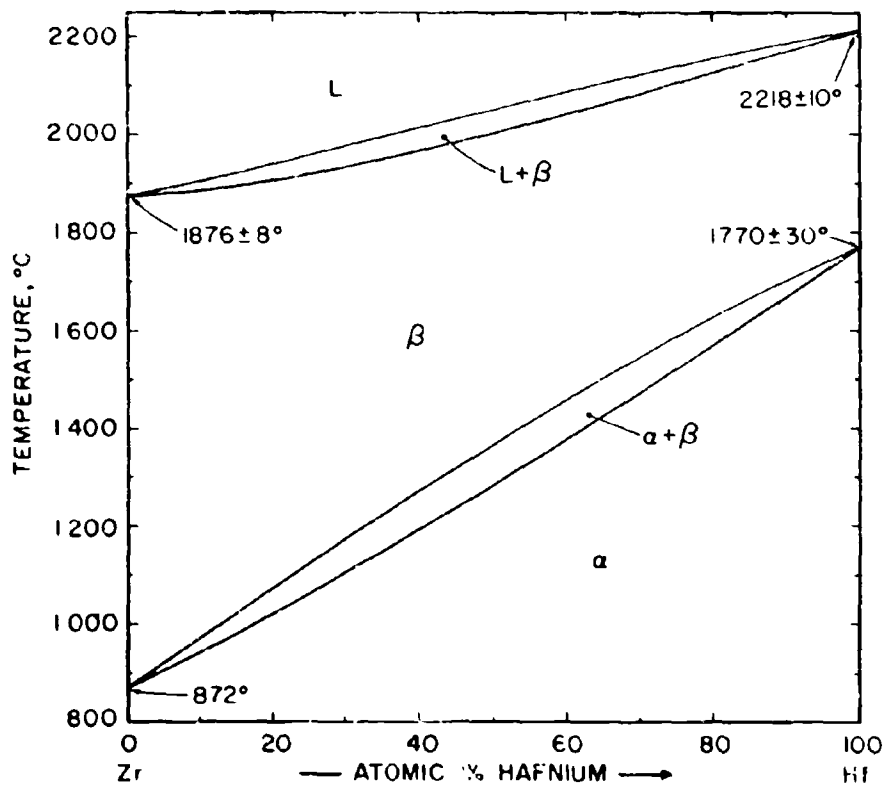

Figure III.A.9.1: Constitution Diagram Zr-Hf.

(Temperature Error Figures Based on Estimated Overall Uncertainty).

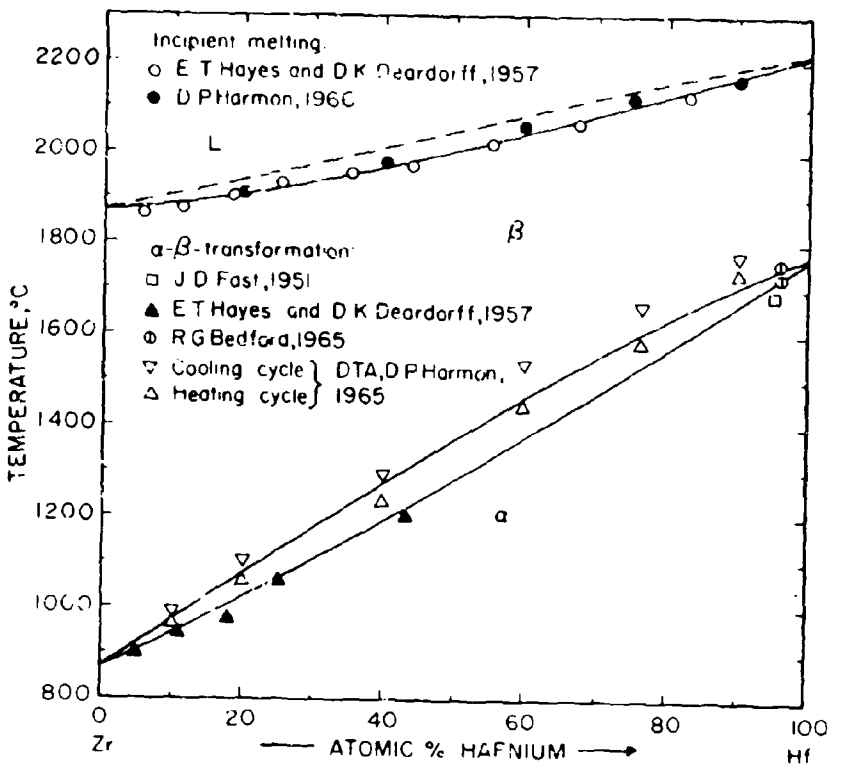

Figure III.A.9.2: Melting and α-β-Transformation Temperatures of Zr-Hf Alloys.

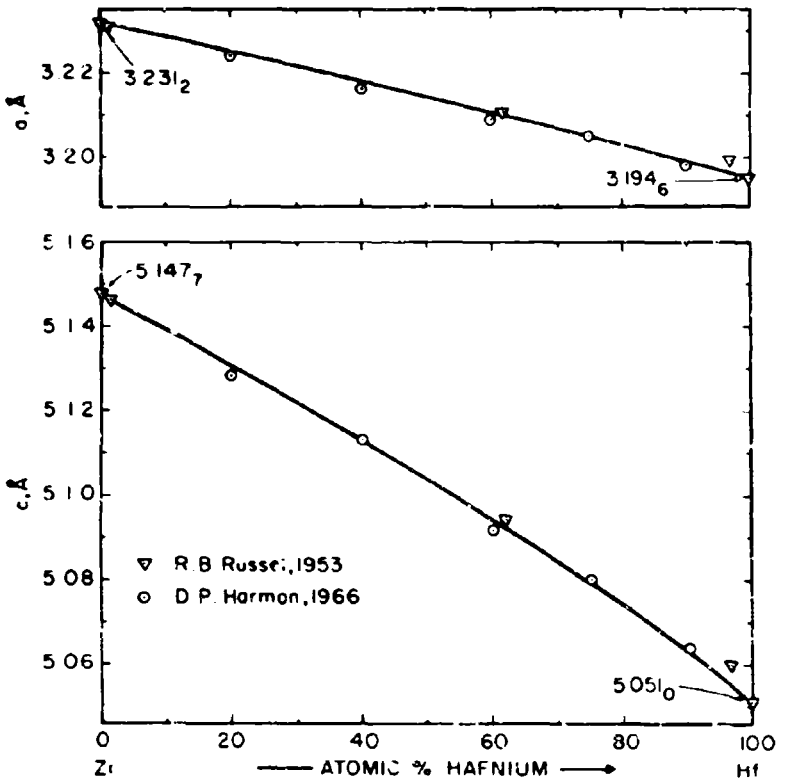

Figure III.A.9.3: Lattice Parameters of the α-(Zr, Hf)-Solid Solution.

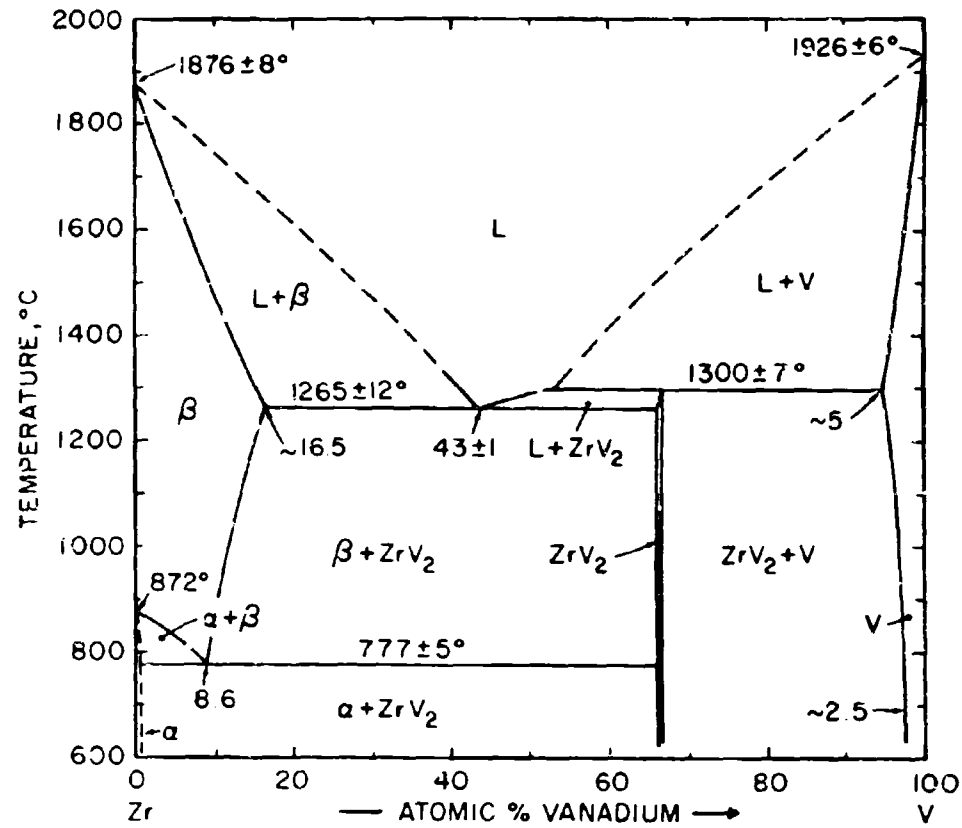

Figure III.A.10.1: Constitution Diagram Zr-V.

(Temperature Error Figures Based on Estimated Overall Uncertainty).

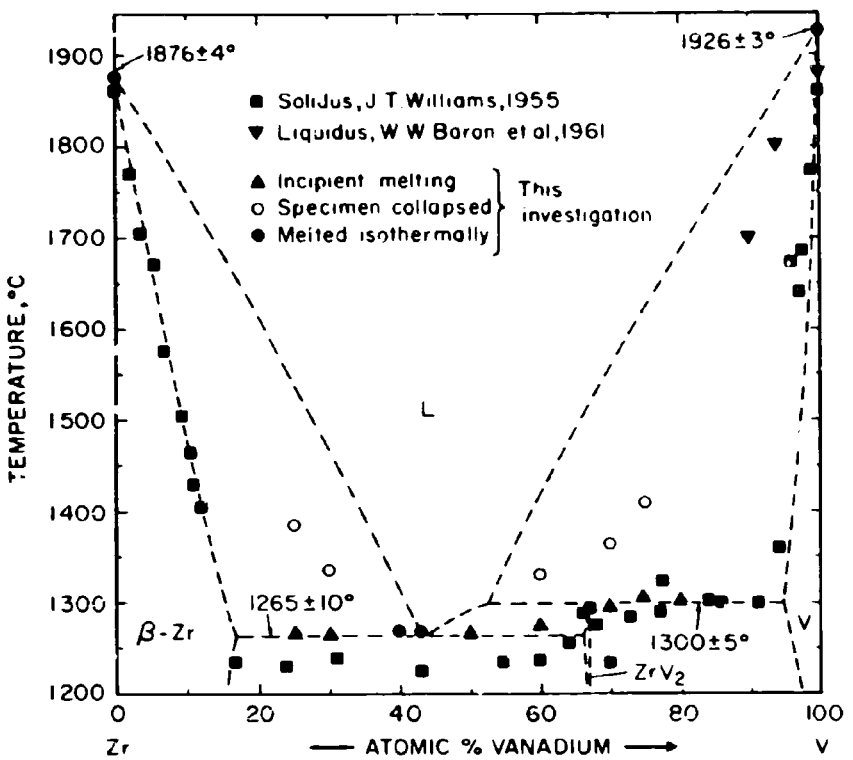

Figure III.A.10.2: Melting Temperatures of Zr-V Alloys.

(Temperature Error Figures Based on Reproducibility).

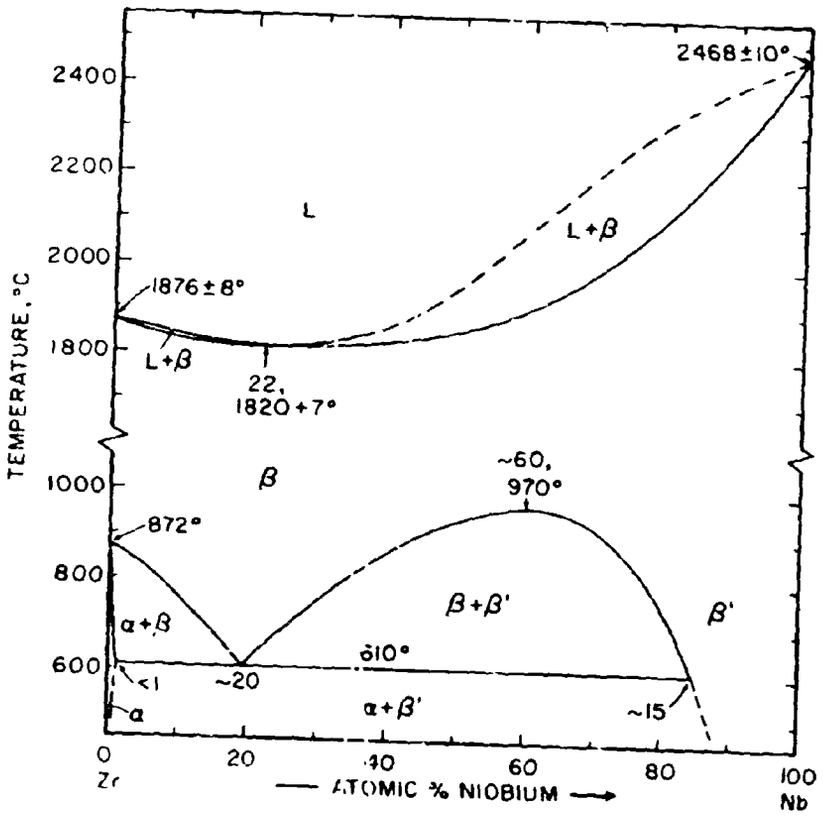

Figure III.A.11.1: Constitution Diagram Zr-Nb.

(Temperature Error Figures Based on Estimated Overall Uncertainty).

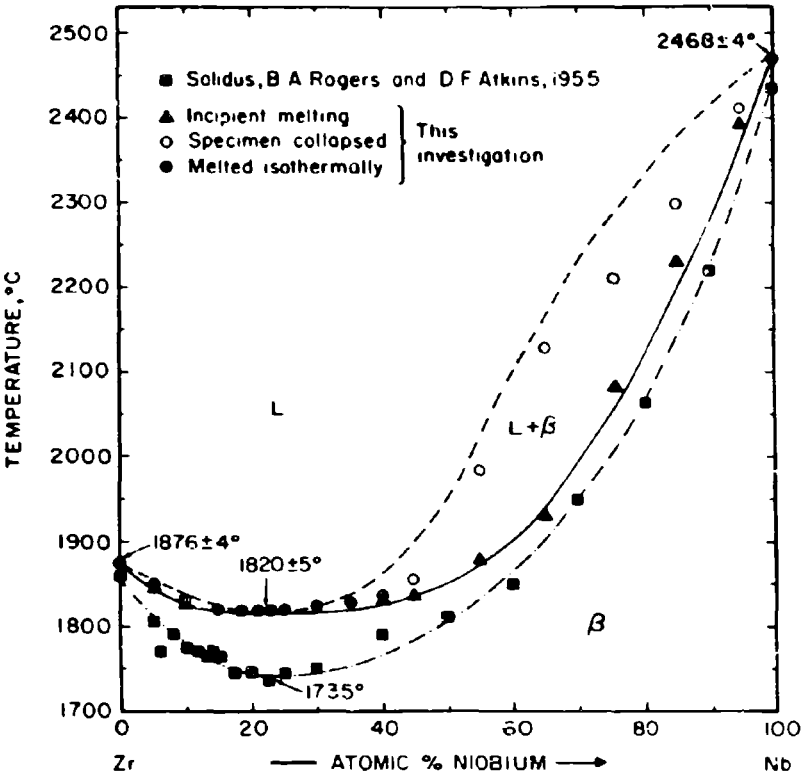

Figure III.A.11.2: Melting Temperatures of Zr-Nb Alloys.

(Temperature Error Figures Based on Reproducibility).

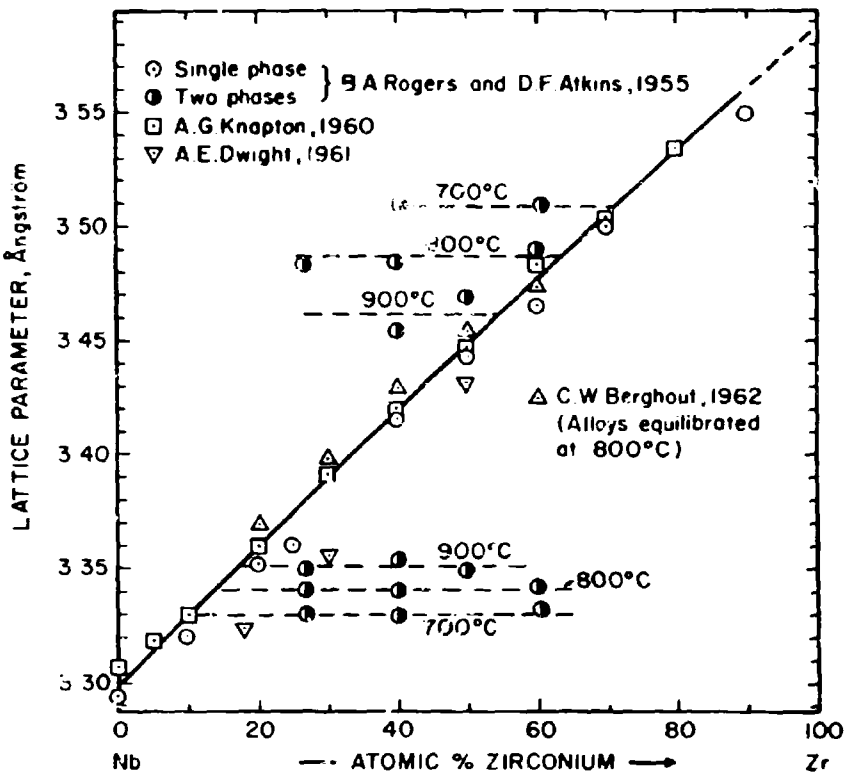

Figure III.A.11.3: Lattice Parameters of the β-(Nb, Zr)-Solid Solution.

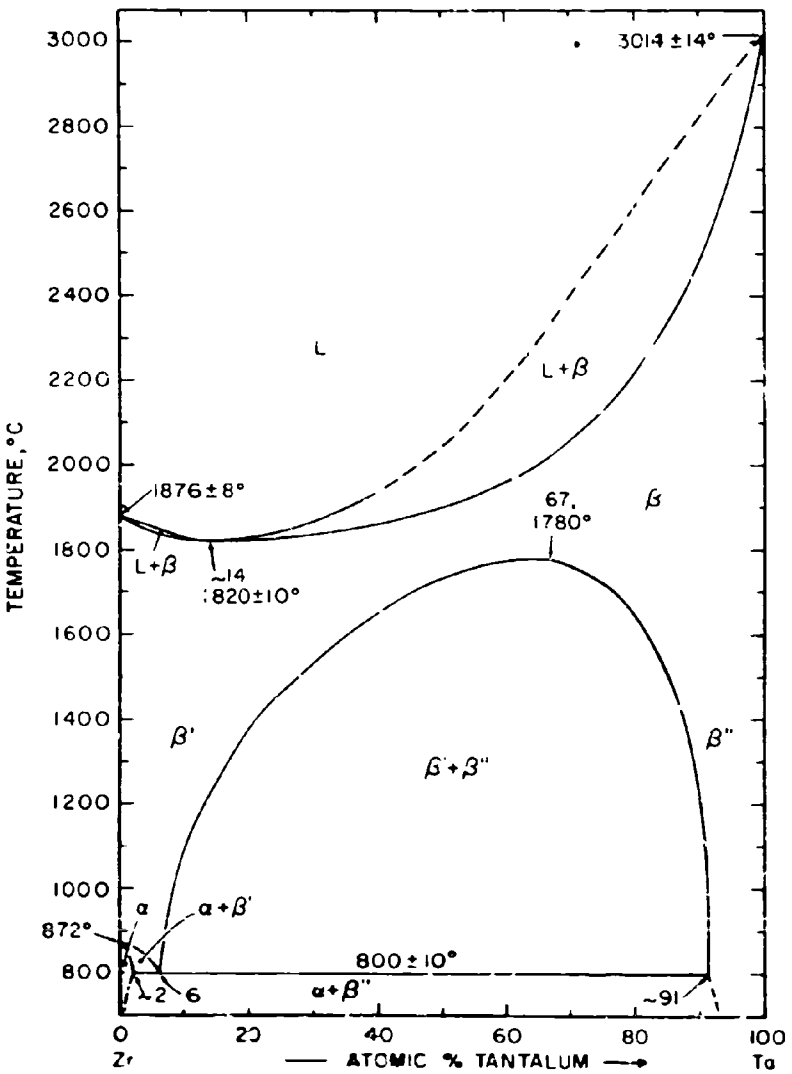

Figure III.A.12.1: Constitution Diagram Zr-Ta.

(Temperature Error Figures Based on Estimated Overall Uncertainty).

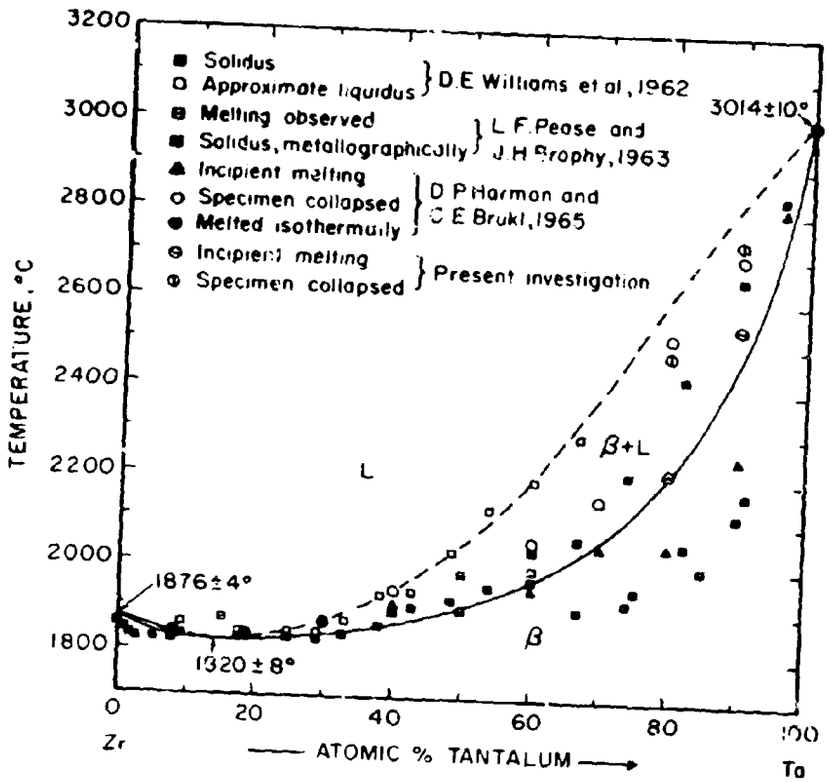

Figure III.A.12.2: Melting Temperatures of Zr-Ta Alloys.

(Temperature Error Figures Based on Reproducibility).

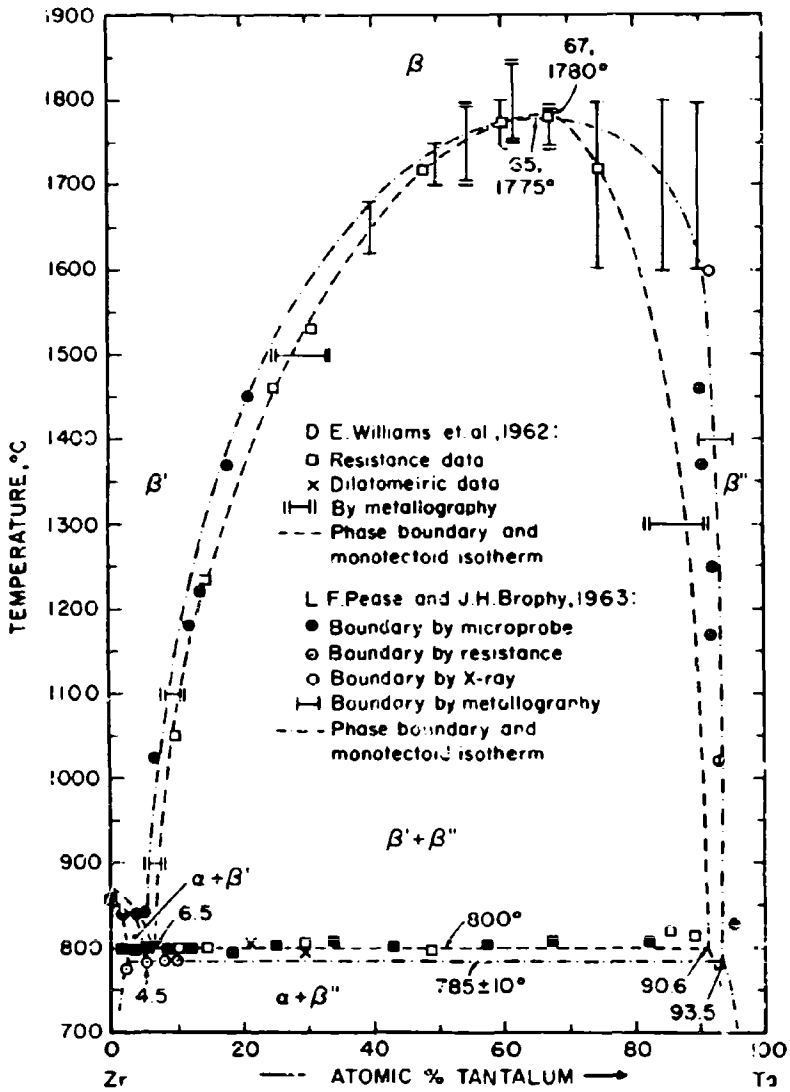

Figure III.A.12.3: Experimental Data for the Miscibility Gap and the Eutectoid Isotherm in the Zr-Ta System.

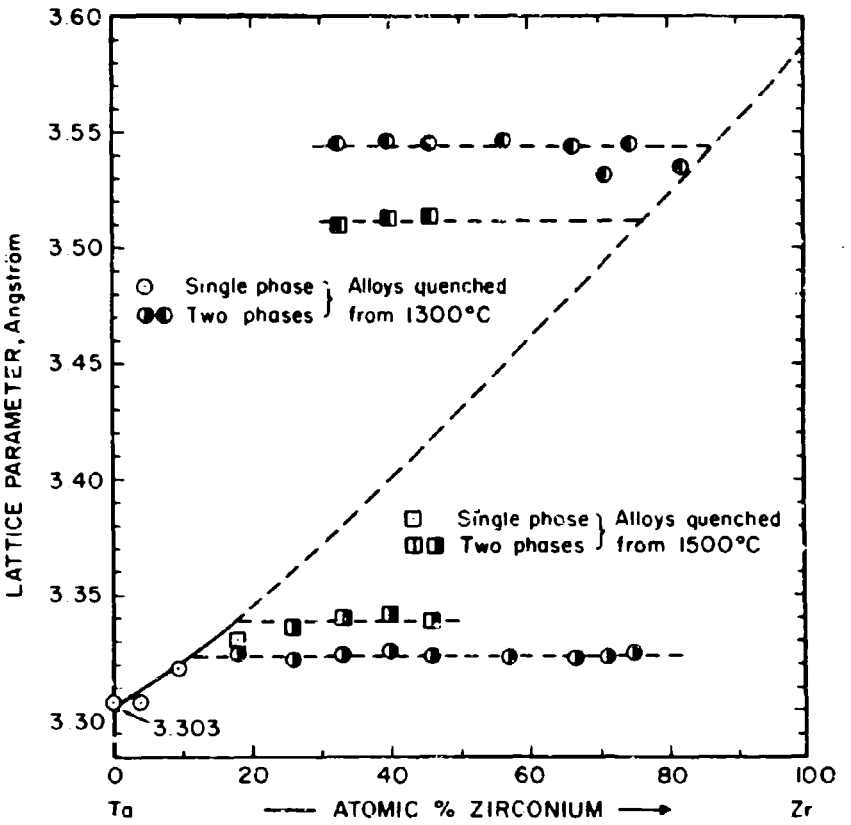

Figure III.A.12.4: Lattice Parameters of the β-(Zr, Ta)-Solid Solution.

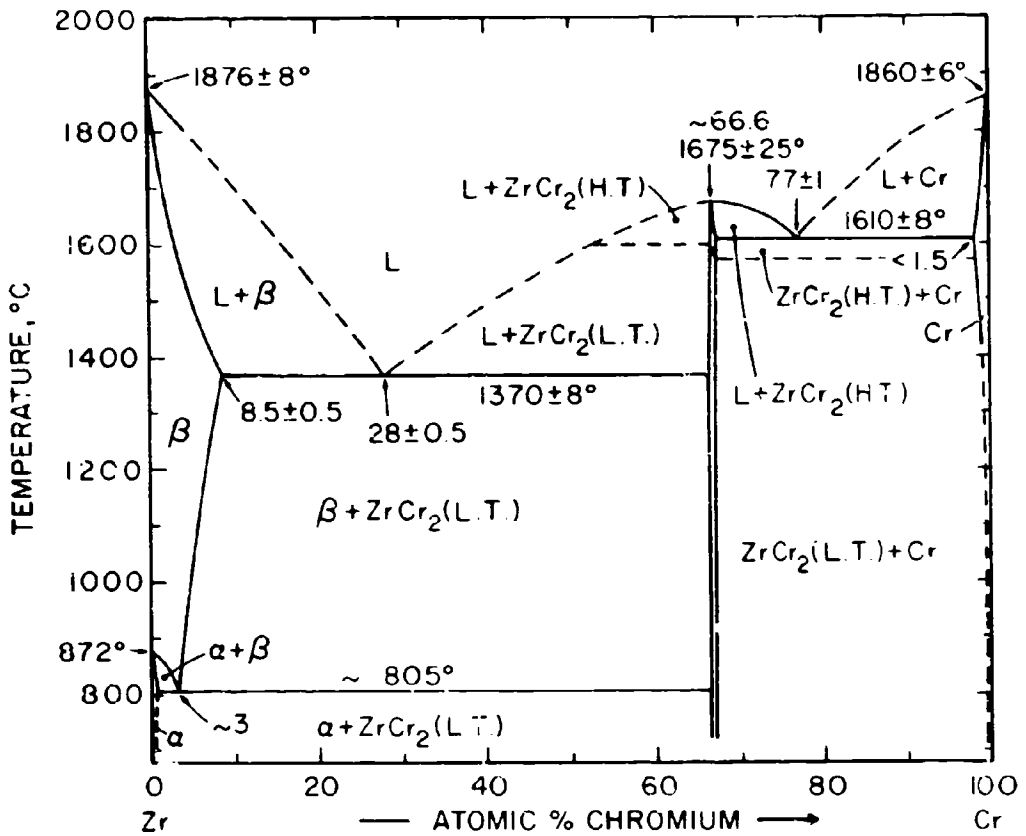

Figure III.A.13.1: Constitution Diagram Zr-Cr.

(Temperature Error Figures Based on Estimated Overall Uncertainty).

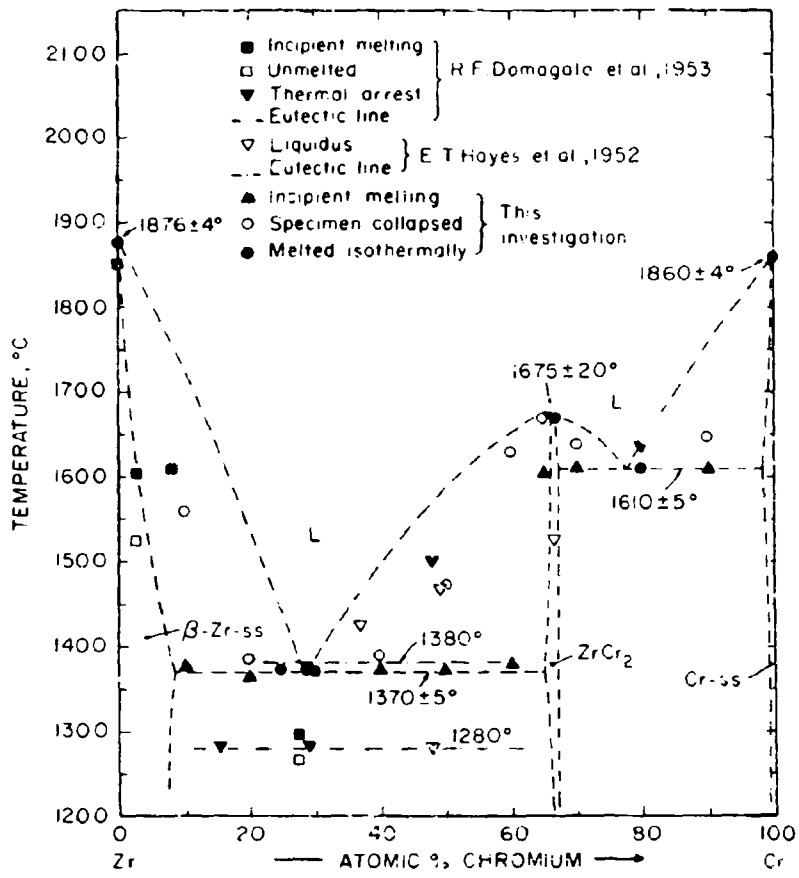

Figure III.A.13.2: Melting Temperatures of Zr-Cr Alloys.

(Temperature Error Figures Based on Reproducibility).

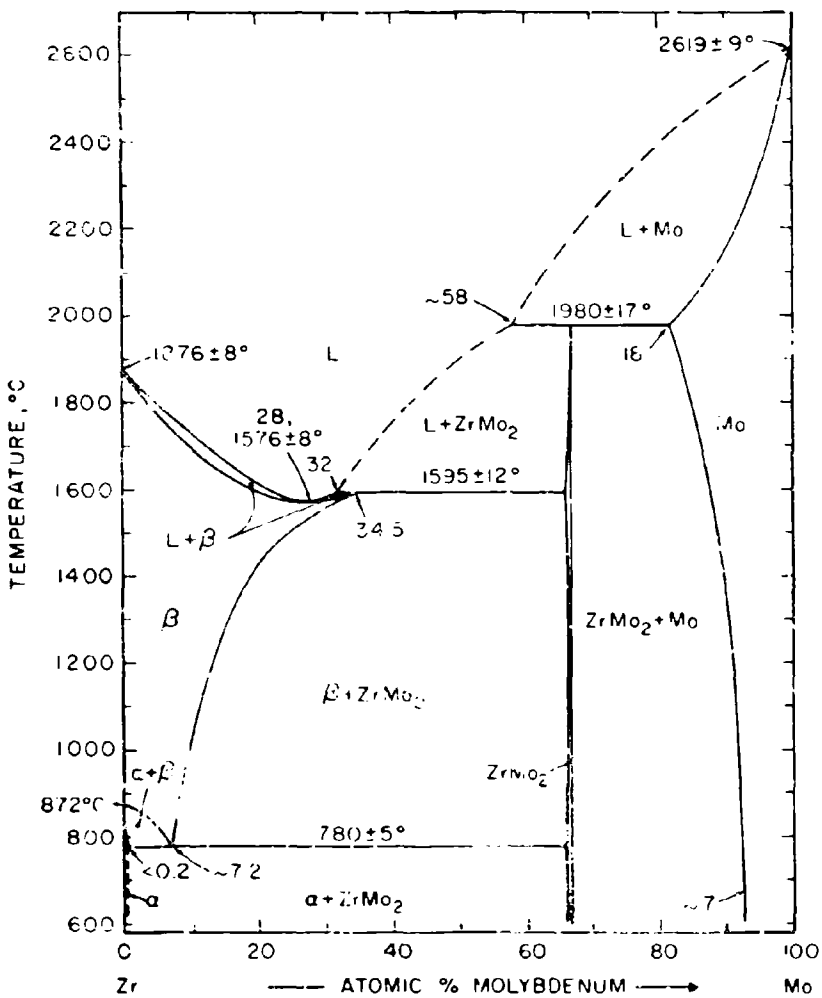

Figure III.A.14.1: Constitution Diagram Zr-Mo.

(Temperature Error Figures Based on Estimated Overall Uncertainty).

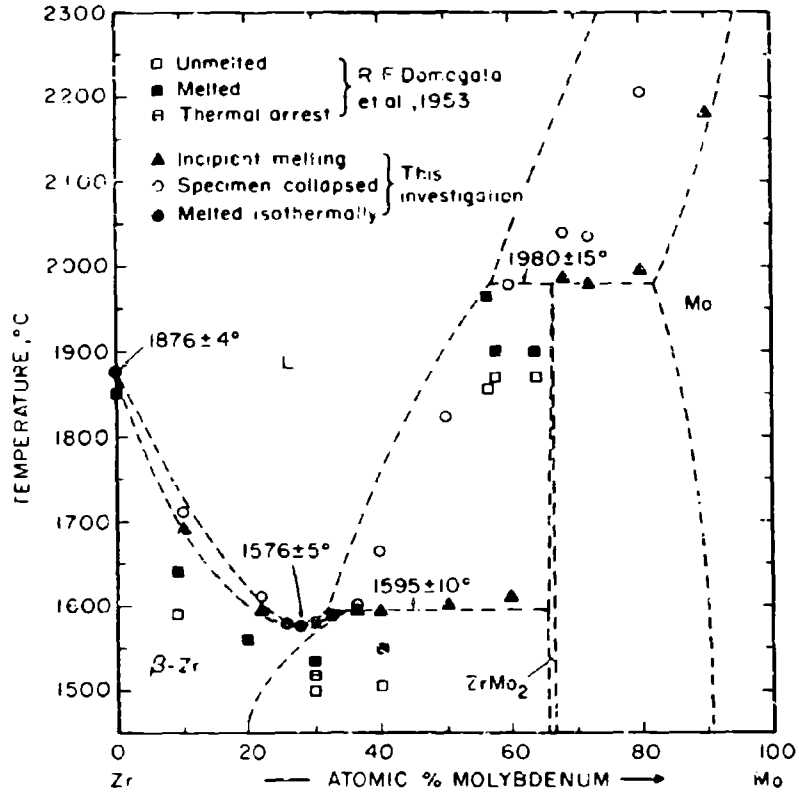

Figure III.A.14.2: Melting Temperatures of Zr-Mo Alloys.

(Temperature Error Figures Based on Reproducibility).

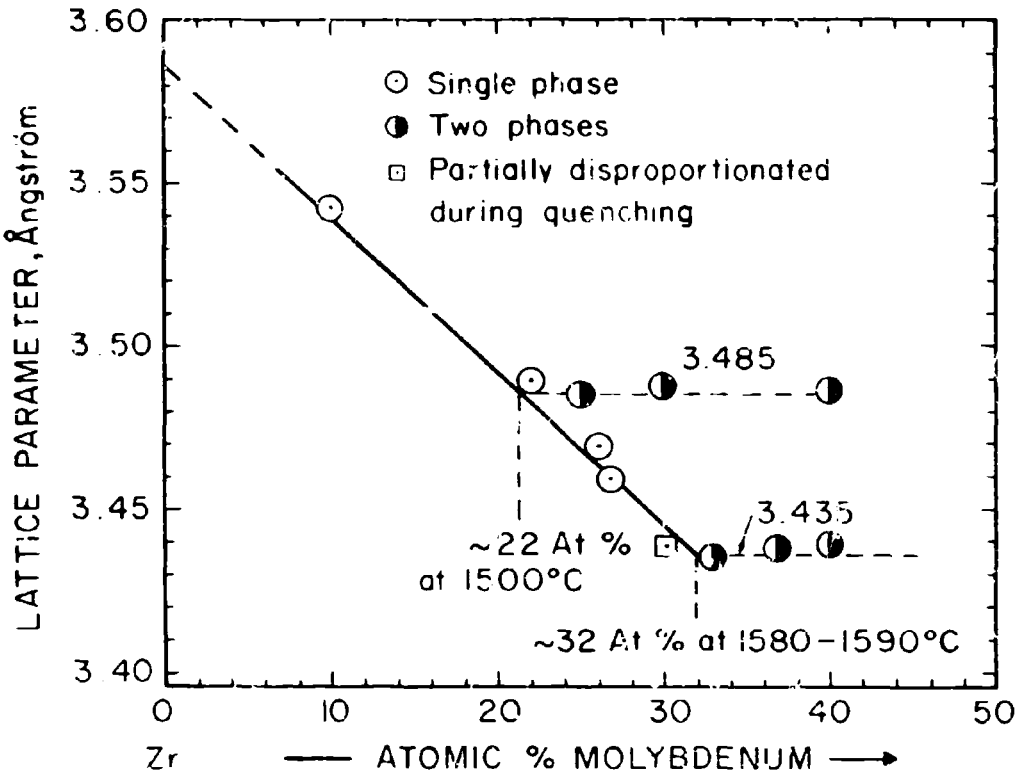

Figure III.A.14.3: Lattice Parameters of the β-Zr Solid Solution.

(Alloys Quenched from the Indicated Temperatures).

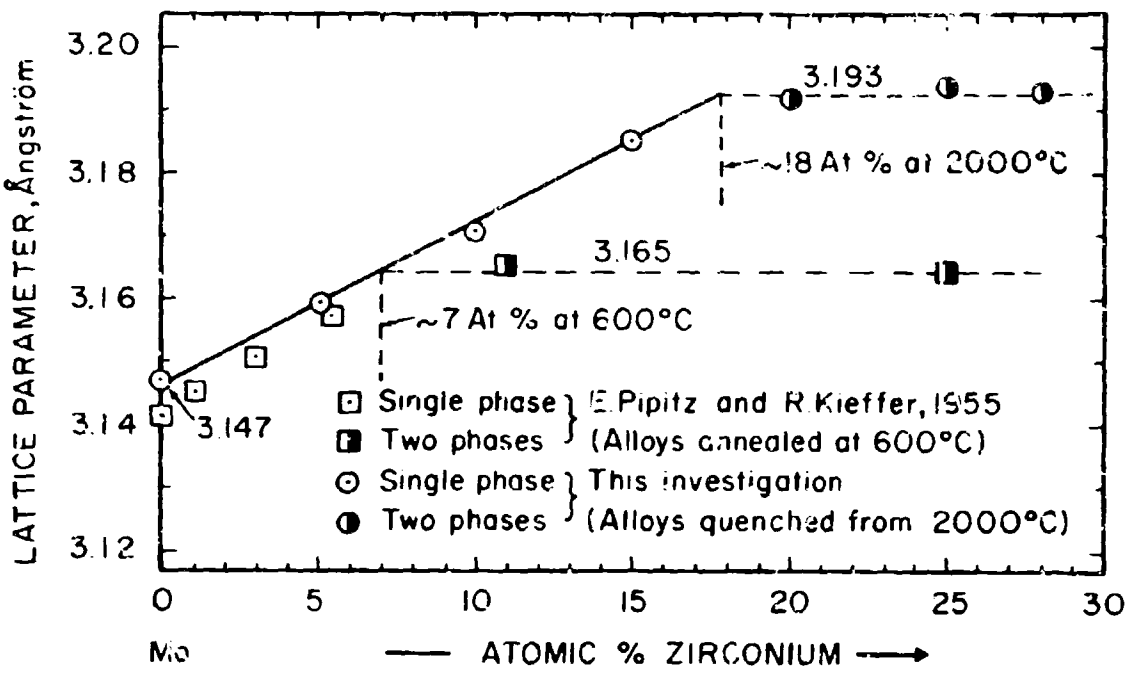

Figure III.A.14.4: Lattice Parameters of the Molybdenum Phase in the (Zr, Mo) System.

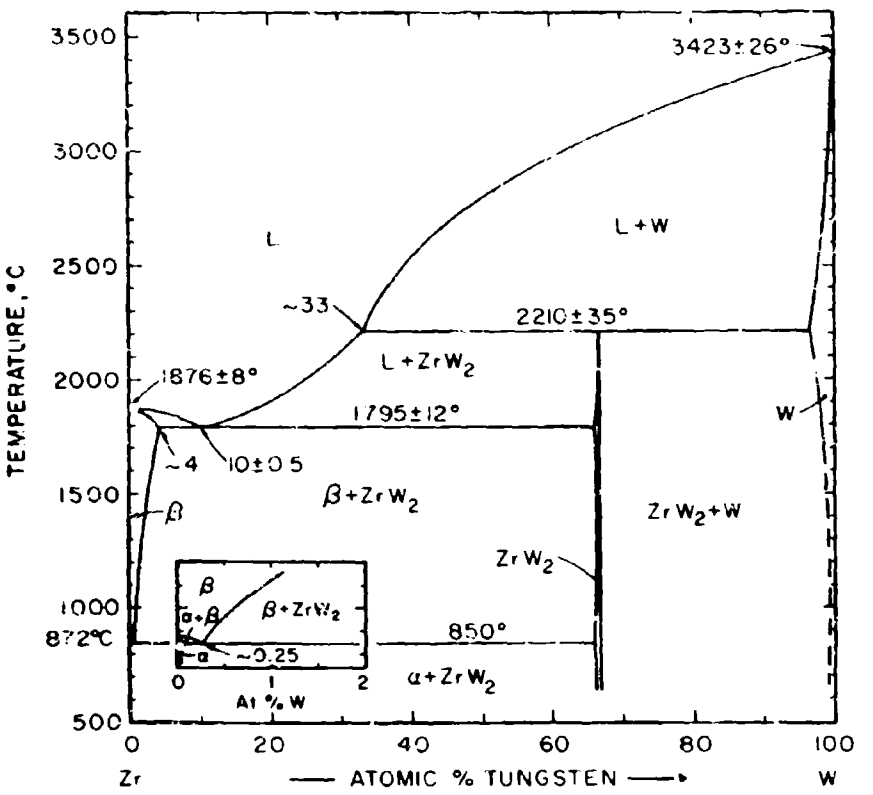

Figure III.A.15.1: Constitution Diagram Zr-W.

(Temperature Error Figures Based on Estimated Overall Uncertainty).

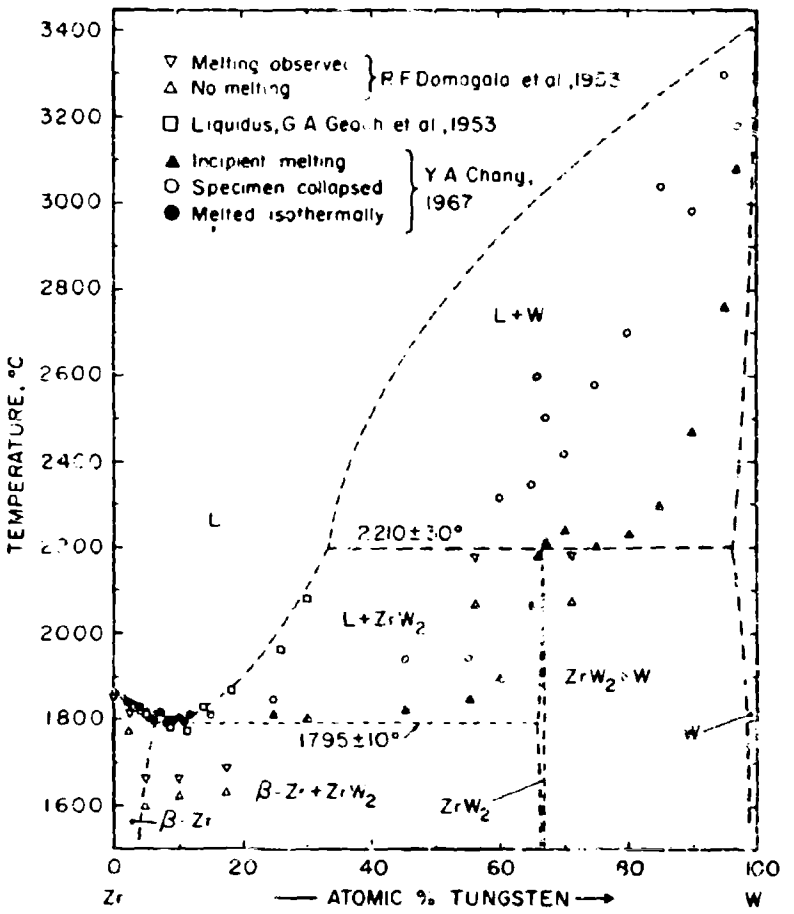

Figure III.A.15.2: Melting Temperatures of Zr-W Alloys.

(Temperature Error Figures Based on Reproducibility).

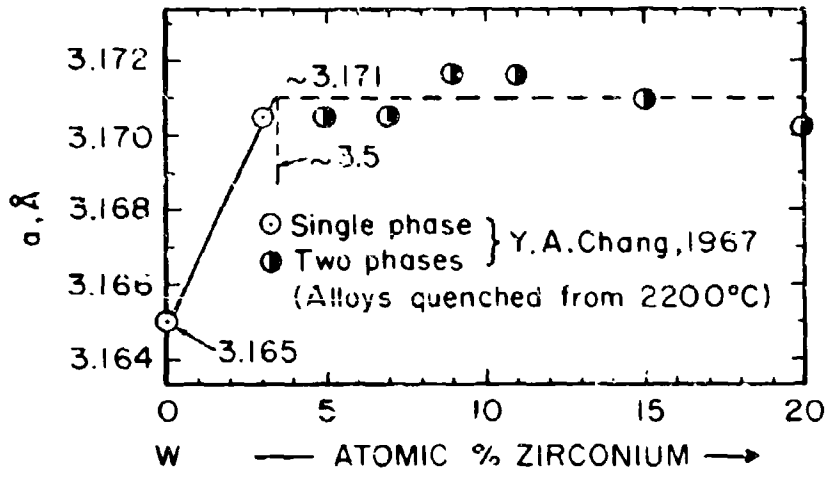

Figure III.A.15.3: Lattice Parameters of the Tungsten Phase in the (Zr, W) System.

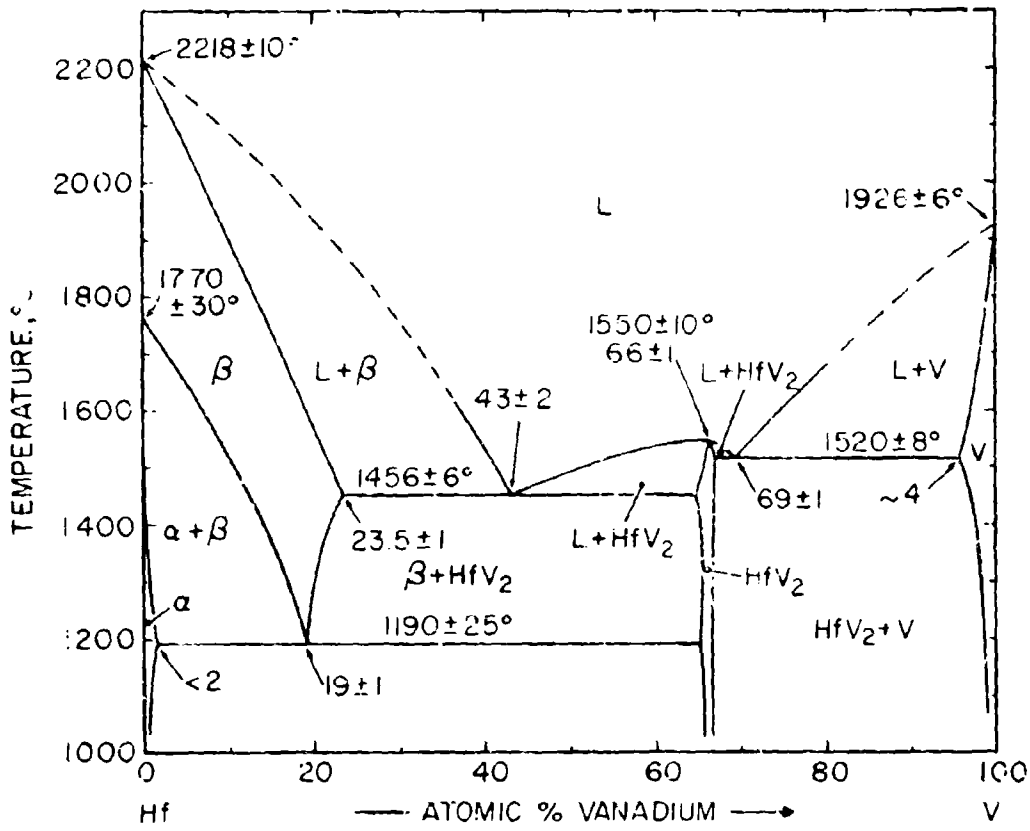

Figure III.A.16.1: Constitution Diagram of the Hf-V System.

(Temperature Error Figures Based on Estimated Overall Uncertainty).

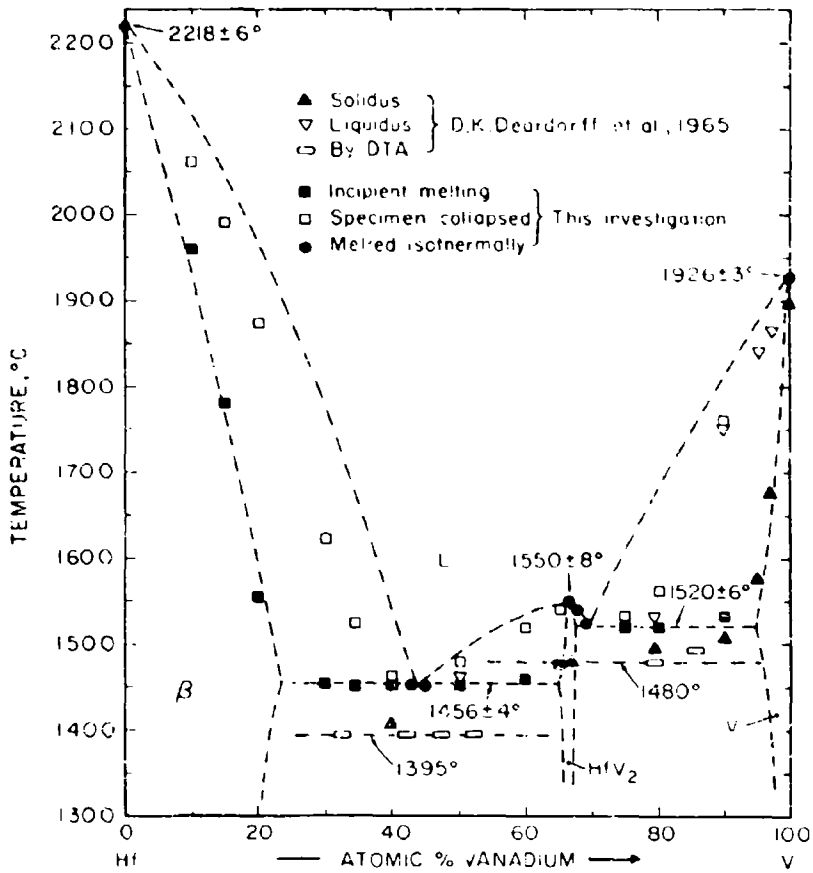

Figure III.A.16.2: Melting Temperatures of Hf-V Alloys.

(Temperature Error Figures Based on Reproducibility).

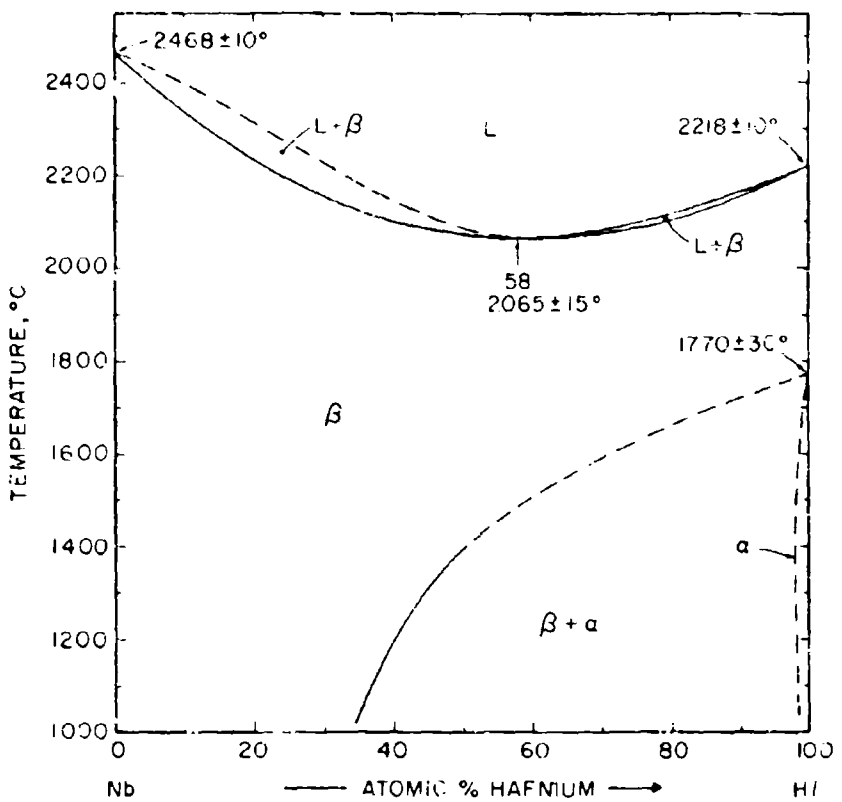

Figure III.A.17.1. Constitution Diagram Nb-Hf.

(Temperature Error Figures Based on Estimated Overall Uncertainty).

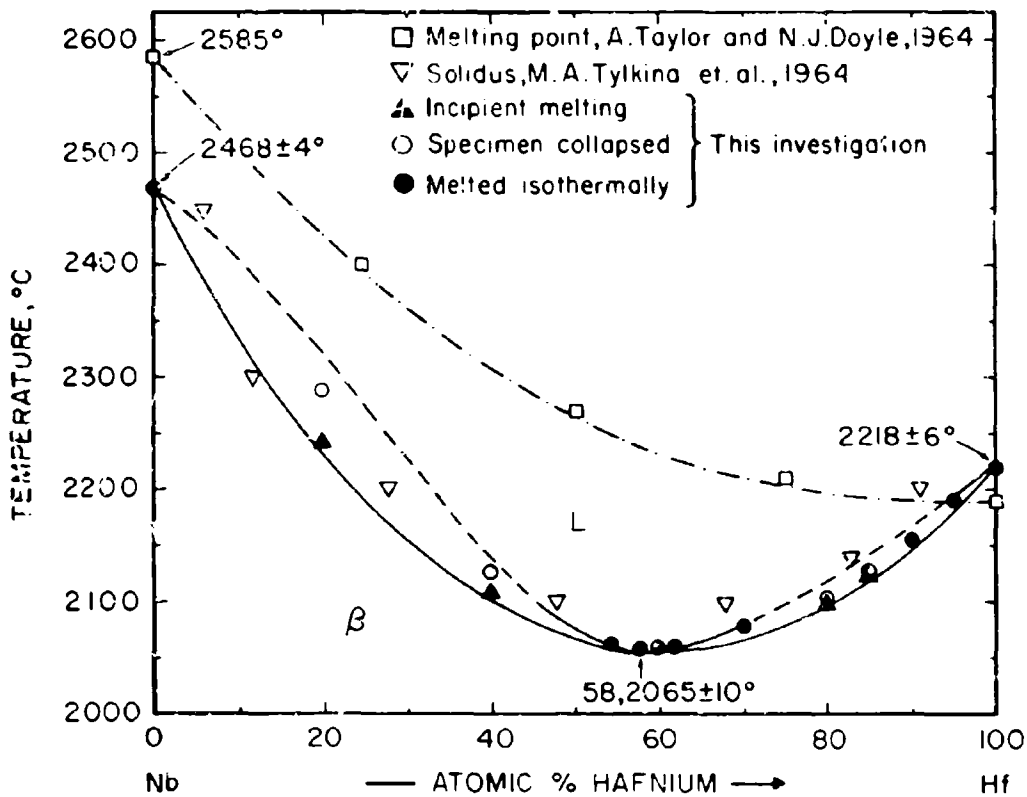

Figure III.A.17.2: Melting Temperatures of Nb-Hf Alloys.

(Temperature Error Figures Based on Reproducibility).

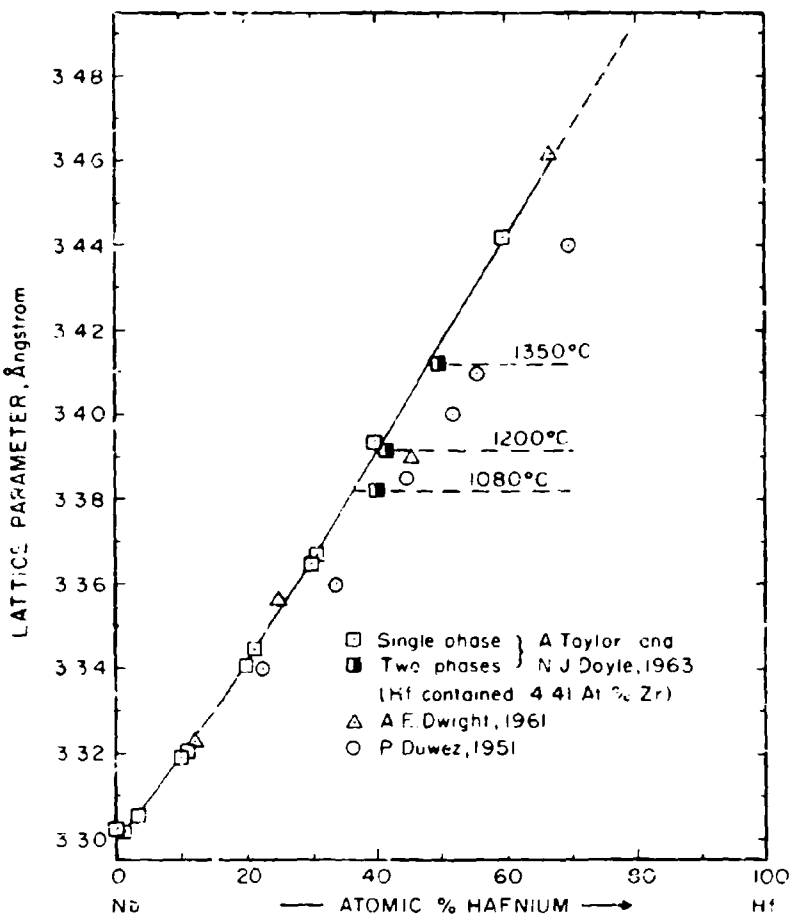

Figure III.A.17.3: Lattice Parameters of the β-(Hf, Nb) Solid Solution.

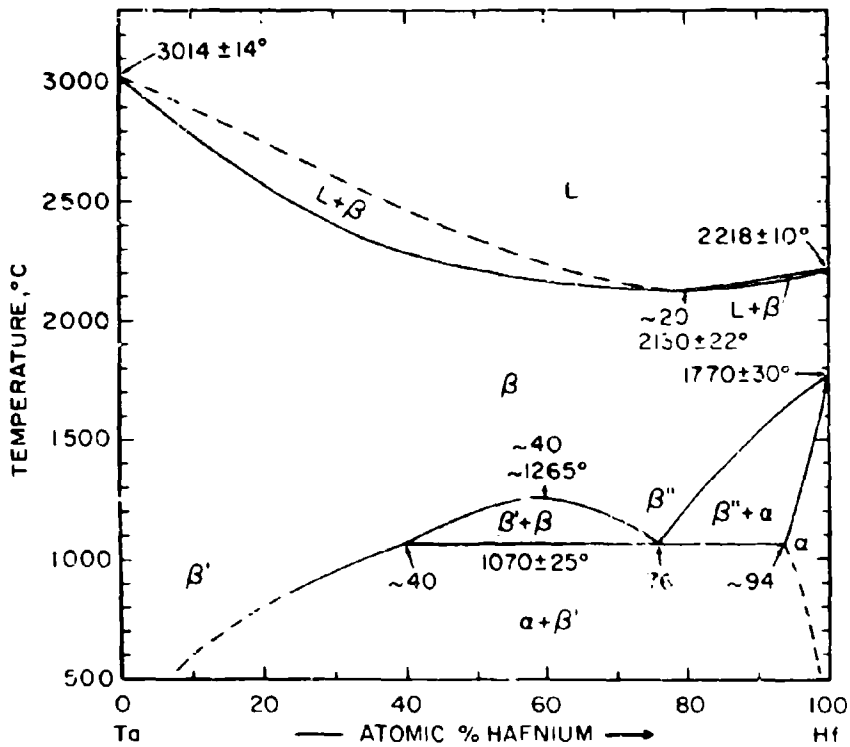

Figure III.A.18.1: Constitution Diagram Hf-Ta.

(After L.L. Oden et al., 1964)

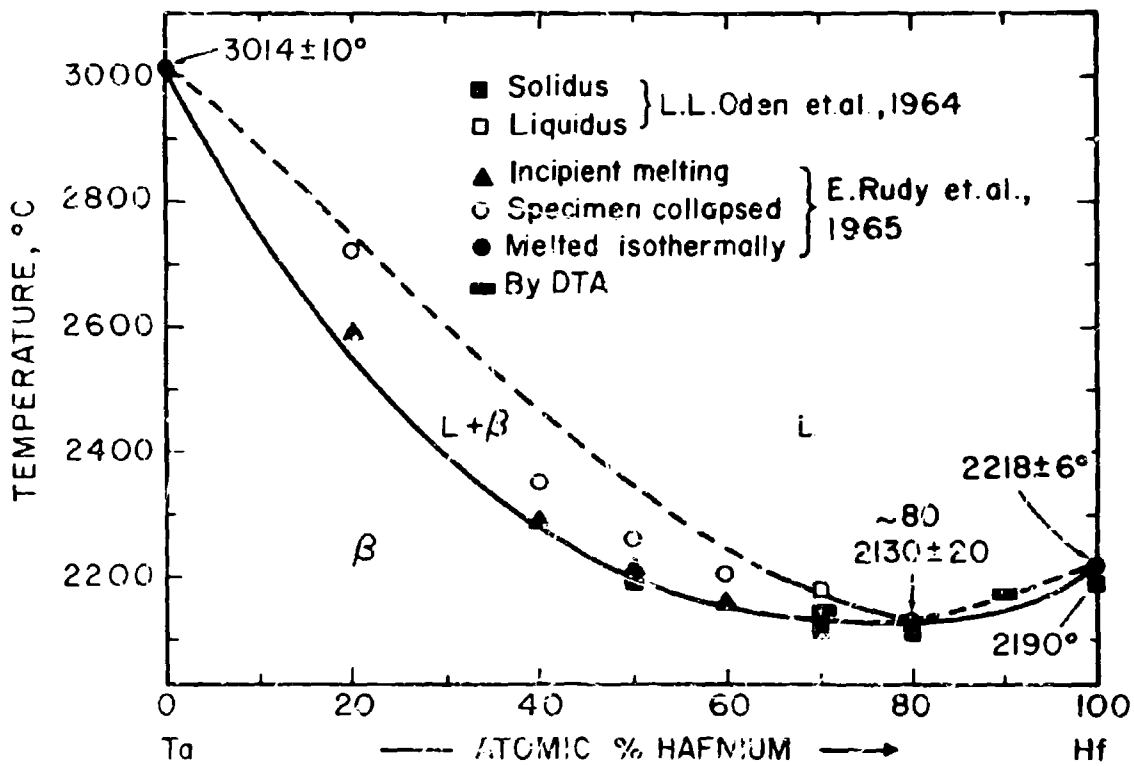

Figure III.A.18.2: Melting Temperatures of Ta-Hf Alloys.

(Temperature Error Figures Based on Reproducibility).

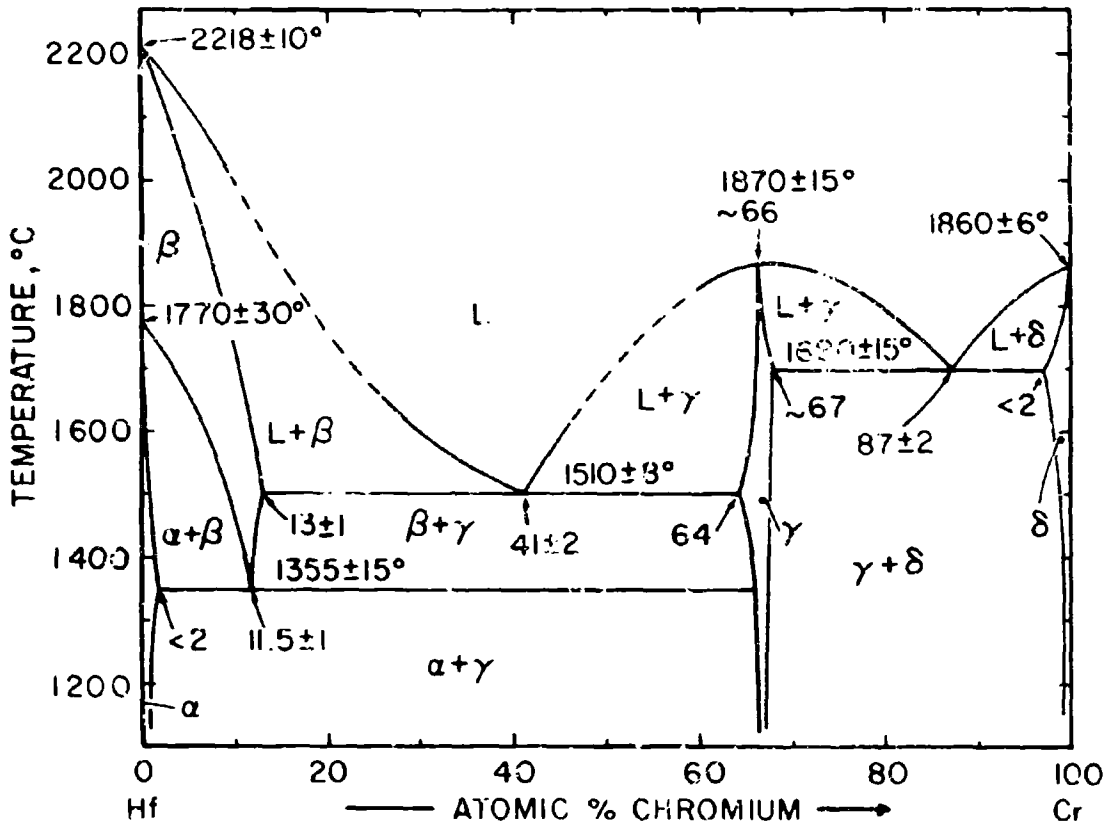

Figure III.A.19.1: Constitution Diagram Hf-Cr.

(Temperature Error Figures Based on Estimated Overall Uncertainty).

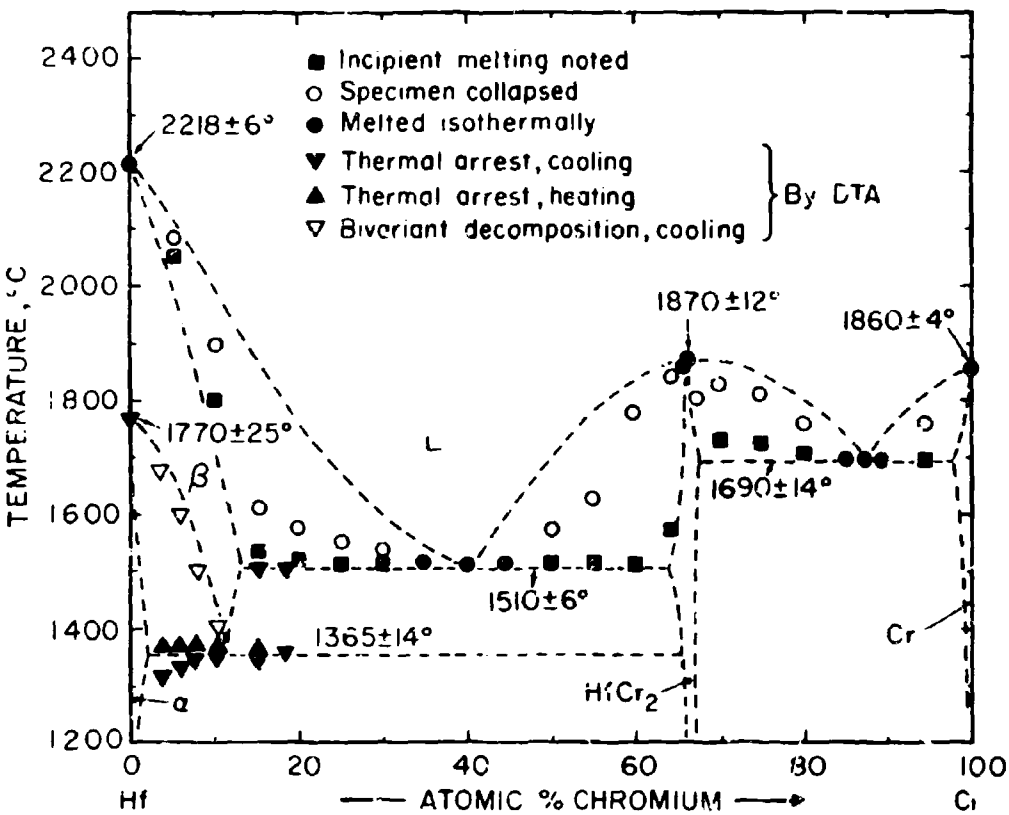

Figure III.A.19.2: Melting Temperatures and Solid State Reactions in the Hf-Cr System.

(Temperature Error Figures Based on Reproducibility).

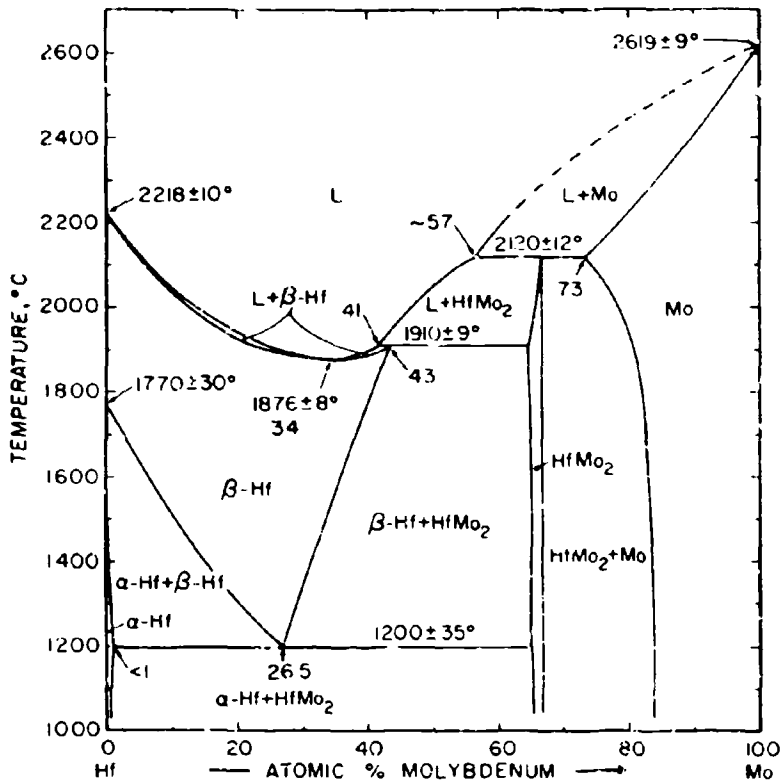

Figure III.A.20.1: Constitution Diagram of the System Hf-Mo.

(Transformation of $HfMo_2$ not Shown. Temperature Error Figures Based on Estimated Overall Uncertainty).

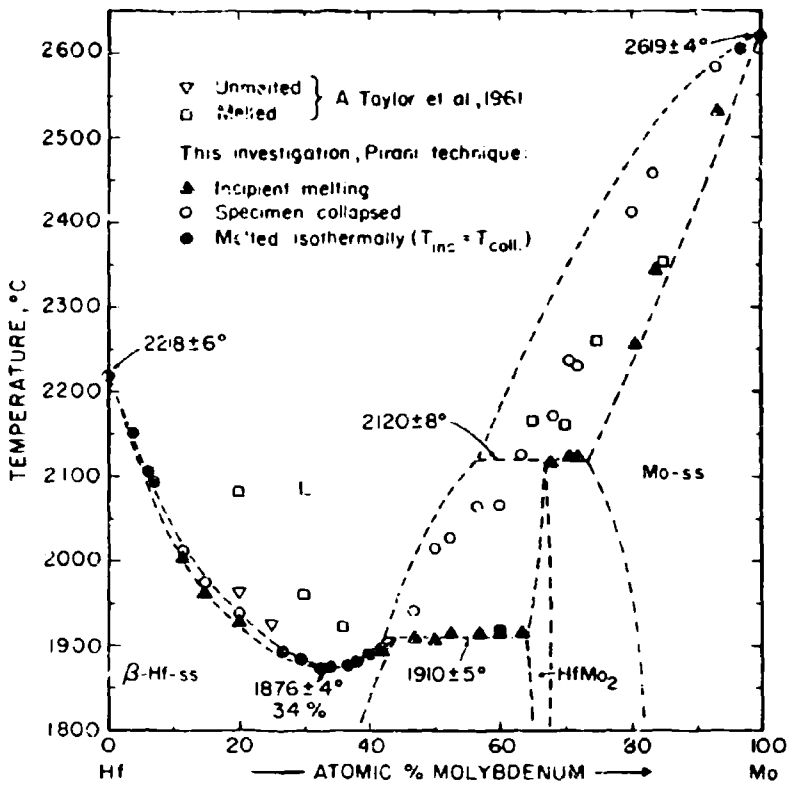

Figure III.A.20.2: Melting Temperatures of Hf-Mo Alloys.

(Temperature Error Figures Based on Reproducibility).

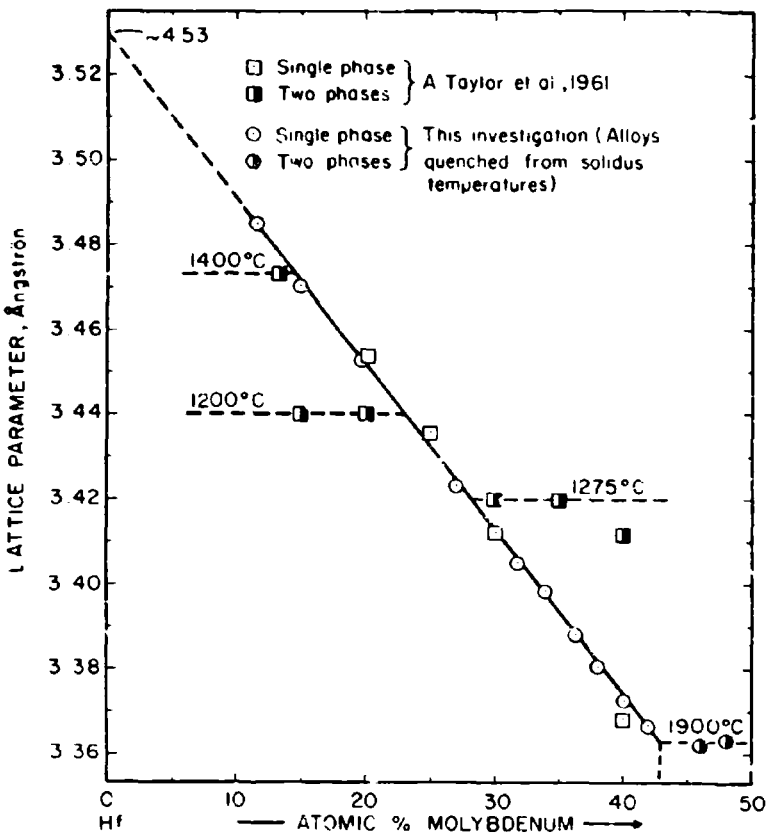

Figure III.A.20.3: Lattice Parameters of the β-Hf Phase in the (Hf, Mo)-System.

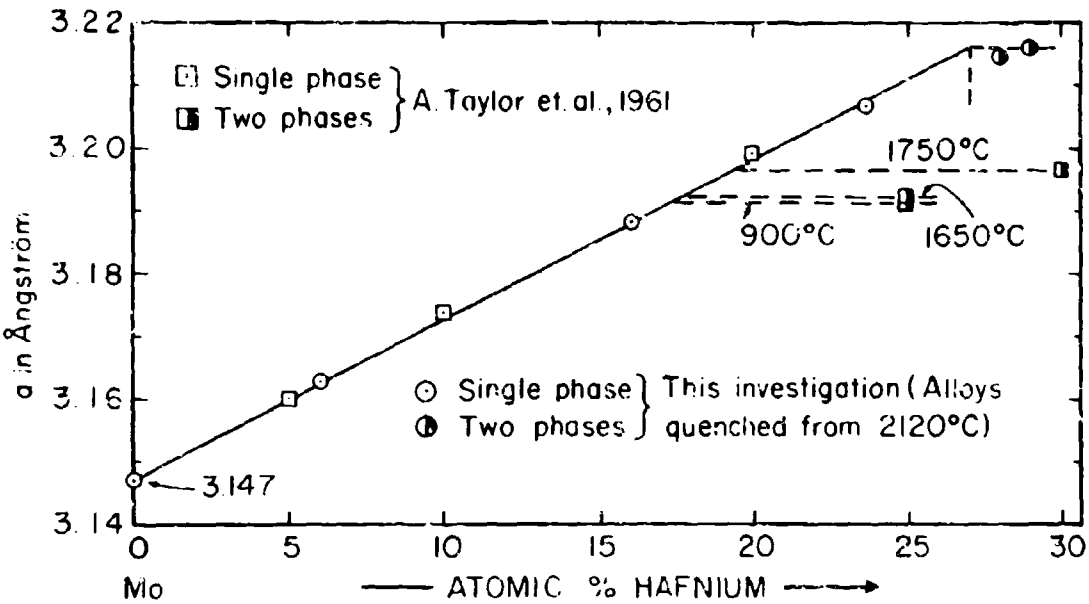

Figure III.A.20.4: Lattice Parameters of the Molybdenum Phase in the (Hf, Mo)-System.

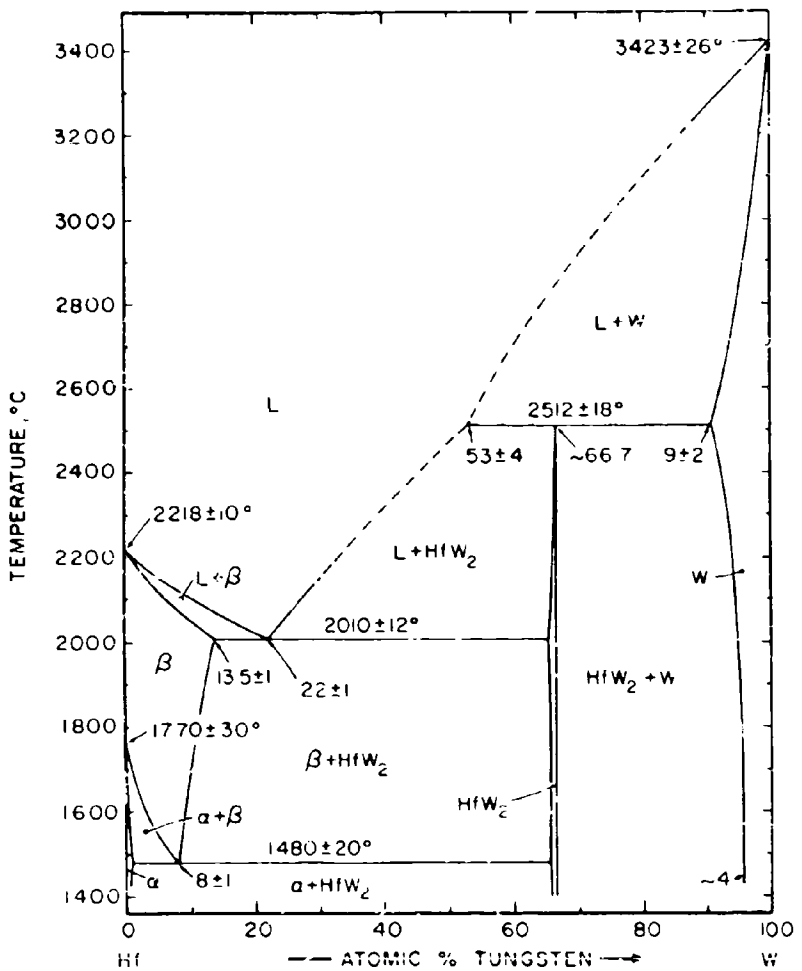

Figure III.A.21.1: Constitution Diagram Hf-W.

(Temperature Error Figures Based on Estimated Overall Uncertainties).

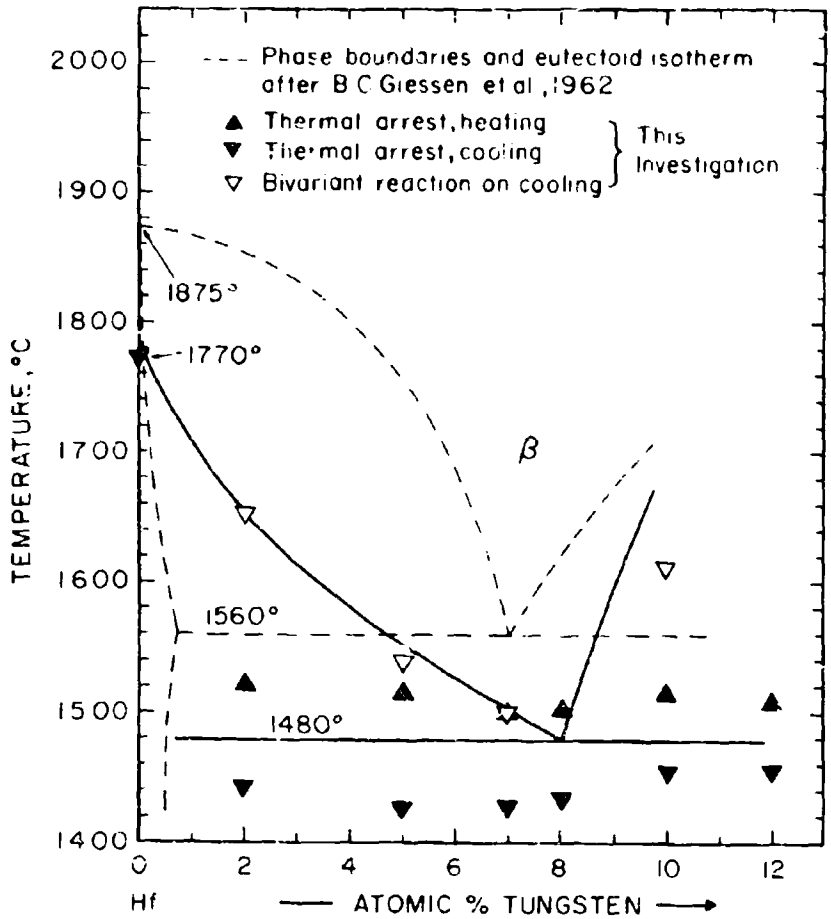

Figure III.A.21.2: Solid State Reactions in the Hf-Rich Region of the (Hf, W)-System.

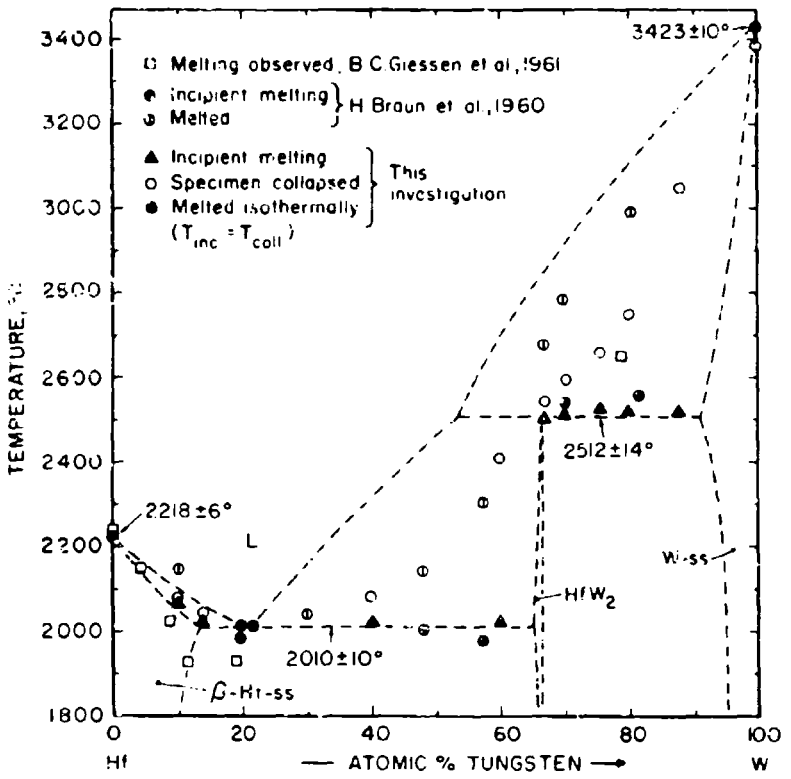

Figure III.A.21.3: Melting Temperatures of Hf-W Alloys.

(Temperature Error Figures Based on Reproducibility).

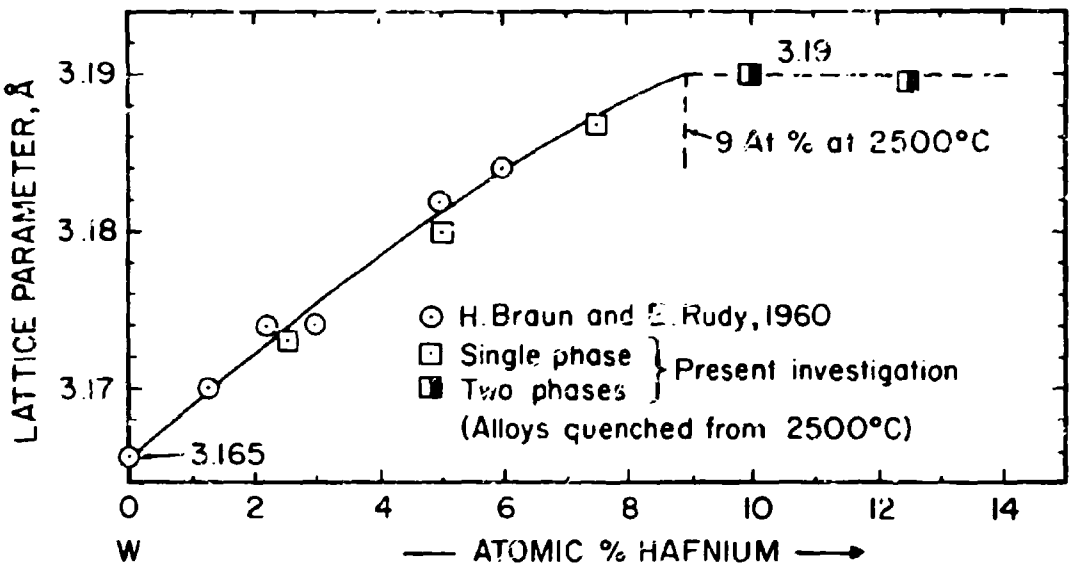

Figure III.A.21.4: Lattice Parameters of the Tungsten Phase in the (Hf, W)-System.

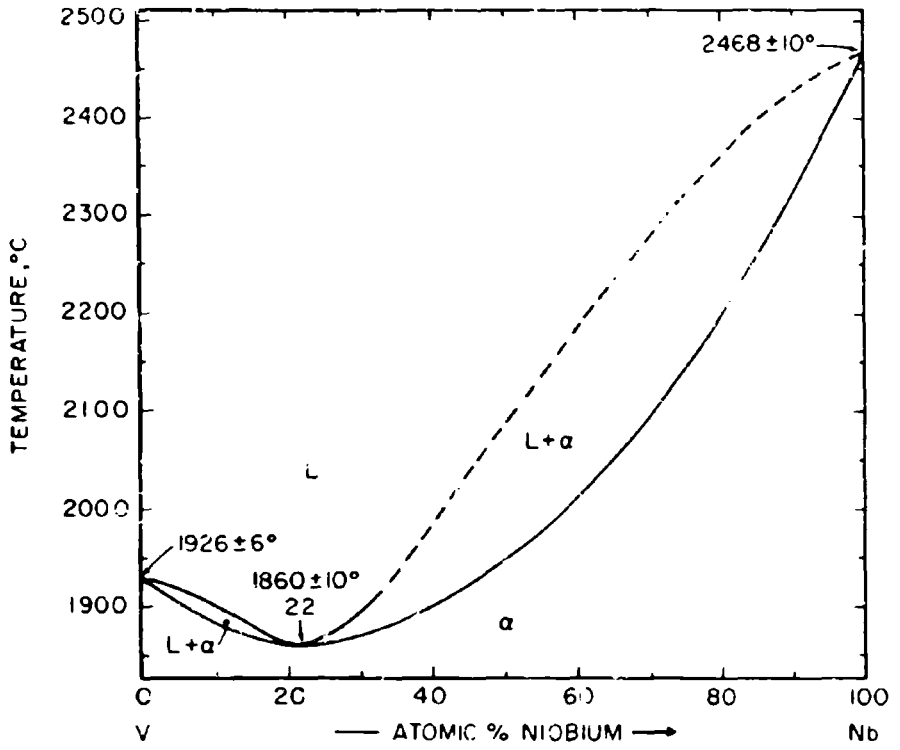

Figure III.A.22.1: Constitution Diagram V-Nb.

(Temperature Error Figures Based on Estimated Overall Uncertainty).

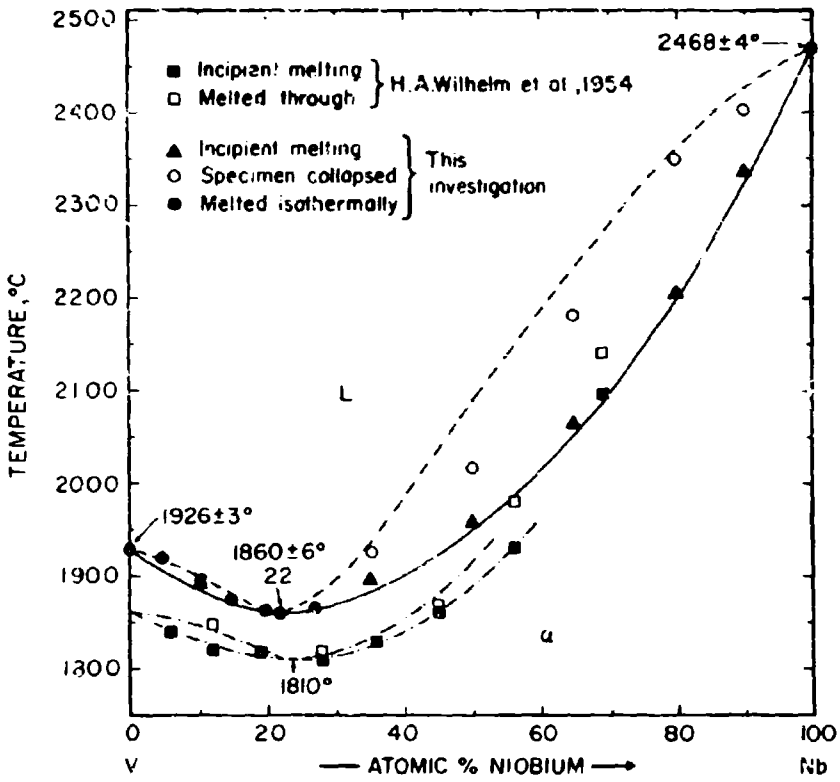

Figure III.A.22.2: Melting Temperatures of V-Nb Alloys.

(Temperature Error Figures Based on Reproducibility).

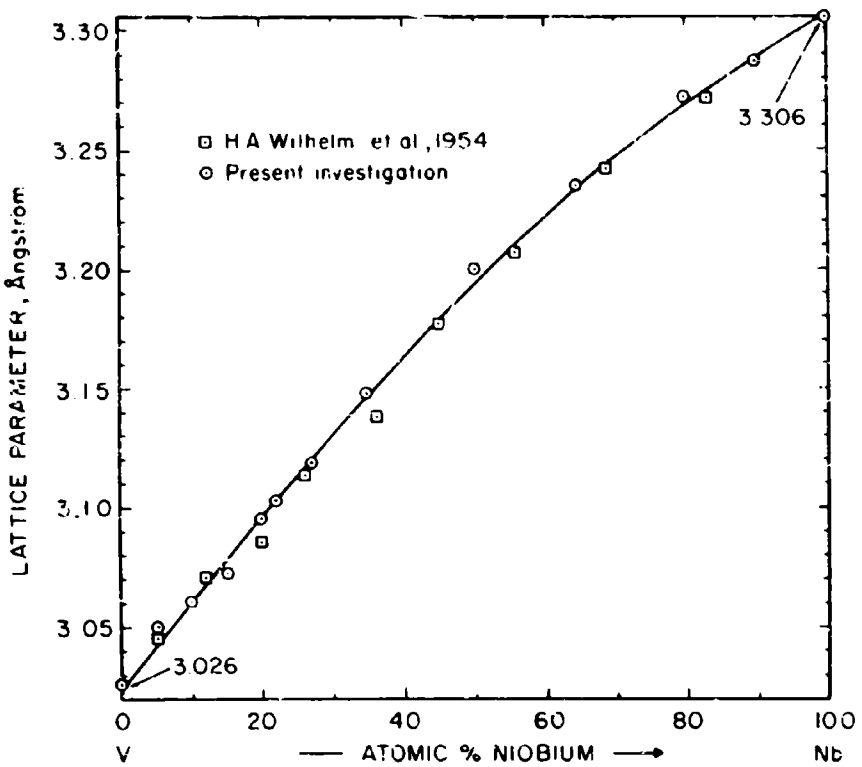

Figure III.A.22.3: Lattice Parameters of the V-Nb Solid Solution.

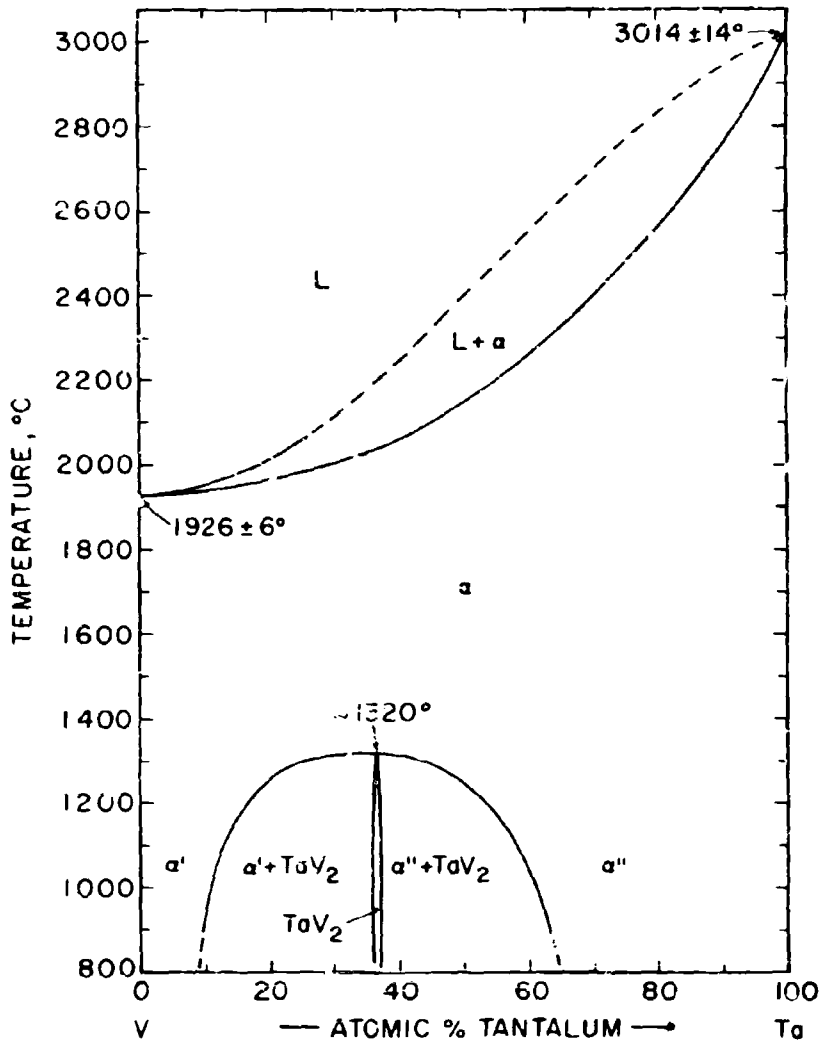

Figure III.A.23.1: Constitution Diagram V-Ta.

(Temperature Error Figures Based on Estimated Overall Uncertainty).

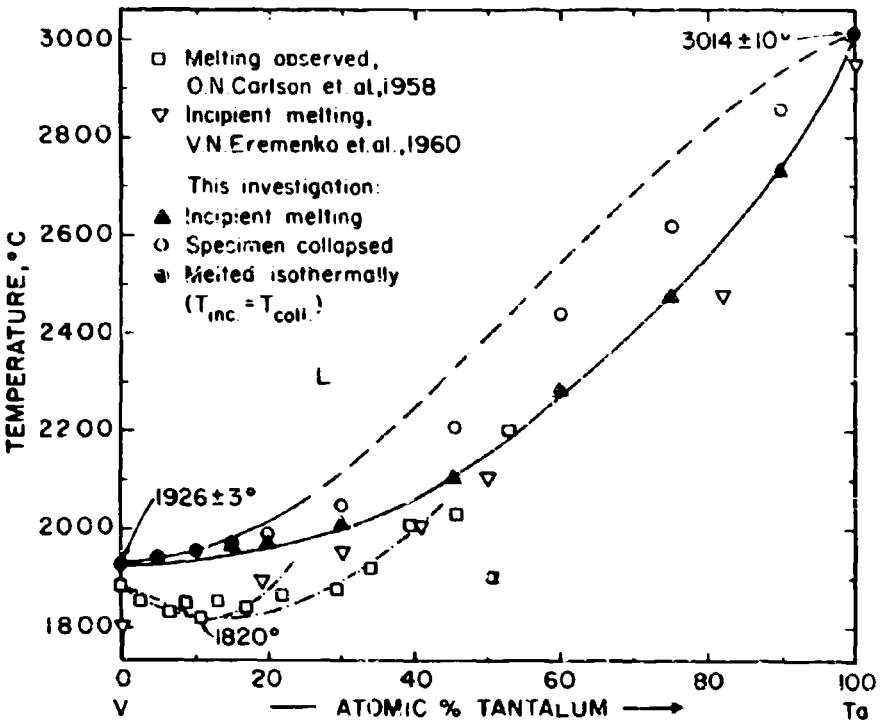

Figure III.A.23.2: Melting Temperatures of V-Ta Alloys.

(Temperature Error Figures Based on Reproducibility).

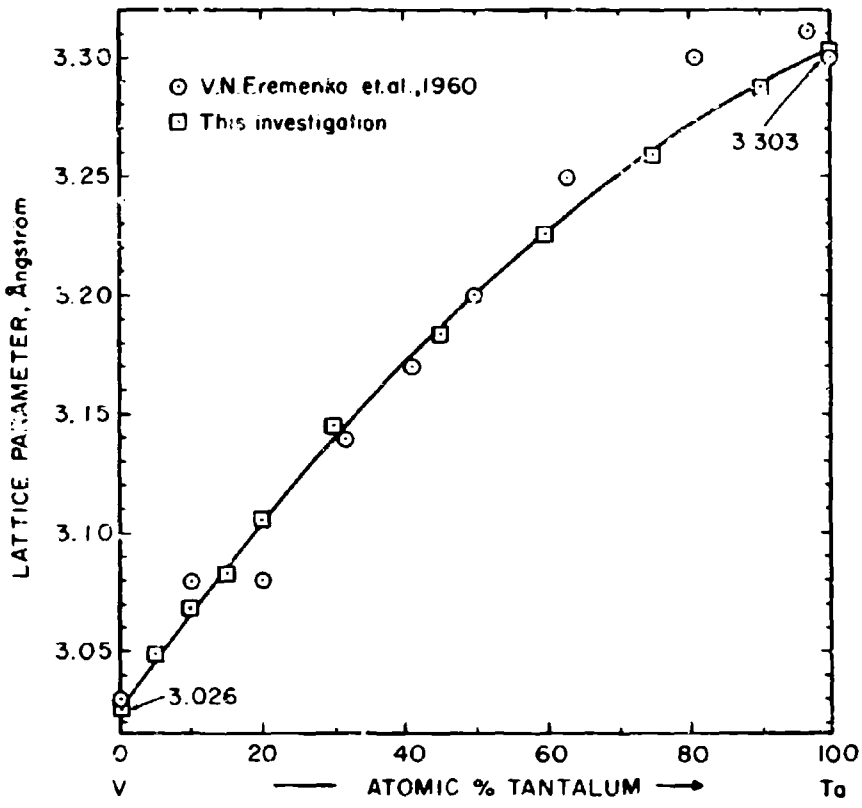

Figure III.A.23.3: Lattice Parameters of the V-Ta Solid Solution.

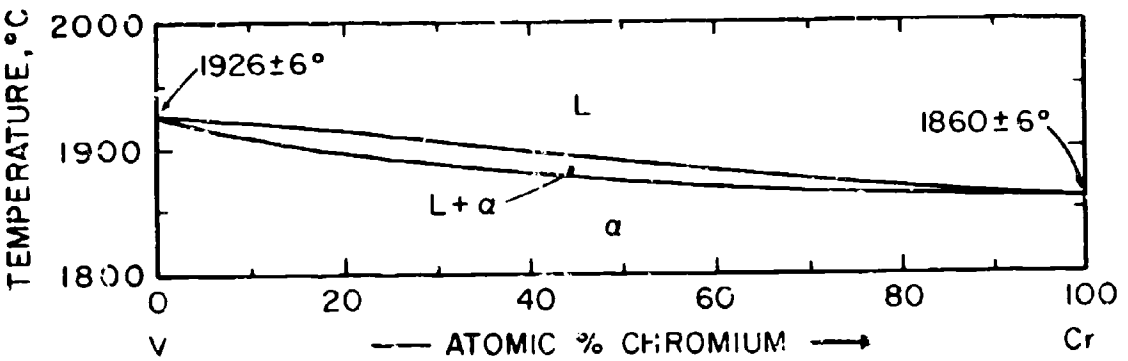

Figure III.A.24.1: Constitution Diagram of the System V-Cr.

(Temperature Error Figures Based on Estimated Overall Uncertainty).

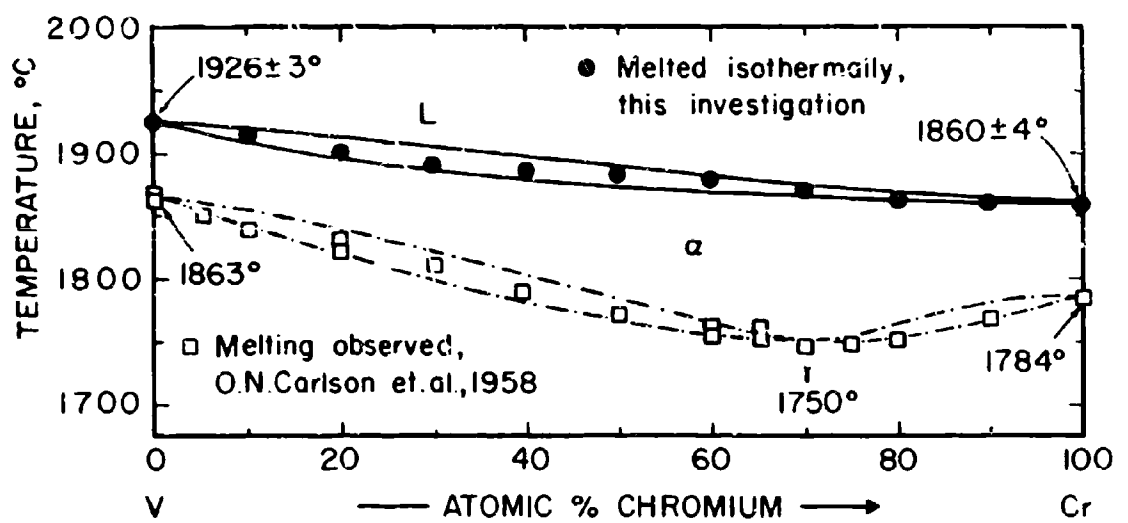

Figure III.A.24.2: Melting Temperatures of V-Cr Alloys.

(Temperature Error Figures Based on Reproducibility).

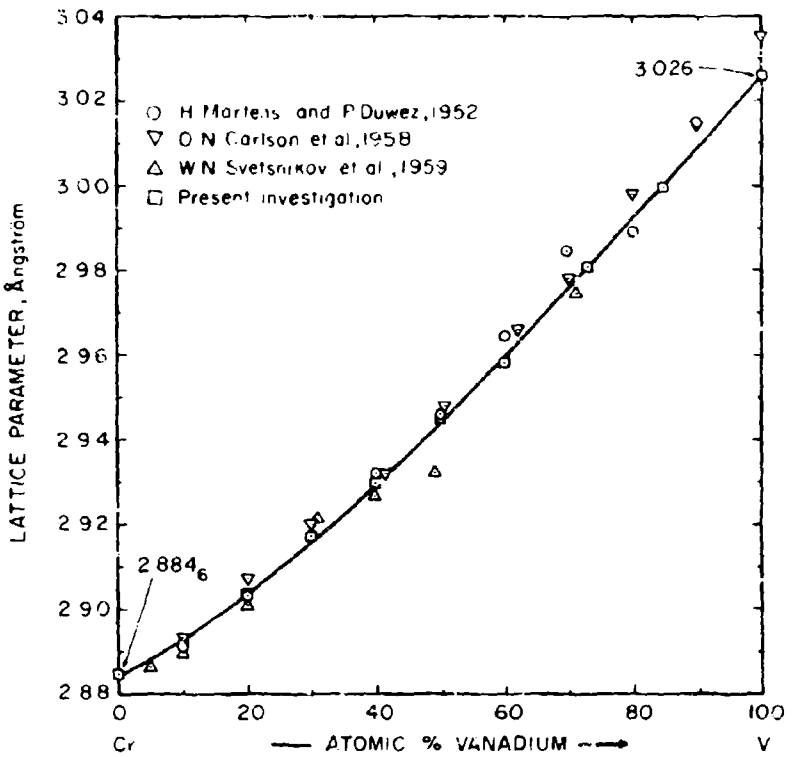

Figure III.A.24.3: Lattice Parameters of the (V,Cr)-Solid Solution.

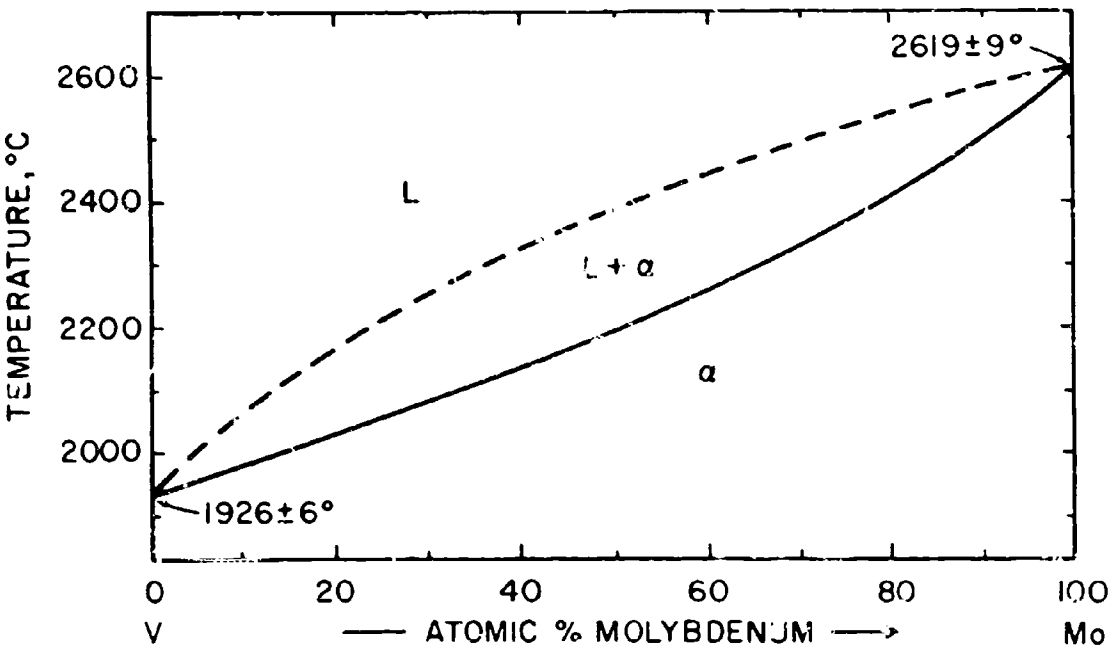

Figure III.A.25.1: Constitution Diagram V-Mo.

(Temperature Error Figures Based on Estimated Overall Uncertainty).

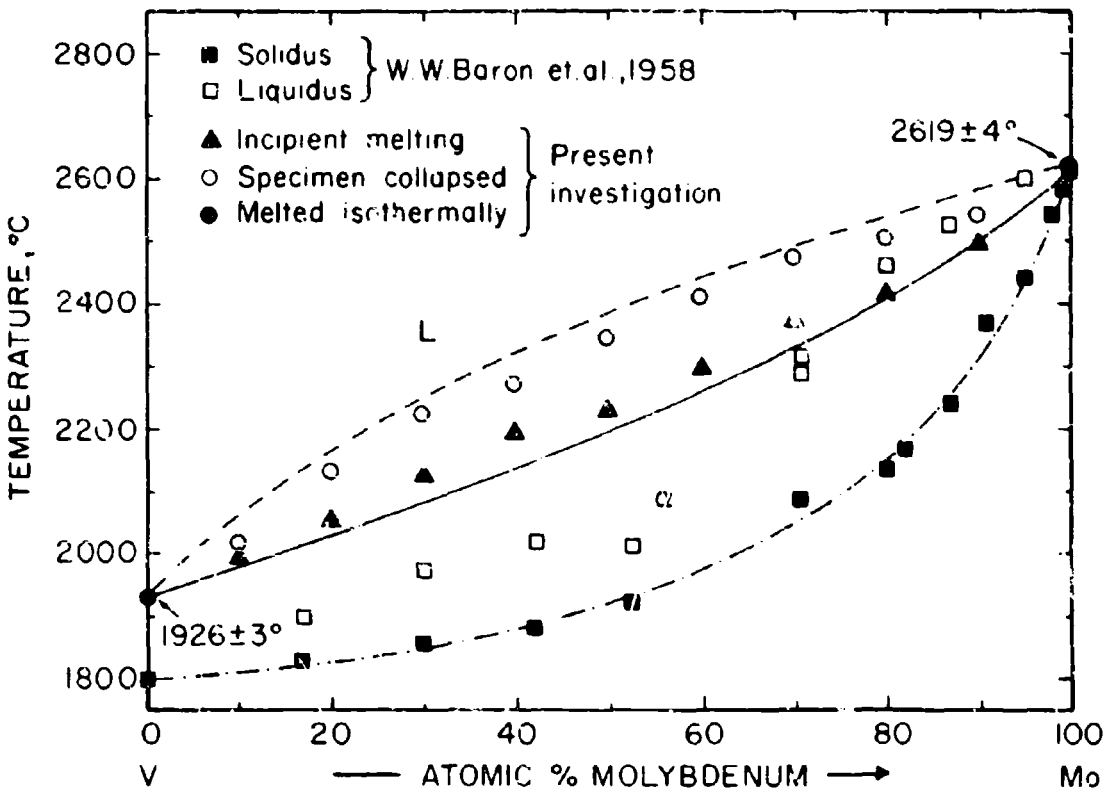

Figure III.A.25.2: Melting Temperatures of V-Mo Alloys.

(Temperature Error Figures Based on Reproducibility).

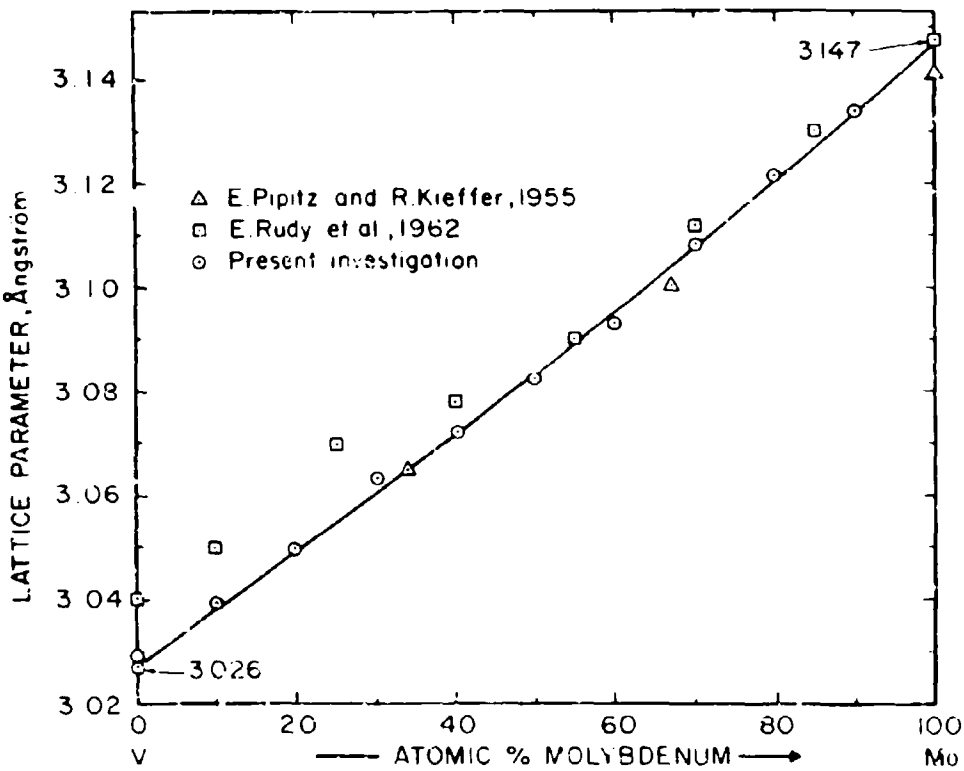

Figure III.A.25.3: Lattice Parameters of V-Mo Alloys.

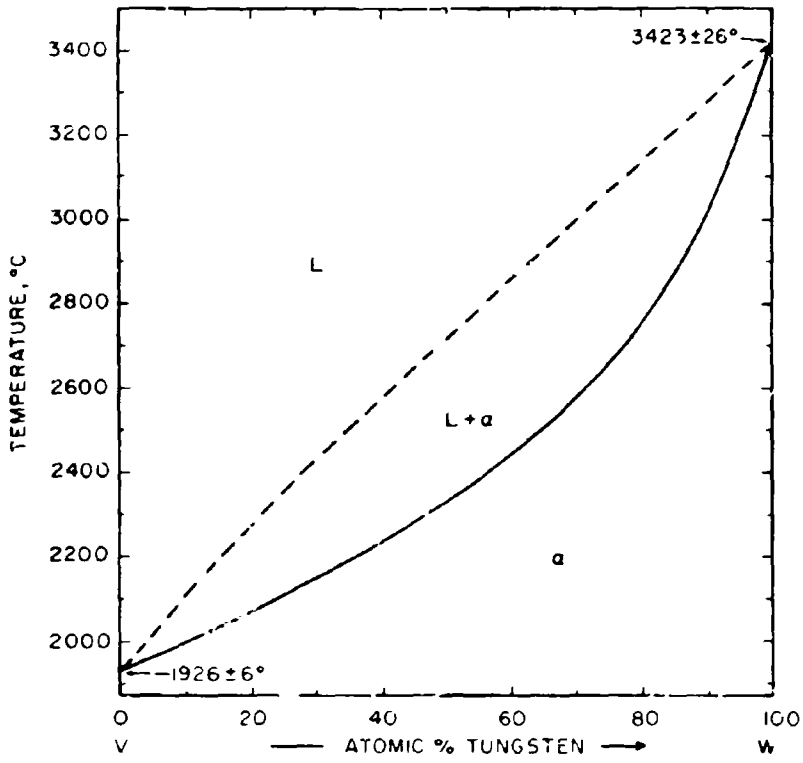

Figure III.A.26.1: Constitution Diagram of the System V-W.

(Temperature Error Figures Based on Estimated Overall Uncertainty).

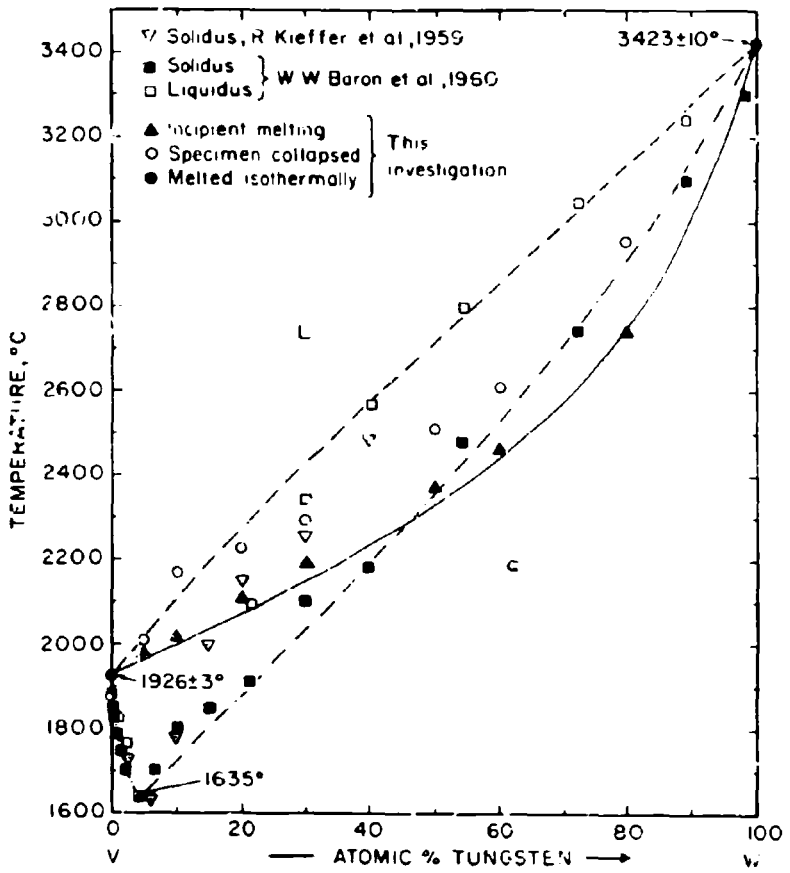

Figure III.A.26.2: Melting Temperatures of V-W Alloys.

(Temperature Error Figures Based on Reproducibility).

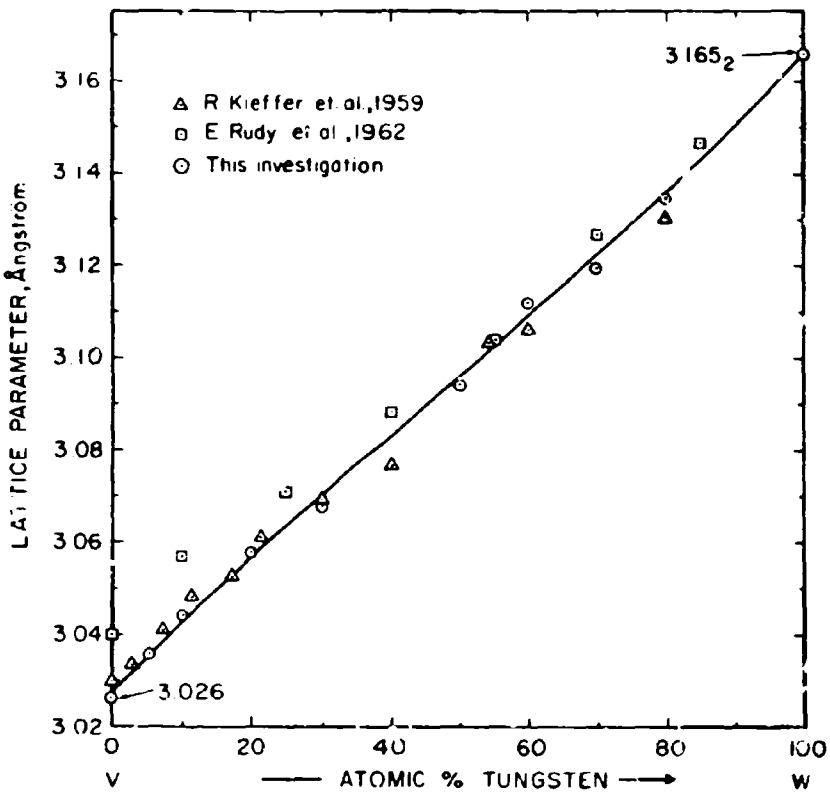

Figure III.A.26.3: Lattice Parameters of V-W Alloys.

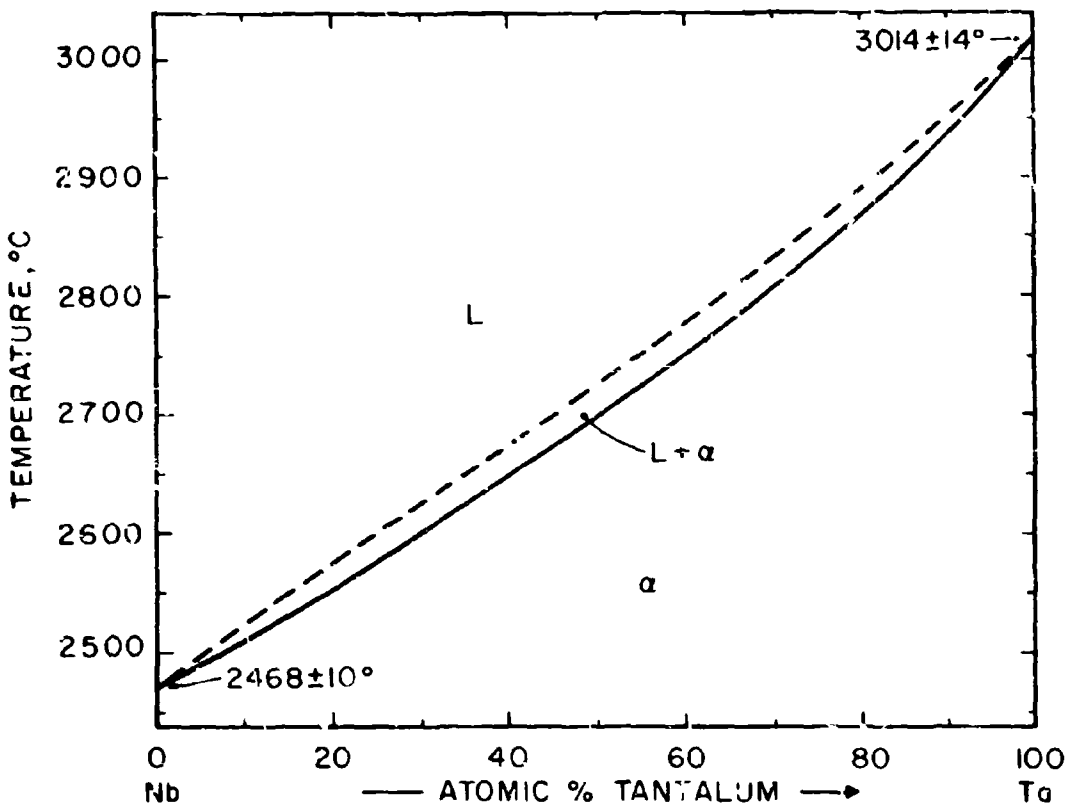

Figure III.A.27.1: Constitution Diagram of the System Nb-Ta.

(Temperature Error Figures Based on Estimated Overall Uncertainty).

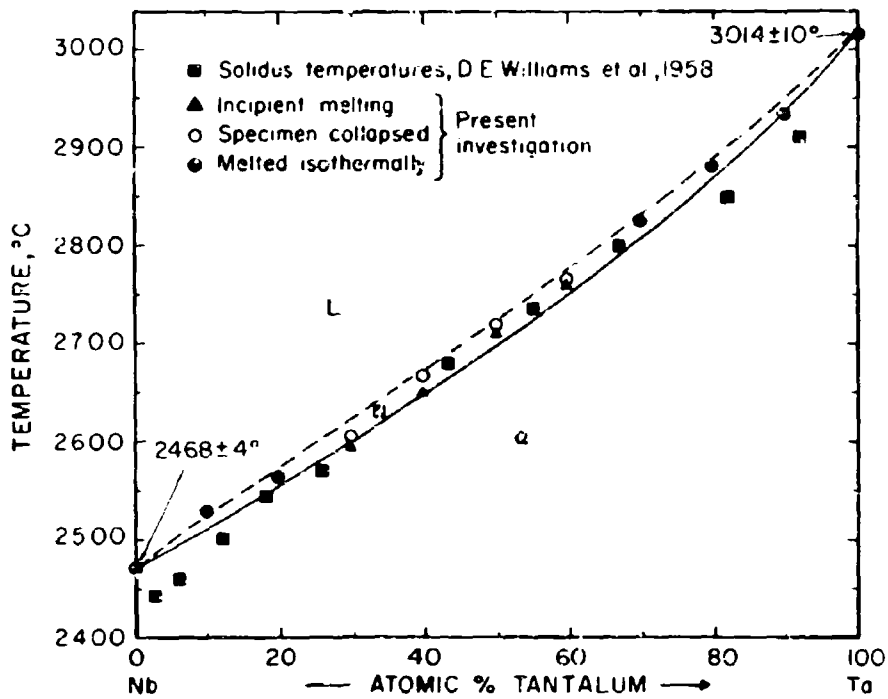

Figure III.A.27.2: Melting Temperatures of Nb-Ta Alloys.

(Temperature Error Figures Based on Reproducibility).

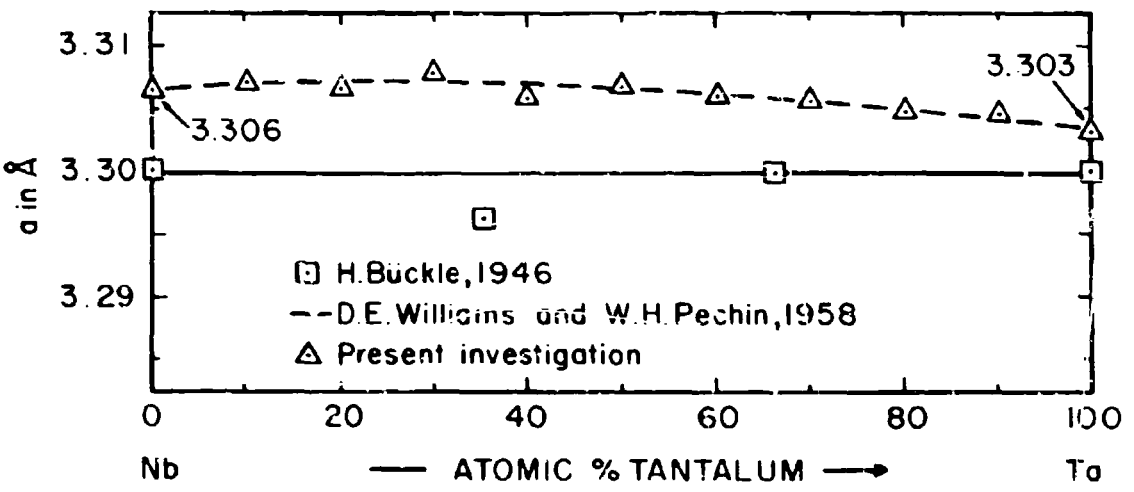

Figure III.A.27.3: Lattice Parameters of Nb-Ta Alloys.

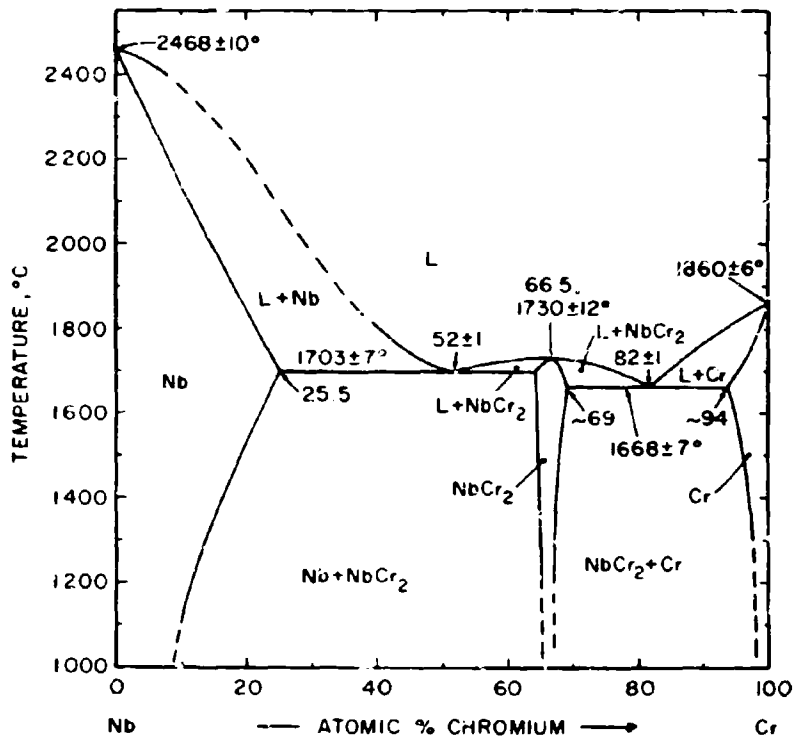

Figure III.A.28.1: Constitution Diagram Nb-Cr.

(Temperature Error Figures Based on Estimated Overall Uncertainty).

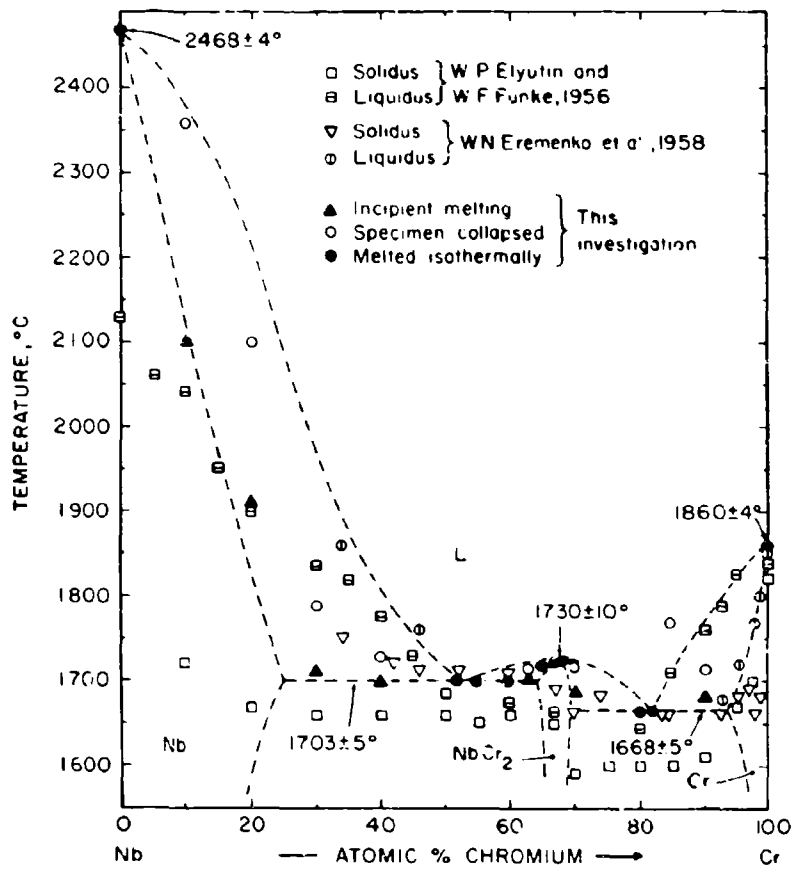

Figure III.A.28.2: Melting Temperatures of Nb-Cr Alloys.

(Temperature Error Figures Based on Reproducibility).

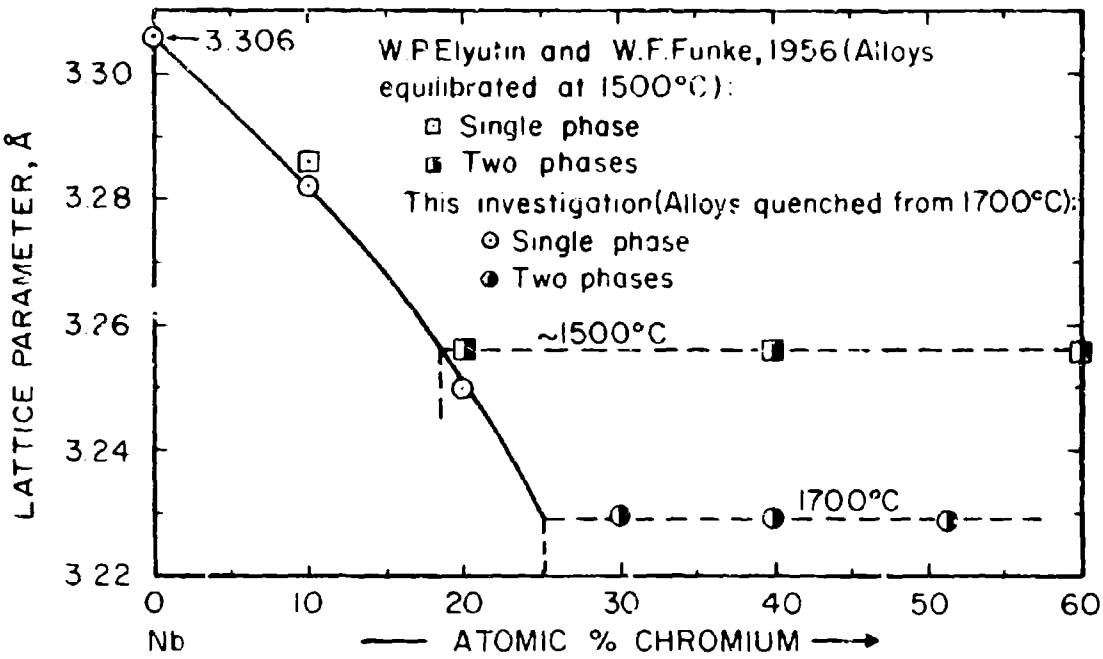

Figure III.A.28.3: Lattice Parameters of the Nb-Cr Solid Solution.

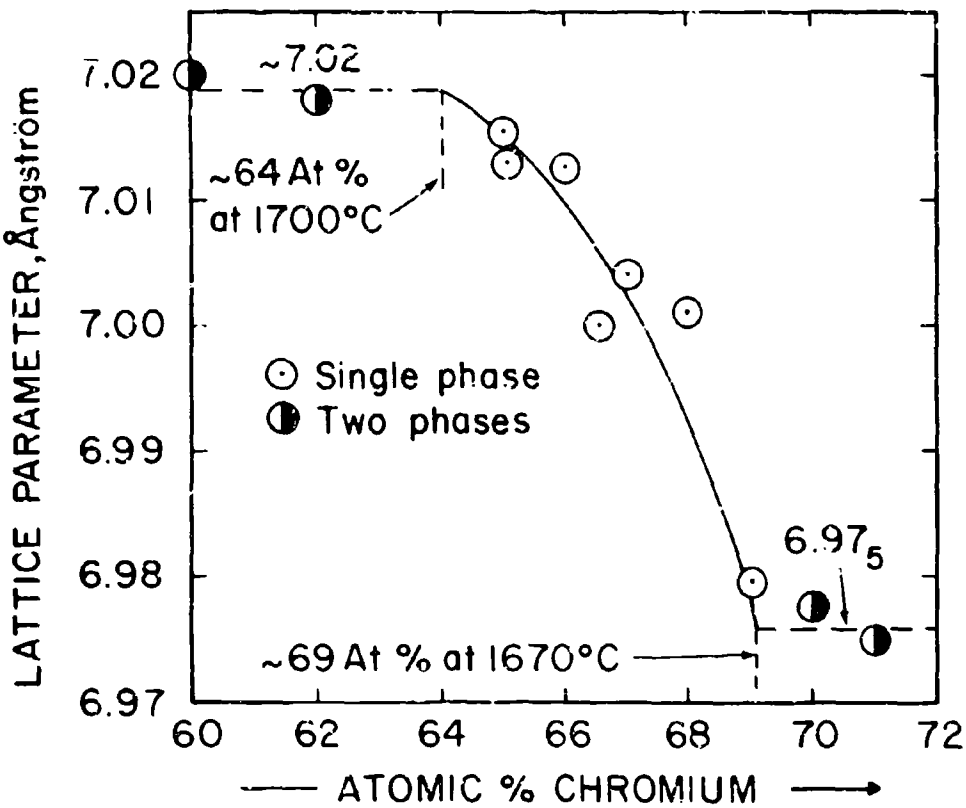

Figure III.A.28.4: Lattice Parameters of the Cubic (C 15) Laves Phase in the Nb-Cr System.

(Alloys Quenched from Solidus Temperatures, this Investigation).

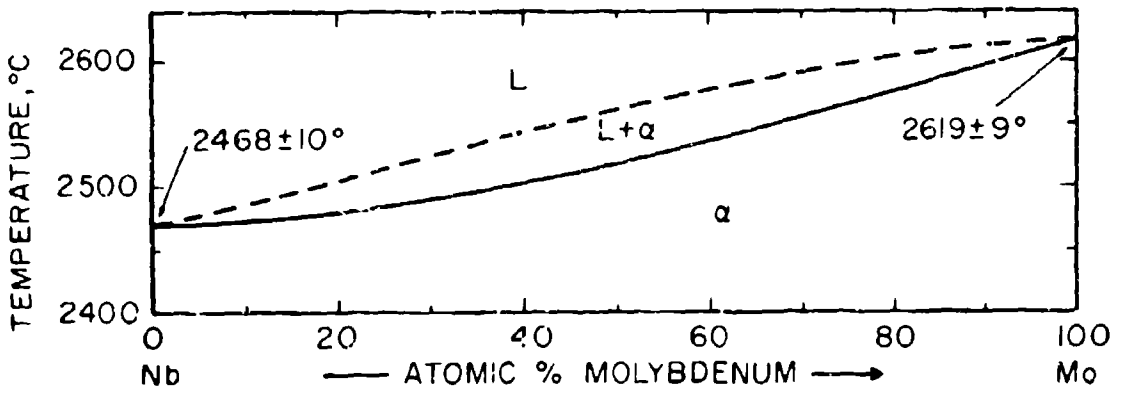

Figure III.A.29.1: Constitution Diagram Nb-Mo.

(Temperature Error Figures Based on Estimated Overall Uncertainty).

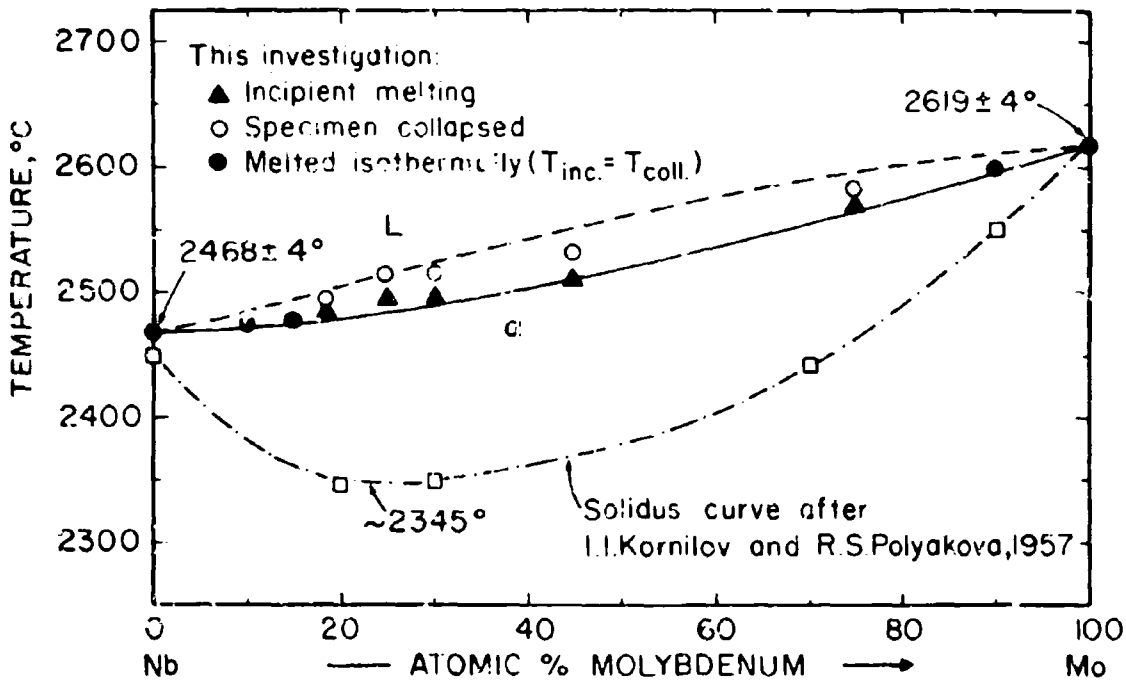

Figure III.A.29.2: Melting Temperatures of Nb-Mo Alloys.

(Temperature Error Figures Based on Reproducibility).

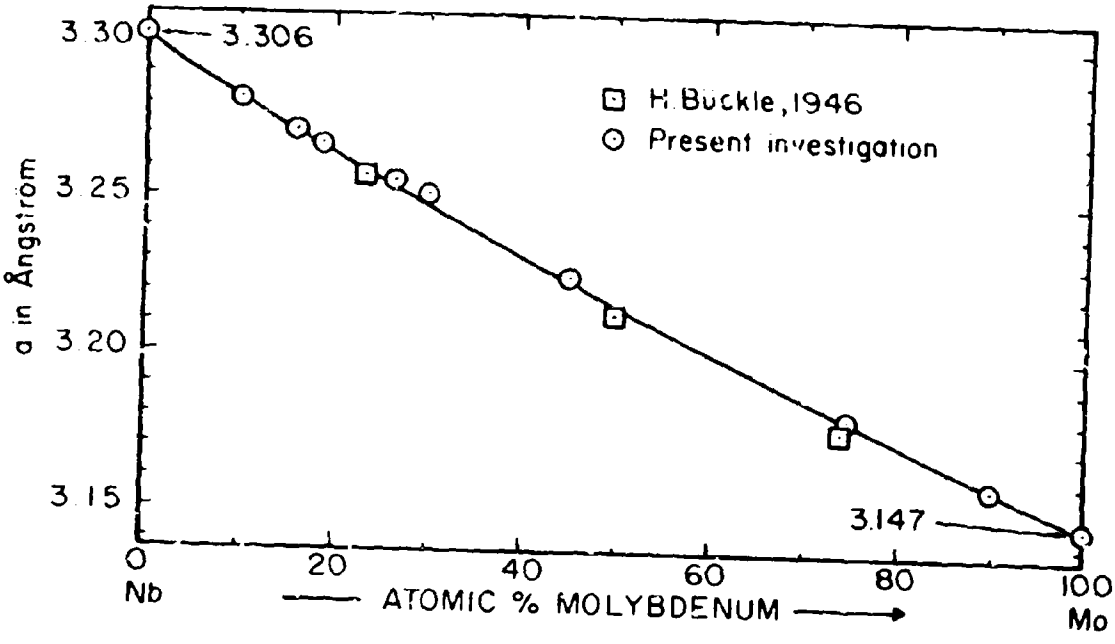

Figure III.A.29.3: Lattice Parameters of Nb-Mo Alloys.

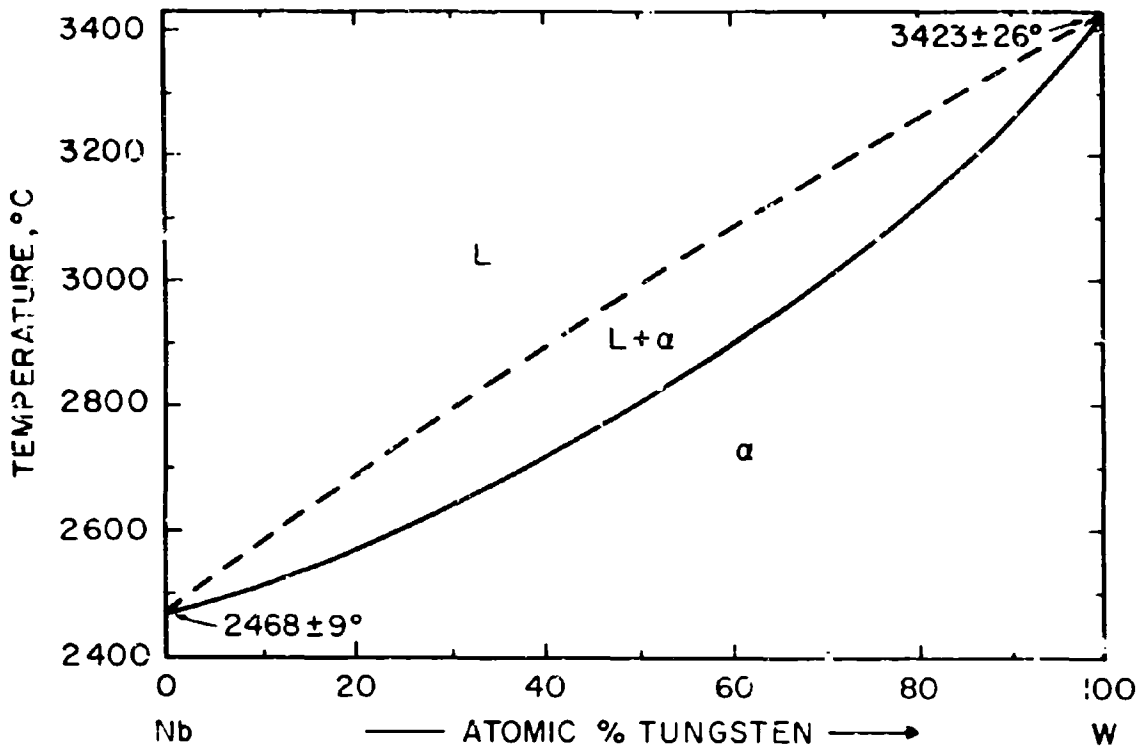

Figure III.A.30.1: Constitution Diagram of the System Nb-W.

(Temperature Error Figures Based on Estimated Overall Uncertainty).

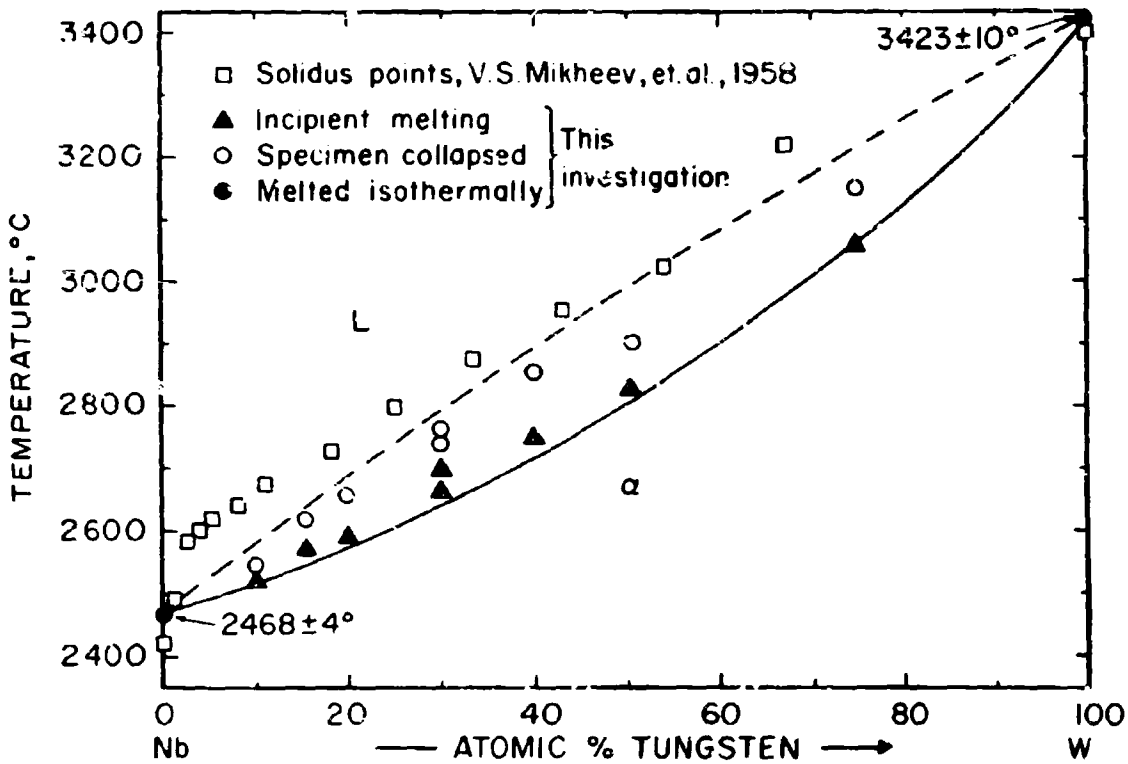

Figure III.A.30.2: Solidus Temperatures of Nb-W Alloys.

(Temperature Error Figures Based on Reproducibility).

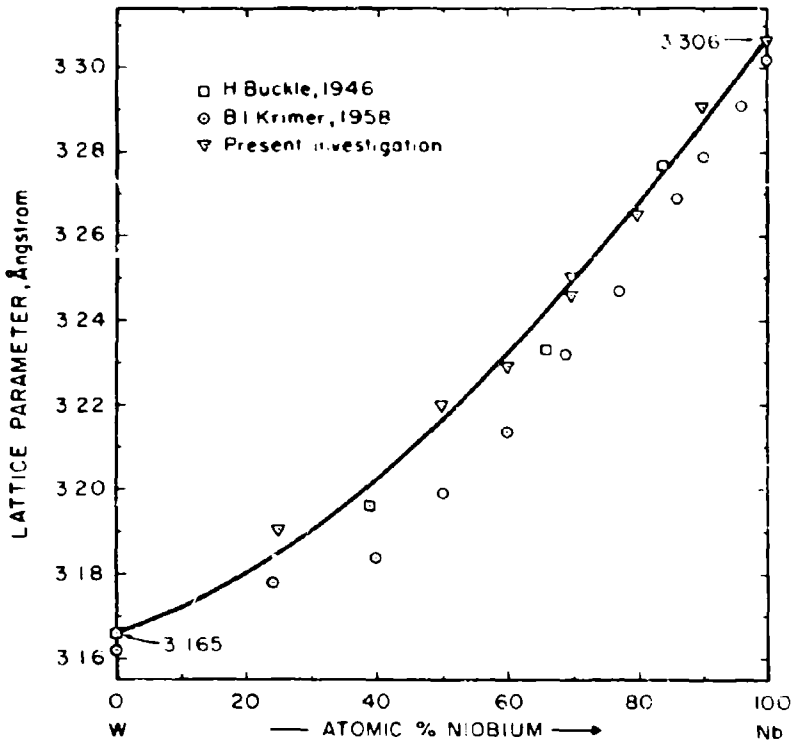

Figure III.A.30.3: Lattice Parameters of the Nb-W Solid Solution.

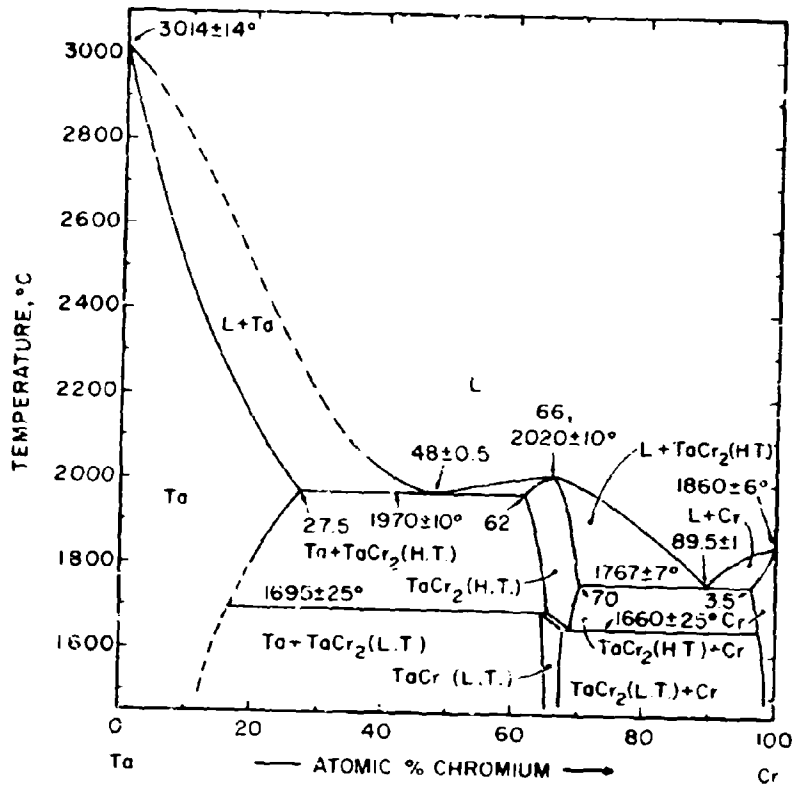

Figure III.A.31.1: Constitution Diagram of the Ta-Cr System.

(Temperature Error Figures Based on Estimated Overall Uncertainty).

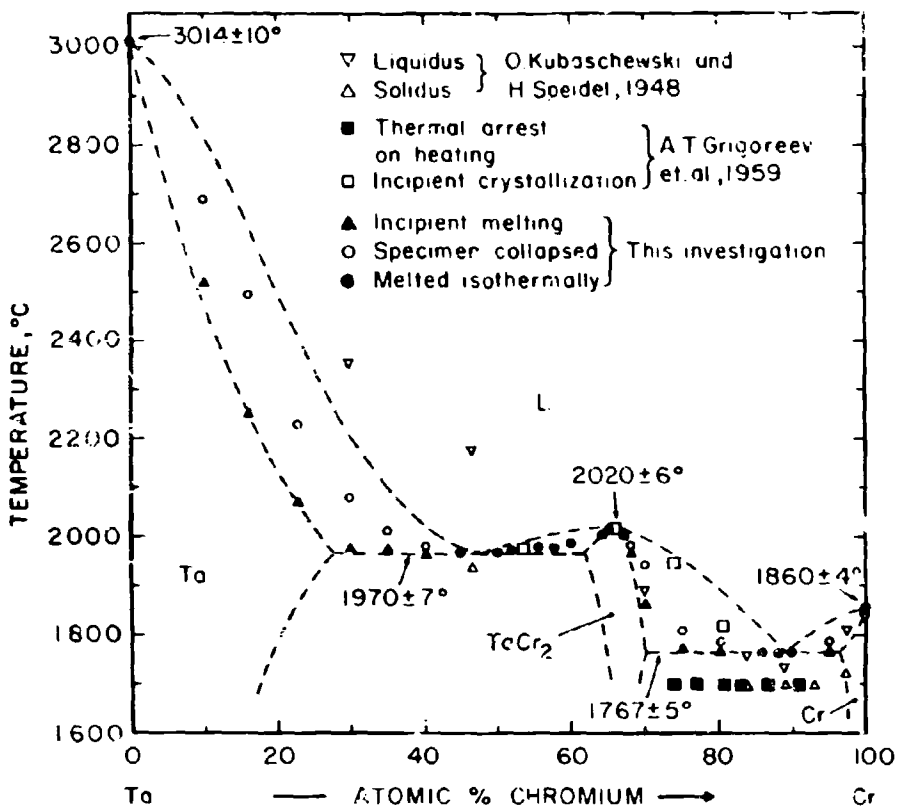

Figure III.A.31.2: Melting Temperatures of Ta-Cr Alloys.

(Temperature Error Figures Based on Reproducibility).

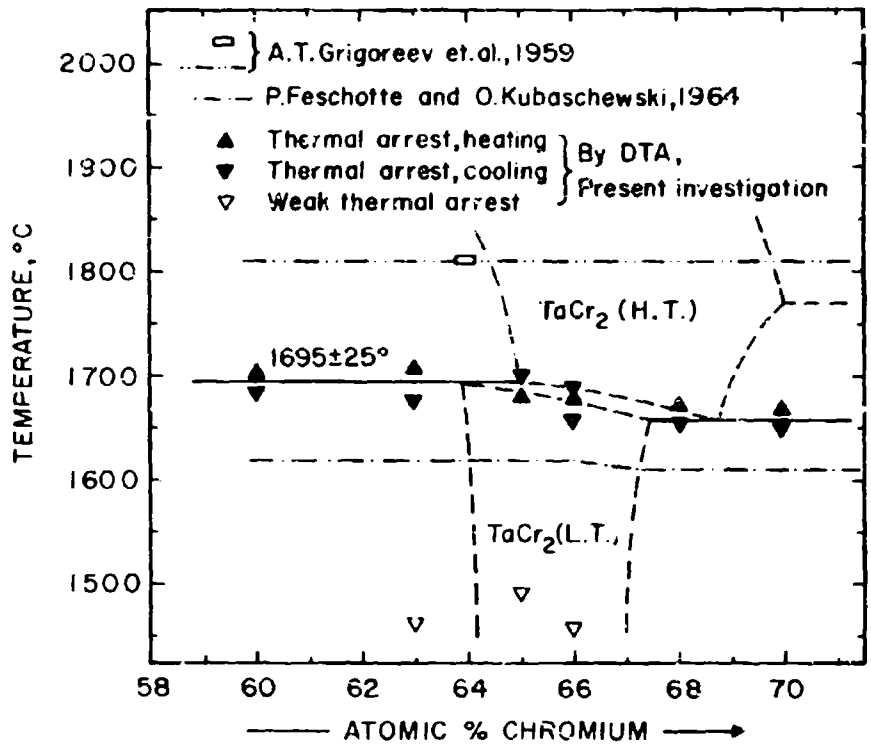

Figure III.A.31.3: Transformation of the $TaCr_2$-Phase.

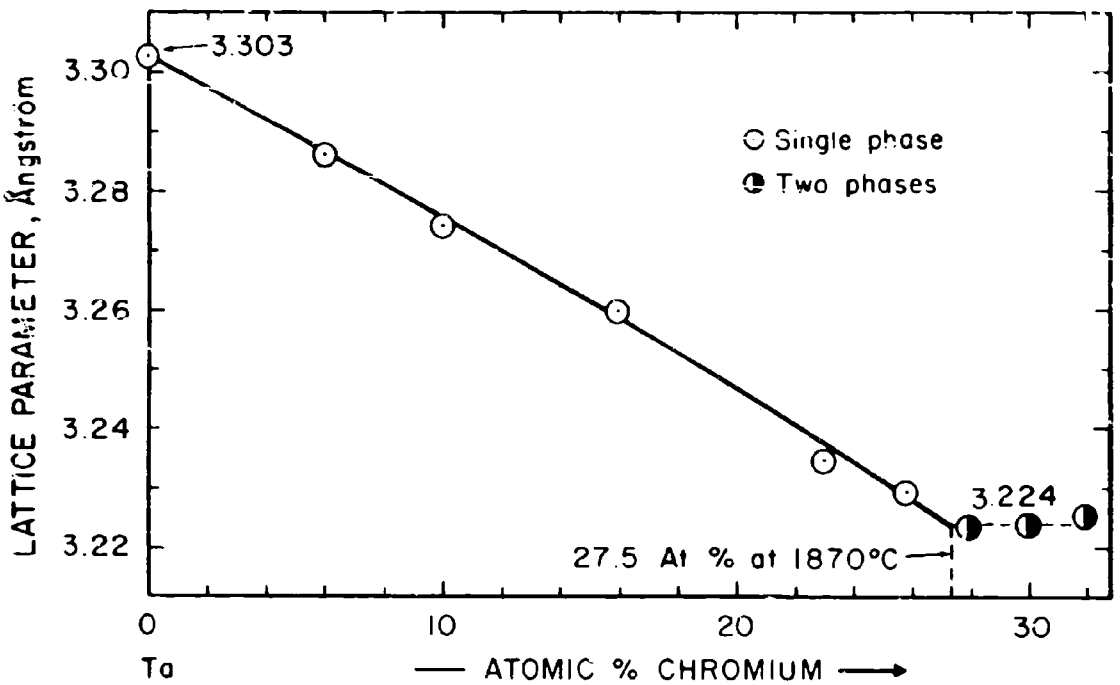

Figure III.A.31.4: Lattice Parameters of the Tantalum Phase in the (Ta, Cr)-System.

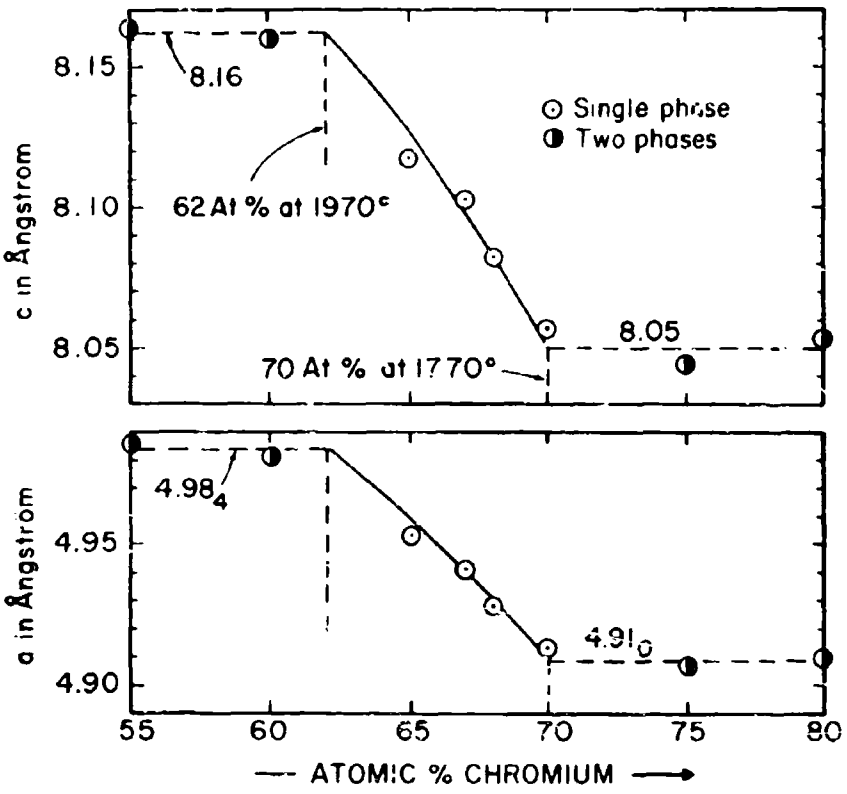

Figure III.A.31.5: Lattice Parameters of the Hexagonal (C 14-Type), High Temperature Modification of $TaCr_2$.

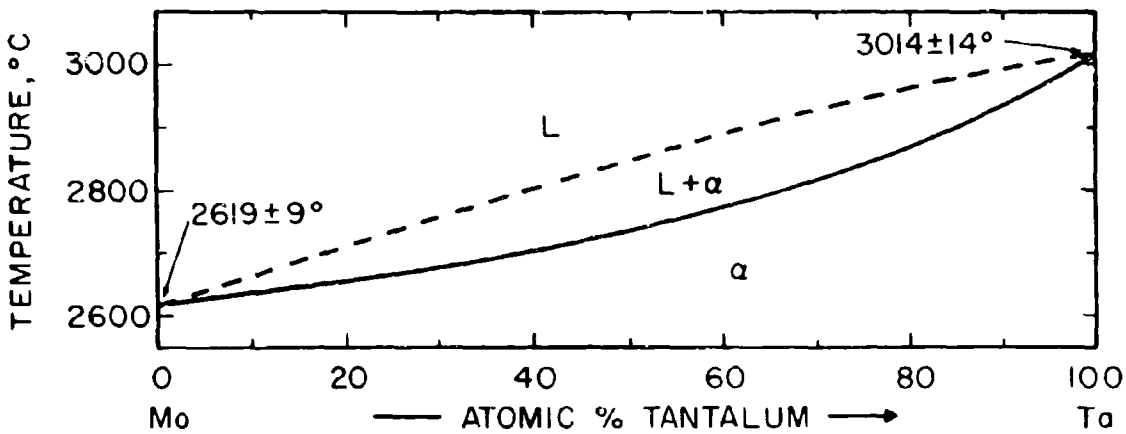

Figure III.A.32.1: Constitution Diagram of the Ta-Mo System.

(Temperature Error Figures Based on Estimated Overall Uncertainty).

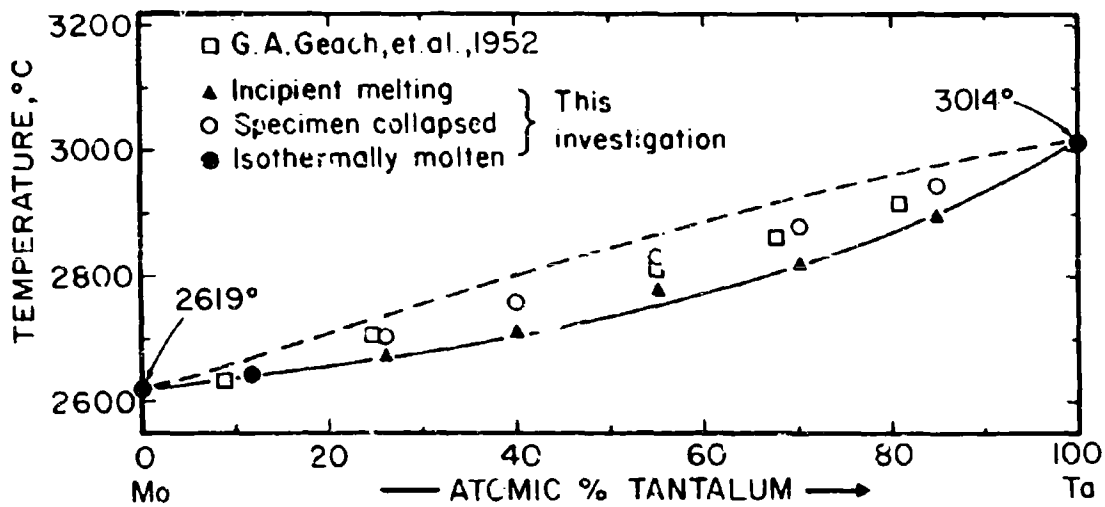

Figure III.A.32.2: Melting Temperatures of Ta-Mo Alloys.

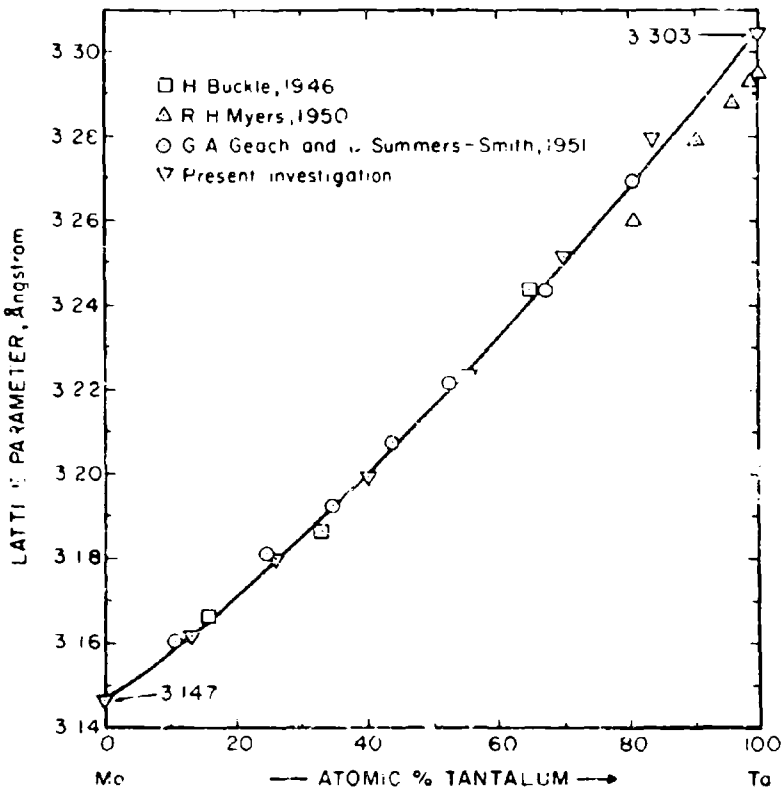

Figure III.A.32.3: Lattice Parameters of the (Ta, Mo)-Solid Solution.

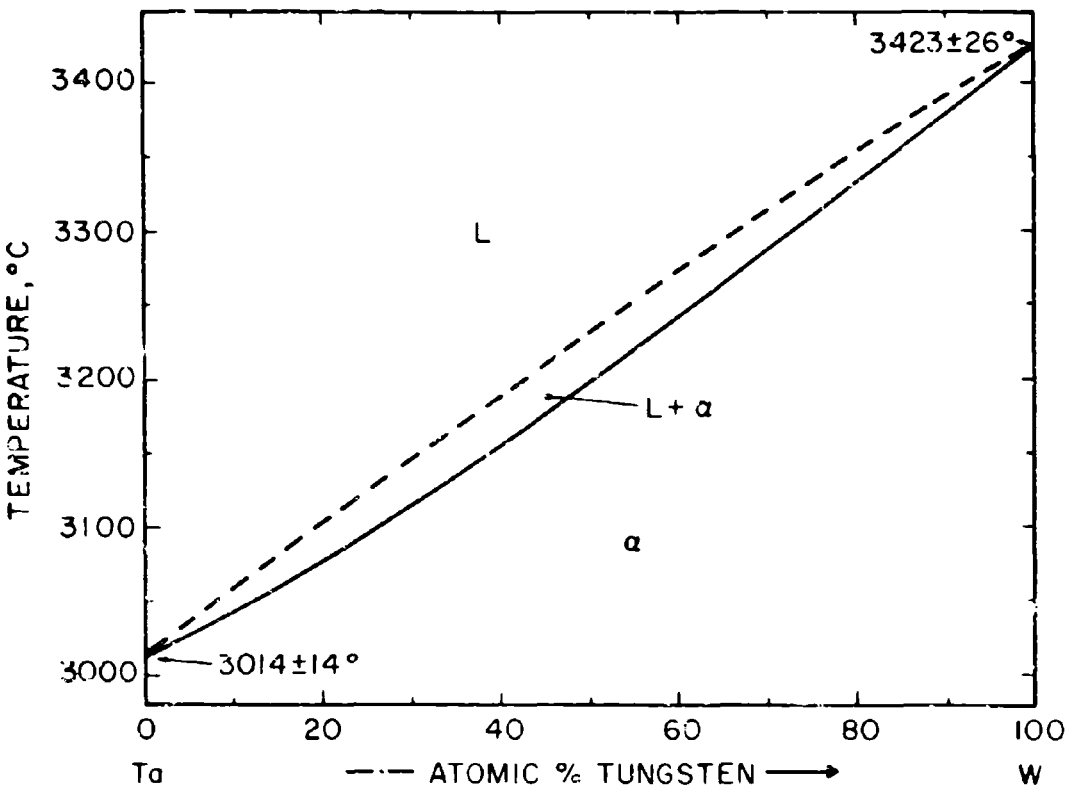

Figure III.A.33.1: Constitution Diagram of the Ta-W System.

(Temperature Error Figures Based on Estimated Overall Uncertainty).

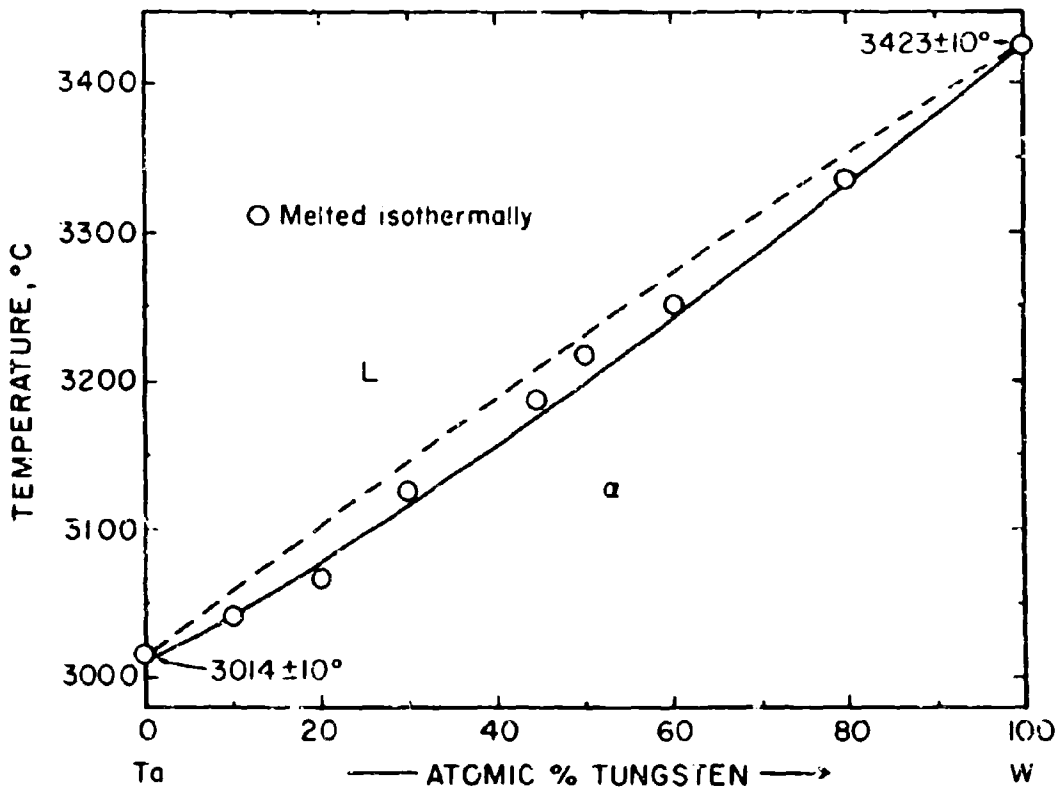

Figure III.A.33.2: Melting Temperatures of Ta-W Alloys.

(Temperature Error Figures Based on Reproducibility).

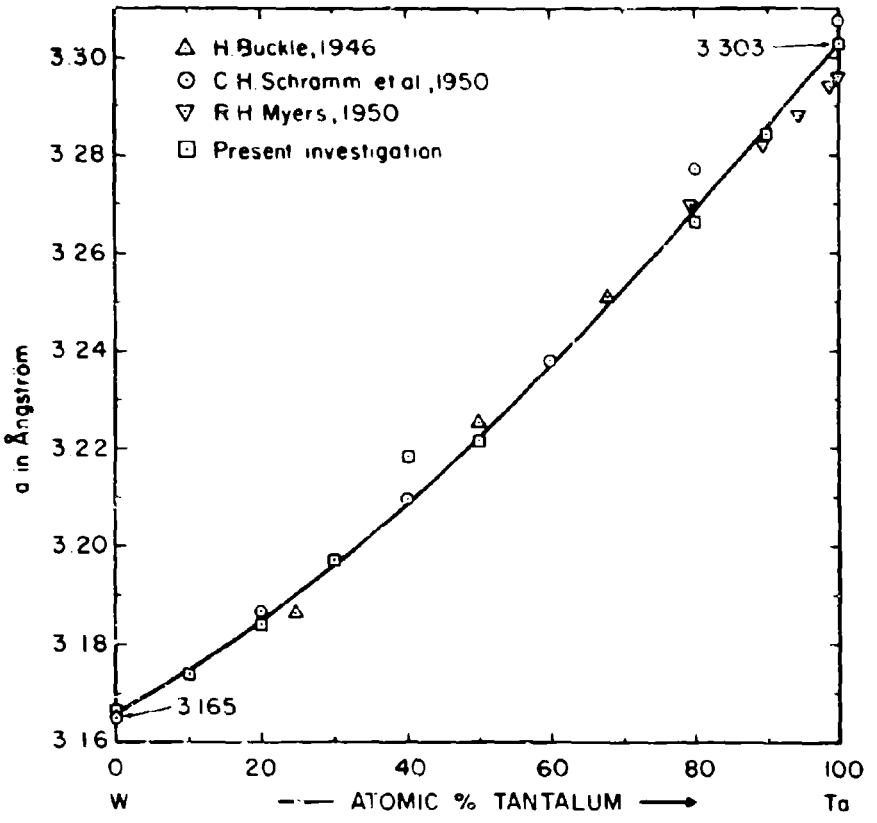

Figure III.A.33.3: Lattice Parameters of Ta-W Alloys.

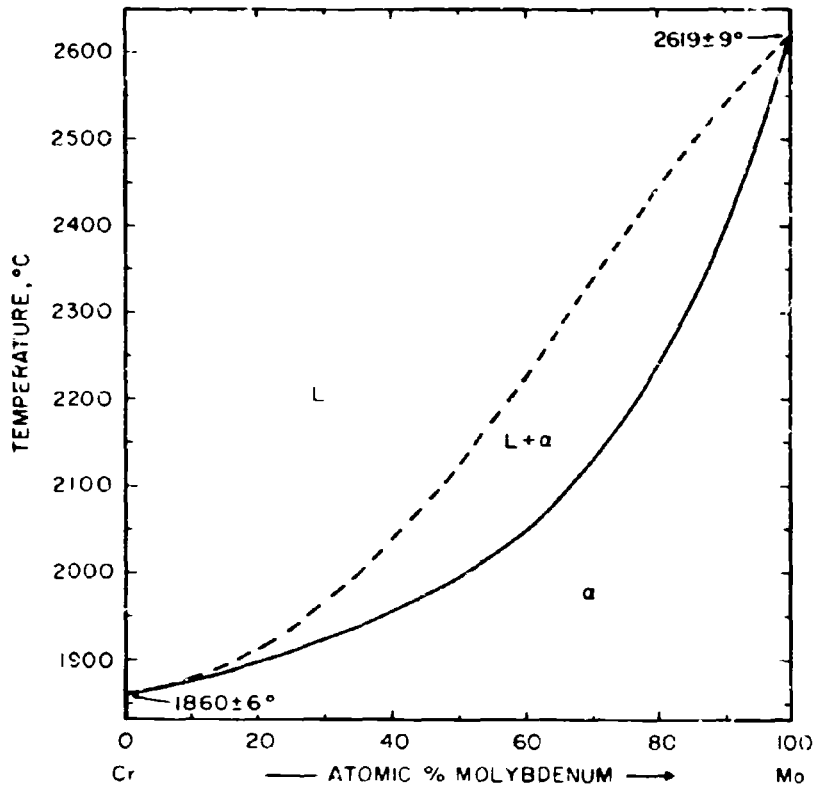

Figure III.A.34.1: Constitution Diagram of the Cr-Mo System.

(Temperature Error Figures Based on Estimated Overall Uncertainties).

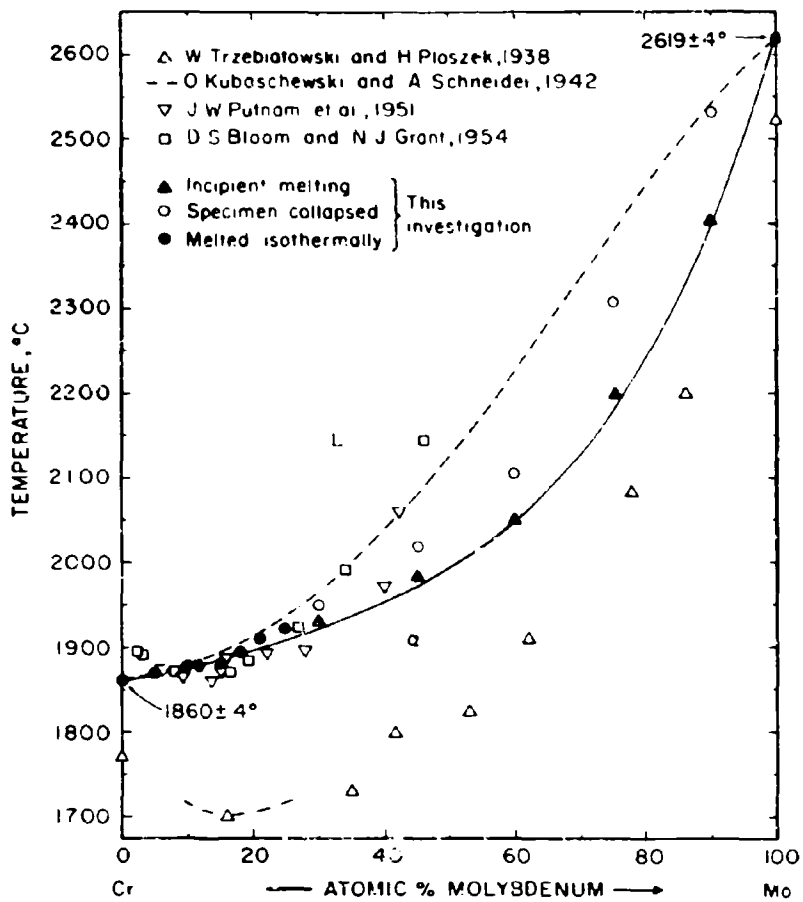

Figure III.A.34.2: Melting Temperatures of Mo-Cr Alloys.

(Temperature Error Figures Based on Reproducibility).

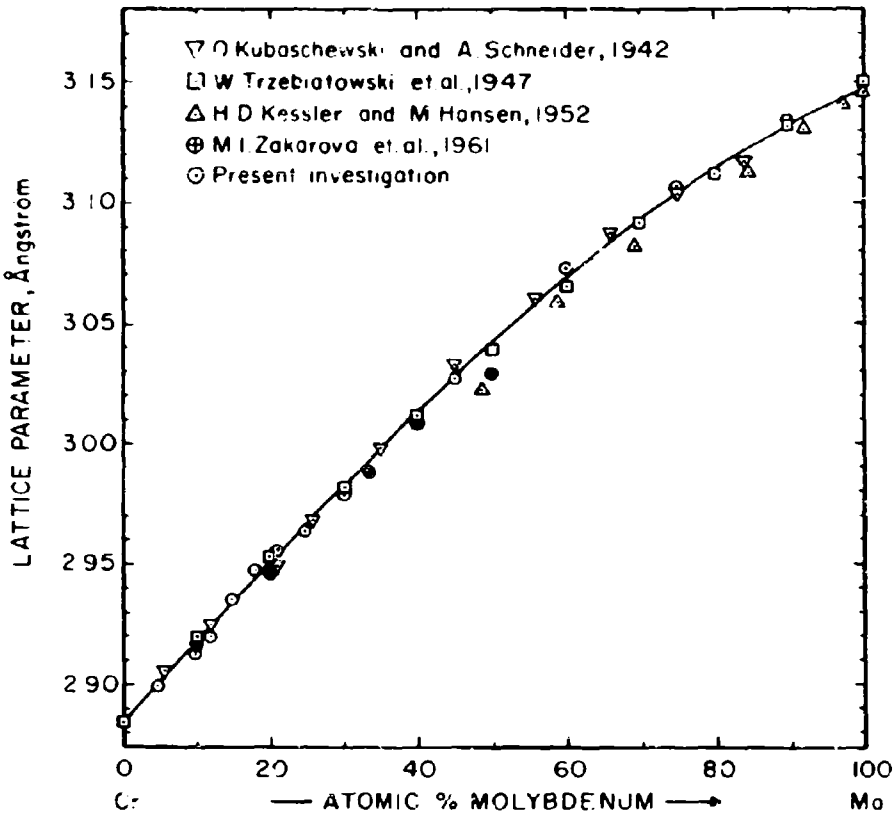

Figure III.A.34.3: Lattice Parameters of Cr-Mo Alloys.

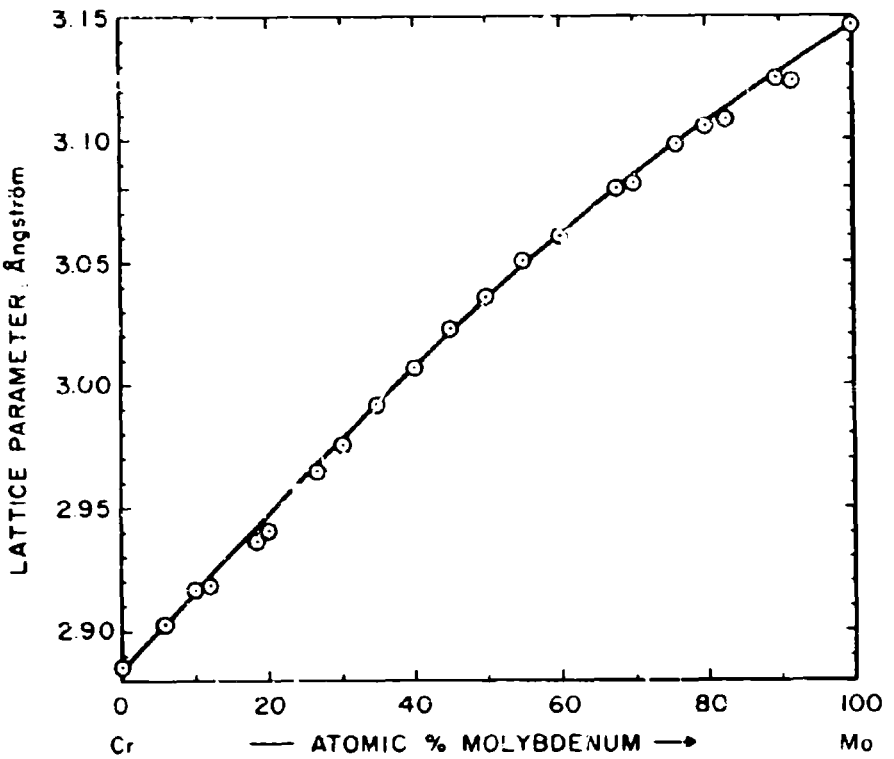

Figure III.A.34.4: Lattice Parameters of Cr-Mo Alloys.

(After S.R. Baen and P. Duwez, 1951).

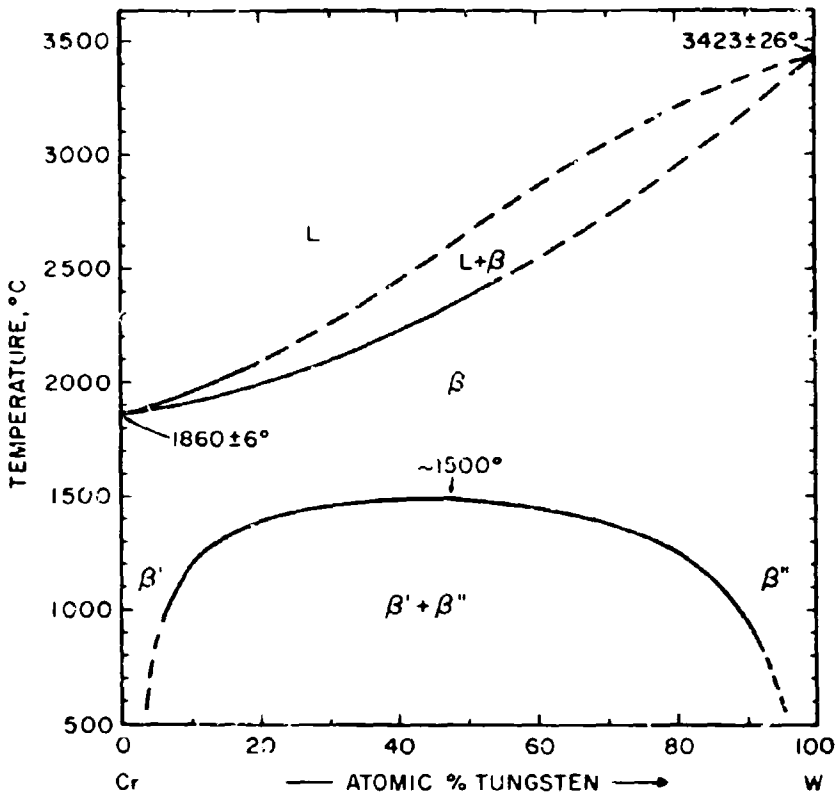

Figure III.A.35.1: Constitution Diagram Cr-W.

(Temperature Error Figures Based on Estimated Overall Uncertainty).

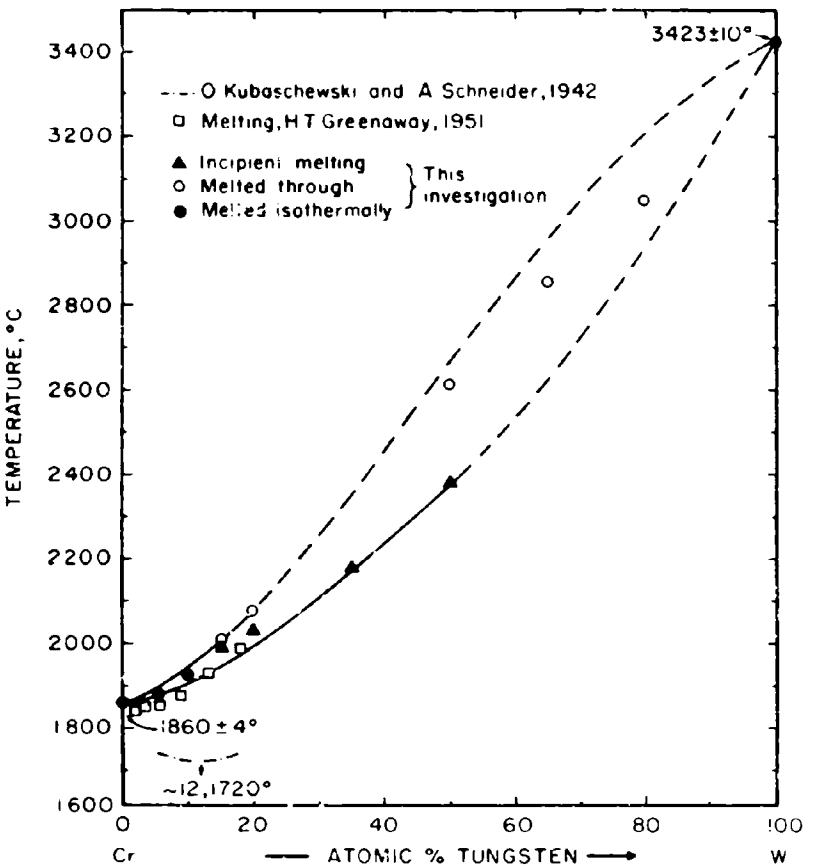

Figure III.A.35.2: Melting Temperatures of Cr-W Alloys.

(Temperature Error Figures Based on Reproducibility).

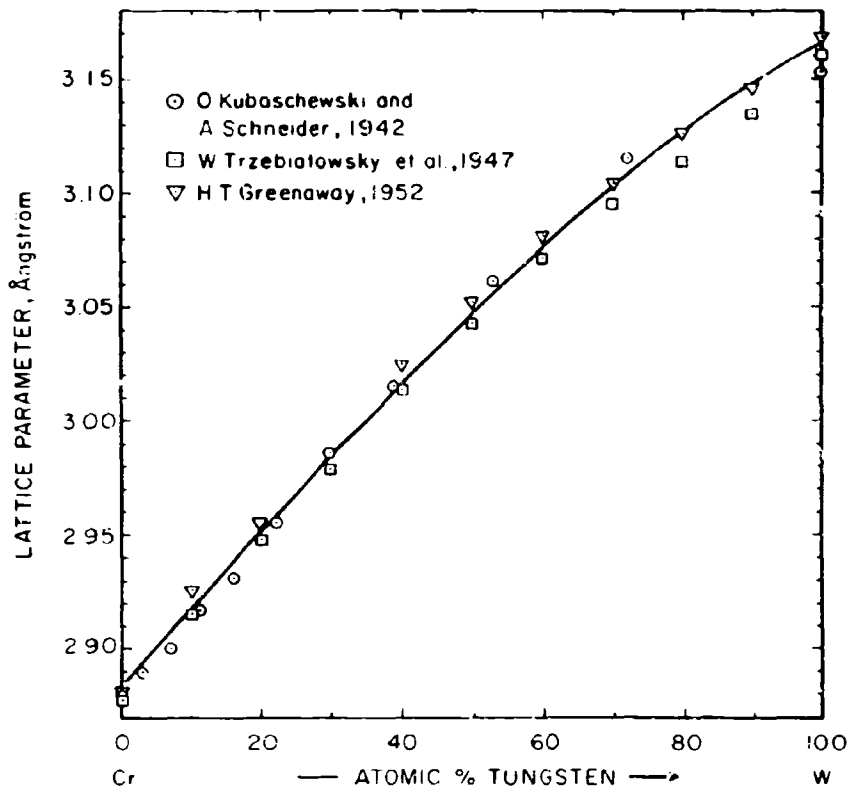

Figure III.A.35.3: Lattice Parameters of Cr-W Alloys.

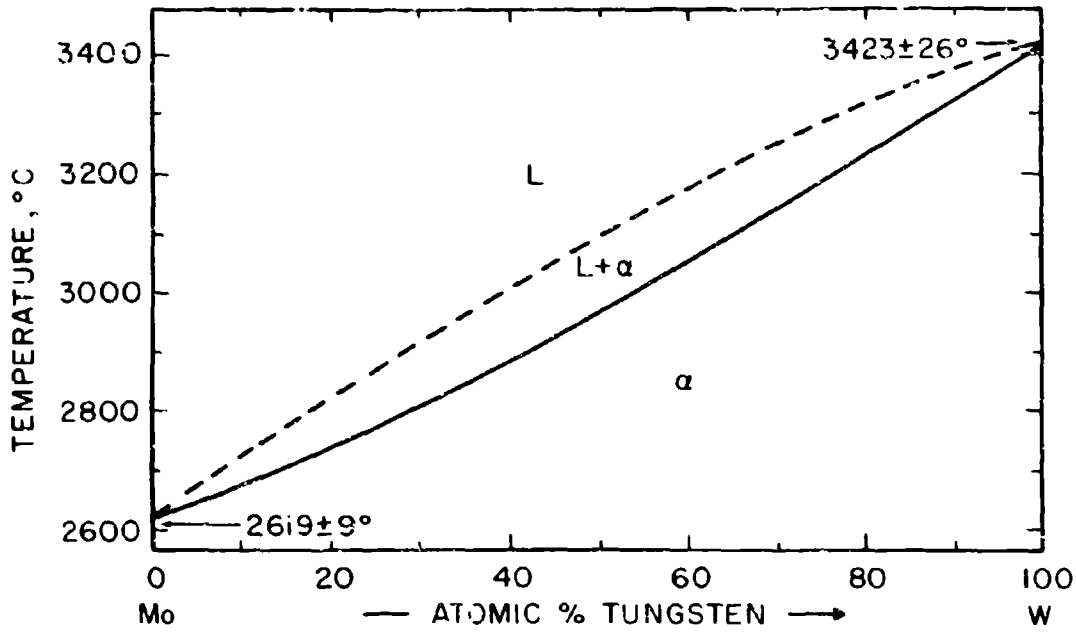

Figure III.A.36.1: Constitution Diagram of the System Mo-W.

(Temperature Error Figures Based on Estimated Overall Uncertainty).

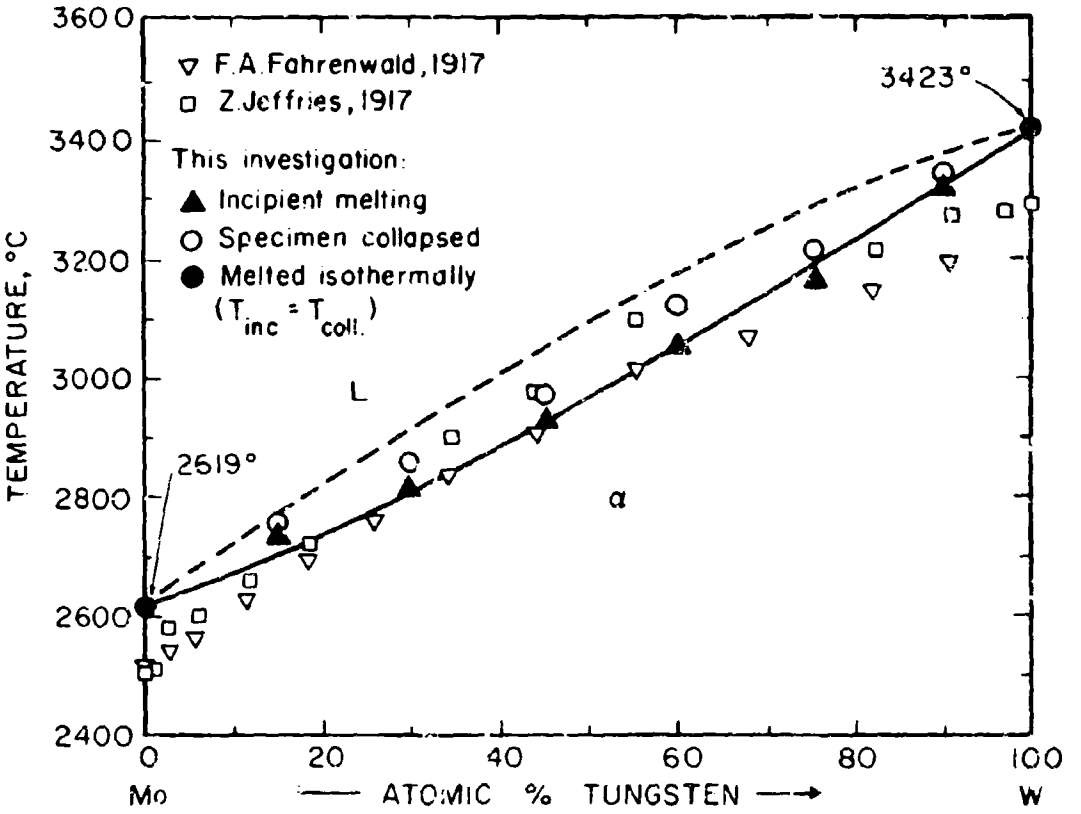

Figure III.A.36.2: Melting Temperatures of Mo-W Alloys.

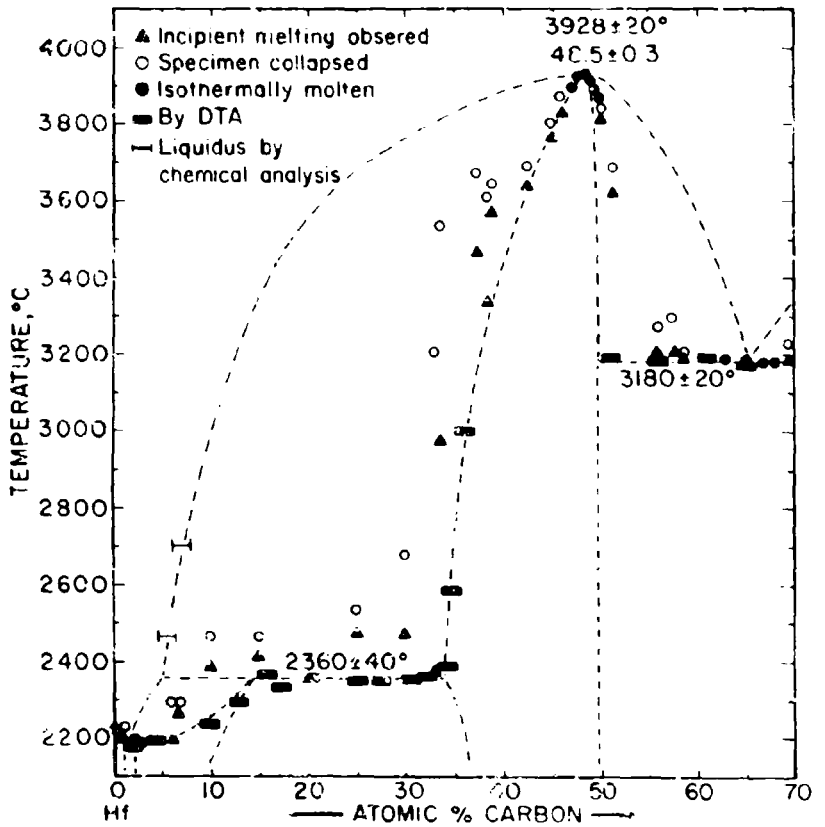

Figure III.B.3.2: Melting Temperatures of Hf-C Alloys.

(Temperature Error Figures Based on Reproducibility).

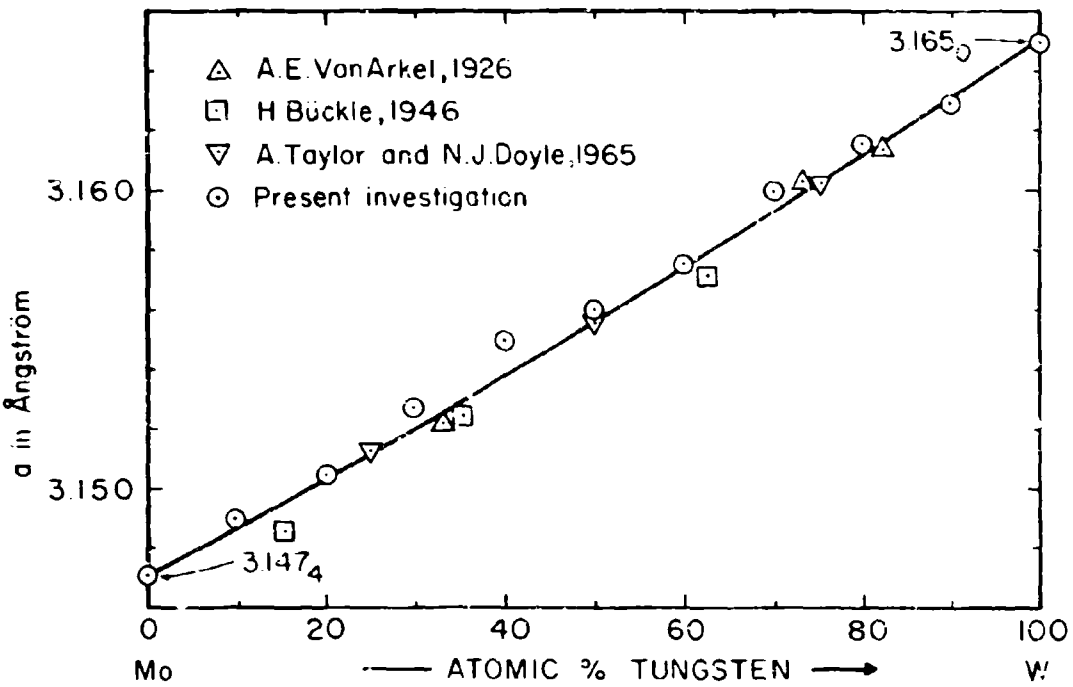

Figure III.A.36.3: Lattice Parameters of Mo-W Alloys.

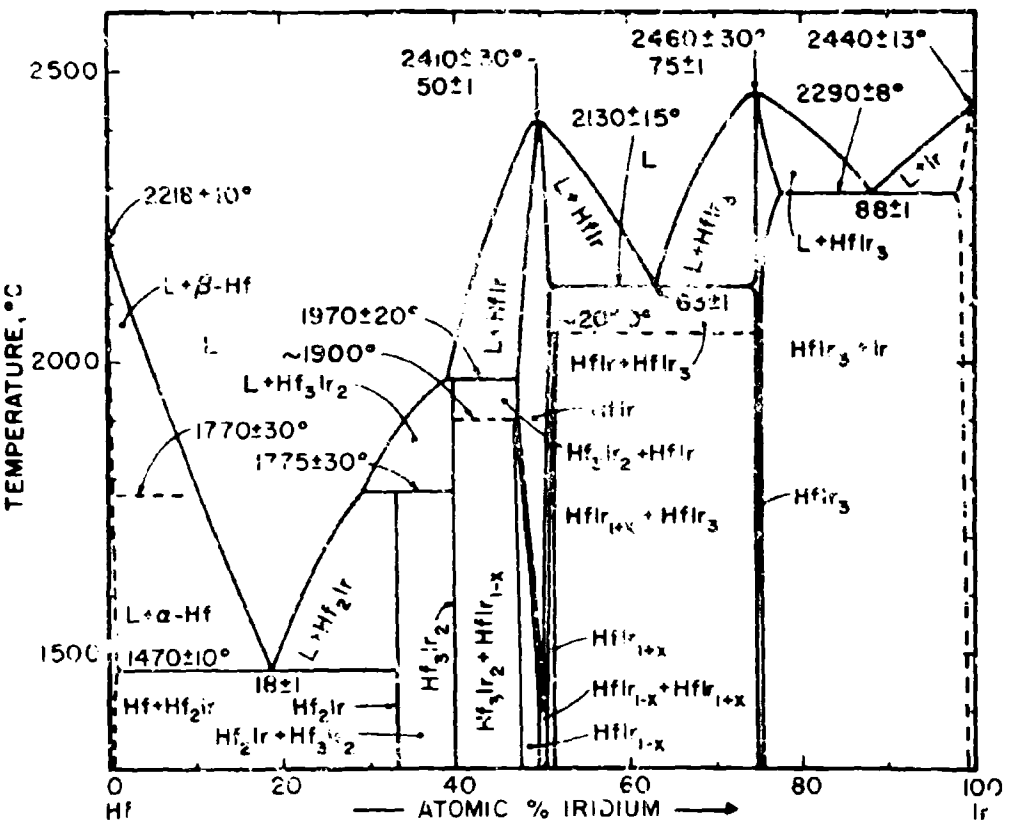

Figure IV.....7.1: Constitution Diagram of the Hf-Ir System.

(Temperature Error Figures Based on Reproducibility).

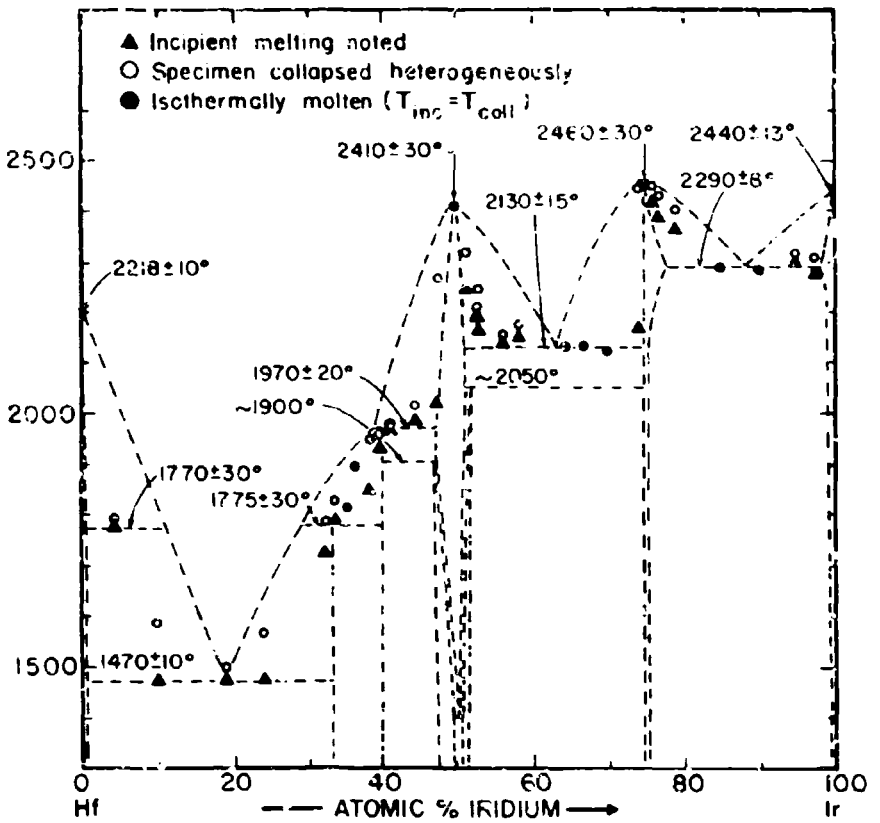

Figure III.A.37.2: Melting Temperatures of Hf-Ir Alloys.

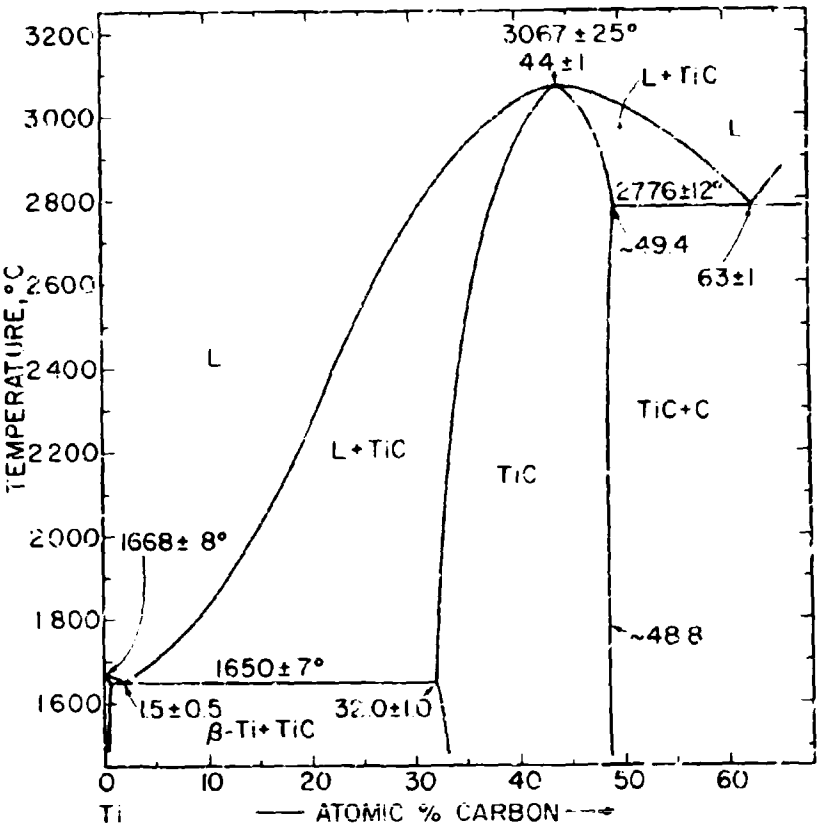

Figure III.B.1.1: Constitution Diagram of the System Ti-C.

(Temperature Error Figures Based on Estimated Overall Uncertainty)

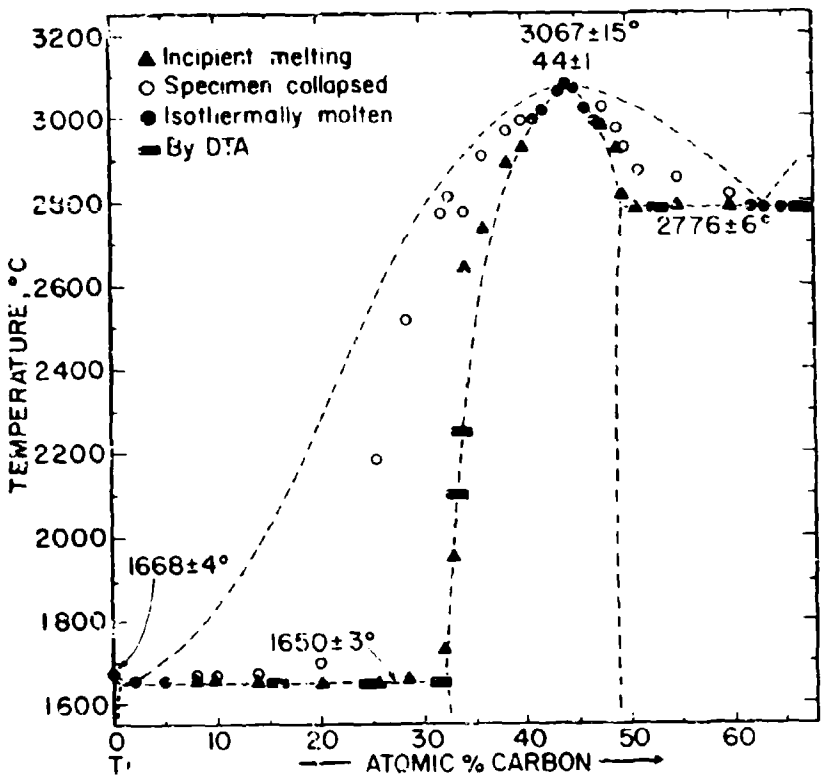

Figure III.B.1.2: Melting Temperatures of Ti-C Alloys

(Temperature Error Figures Based on Estimated Overall Uncertainty).

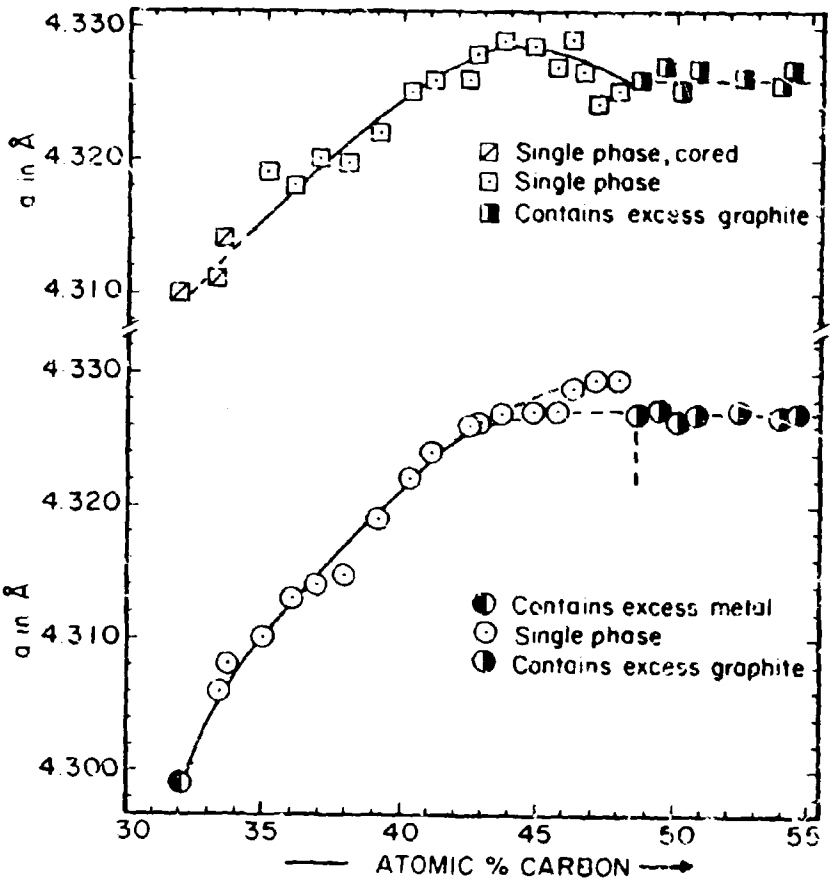

Figure III.B.1.3: Lattice Parameters of Titanium Monocarbide.

⊡ – Quenched from Slightly Above Solidus Temperatures.

⊙ – Melted Samples Reannealed for 40 hrs at 1350°C.

Maximum Concentration Uncertainty: ± 0.4 At.% C.

Maximum Uncertainty in Lattice Parameters: ± 0.0008 Å

Combined Content of Oxygen + Nitrogen: < 150 ppm

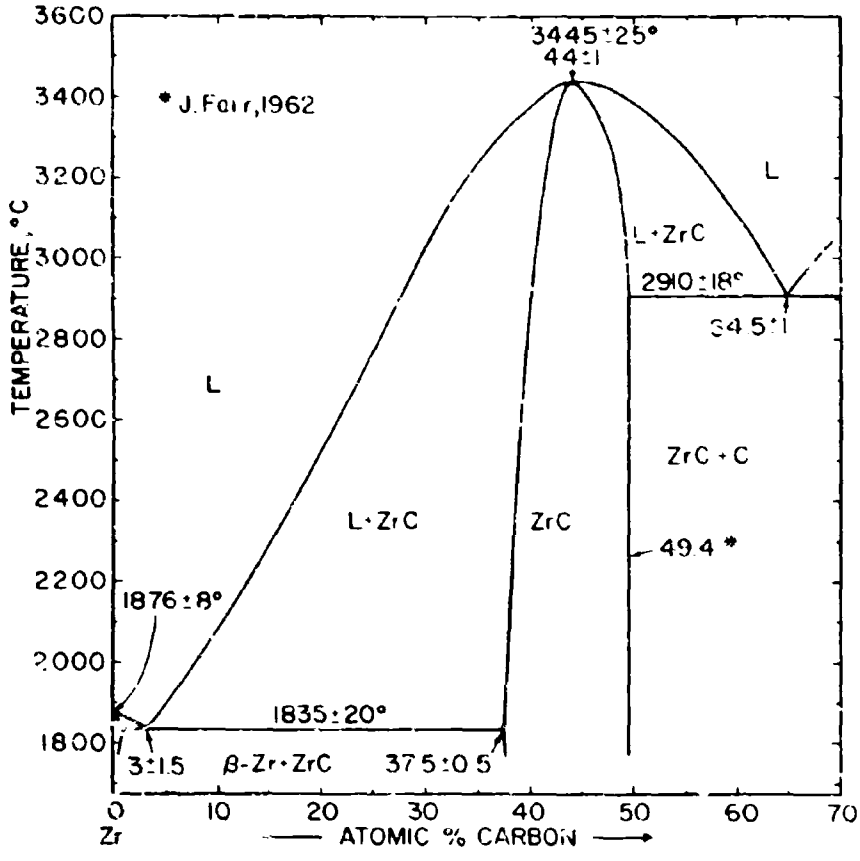

Figure III.B.2.1: Constitution Diagram of the Zr-C System.

(Temperature Error Figures Based on Estimated Overall Uncertainty).

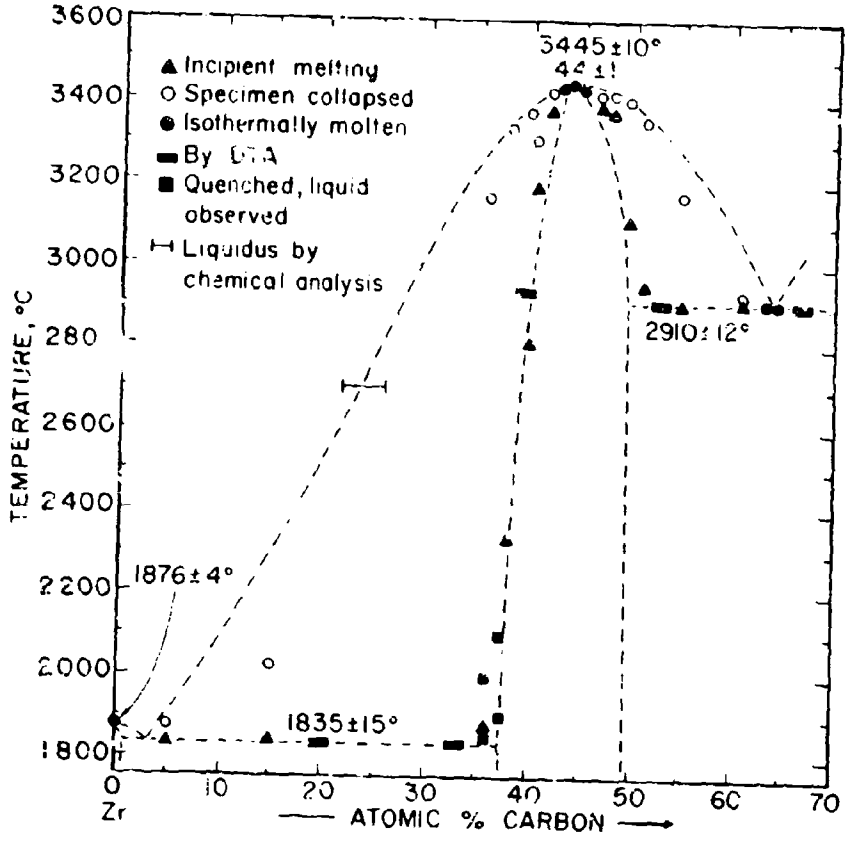

Figure III.B.2.2. Melting Temperatures of Zr-C Alloys.

(Temperature Error Figures Based on Reproducibility).

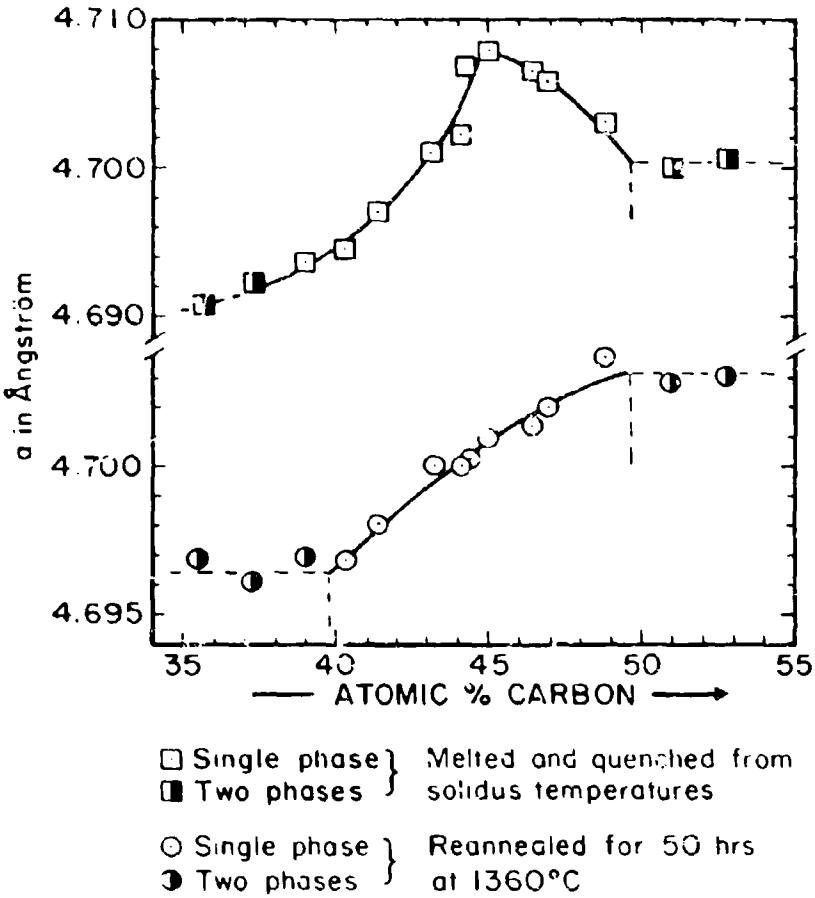

Figure III.B.2.3: Lattice Parameters of the Zirconium Monocarbide Phase.

Concentration Uncertainty: ± 0.2 At.% C.

Lattice Parameters: ± 0.0003 Å

Oxygen + Nitrogen: < 150 ppm

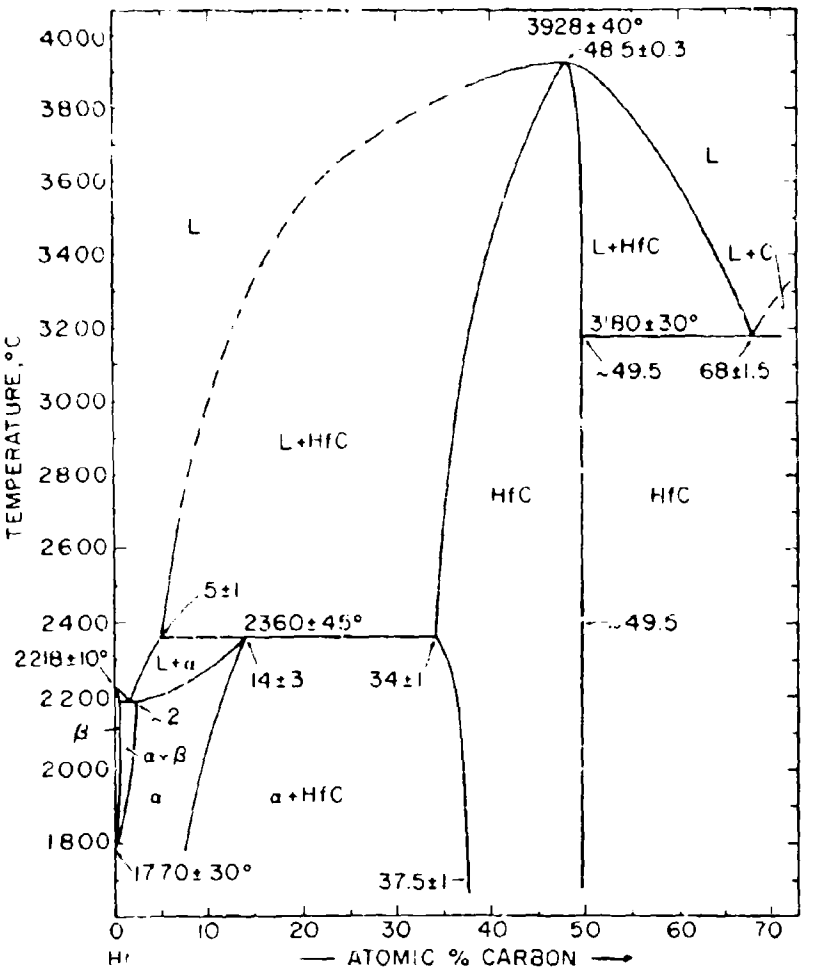

Figure III.B.3.1: Constitution Diagram of the System Hf-C.

(Temperature Error Figures Based on Estimated Overall Uncertainty).

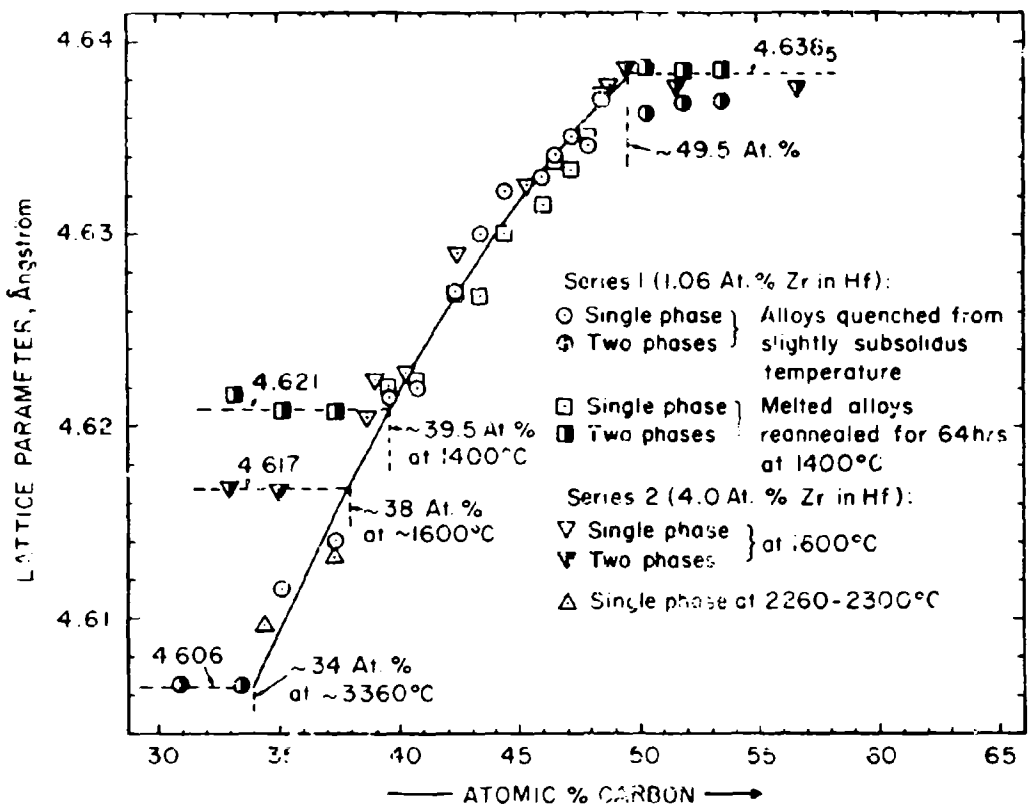

Figure III.B.3.3: Lattice Parameters of the Hafnium Monocarbide Phase.

(All Parameters Extrapolated to Zero Zirconium Content).

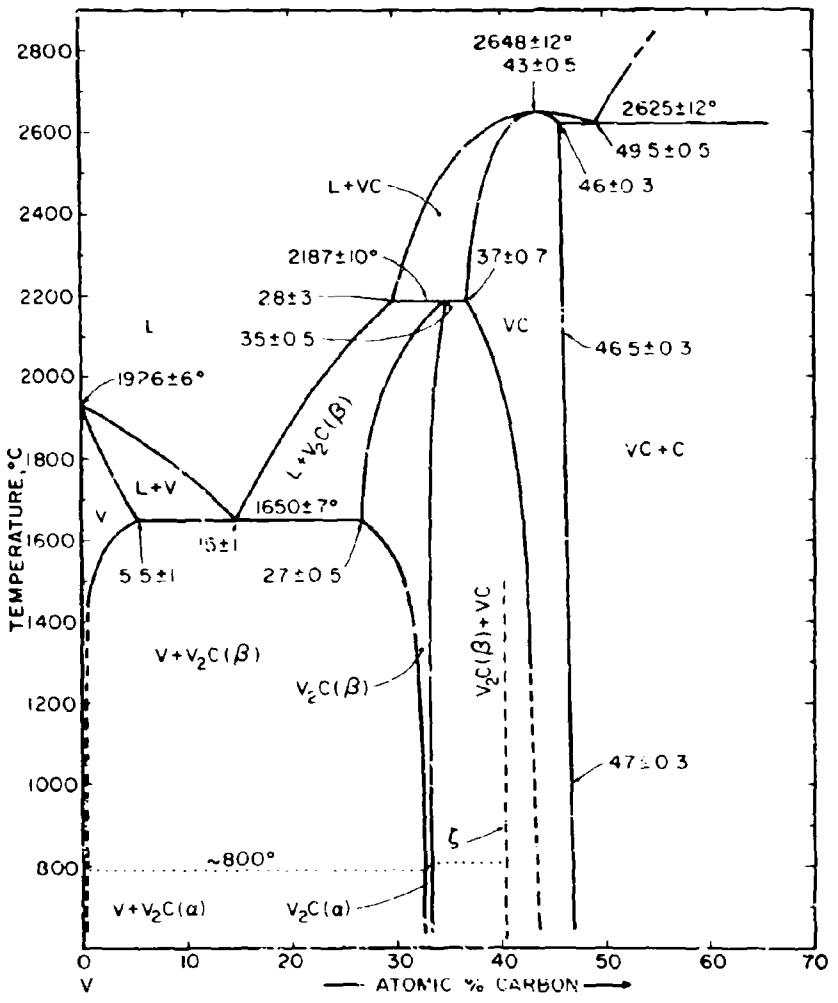

Figure III.B.4.1: Constitution Diagram of the System V-C.

(Temperature Error Figures Based on Estimated Overall Uncertainty).

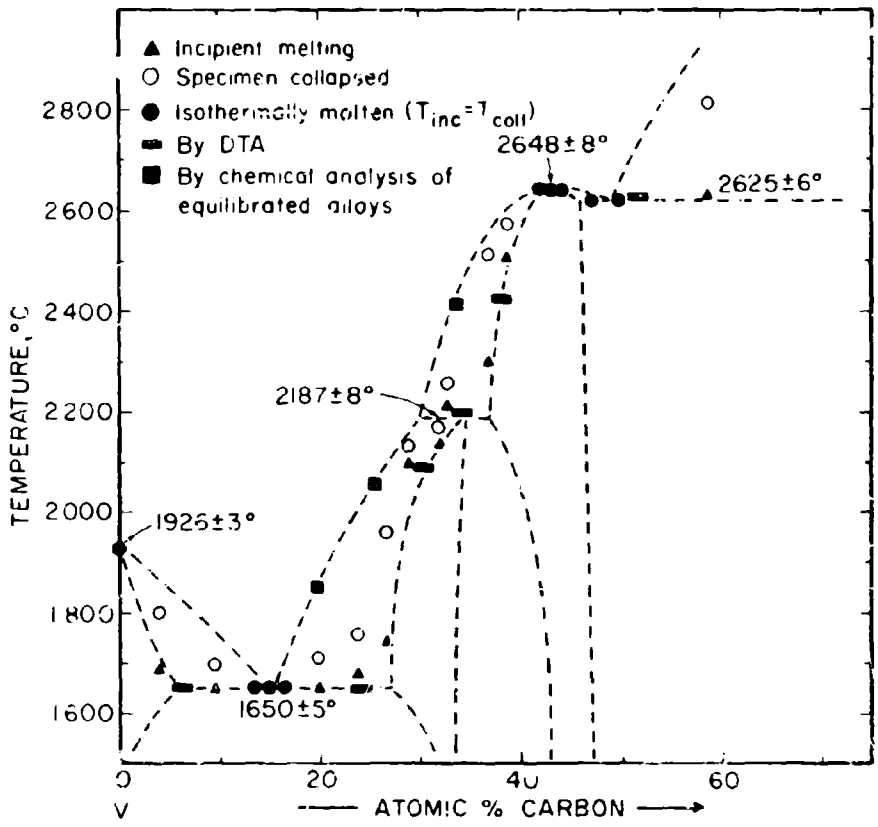

Figure III.B.4.2: Melting Temperatures of V-C Alloys.

(Temperature Error Figures Based on Reproducibility).

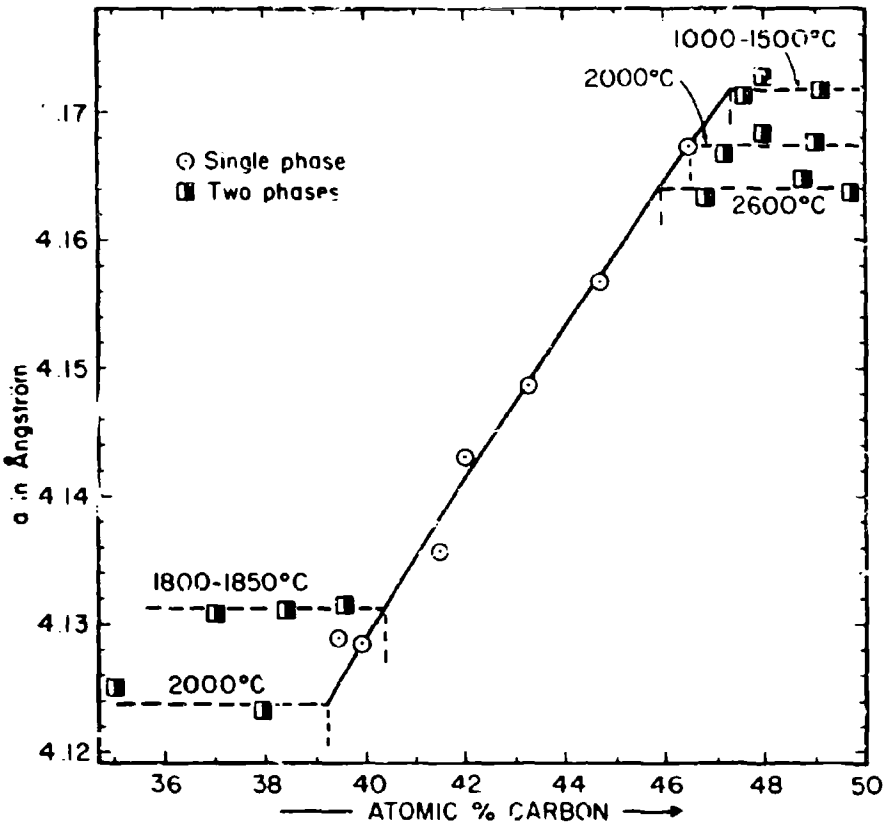

Figure III.B.4.3: Lattice Parameters of the Vanadium Monocarbide Phase.

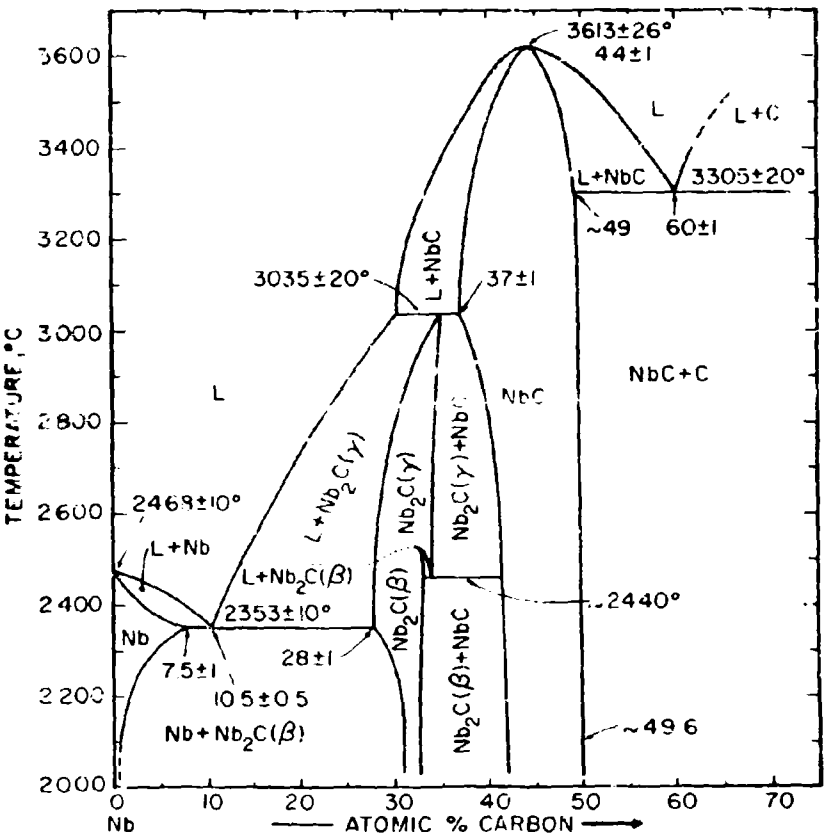

Figure III.B.5.1: Constitution Diagram of the System Nb-C.

(Additional Transformation of Nb_2C at 1230°C not Shown. Temperature Error Figures Based on Estimated Overall Uncertainty).

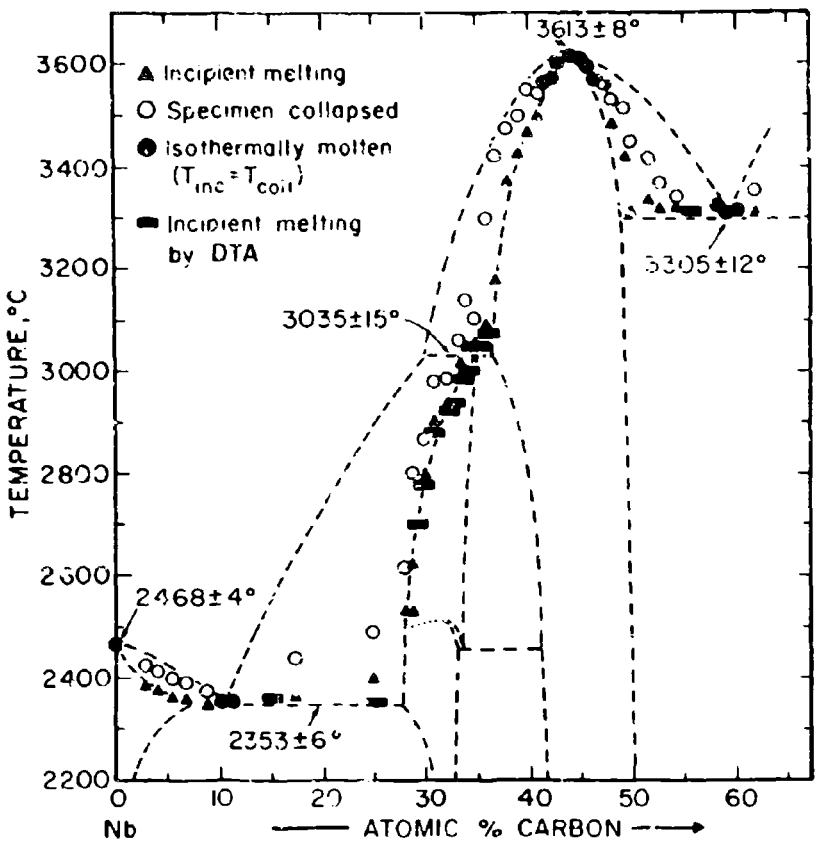

Figure III.B.5.2: Melting Temperatures of Nb-C Alloys.

(Temperature Error Figures Based on Reproducibility).

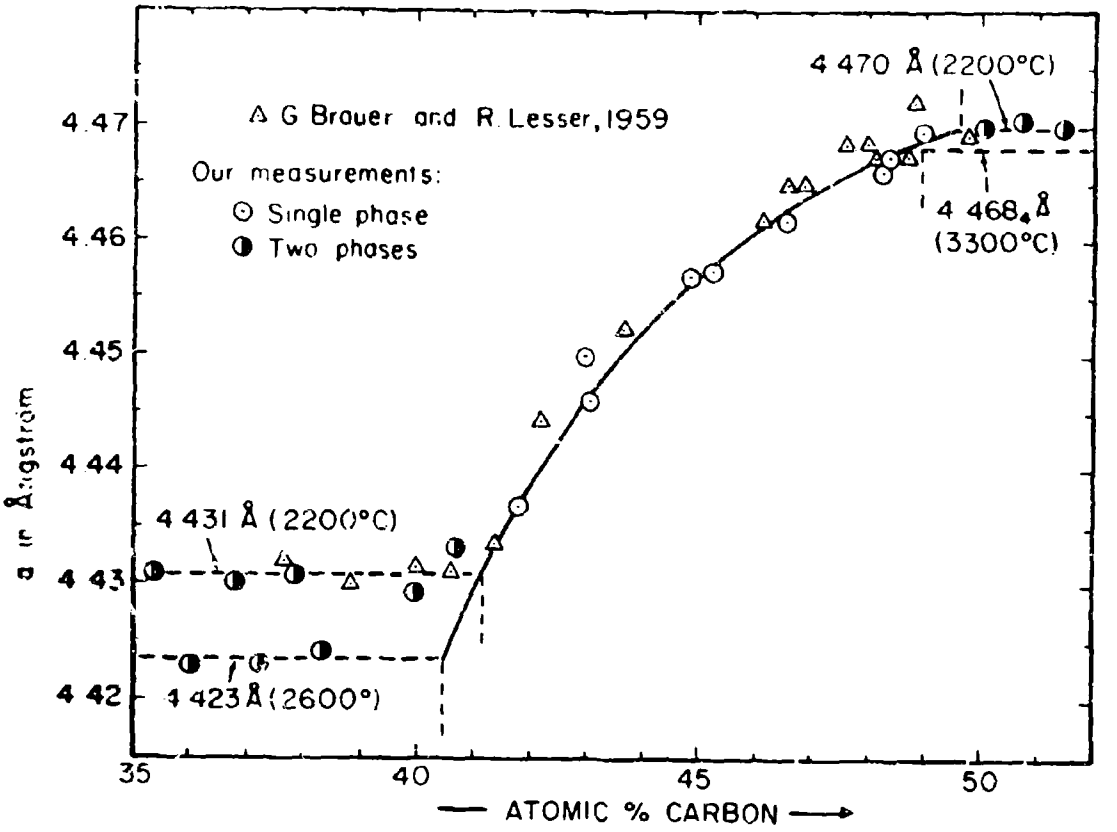

Figure III.B.5.3: Lattice Parameters of the Niobium Monocarbide Phase.

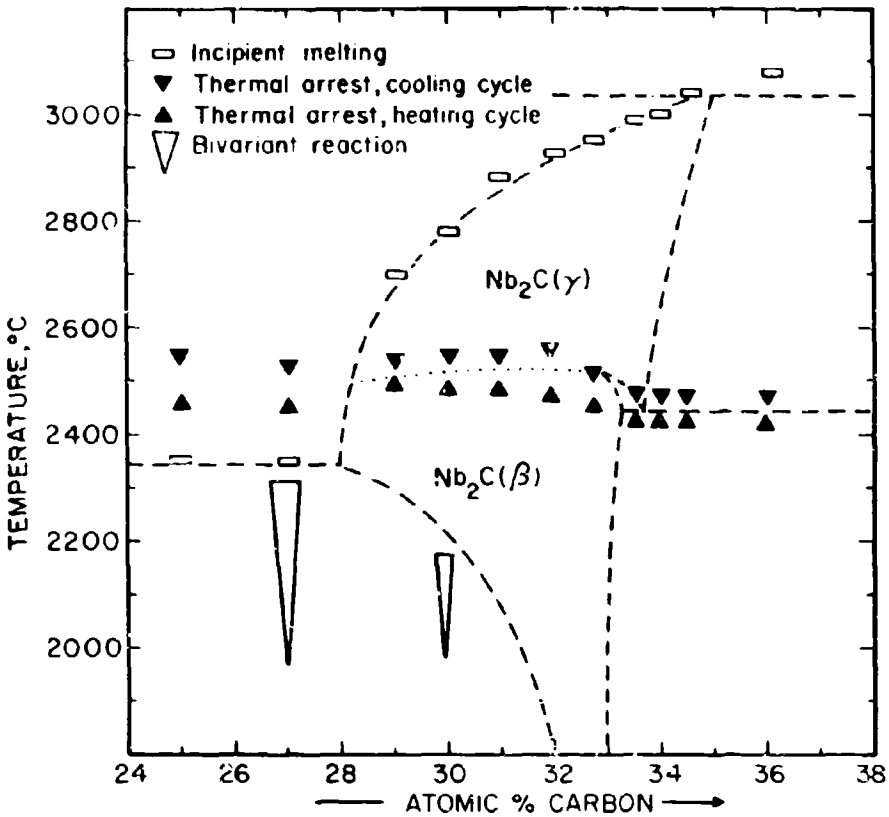

Figure III.B.5.4: High Ternperature Transformation and Incipient Melting in Nb_2C.

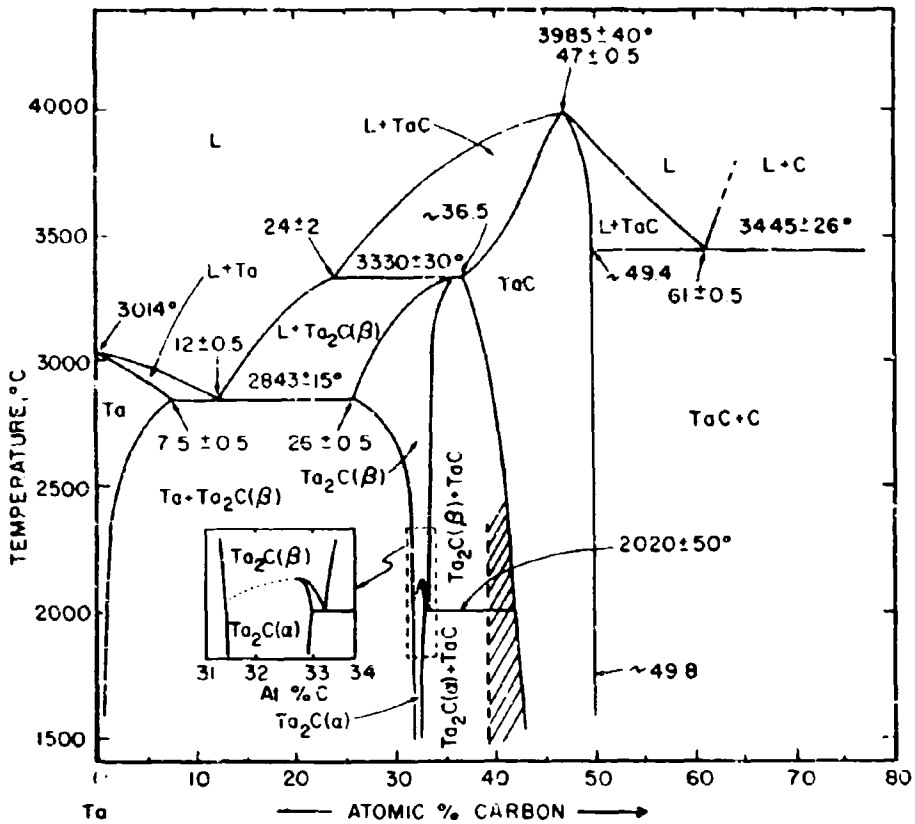

Figure III.B.6.1: Constitution Diagram of the System Ta-C.

(Temperature Error Figures Based on Estimated Overall Uncertainties).

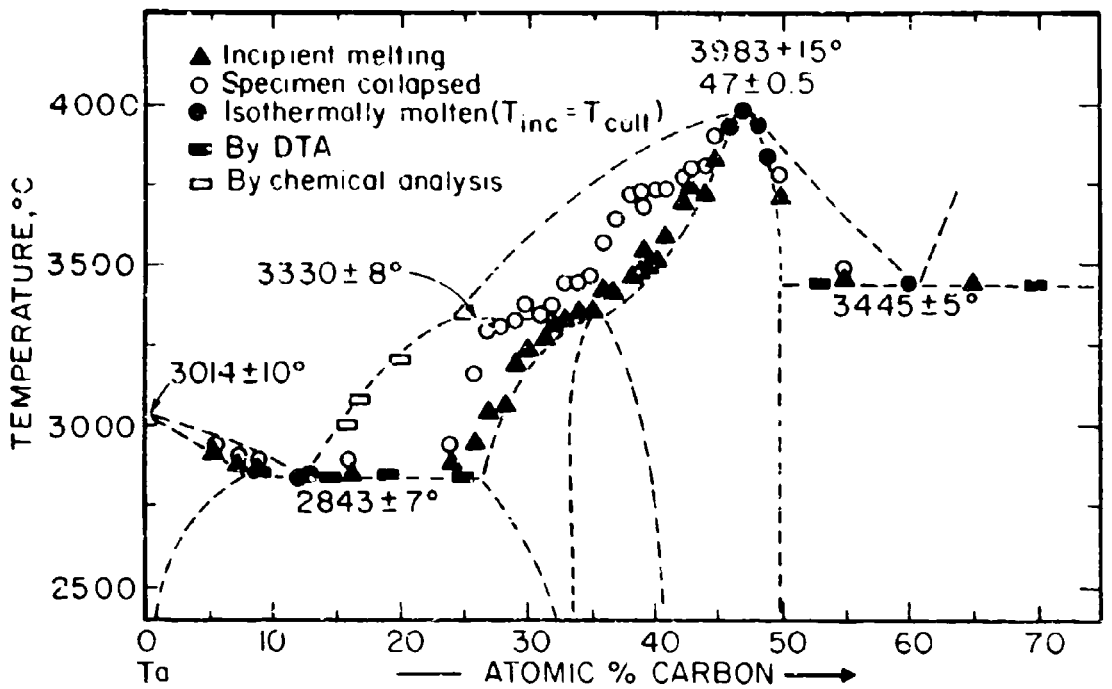

Figure III.B.6.2: Melting Temperatures of Ta-C Alloys.

(Temperature Error Figures Based on Reproducibility).

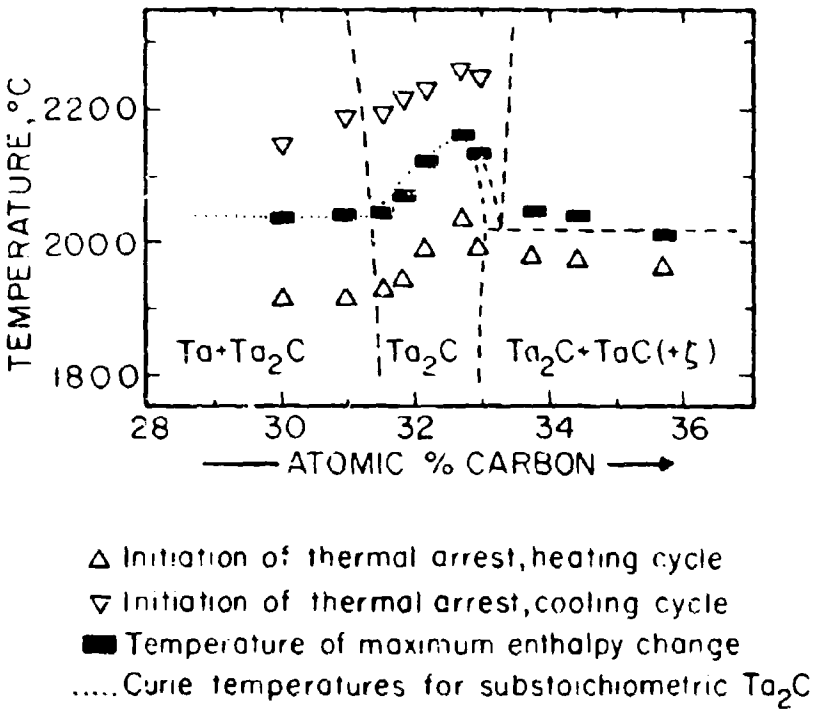

Figure III.B.6.3: Order-Disorder Transformation Temperatures in Ta_2C as Determined by Differential Thermal Analysis.

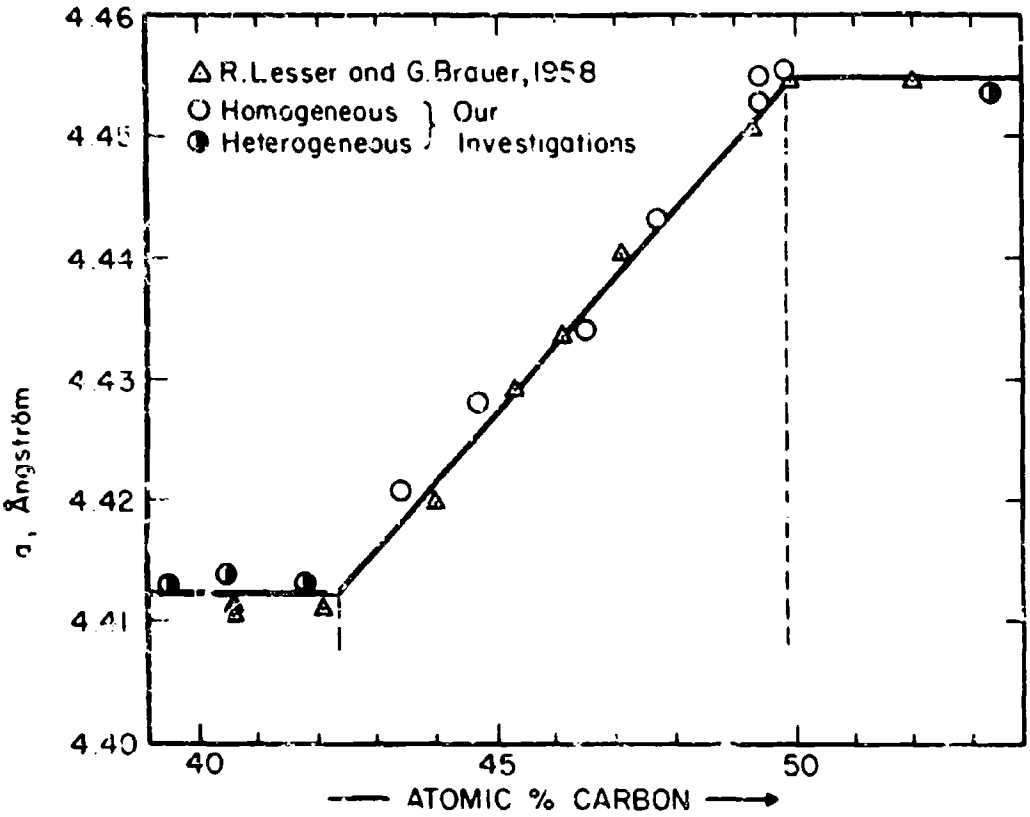

Figure III.B.6.4: Lattice Parameters of Tantalum-Monocarbide.

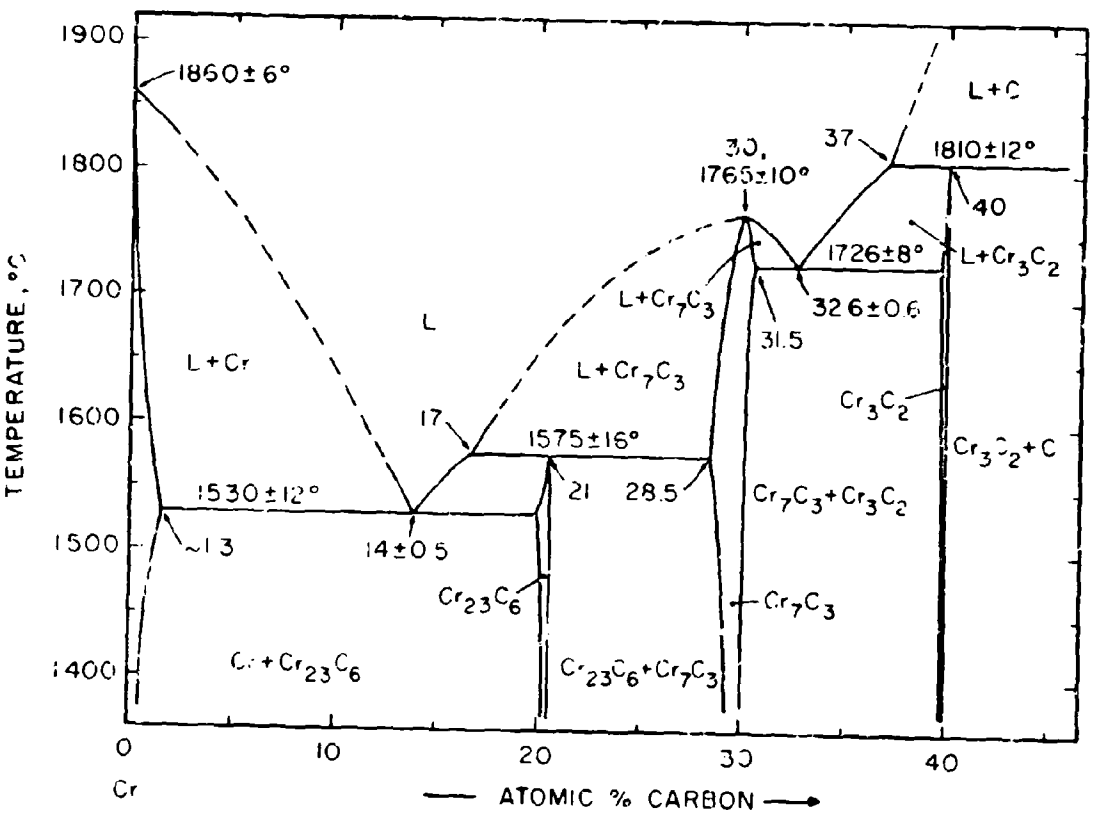

Figure III.B.7 1: Constitution Diagram of the Chromium-Carbon System.

(Temperature Error Figures Based on Estimated Overall Uncertainty).

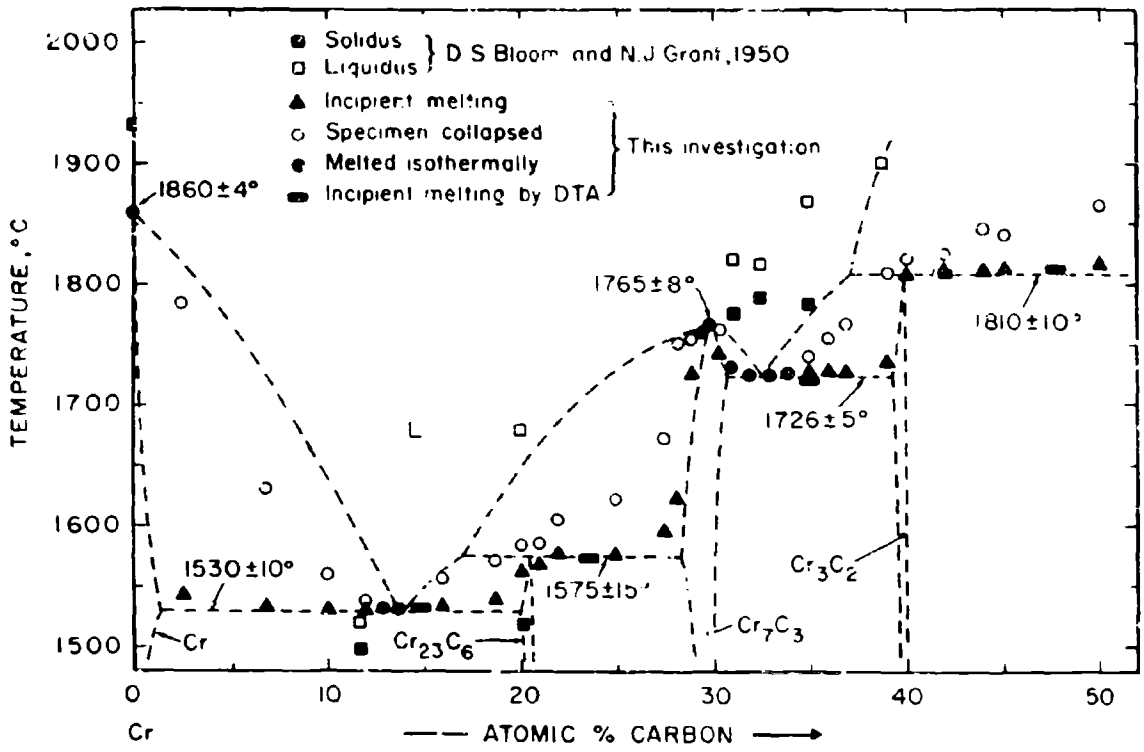

Figure III.B.7.2: Melting Temperatures of Chromium-Carbon Alloys.

(Temperature Error Figures Based on Reproducibility)

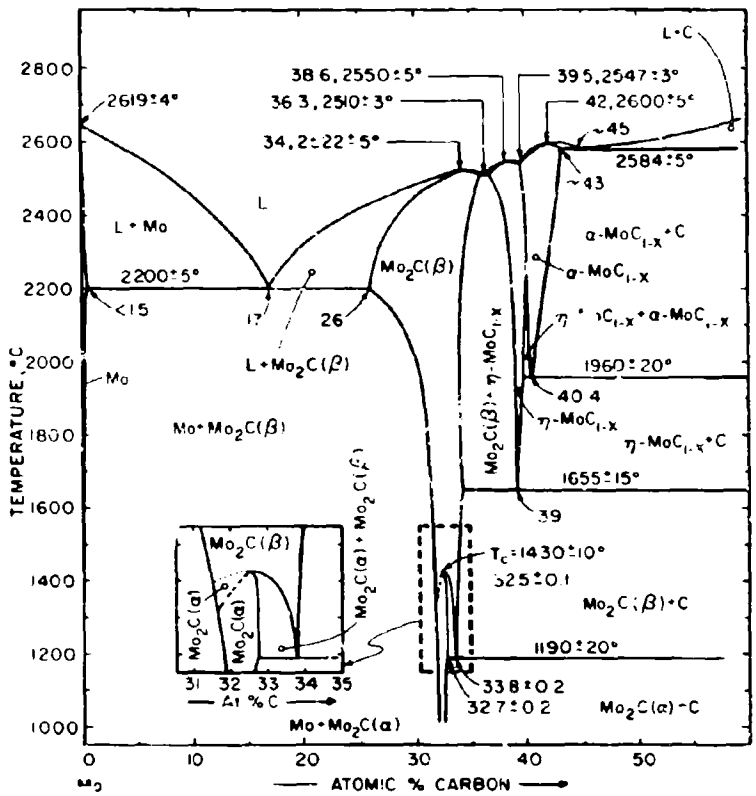

Figure III.B.8.1: Constitution Diagram of the Mo-C System.

(Quoted Temperature Error Figures Based on Reproducibility).

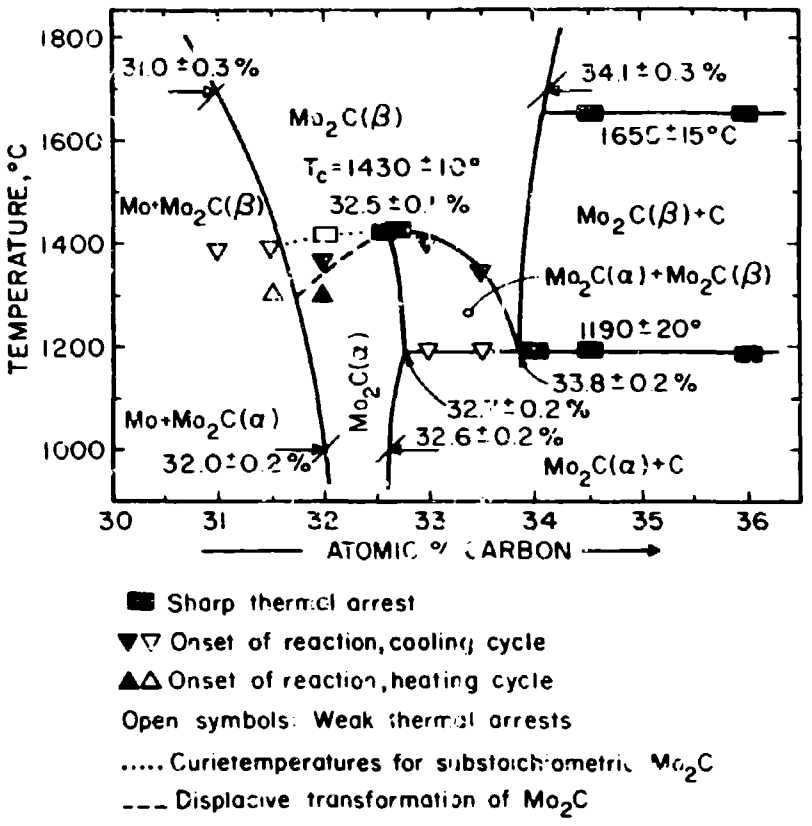

Figure III.B.8.2: Summary of DTA-Results Concerning the α-β-Transition in Mo_2C.

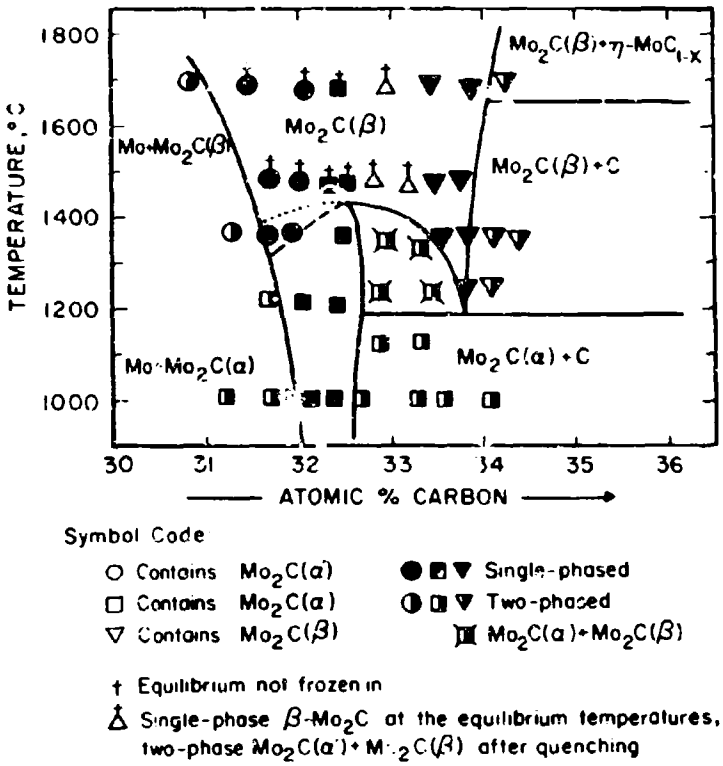

Figure III.B.8.3: Order-Disorder Transformation in Mo_2C: Summary of X-ray and Metallographic Results.

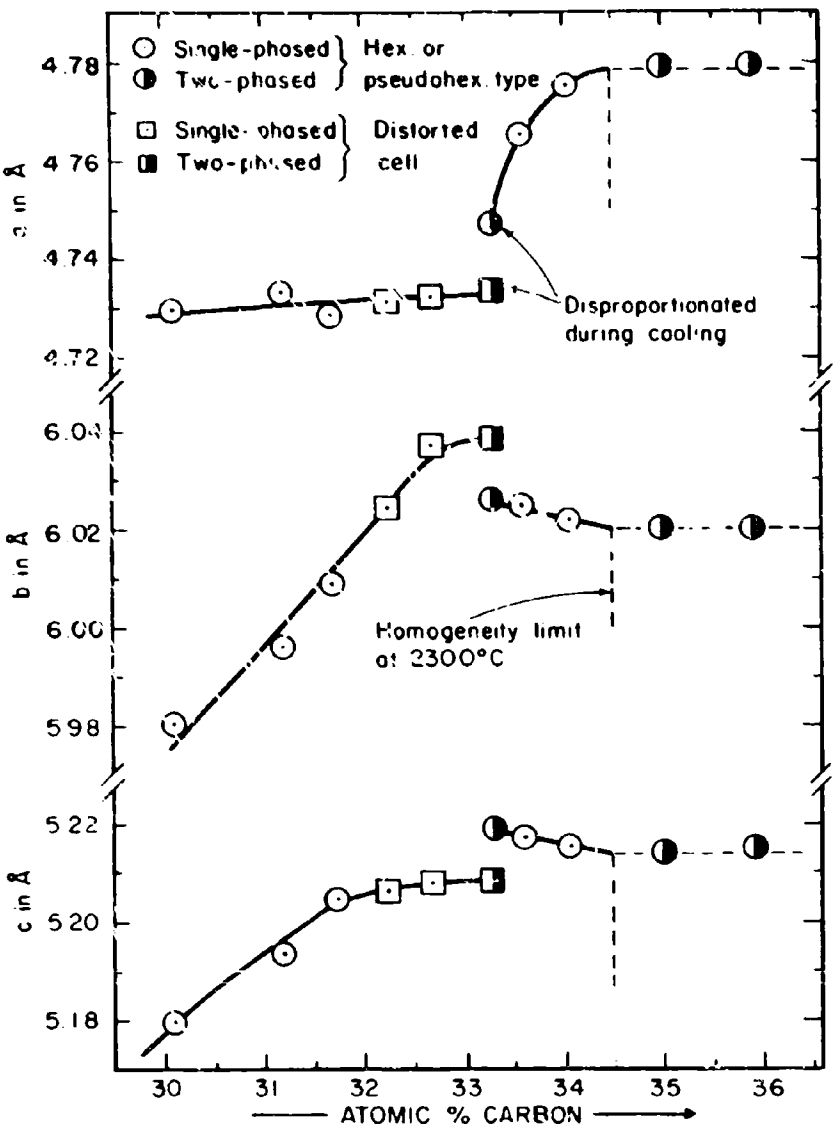

Figure III.B.8.4: Lattice Parameters of Mo_2C Cooled at Approximately 100°C per Second from 2300°C.

(Orthorhombic Axes)

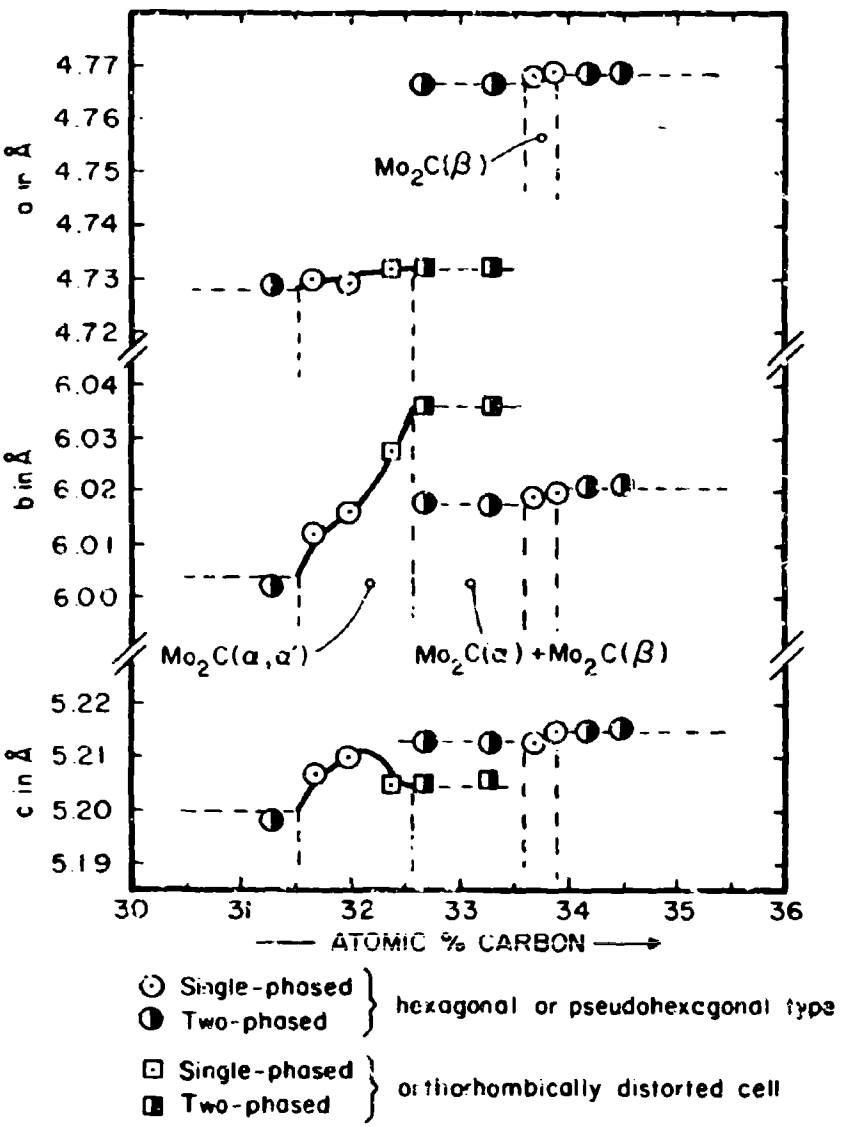

Figure III.B.8.5: Lattice Parameters of Mo_2C. Alloys Quenched After Equilibration at 1350°C.

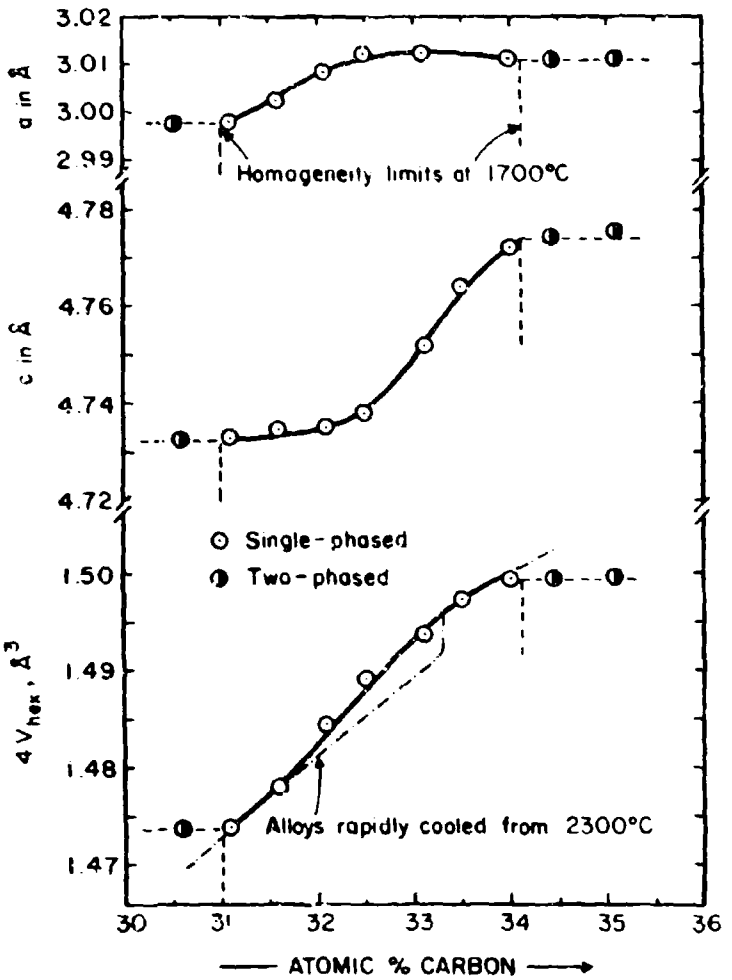

Figure III.B.8.6: Lattice Parameters and Unit Cell Volume of Mo_2C in Tin-Quenched (1700°C) Alloys.

Indexing According to L'3-Type.

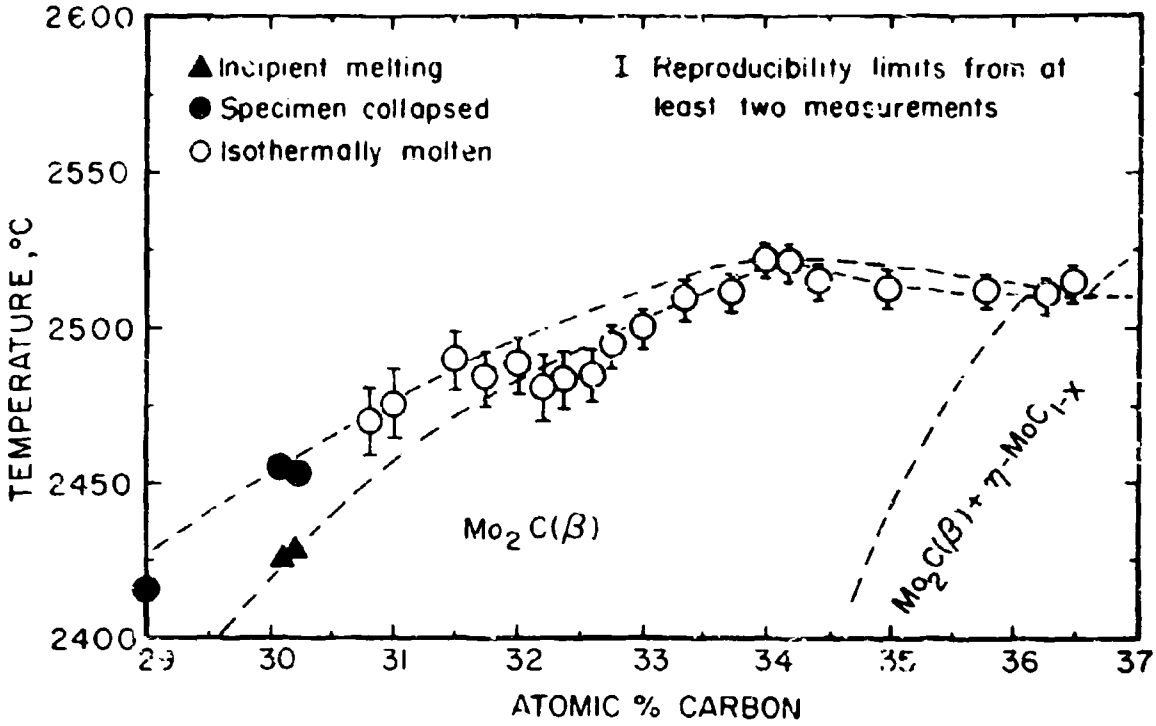

Figure III.B.8.7: Melting Temperatures of the Mo_2C-Phase.

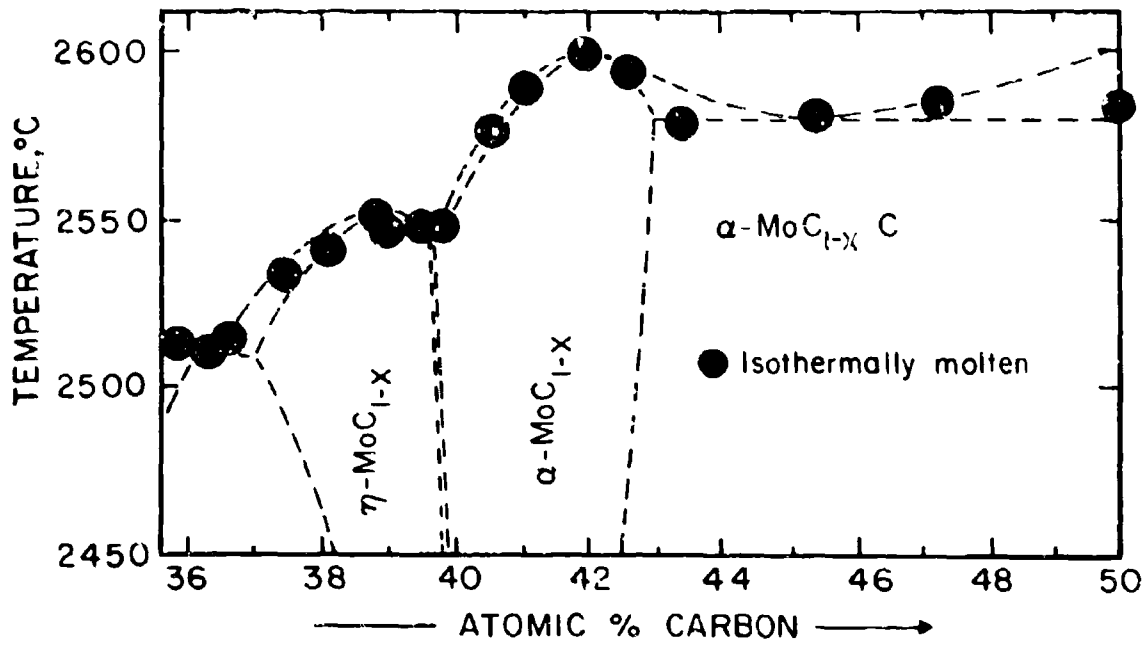

Figure III.B.8.8: Melting in Carbon-Rich Mo-C Alloys.

Reproducibility Limits of Experimental Points: ± 5°C; ± 0.3 At.% C.

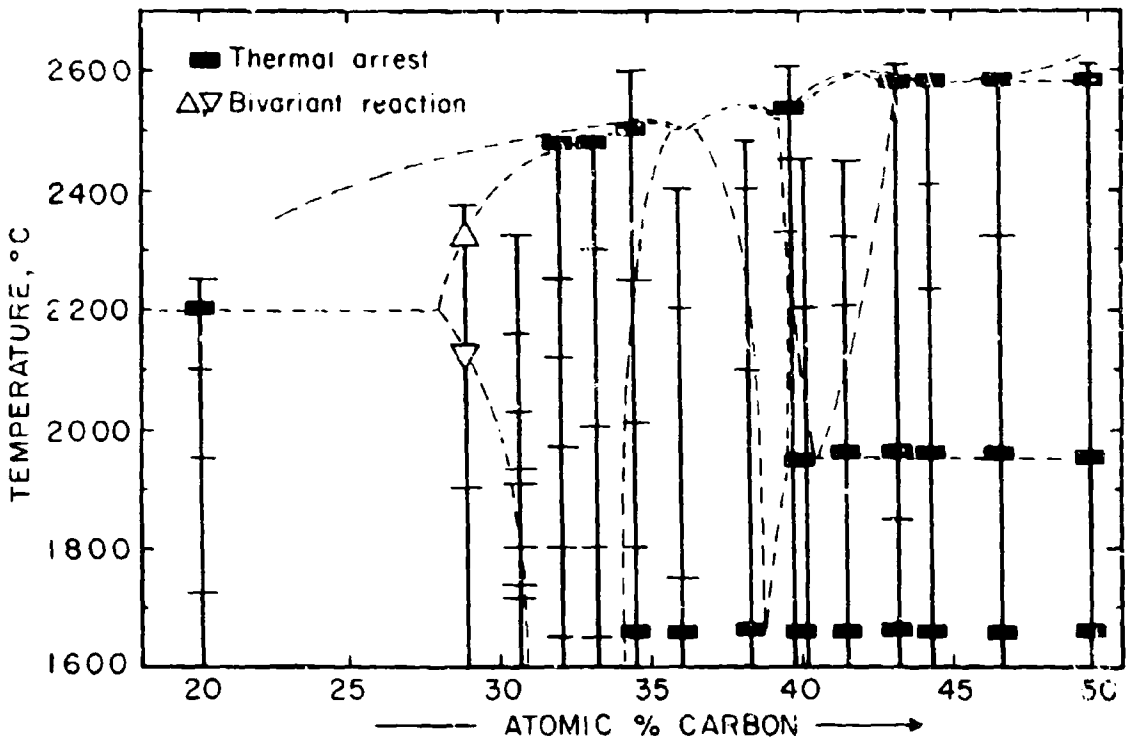

Figure III.B.8.9: Summary of Differential-Thermoanalytical Studies in the Mo-C System.

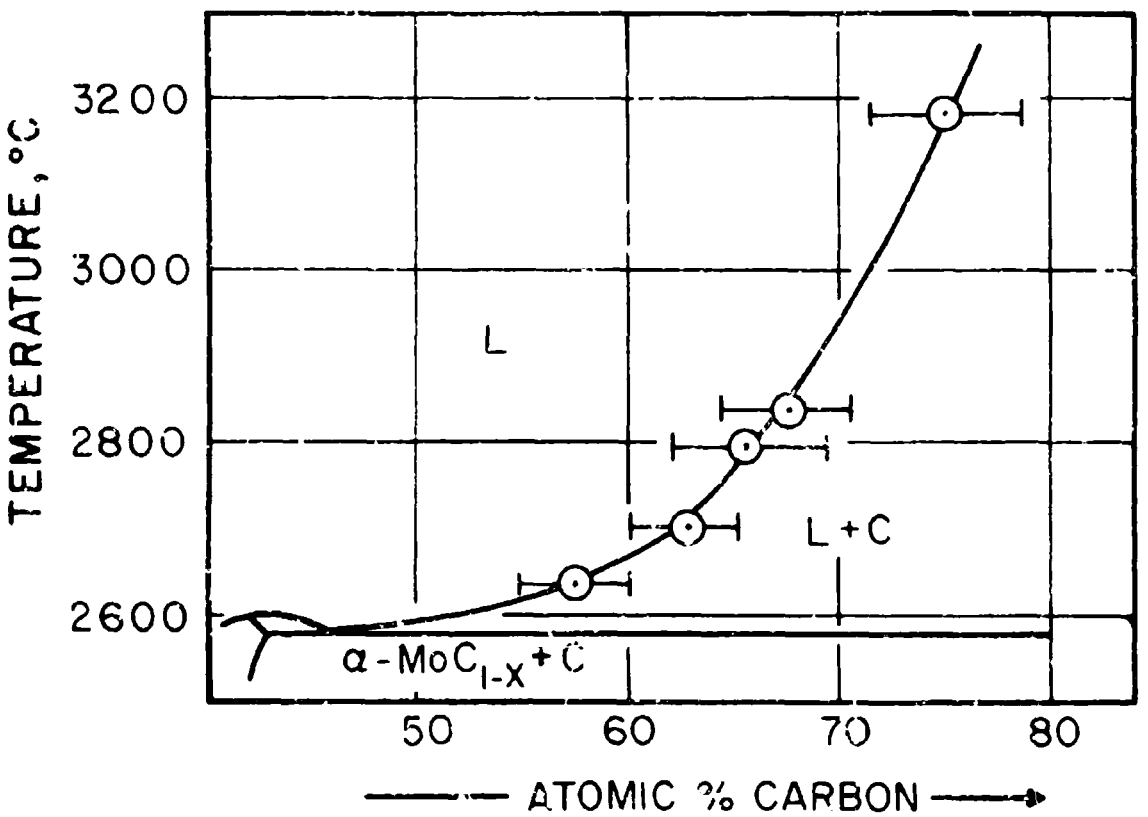

Figure III.B.8.10: Composition of the Carbon-Saturated Melt as a Function of Temperature.

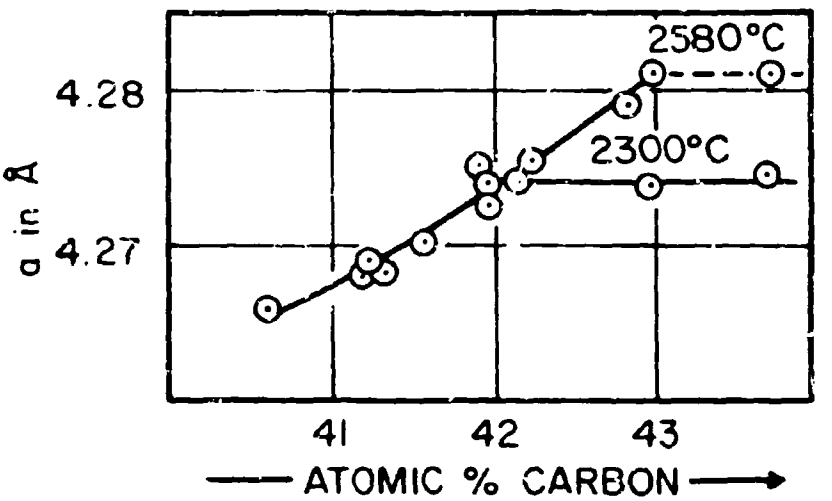

Figure III.B.8.11: Lattice Parameters of the Cubic High Temperature Phase in the Mo-C System.

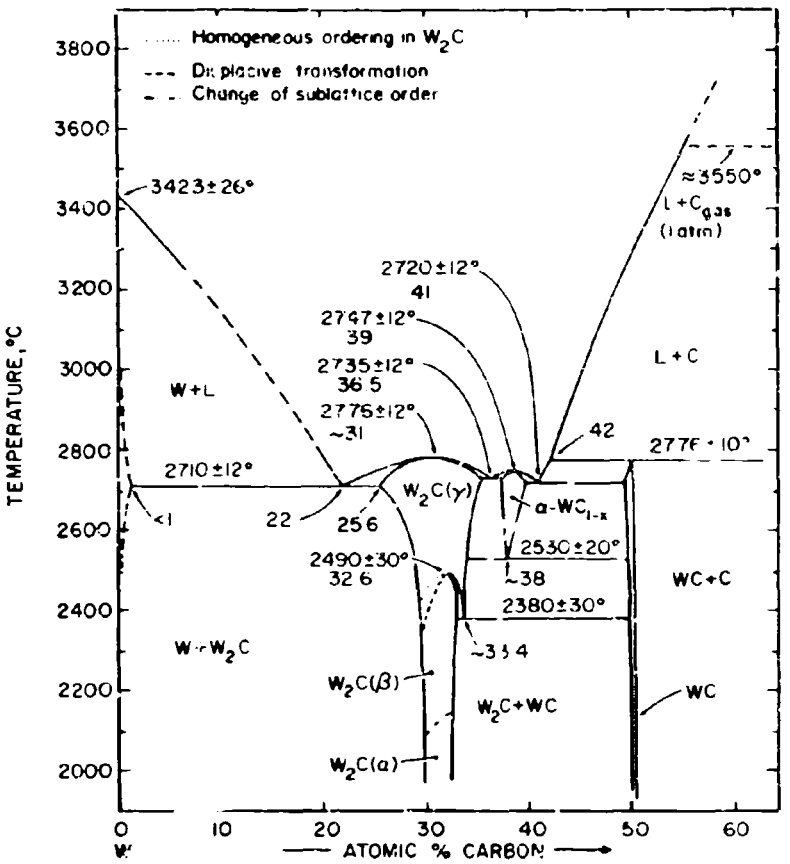

Figure III.B.9 Constitution Diagram W-C.

Temperature Error Figures Based on Estimated Overall Uncertainty).

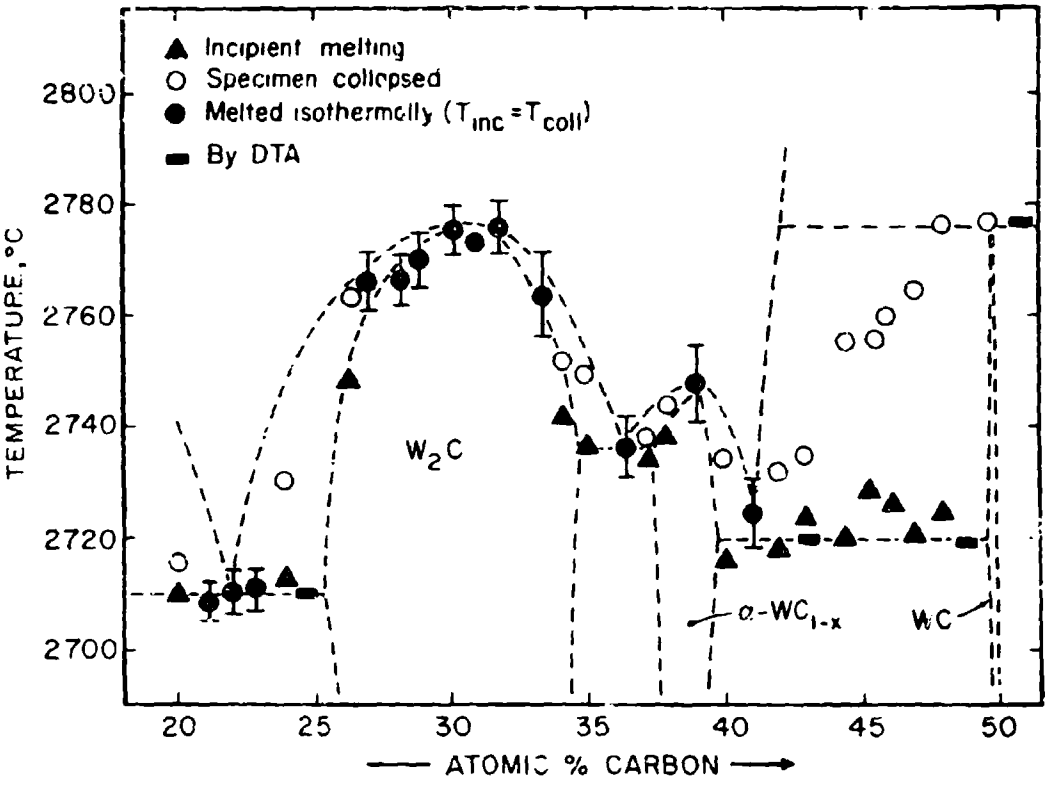

Figure III.B.9.2: Melting Temperatures of W-C Alloys.

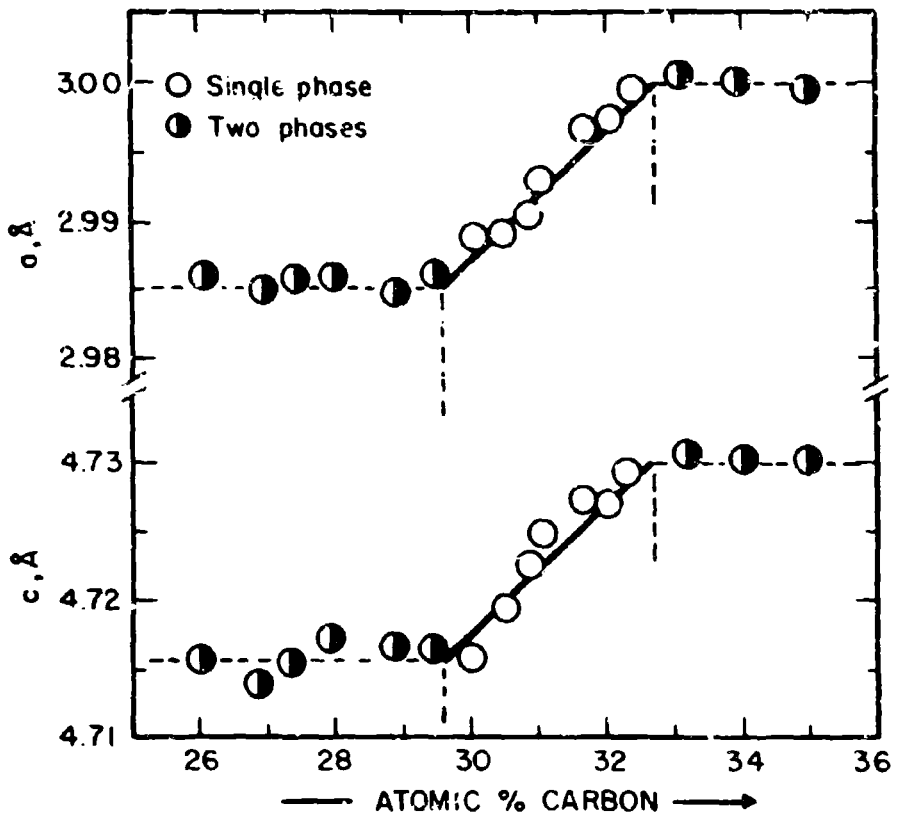

Figure III.B.9.3: Lattice Parameters of the W_2C-Phase.

Alloys Cooled at ~100°C per Second from 2200°C. Indexing According to L'3-Type.

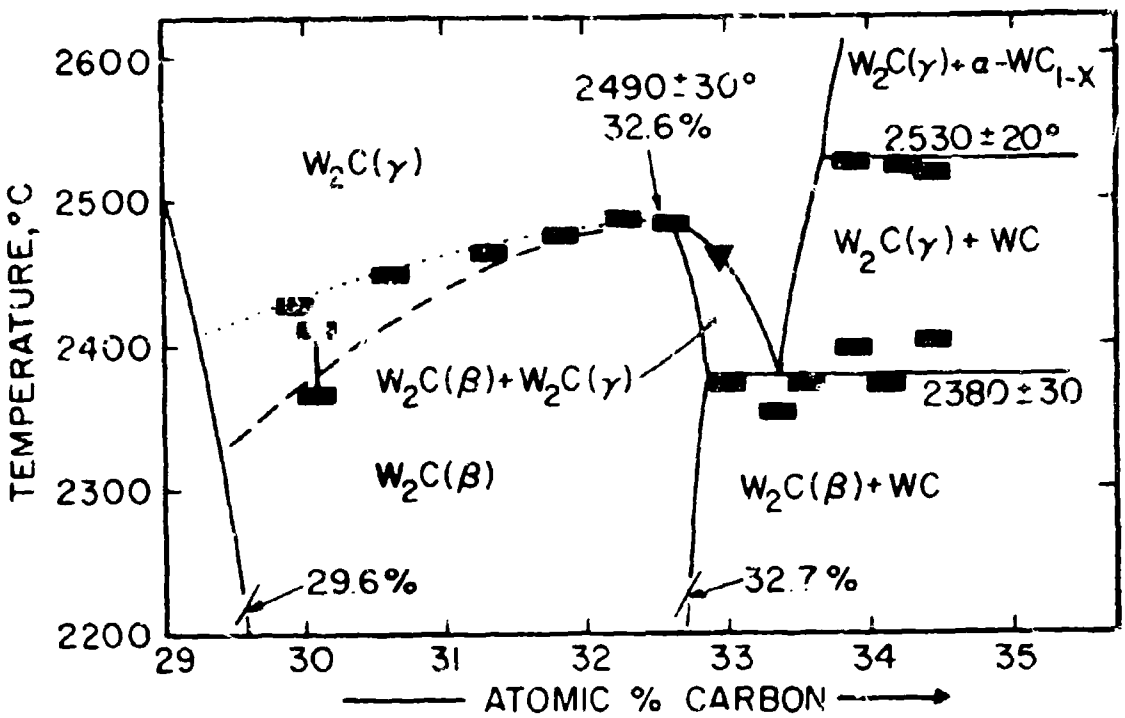

Figure III.B.9.4: Summary of DTA-Results Concerning the Order-Disorder Transition in W_2C.

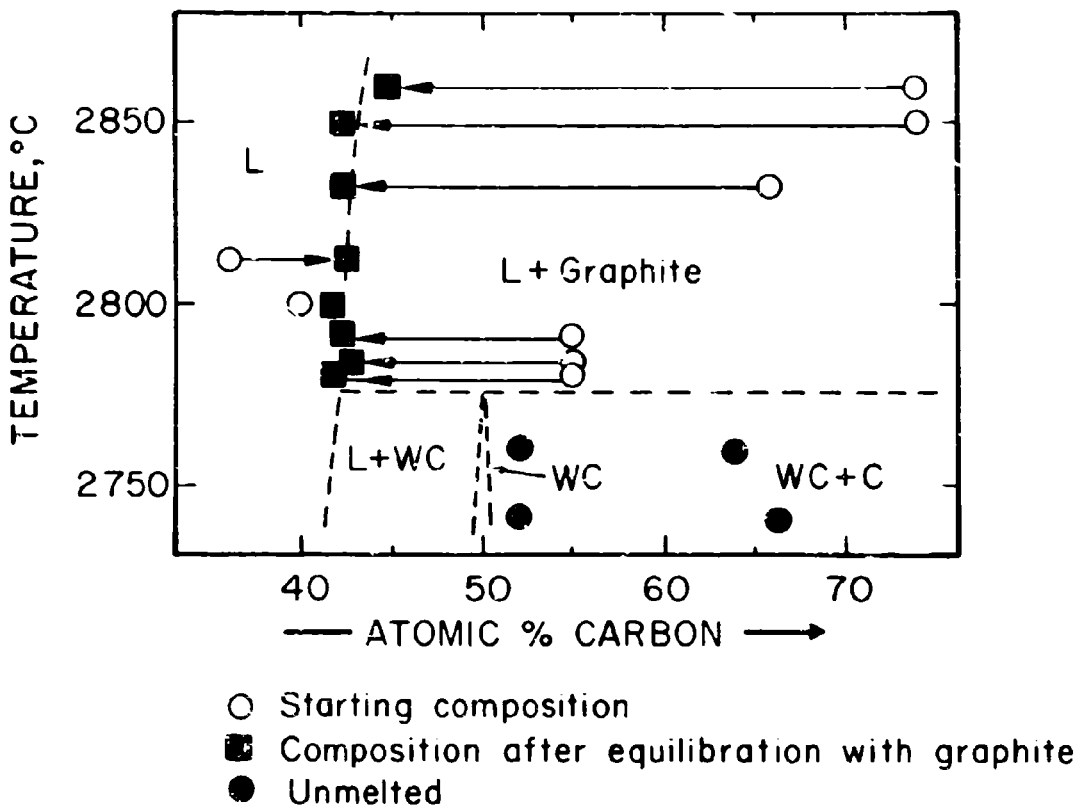

Figure III.B.9.5: W-C: Composition of the Peritectic Melt Near the Decomposition Temperature of Tungsten Monocarbide.

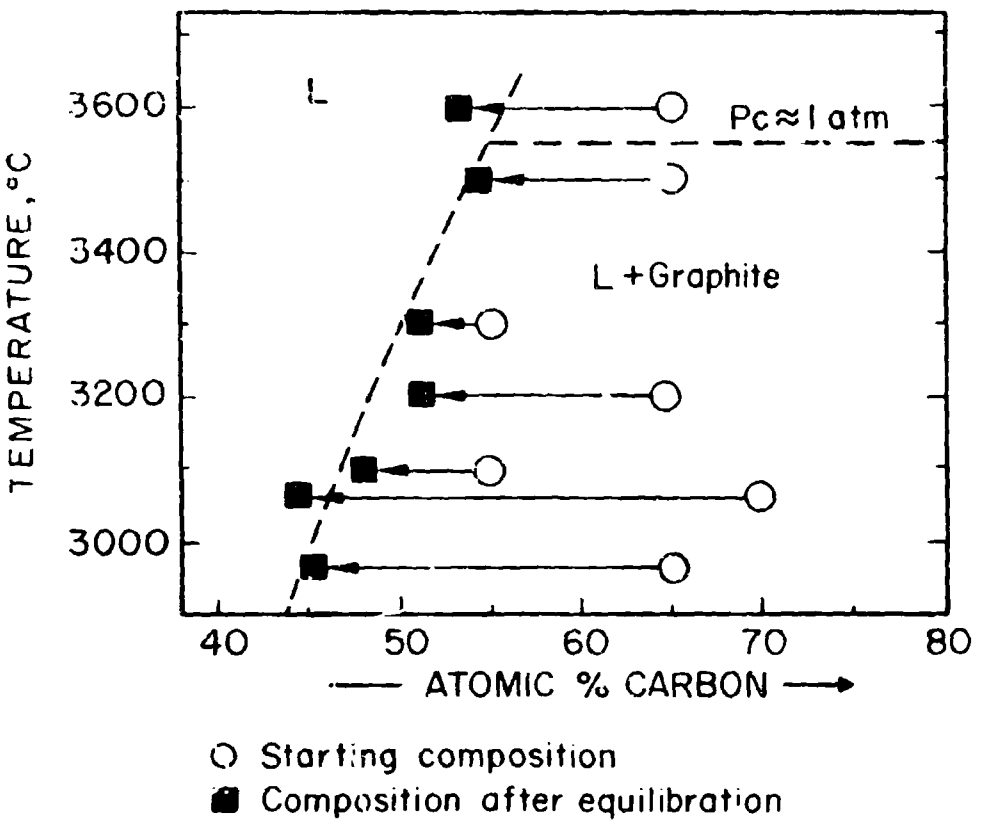

Figure III.B.9.6: W-C: Composition of the Carbon-Saturated Melt as a Function of Temperature.

C. BINARY TRANSITION METAL-BORON SYSTEMS

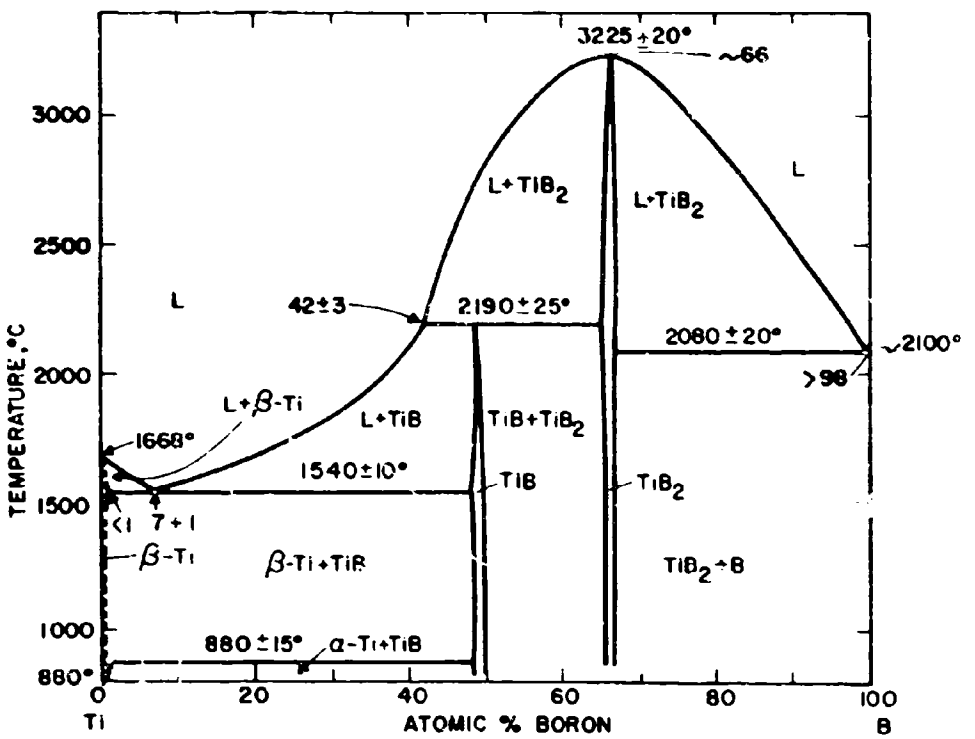

Figure III.C.1.1. Constitution Diagram of the Ti-B System

(Temperature Error Figures Based on Reproducibility)

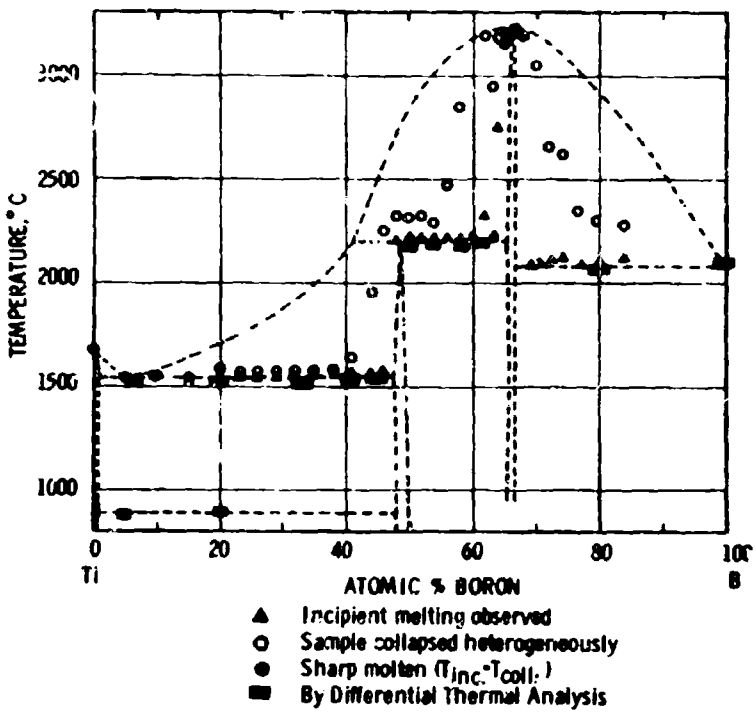

Figure III.C.1.2: Melting Temperatures of Ti-B Alloys.

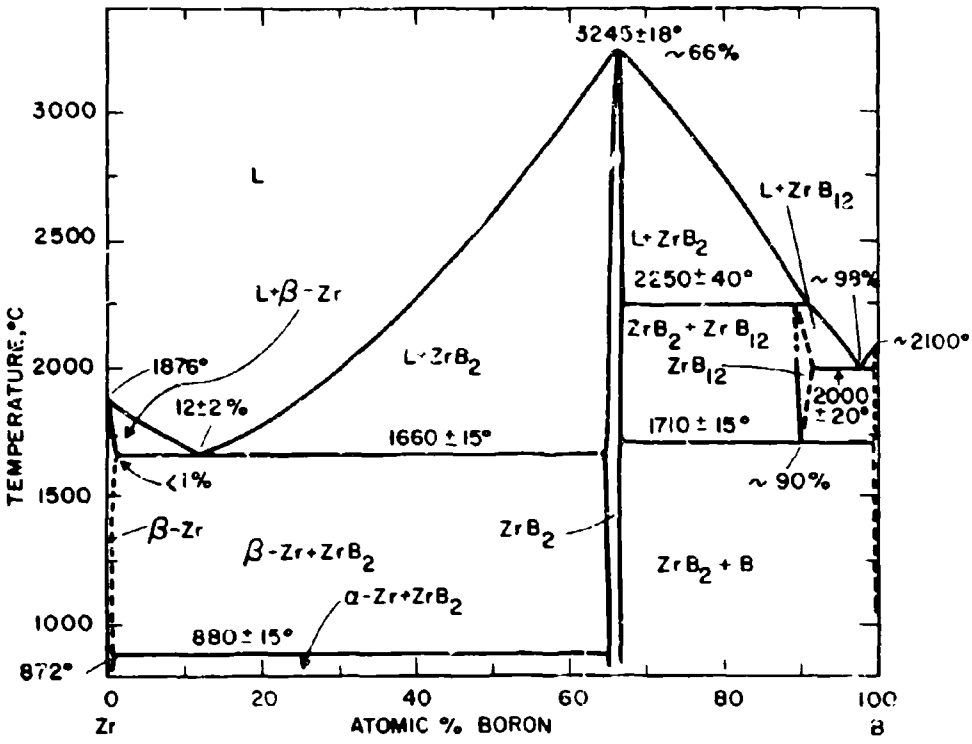

Figure III.C.2.1: Constitution Diagram of the Zr-B System.

(Temperature Error Figures Based on Reproducibility).

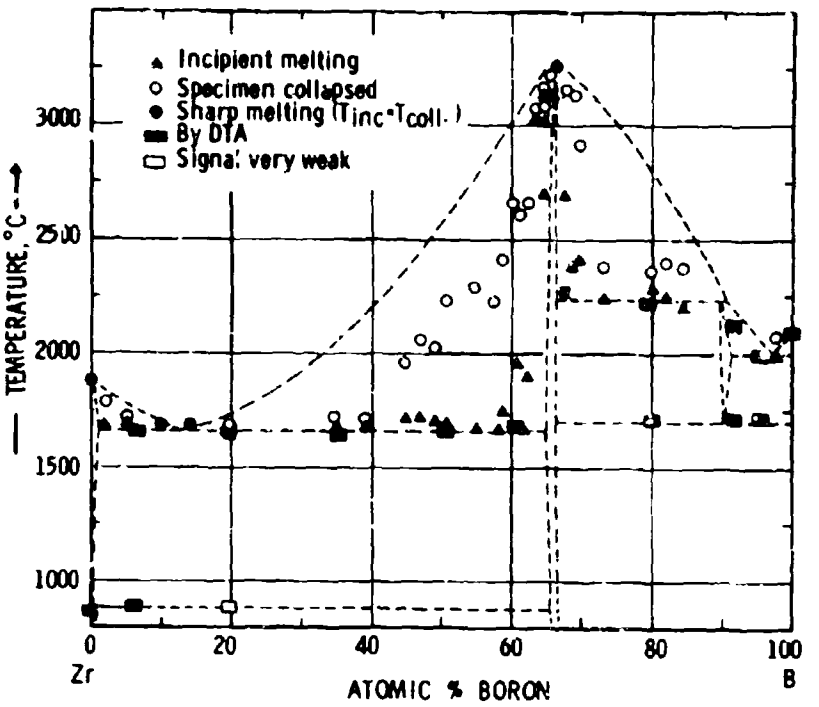

Figure III.C.2.2: Melting Temperatures of Zr-B Alloys.

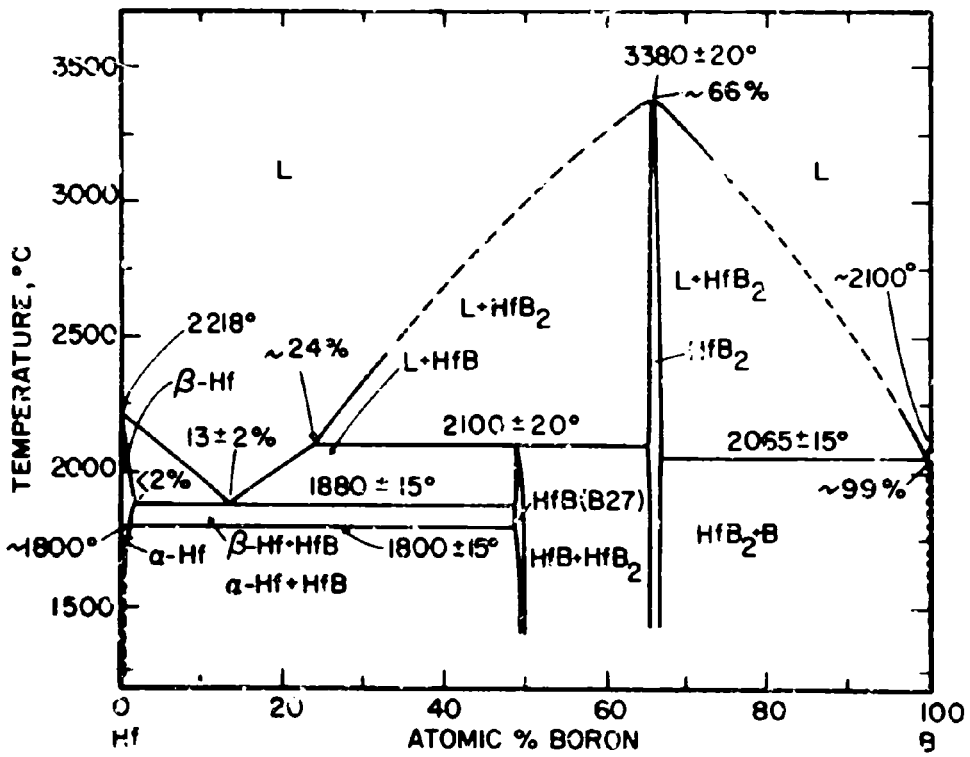

Figure III.C.3.1: Constitution Diagram of the Hf-B System.

(Temperature Error Figures Based on Reproducibility).

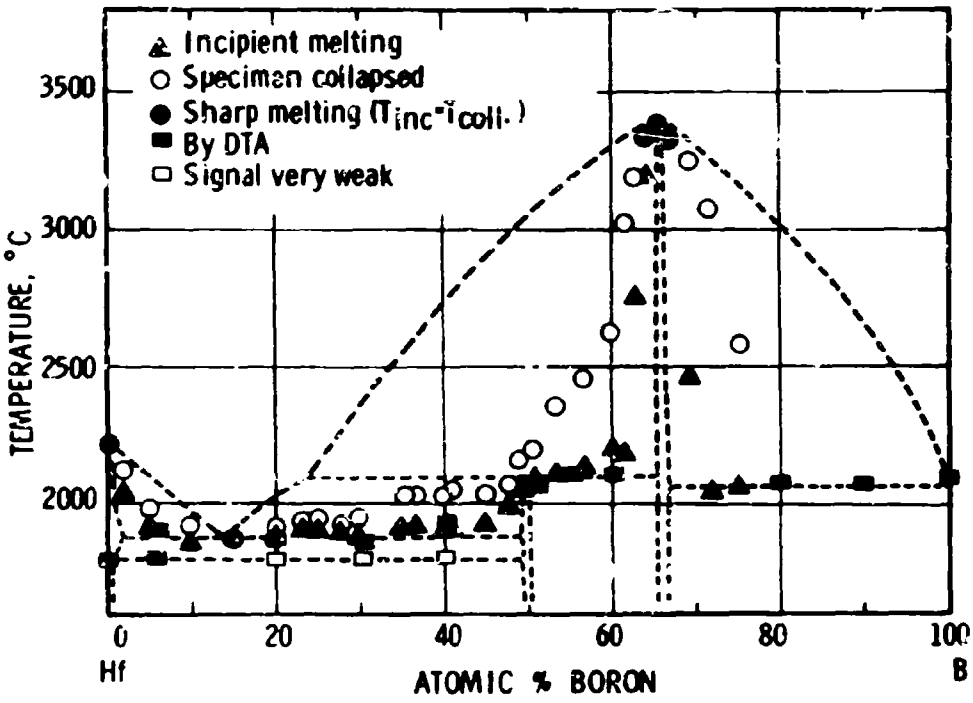

Figure III.C.3.2: Melting Temperatures of Hf-B Alloys.

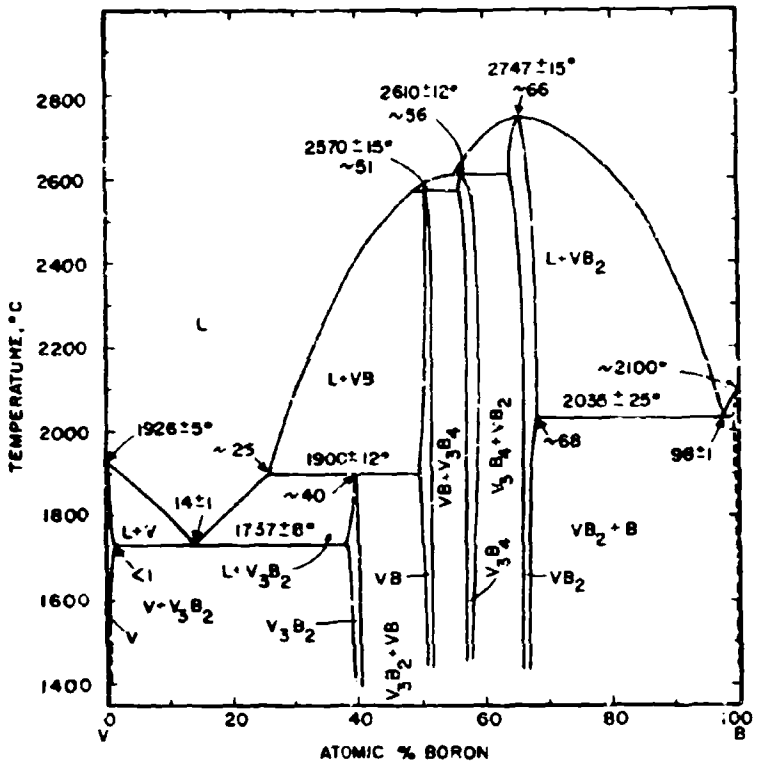

Figure III.C.4.1: Constitution Diagram of the System V-B.

(Temperature Error Figures Based on Reproducibility).

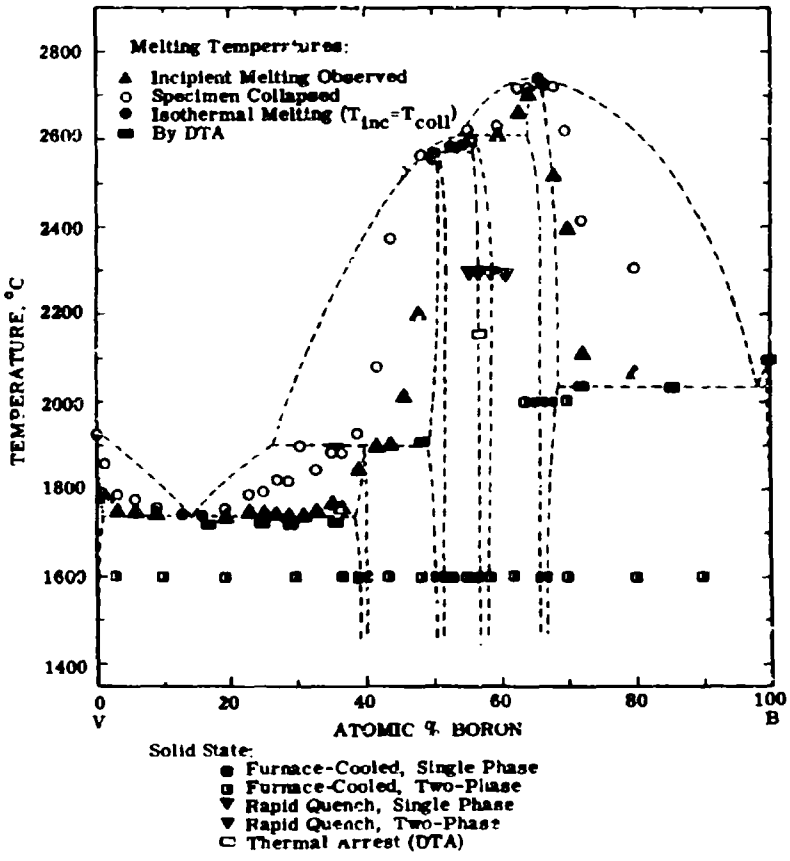

Figure III.C.4.2. Melting Temperatures and Qualitative Phase Evaluation of V-B Alloys.

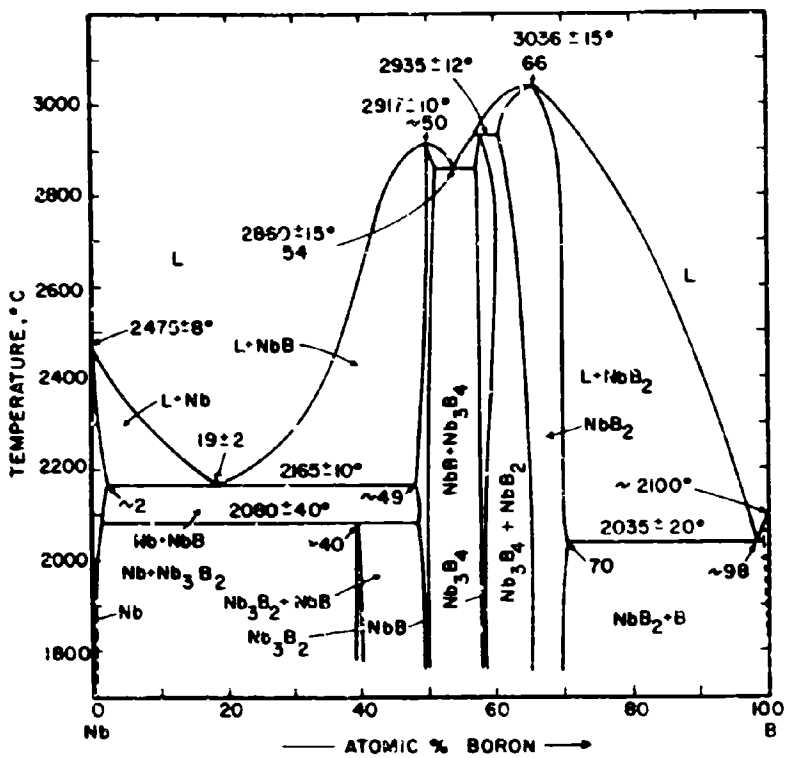

Figure III.C.5.1: Constitution Diagram of the Nb-B System.

(Temperature Error Figures Based on Reproducibility).

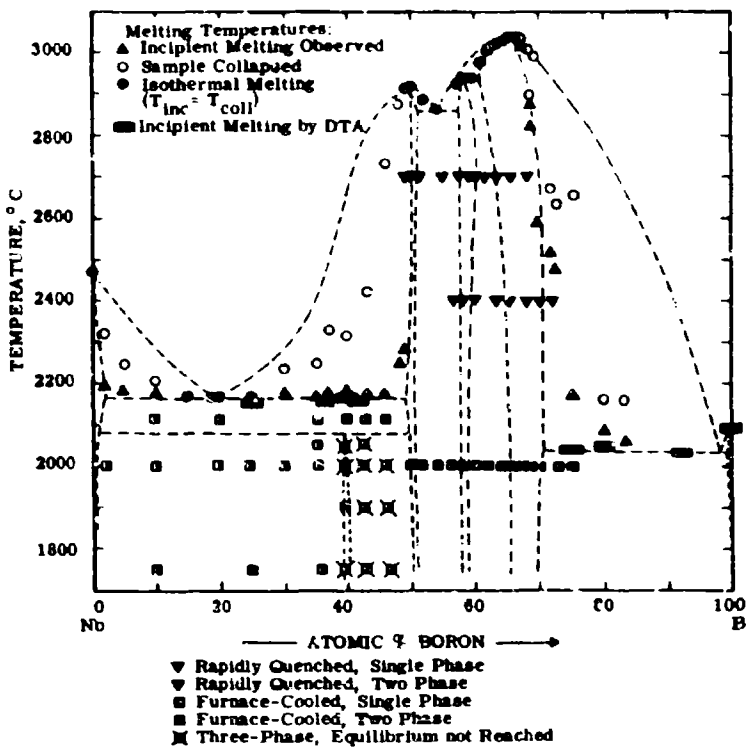

Figure III.C.5.2: Melting Temperatures and Qualitative Phase Evaluation of Nb-B Alloys.

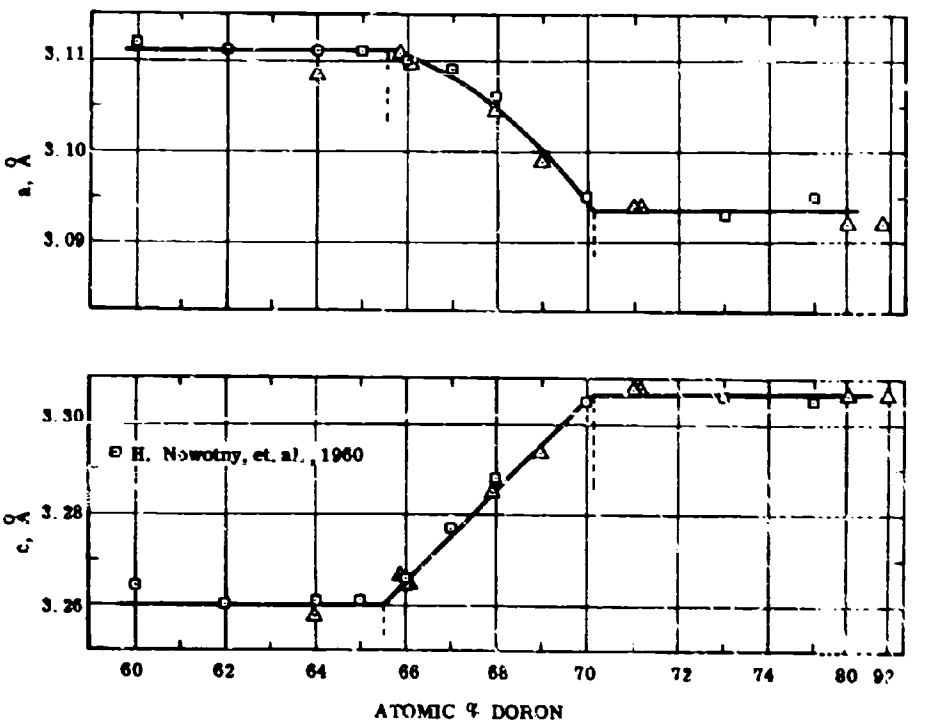

Figure III.C.5.3: Lattice Parameters of Niobium Diboride.

(Alloys Equilibrated at 2000°C).

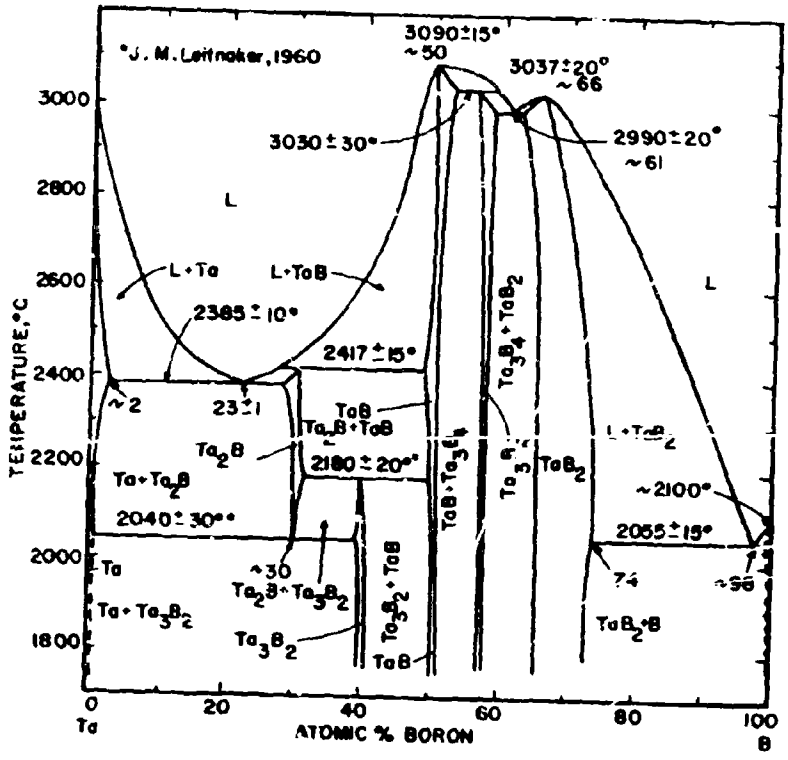

Figure III.C.6.1: Constitution Diagram of the Ta-B System.

(Temperature Error Figures Based on Reproducibility).

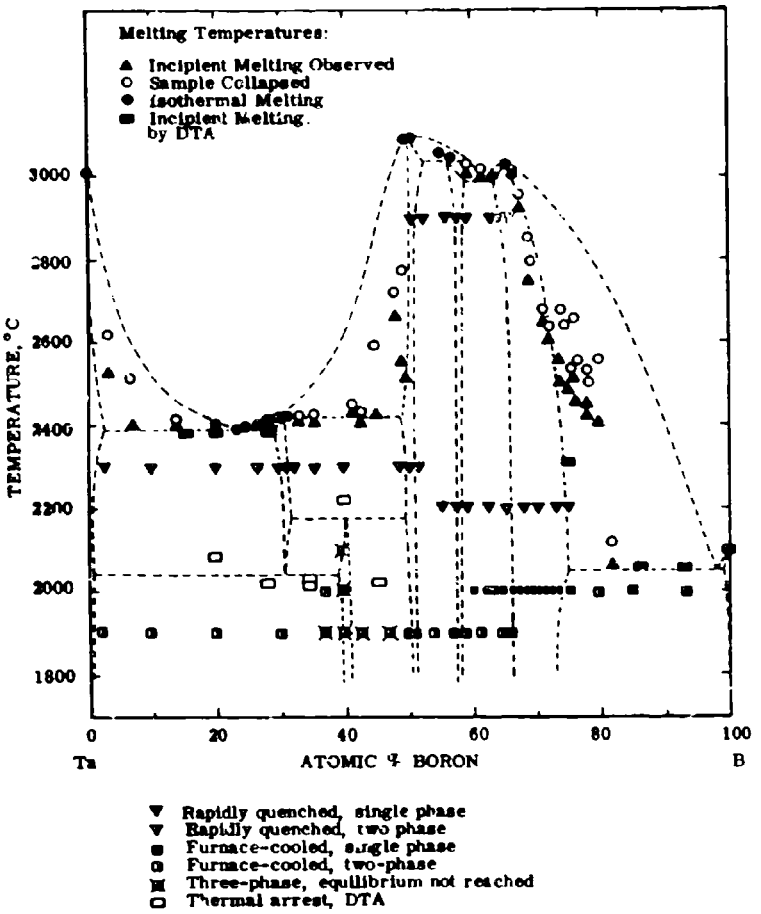

Figure III.C.6.2: Melting Temperatures and Qualitative Phase Evaluation of Ta-B Alloys.

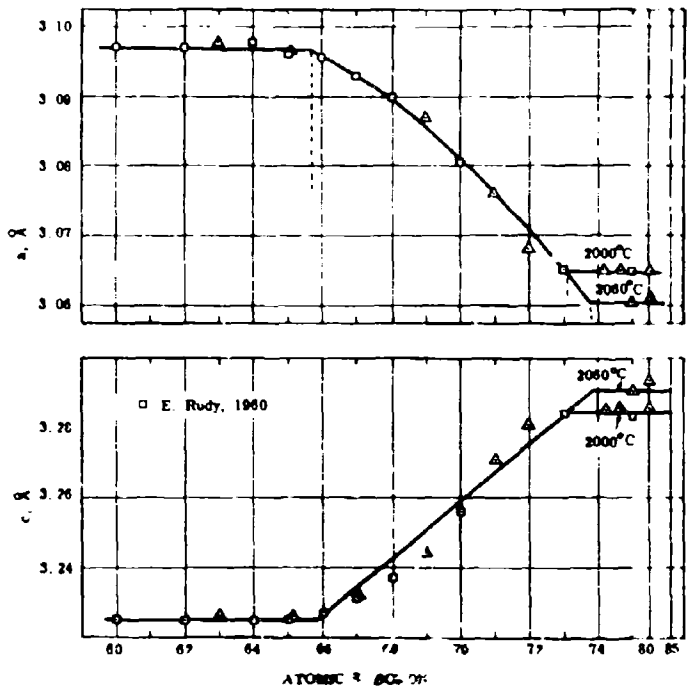

Figure III.C.6.3: Lattice Parameters of Tantalum Diboride.

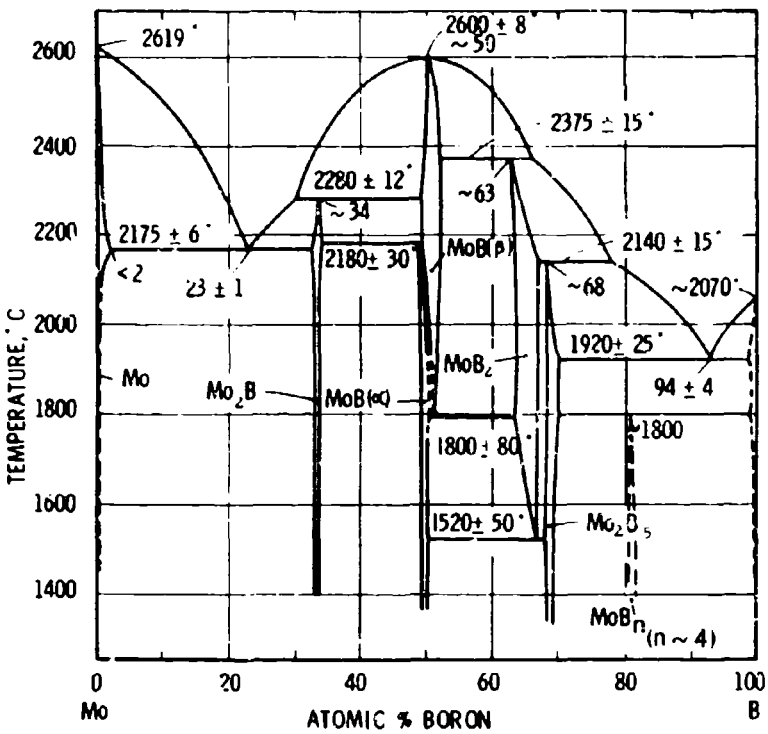

Figure III.C.7.1: Constitution Diagram of the Mo-B System.

(Temperature Error Figures Based on Reproducibility).

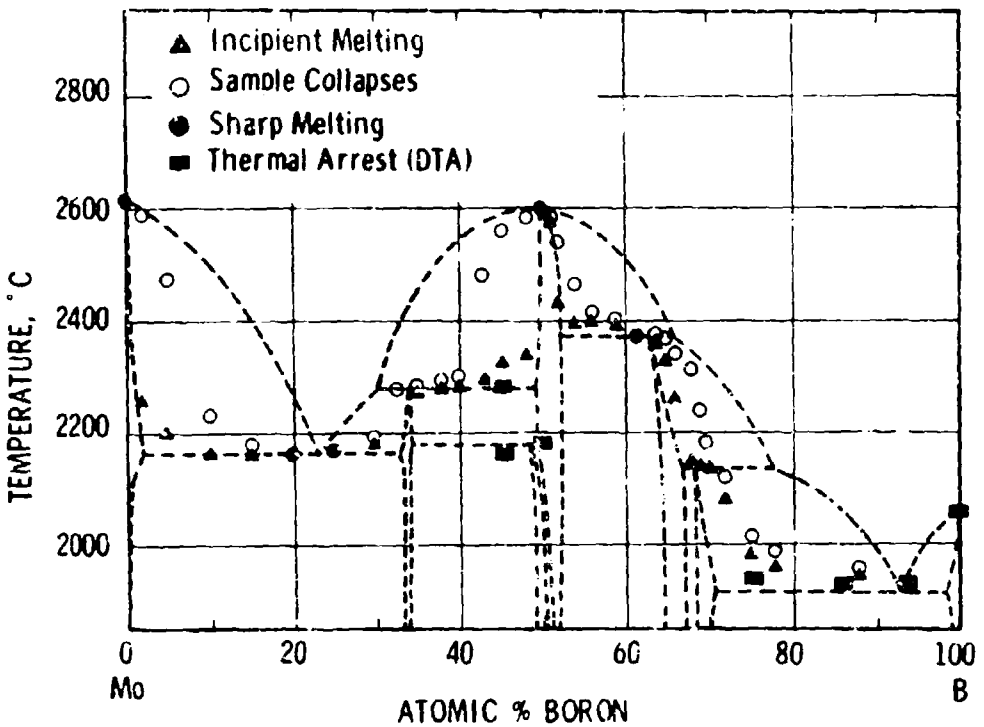

Figure III.C.7.2: Melting Temperatures of Mo-B Alloys.

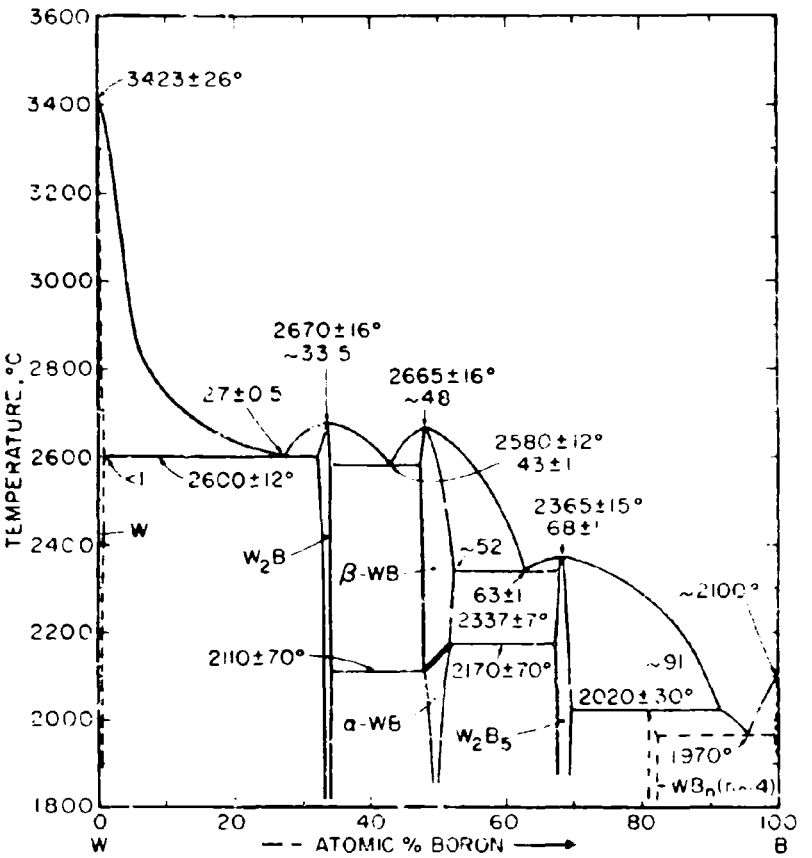

Figure III.C.8.1: Constitution Diagram of the W-B System.

(Temperature Error Figures Based on Reproducibility).

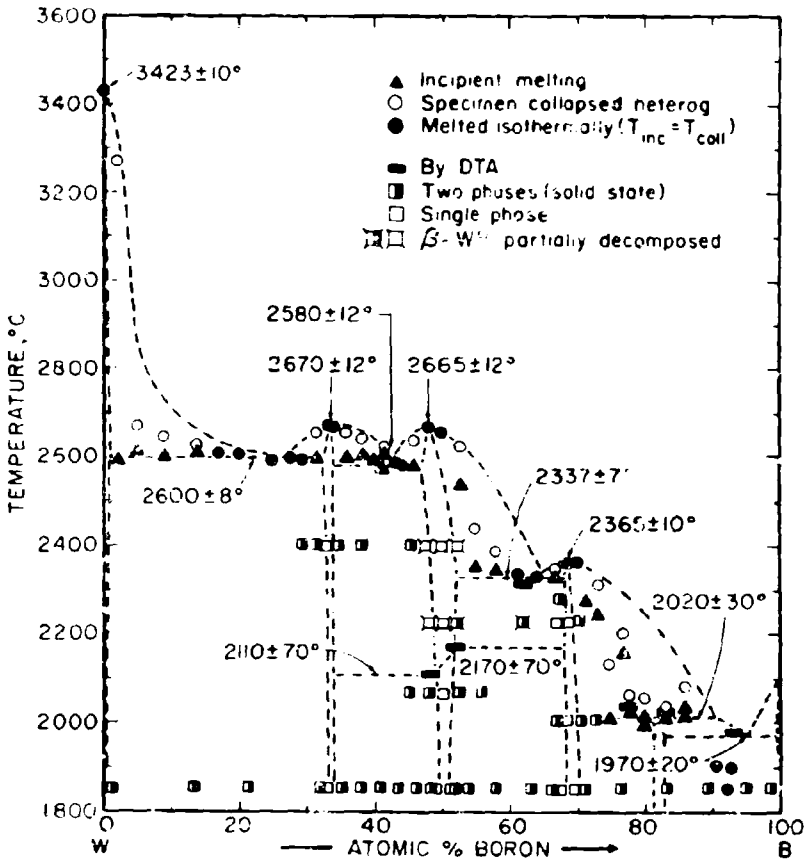

Figure III.C.8.2: Melting Temperatures and Qualitative Phase Evaluation of W-B Alloys.

D. BINARY TRANSITION METAL-SILICON SYSTEMS

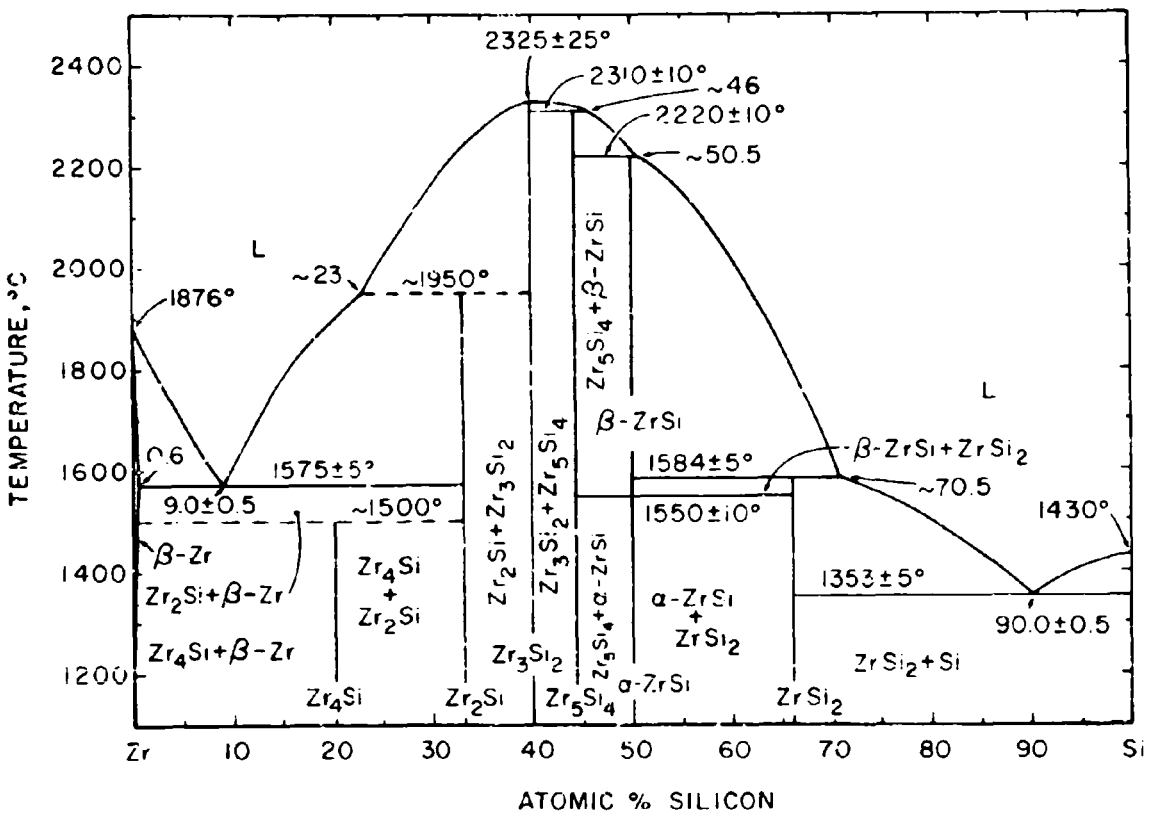

Figure III.D.1.1: Constitution Diagram of the System Zr-Si.

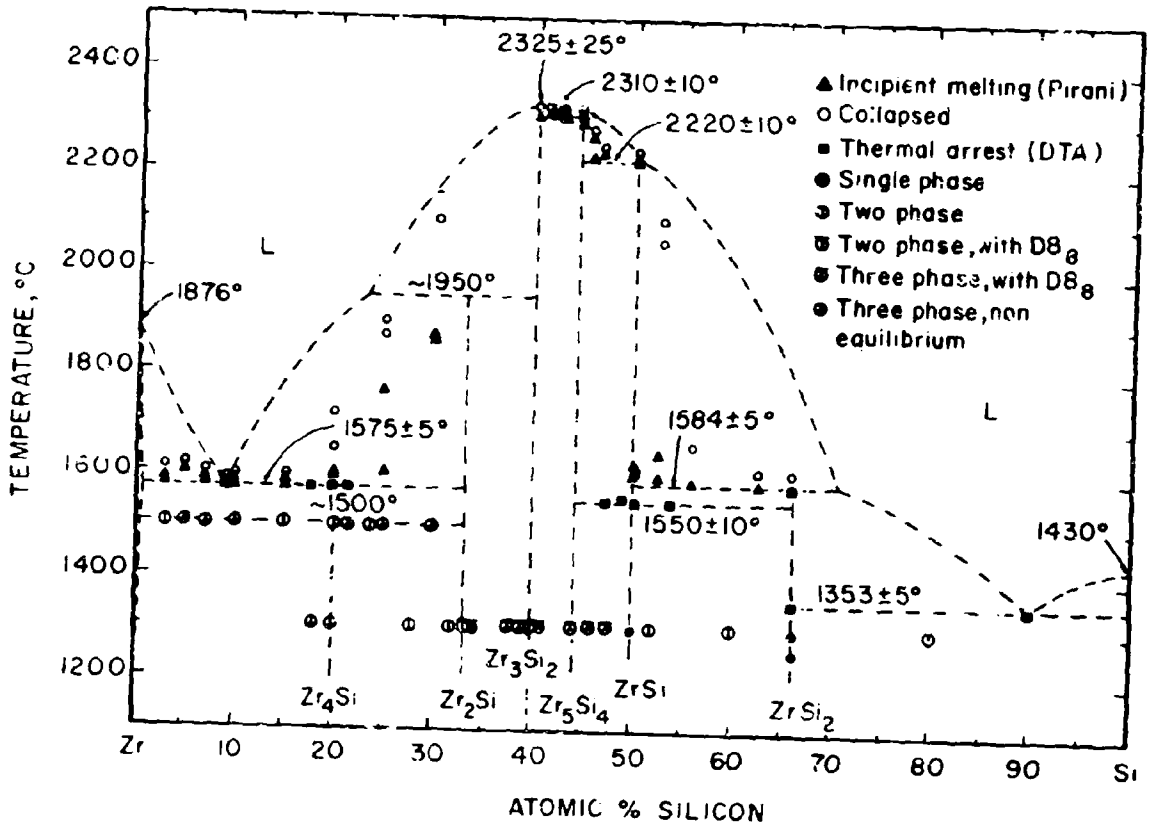

Figure III.D.1.2: Melting Temperatures of Zr-Si Alloys and Qualitative Phase Evaluation of Solid State Equilibrated Alloys.

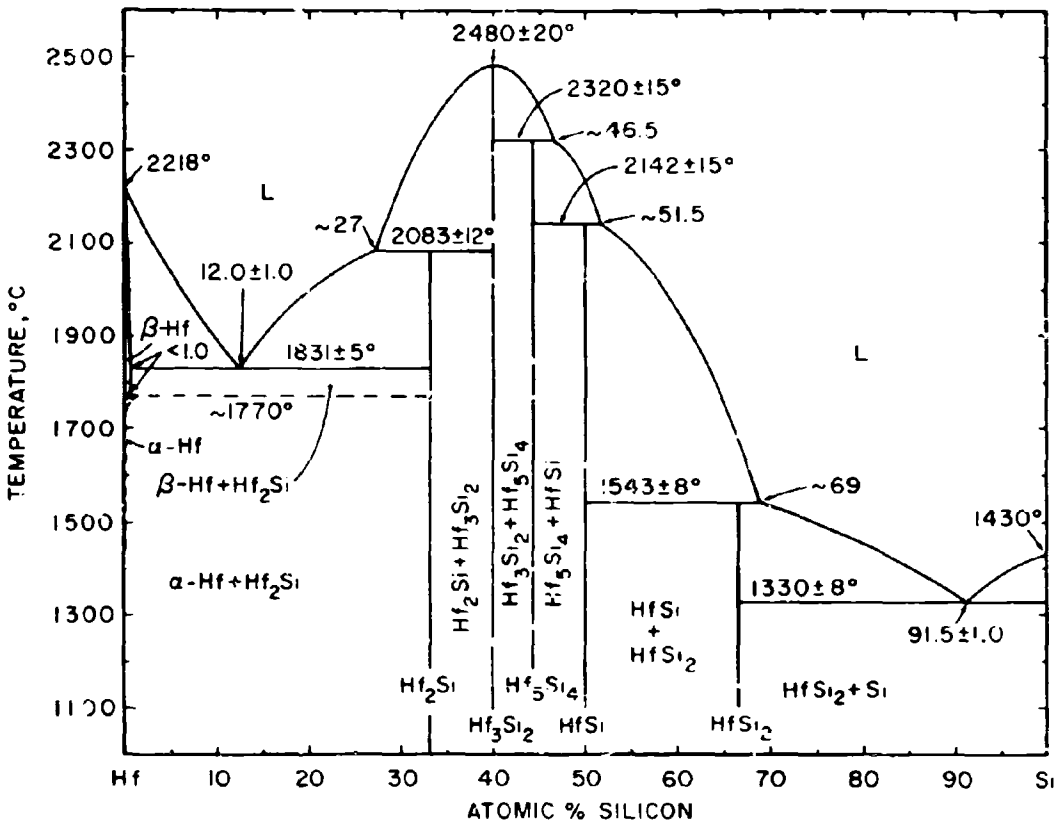

Figure III.D.2.1: Constitution Diagram of the Hf-Si System.

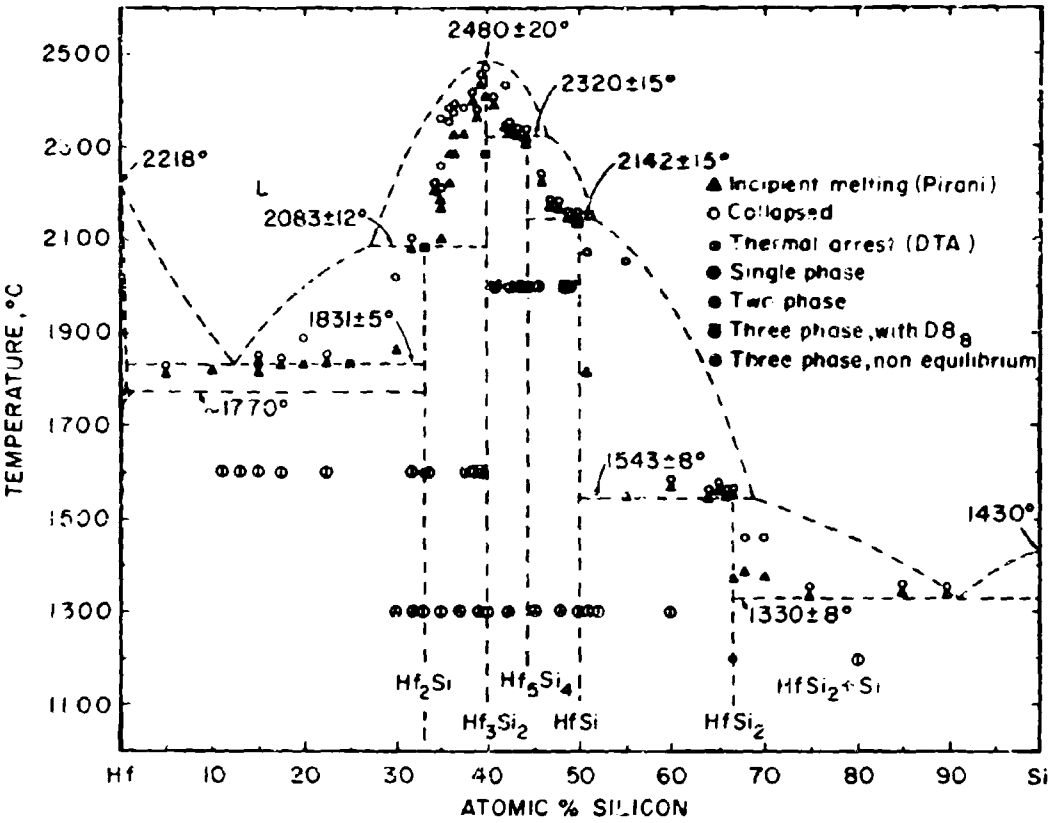

Figure III.D.2.2: Melting Temperatures of Hf-Si Alloys and Qualitative Phase Evaluation of Solid State Equilibrated Alloys.

E. TERNARY TRANSITION METAL-CARBON SYSTEMS

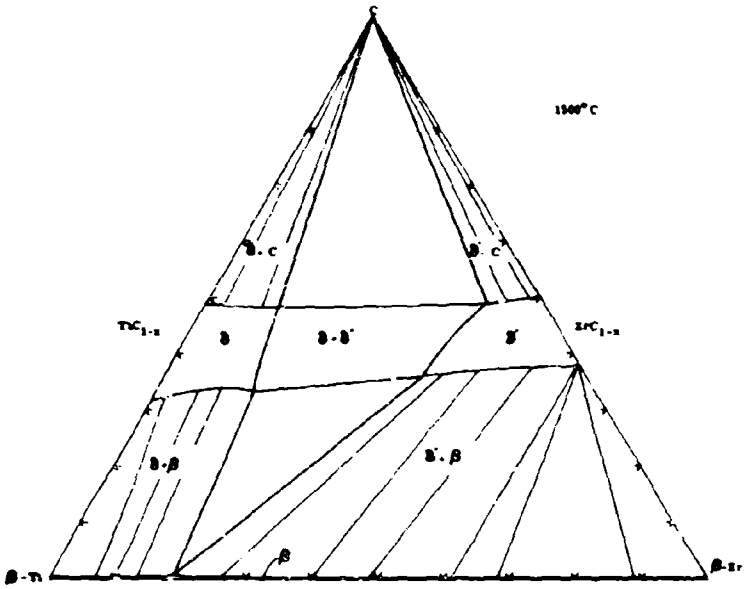

Figure III.E.1.1: Isothermal Section of the Ti-Zr-C System at 1500°C.

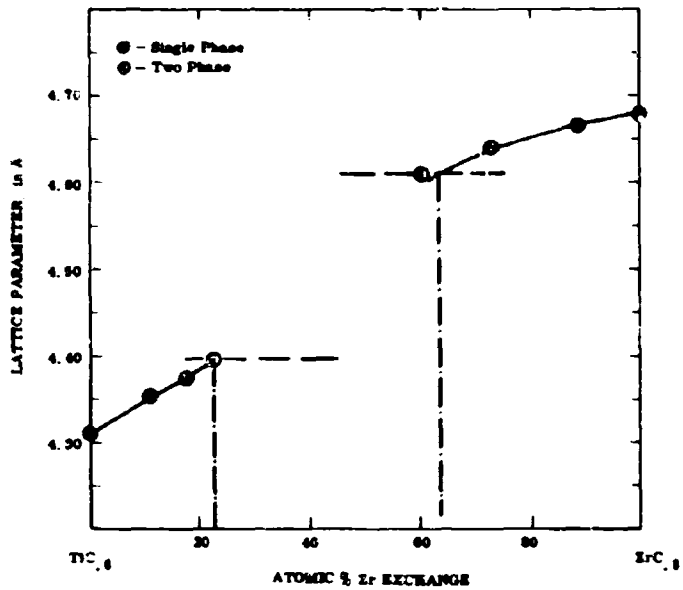

Figure III.E.1.2: Lattice Parameters of the Monocarbide Solution at 37.5 At.% C. Alloys Equilibrated at 1500°C.

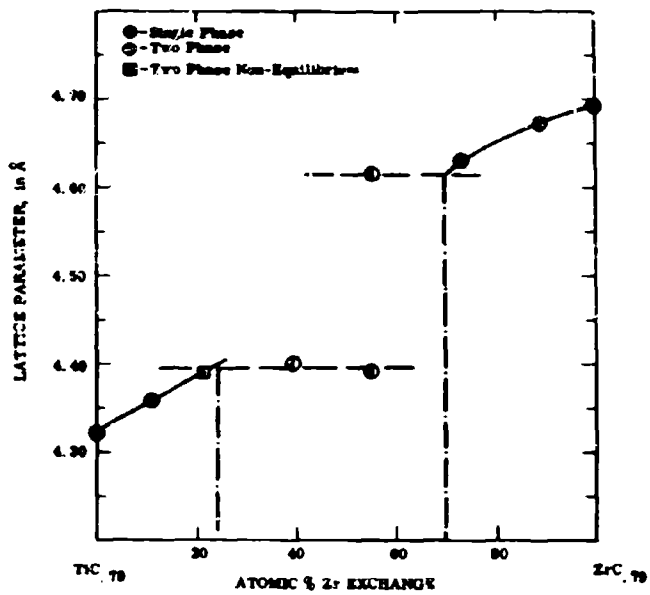

Figure III.E.1.3: Lattice Parameters of the Monocarbide Solution at 44 At.% C. Alloys Equilibrated at 1500°C.

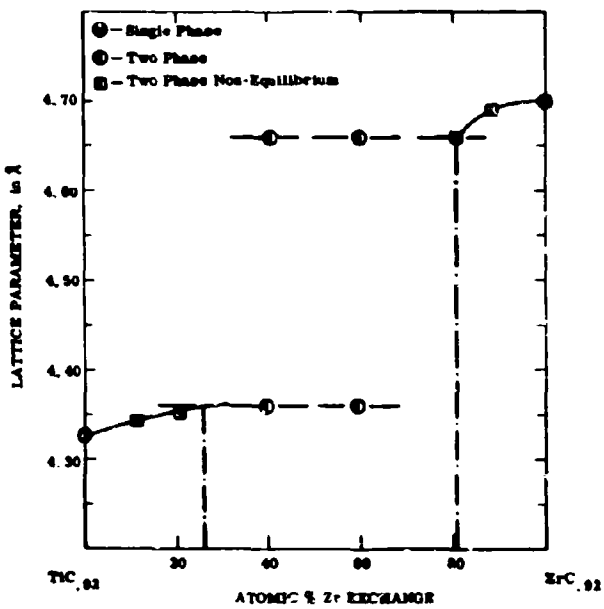

Figure III.E.1.4: Lattice Parameters of the Monocarbide Solid Solution at 48 At.% C. Alloys Equilibrated at 1500°C.

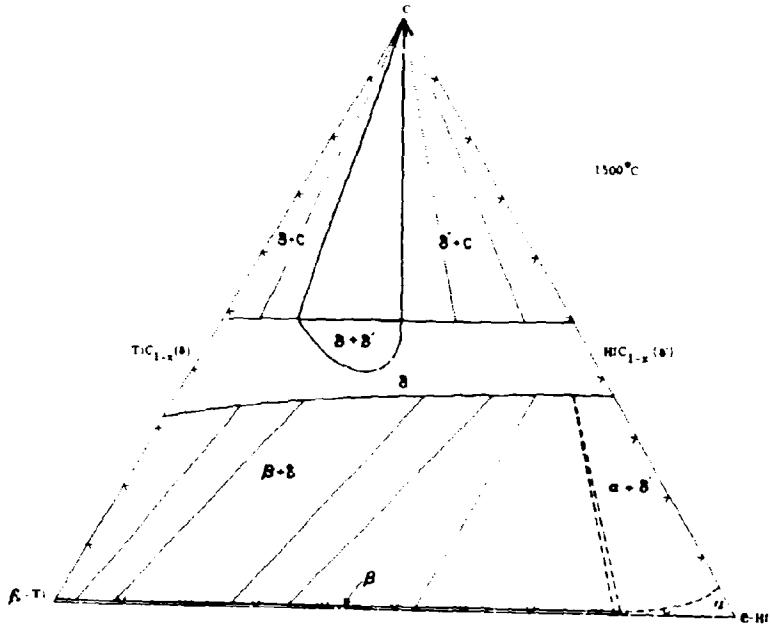

Figure III.E.2.1: Isothermal Section of the Ti-Hf-C System at 1500°C.

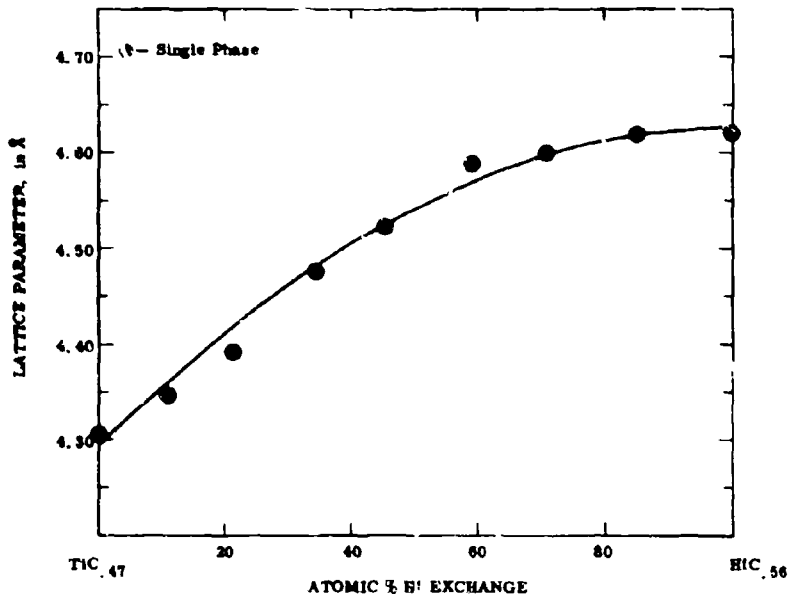

Figure III.E.2.2: Lattice Parameters of the (Ti, Hf)C_{1-x} - Solid Solution at 32-36 At.% C. Alloys Equilibrated at 1500°C.

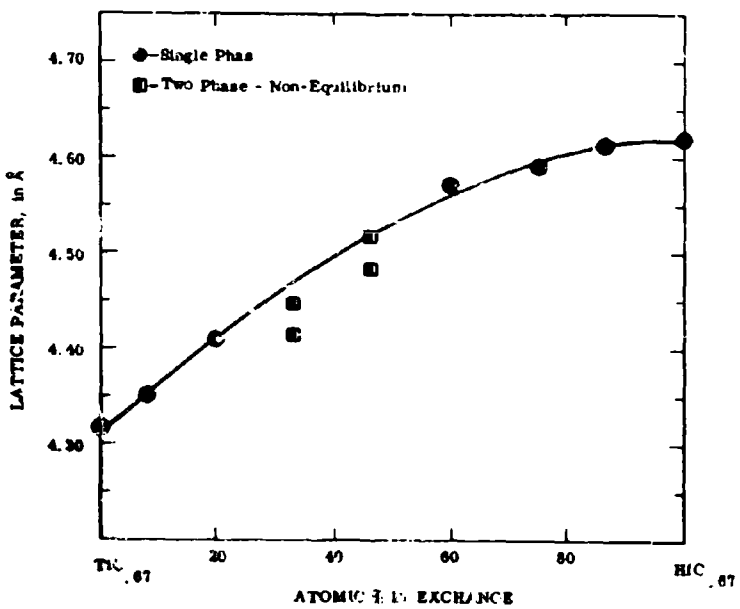

Figure III.E.2.3: Lattice Parameters of the (Ti, Hf)C_{1-x} - Solid Solution at 40 At.% C. Alloys Equilibrated at 1500°C.

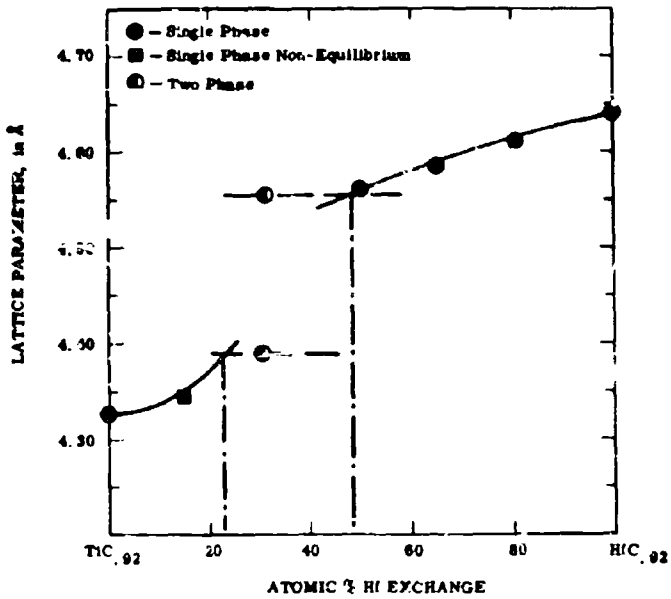

Figure III.E.2.4: Lattice Parameters of the $(Ti,Hf)C_{1-x}$ Solid Solution at 48 At.% C. Alloys Equilibrated at 1500°C.

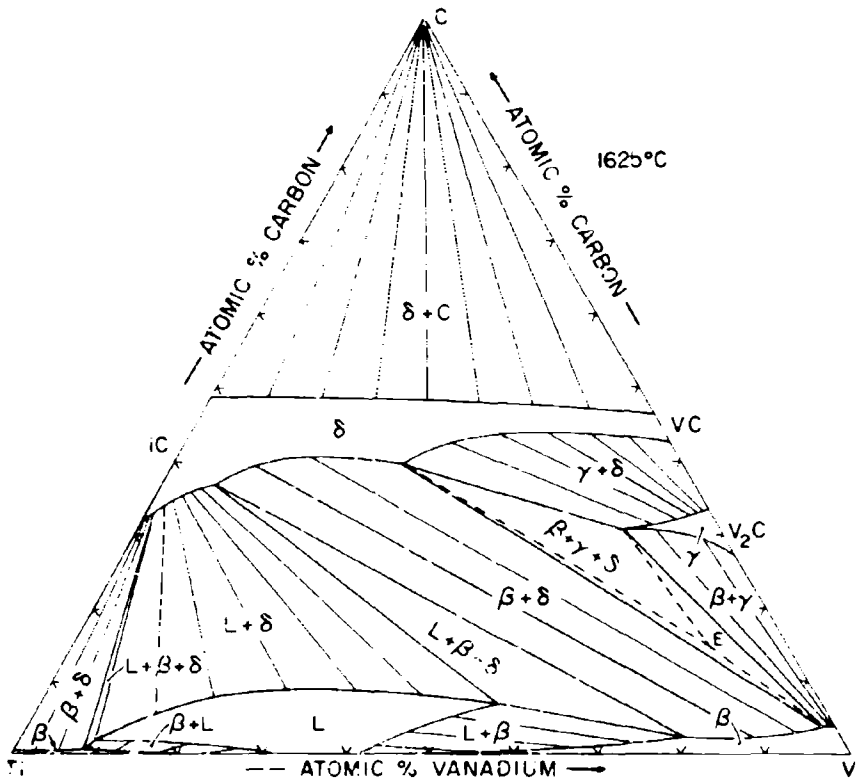

Figure III.E.3.11. Isothermal Section of the Ti-V-C System at 1625°C

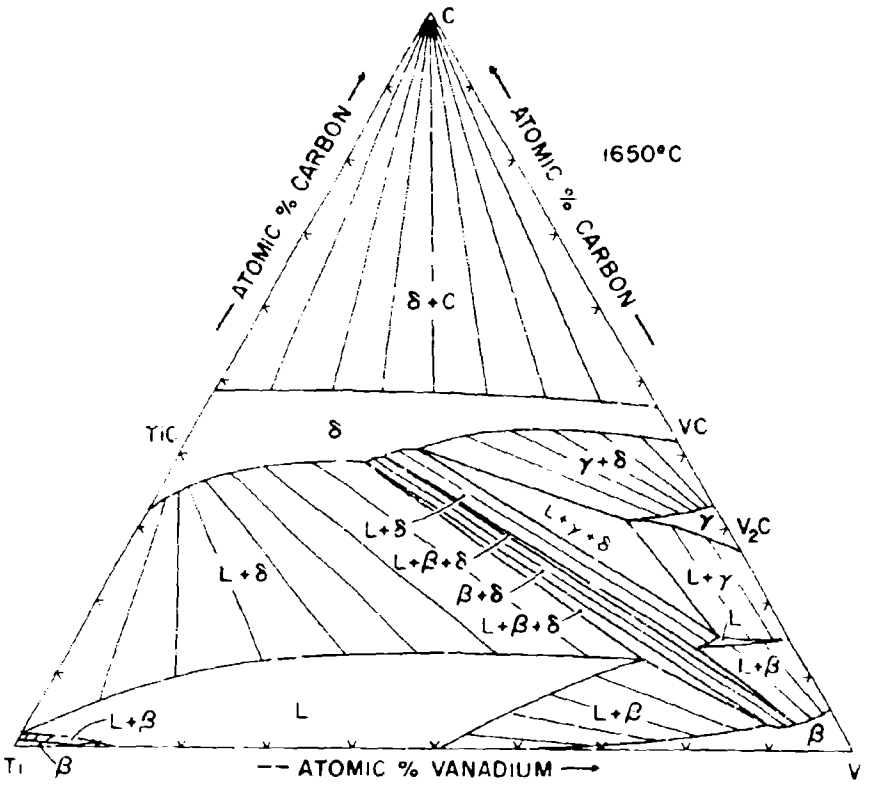

Figure III.E.3.12. Isothermal Section of the Ti-V-C System at 1650°C

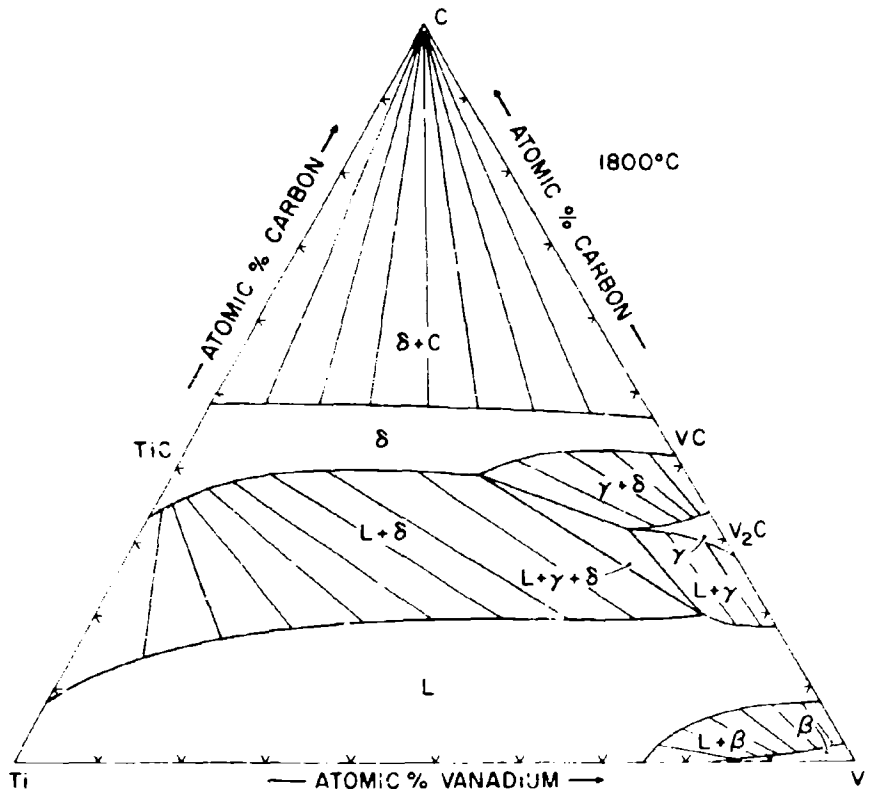

Figure III.E.3.13. Isothermal Section of the Ti-V-C System at 1800° C

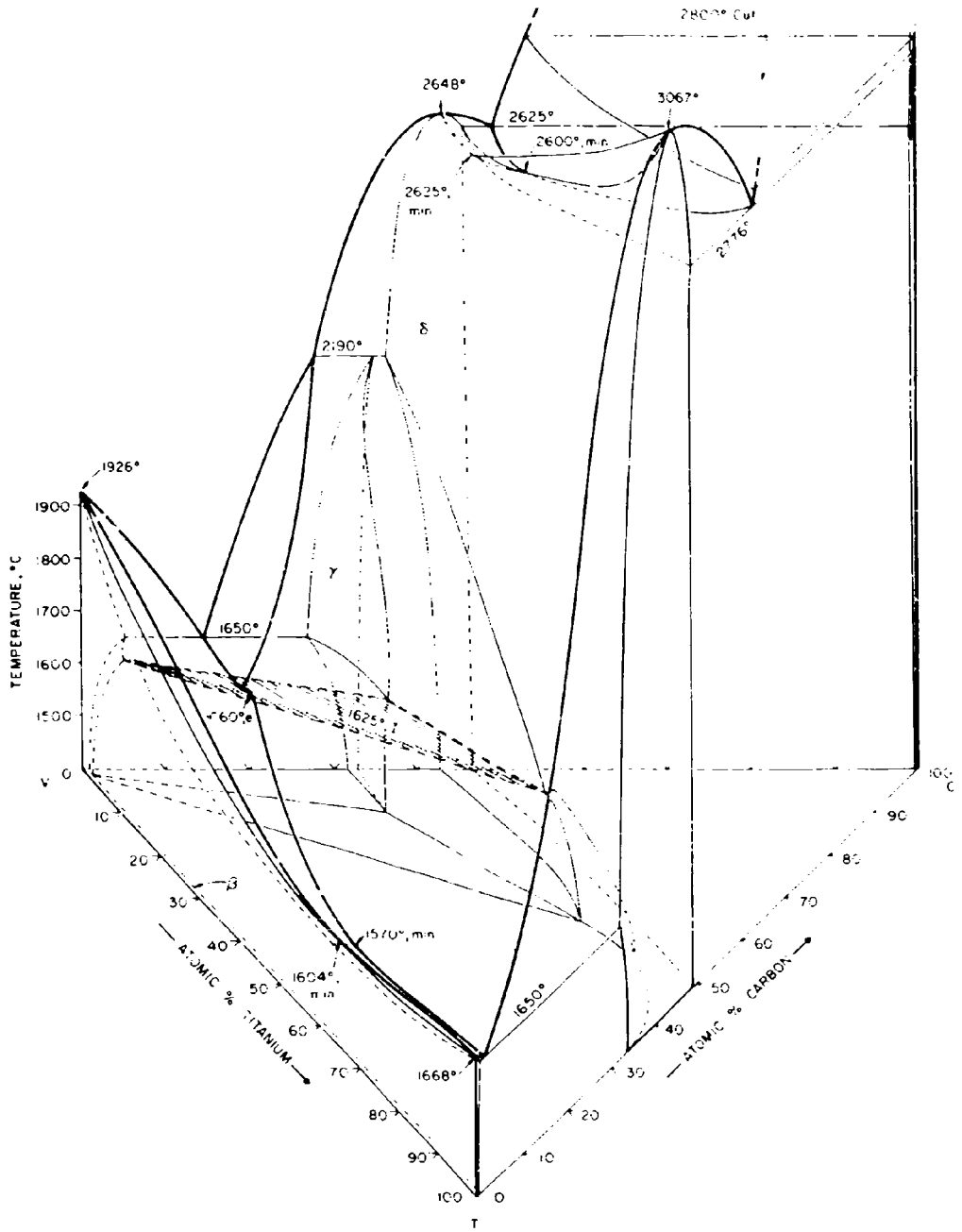

Figure III.E.3.1. Isometric View of the Ti-V-C System

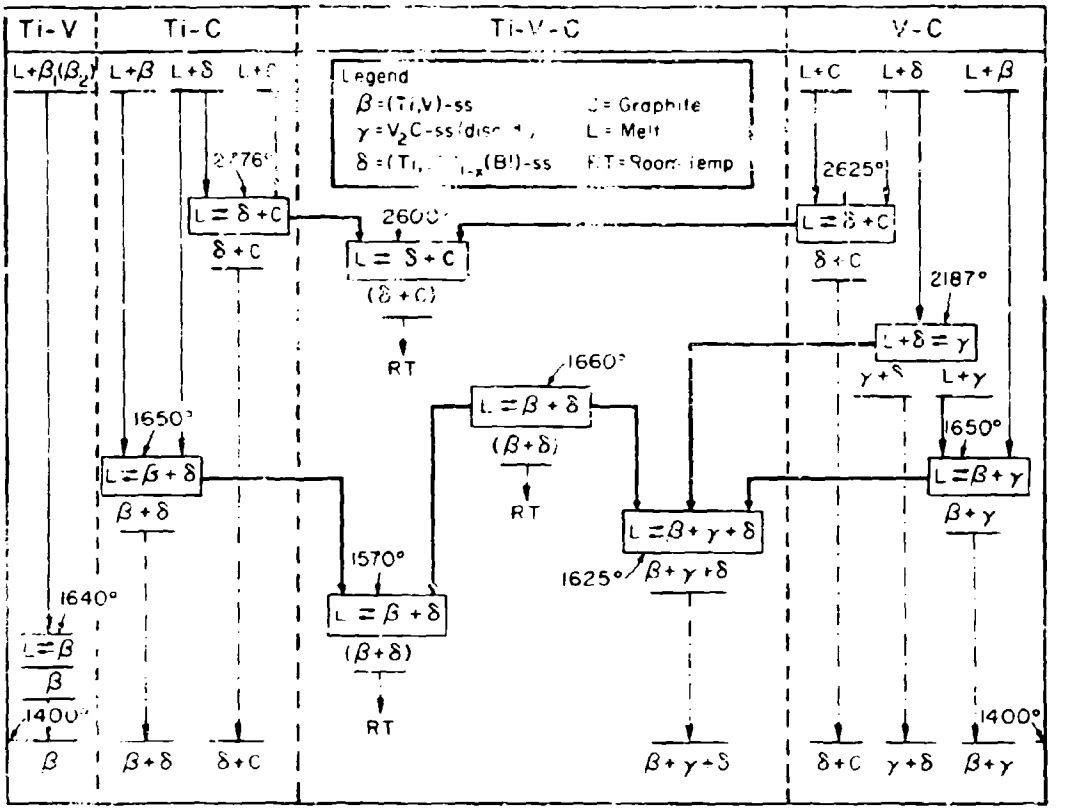

Figure III.E.3.2. Reaction Diagram for the Ti-V-C System

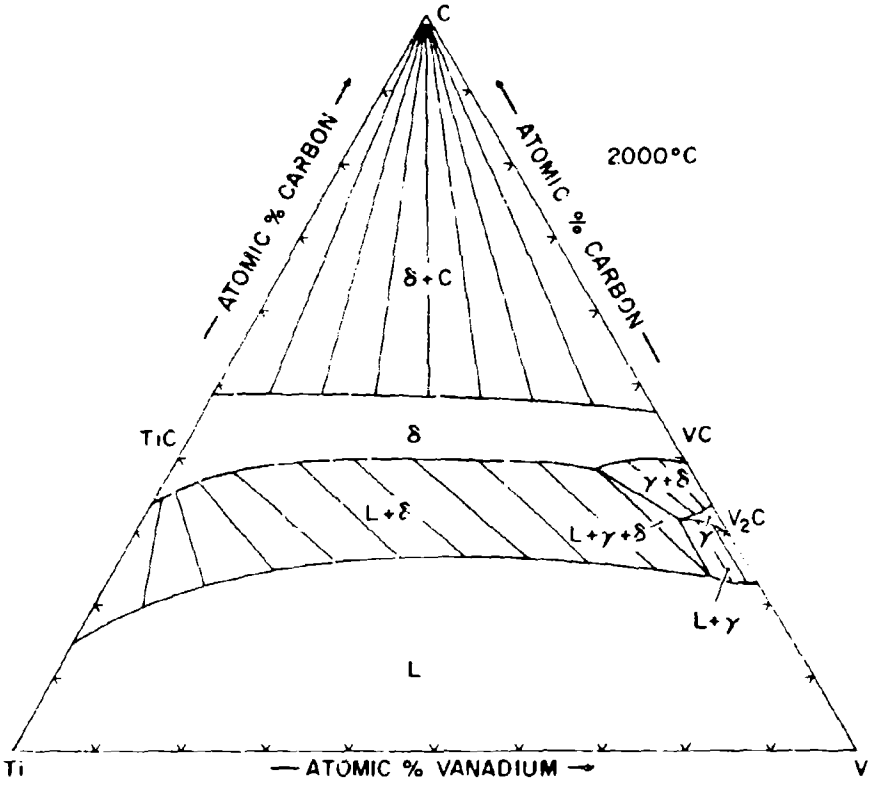

Figure III.E.3.14. Isothermal Section of the Ti-V-C System at 2000°C.

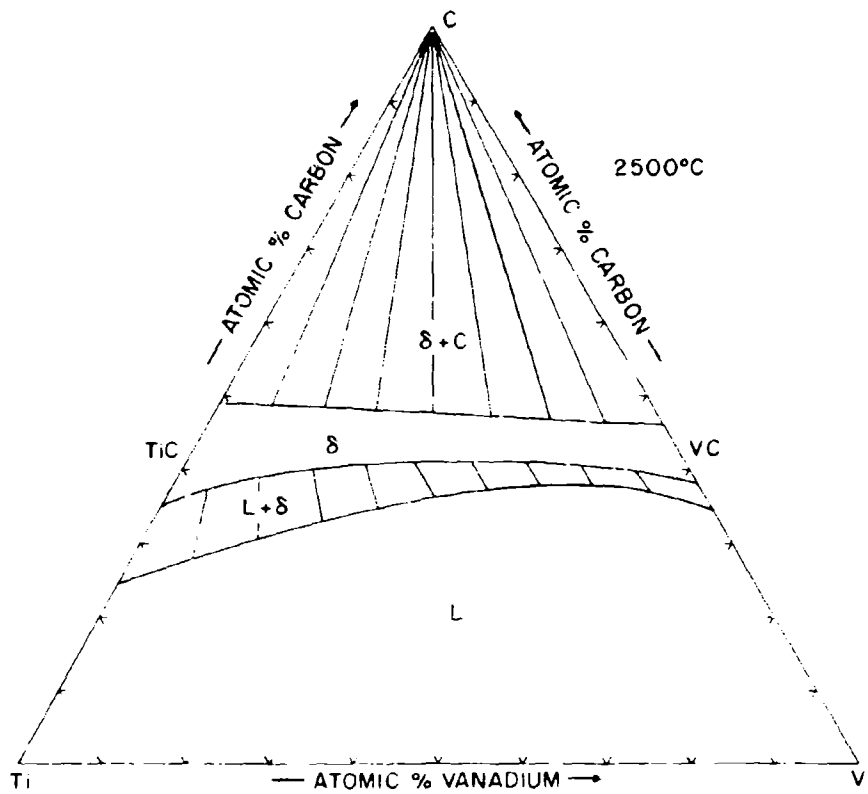

Figure III.E.3.15. Isothermal Section of the Ti-V-C System at 2500°C.

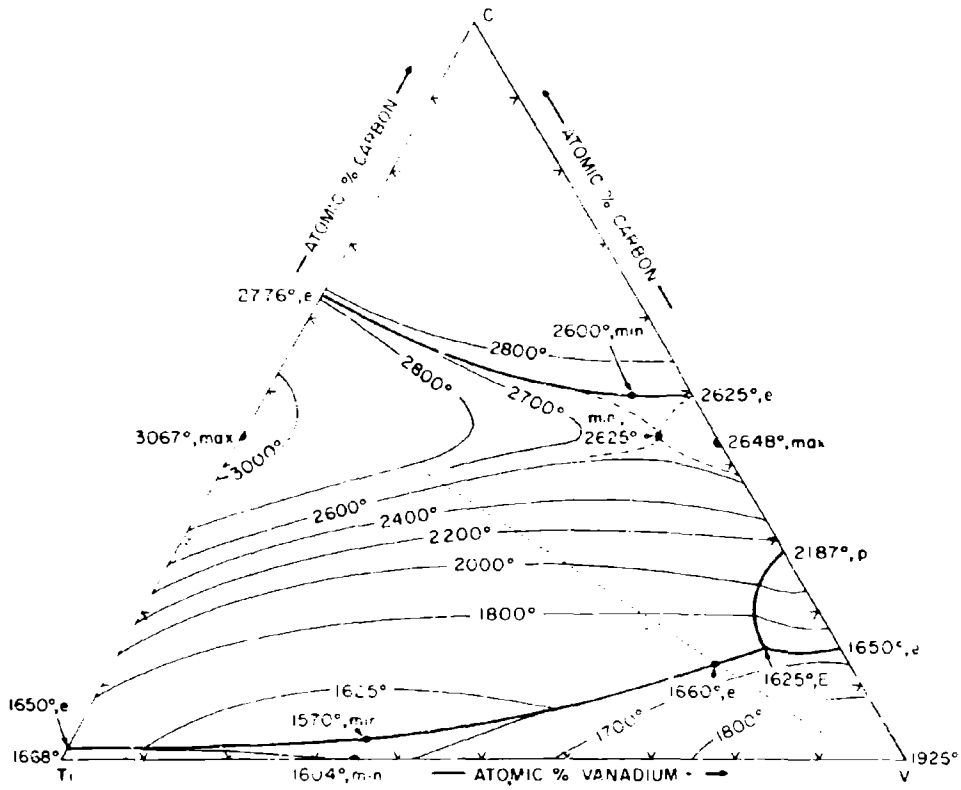

Figure III.E.3.3. Liquidus Projections in the Ti-V-C System.

Dotted: Pseudobinary Eutectic Line

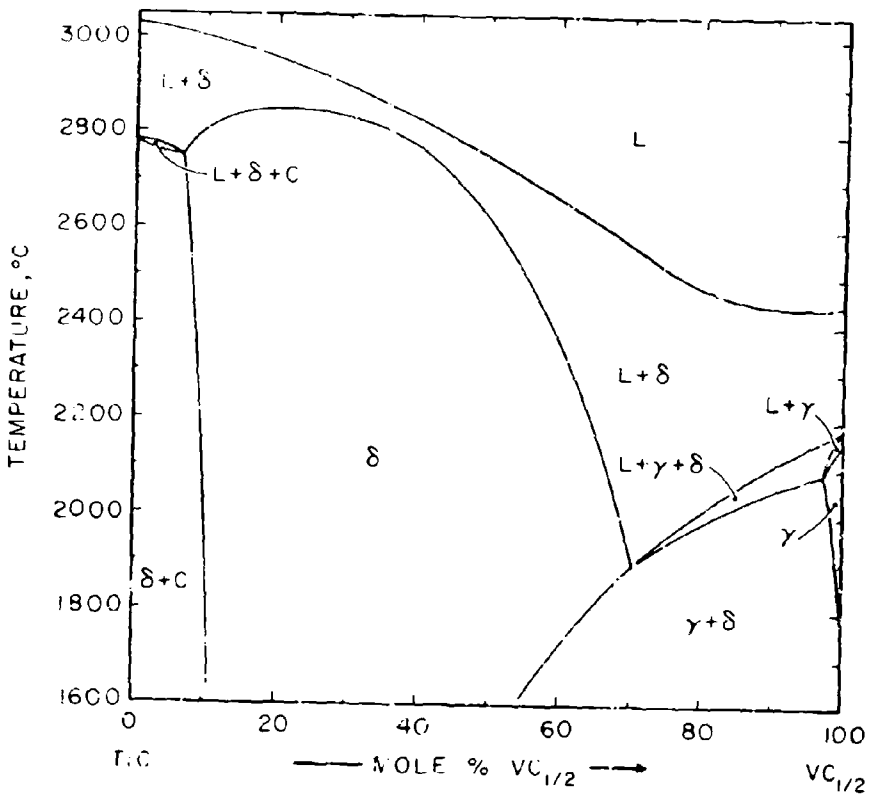

Figure III.E.3.4. Isopleth TiC-$VC_{1/2}$

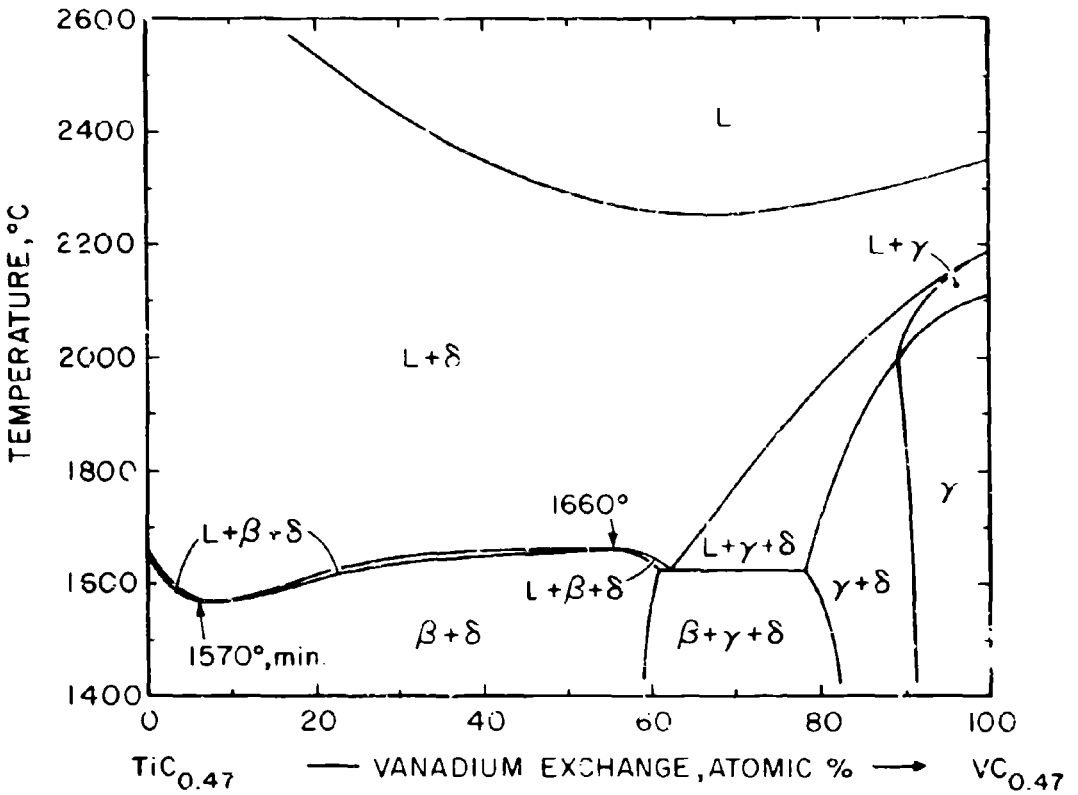

Figure III.E.3.5. Isopleth at 32 At.% C

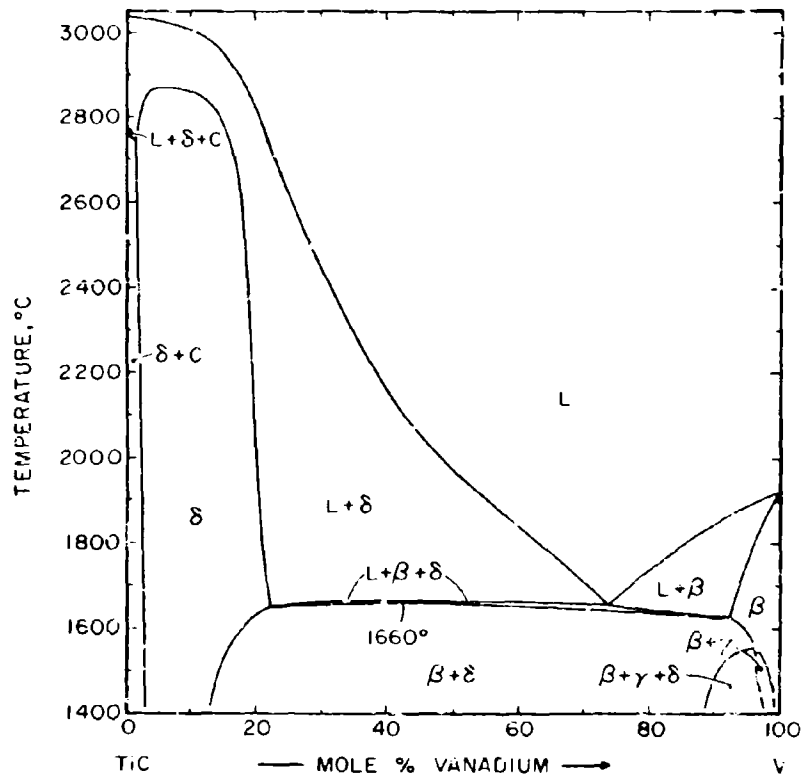

Figure III.E.3.6. Isopleth TiC-V

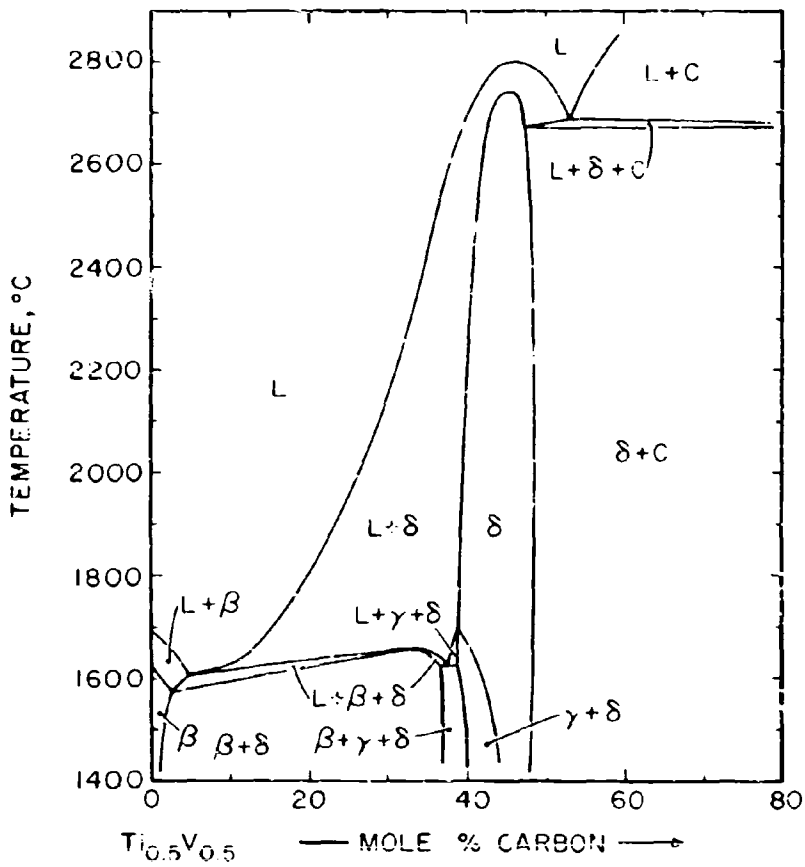

Figure III.E.3.7. Isopleth $Ti_{0.5}V_{0.5}$-C

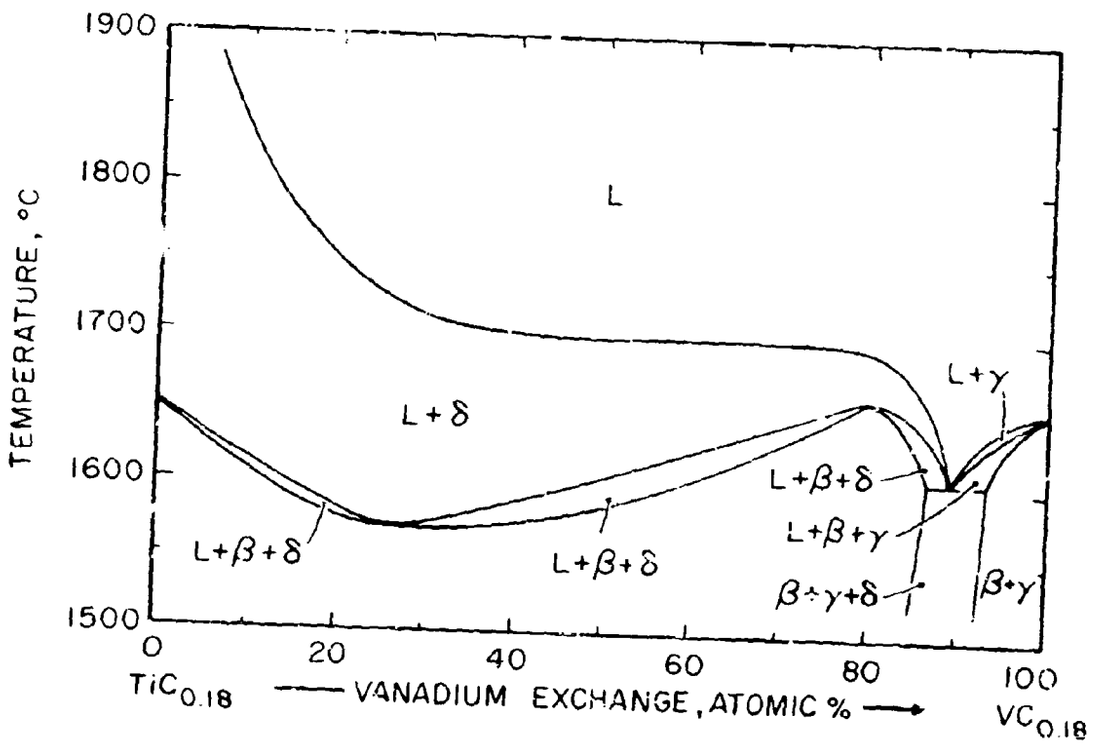

Figure III.E.3.8. Isopleth at 15 At.% C

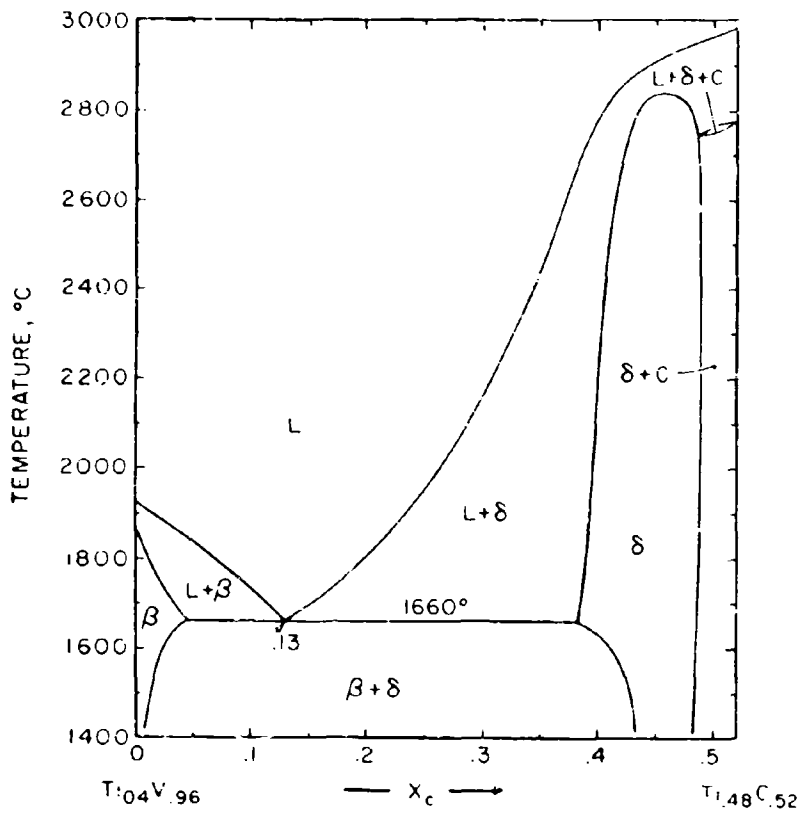

Figure III.E.3.9. Isopleth Along the Pseudobinary Section Metal + Monocarbide

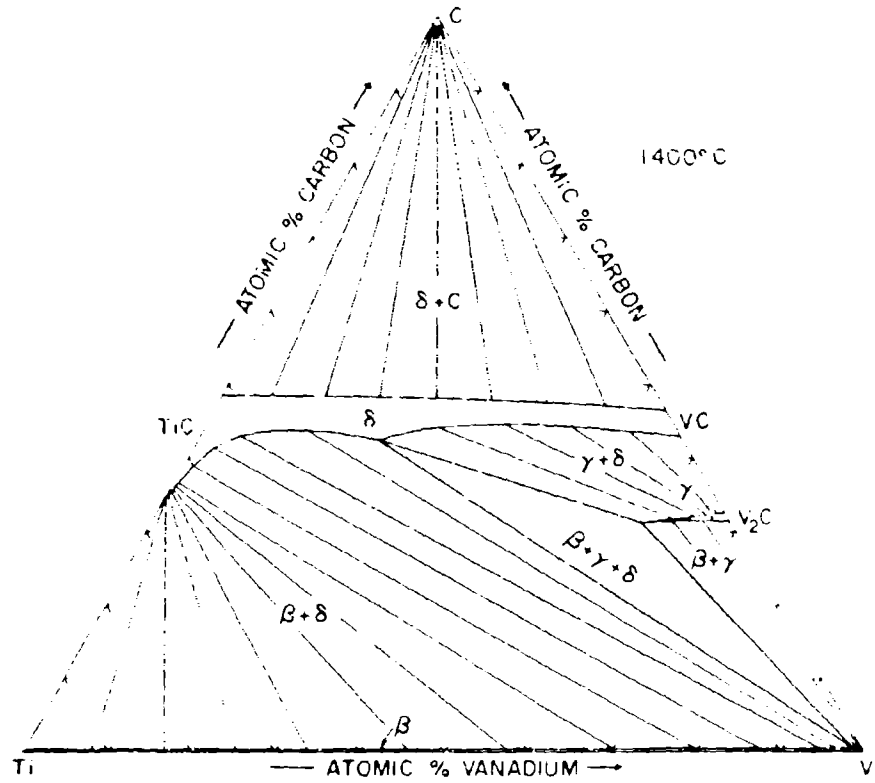

Figure III.E.3.10. Isothermal Section of the Ti-V-C System at 1400° C

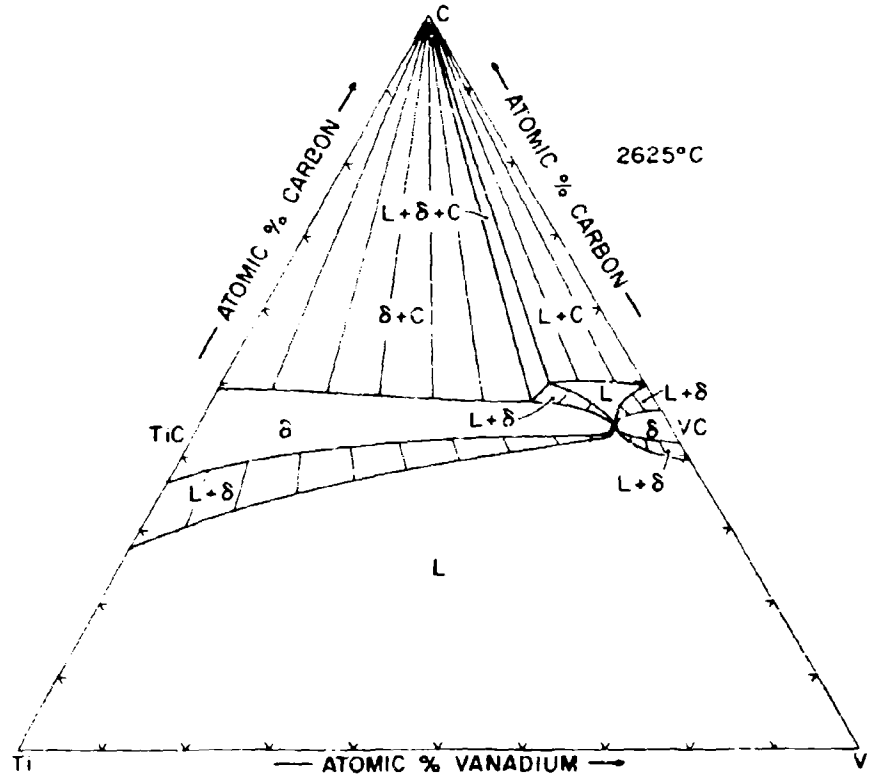

Figure III.E.3.16. Isothermal Section of the Ti-V-C System at 2625°C

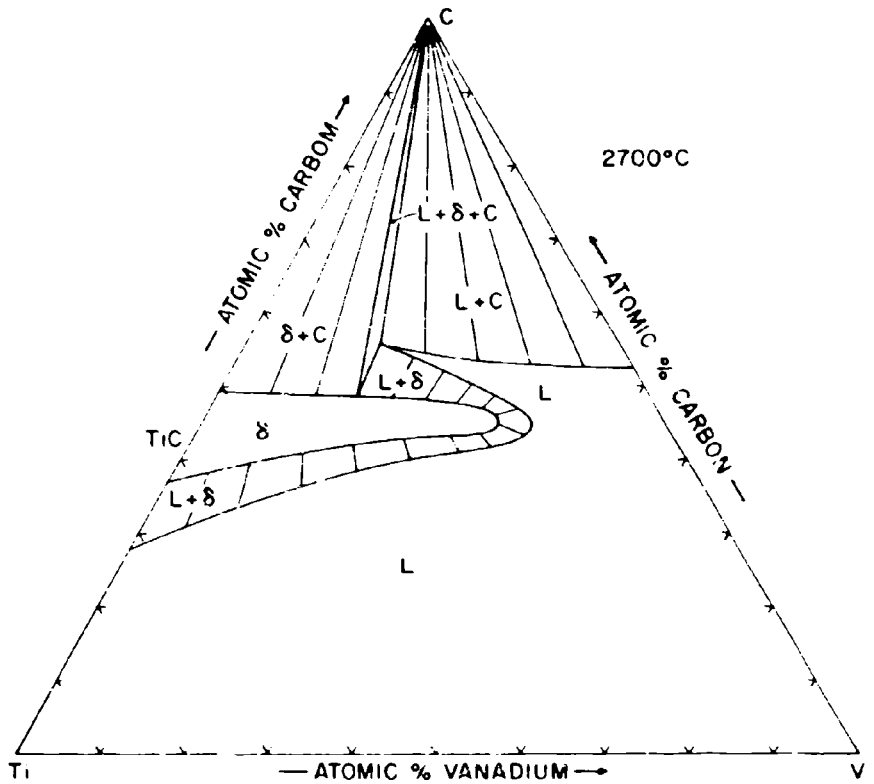

Figure III.E.3.17. Isothermal Section of the Ti-V-C System at 2700°C

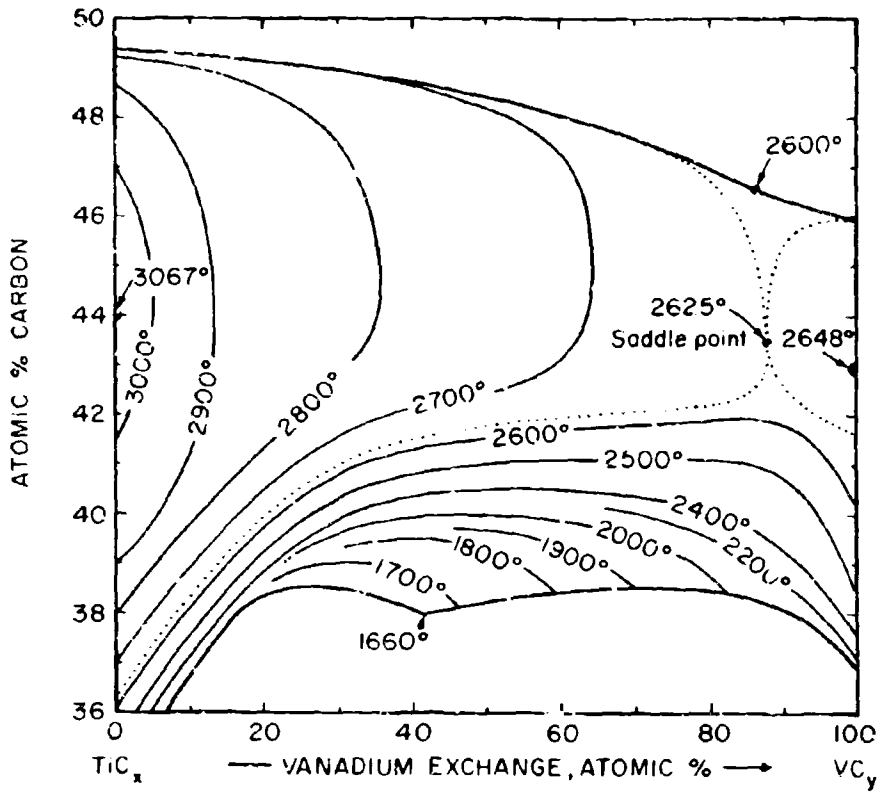

Figure III.E.3.18. Solidus Isotherms for the Monocarbide Solid Solution

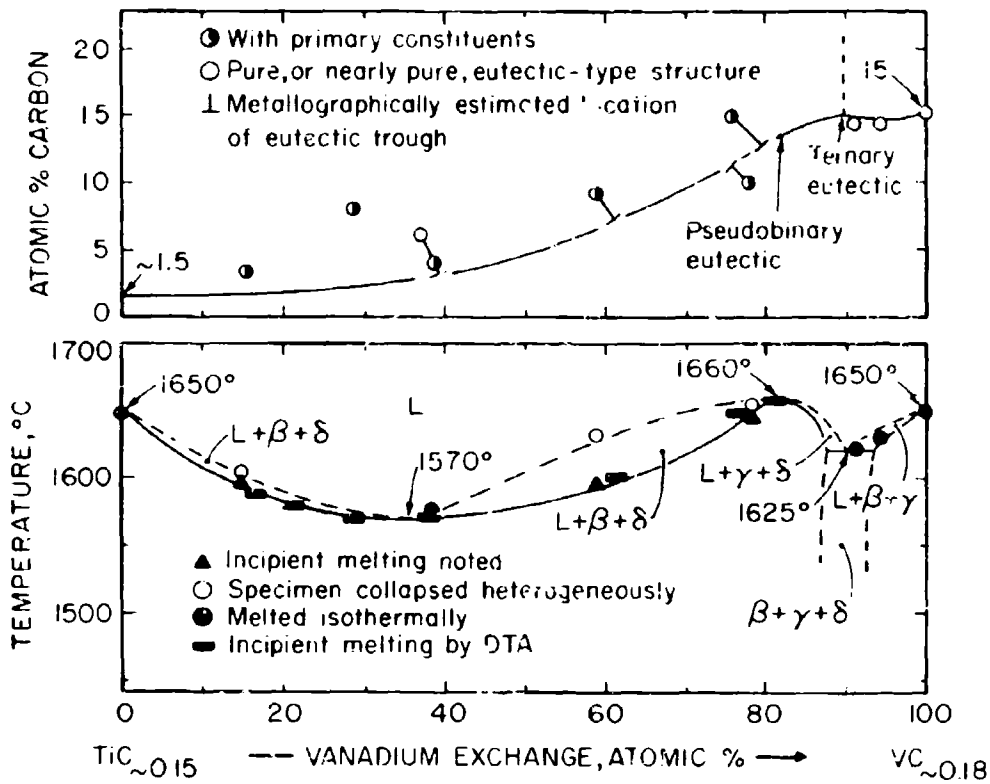

Figure III.E.3.19. Experimental Melting Temperatures in Alloys Located Along the Metal-Rich Eutectic Trough

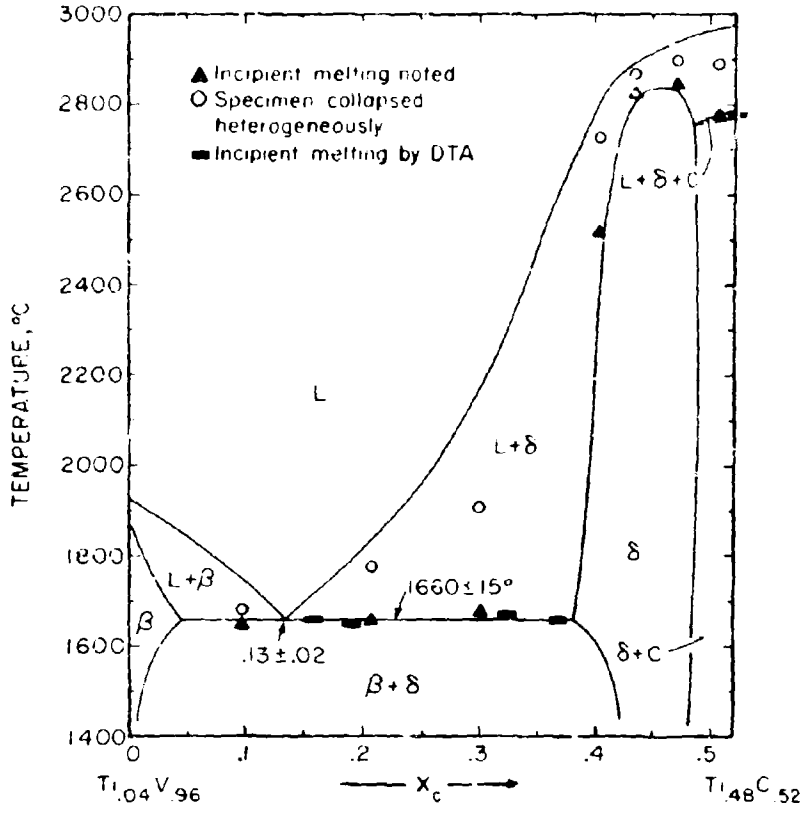

Figure III.E.3.2(. Experimental Melting Temperatures in Alloys Located at the Pseudobinary Section Metal + Monocarbide Phase

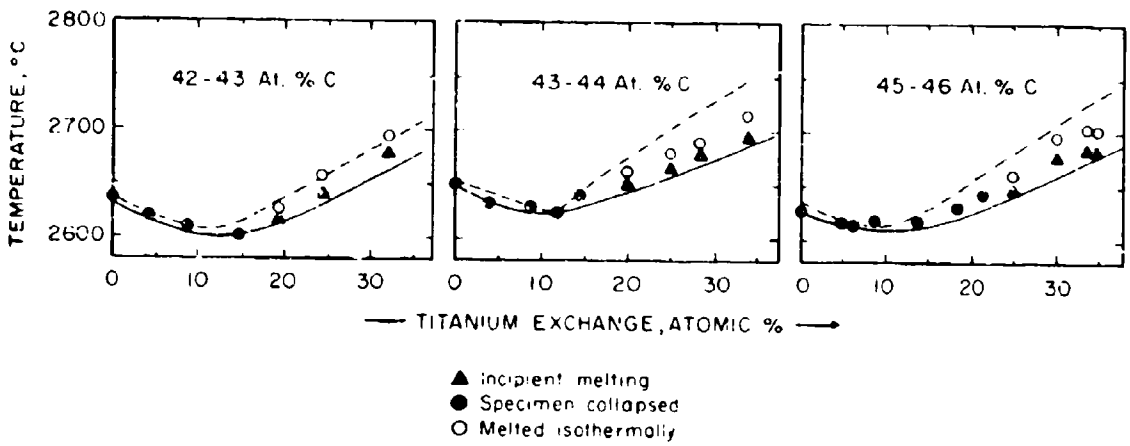

Figure III.E.3.21. Melting Temperatures of the Monocarbide Solution Near the Vanadium-Carbon Binary

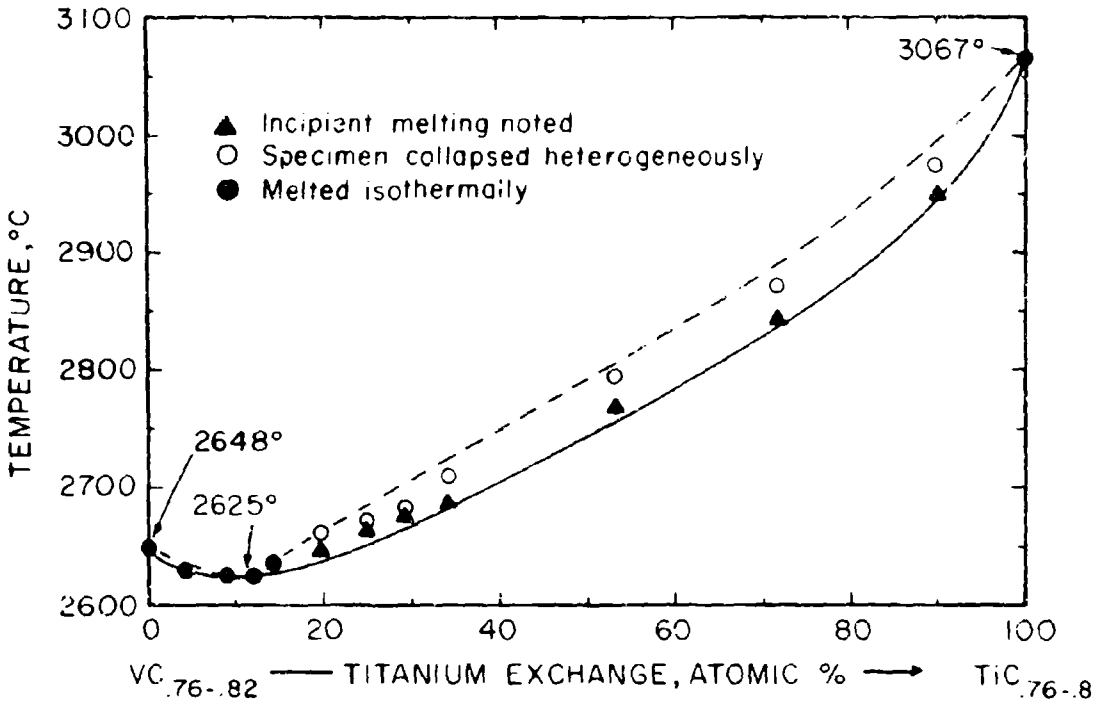

Figure III.E.3.22. Maximum Solidus Temperatures of the $(Ti,V)C_{1-x}$ (B1) Solid Solution

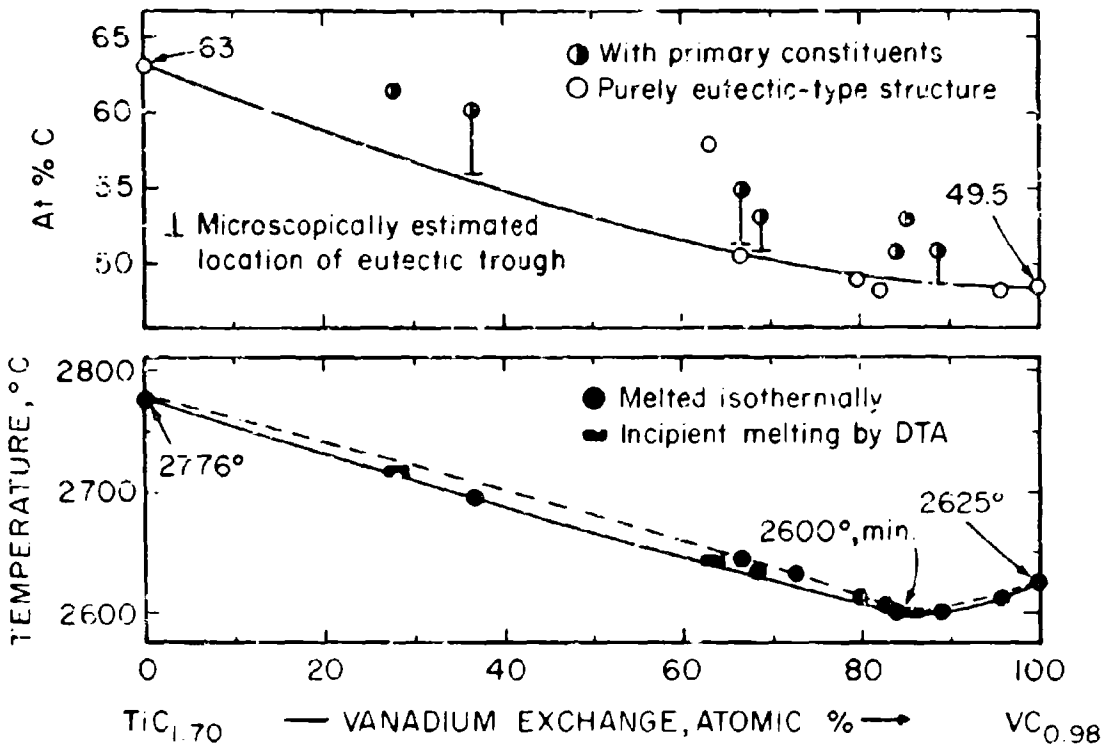

Figure III.E.3.23. Melting Along the Monocarbide + Graphite Eutectic Trough

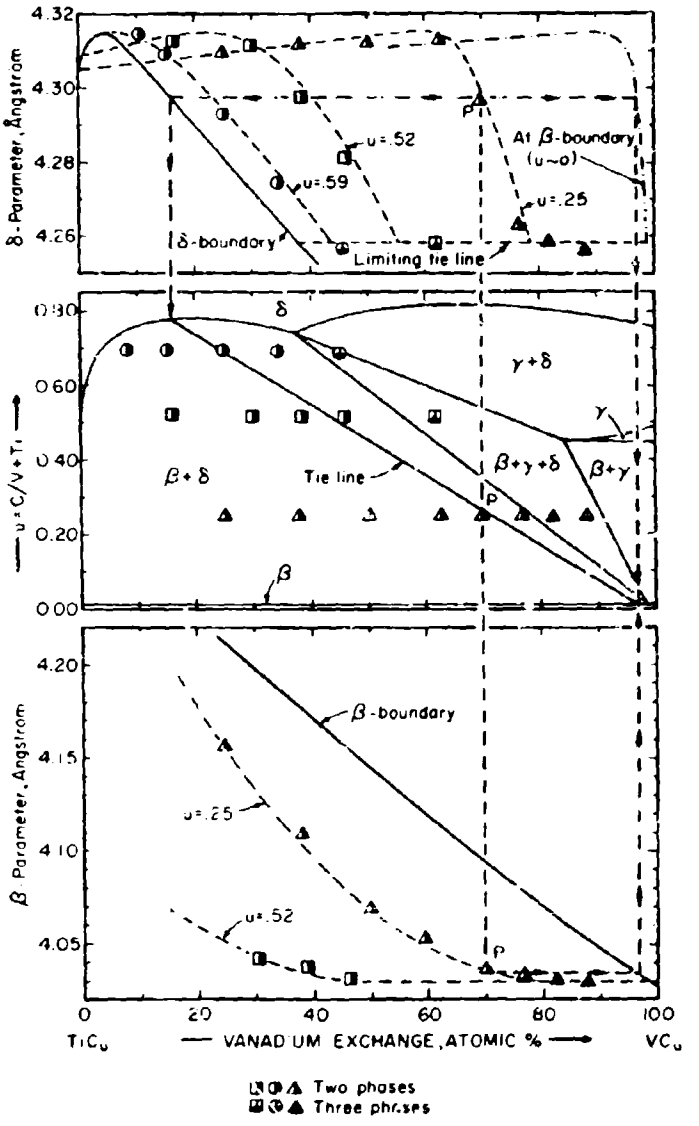

Figure III.E.3.24. Ti-V-C: Determination of the Tie Line Distribution in the Two-Phase Field β+δ by Lattice Parameter Measurements on Two-Phased, β+δ, and Three-Phased, β+γ+δ, Alloys. (Samples Equilibrated at 1400°C)

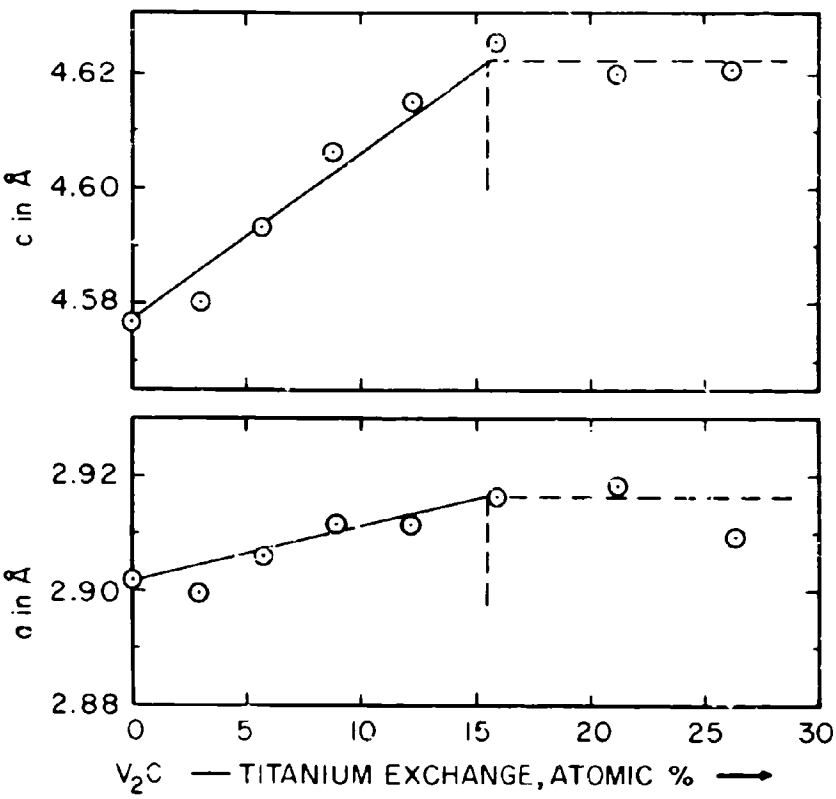

Figure III.E.3.25. Lattice Parameters of the $(Ti,V)_2C$-Phase

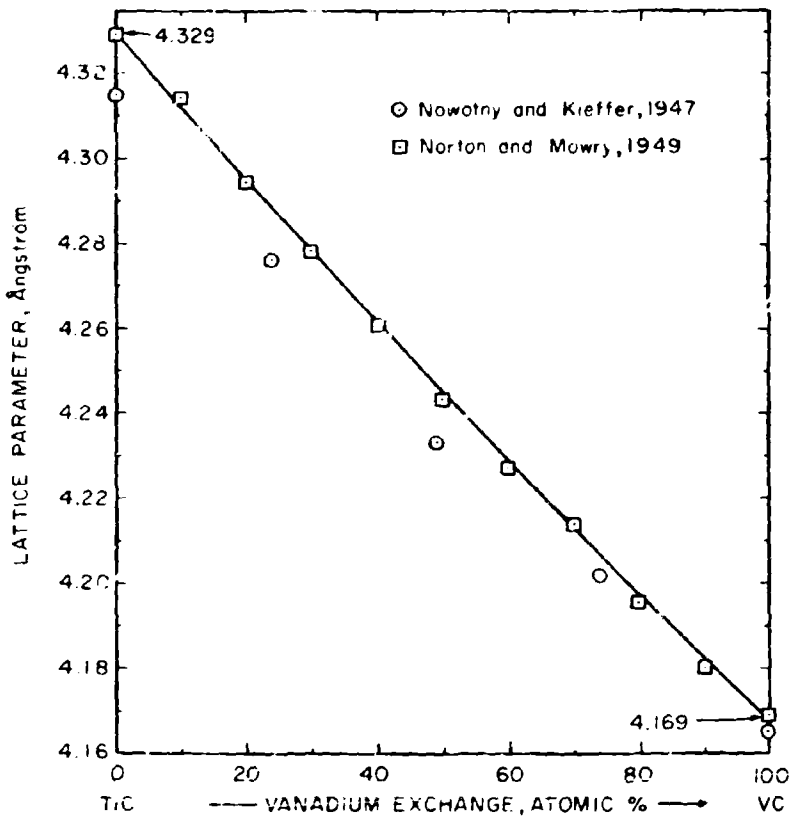

Figure III.E.3.26. Lattice Parameters of the Carbon-Saturated Monocarbide Solution (Literature Data)

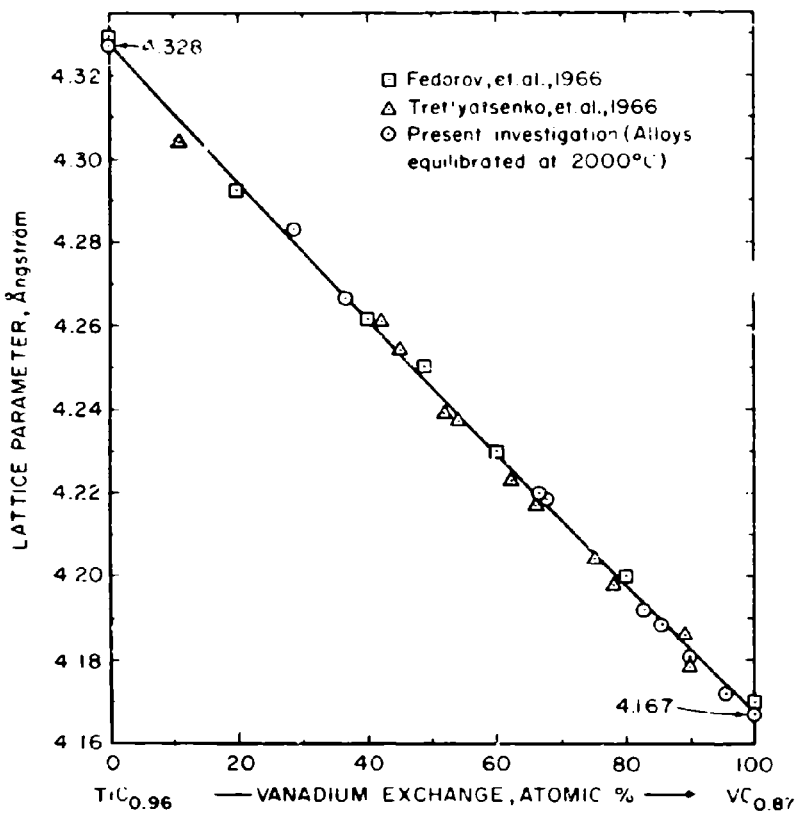

Figure III.E.3.27. Lattice Parameters of the Carbon-Saturated Monocarbide (Literature and Own Data)

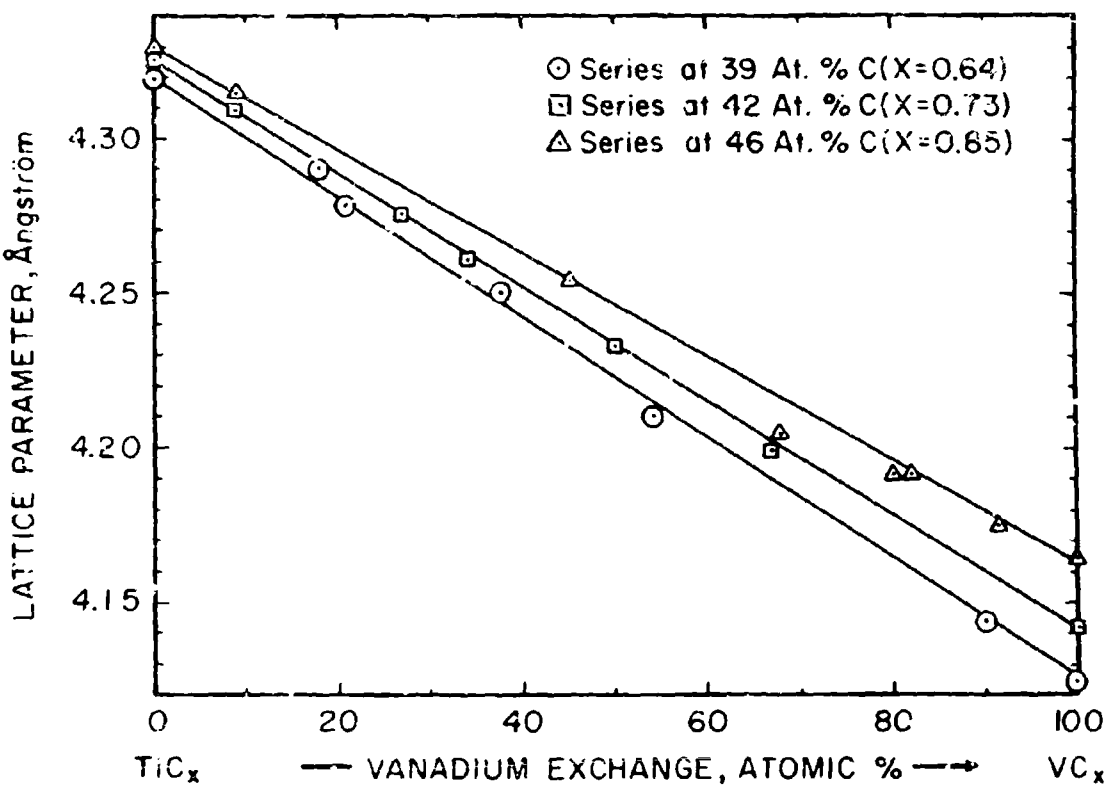

Figure III.E.3.28. Lattice Parameters of the (Ti,V)C_{1-x}(B1)-Solid Solution at Various Carbon Defects

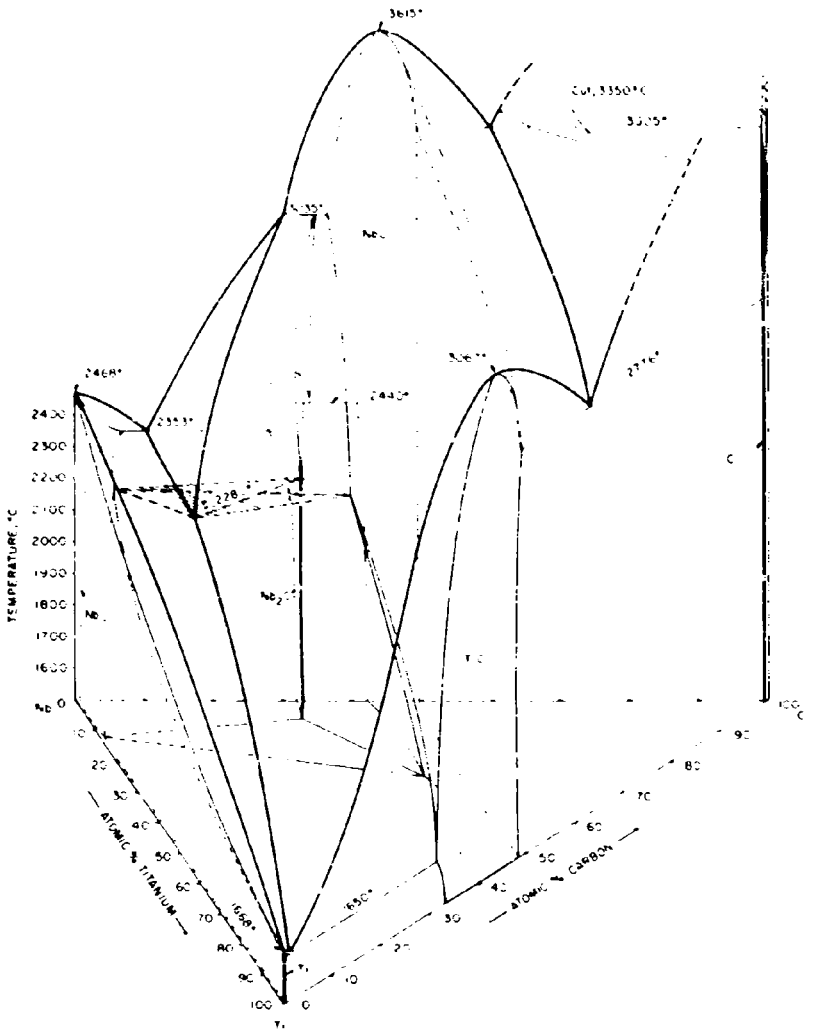

Figure III.E.4.1. Isometric View of the Ti-Nb-C System.
(Continuation of the Order-Disorder Transition in Nb_2C into the Ternary Disregarded)

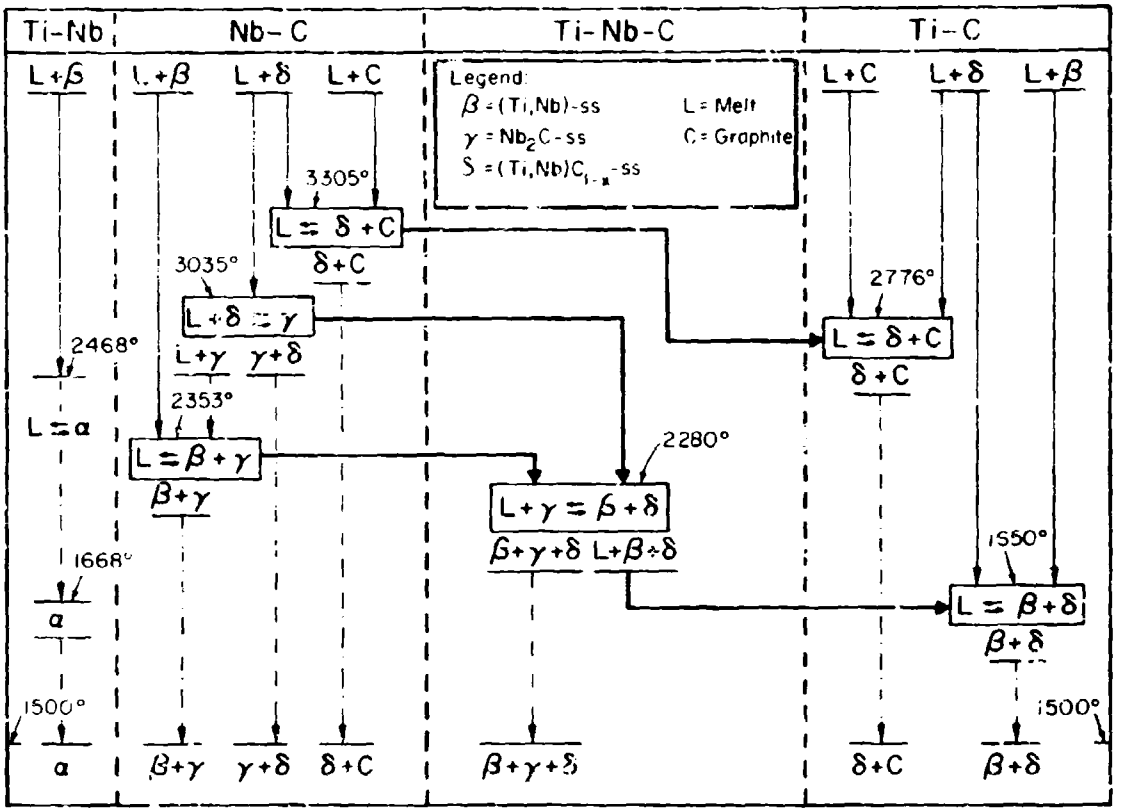

Figure III.E.4.2. Reaction Diagram for the Ti-Nb-C System

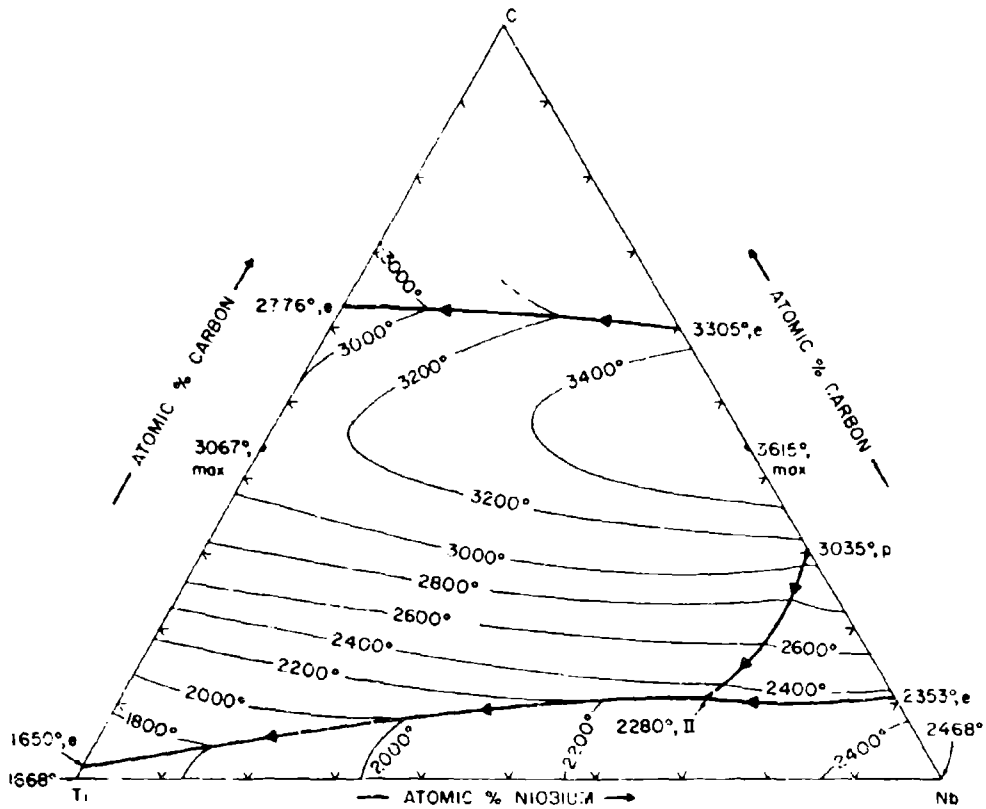

Figure III.E.4.3. Liquidus Projections in the Ti-Nb-C System

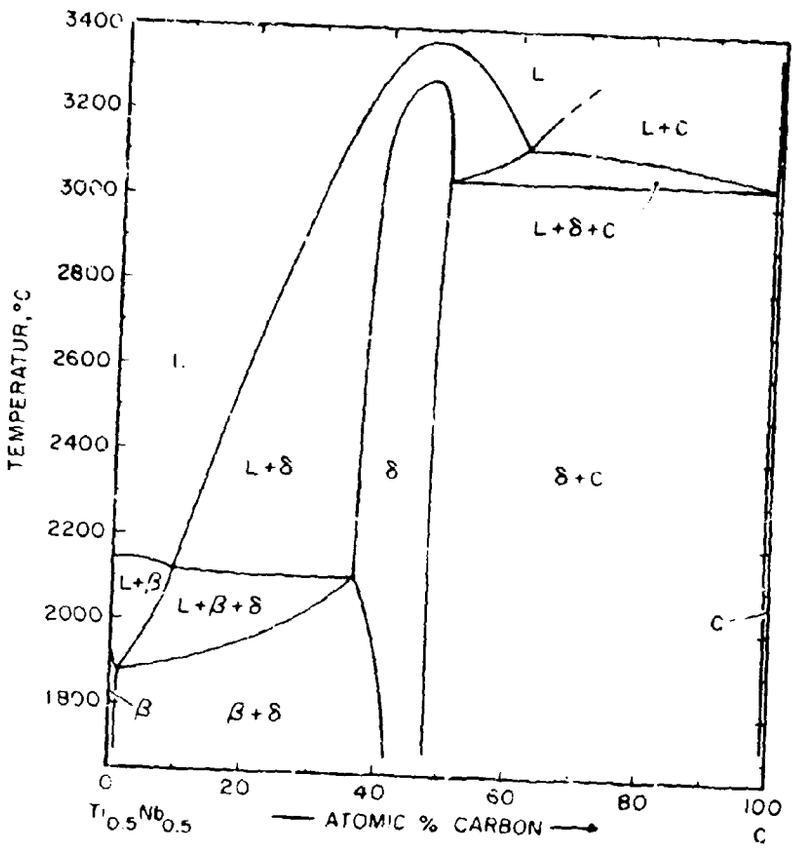

Figure III.E.4.4. Isopleth $Ti_{0.5}Nb_{0.5}$-C

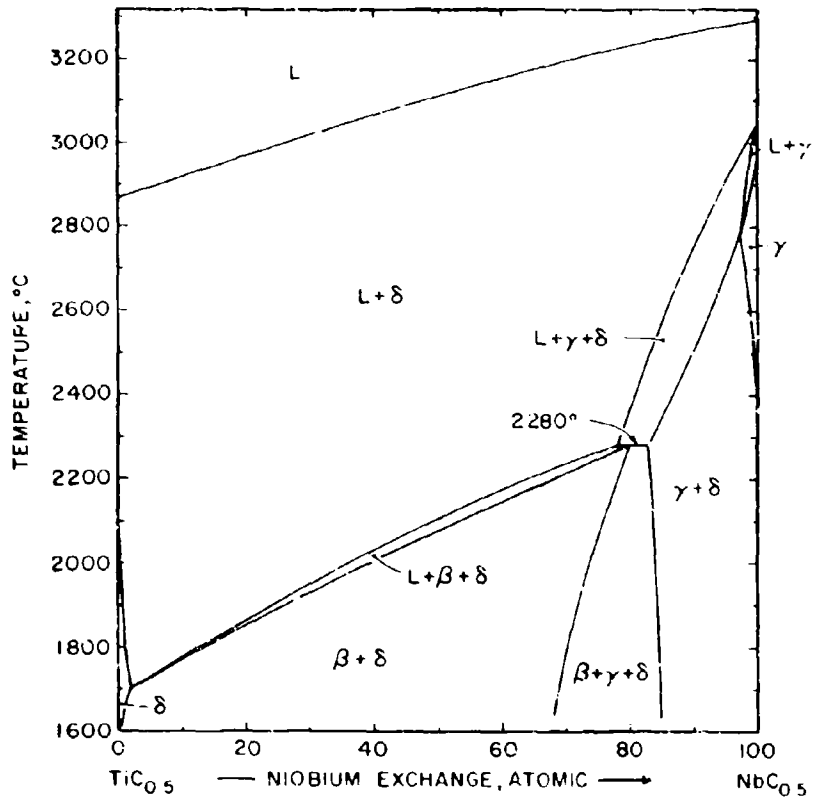

Figure III.E.4.5. Isopleth at 33.3 At.% C

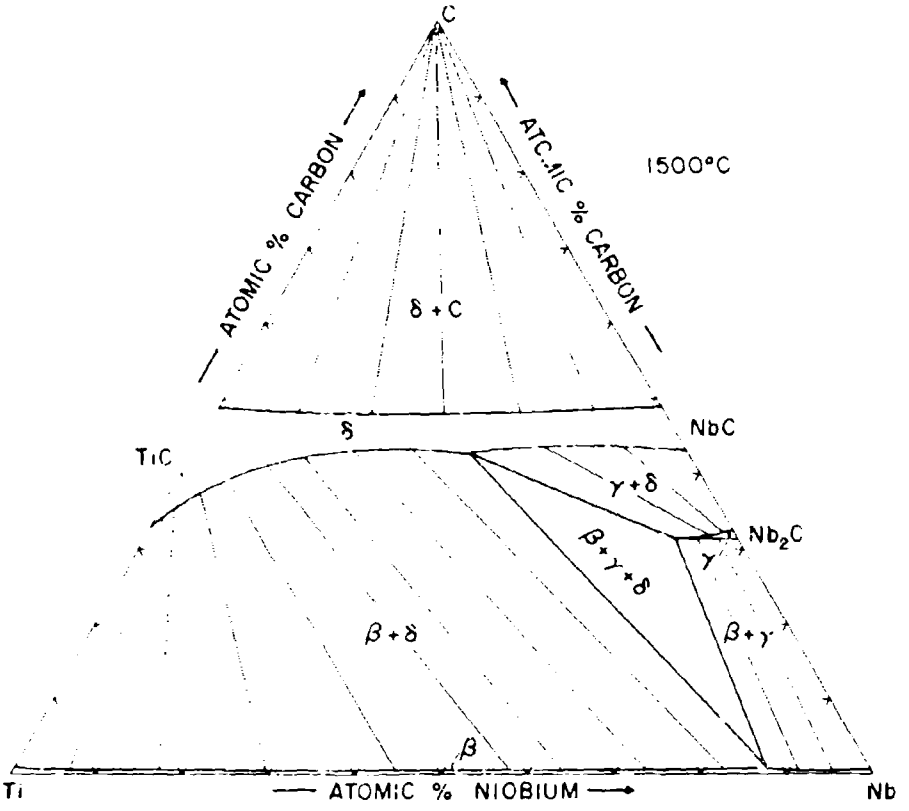

Figure III.E.4.6. Isothermal Section of the Ti-Nb-C System at 1500°C

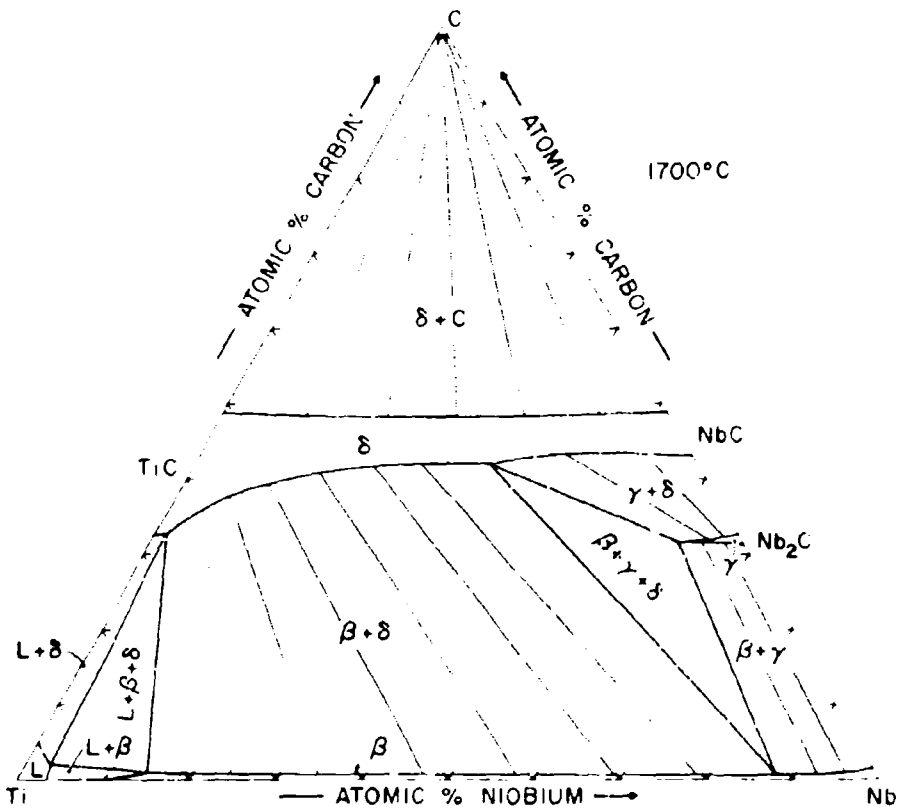

Figure III.E.4.7. Isothermal Section of the Ti-Nb-C System at 1700° C

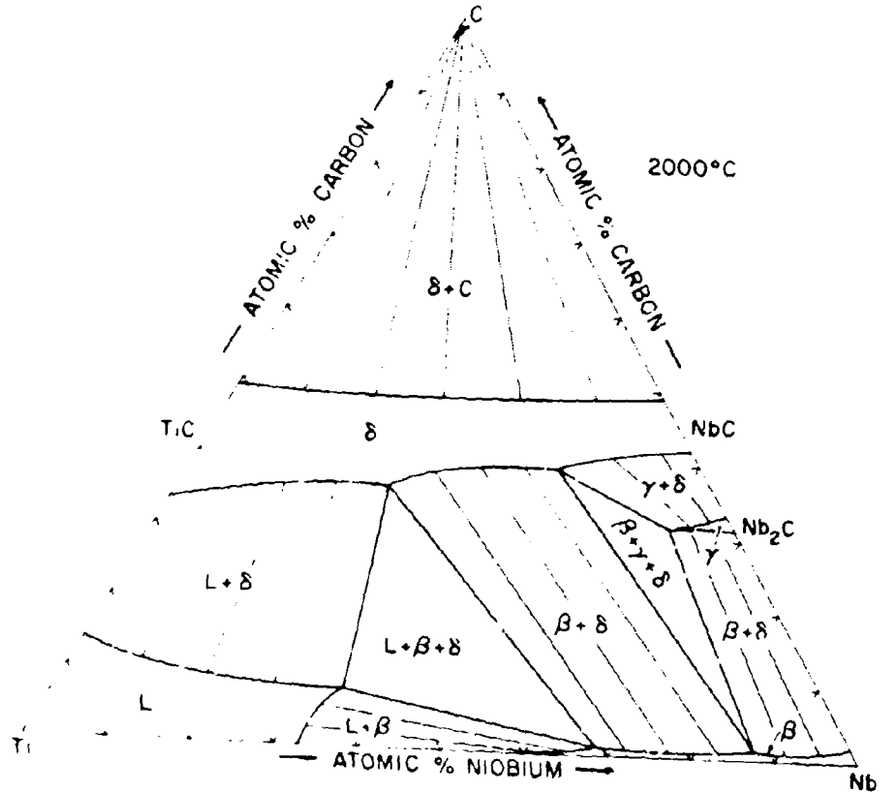

Figure III.E.4.8. Isothermal Section of the Ti-Nb-C System at 2000°C

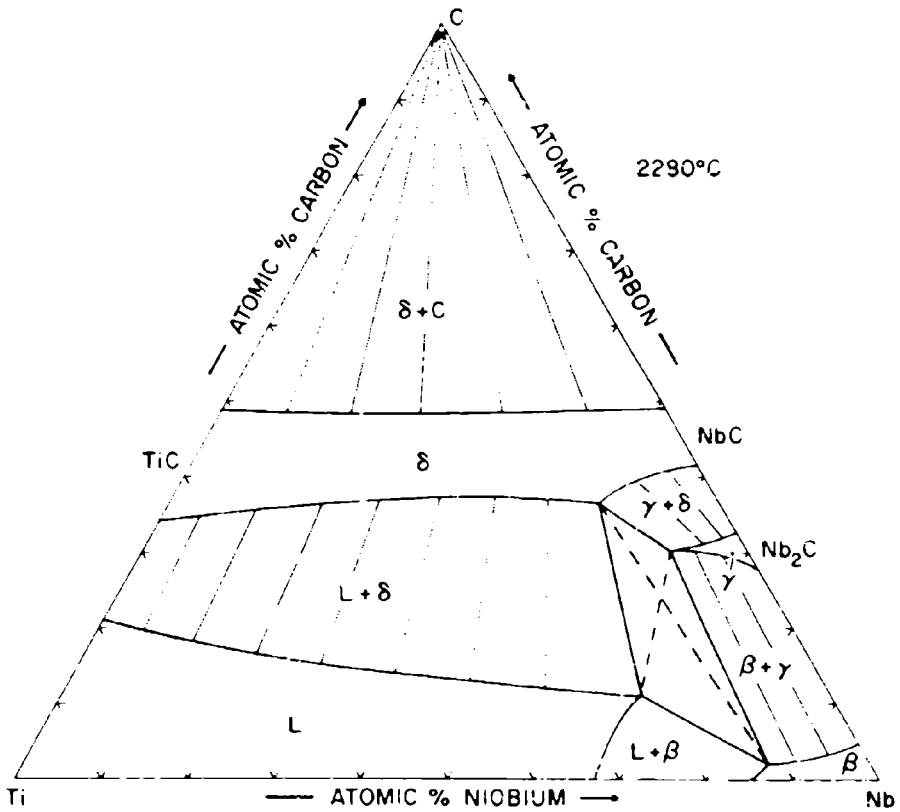

Figure III.E.4.9. Isothermal Section of the Ti-Nb-C System at 2280° C

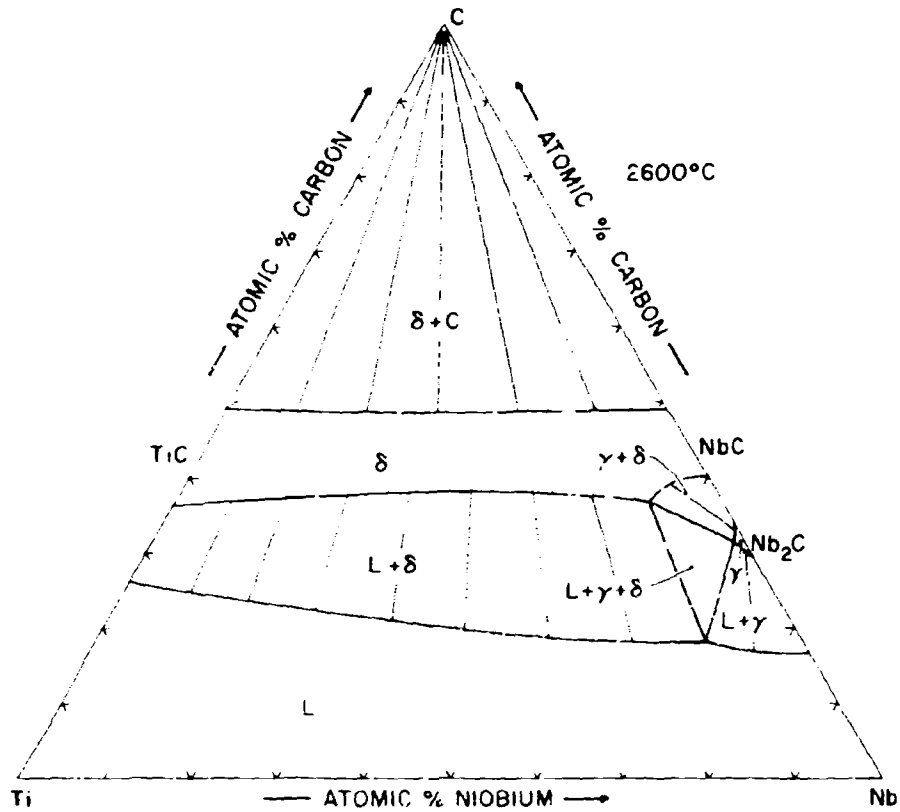

Figure III.E.4.10. Isothermal Section of the Ti-Nb-C System at 2600° C

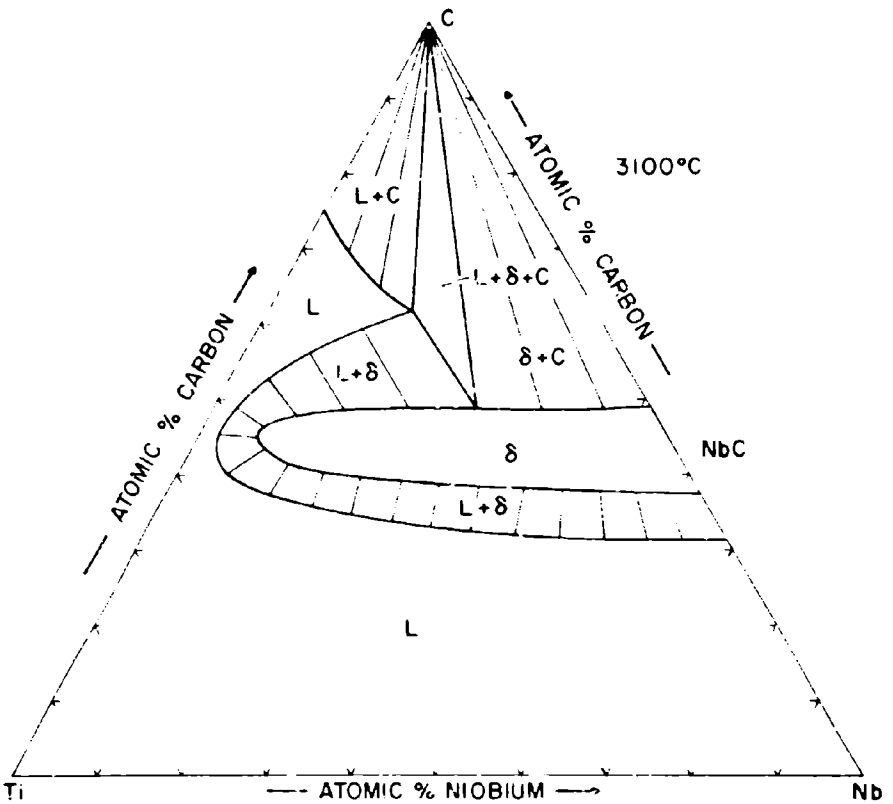

Figure III.E.4.11. Isothermal Section of the Ti-Nb-C System at 3100°C

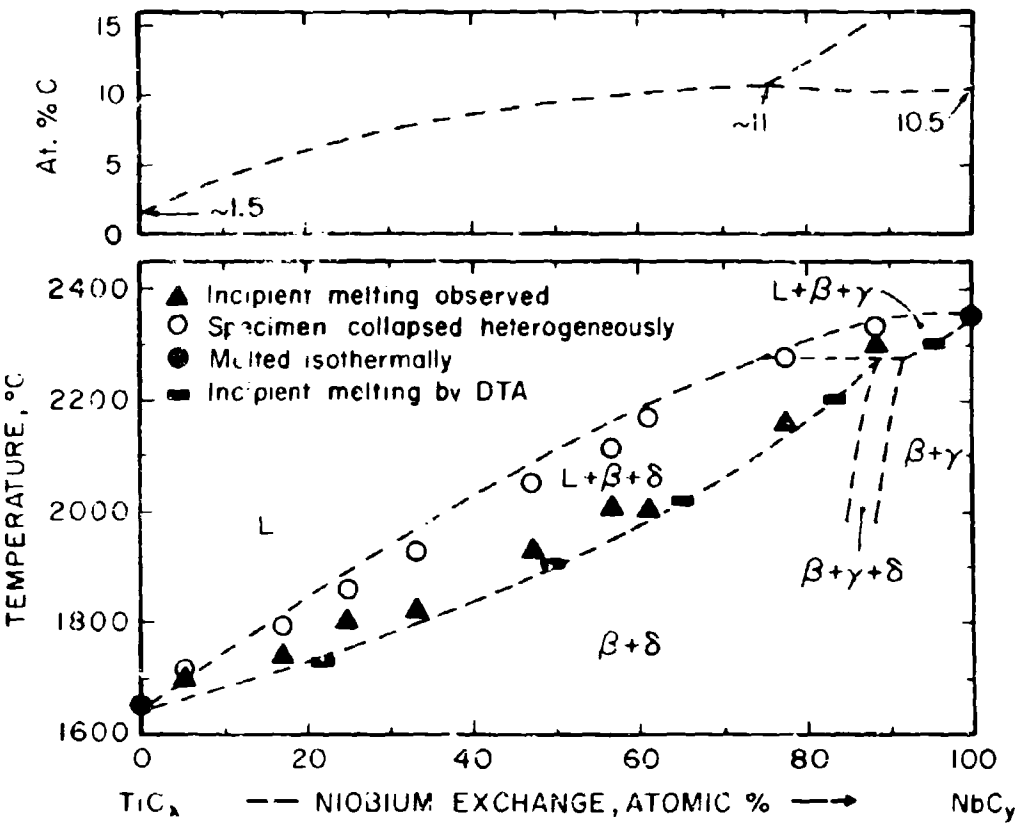

Figure III.E.4.12. Observed Melting Temperatures in Alloys Located Along the Metal-Rich Eutectic Trough

(Top: Microscopically estimated location of eutectic trough)

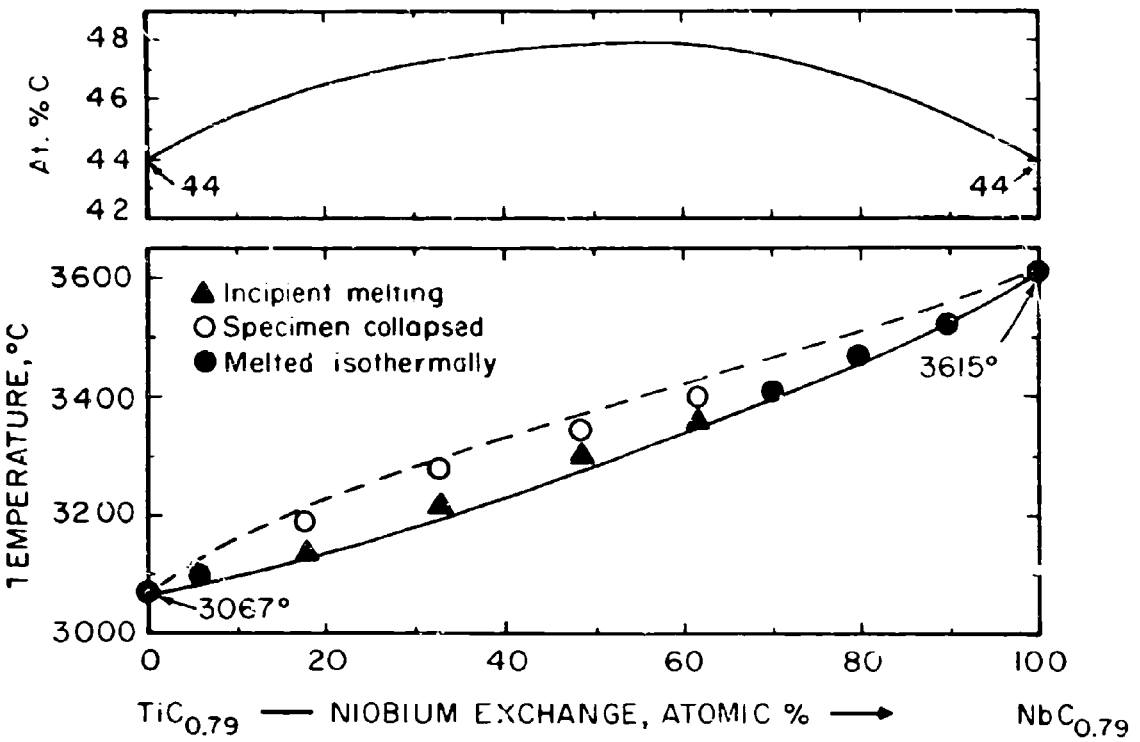

Figure III.E.4.13. Maximum Solidus Temperatures With Composition Line (Top) for the $(Ti,Nb)C_{1-x}$ (B1) Solid Solution

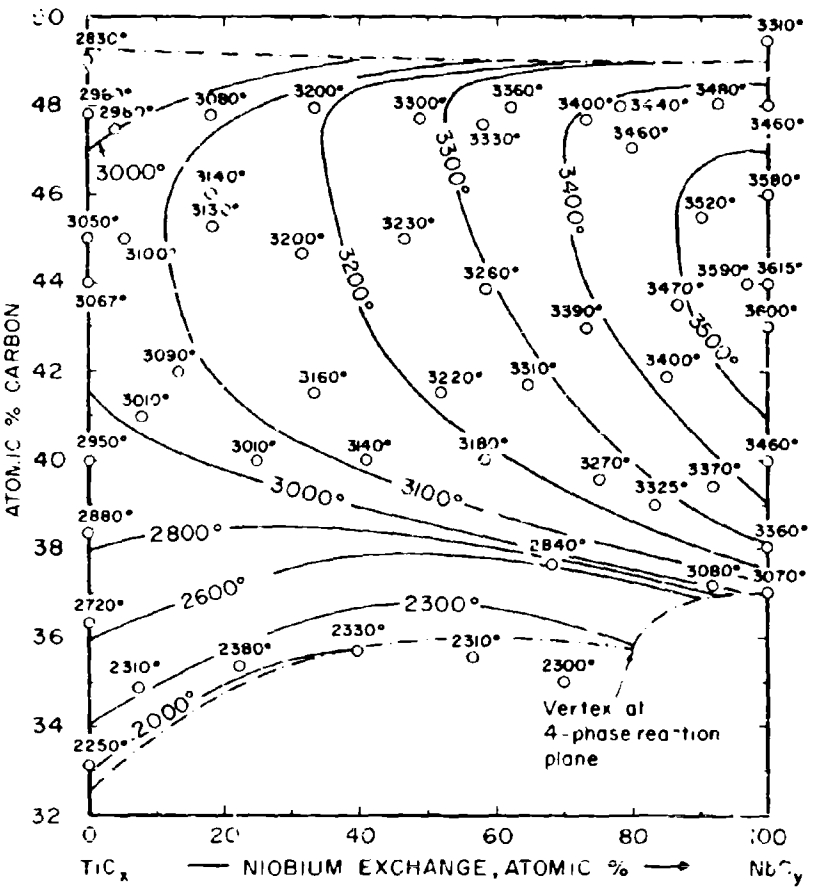

Figure III.E.4.14. Solidus Isotherms for the Monocarbide Solid Solution

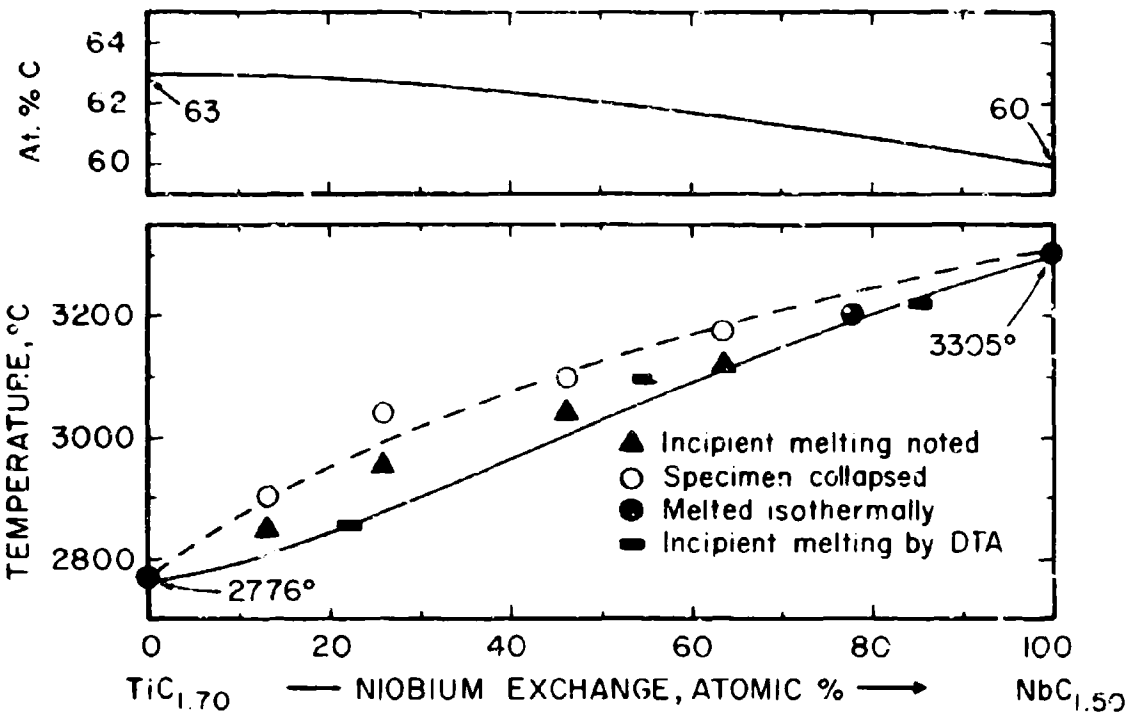

Figure III.E.4.15. Experimental Melting Temperatures Along the Monocarbide + Graphite Eutectic Trough.

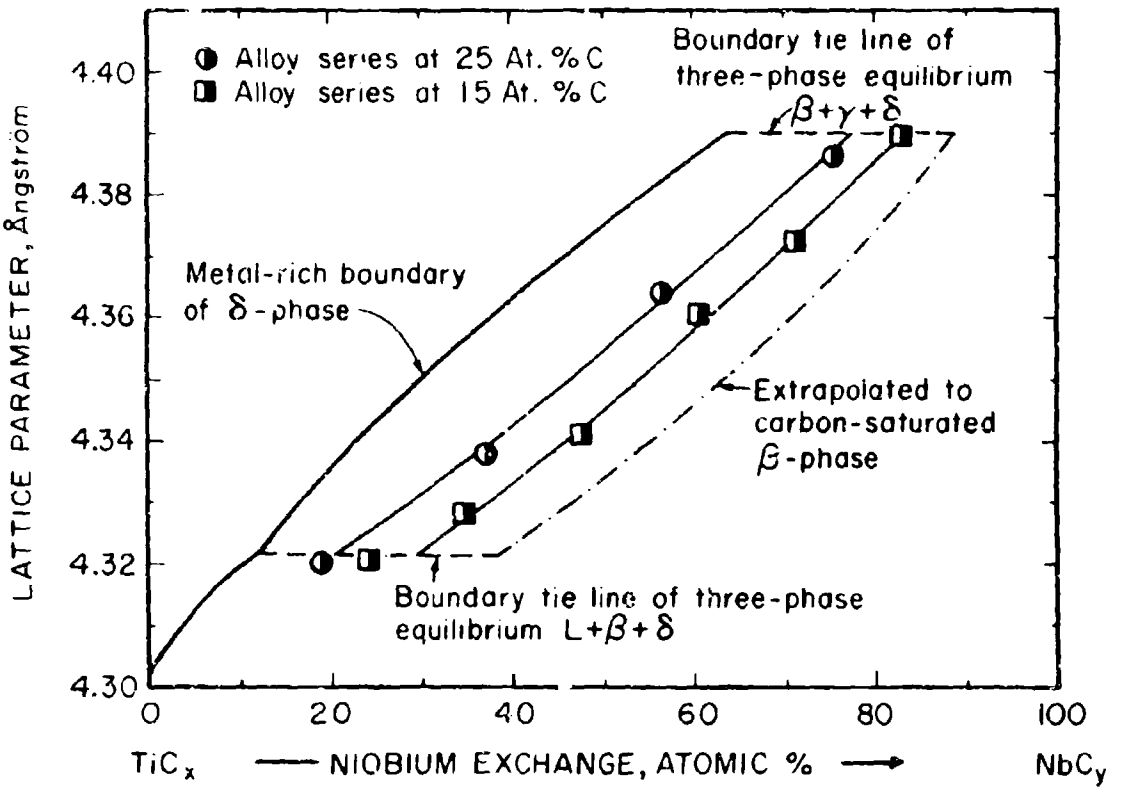

Figure III.E.4.16. Determination of the Tie Line Distribution in the Two-Phase Field β+δ by Monocarbide Lattice Parameter Measurements in Two-Phased, β+δ, Alloys.

(Alloys equilibrated at 1800° C)

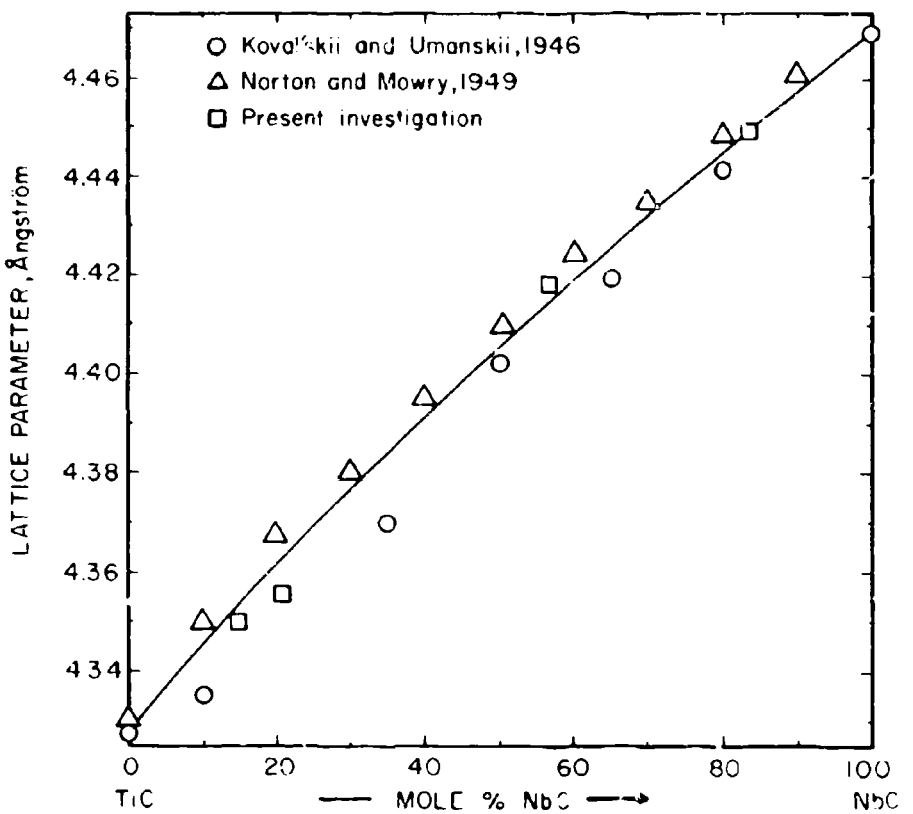

Figure III.E.4.17. Lattice Parameters of the Carbon-Saturated Monocarbide Phase (Literature and Own Data)

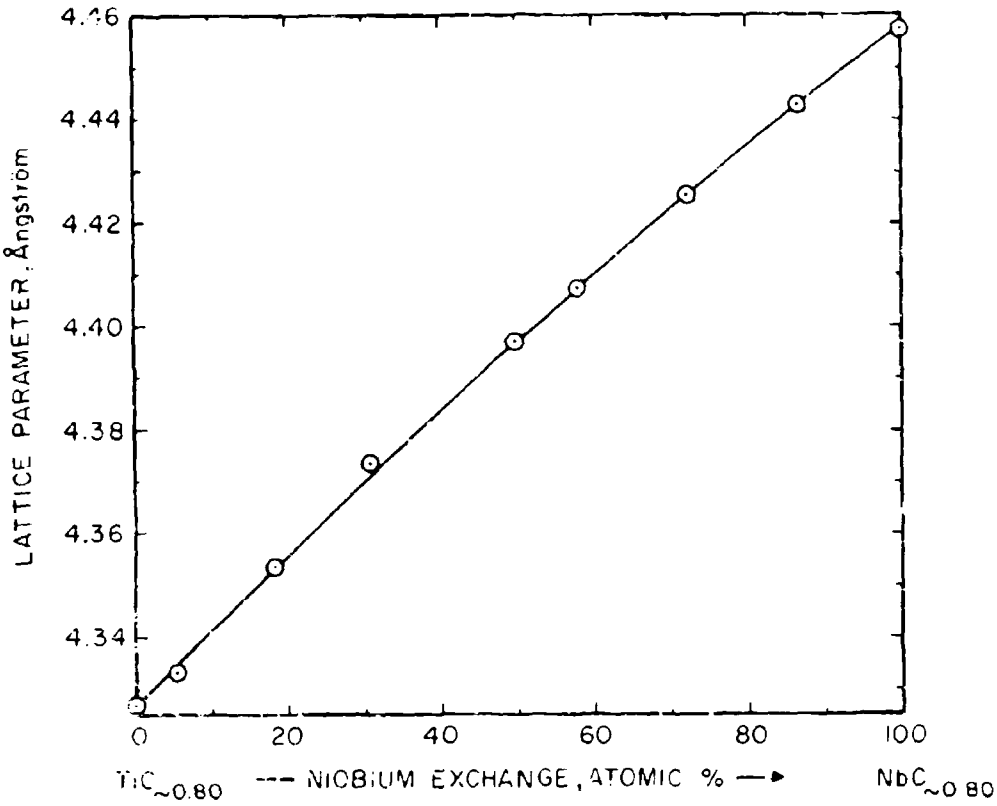

Figure III.E.4.18. Lattice Parameters of the Monocarbide Solution at 44 At.% C

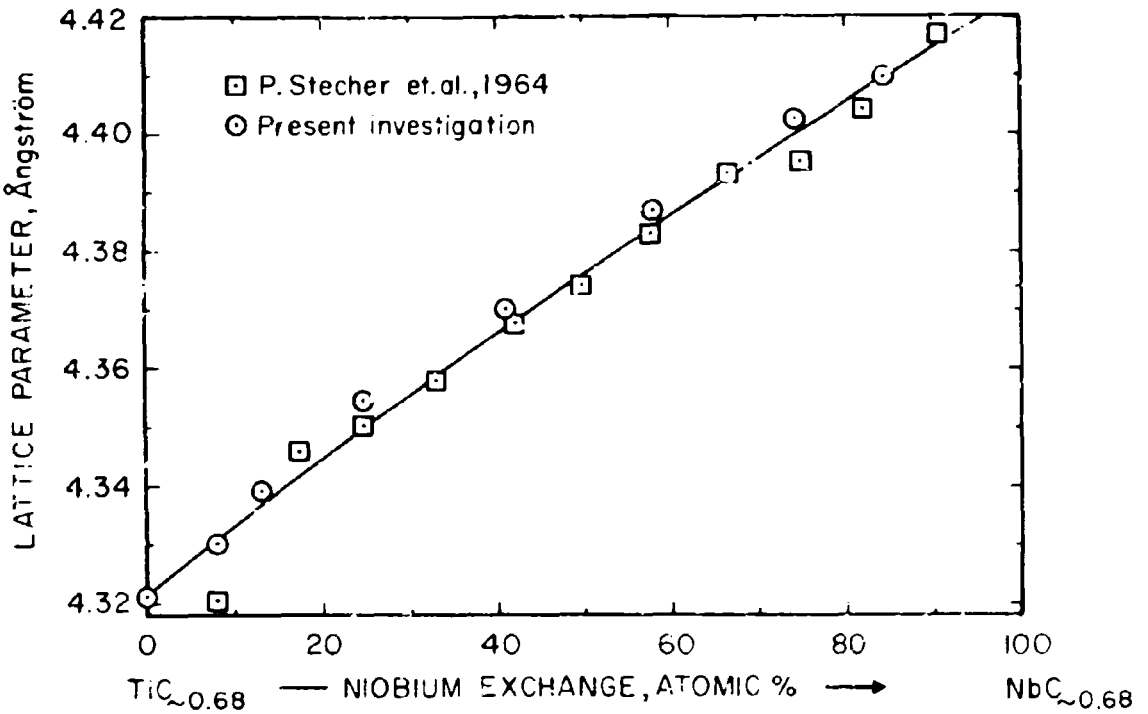

Figure III.E.4.19. Lattice Parameters of the Monocarbide Solution at 40 At.% C.

(Literature and Own Data)

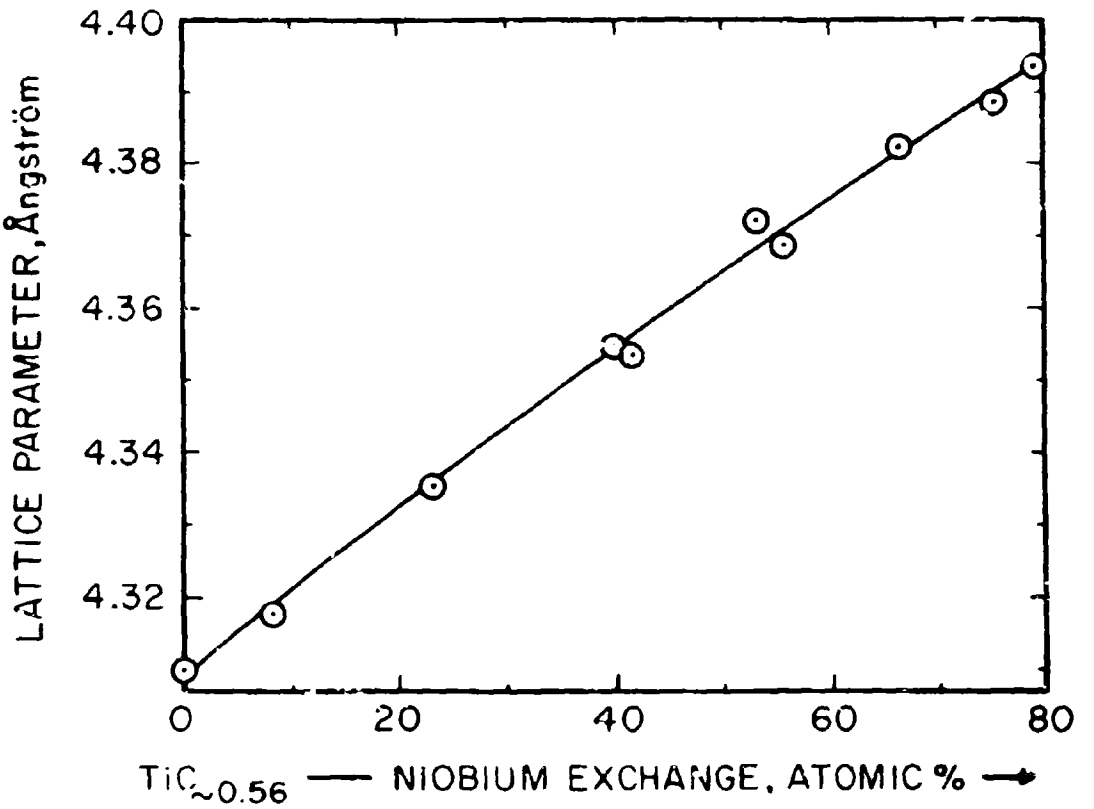

Figure III.E.4.20. Lattice Parameters of the Monocarbide Solution at 36 At.% C

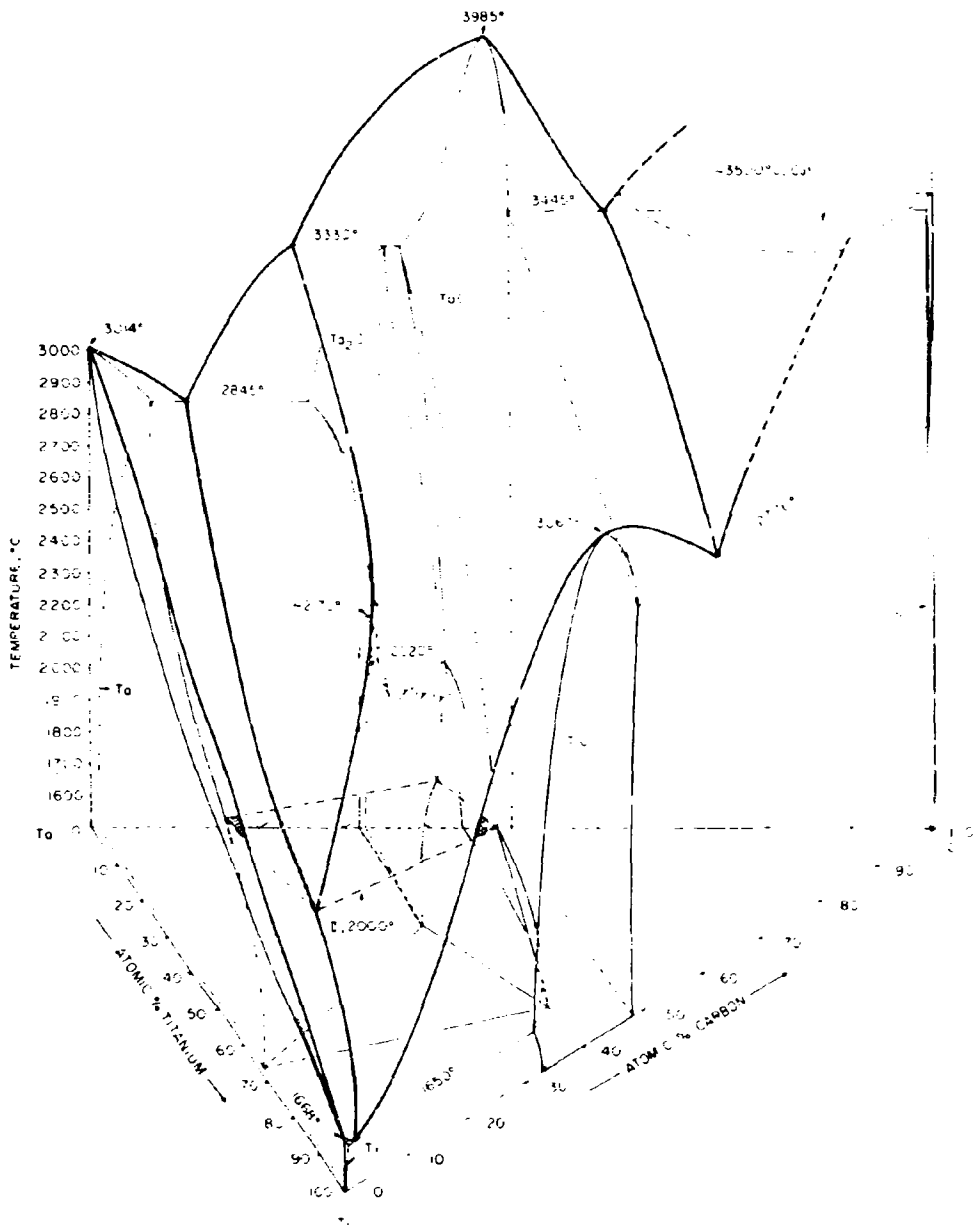

Figure III.E.5.1. Isometric View of the Ti-Ta-C System

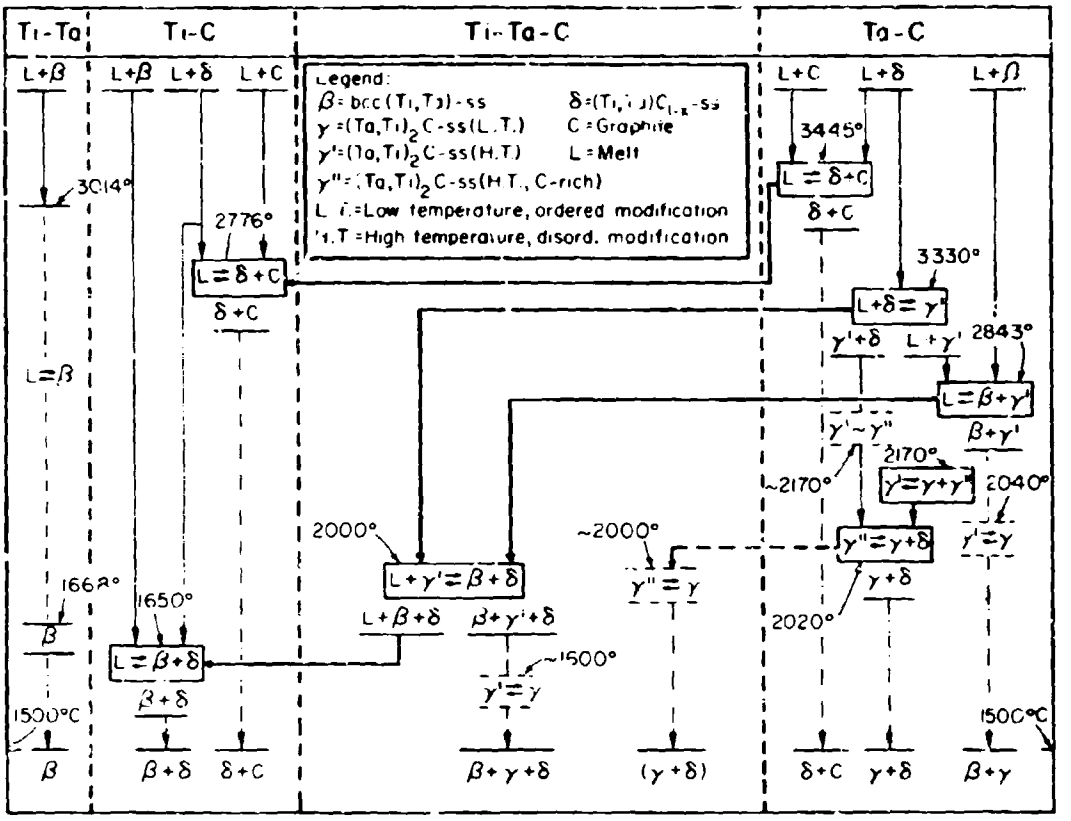

Figure III.E.5.2. Reaction Diagram for the Ti-Ta-C System

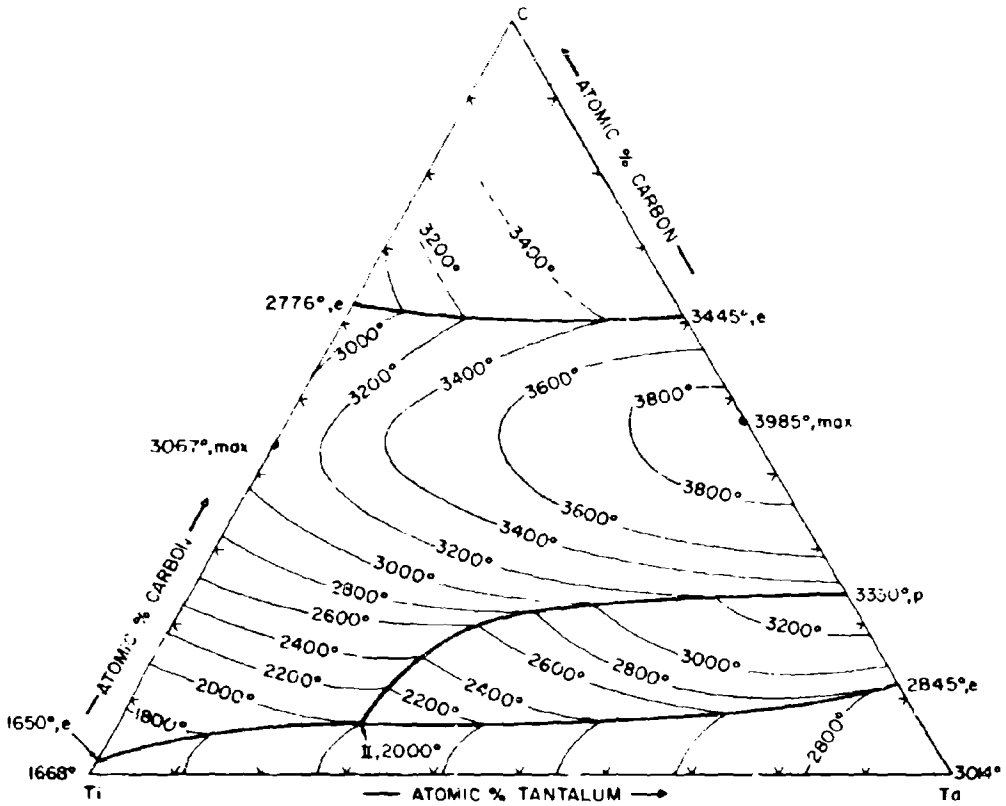

Figure III.E.5.3. Liquidus Projections in the Ti-Ta-C Systems

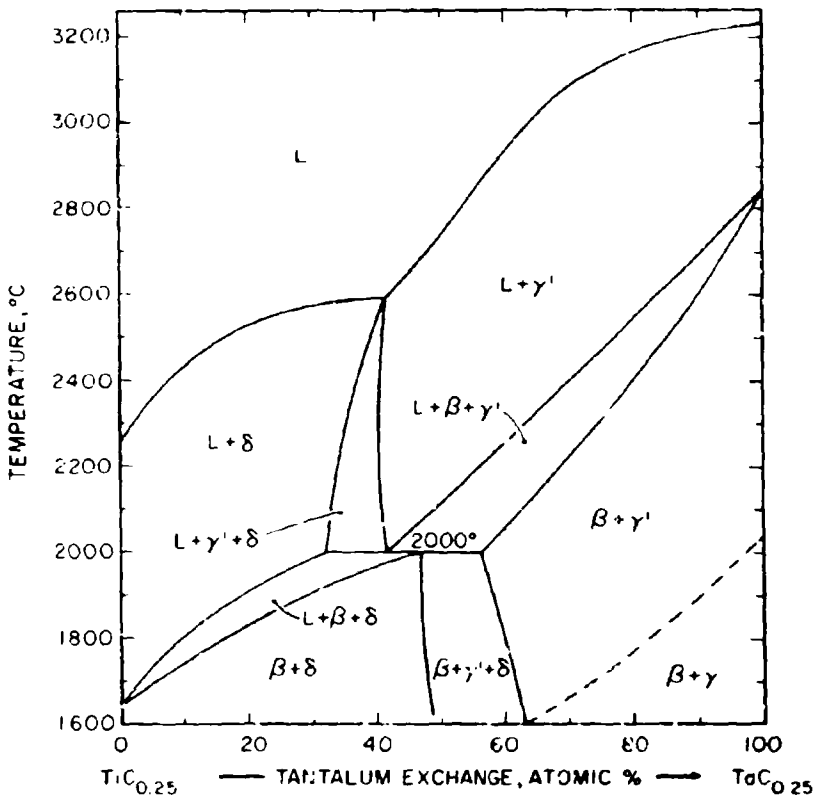

Figure III.E.5.4. Isopleth at 20 At.% C

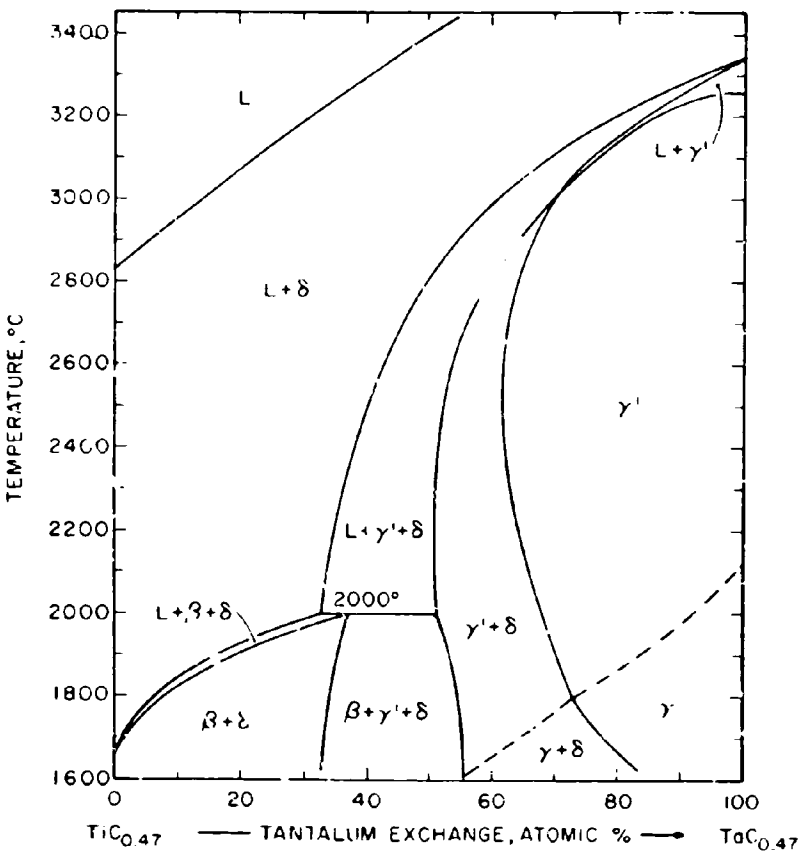

Figure III.E.5.5. Isopleth at 32 At.% C

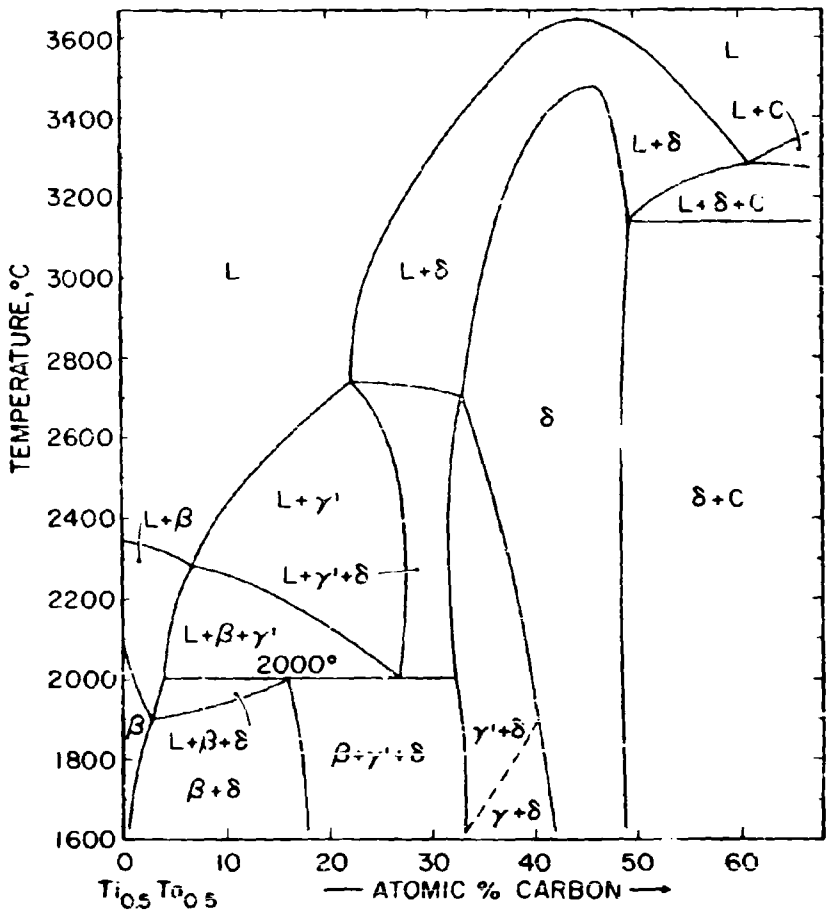

Figure III.E.5.6. Isopleth $Ti_{0.5}Ta_{0.5}$-C

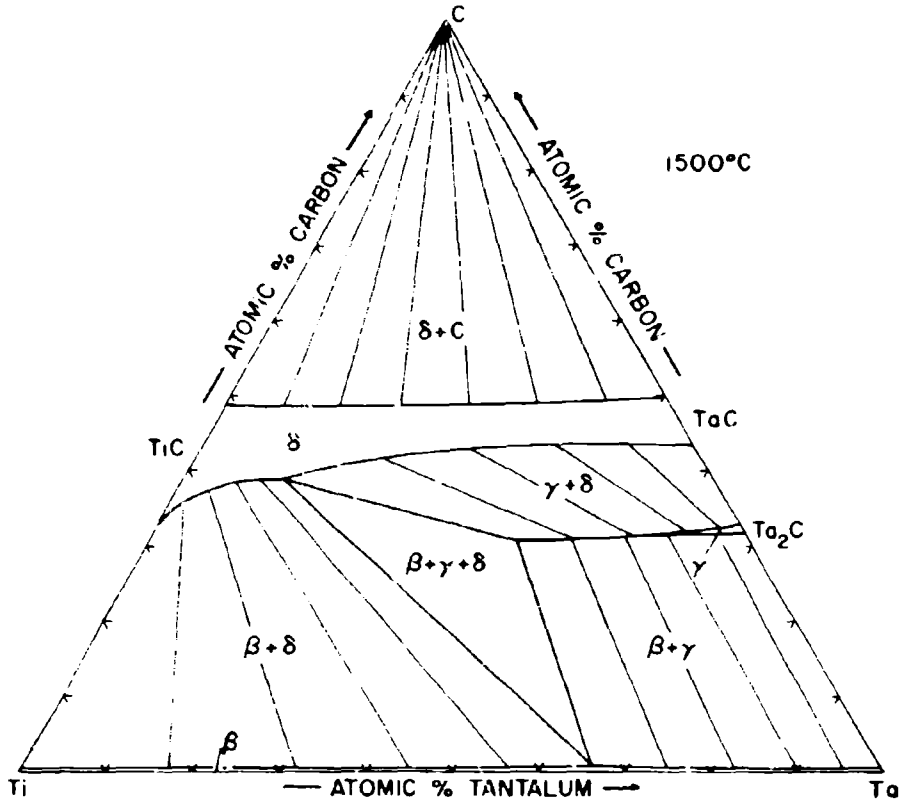

Figure III.E.5.7. Isothermal Section of the Ti-Ta-C System at 1500°C

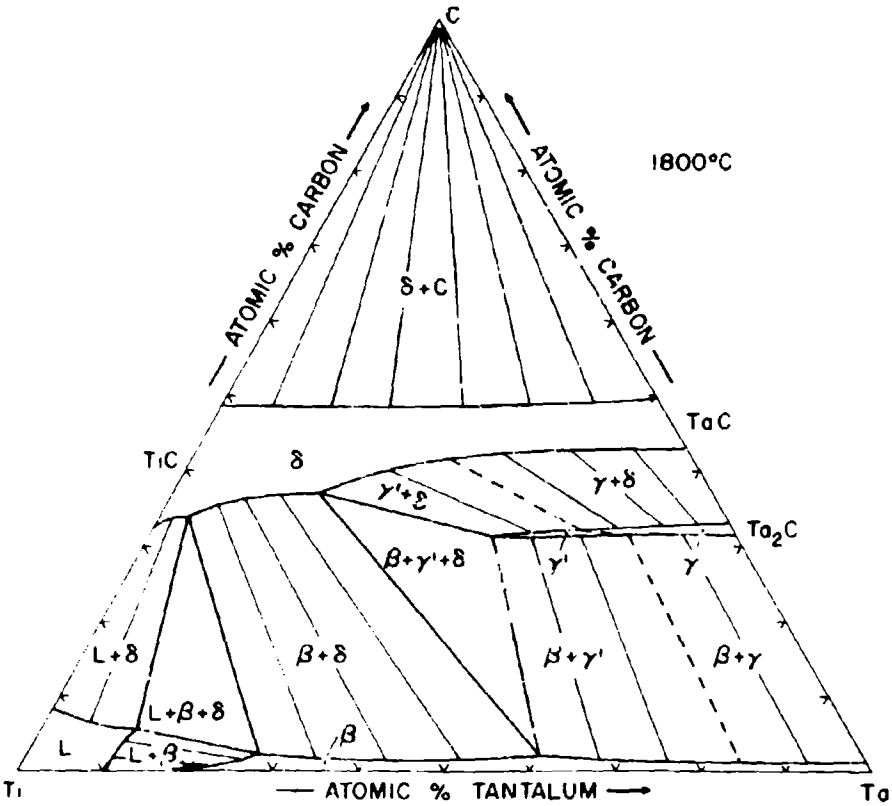

Figure III.E.5.8. Isothermal Section of the Ti-Ta-C System at 1800° C

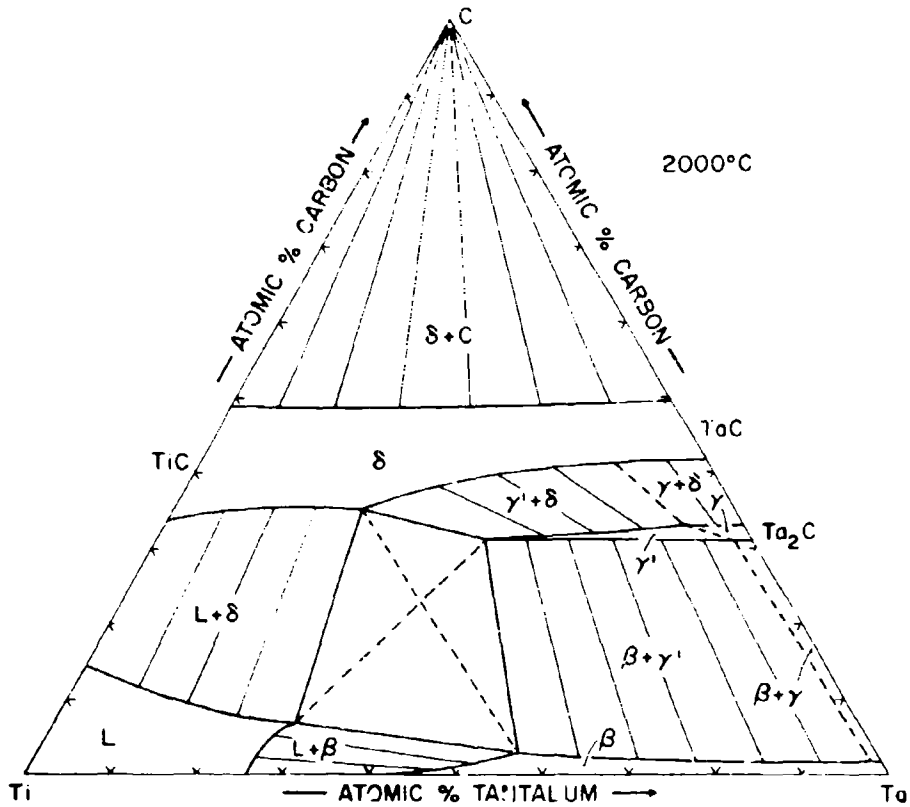

Figure III.E.5.9. Isothermal Section of the Ti-Ta-C System at 2000° C

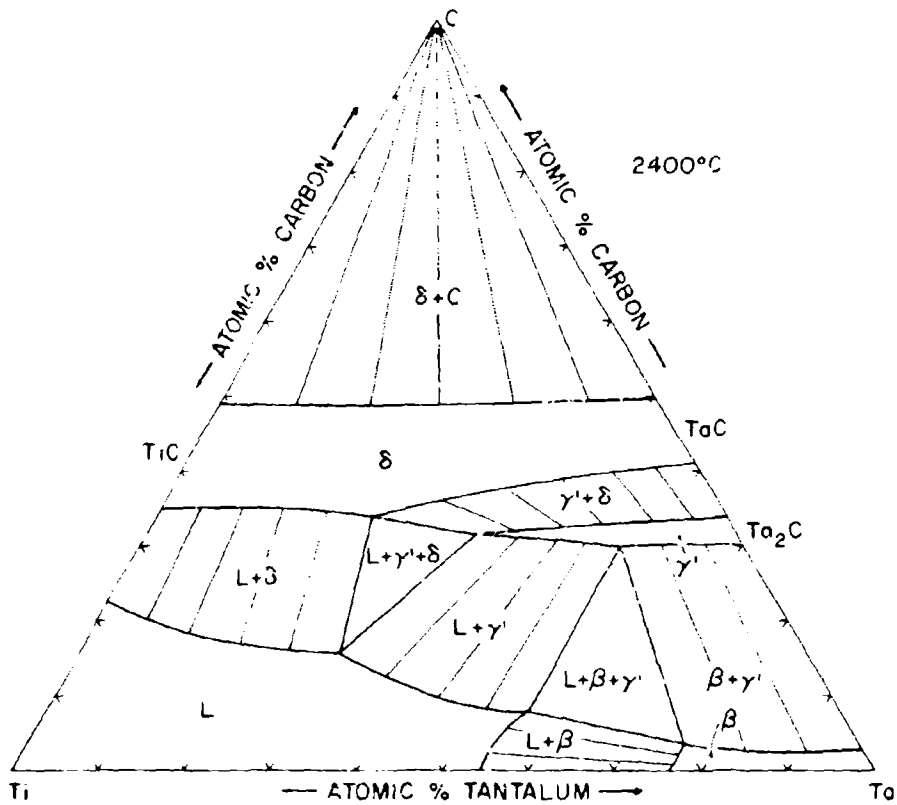

Figure III.E.5.10. Isothermal Section of the Ti-Ta-C System at 2400°C

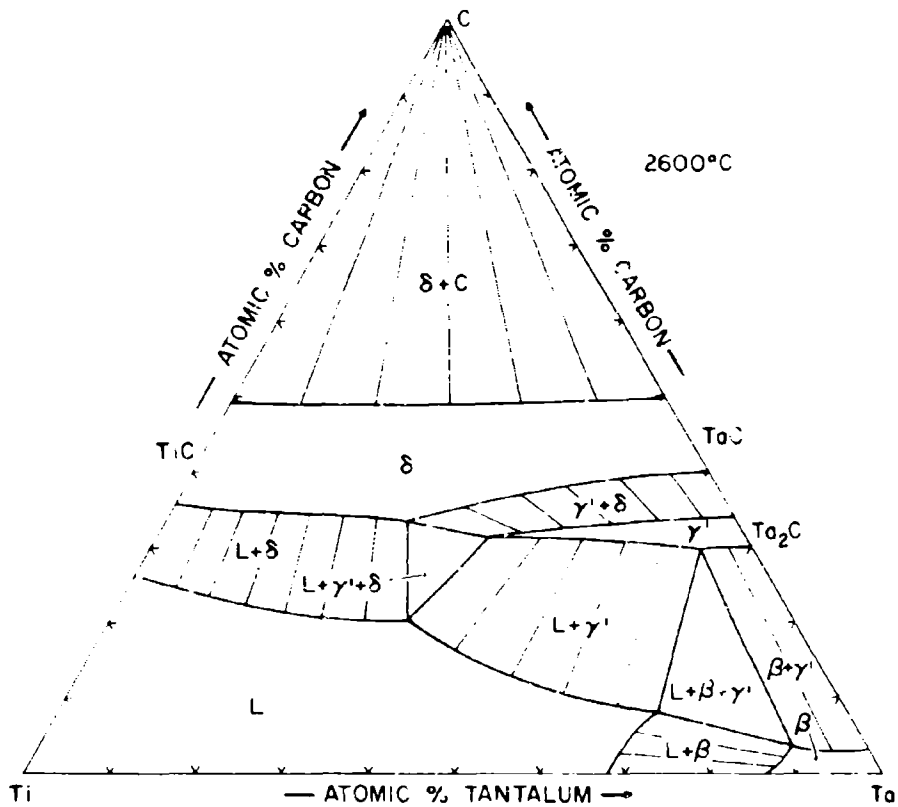

Figure III.E.5.11. Isothermal Section of the Ti-Ta-C System at 2600° C

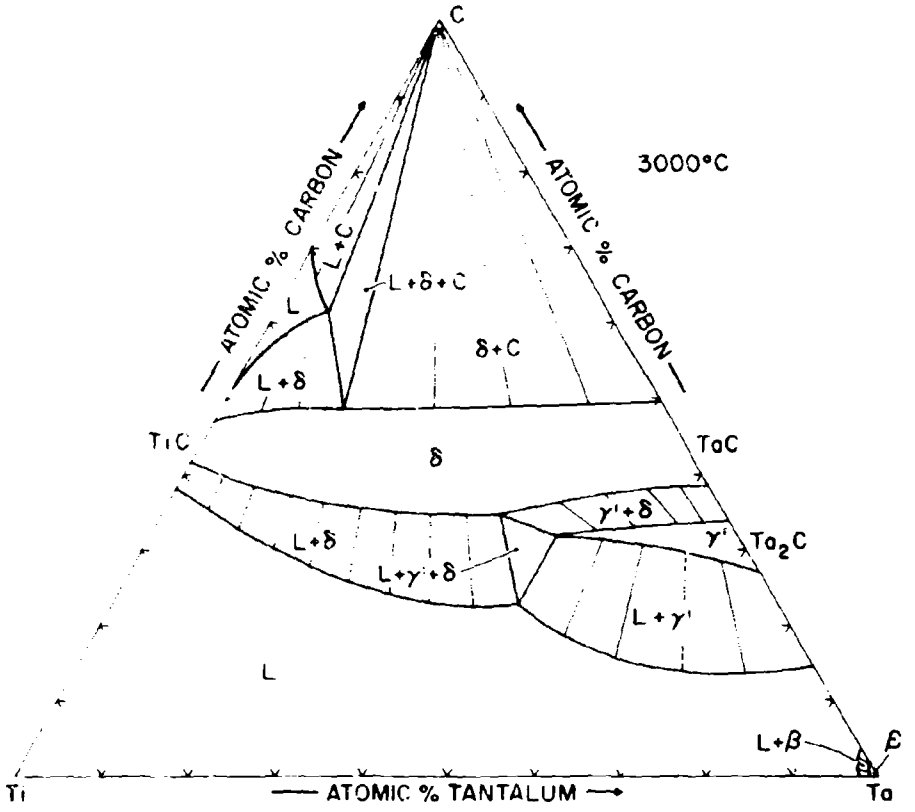

Figure III. E. 5. 12. Isothermal Section of the Ti-Ta-C System at 3000° C

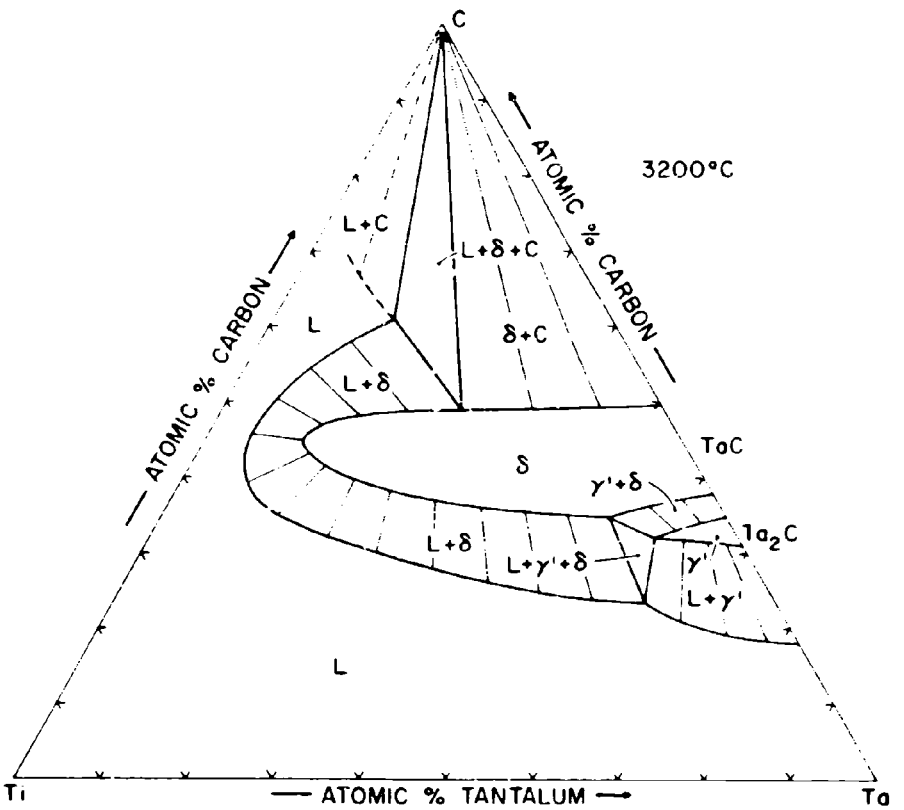

Figure III.E.5.13. Isothermal Section of the Ti-Ta-C System at 3200° C

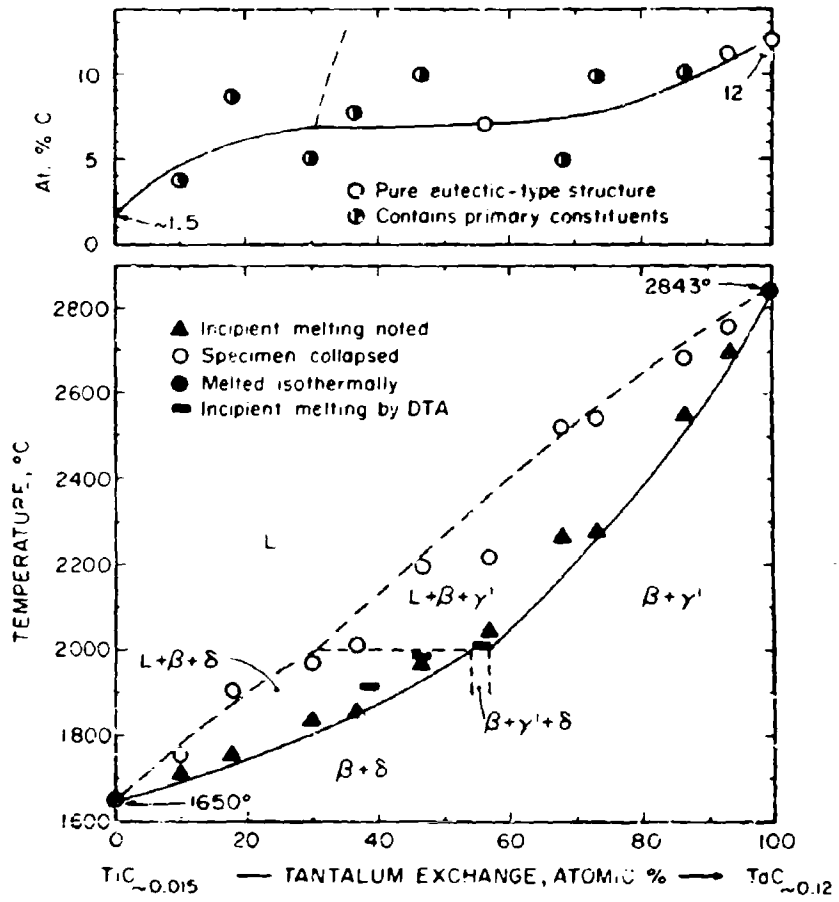

Figure III.E.5.14. Observed Melting Temperatures in Alloys Located Along the Metal-Rich Eutectic Trough.

Top: Microscopically Estimated Location of Eutectic Trough

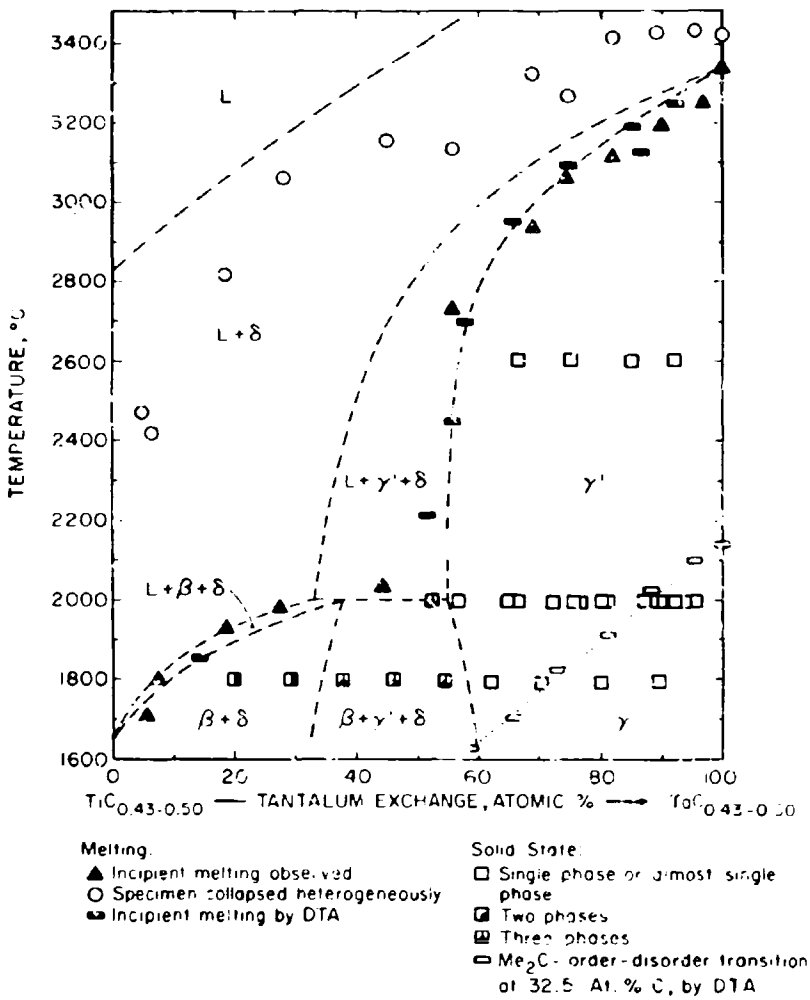

Figure III.E.5.15. Experimental Melting Temperatures, Solid State Reactions, and Qualitative Phase Evaluation of Solid State-Equilibrated Alloys Containing Between 30 and 33.3 At.% C

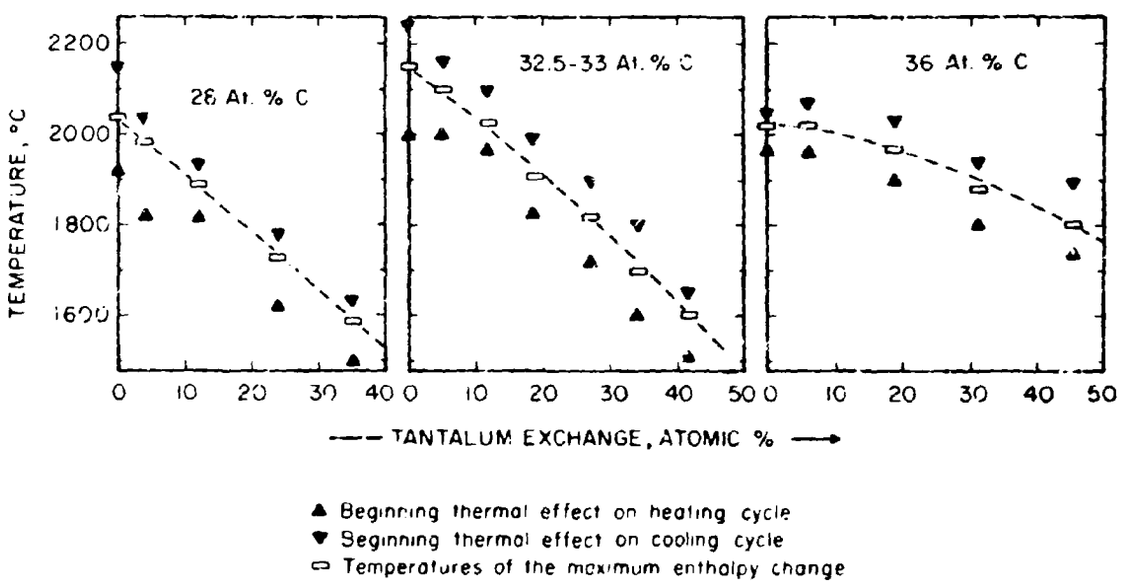

Figure III.E.5.16. Observed Order-Disorder Transformation Temperatures in the Subcarbide, $(Ta,Ti)_2C$, Phase.

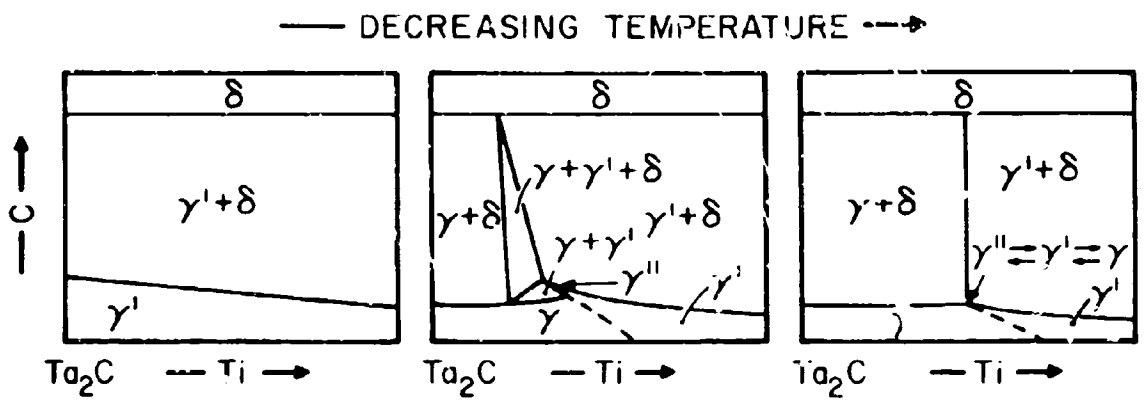

Figure III.E.5.17. Diagrammatic Illustration of the Termination of the Heterogeneous Order-Disorder Transition in Ta_2C in a Limiting Tie Line by Titanium Substitution

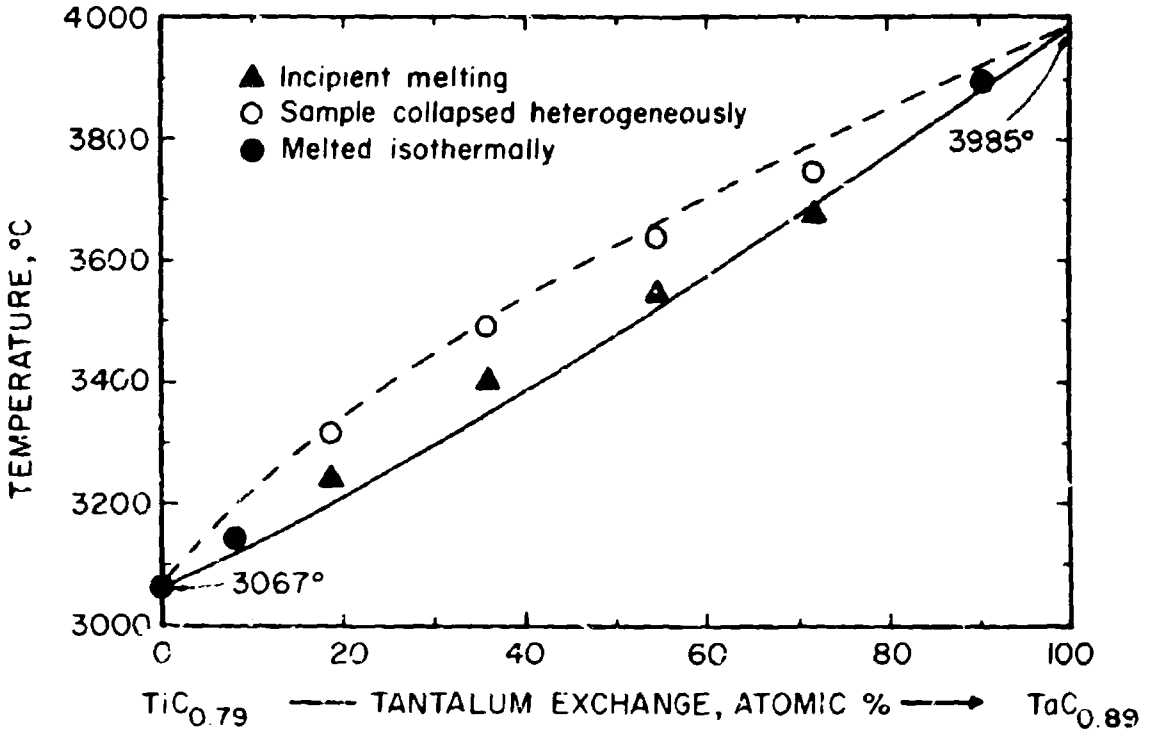

Figure III.E.5.18. Maximum Solidus Temperatures of the Monocarbide Phase

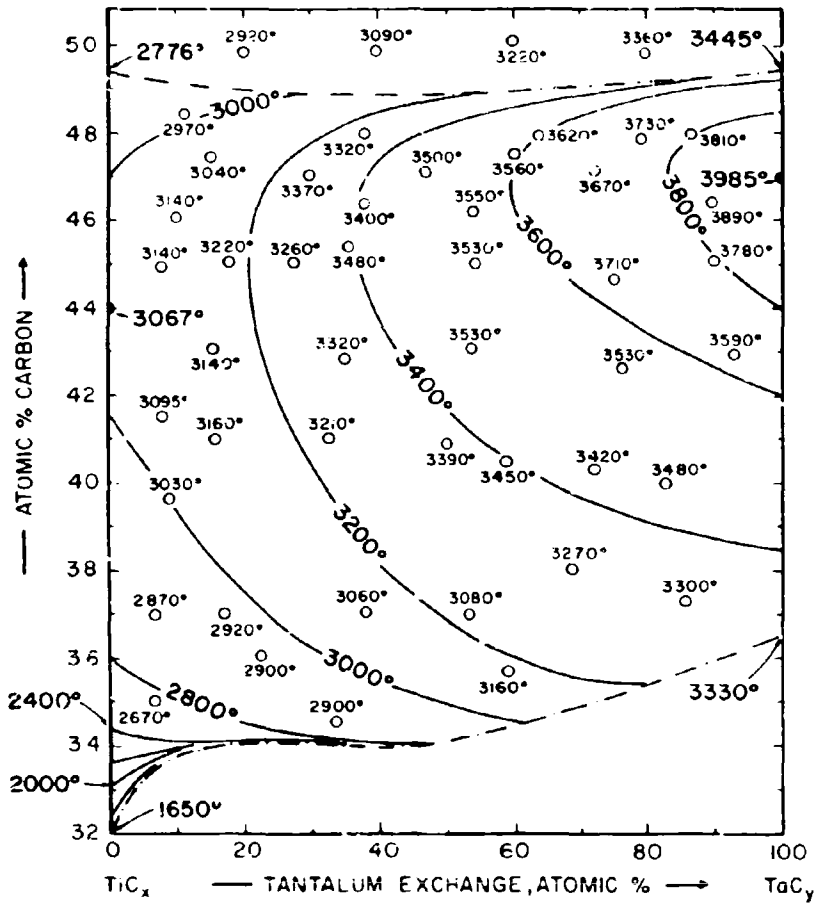

Figure III.E.5.19. Experimental Solidus Points and Solidus Isotherms for the Carbon-Deficient Monocarbide Solutions

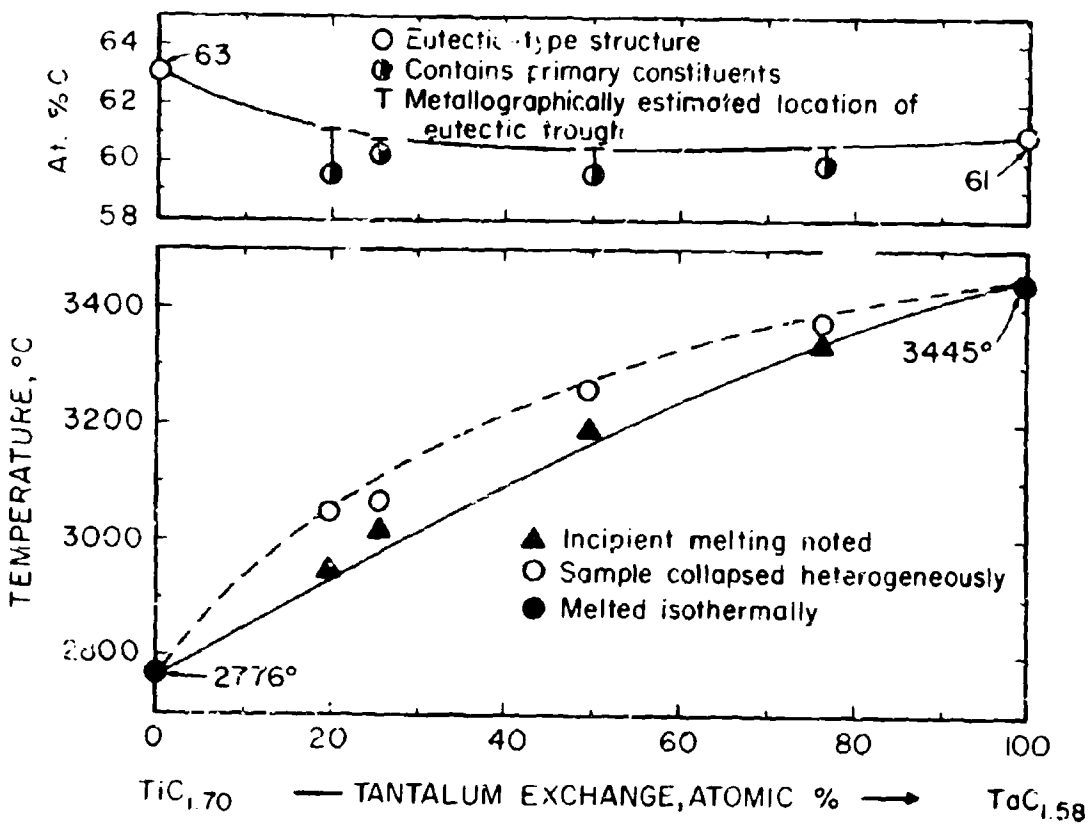

Figure III.E.5.20. Experimental Melting Temperatures in Monocarbide + + Graphite Alloys and Location of the Eutectic Trough.

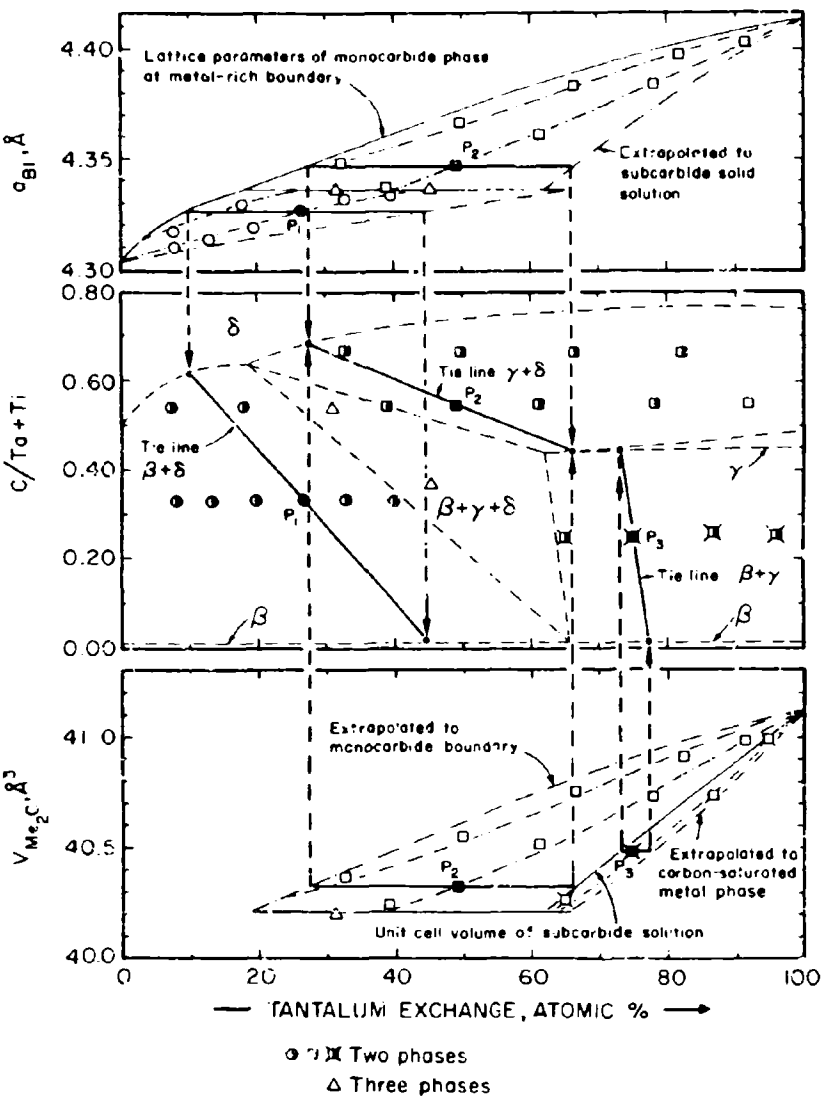

Figure III.E.5.21. Determination of the Tie Line Distribution in the Three Two-Phase Fields by Lattice Parameter Measurements on the Coexisting Phases.

(Alloys equilibrated at 1500° C)

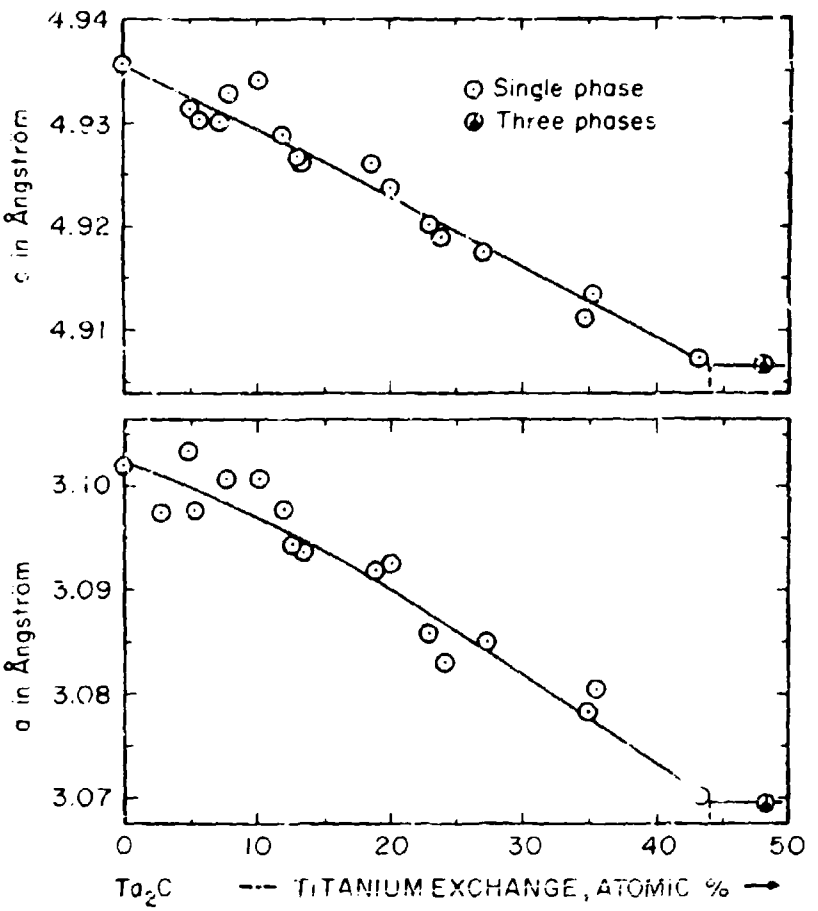

Figure III.E.5.22. Lattice Parameters of the Subcarbide, $(Ta,Ti)_2C$, Phase.

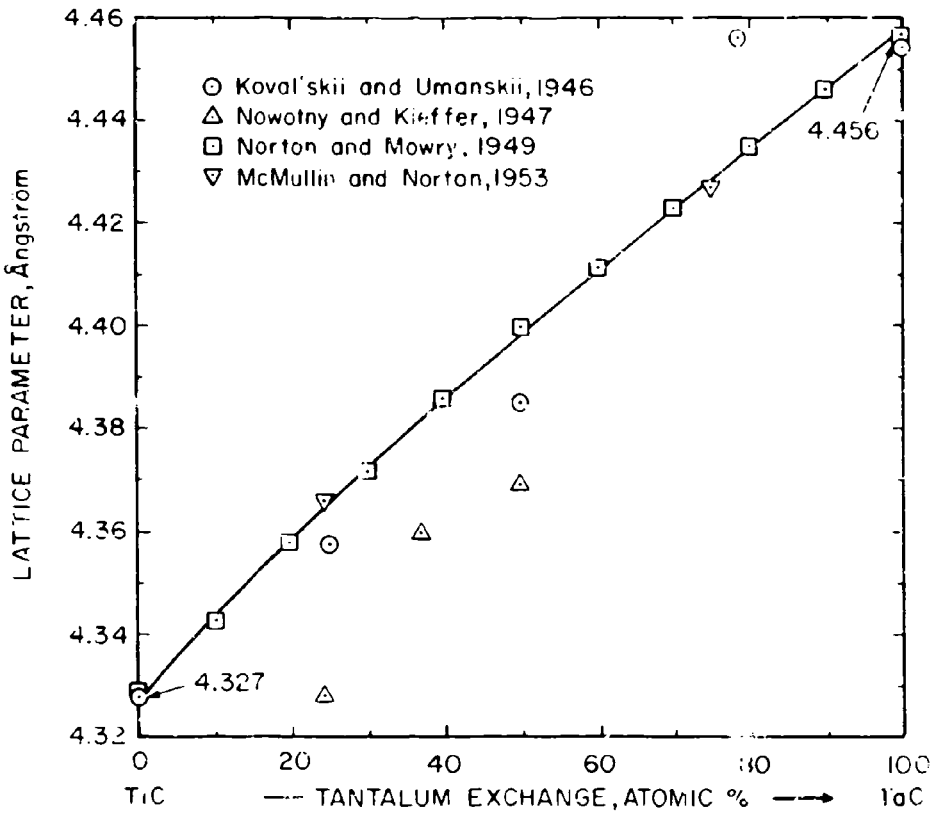

Figure III.E.5.23. Lattice Parameters of the Carbon-Saturated Monocarbide (B1) Solution. (Literature Data)

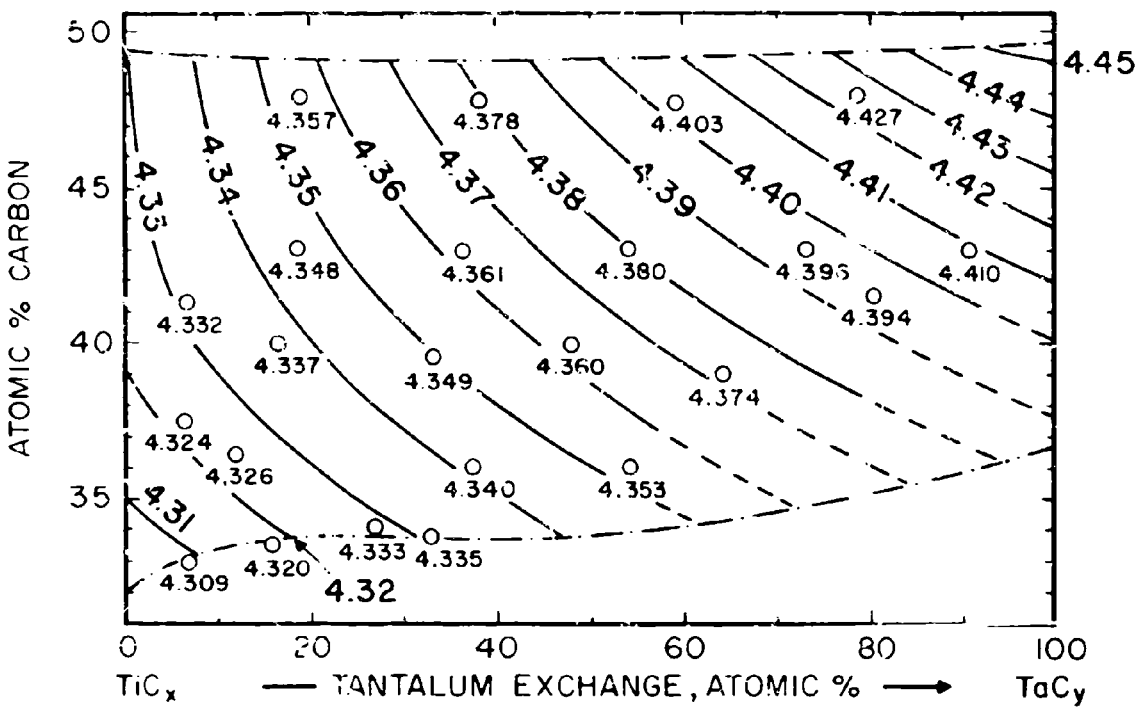

Figure III.E.5.24. Observed Lattice Parameters and Isoparametric Lines for the Carbon-Deficient Monocarbide Solid Solution

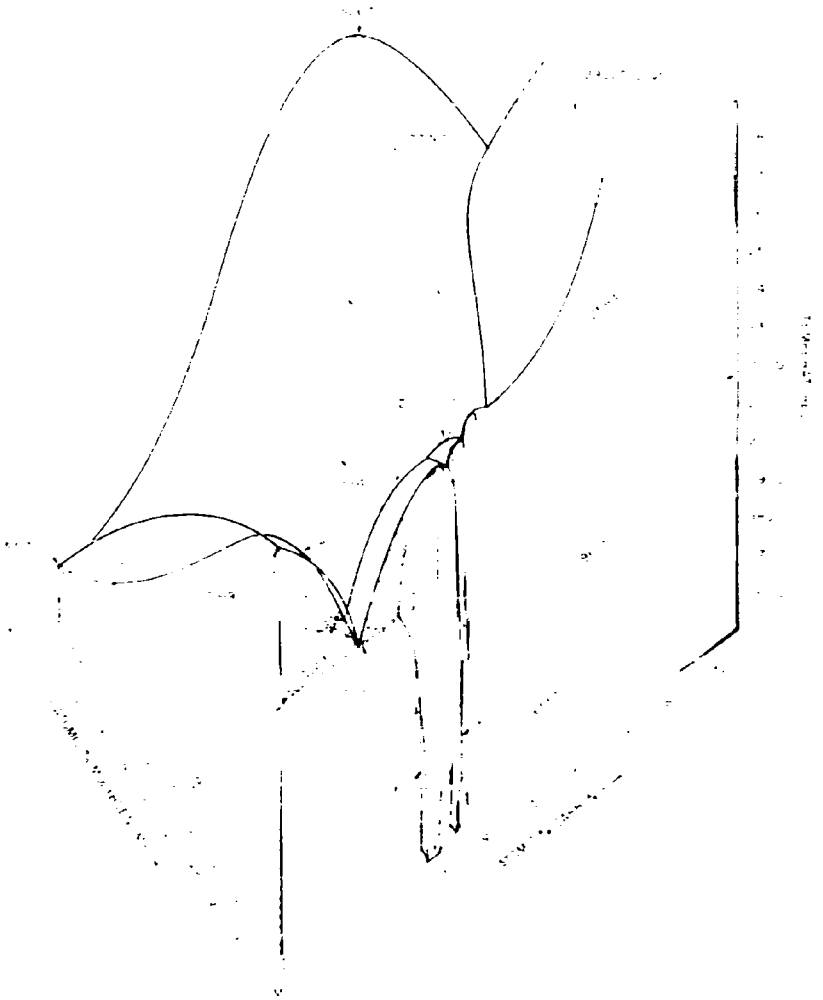

Figure III.E.6.1. Isometric View of the Ti-Mo-C System

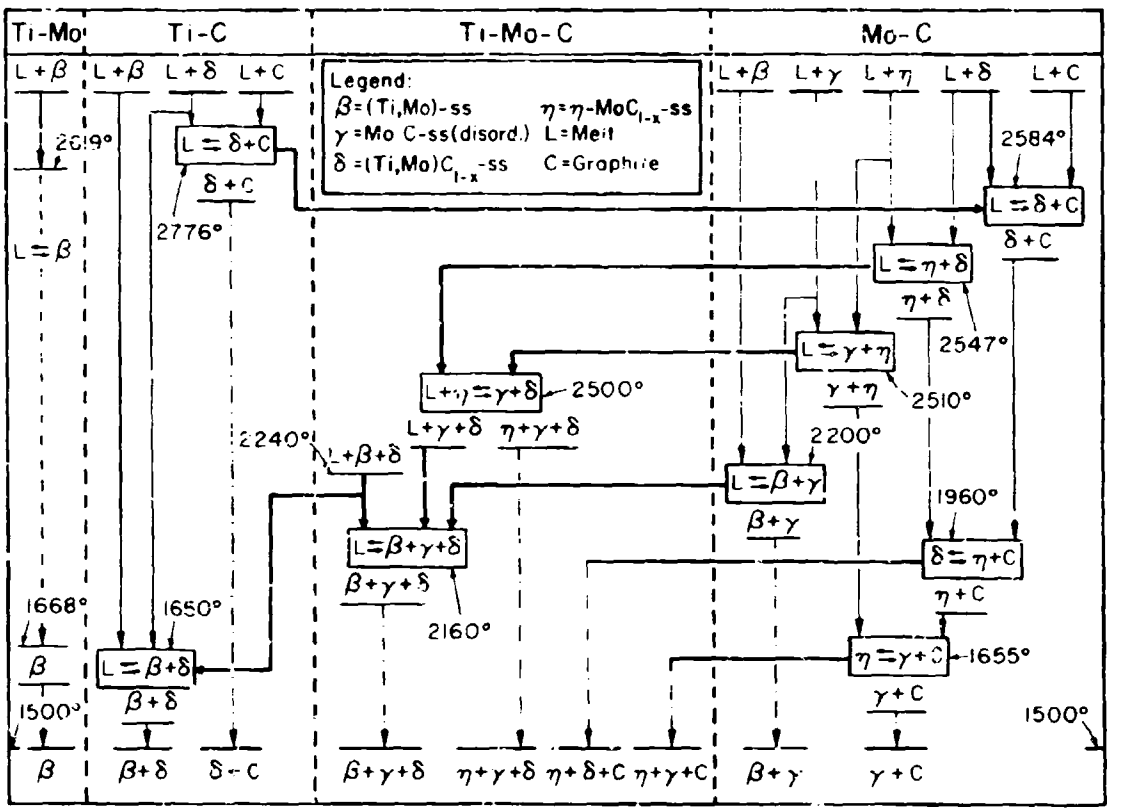

Figure III.E.6.2. Reaction Diagram for the Ti-Mo-C System

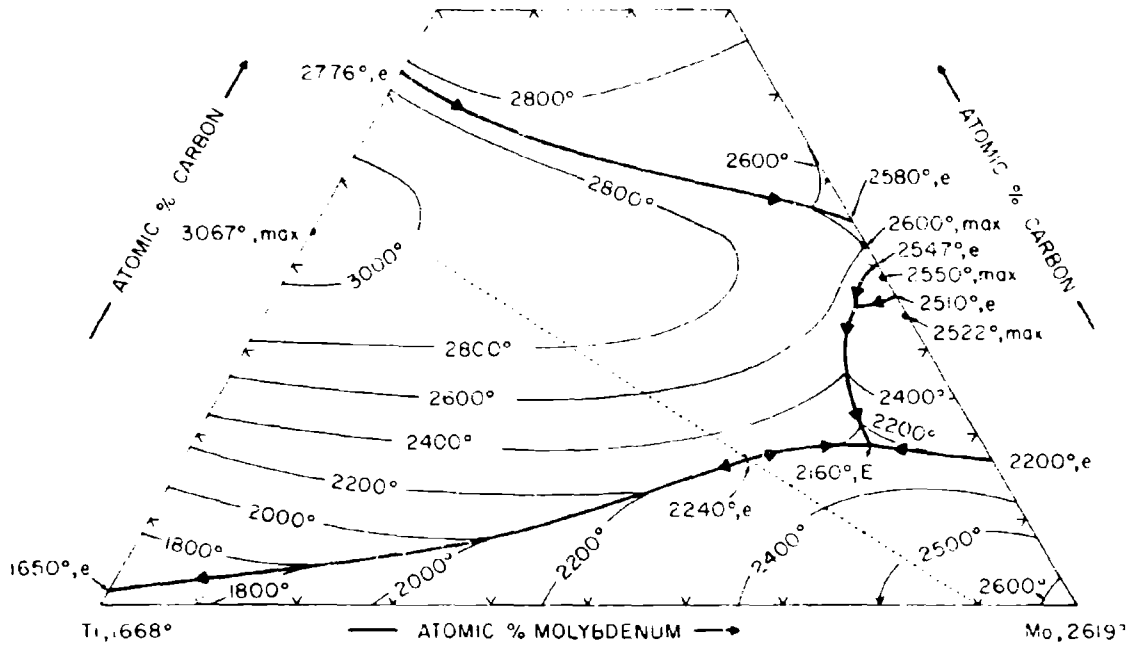

Figure III.E.6.3. Liquidus Projections in the Ti-Mo-C System

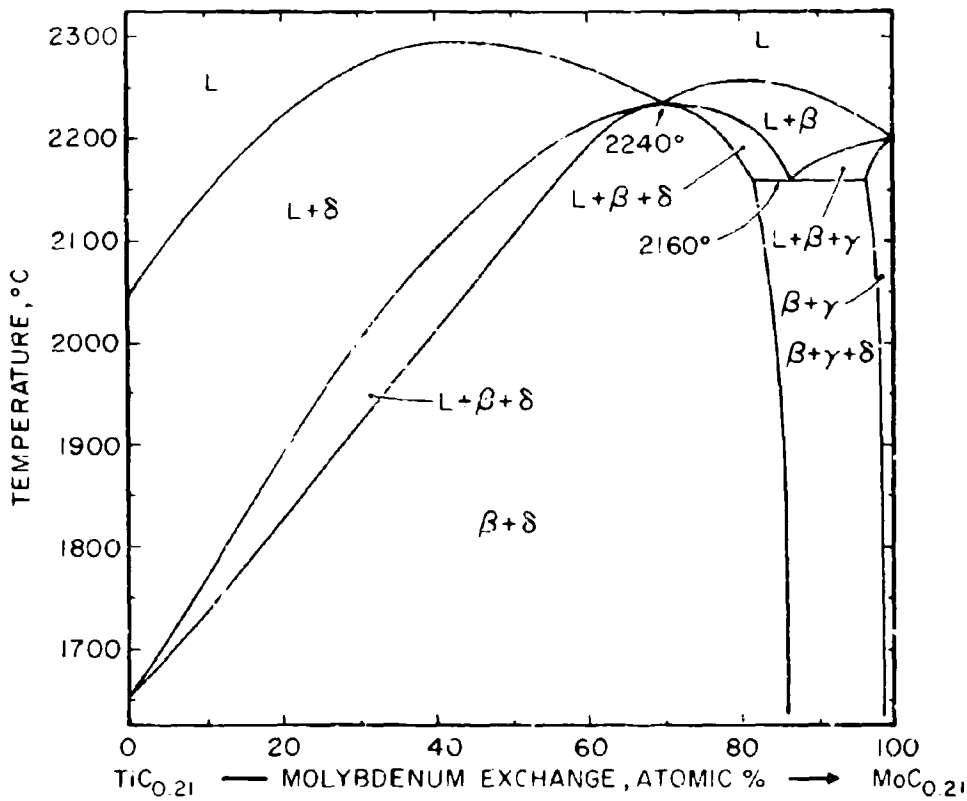

Figure III.E.6.4. Isopleth at 17 At.% C

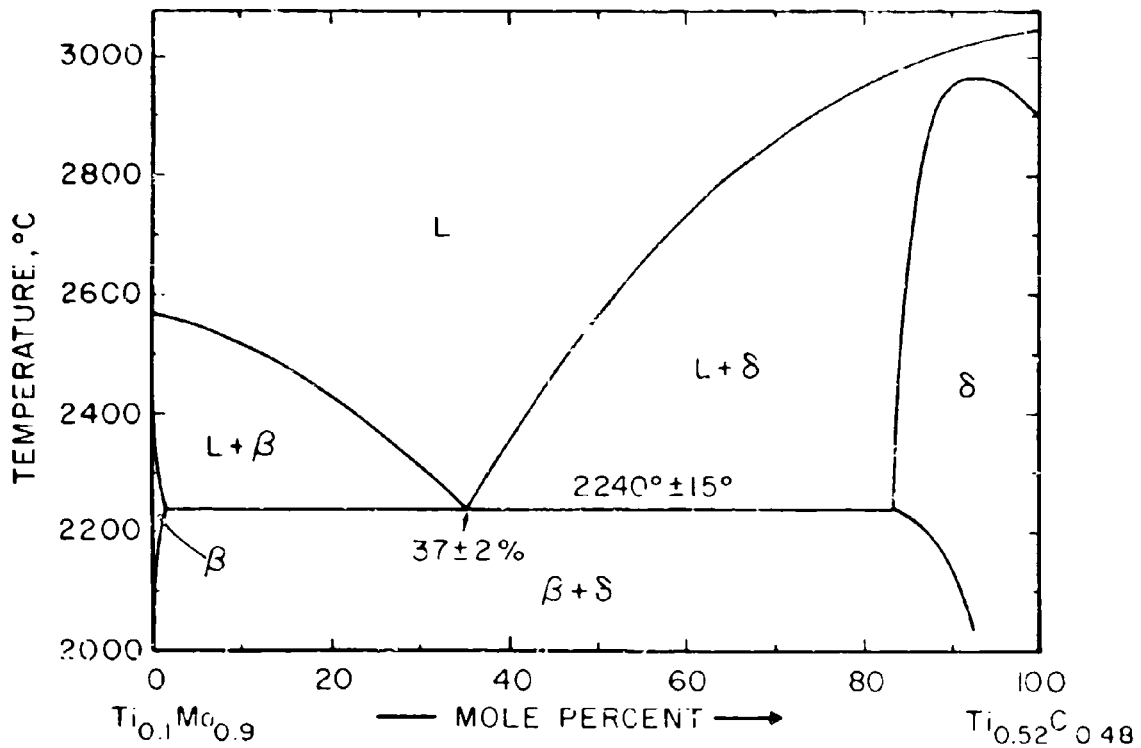

Figure III.E.6.5. Isopleth Along the Pseudobinary Section Metal + Monocarbide Phase

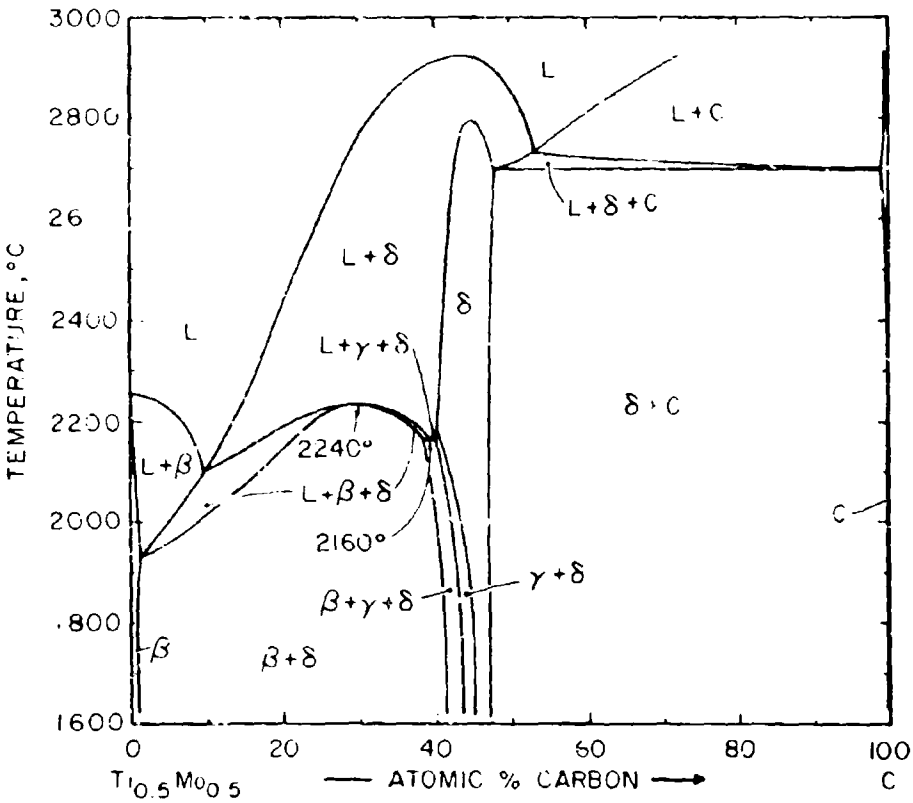

Figure III.E.6.6. Isopleth $Ti_{0.5}Mo_{0.5}$-C

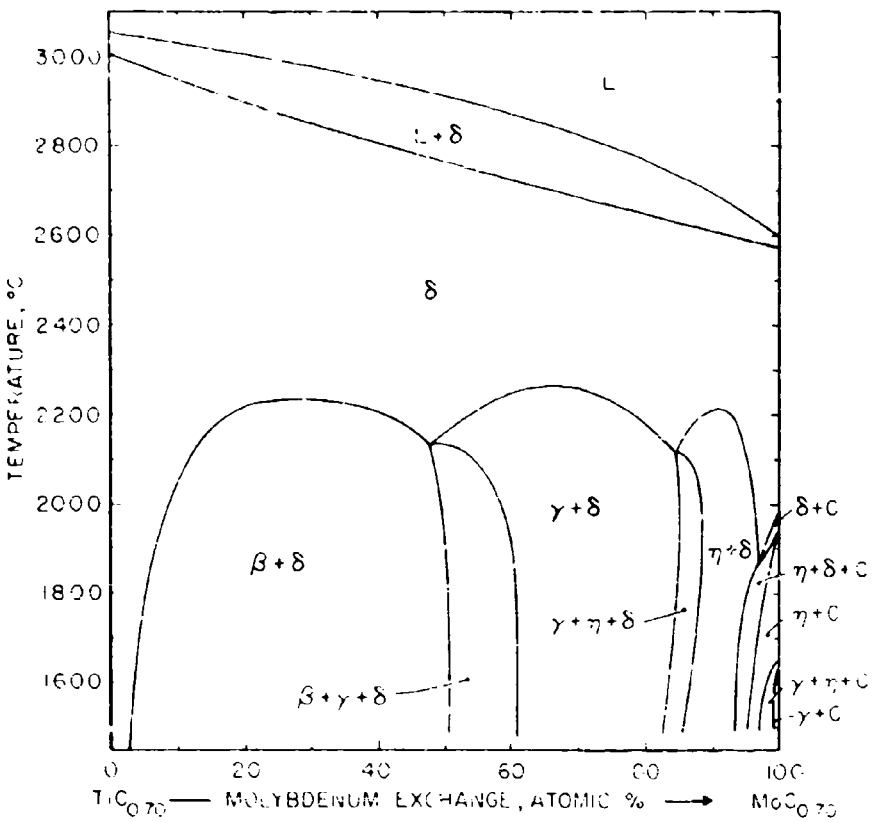

Figure III.E.6.7. Isopleth at 41 At.% C

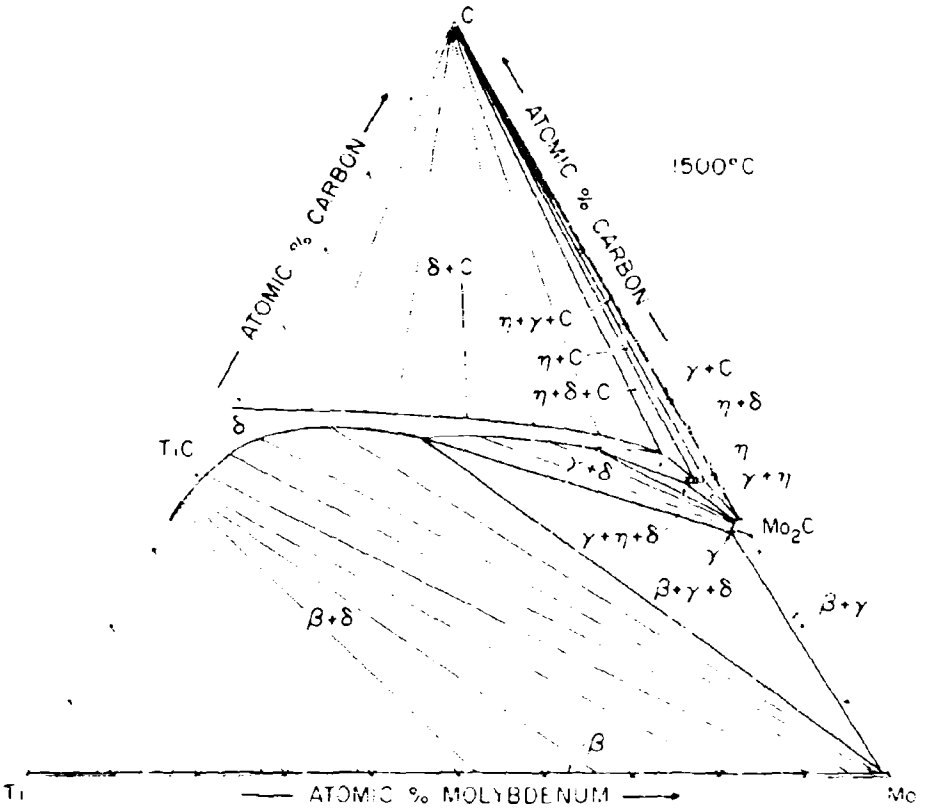

Figure III.E.6.8. Isothermal Section of the Ti-Mo-C System at 1500° C

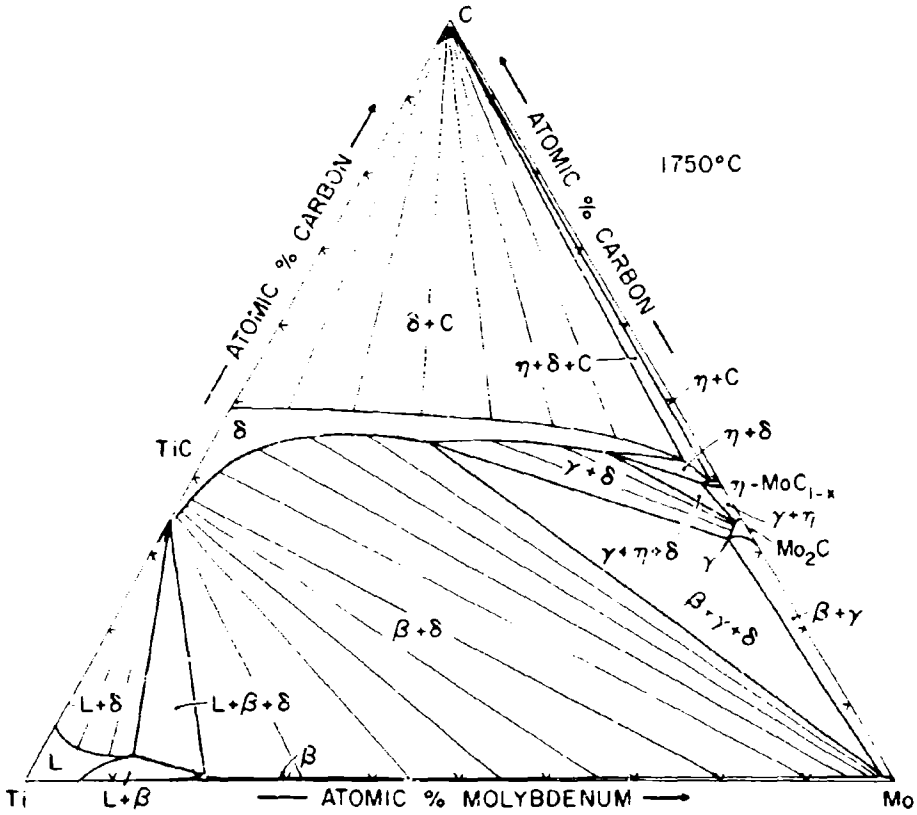

Figure III.E.6.9. Isothermal Section of the Ti-Mo-C System at 1750°C

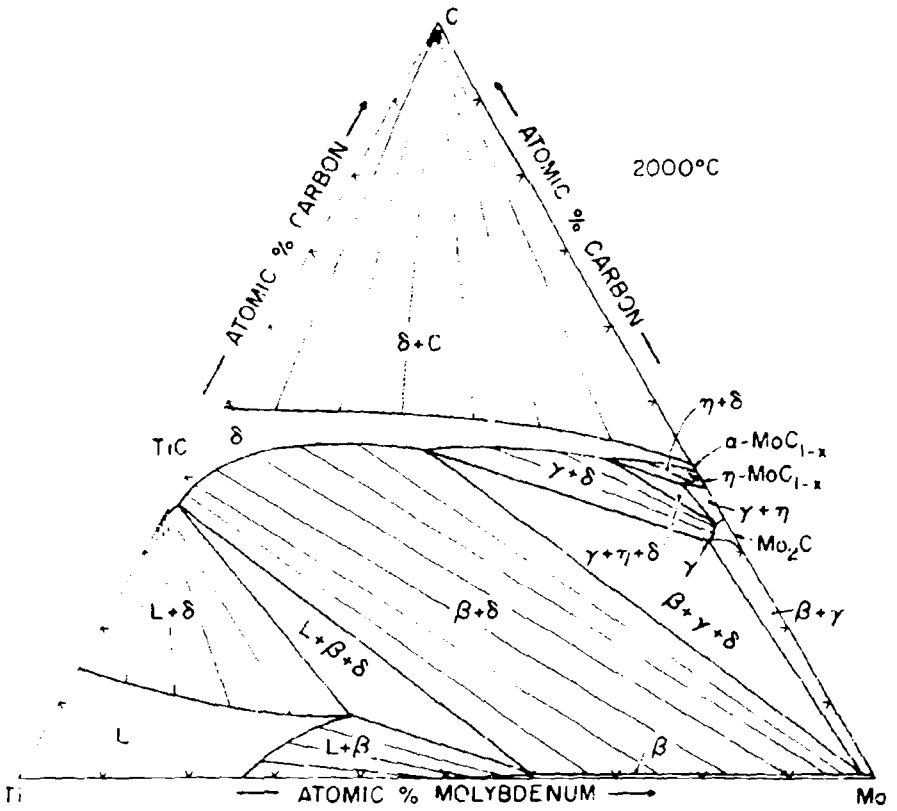

Figure III.E.5.10. Isothermal Section of the Ti-Mo-C System at 2000°C

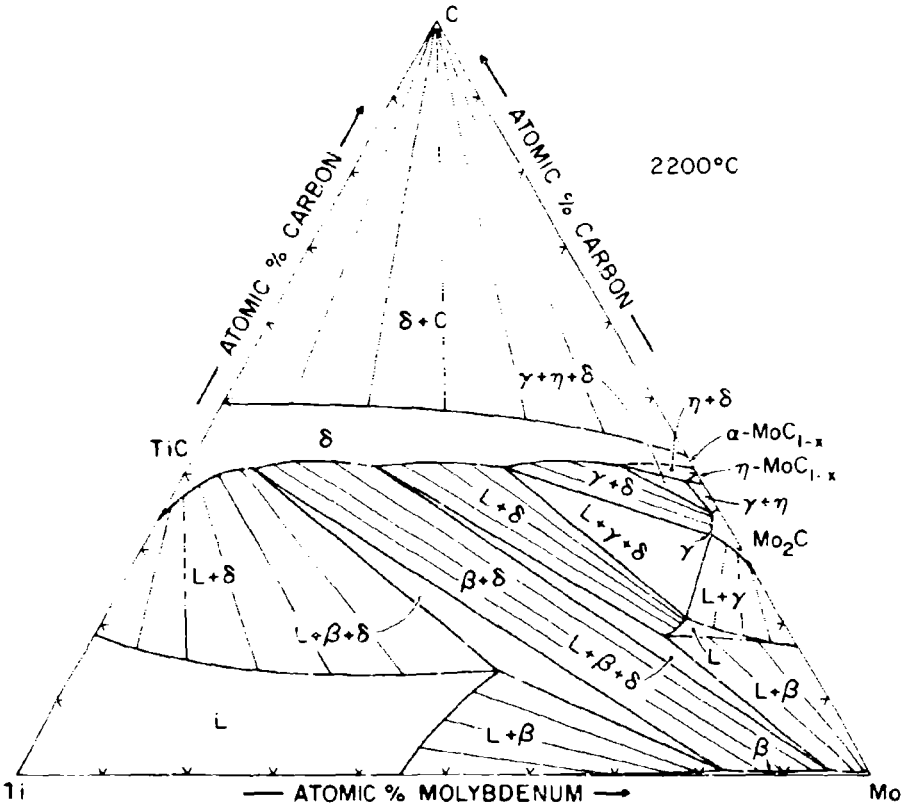

Figure III.E.6.11. Isothermal Section of the Ti-Mo-C System at 2200° C

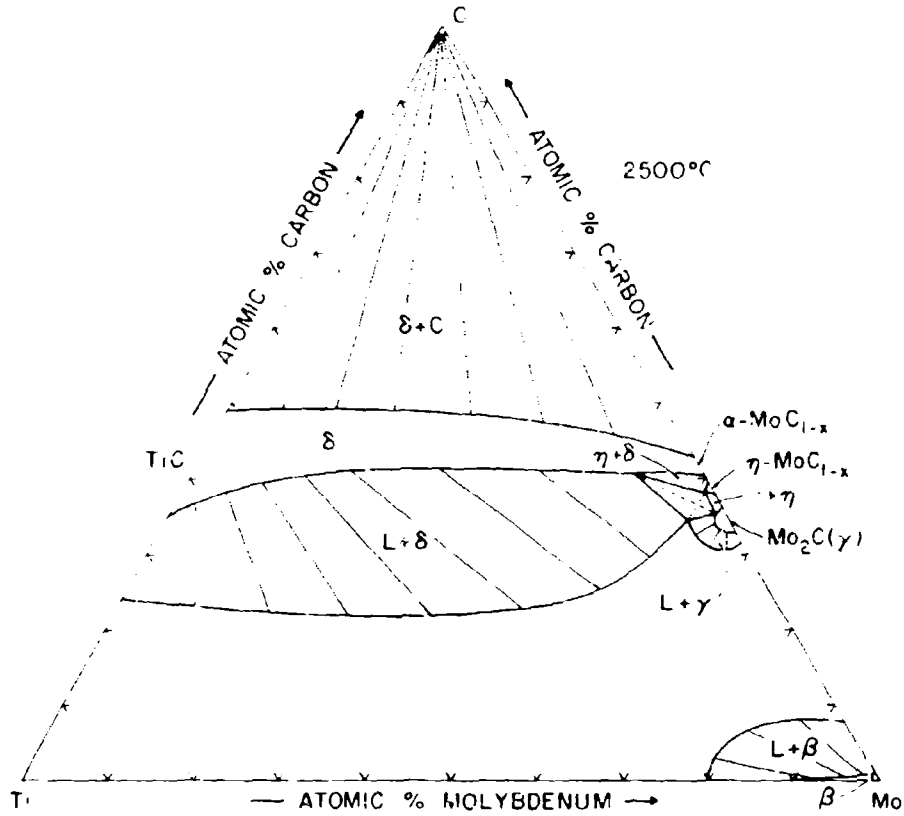

Figure III.E.6.12. Isothermal Section of the Ti-Mo-C System at 2500° C

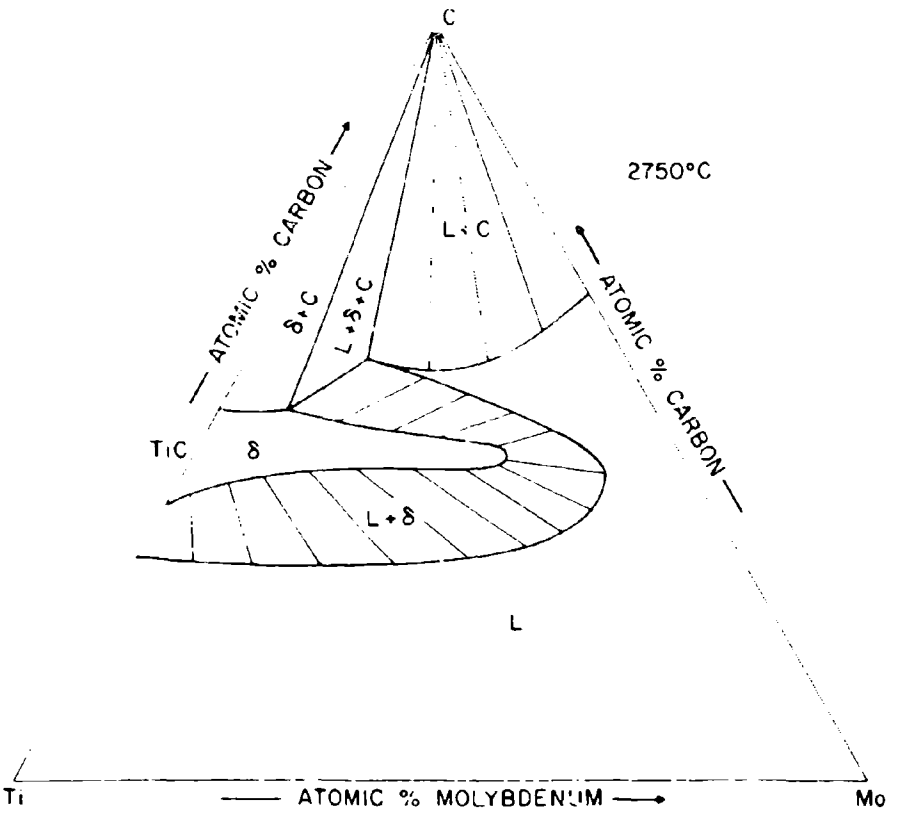

Figure III.E.6.13. Isothermal Section of the Ti-Mo-C System at 2750° C

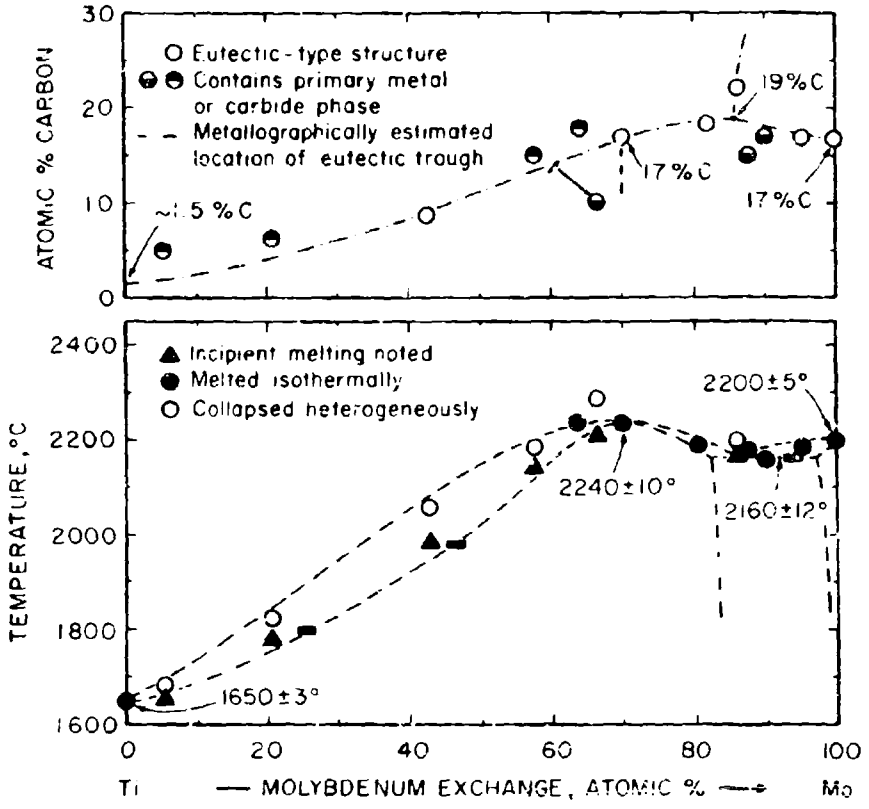

Figure III.E.6.14. Experimental Melting Temperatures of Ti-Mo-C Alloys Located Along the Metal-Rich Eutectic Trough.

Top: Microscopically Estimated Location of Eutectic Trough

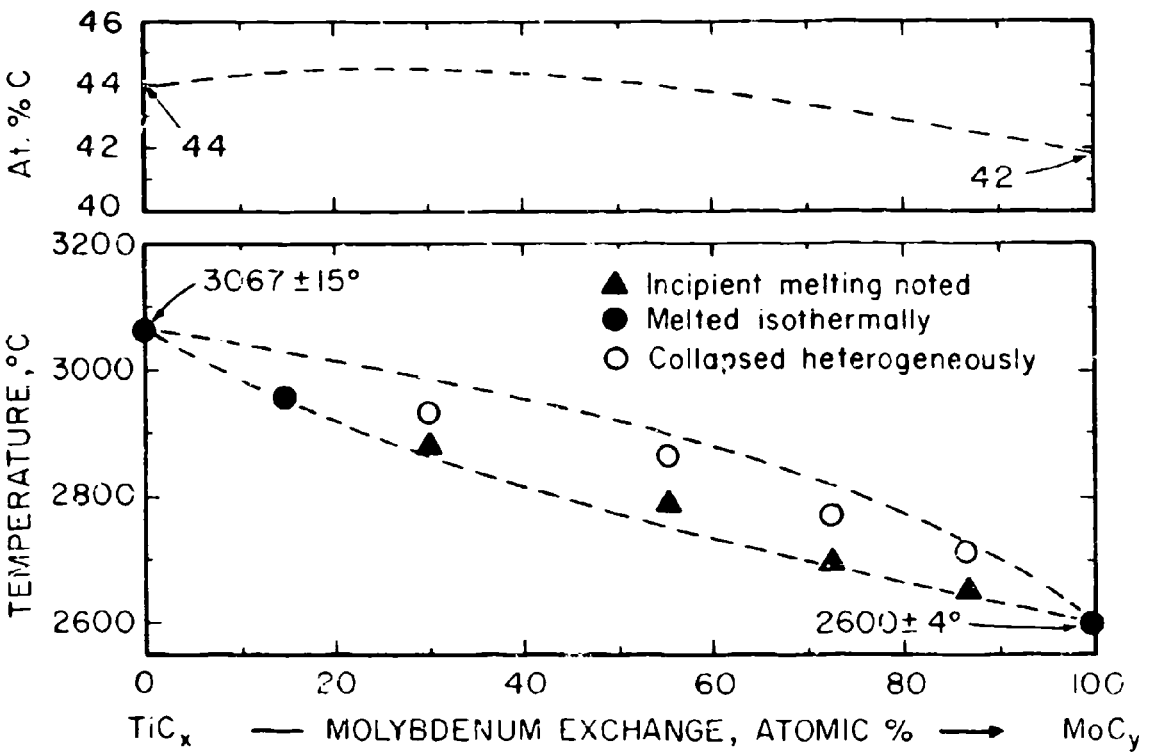

Figure III.E.6.15. Maximum Solidus Temperatures and Composition Line for the (Ti,Mo)C_{1-x} (B1) Solid Solution

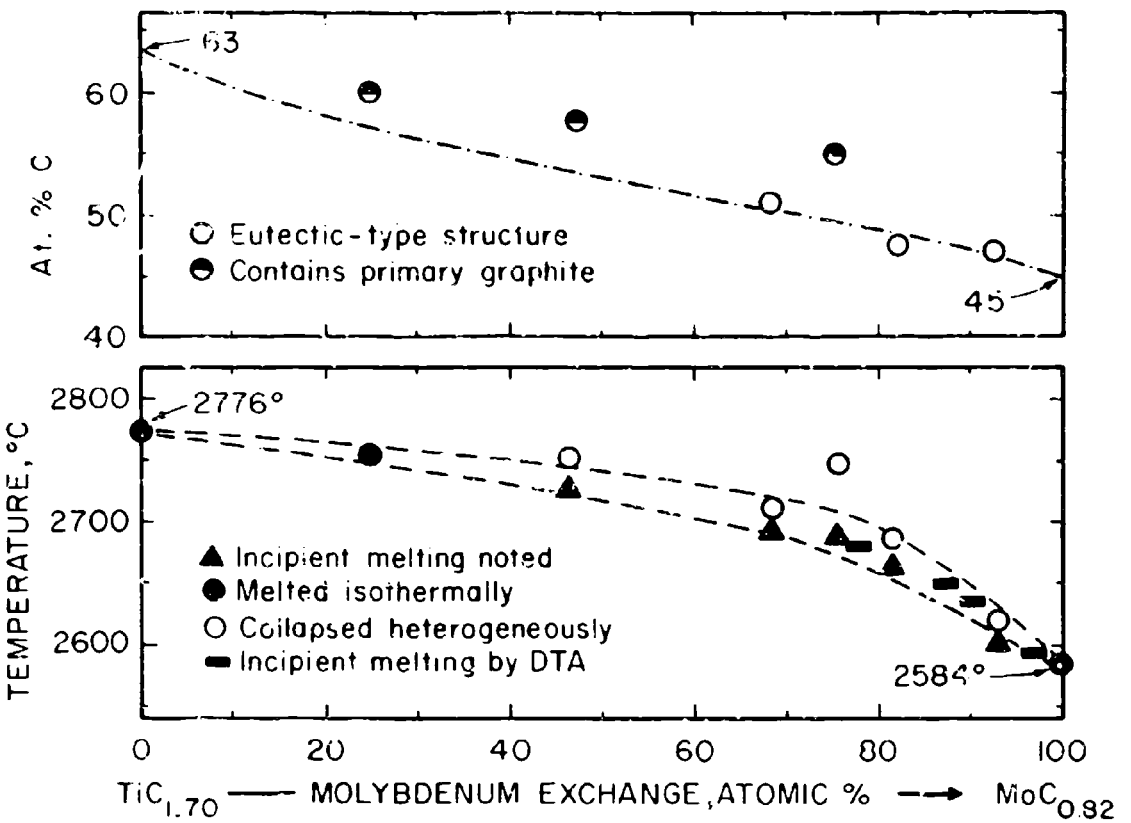

Figure III.E.6.16. Experimental Melting Temperatures of Alloys Located Along the Monocarbide + Graphite Eutectic Trough.

Top: Microscopically Estimated Location of Eutectic Trough

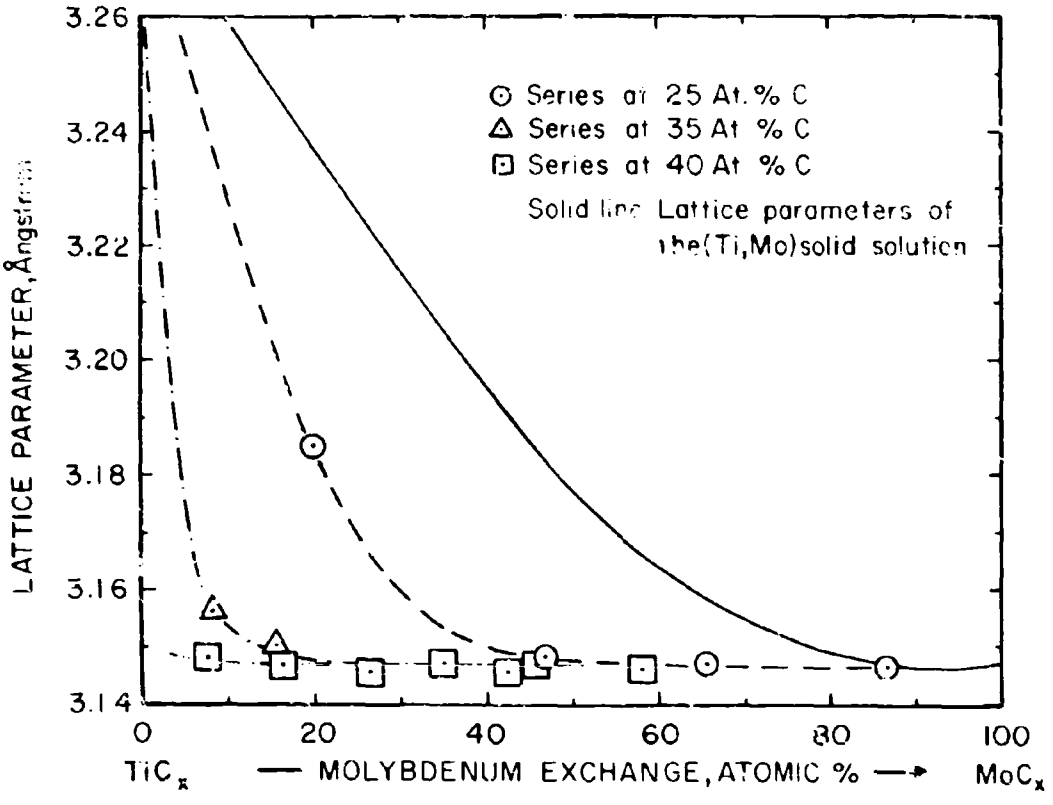

Figure III.E.6.17. Determination of the Tie Line Distribution in the Two-Phase Field β+δ by Metal Lattice Parameter Measurements in Two-Phased, β+δ, Alloys.

(Alloys Equilibrated at 1500° C)

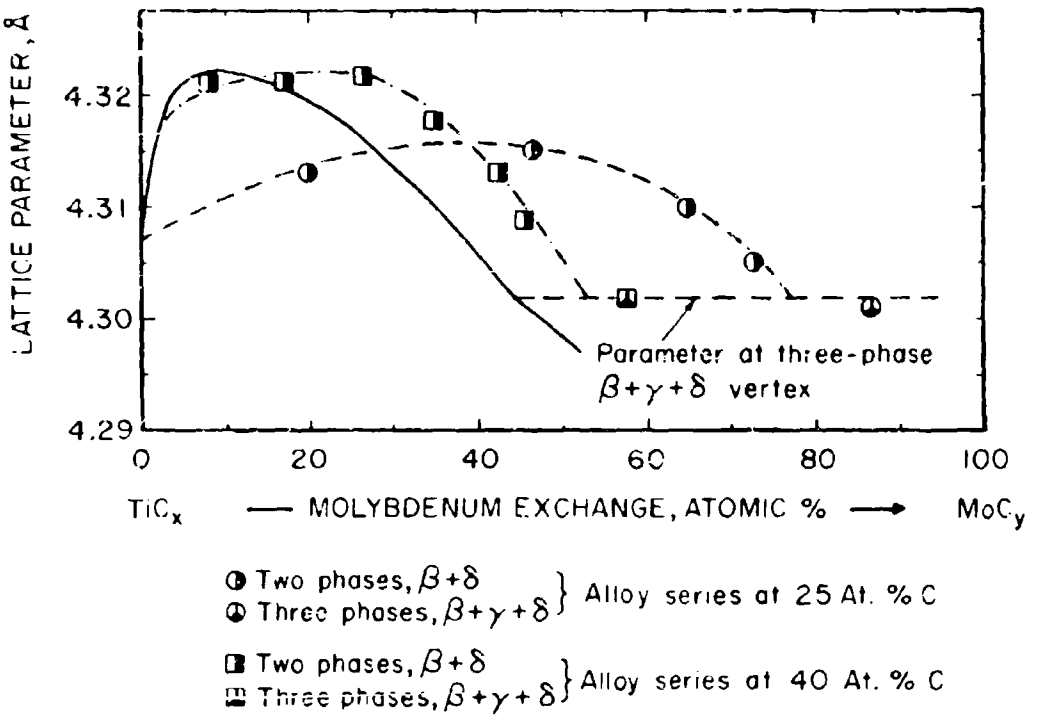

Figure III.E.6.18. Determination of the Coexisting Monocarbide Compositions in Two-Phase, $\beta+\delta$, Alloys by Lattice Parameter Measurements

(Alloys Equilibrated at 1500° C)

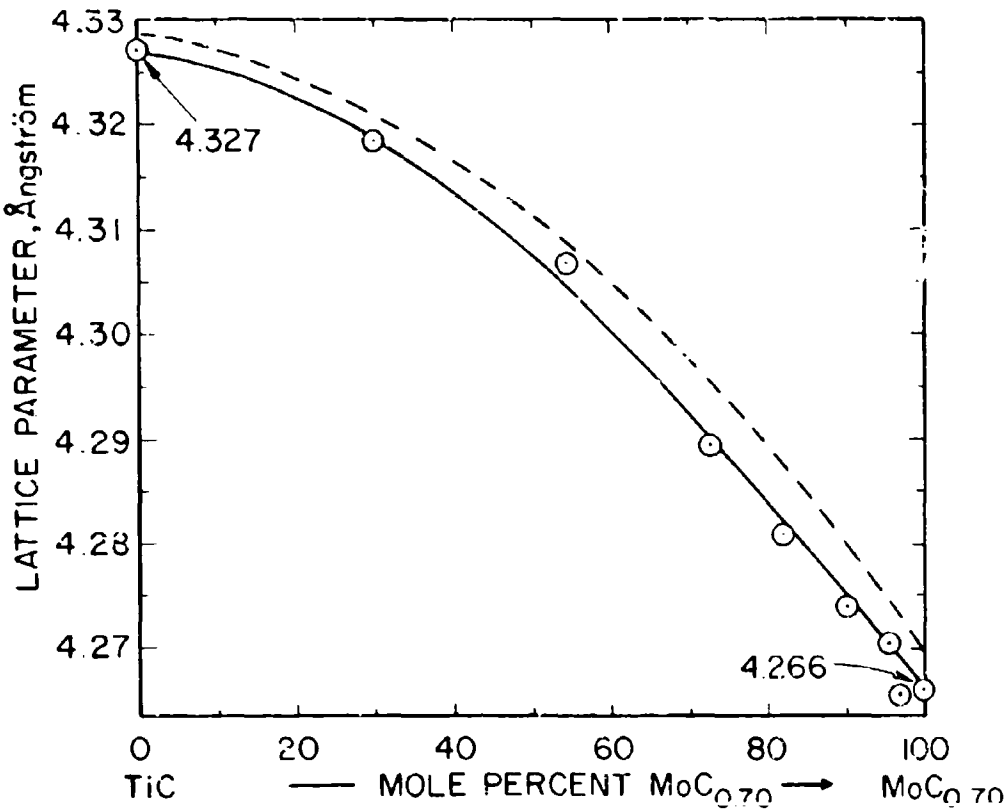

Figure III.E.6.19. Lattice Parameters of the Monocarbide Phase Along the Section TiC-$MoC_{0.70}$

Dashed Line: Calculated (see report reference)

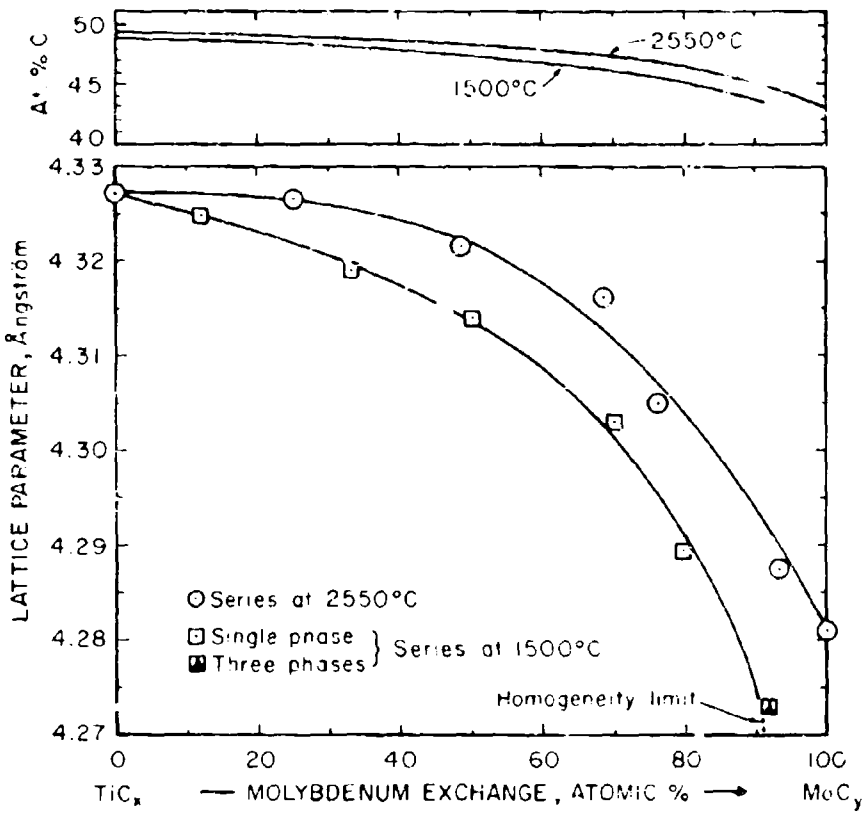

Figure III.E.6.20. Lattice Parameters of the Carbon-Saturated Monocarbide Phase in Alloys Equilibrated at 1500° C and 2550° C

Top: Analytically Determined Phase Boundaries

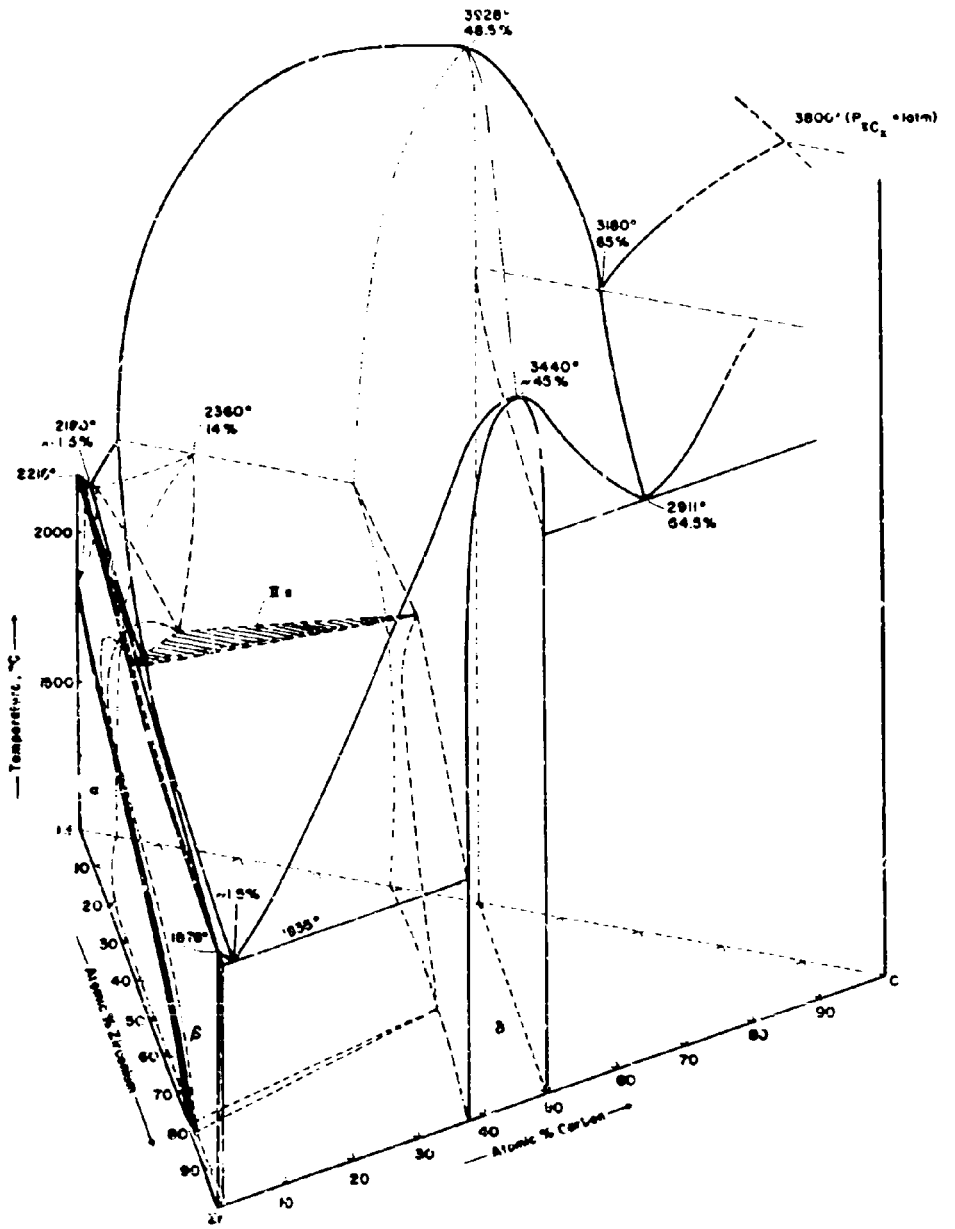

Figure III.E.7.1: Isometric View of the Zr-Hf-C System

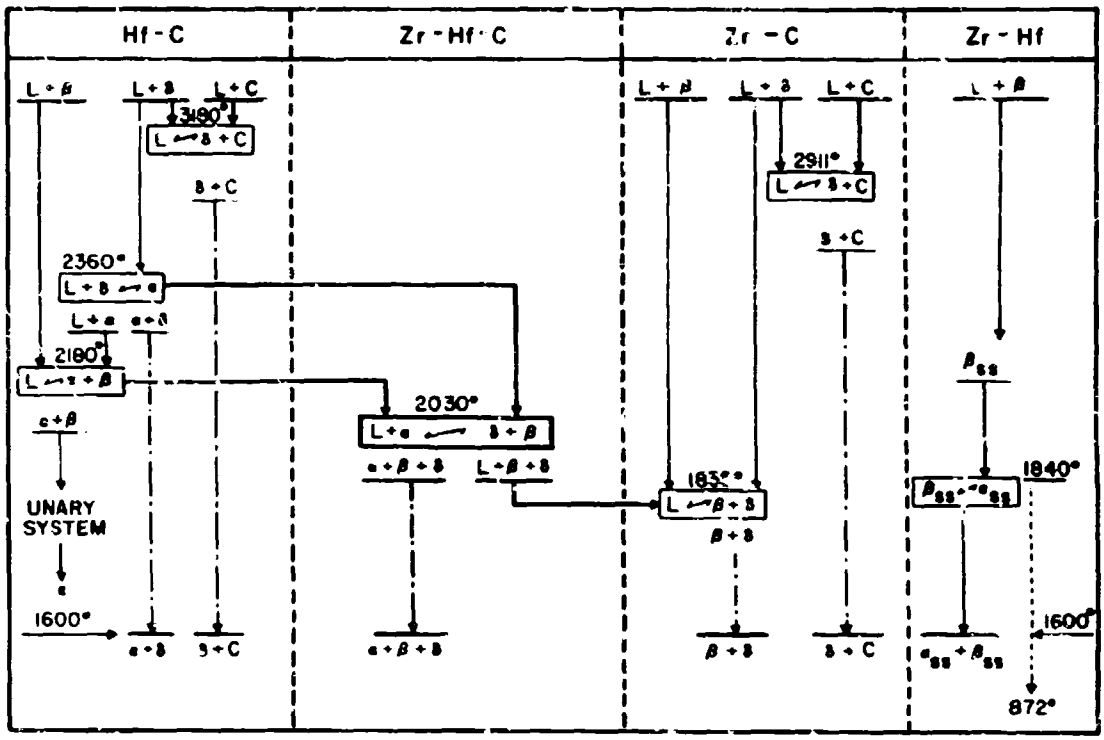

Figure III.E.7.2. Reaction Diagram for Ternary Zr-Hf-C Alloys

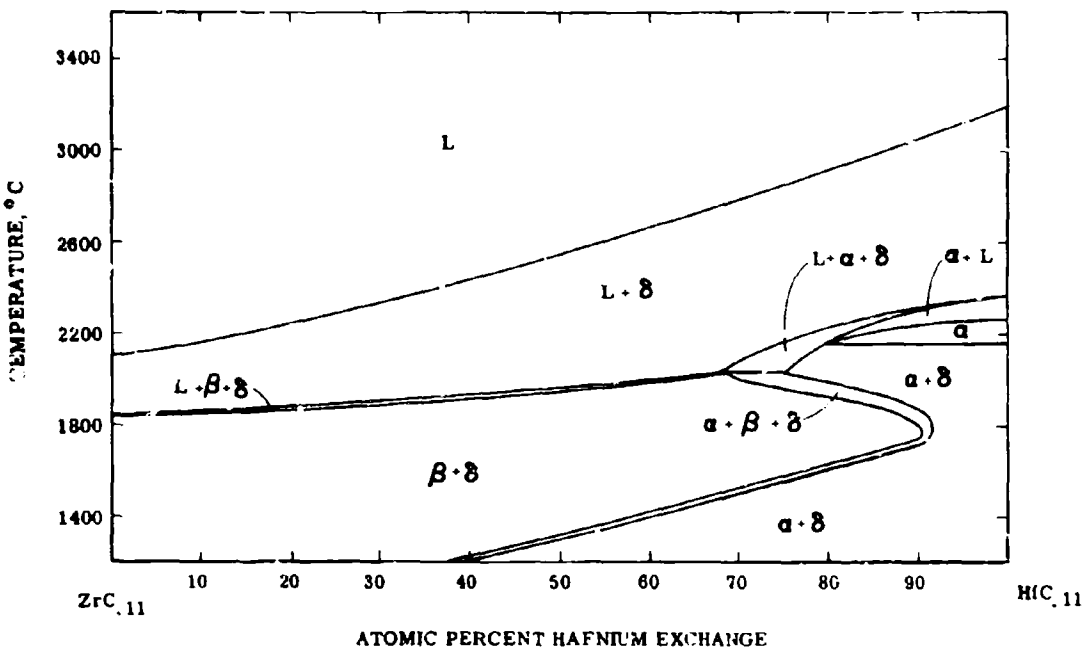

Figure III.E.7.3. Zr-Hf-C: Isopleth at 10 At.% C

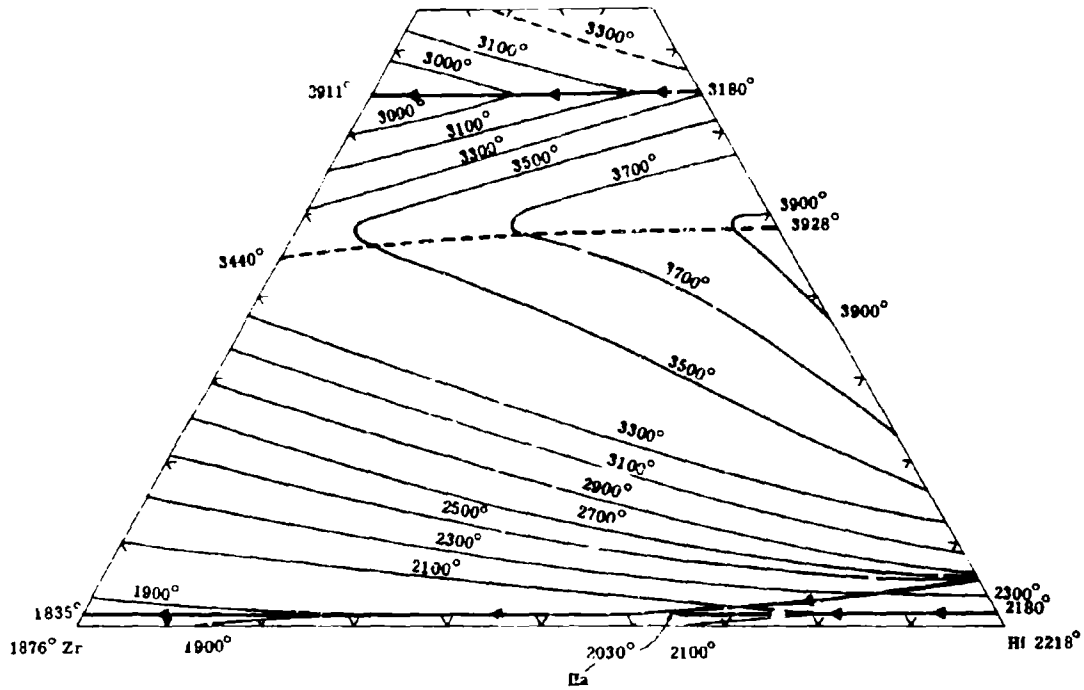

Figure III.E.7.1. Liquidus Projections in the Zr-Hf-C System

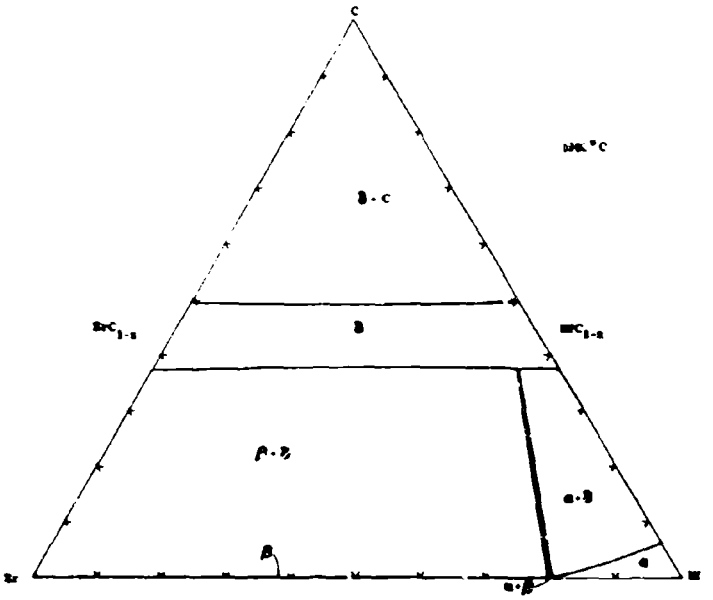

Figure III.E.7.5. Isothermal Section of the Zr-Hf-C System at 1600° C

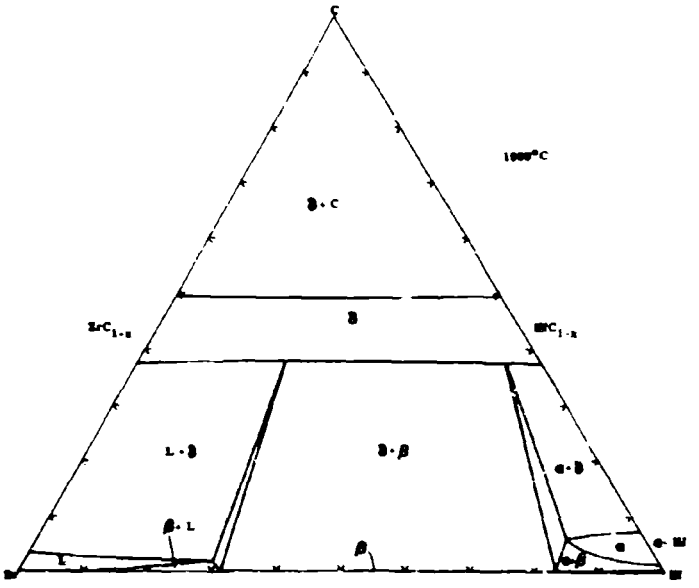

Figure III.E.7.6. Isothermal Section of the Zr-Hf-C System at 1900° C

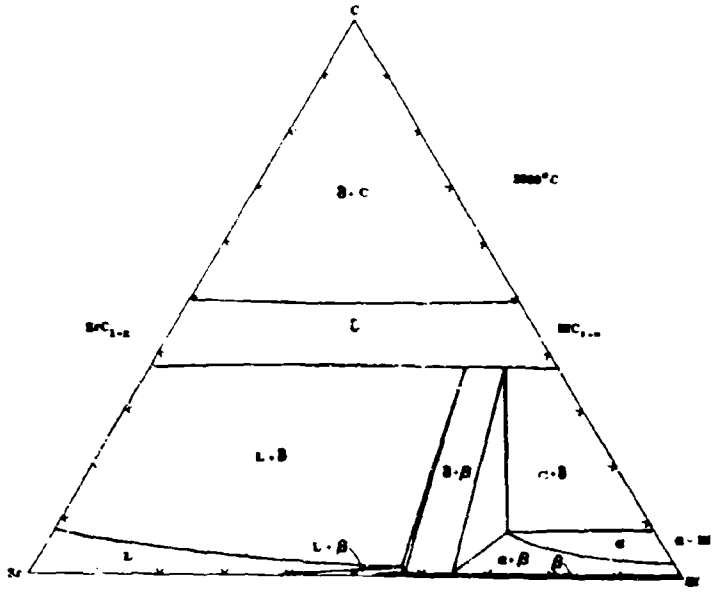

Figure III.E.7.7. Isothermal Section of the Zr-Hf-C System at 2000°C

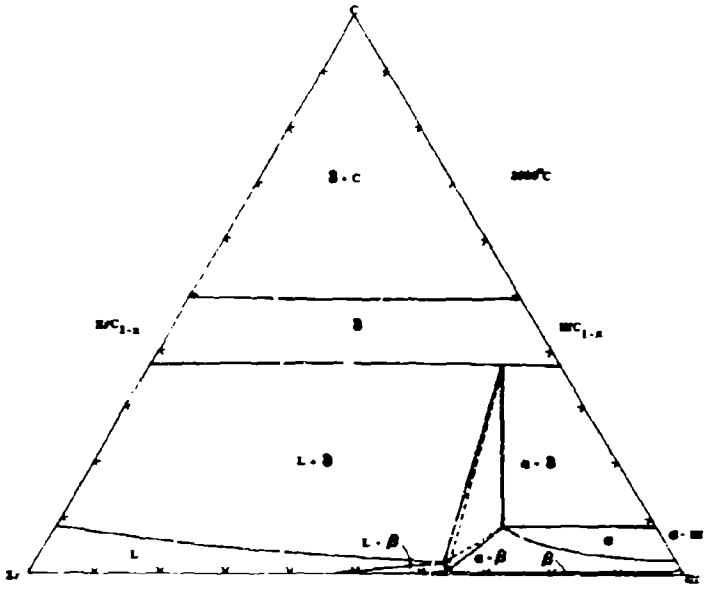

Figure III.E.7.8. Isothermal Section of the Zr-Hf-C System at 2030°C

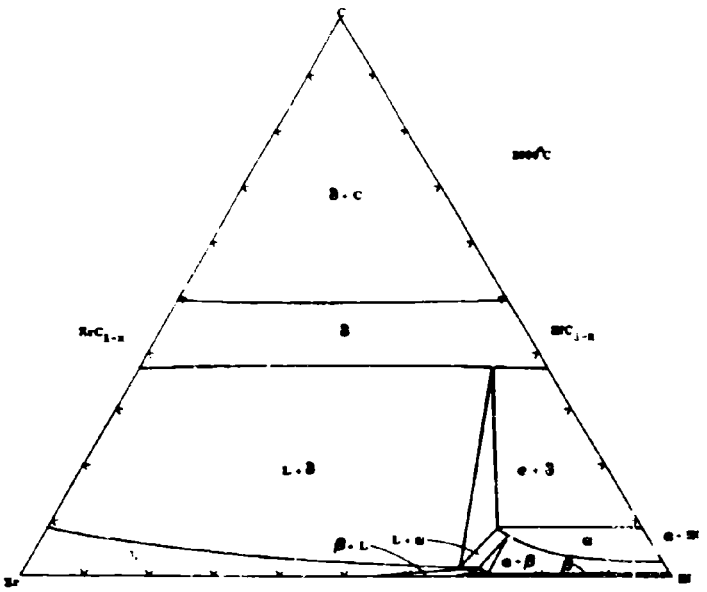

Figure III.E.7.9. Isothermal Section of the Zr-Hf-C System at 2060° C

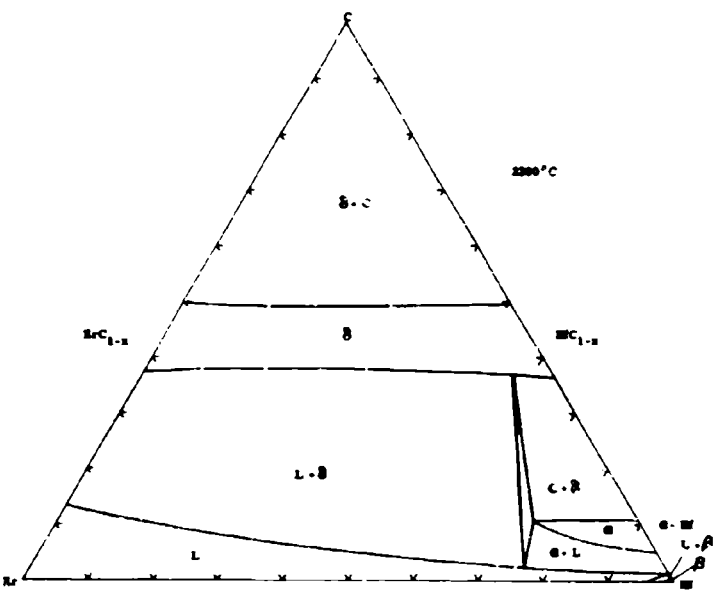

Figure III.E.7.10. Isothermal Section of the Zr-Hf-C System at 2200° C

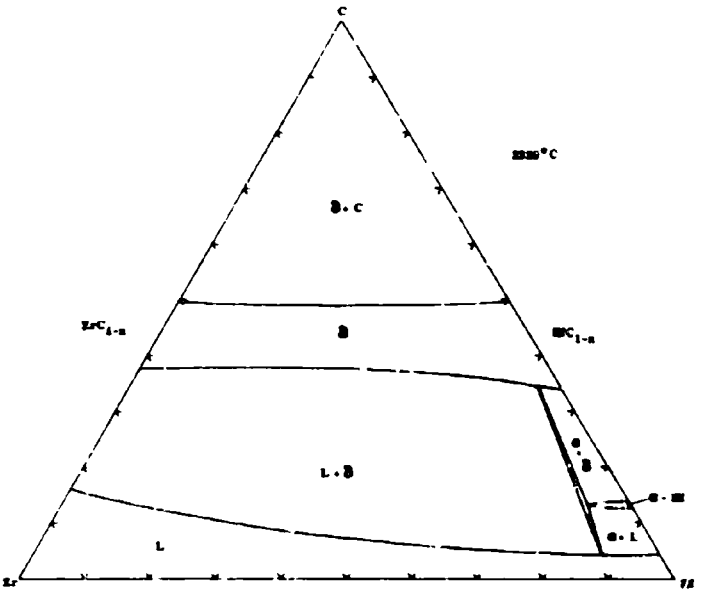

Figure III.E.7.11. Isothermal Section of the Zr-Hf-C System at 2320°C

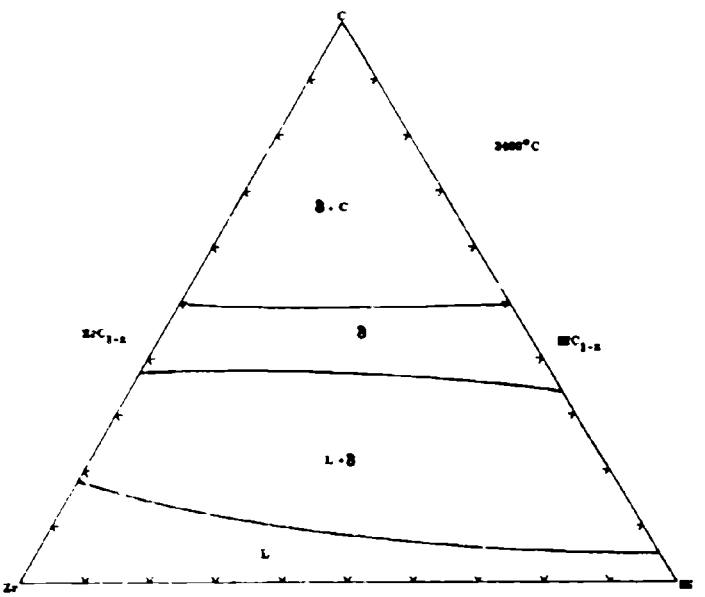

Figure III.E.7.12. Isothermal Section of the Zr-Hf-C System at 2400°C

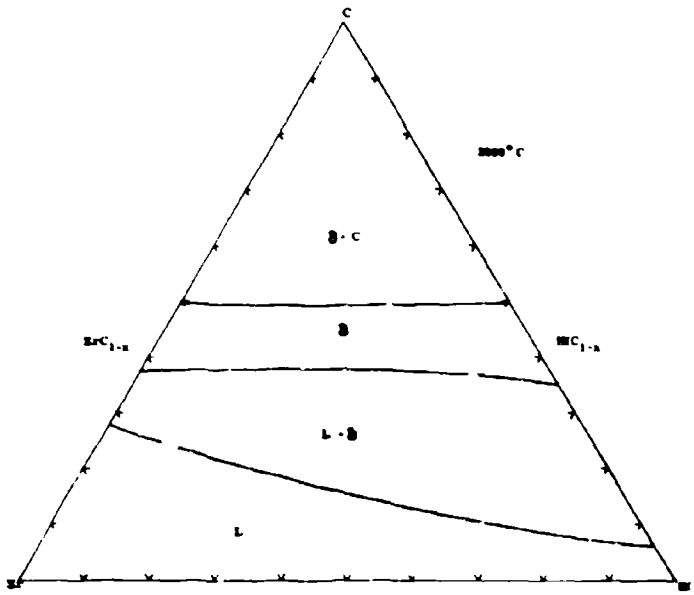

Figure III.E.7.13. Isothermal Section of the Zr-Hf-C System at 2800° C

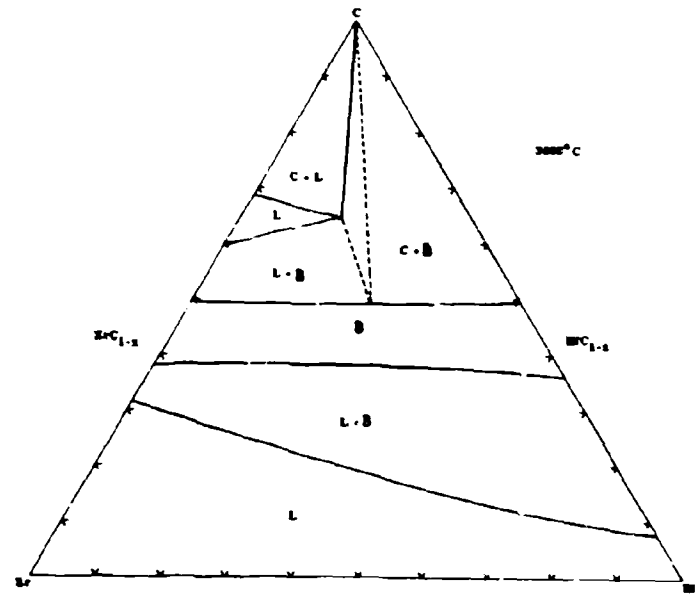

Figure III.E.7.14. Isothermal Section of the Zr-Hf-C System at 3000° C

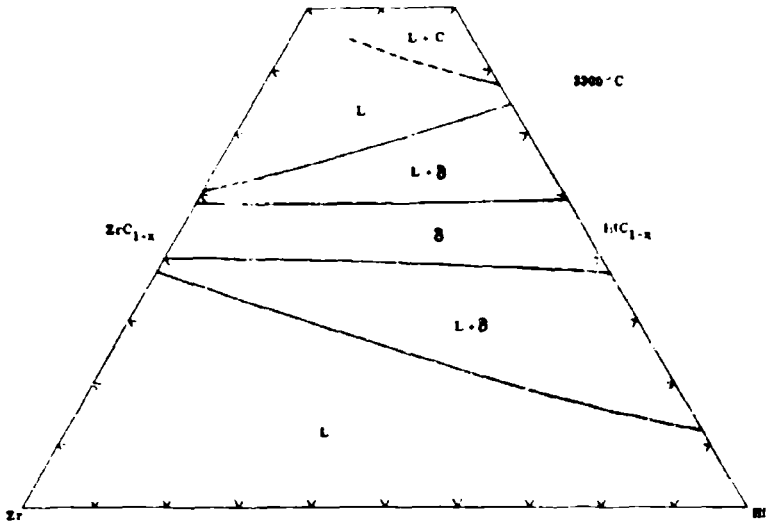

Figure III.E.7.15. Isothermal Section of the Zr-Hf-C System at 3300° C

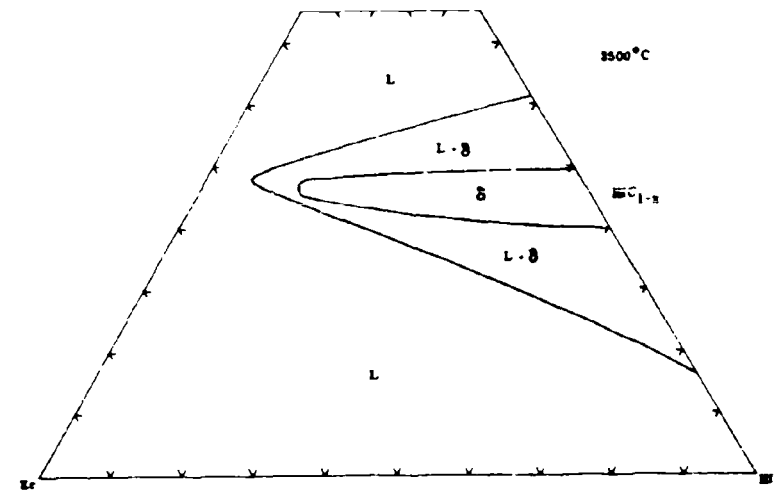

Figure III.E.7.16. Isothermal Section of the Zr-Hf-C System at 3500° C

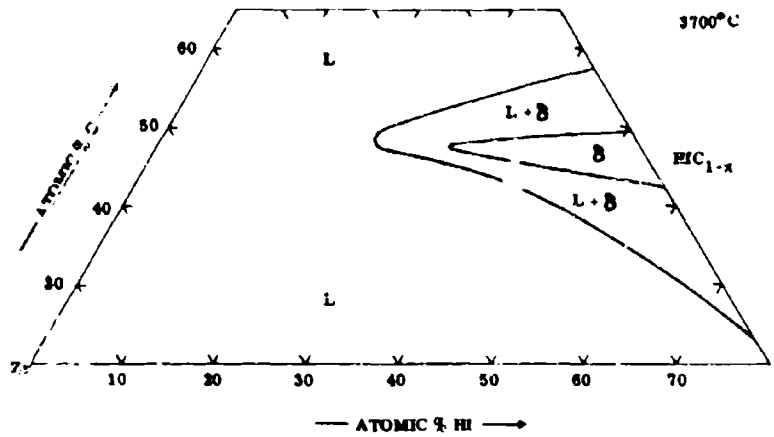

Figure III.E.7.17. Isothermal Section of the Zr-Hf-C System at 3700°C

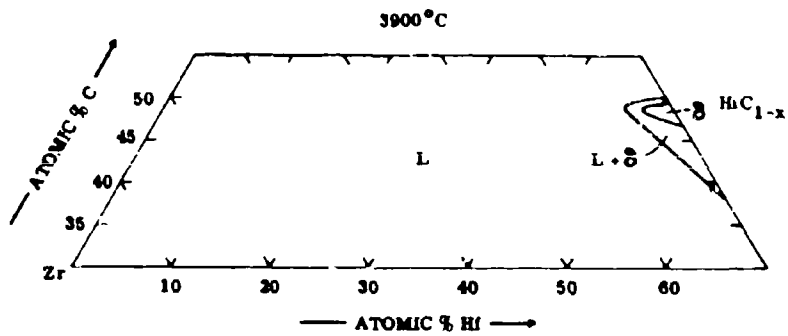

Figure III.E.7.18. Isothermal Section of the Zr-Hf-C System at 3900°C

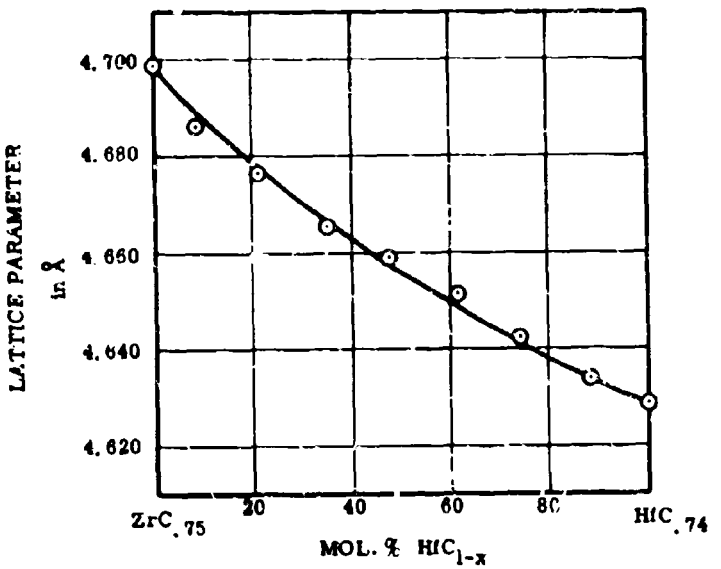

Figure III.E.7.19. Lattice Parameters of $(Zr,Hf)C_{.74-.75}$

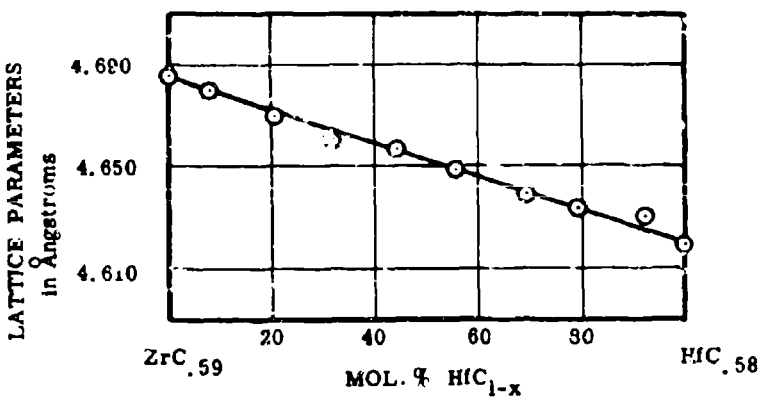

Figure III.E.7.20. Lattice Parameters of $(Zr,Hf)C_{0.58-.59}$

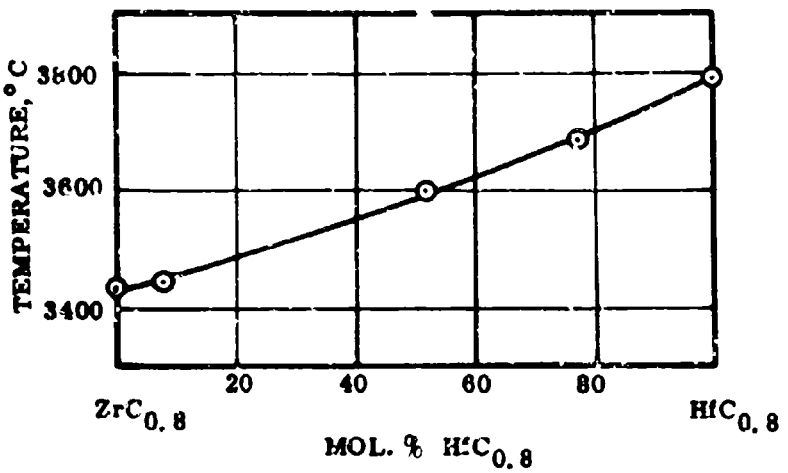

Figure III.E.7.21. Melting Temperatures of Monocarbide Alloys at $(Zr,Hf)C_{0.8}$

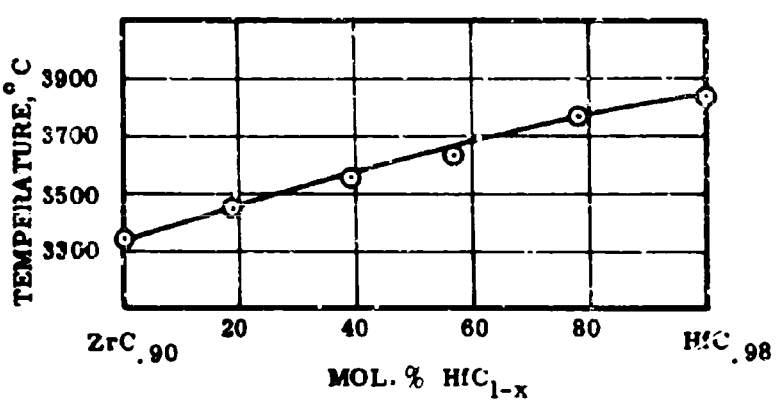

Figure III.E.7.22. Melting Temperatures of Monocarbide Alloys at $(Zr,Hf)C_{.90-.98}$

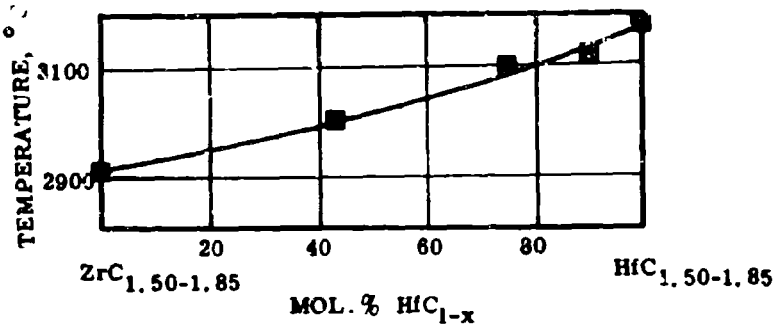

Figure III.E.7.23. Melting Along the Monocarbide + Graphite Eutectic Trough

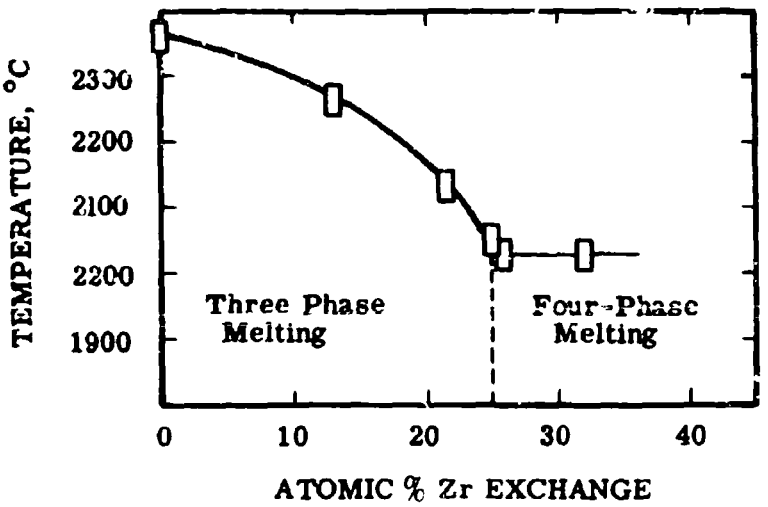

Figure III.E.7.24. Zr-Hf-C. Incipient Melting of the α-(Zr,Hf,C)-Phase

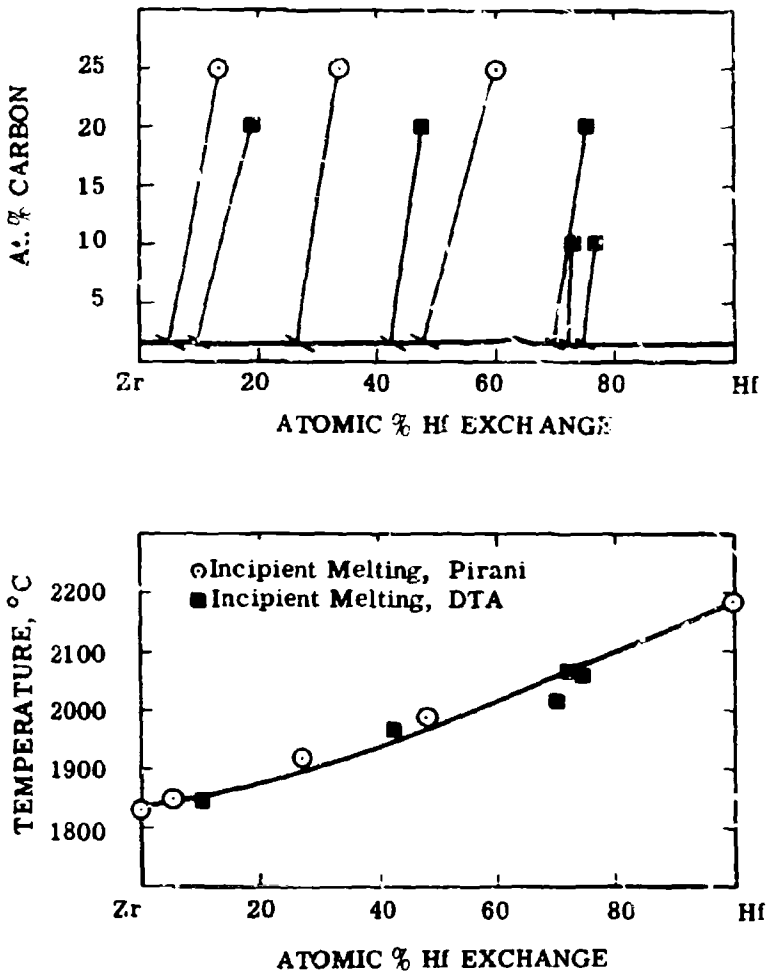

Figure III.E.7.25. Bivariant Melting in Metal-Rich Zr-Hf-C Alloys and Location of the Metal-Rich Eutectic Trough

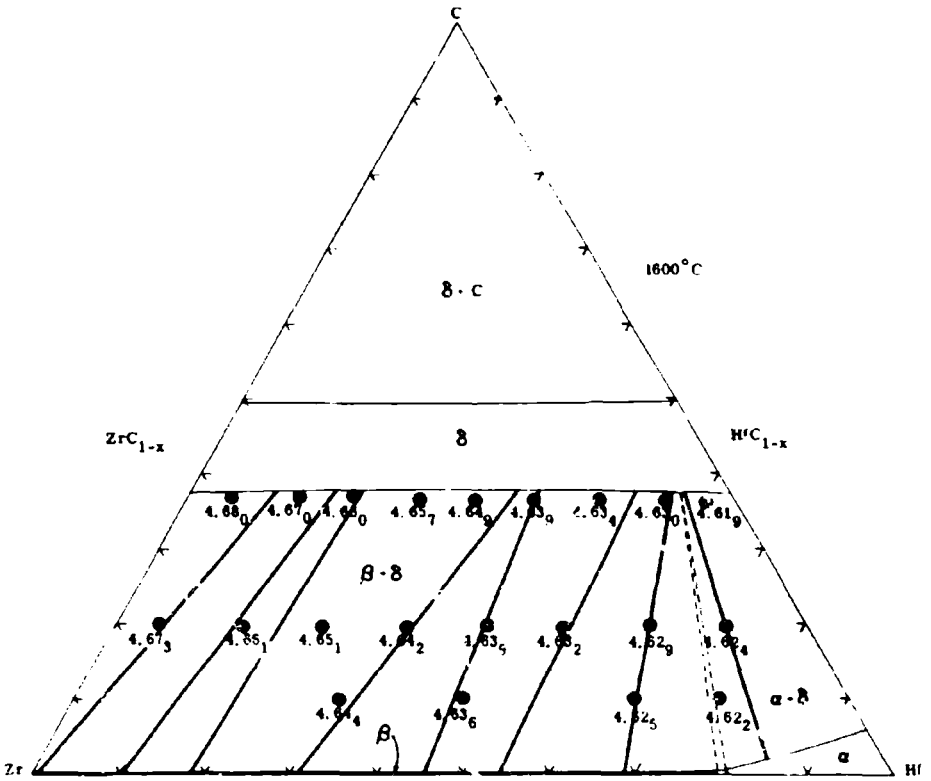

Figure III.E.7.26. Zr-Hf-C. Monocarbide Lattice Parameters (in Ångström) and Tie Lines in the Metal + Monocarbide Region.

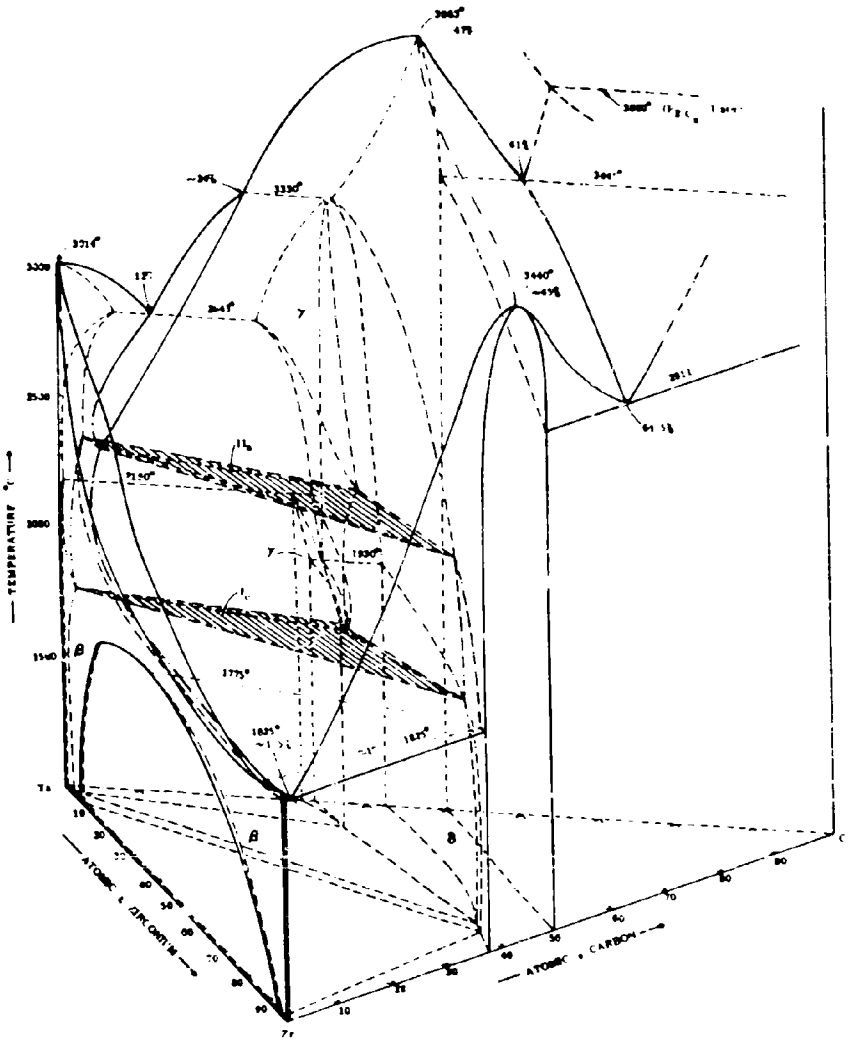

Figure III.E.8.1. Isometric View of the Zr-Ta-C System

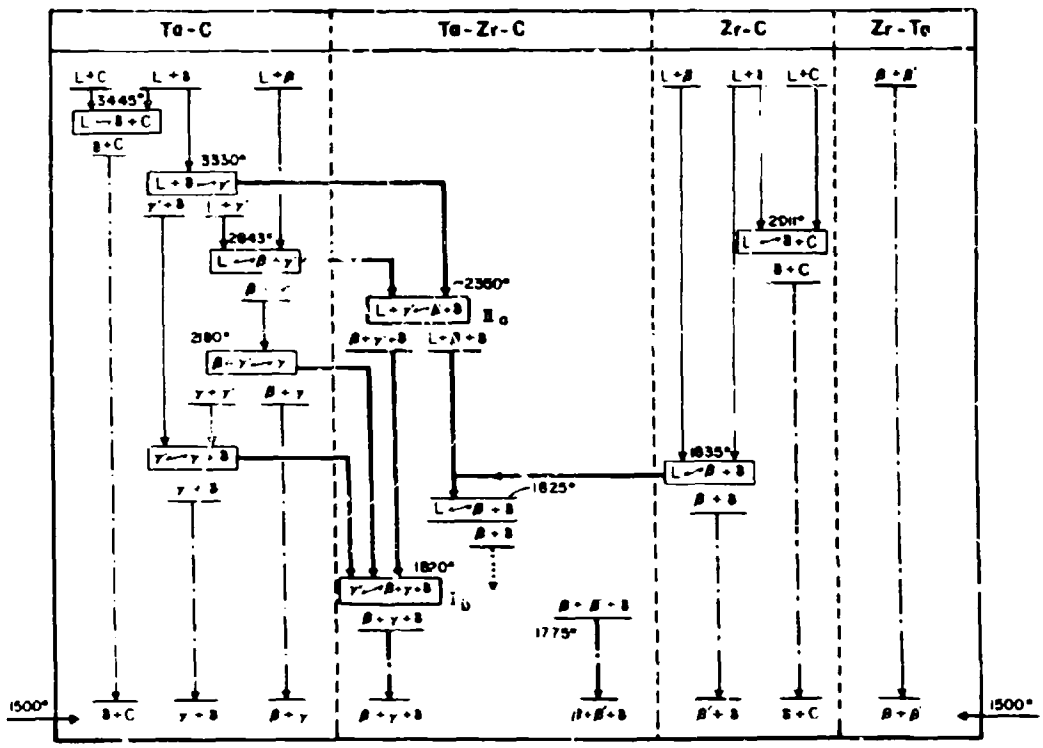

Figure III.E.8.2. Reaction Diagram for Zr-Ta-C Alloys

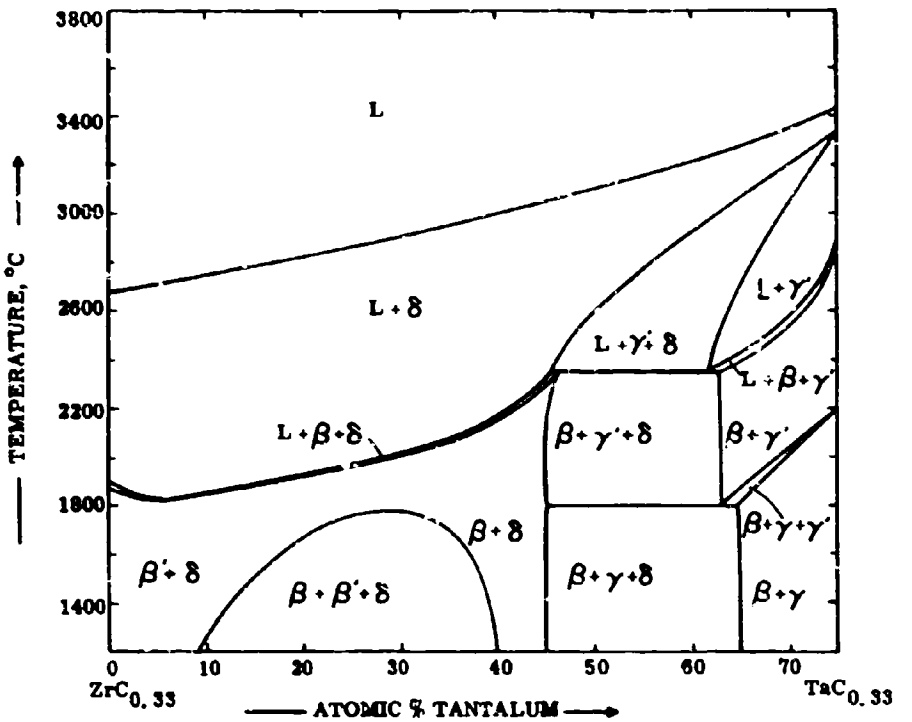

Figure III.E.8.3. Zr-Ta-C: Isopleth at $ZrC_{0.33}$-$TaC_{0.33}$

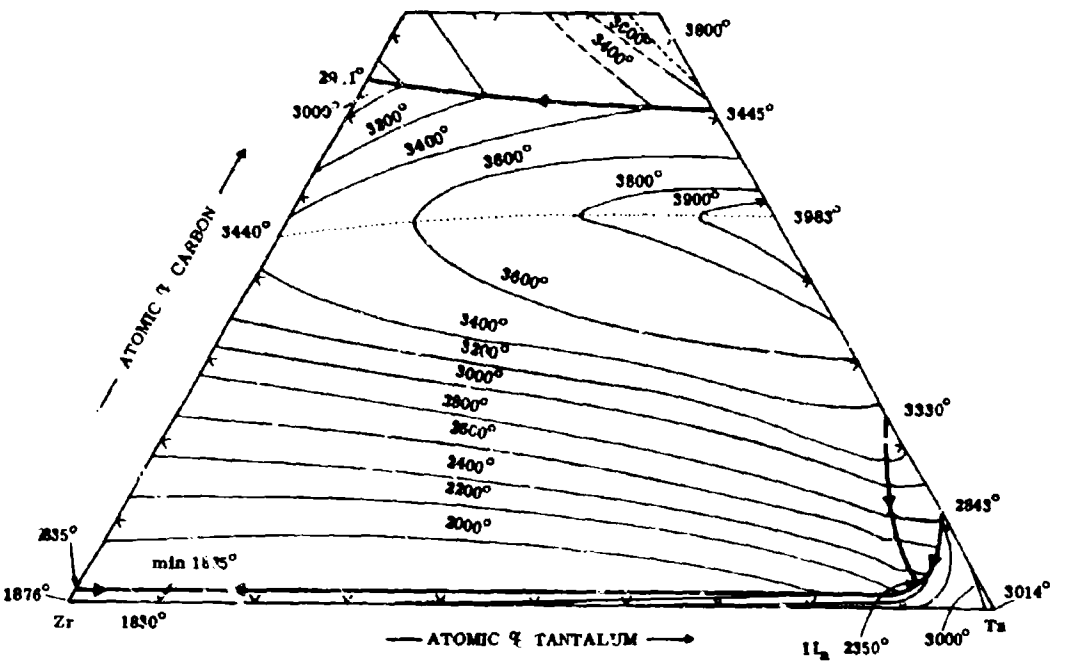

Figure III.E.8.4. Liquidus Projections in the Zr-Ta-C System

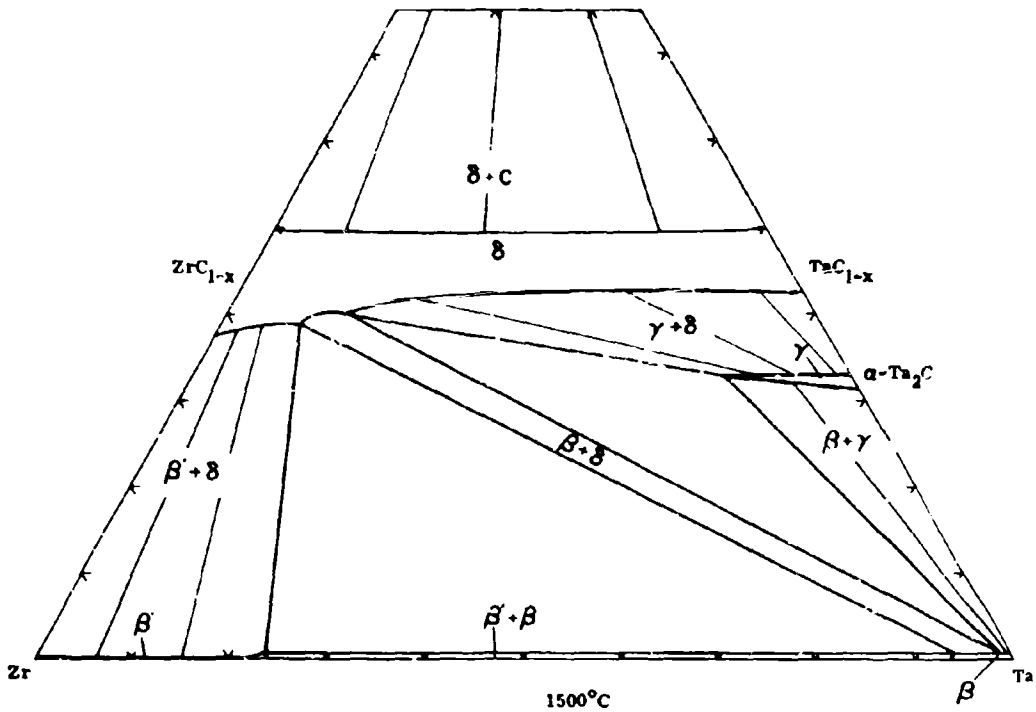

Figure III.E.8.5. Isothermal Section of the Zr-Ta-C System at 1500° C

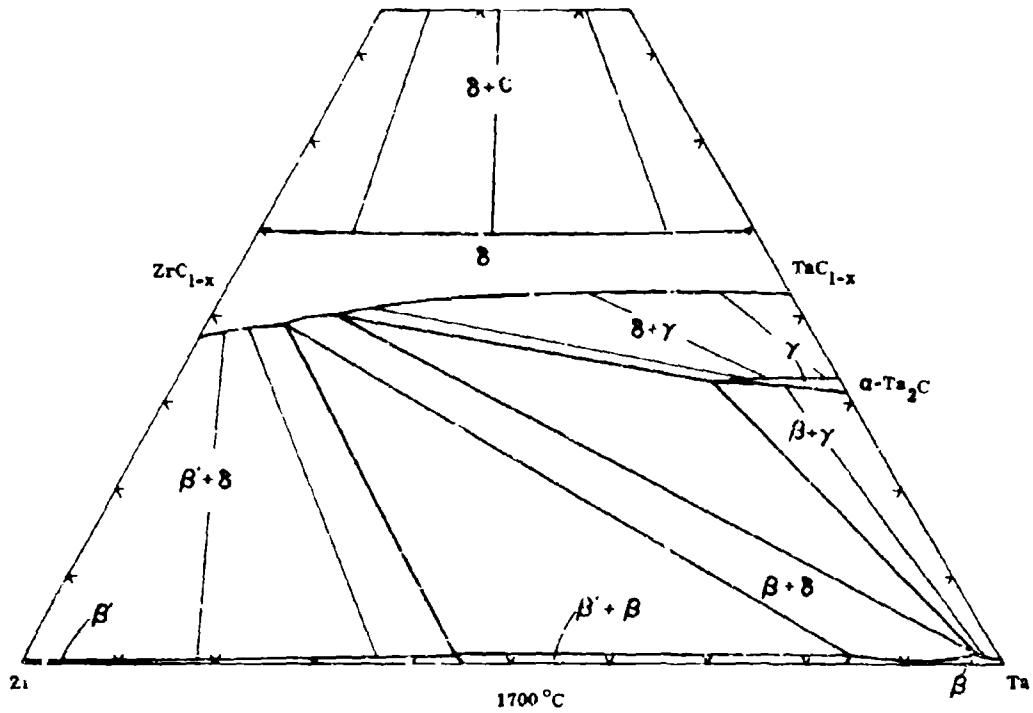

Figure III.E.8.6. Isothermal Section of the Zr-Ta-C System at 1700° C

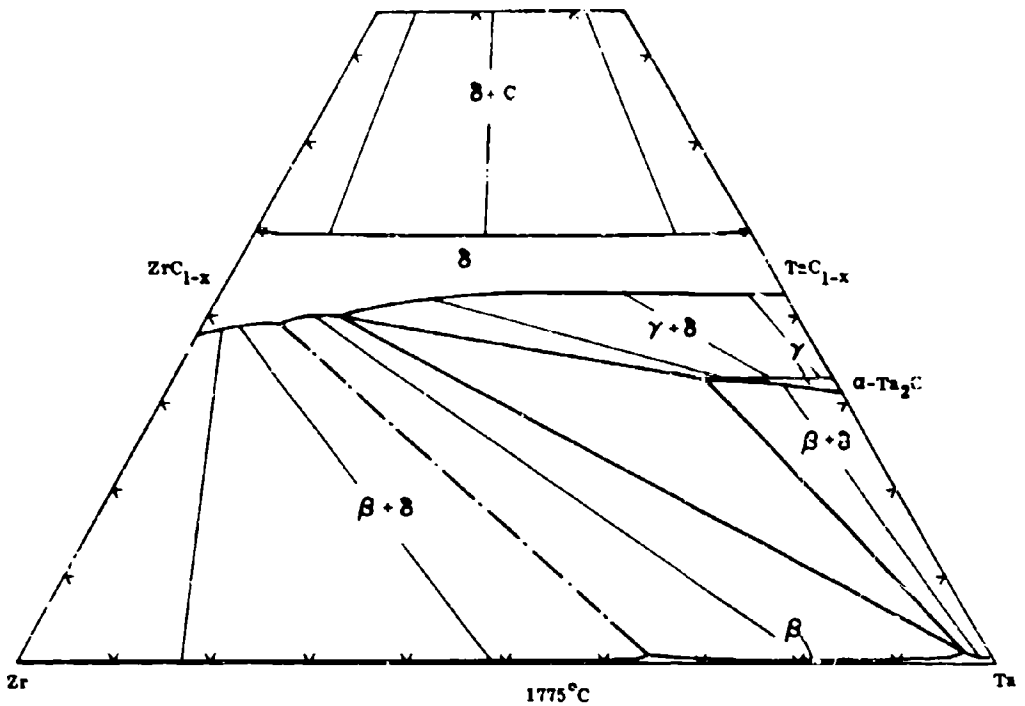

Figure III.E.8.7. Isothermal Section of the Zr-Ta-C System at 1775°C

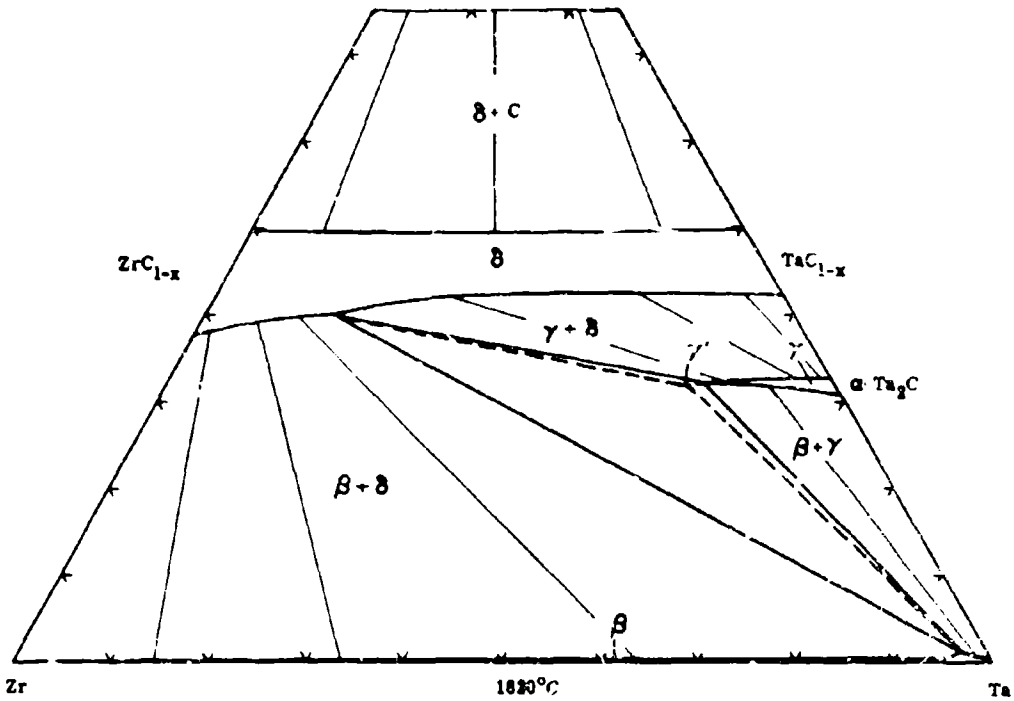

Figure III.E.8.8. Isothermal Section of the Zr-Ta-C System at 1820° C

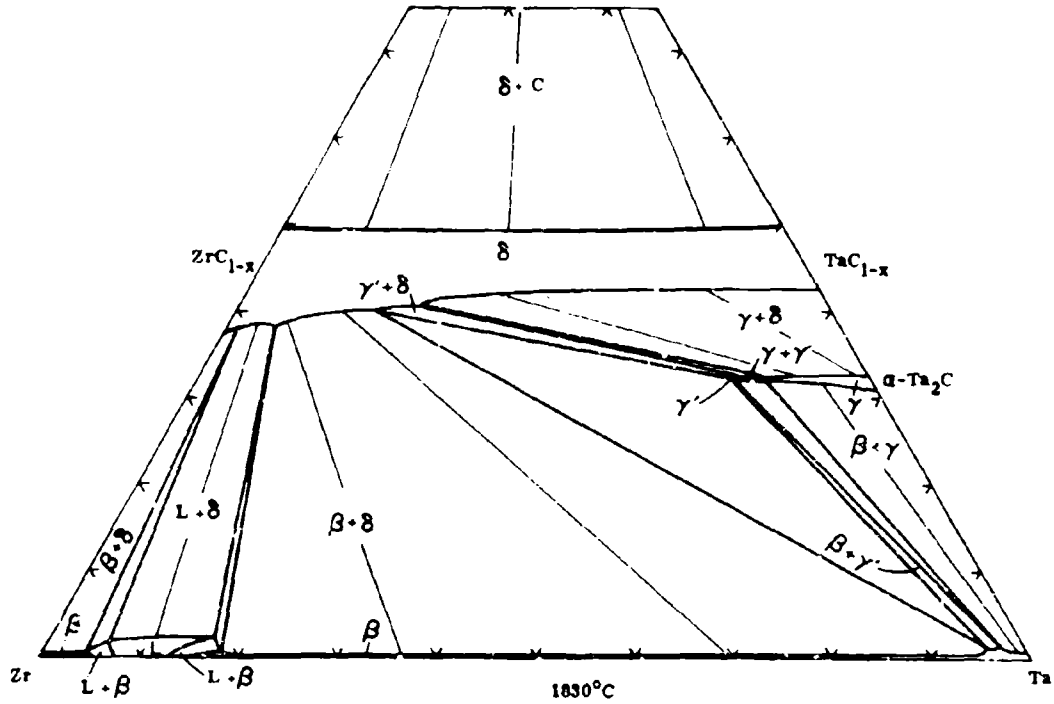

Figure III.E.8.c. Isothermal Section of the Zr-Ta-C System at 1830°C

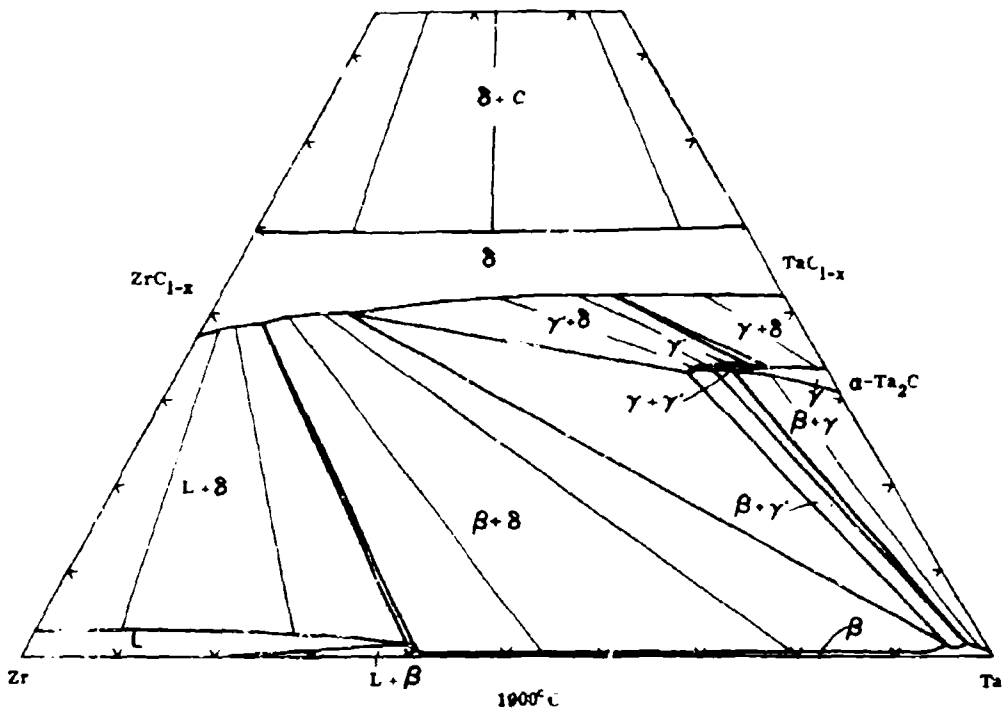

Figure III.E.8.10. Isothermal Section of the Zr-Ta-C System at 1900°C

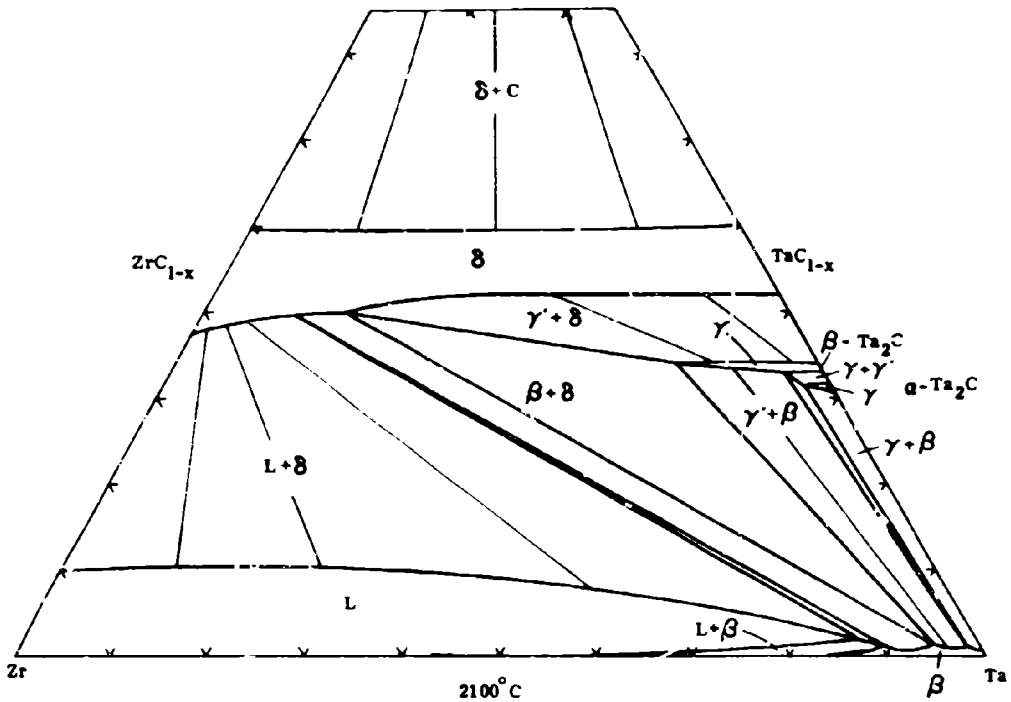

Figure III.E.8.11. Isothermal Section of the Zr-Ta-C System at 2100°C

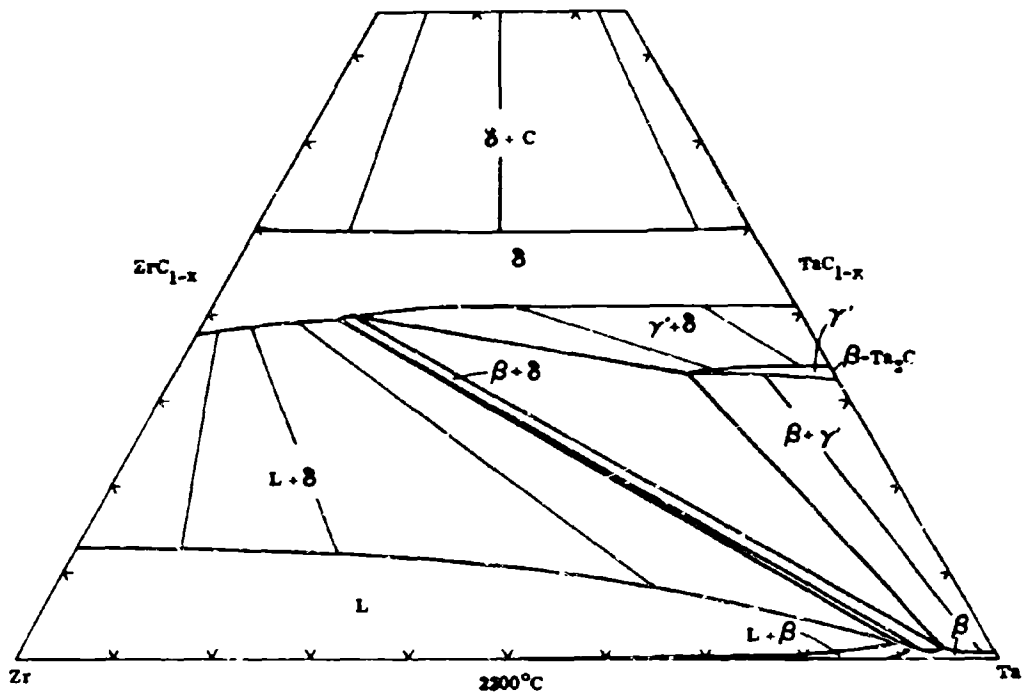

Figure III.E.8.12. Isothermal Section of the Zr-Ta-C System at 2200° C

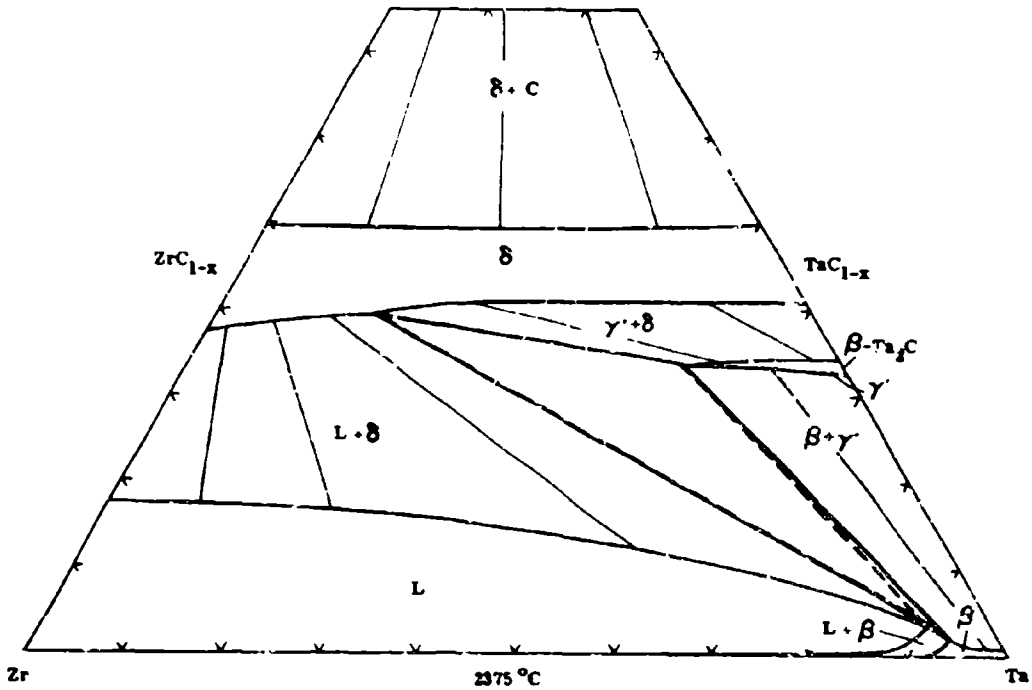

Figure III.E.8.13. Isothermal Section of the Zr-Ta-C System at 2375° C

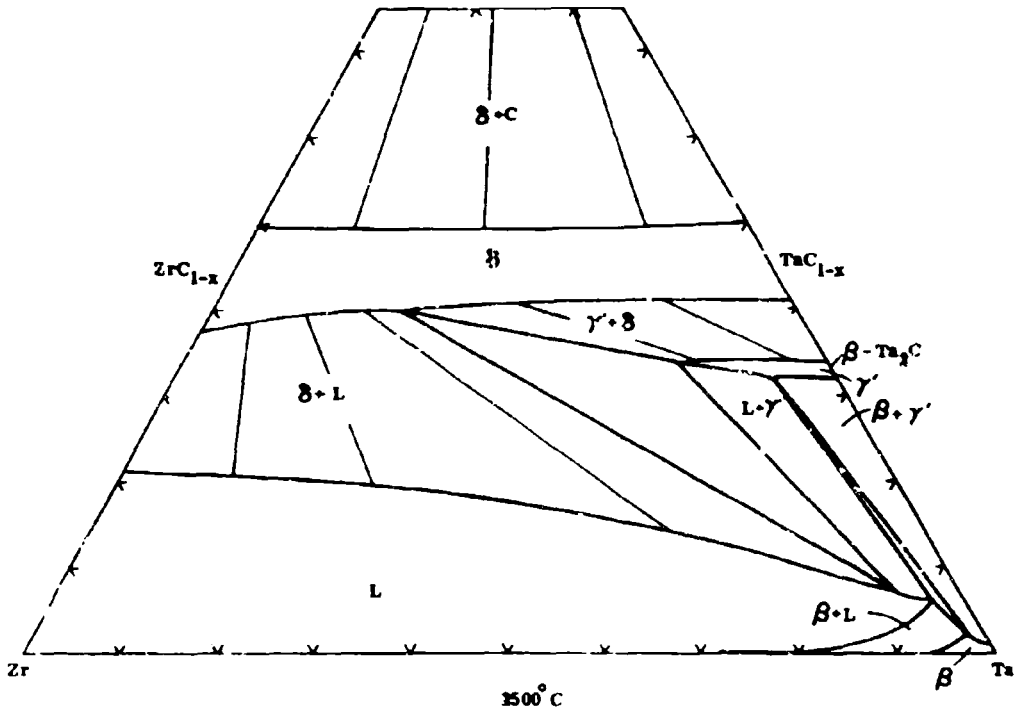

Figure III.E.8.14. Isothermal Section of the Zr-Ta-C System at 2500°C

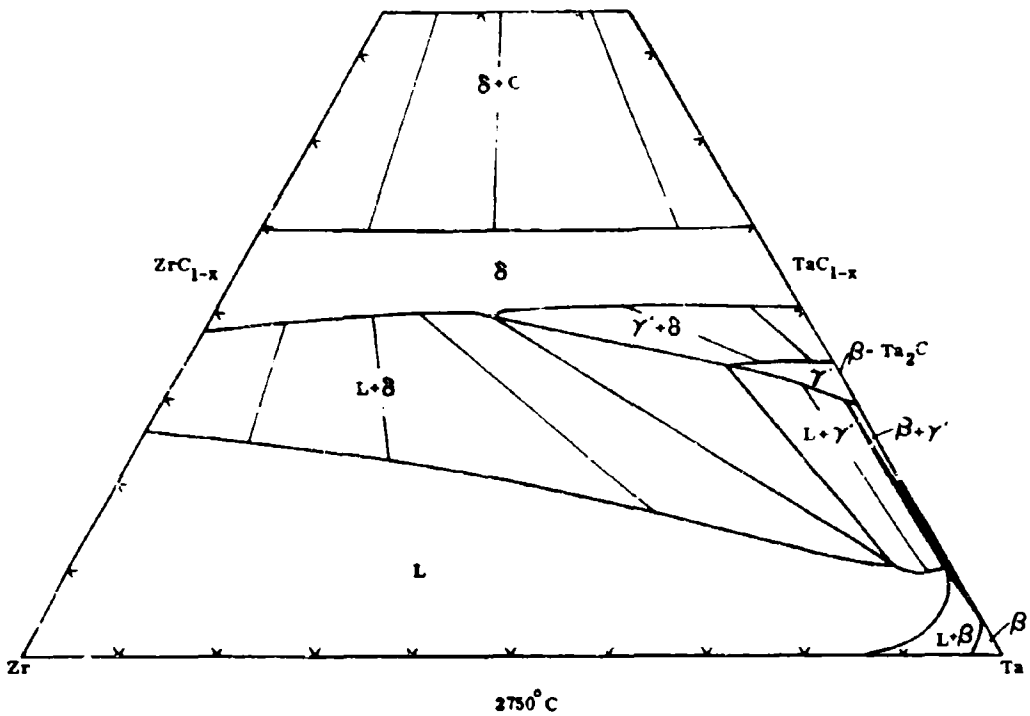

Figure III.E.8.15. Isothermal Section of the Zr-Ta-C System at 2750°C

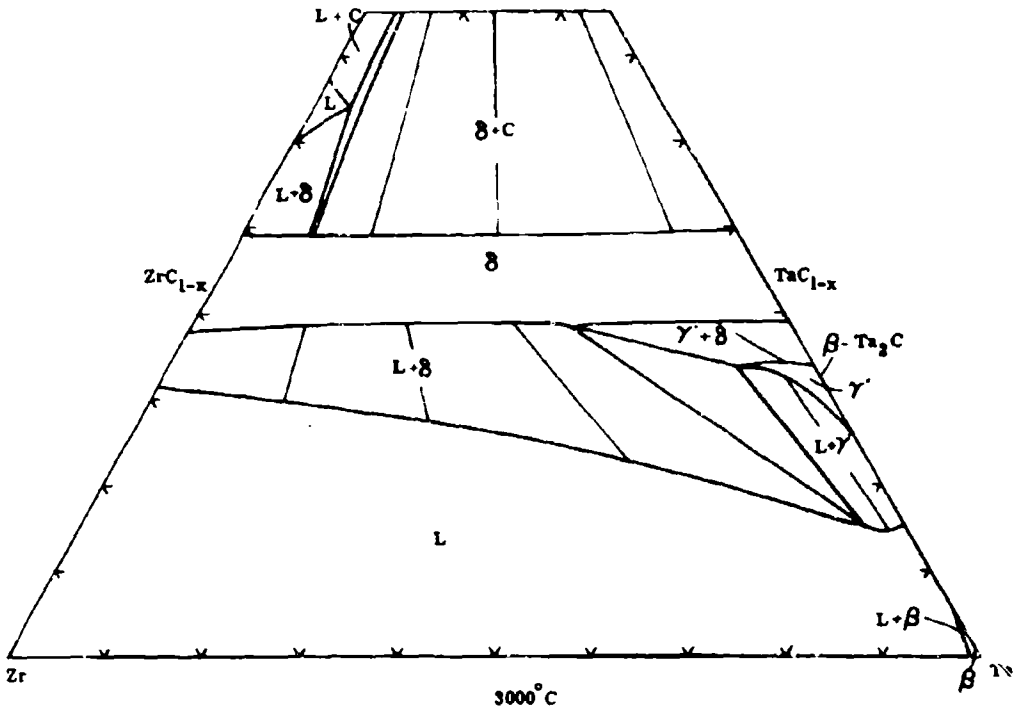

Figure III.E.8.16. Isothermal Section of the Zr-Ta-C System at 3000° C

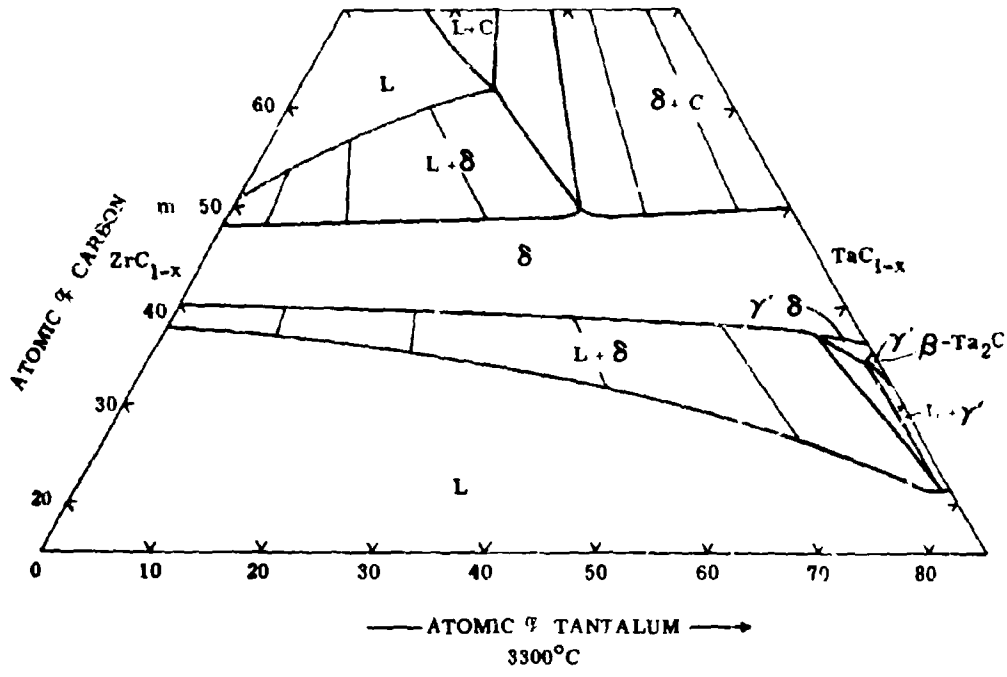

Figure III.E.8.17. Isothermal Section of the Zr-Ta-C System at 3300° C

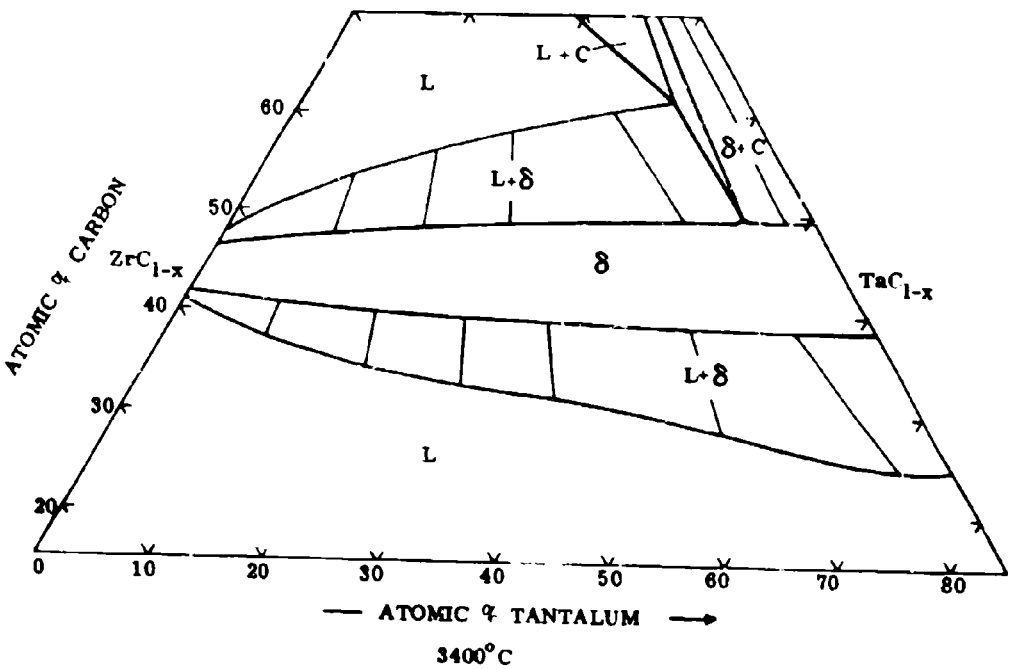

Figure III.E.8.18. Isothermal Section of the Zr-Ta-C System at 3400° C

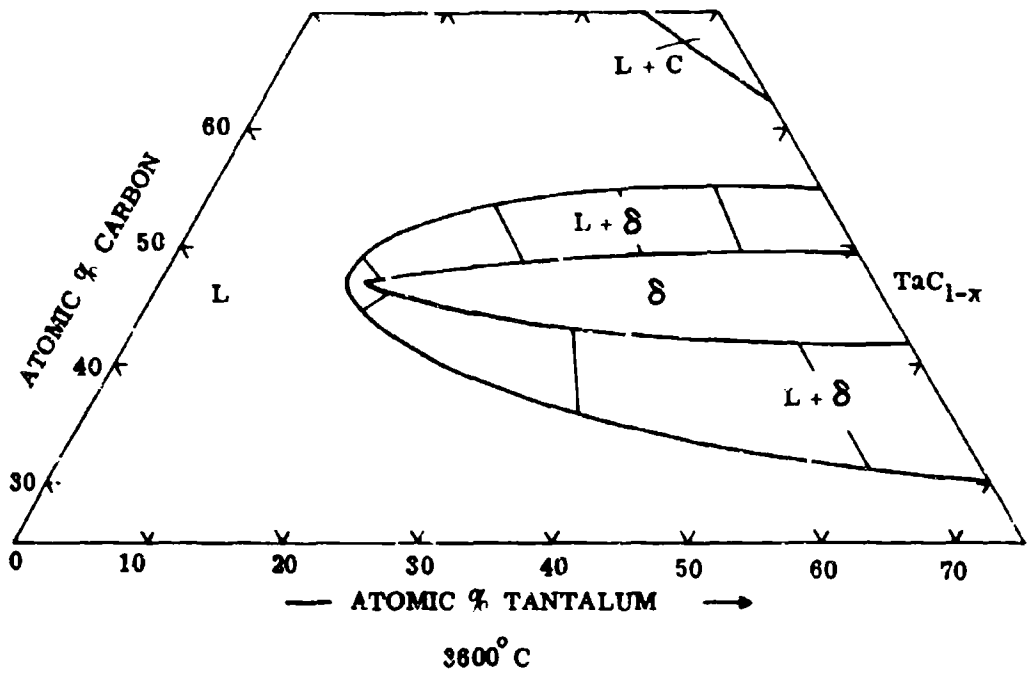

Figure III.E.8.19. Isothermal Section of the Zr-Ta-C System at 3600° C

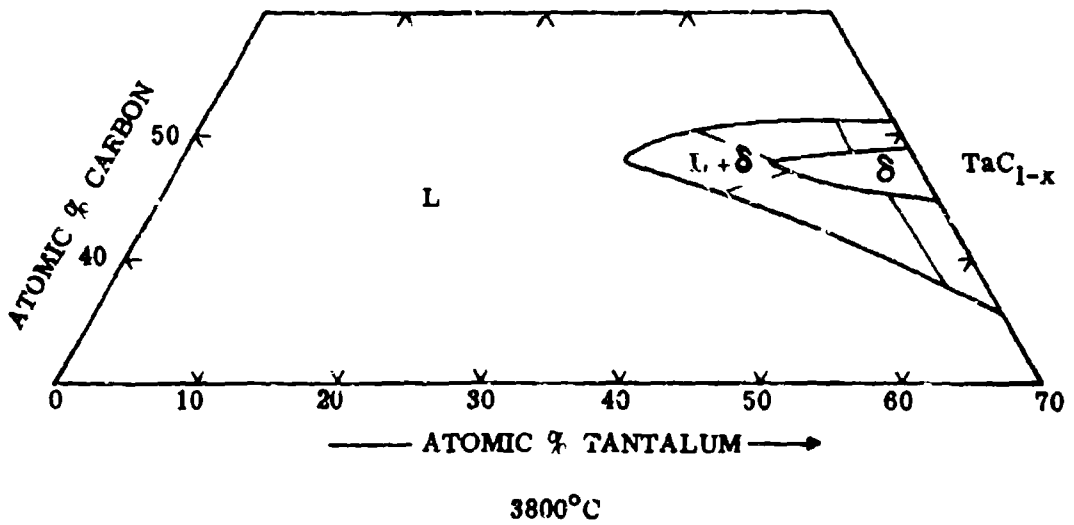

Figure III.E.8.20. Isothermal Section of the Zr-Ta-C System at 3800°C

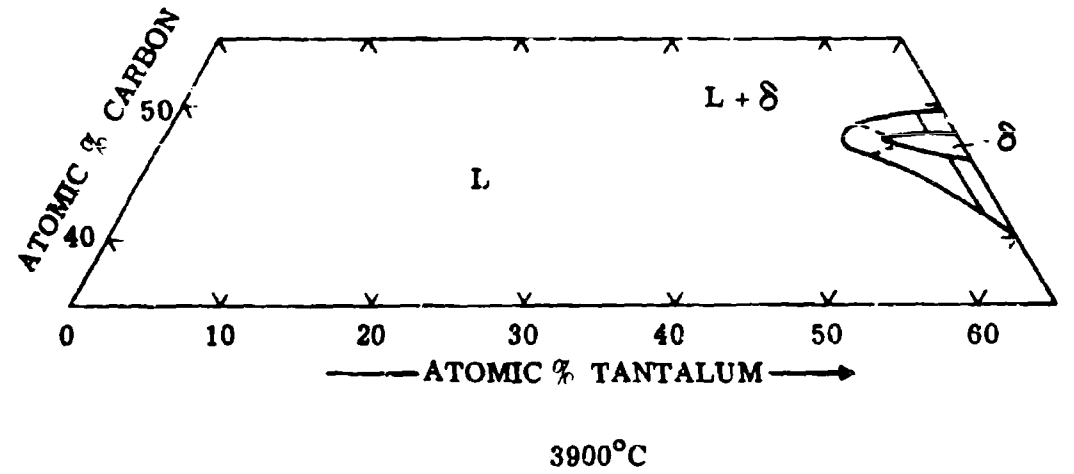

Figure III.E.8.21. Isothermal Section of the Zr-Ta-C System at 3900°C

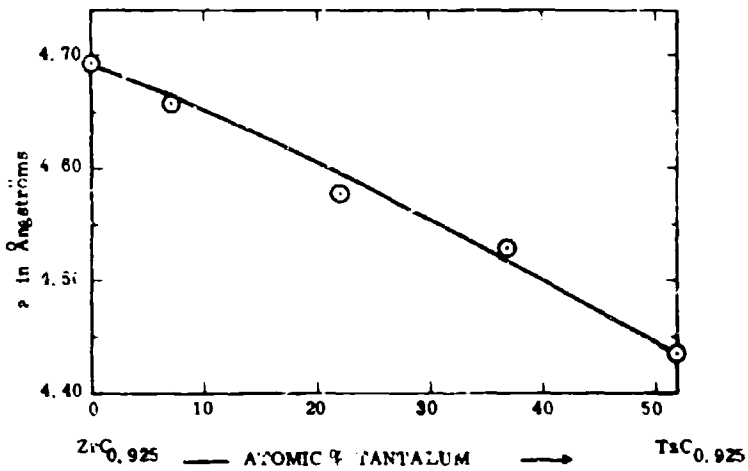

Figure III.E.8.22. Lattice Parameters of the $(Zr,Ta)C_{1-x}$ Solid Solution at 48 At.% C.

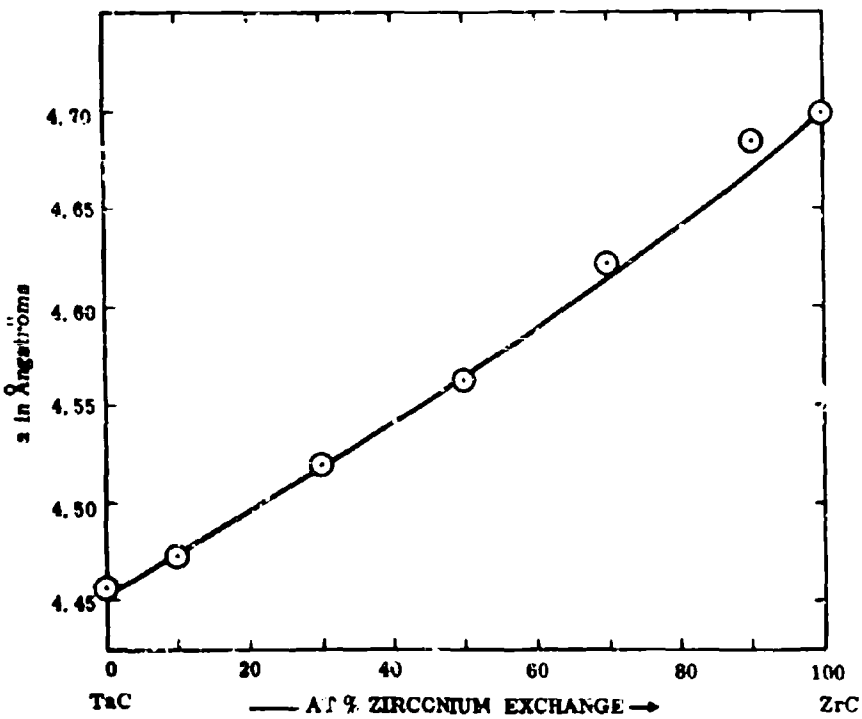

Figure III.E.8.23. Lattice Parameters of the Monocarbide Solid Solution at 50 At.% C. Alloys Quenched from Above 3000°C

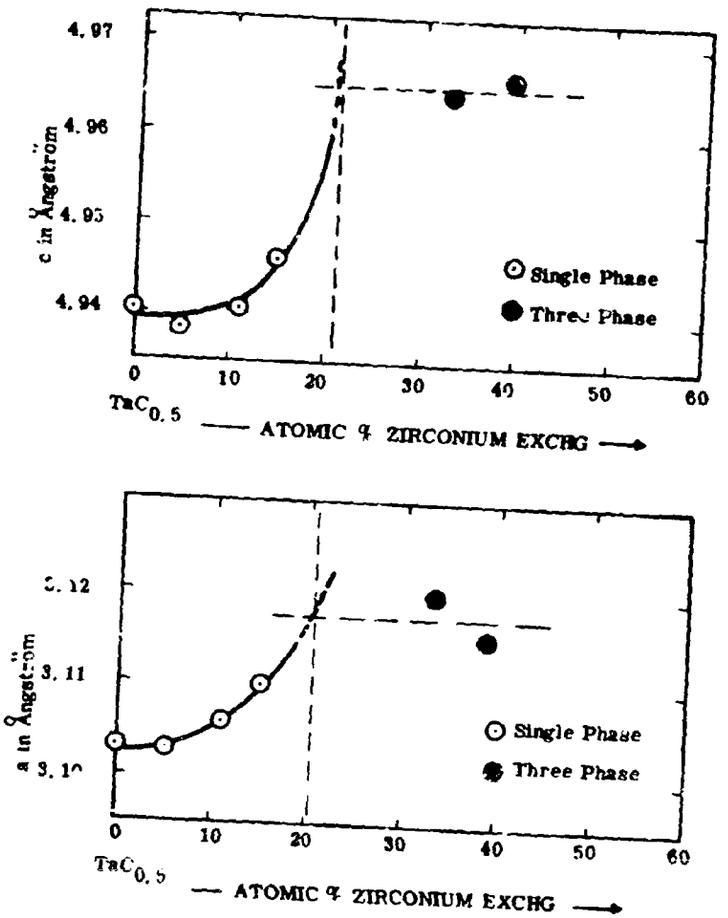

Figure III.E.8.24. Lattice Parameters of the Ta_2C-Phase in 1500°C-Equilibrated Alloys.

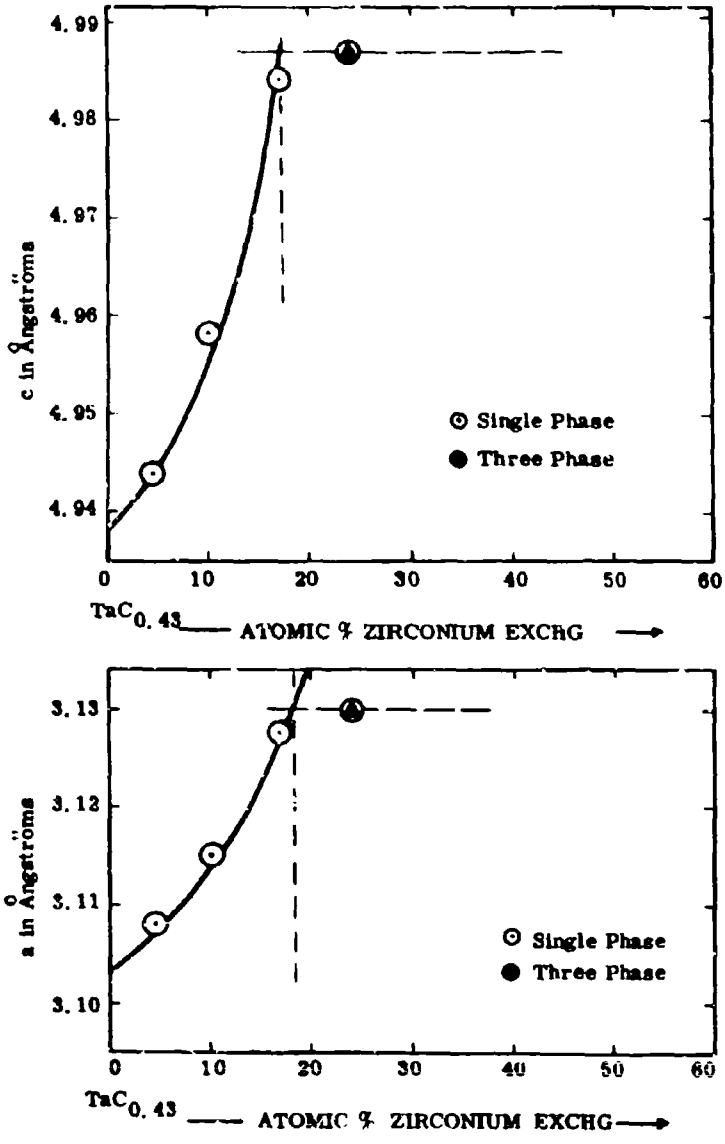

Figure III.E.8.25. Lattice Parameters of the Ta_2C-Phase in Alloys which were Quenched from above 2400° C

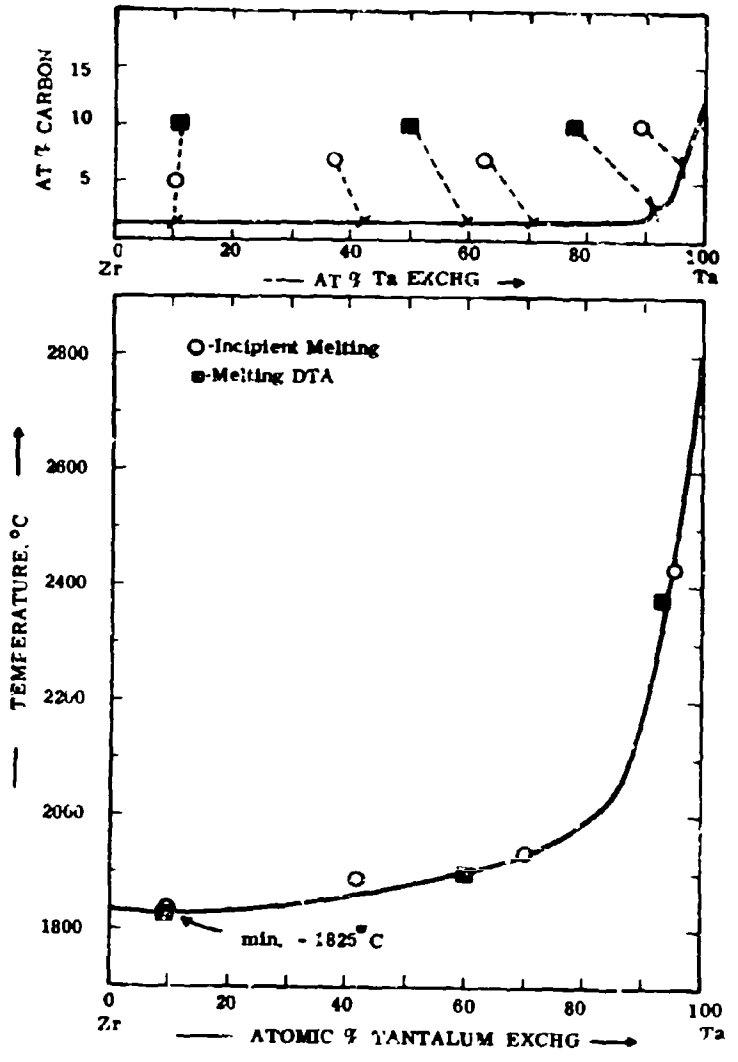

Figure III.E.8.26. Composition (Top) and Temperatures of the Metal-Rich Eutectic Trough in the Zr-Ta-C System

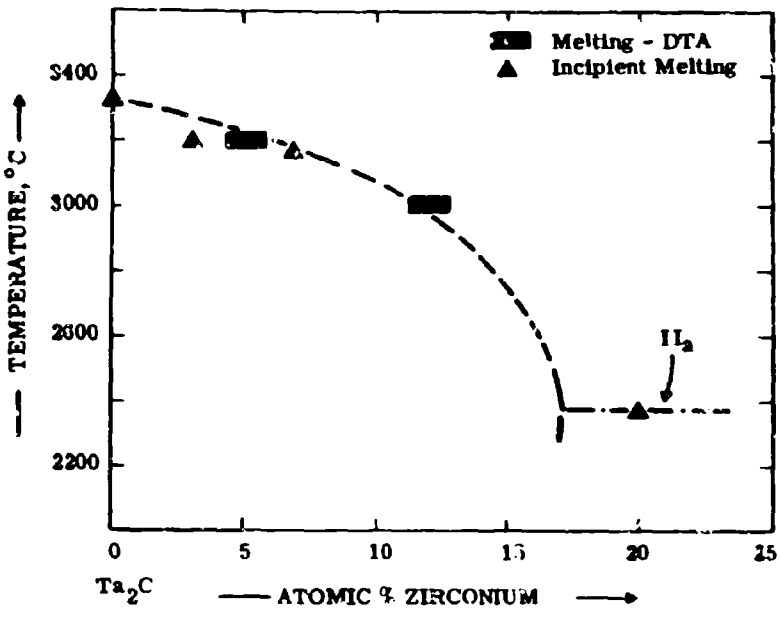

Figure III.E.8.27. Approximate Solidus Temperatures of the $(Ta,Zr)_2C$ Phase

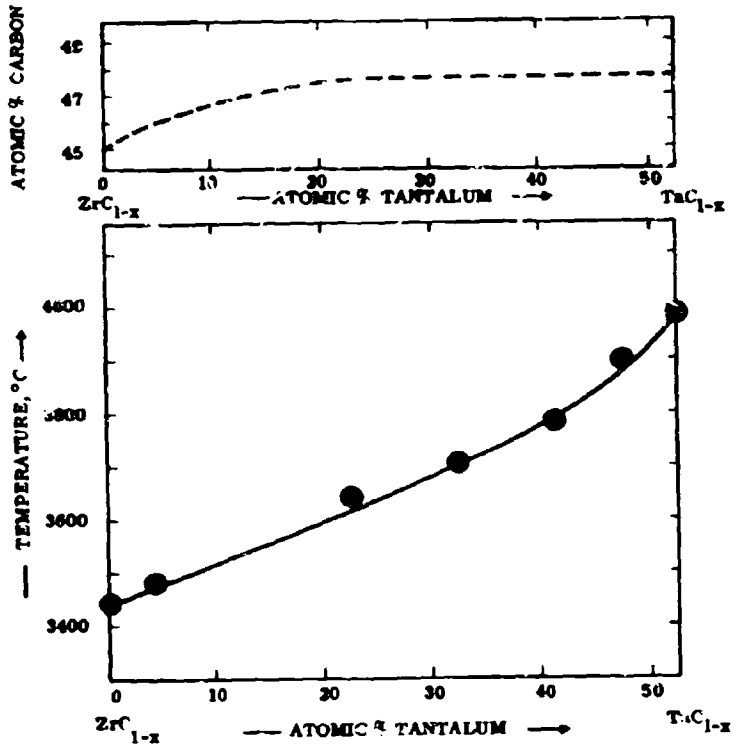

Figure III.E.8.28. Composition of the Maximum Solidus (Top) and Maximum Solidus Temperature of the $(Zr,Ta)C_{1-x}$ Solid Solution

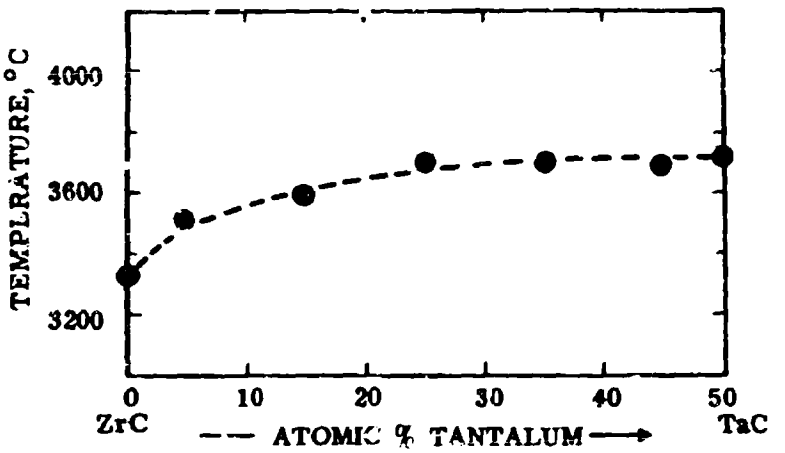

Figure III.E.8.29. Collapsing Temperatures of the Zr-Ta-C Alloy Series Located at 50 At.% C.

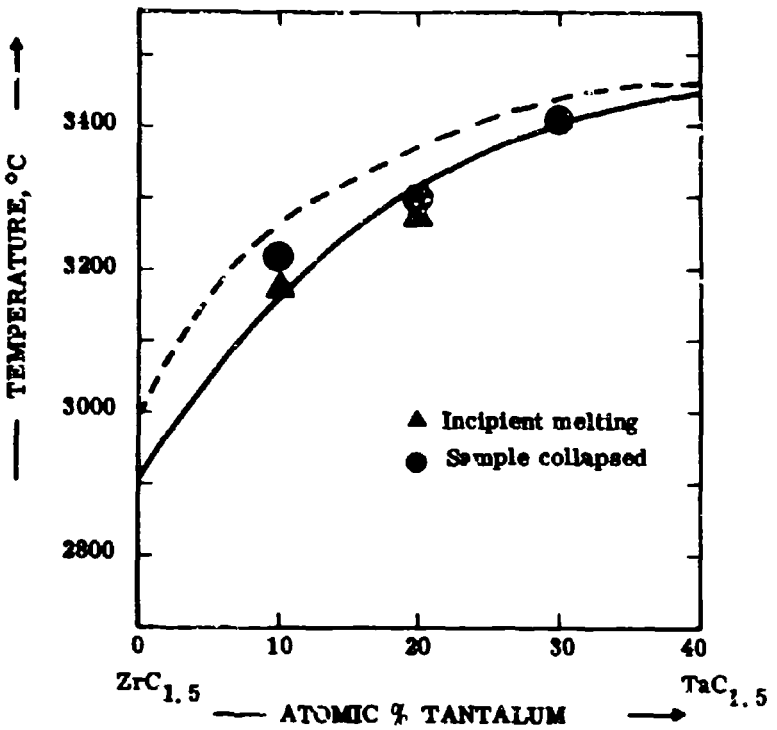

Figure III.E.8.30. Melting Along the Monocarbide + Graphite Eutectic Trough

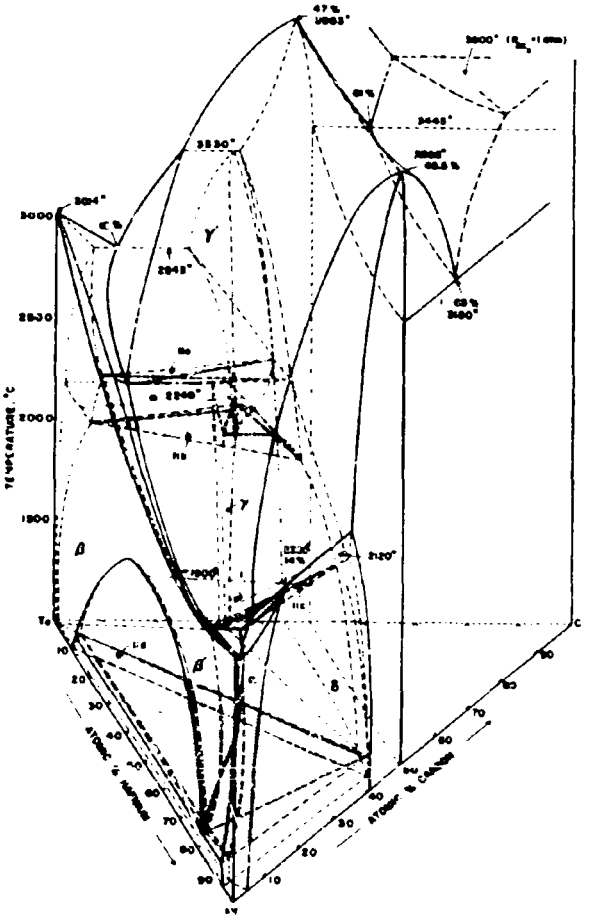

Figure III.E.9.1. Isometric View of the Ta-Hf-C System

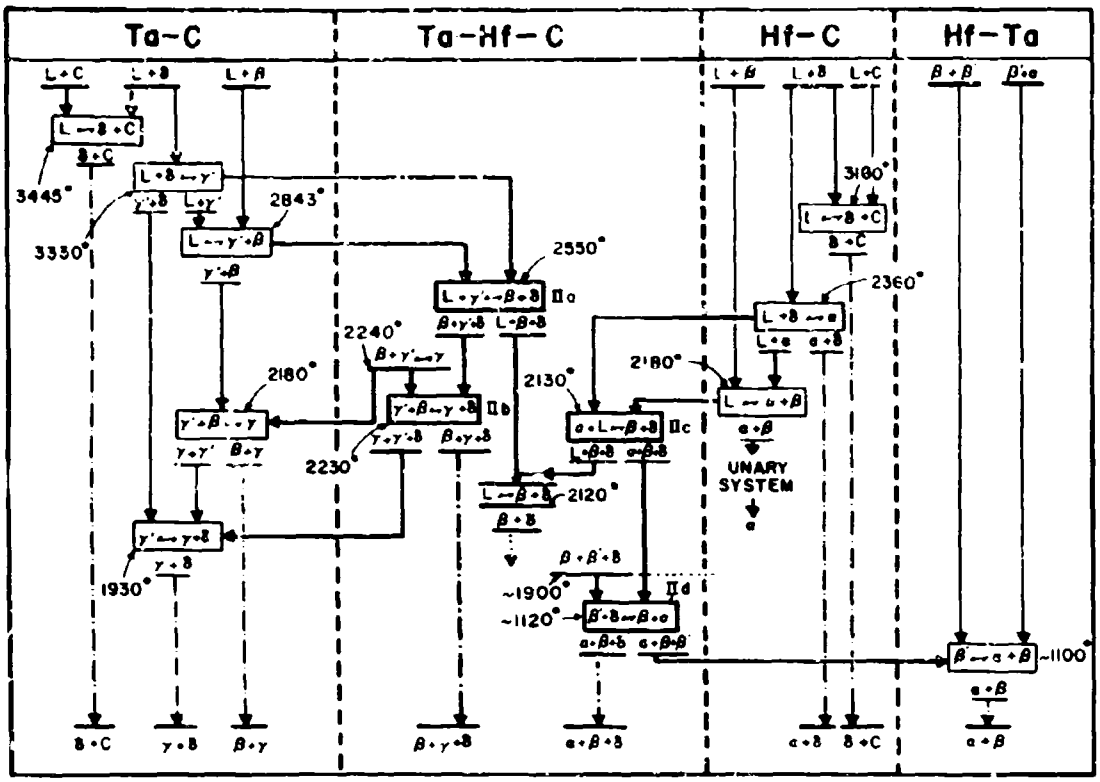

Figure III.E.9.2. Reaction Diagram for the Ta-Hf-C System

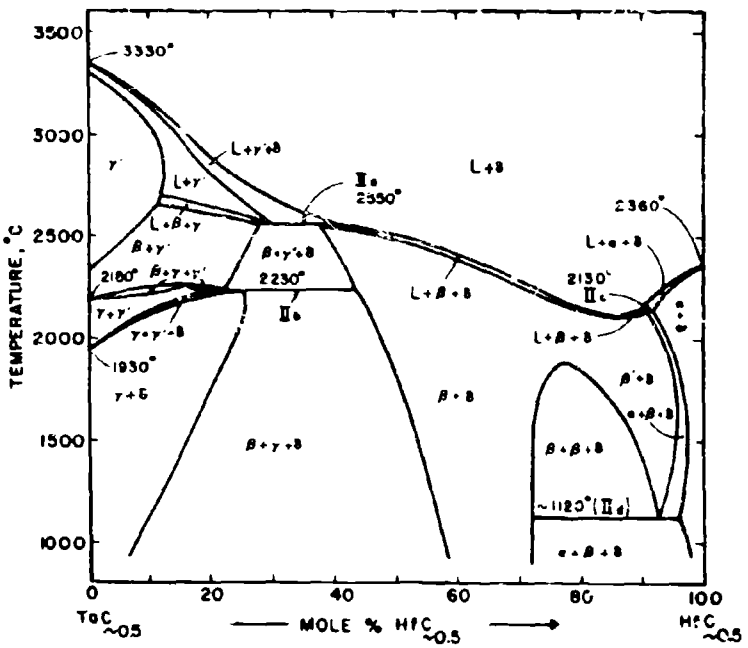

β,β' : bcc,(Ta,Hf)-solid solution
α : hcp,α-Hf solid solution
γ : α-Ta_2C-ss (hex)
γ' : β-Ta_2C-ss (hex)
δ : $(Ta,Hf)C_{1-x}$-ss (cub., B1)

Figure III.E.9.3. Ta-Hf-C: Isopleth at 33 At.% C

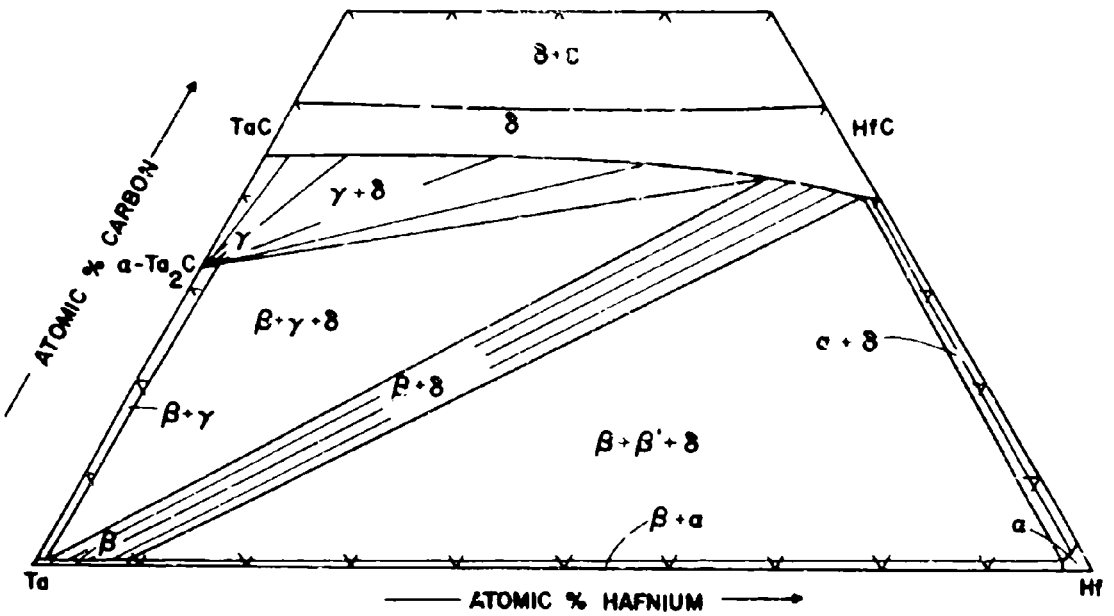

Figure III.E.9.4. Isothermal Section of the Ta-Hf-C System at 1000° C

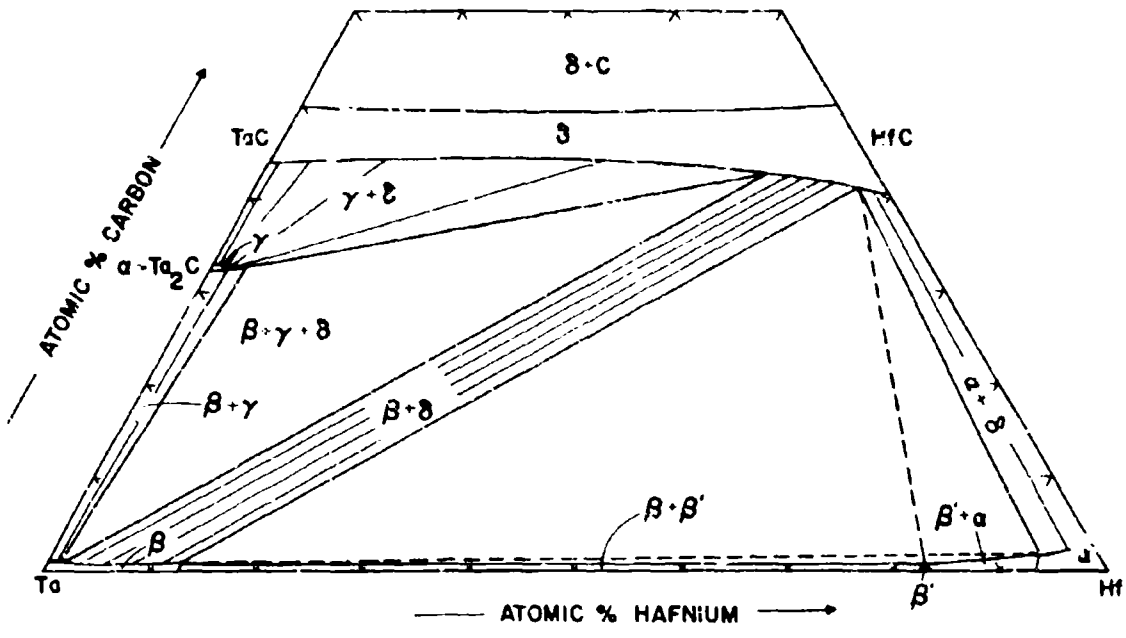

Figure III.E.9.5. Isothermal Section of the Ta-Hf-C System at 1120°C

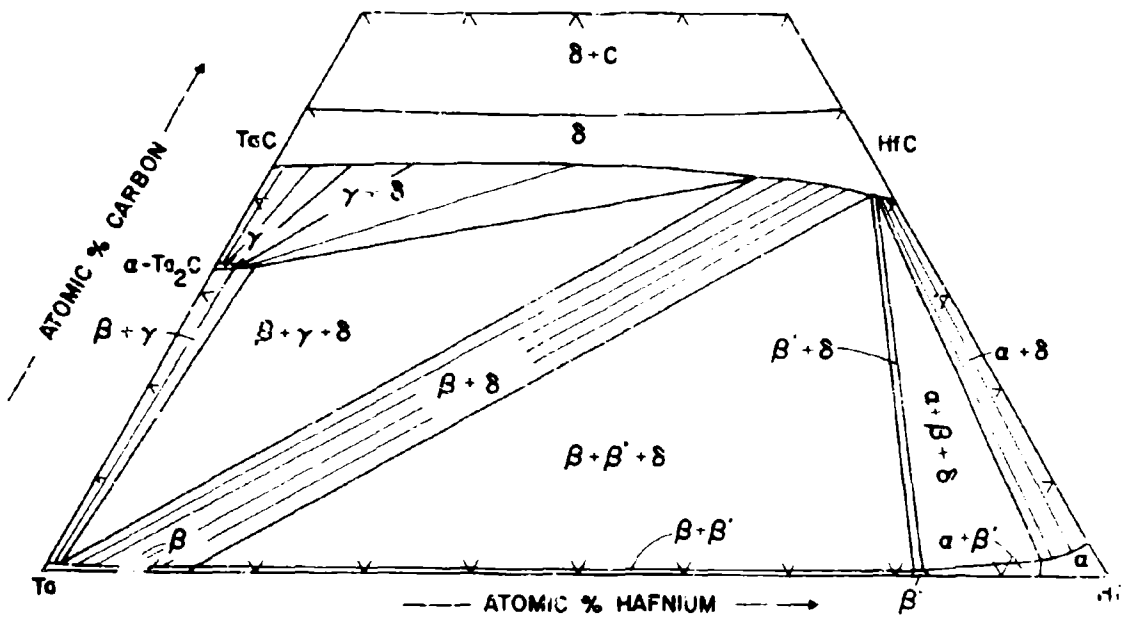

Figure III.E.9.6. Isothermal Section of the Ta-Hf-C System at 1150° C

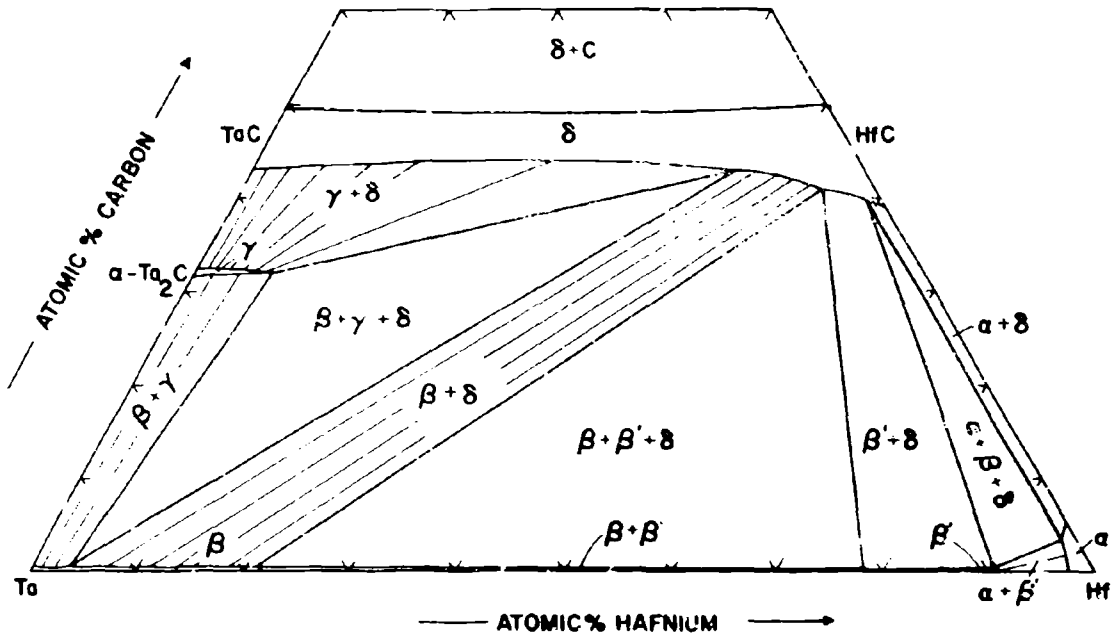

Figure III.E.9.7. Isothermal Section of the Ta-Hf-C System at 1550° C

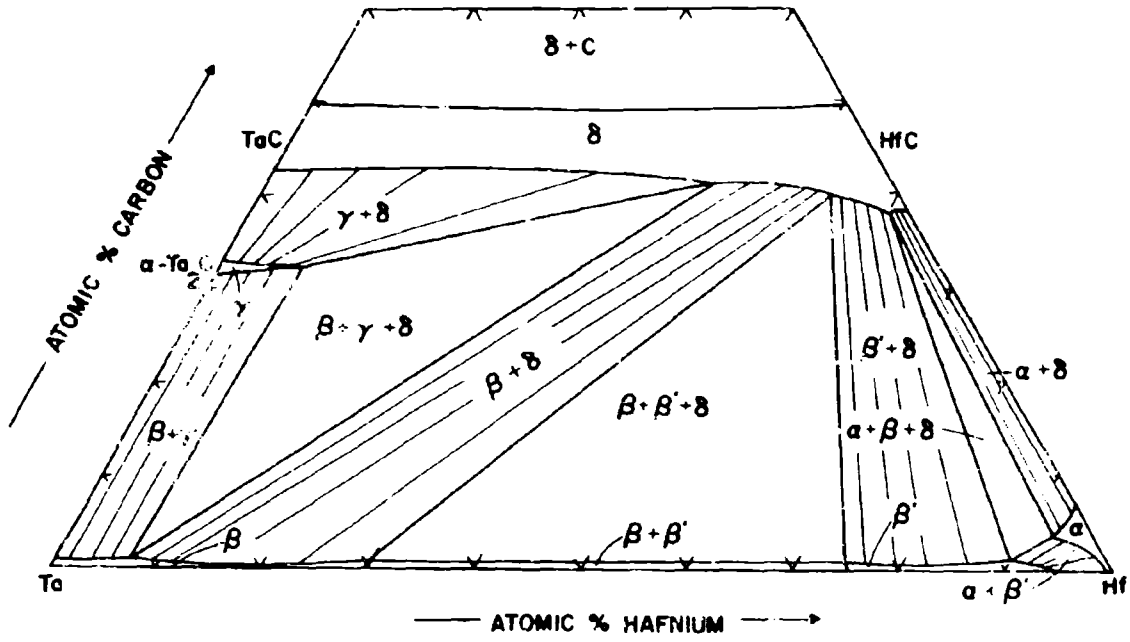

Figure III.E.9.8. Isothermal Section of the Ta-Hf-C System at 1750° C

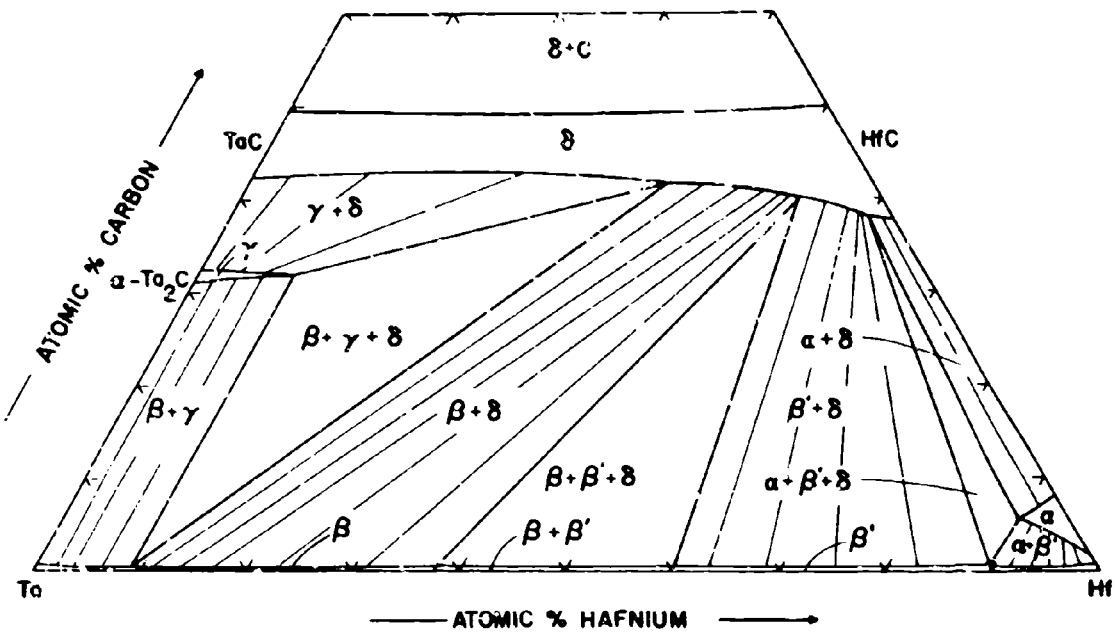

Figure III.E.9.9. Isothermal Section of the Ta-Hf-C System at 1850°C

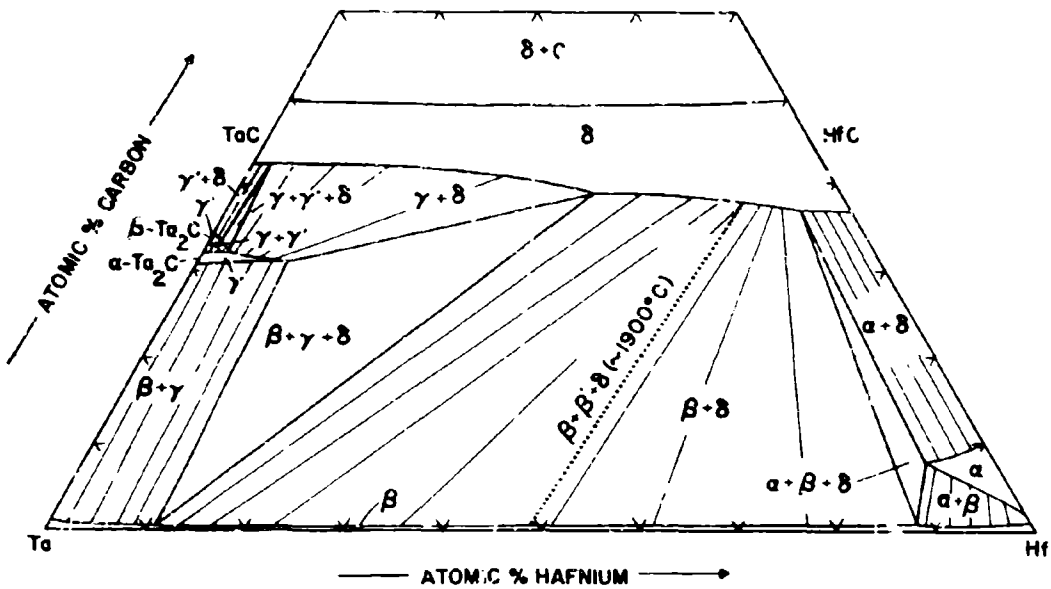

Figure III.E.9.10. Isothermal Section of the Ta-Hf-C System at 2000° C

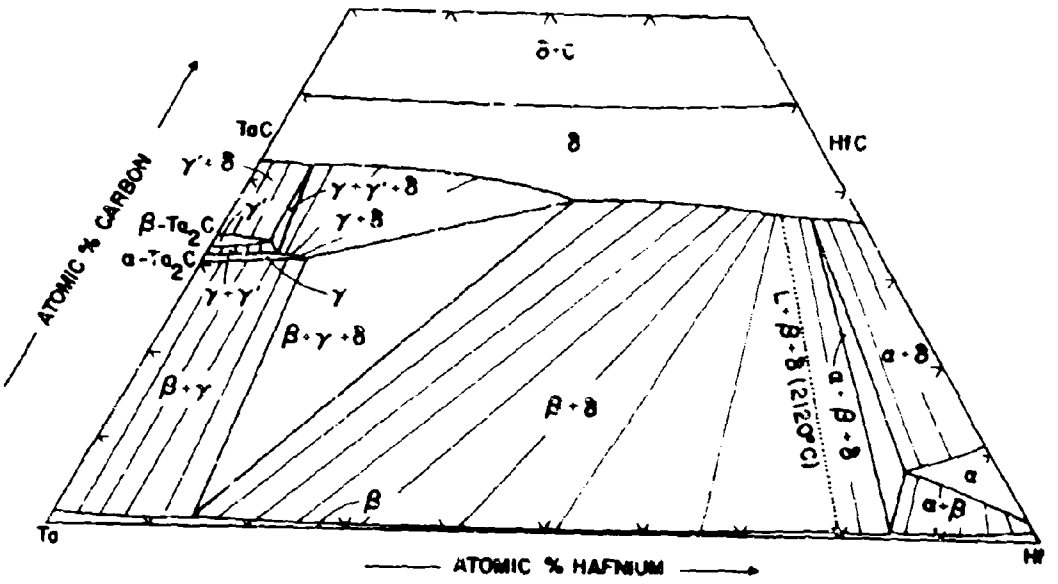

Figure III.E.9.11. Isothermal Section of the Ta-Hf-C System at 2110°C

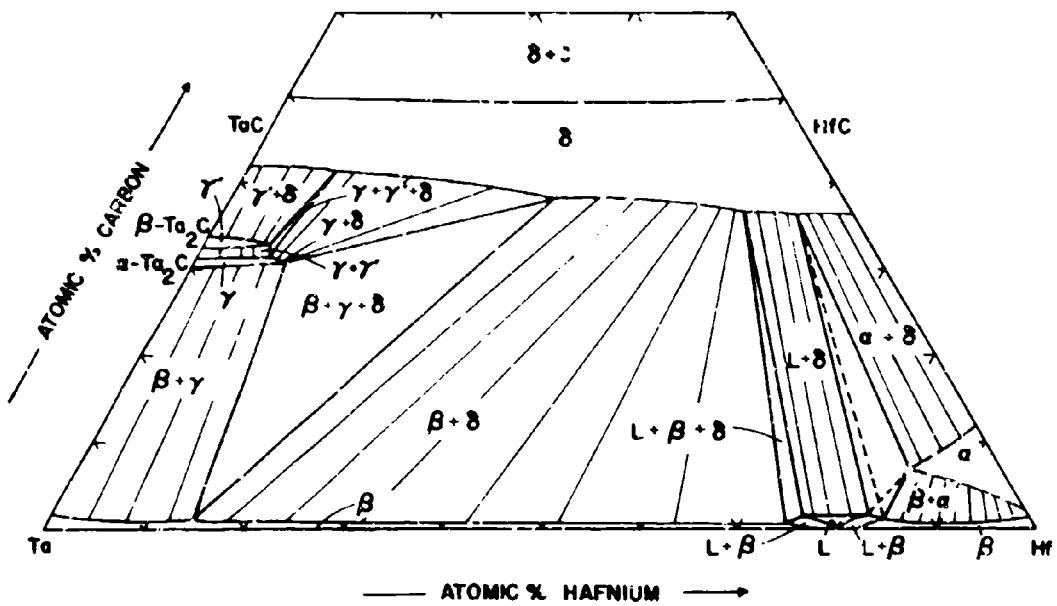

Figure III.E.9.12. Isothermal Section of the Ta-Hf-C System at 2130°C

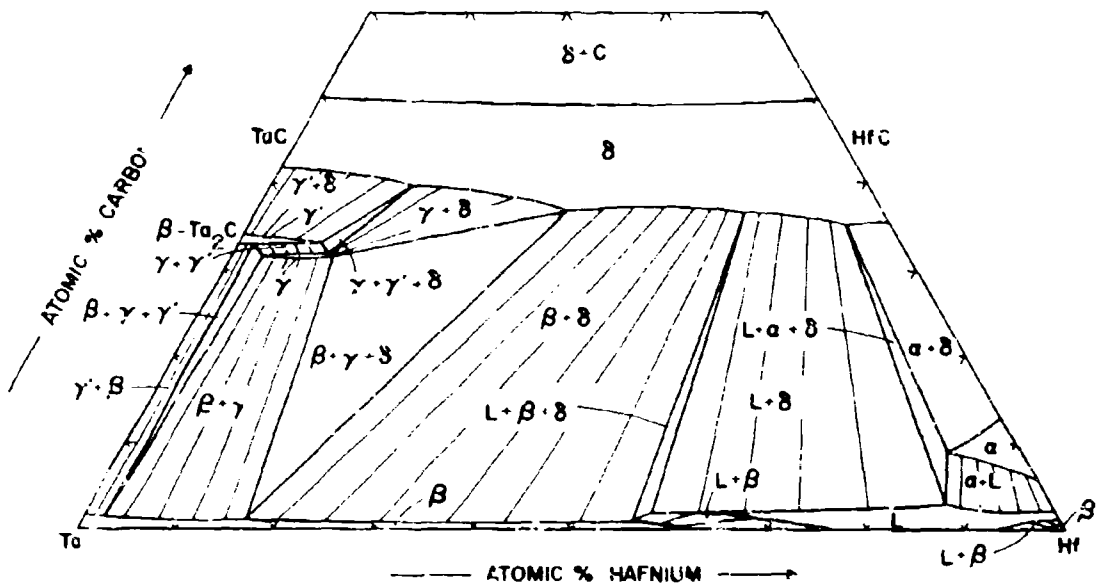

Figure III.E.9.13. Isothermal Section of the Ta-Hf-C System at 2200° C

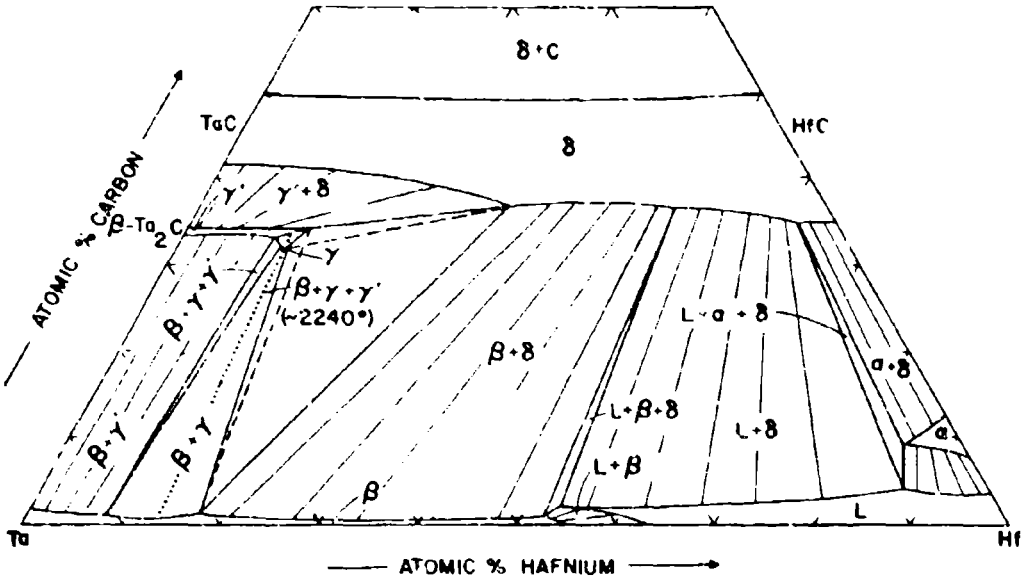

Figure III.E.9.14. Isothermal Section of the Ta-Hf-C System at 2230°C

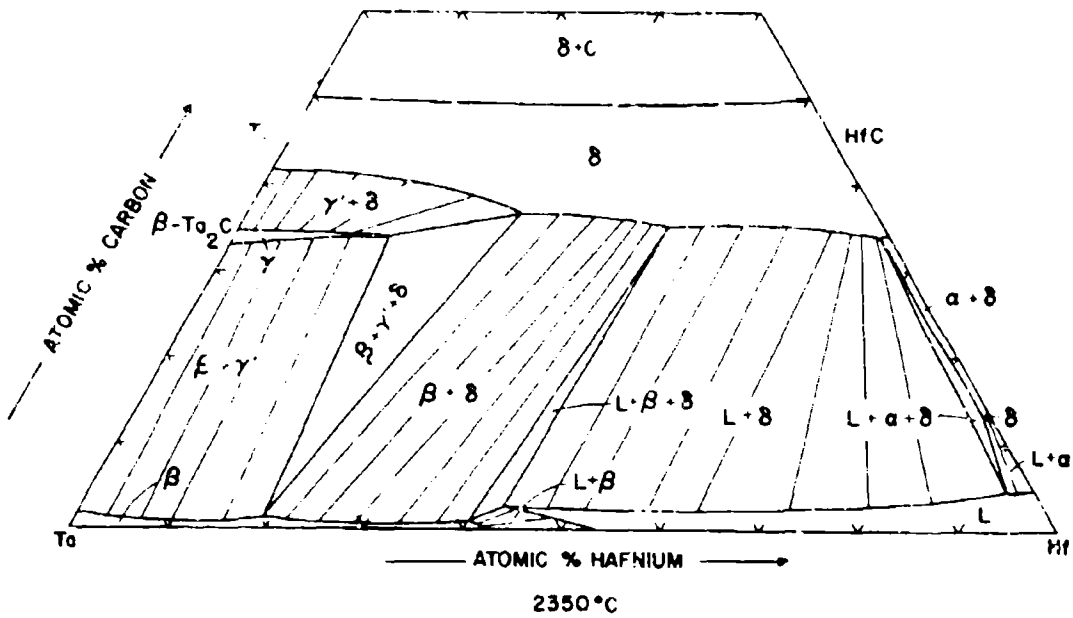

Figure III.E.9.15. Isothermal Section of the Ta-Hf-C System at 2350 °C

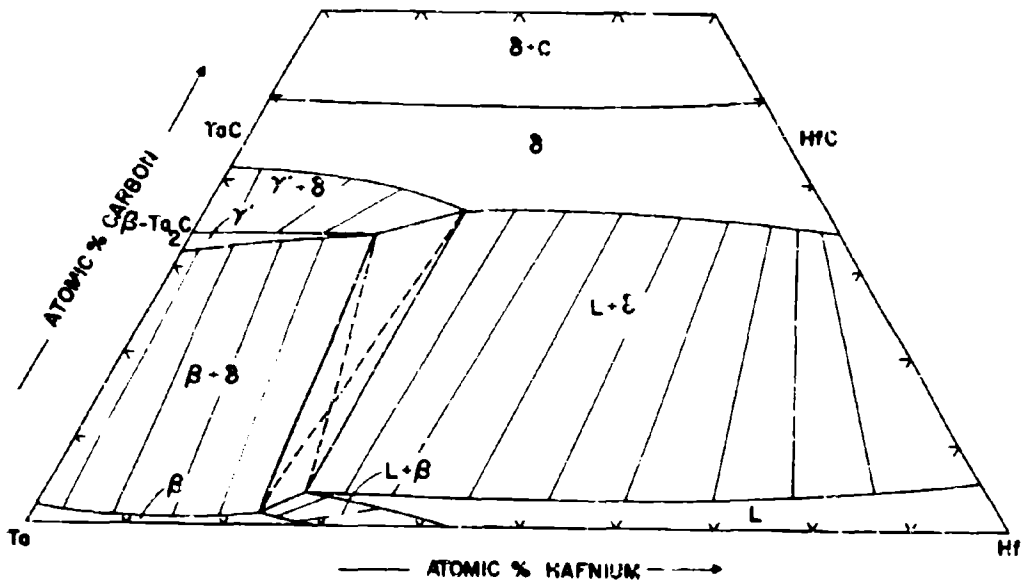

Figure III.E.9.16. Isothermal Section of the Ta-Hf-C System at 2550° C

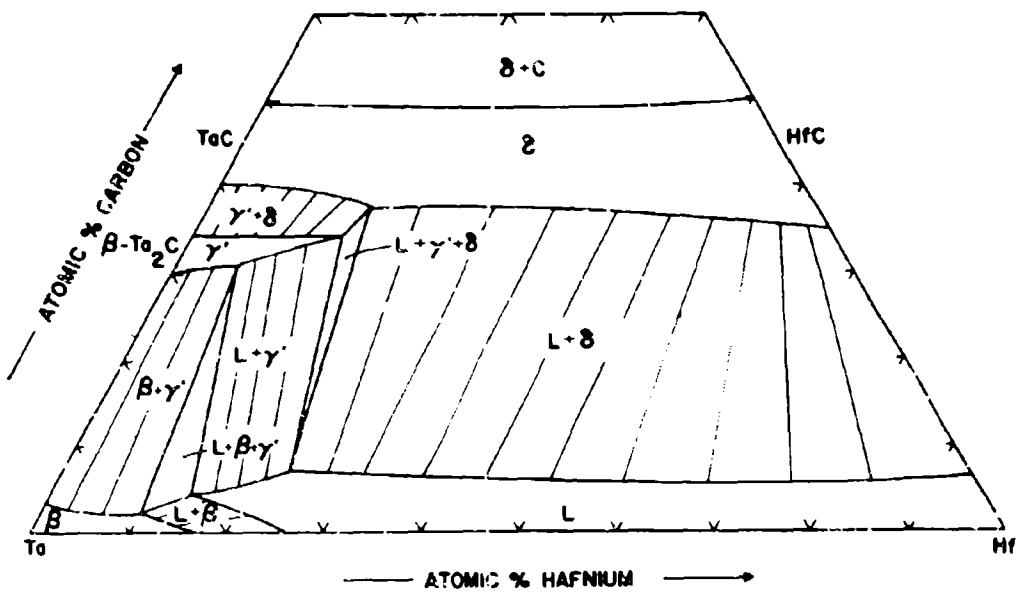

Figure III.E.9.17. Isothermal Section of the Ta-Hf-C System at 2700°C

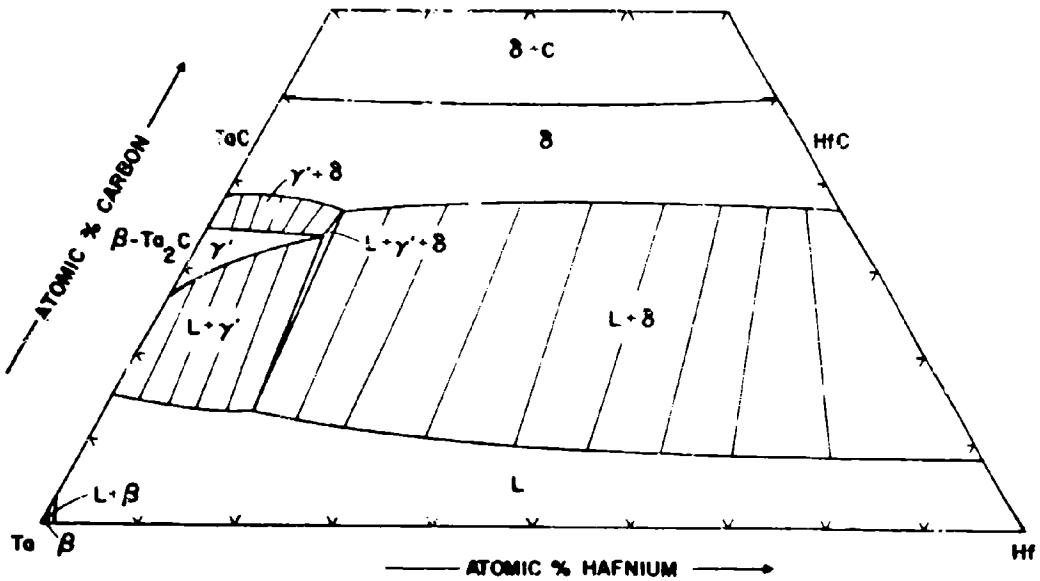

Figure III.E.9.18. Isothermal Section of the Ta-Hf-C System at 3000° C

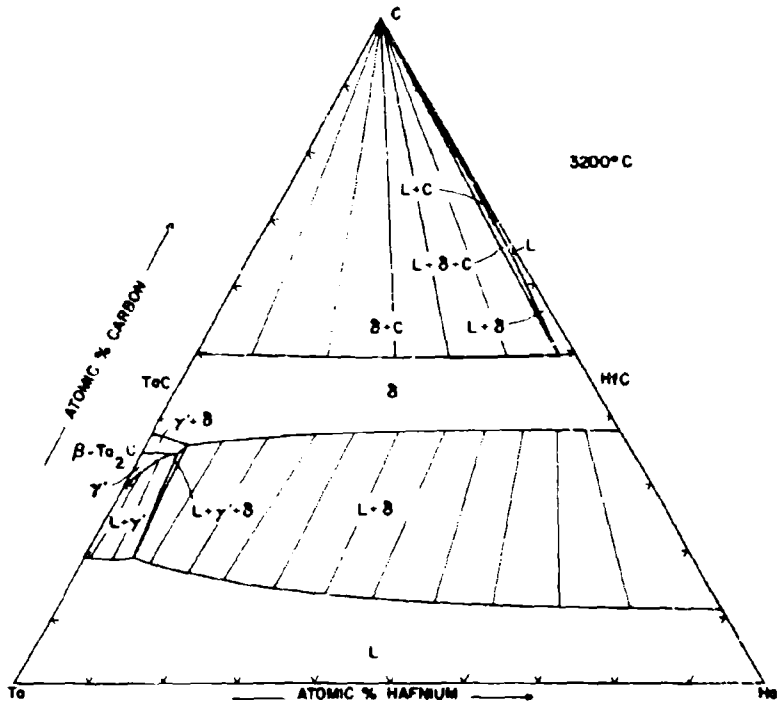

Figure III.E.9.19. Isothermal Section of the Ta-Hf-C System at 3200° C

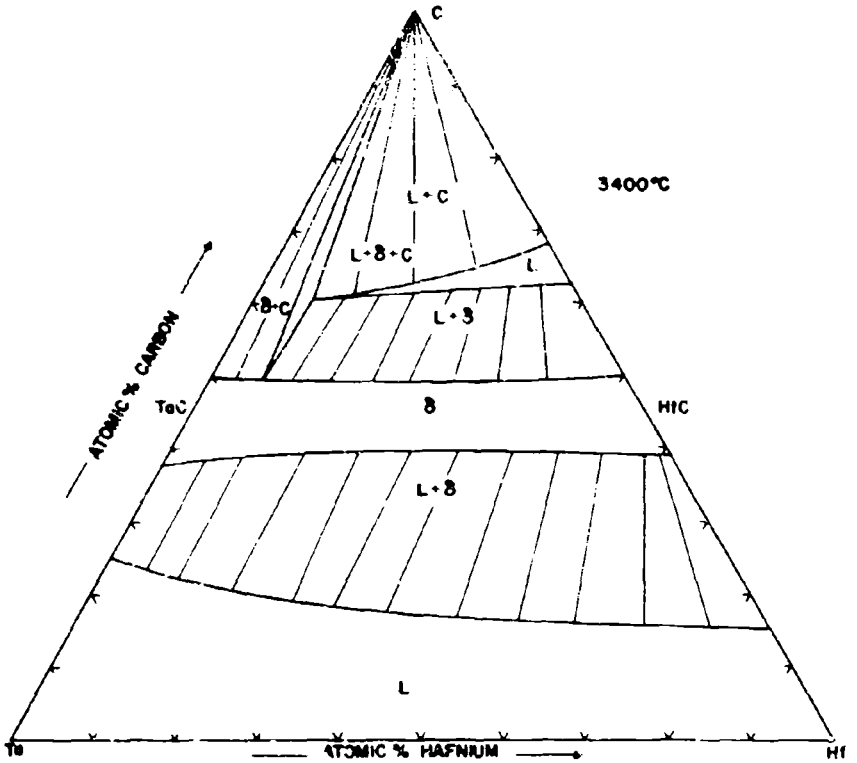

Figure III.E.9.20. Isothermal Section of the Ta-Hf-C System at 3400° C

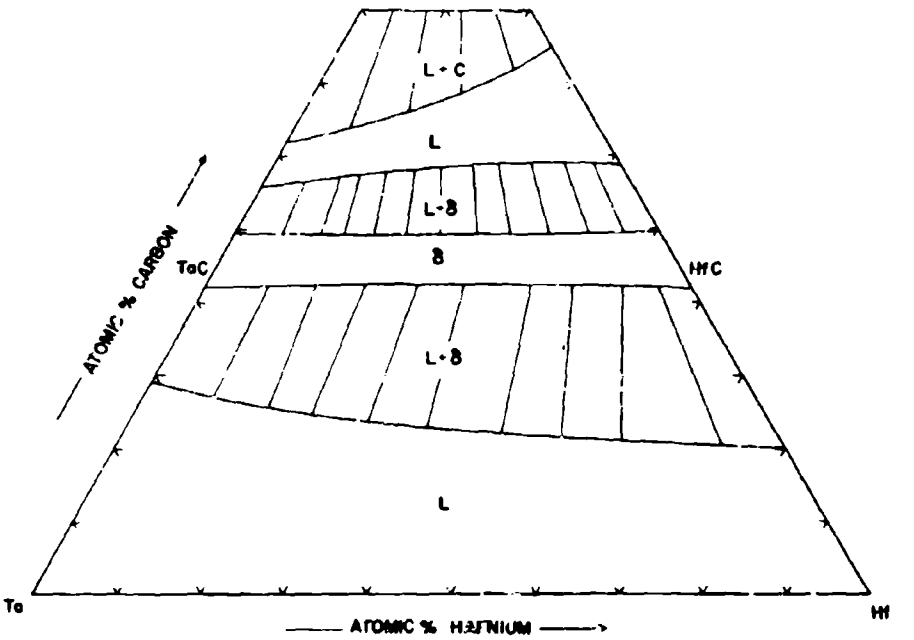

Figure III.E.9.21. Isothermal Section of the Ta-Hf-C System at 3600°C

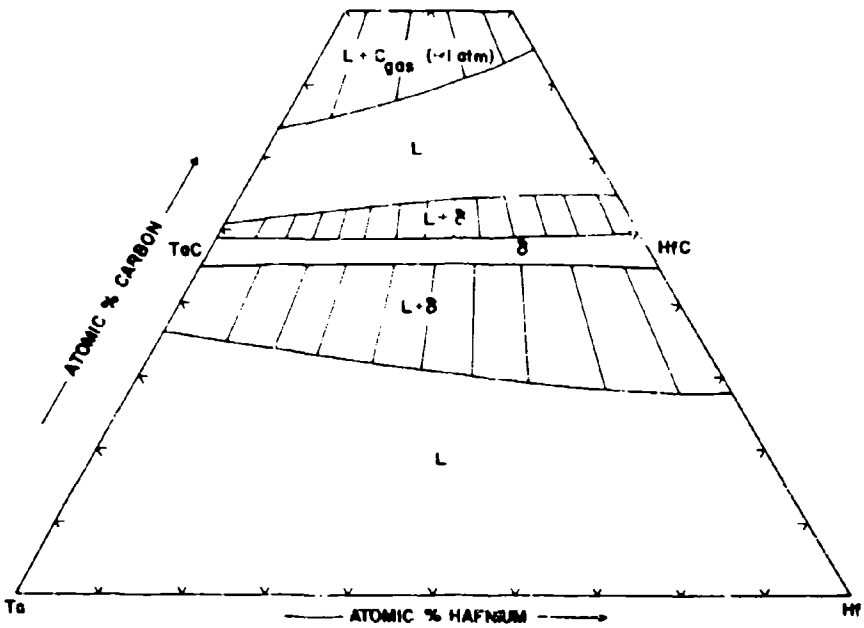

Figure III.E.9.22. Isothermal Section of the Ta-Hf-C System at 3800° C

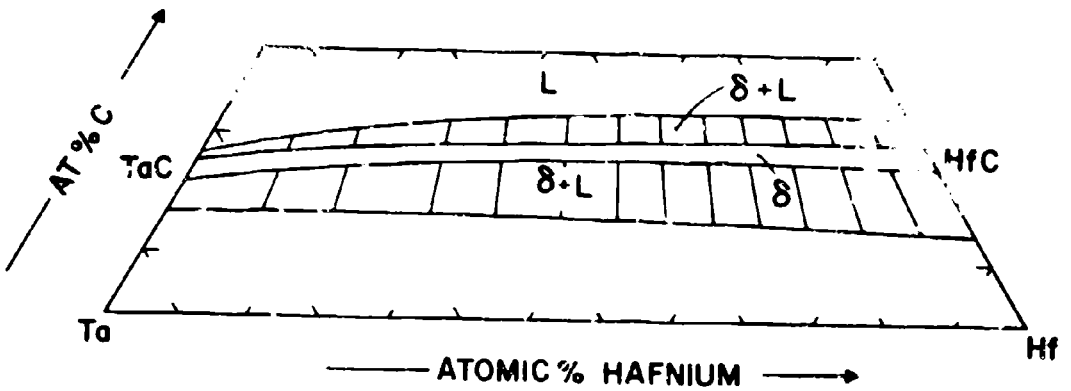

Figure III.E.9.23. Isothermal Section of the Ta-Hf-C System at 3900°C

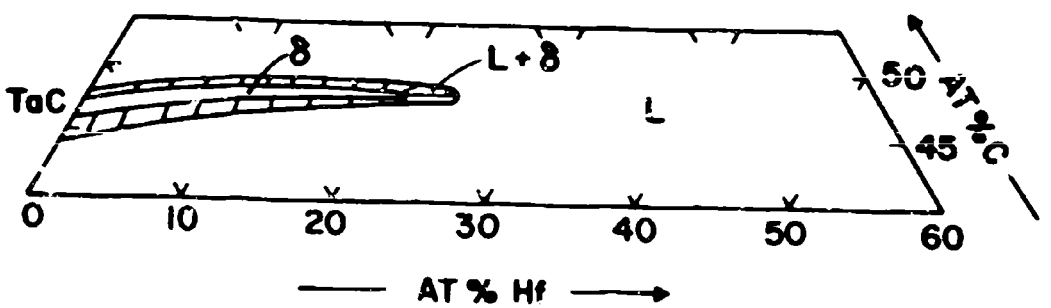

Figure III.E.9.24. Isothermal Section of the Ta-Hf-C System at 3950°C

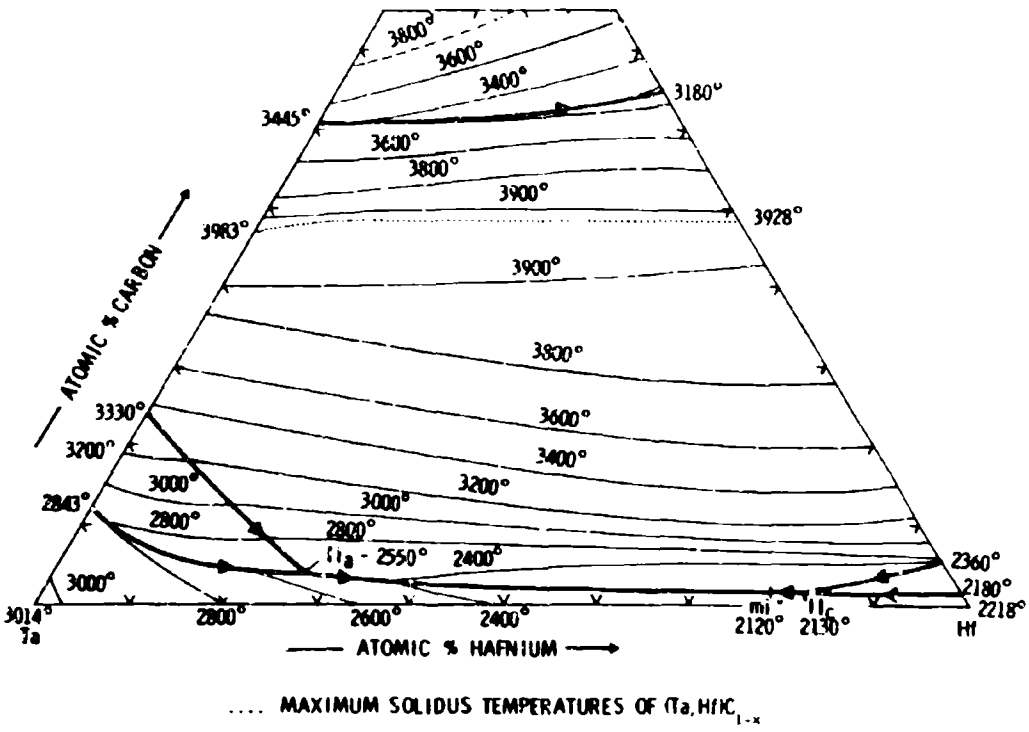

Figure III.E.9.25. Liquidus Projections for the Ta-Hf-C System, Partially Estimated

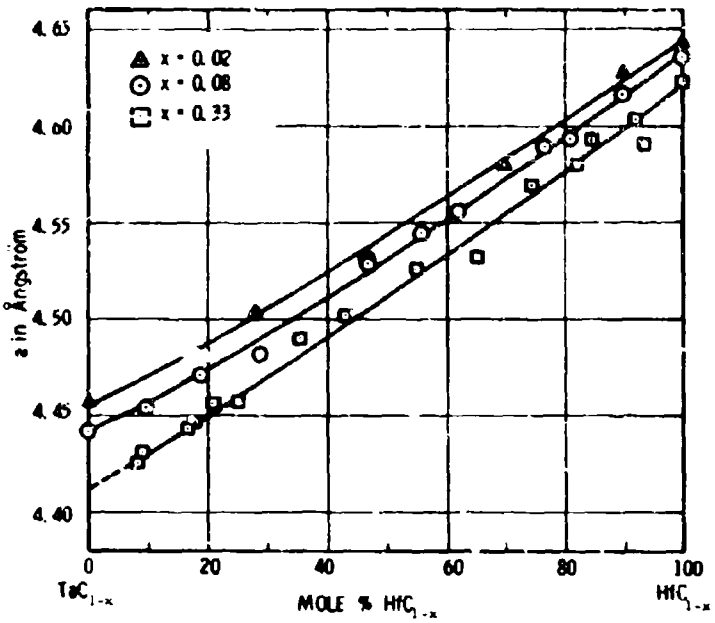

Figure III.E.9.26. Lattice Parameters of the (Ta,Hf)C_{1-x} Solid Solution as a Function of the Carbon Defect

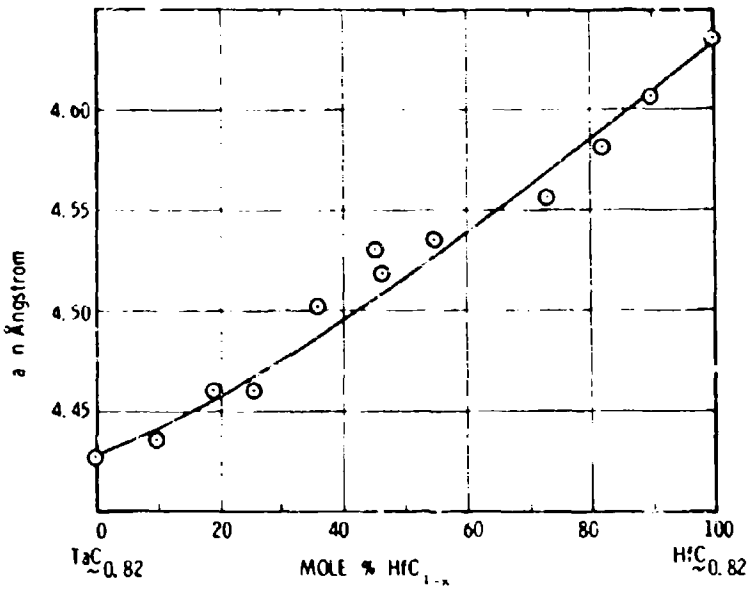

Figure III.E.9.27. Lattice Parameters of the Monocarbide Solid Solution at a Carbon Defect of 5 At.%

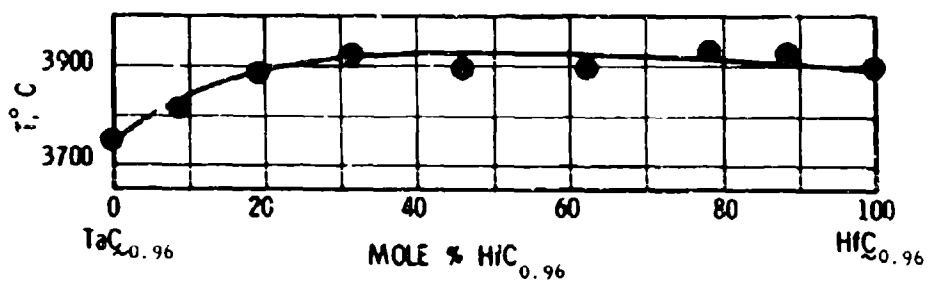

Figure III.E.9.28. Solidus Temperatures for the $(Ta,Hf)C_{1-x}$ Solid Solution at a Carbon Defect of Approximately 1 At.%

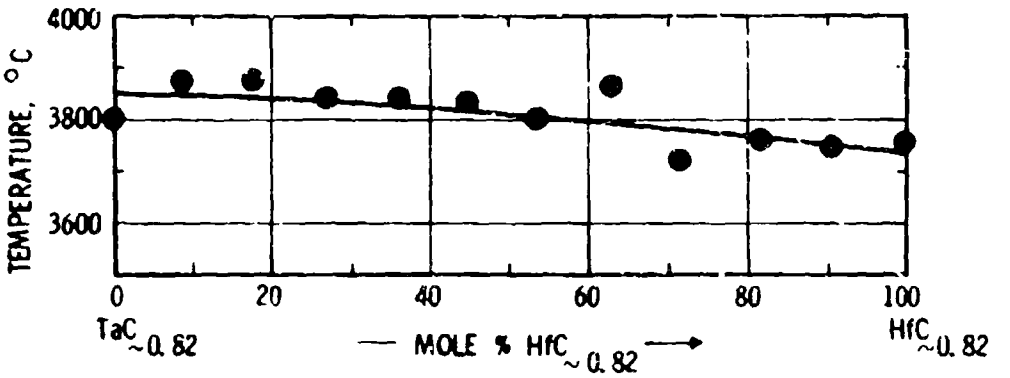

Figure III.E.9.29. Solidus Temperatures of the $(Ta,Hf)C_{1-x}$ Solid Solution at a Carbon Defect of 5 At.%

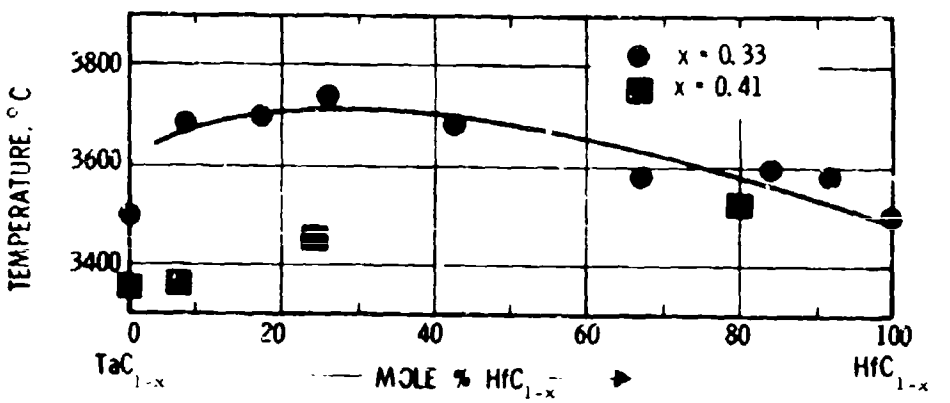

Figure III.E.9.30. Solidus Temperatures of the Hafnium and Tantalum Monocarbide Solid Solution at Carbon Defects of 10 and 13 At.%

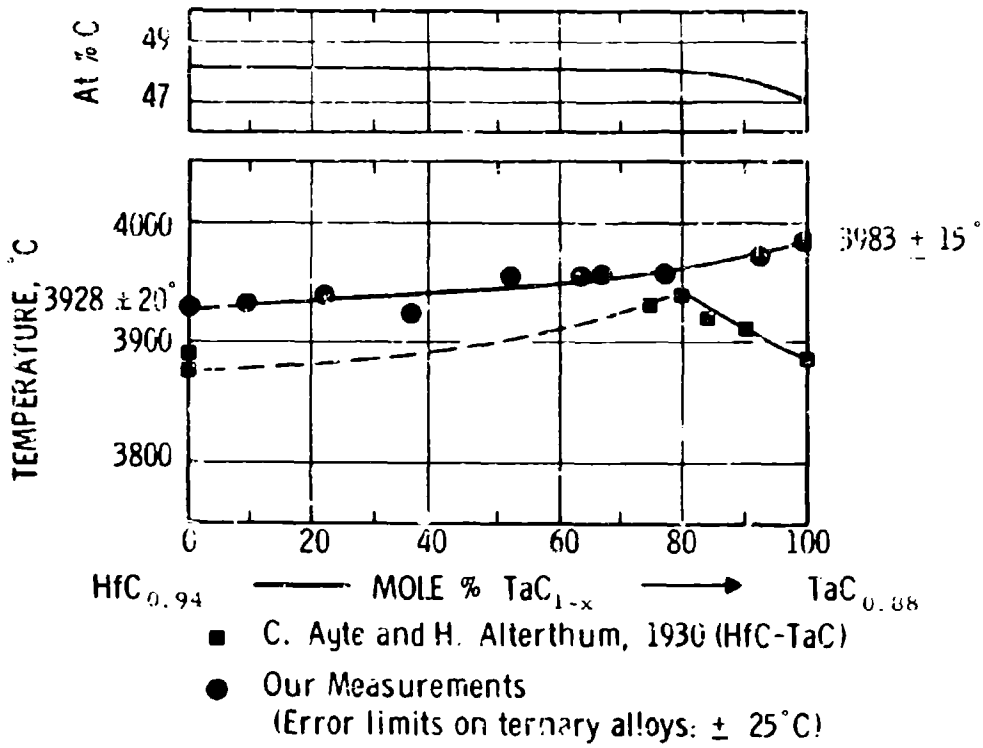

Figure III.E.9.31. Maximum Solidus Temperatures of the Monocarbide Solid Solutions

Top: Composition (± 0.3 At.%) of the Maximum Solidus

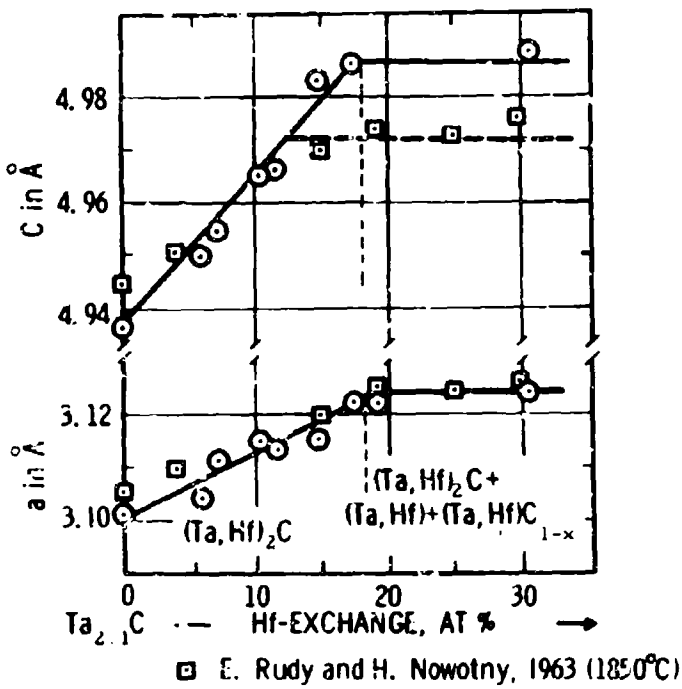

Figure III.E.9.32. Variation of the Lattice Parameters of the Ta_2C-Phase with the Hafnium Content. Alloys Equilibrated at 2000° C

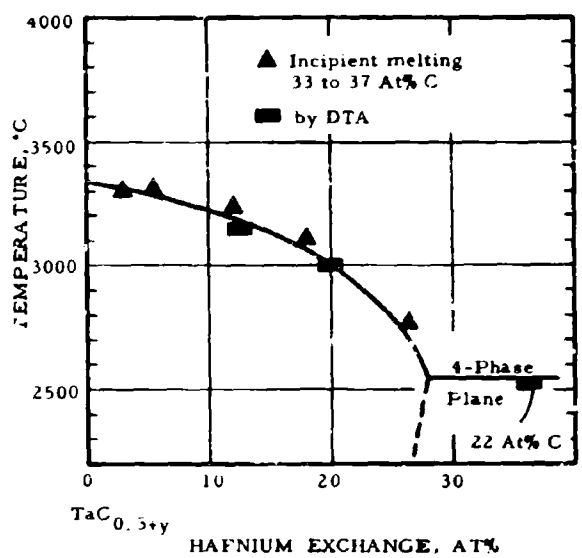

Figure III.E.9.33. Approximate Solidus Curve for the $(Ta,Hf)_2C$ Solid Solution

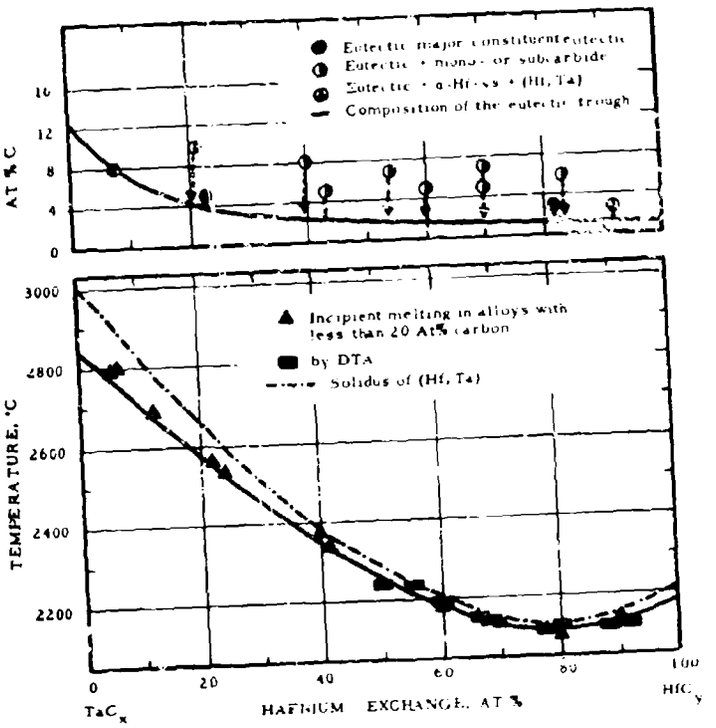

Figure III.E.9.34. Composition (Top) and Temperatures of the Eutectic Trough in the Metal-Rich Portion of the Tantalum-Hafnium-Carbon System

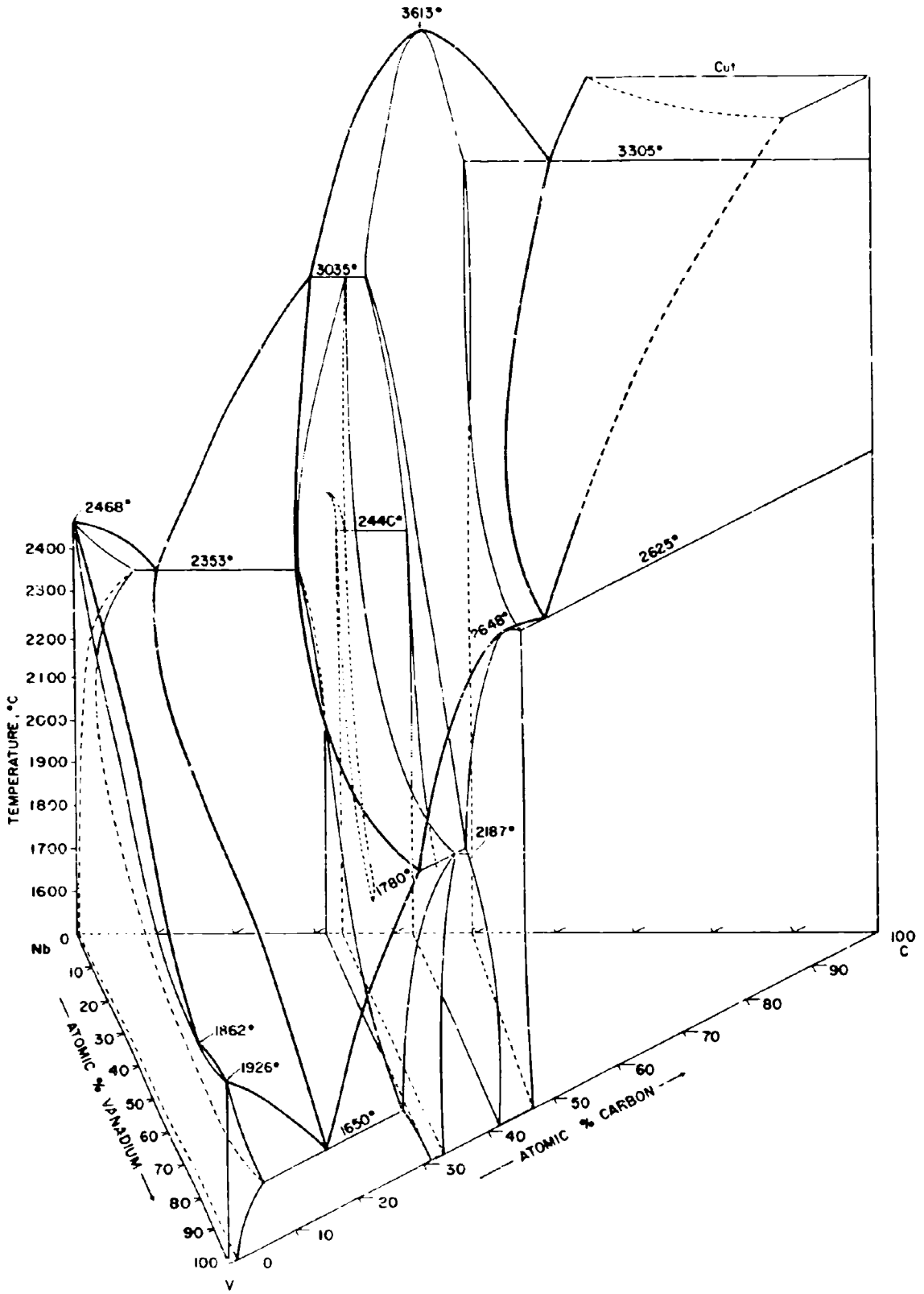

Figure III.E.10.1. Constitution Diagram of the System V-Nb-C

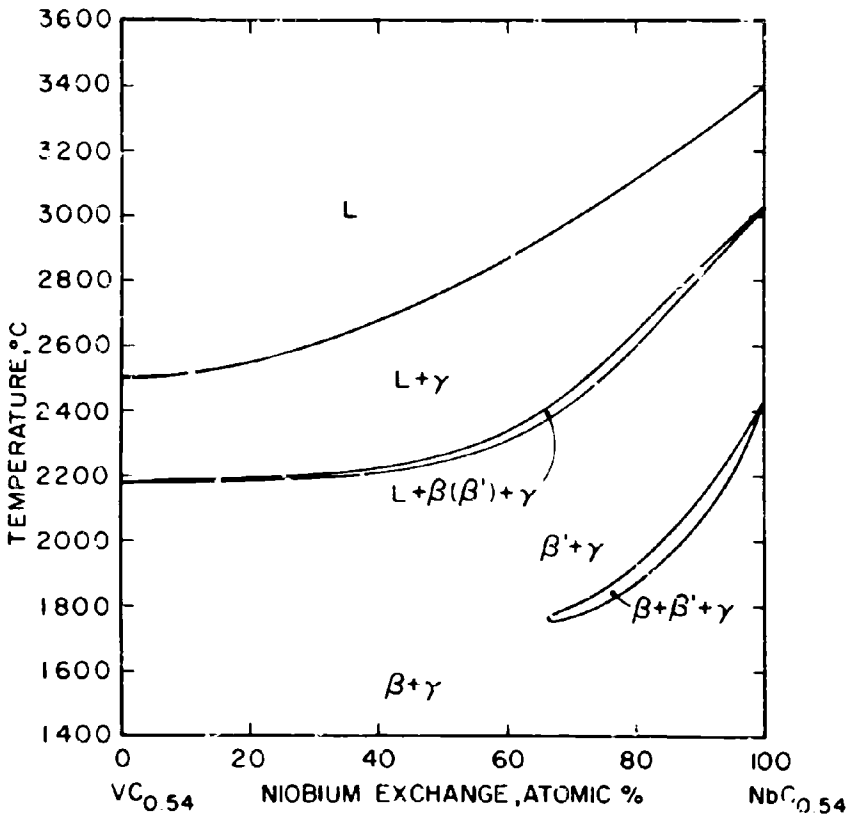

Figure III.E.10.2. Isopleth at $VC_{0.54}$-$NbC_{0.54}$

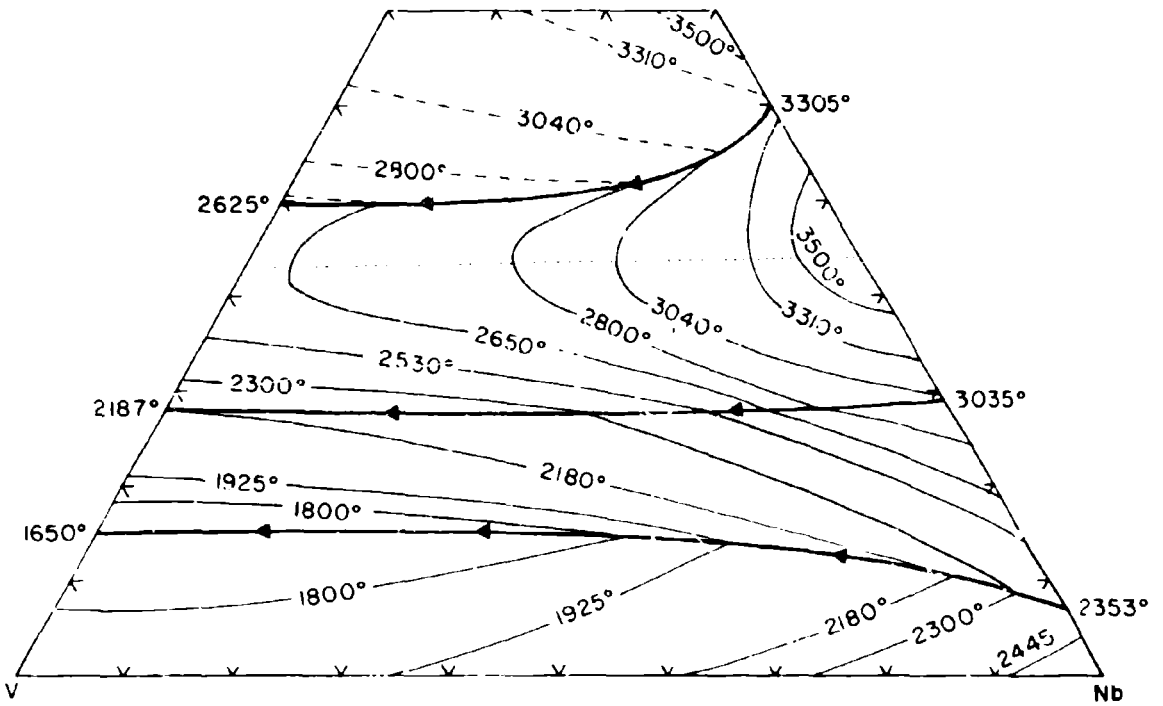

Figure III.E.10.3. Liquidus Projections in the V-Nb-C System

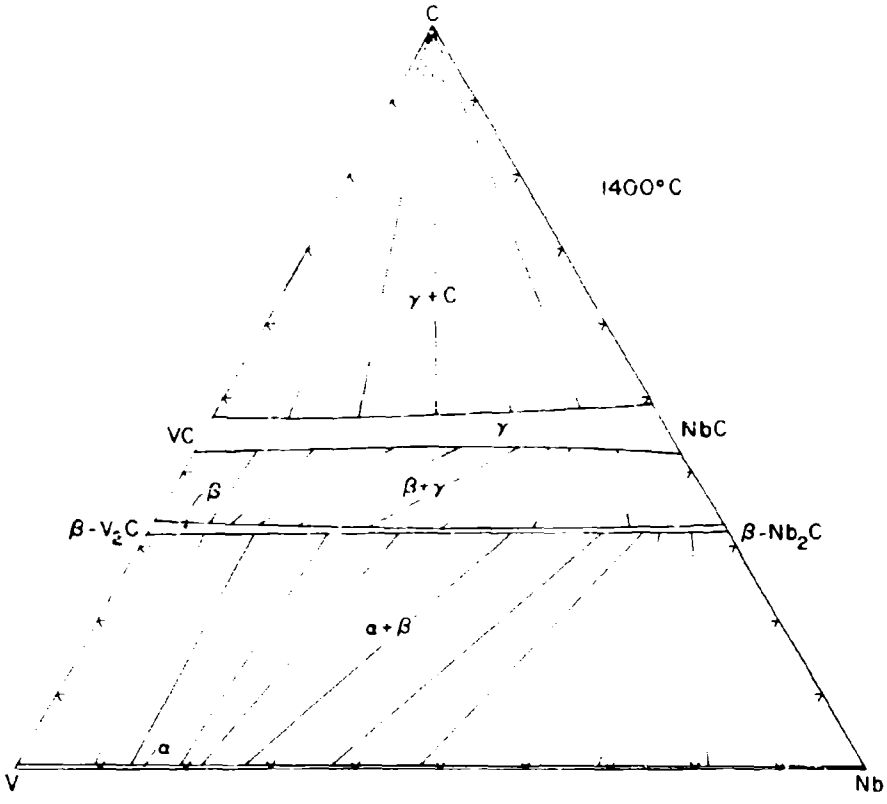

Figure III.E.10.4. Isothermal Section of the V-Nb-C System at 1400°C

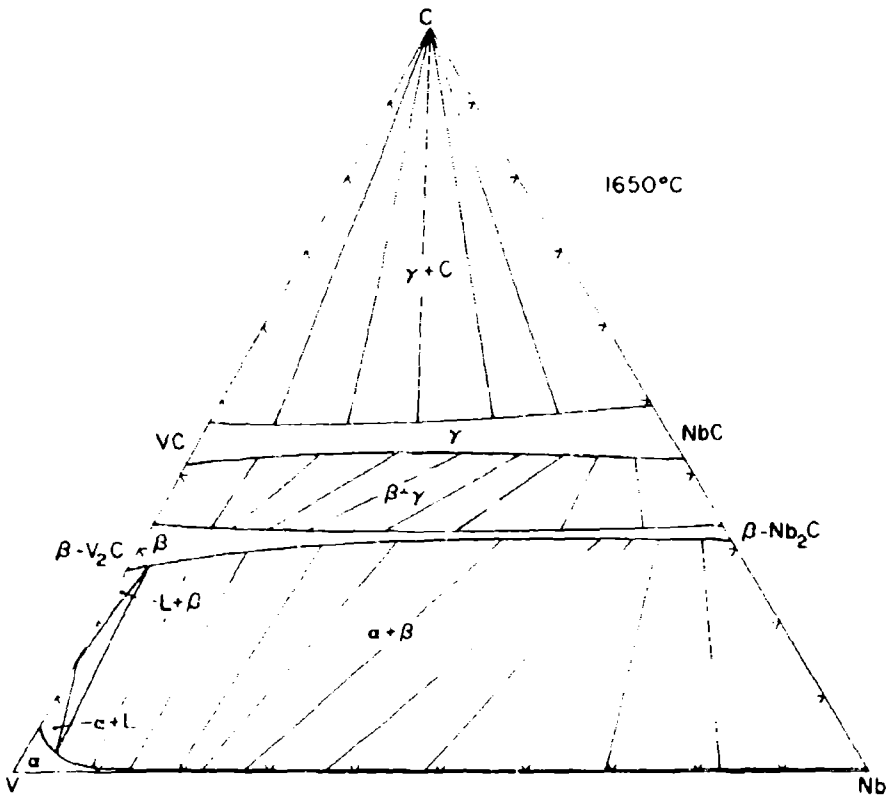

Figure III.E.10.5. Isothermal Section of the V-Nb-C System at 1650°C

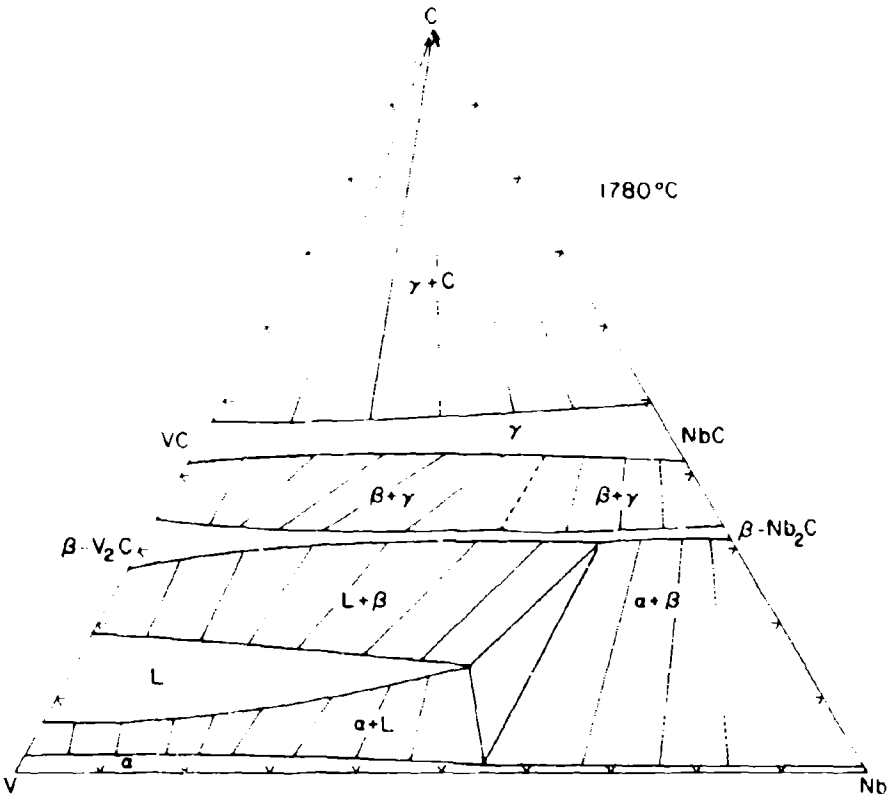

Figure III.E.10.6. Isothermal Section of the V-Nb-C System at 1780° C

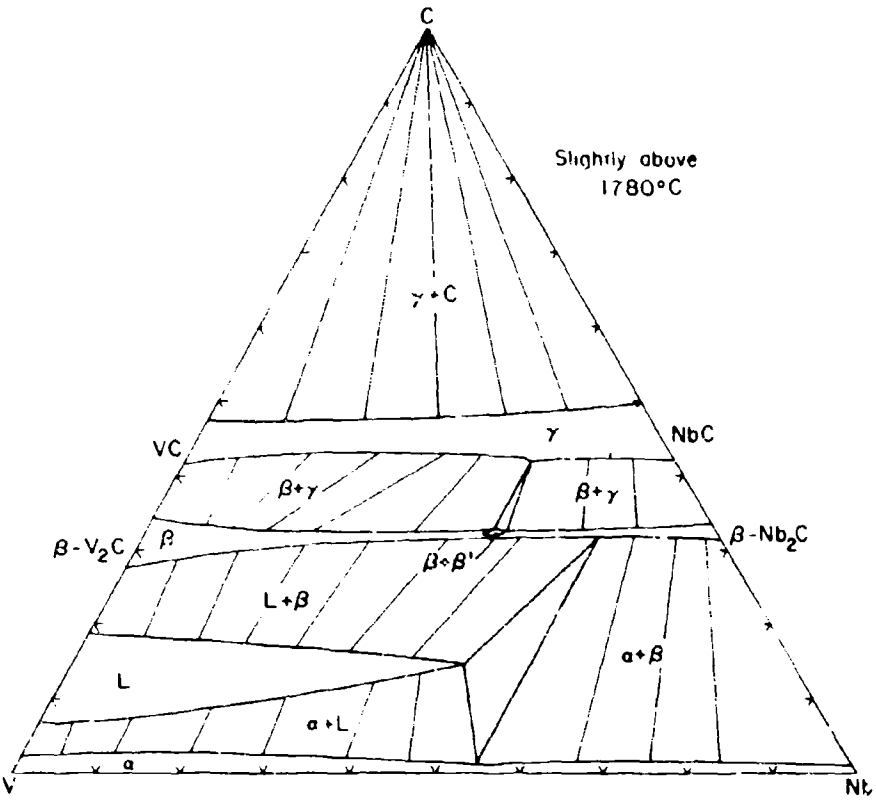

Figure III.E.10.7. Isothermal Section of the V-Nb-C System Slightly Above 1780°C

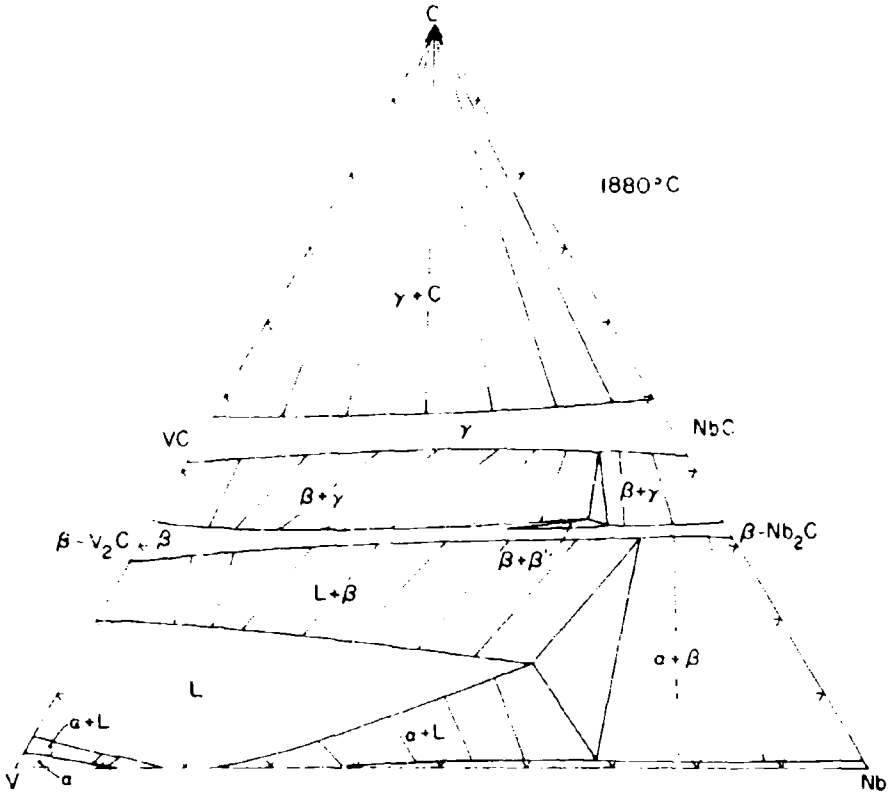

Figure III.E.10.8. Isothermal Section of the V-Nb-C System at 1880° C

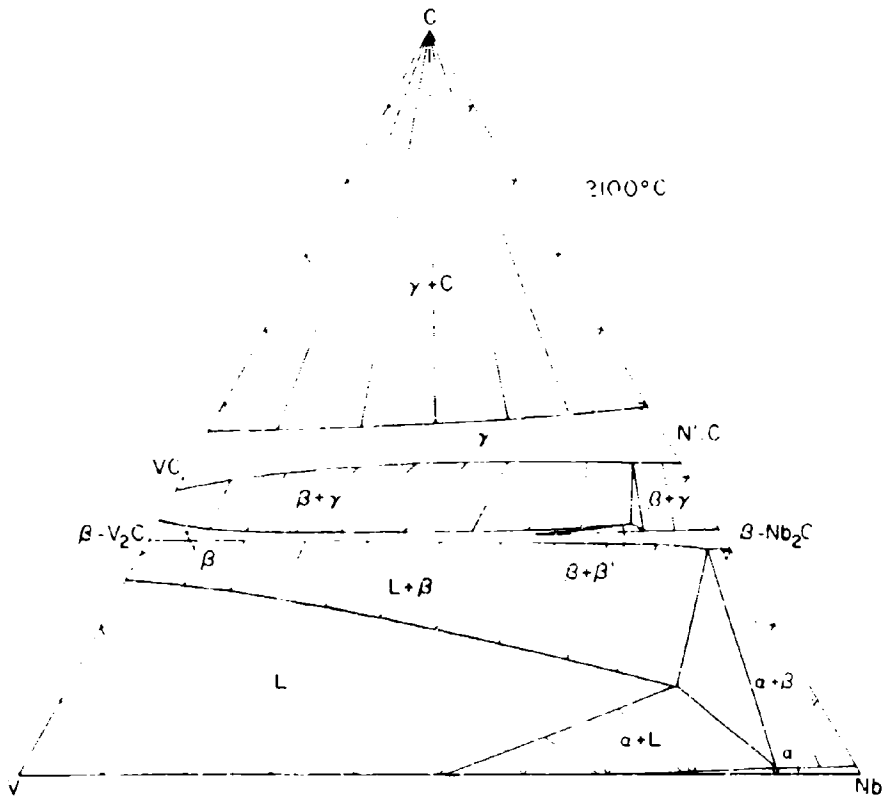

Figure III.E.10.9. Isothermal Section of the V-Nb-C System at 2100°C

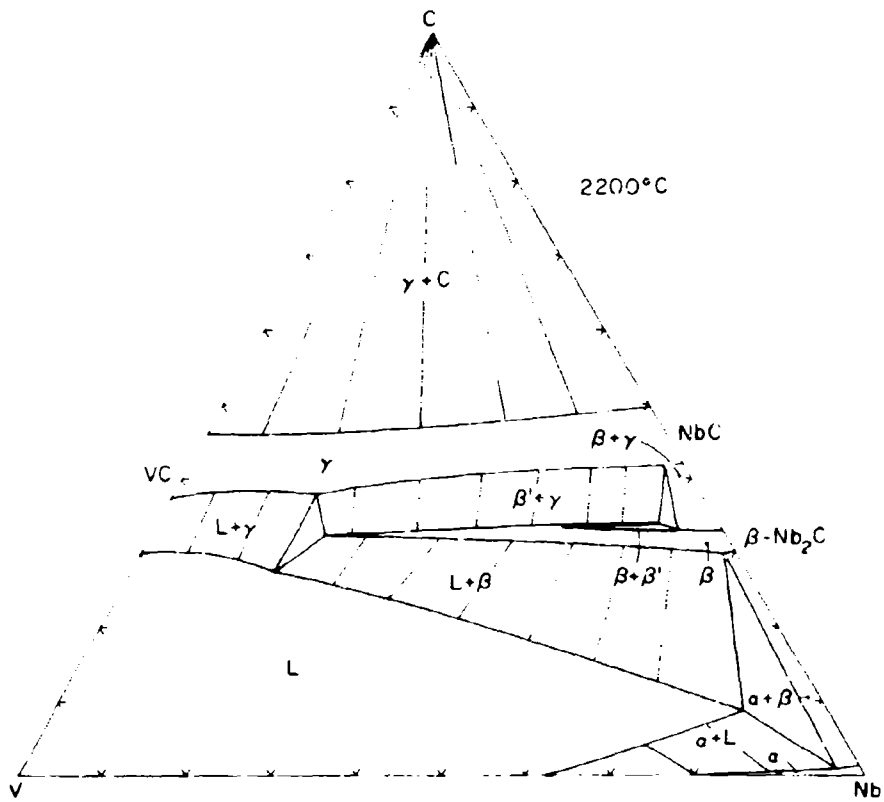

Figure III.E.10.10. Isothermal Section of the V-Nb-C System at 2200°C

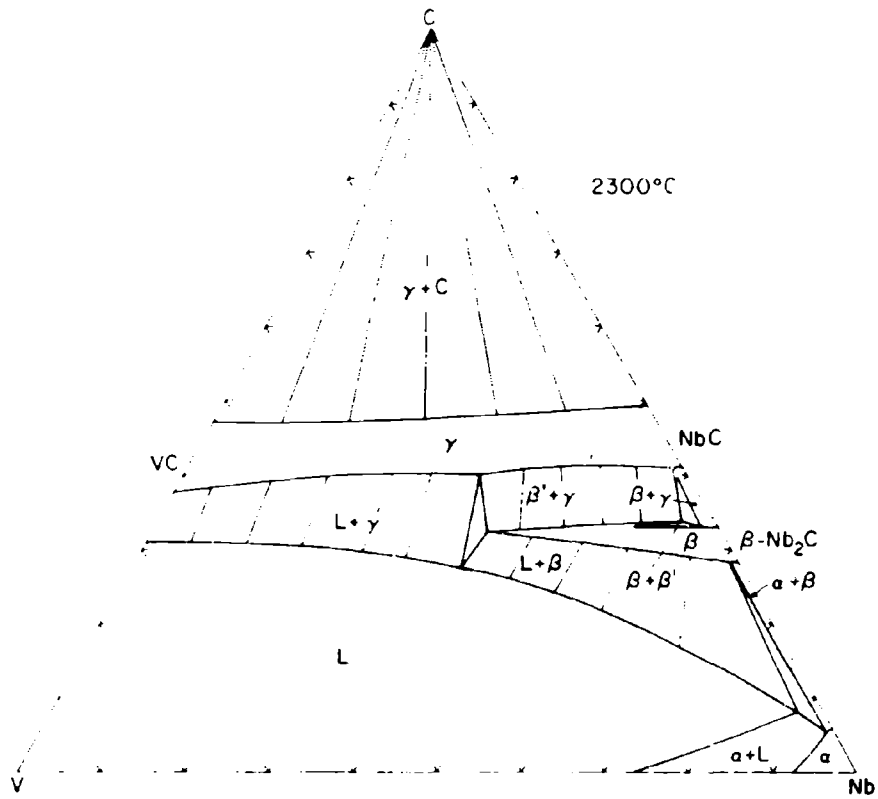

Figure III.E.10.11. Isothermal Section of the V-Nb-C System at 2300° C

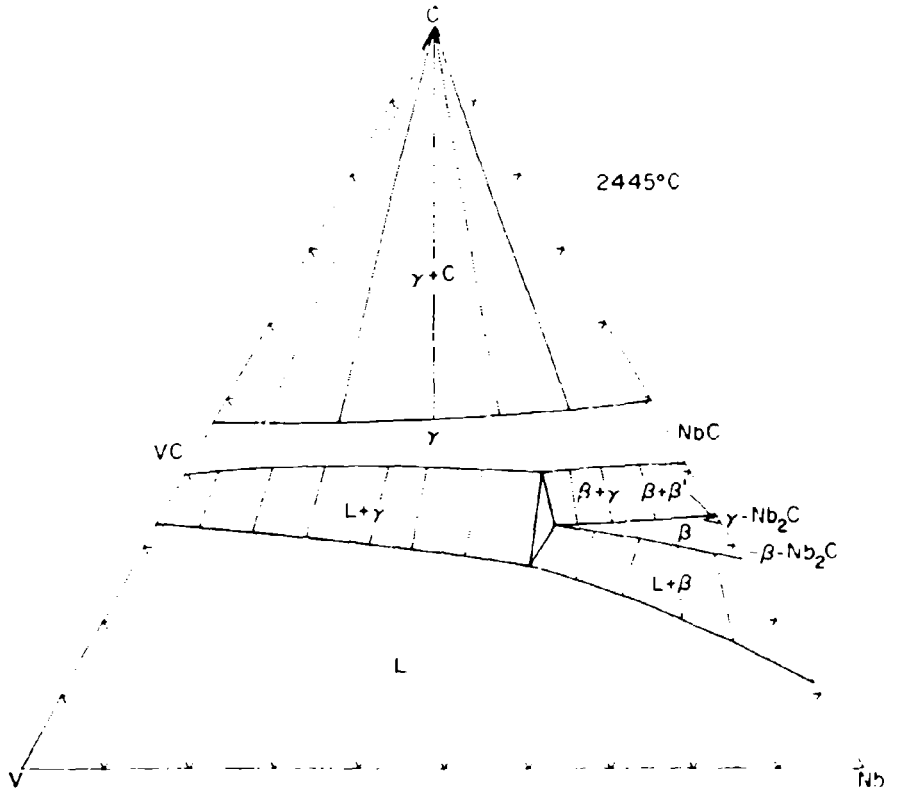

Figure III.E.10.12. Isothermal Section of the V-Nb-C System at 2445° C

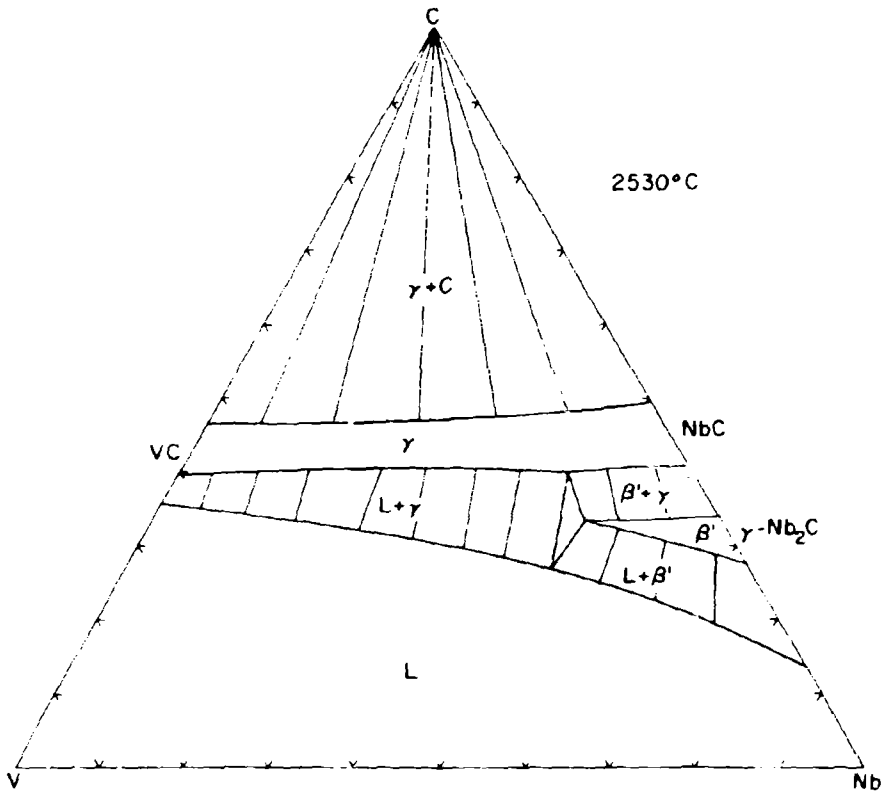

Figure III.E.10.13. Isothermal Section of the V-Nb-C System at 2530°C

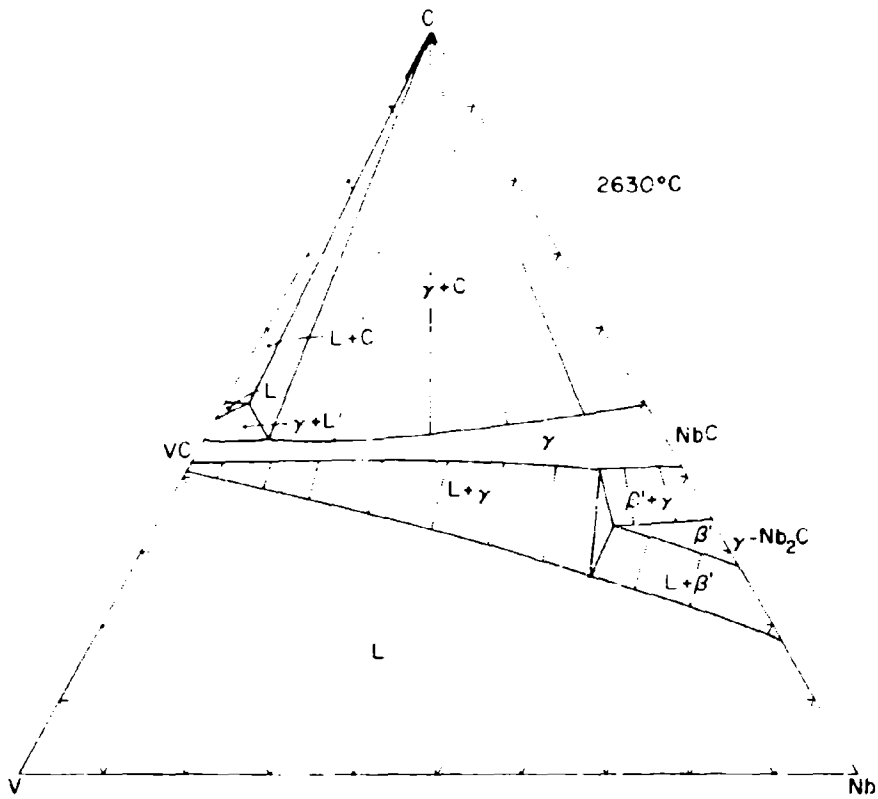

Figure III.E.10.14. Isothermal Section of the V-Nb-C System at 2630°C

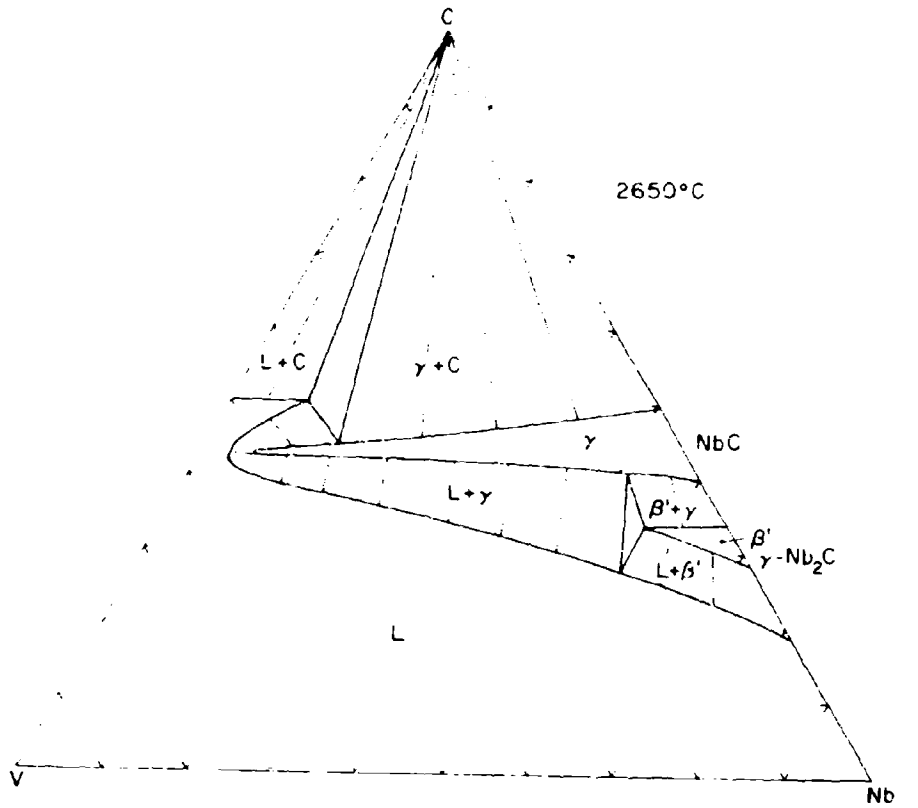

Figure III.E.10.15. Isothermal Section of the V-Nb-C System at 2650°C

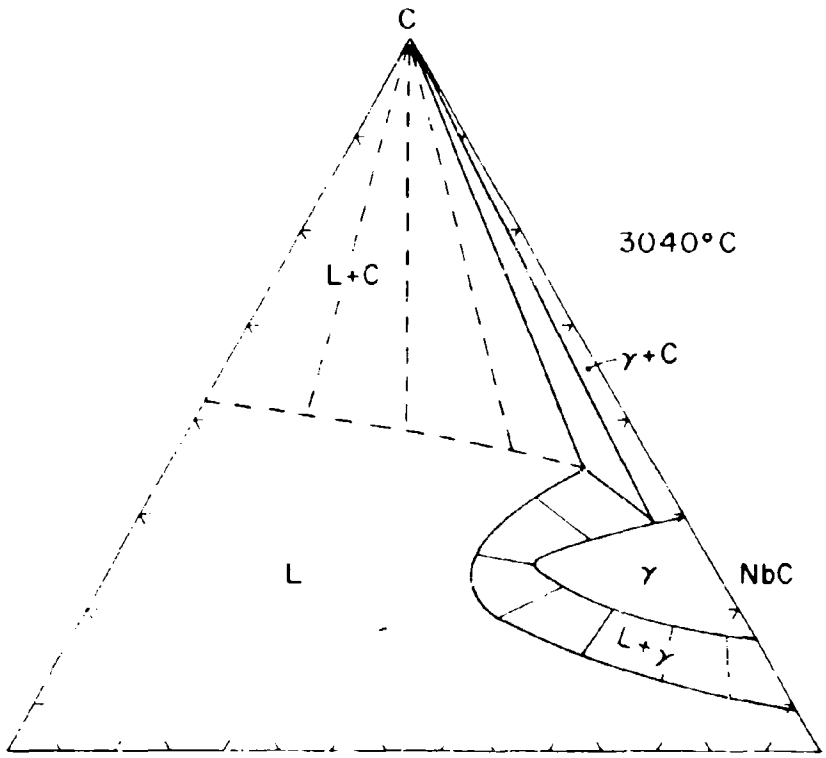

Figure III.E.10.16. Isothermal Section of the V-Nb-C System at 3040°C

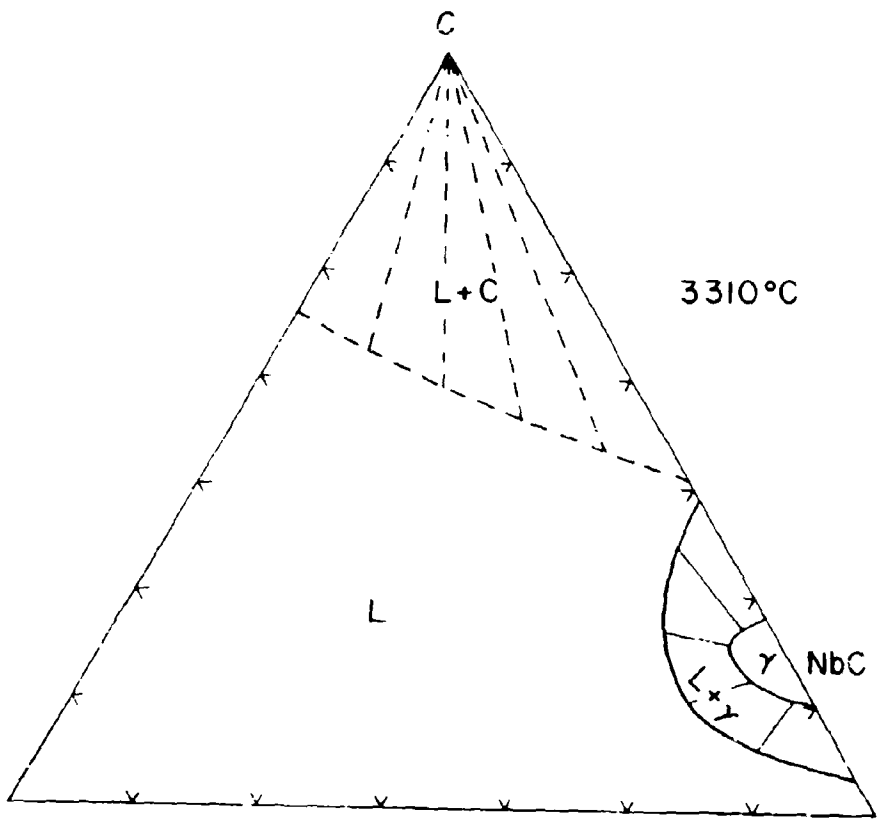

Figure III.E.10.17. Isothermal Section of the V-Nb-C System at 3310°C

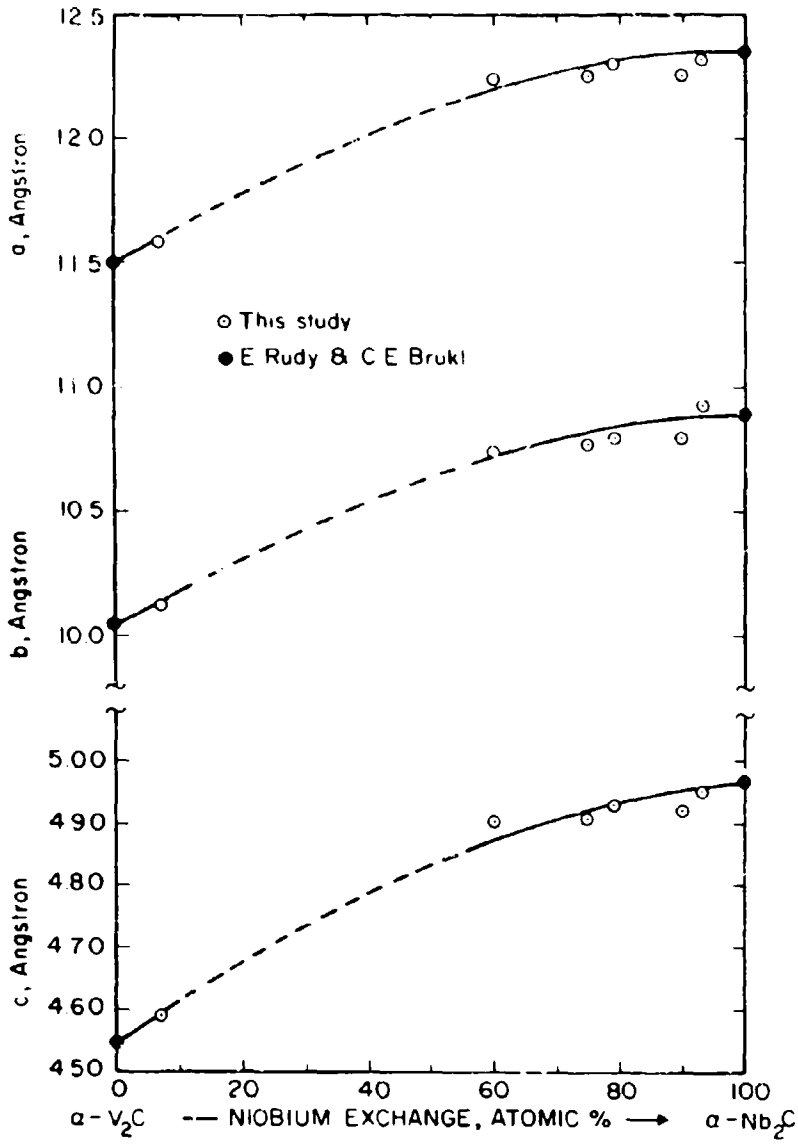

Figure III.E.10.18. Lattice Parameters of the Ternary, Orthorhombic Subcarbide Solid Solution

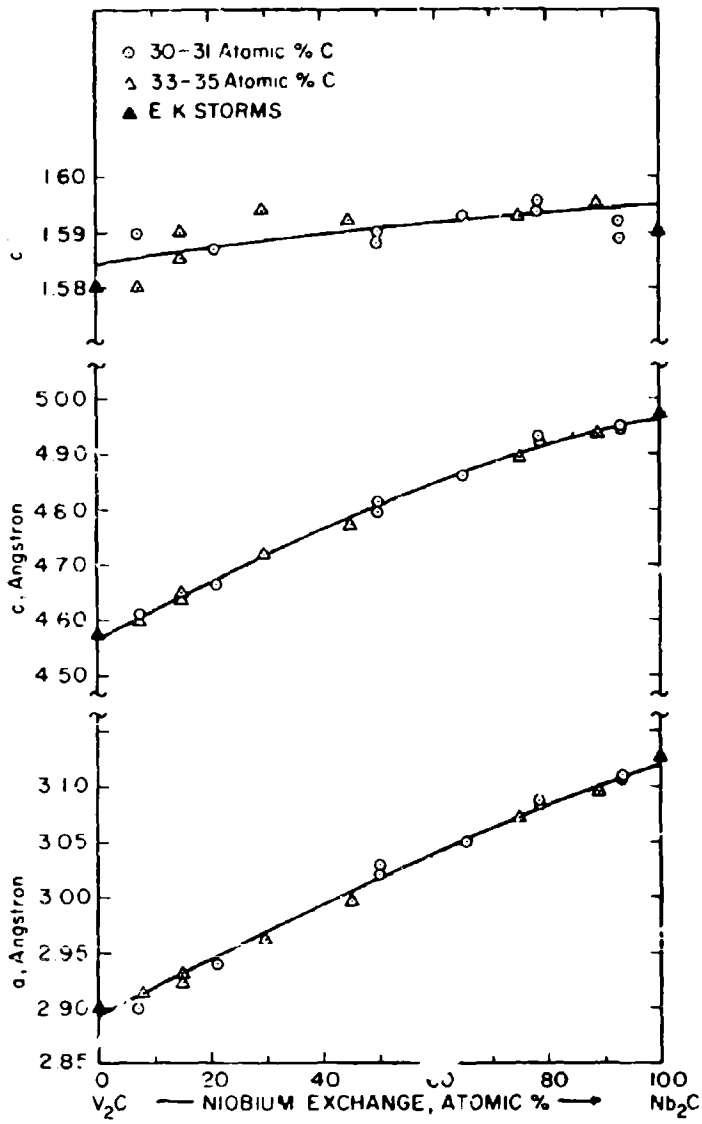

Figure III.E.10.19. Lattice Parameters of the Ternary Hexagonal Subcarbide Solid Solution

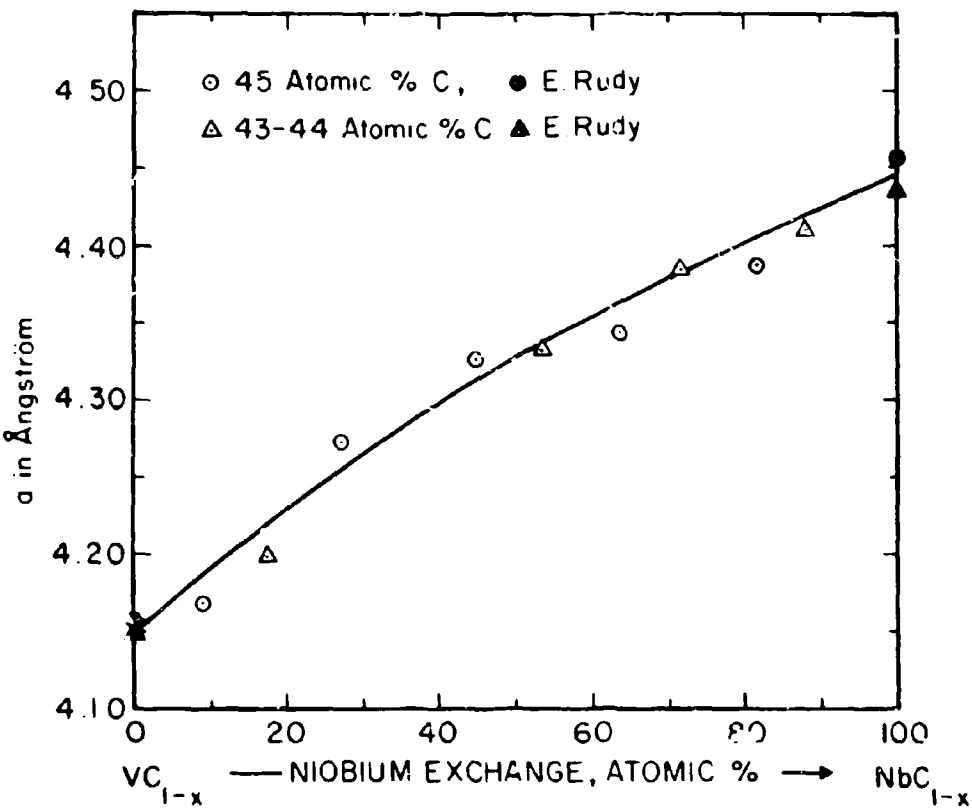

Figure III.E.10.20. Lattice Parameters of the Monocarbide Solid Solution

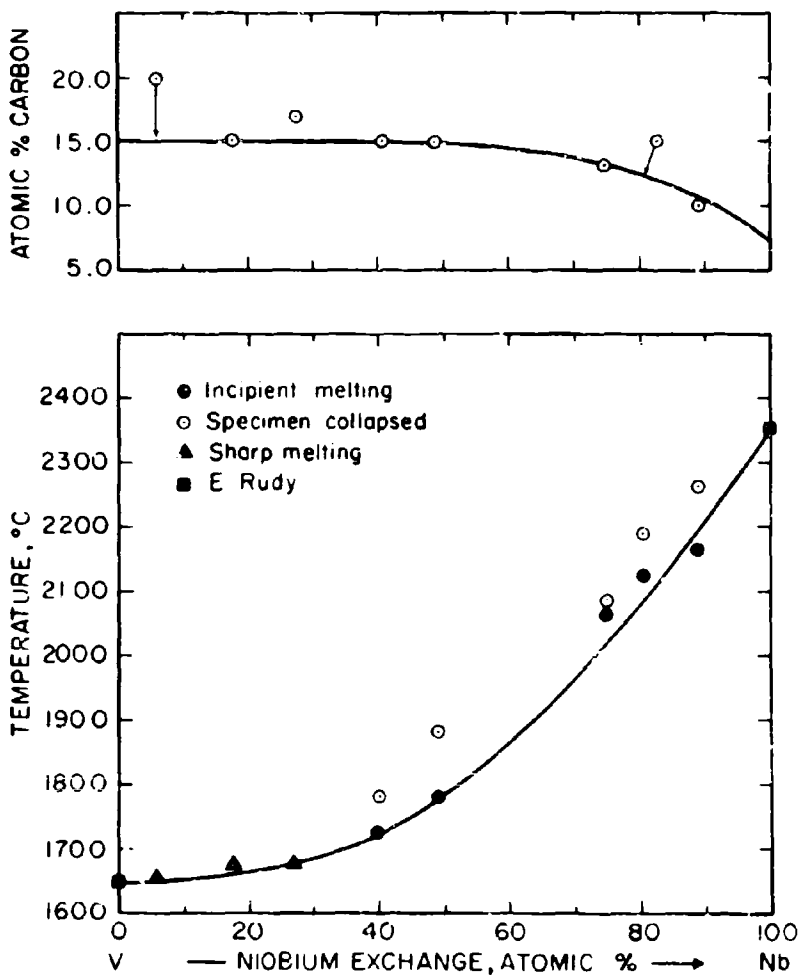

Figure III.E.10.21. Location (Top) and Melting Temperatures (Bottom) of V-Nb-C Alloys Located Along the Me + Me_2C Eutectic Trough

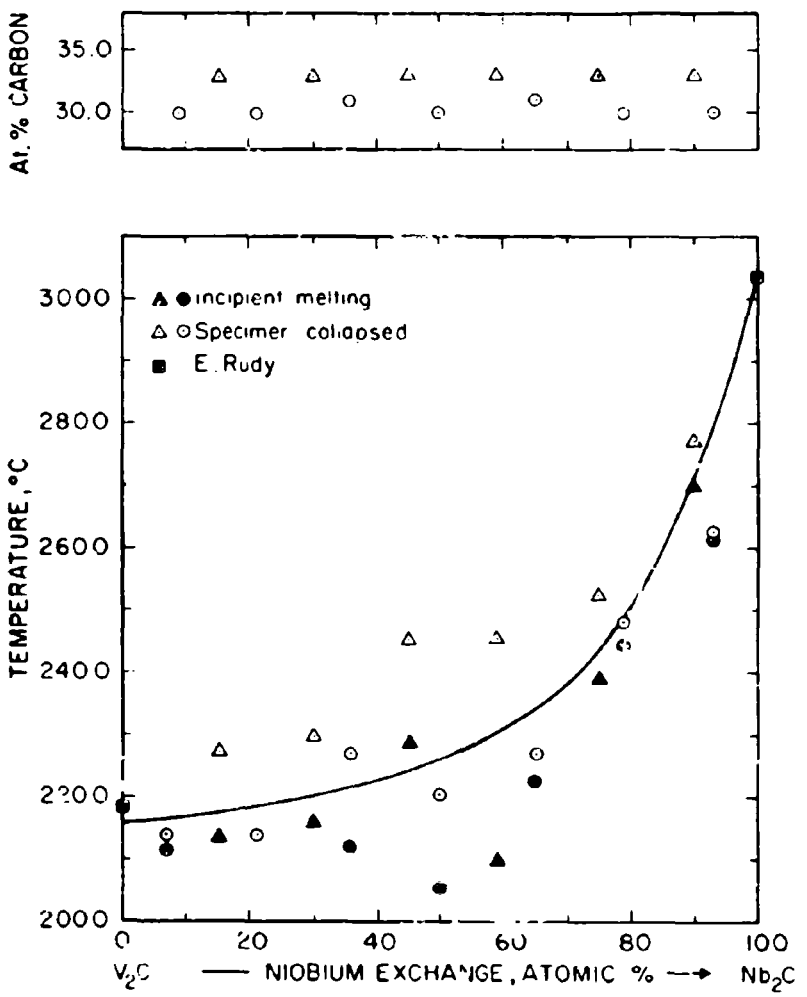

Figure III.E.10.22. Melting Temperatures of the Subcarbide, $(V,Nb)_2C$, Solid Solution.

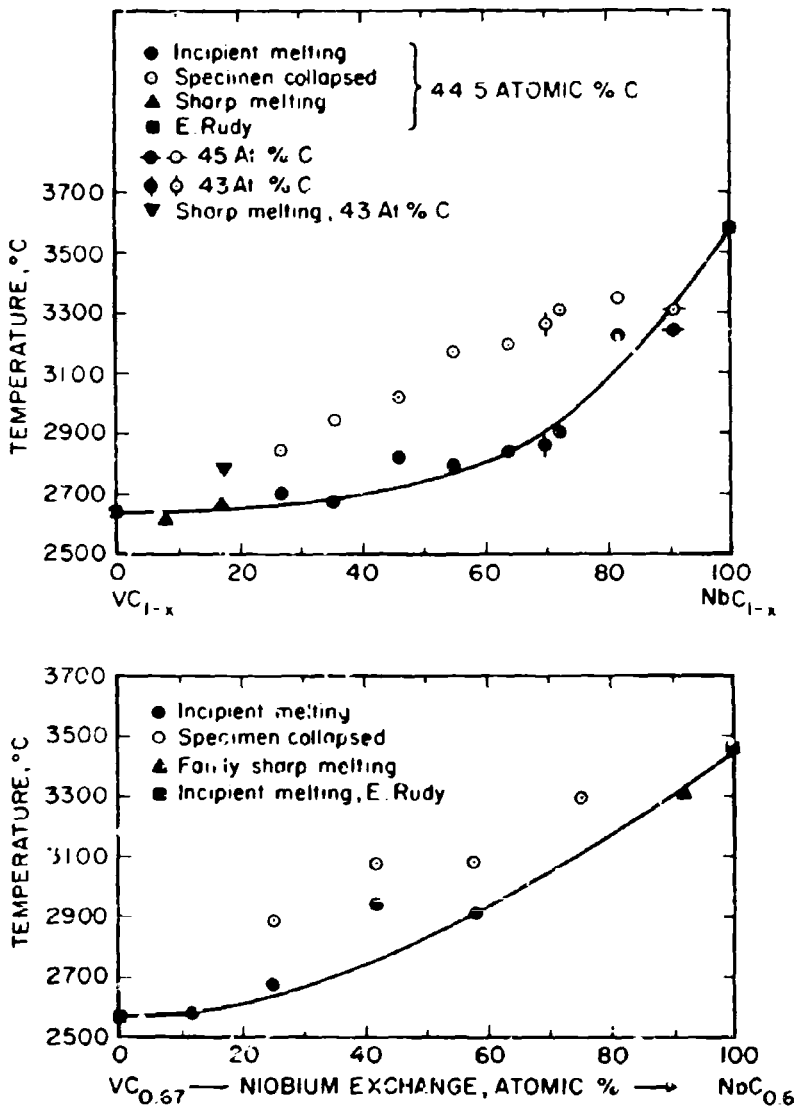

Figure III.E.10.23. Melting Temperatures of the Monocarbide, $(V,Nb)C_{1-x}$, Solid Solution at Various Carbon Defects

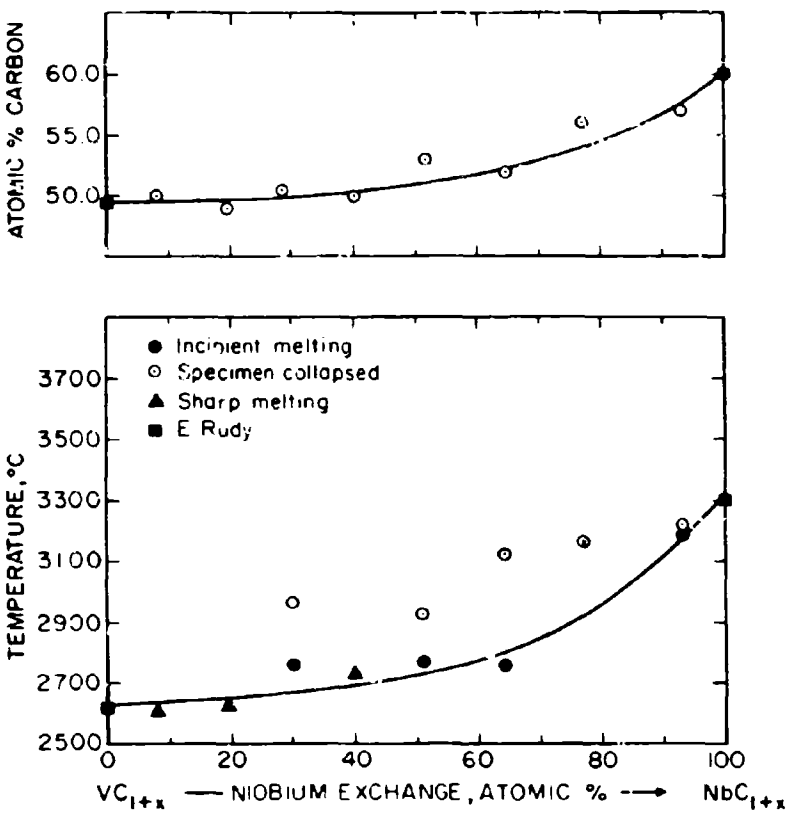

Figure III.E.10.24. Location (Top) and Melting Temperatures (Bottom) of V-Nb-C Alloys Located Along the Monocarbide + Graphite Eutectic Trough

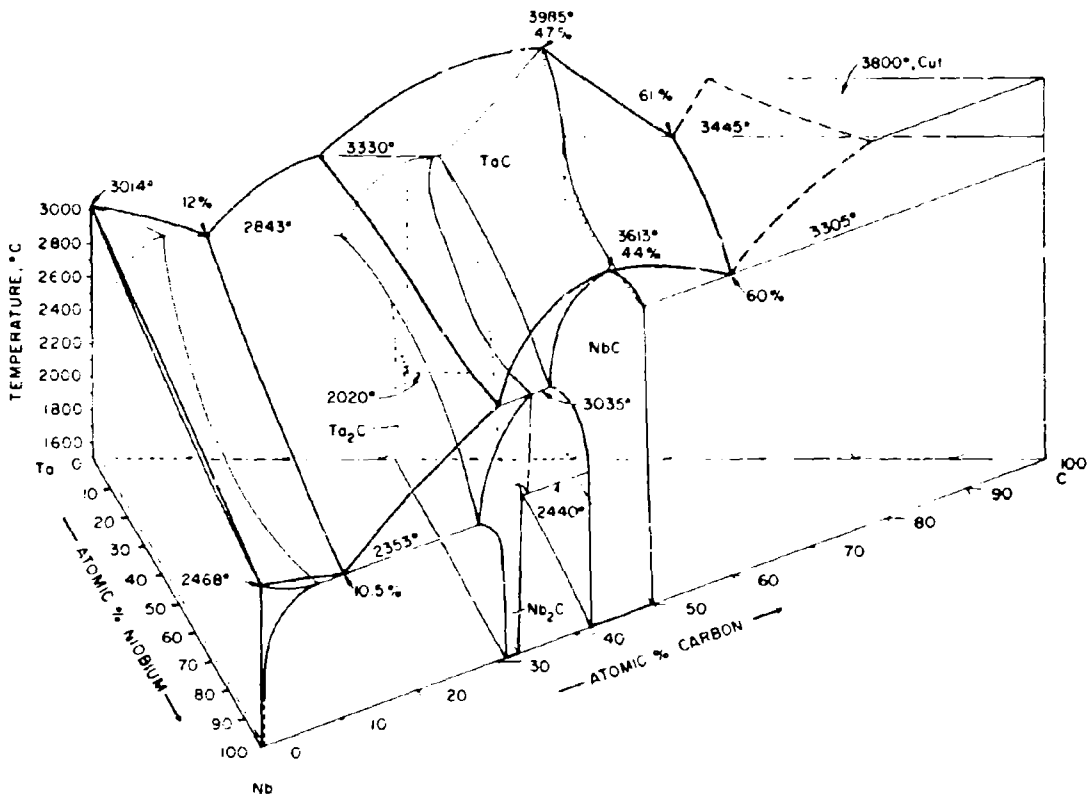

Figure III.E.11.1 Isometric View of the Nb-Ta-C System

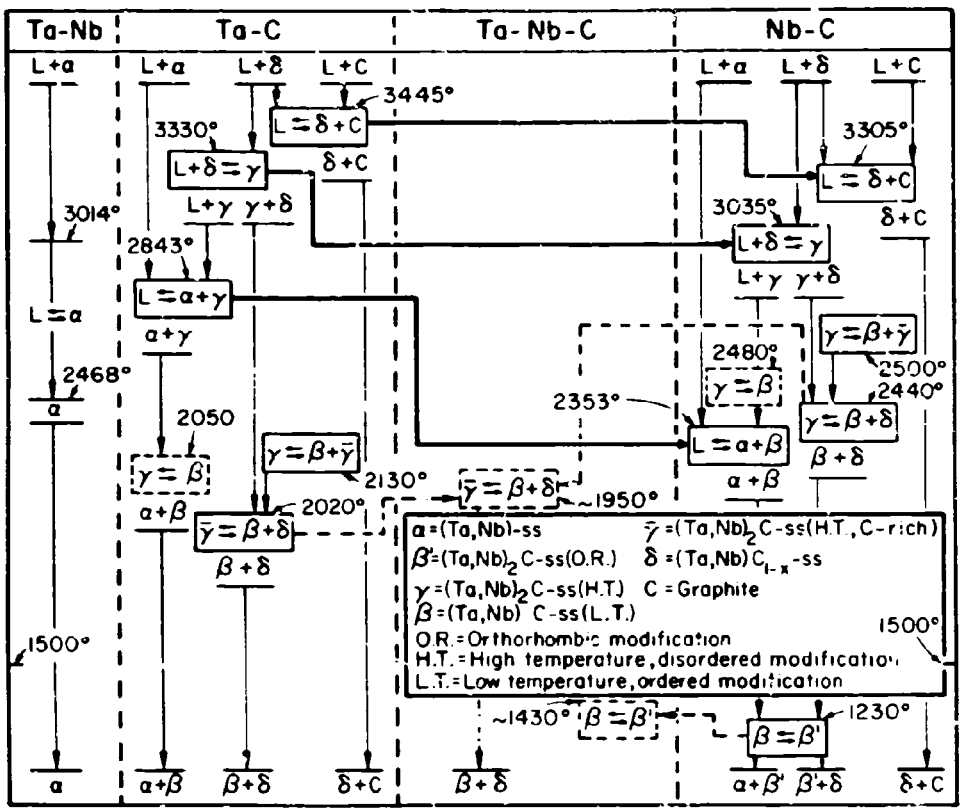

Figure III.E.11.2. Reaction Diagram for the Nb-Ta-C System

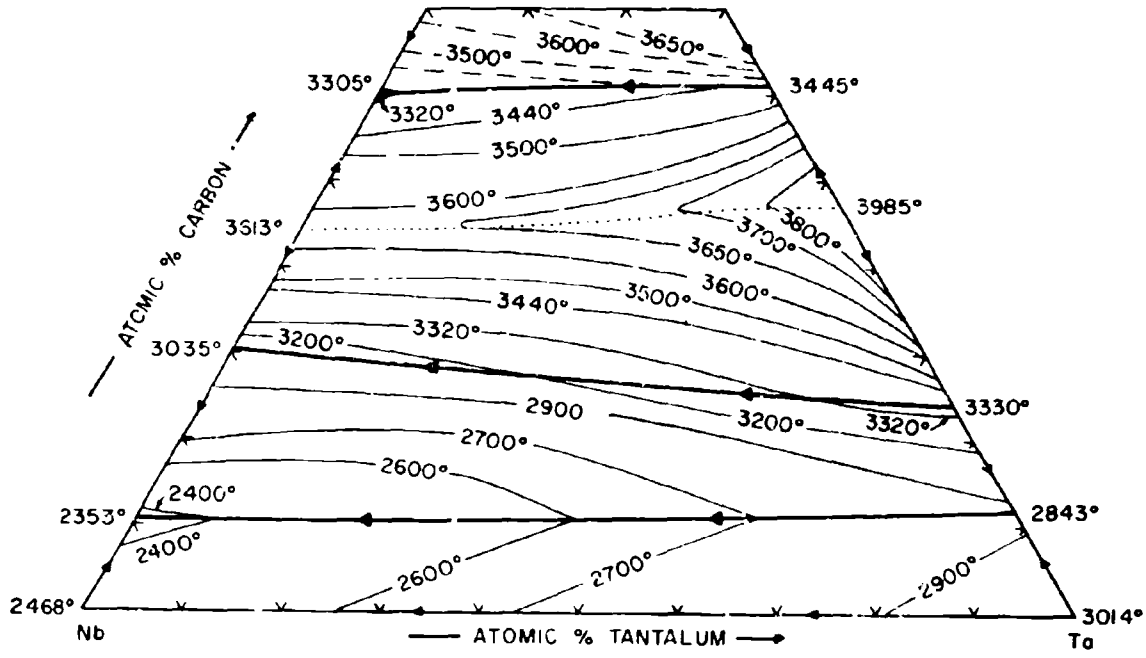

Figure III.E.11.3. Liquidus Projections in the Nb-Ta-C System

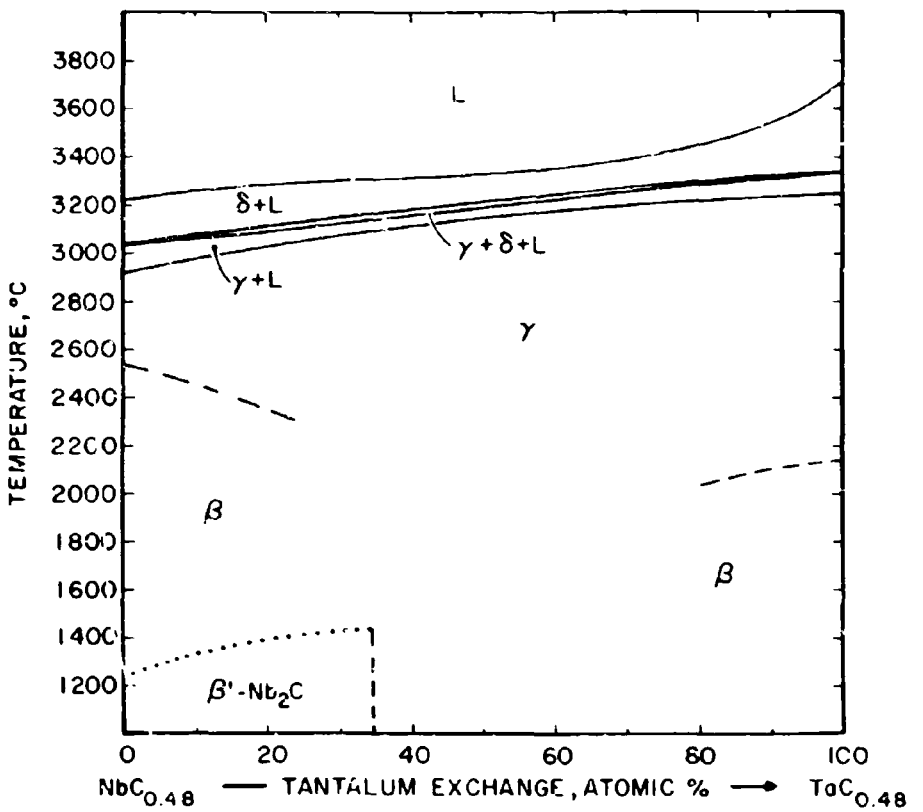

Figure III.E.11.4. Isopleth at 32.5 At.% C

Dashed: Order-Disorder Transformation Temperatures in the $(Nb,Ta)_2C$ Phase

Dotted: Change of Order in Nb_2C-Rich Alloys

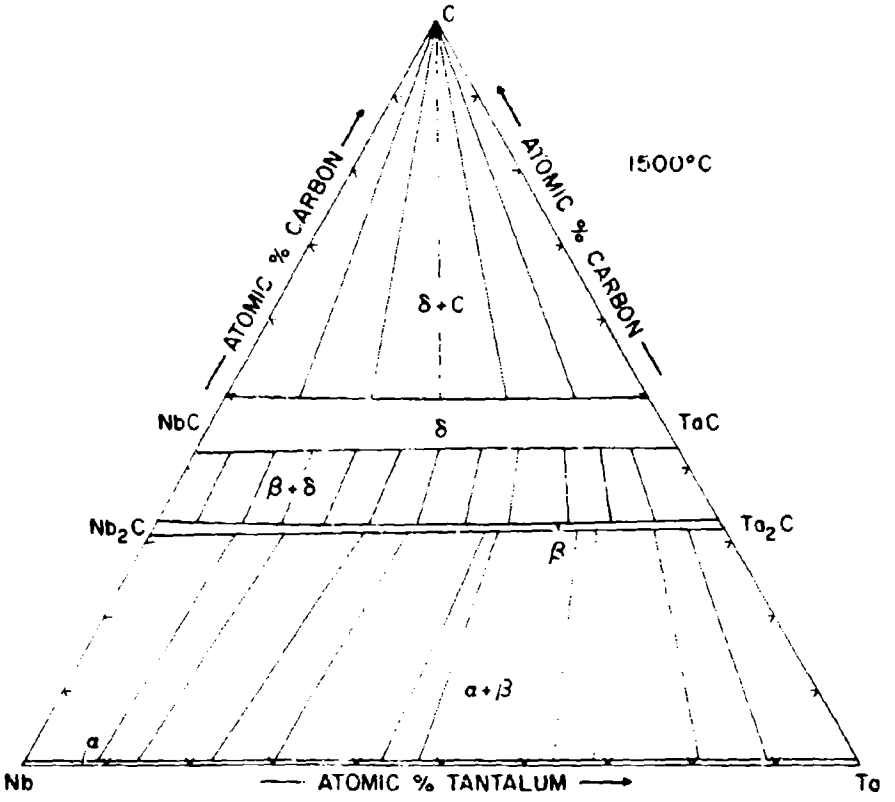

Figure III.E.11.5. Isothermal Section of the Nb-Ta-C System at 1500° C

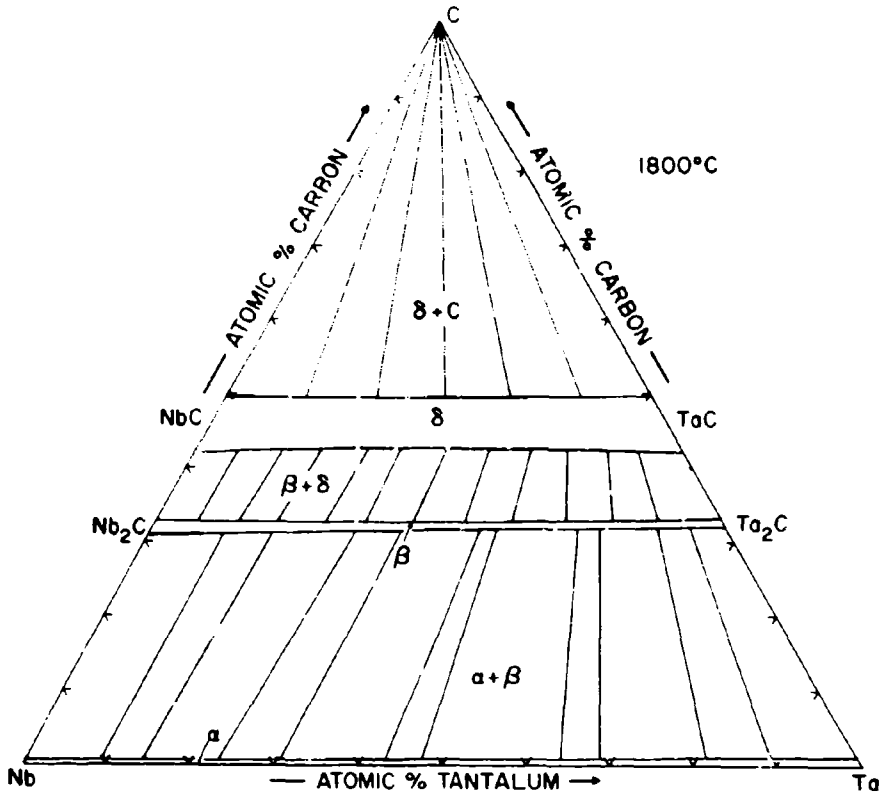

Figure III.E.11.6. Isothermal Section of the Nb-Ta-C System at 1800° C

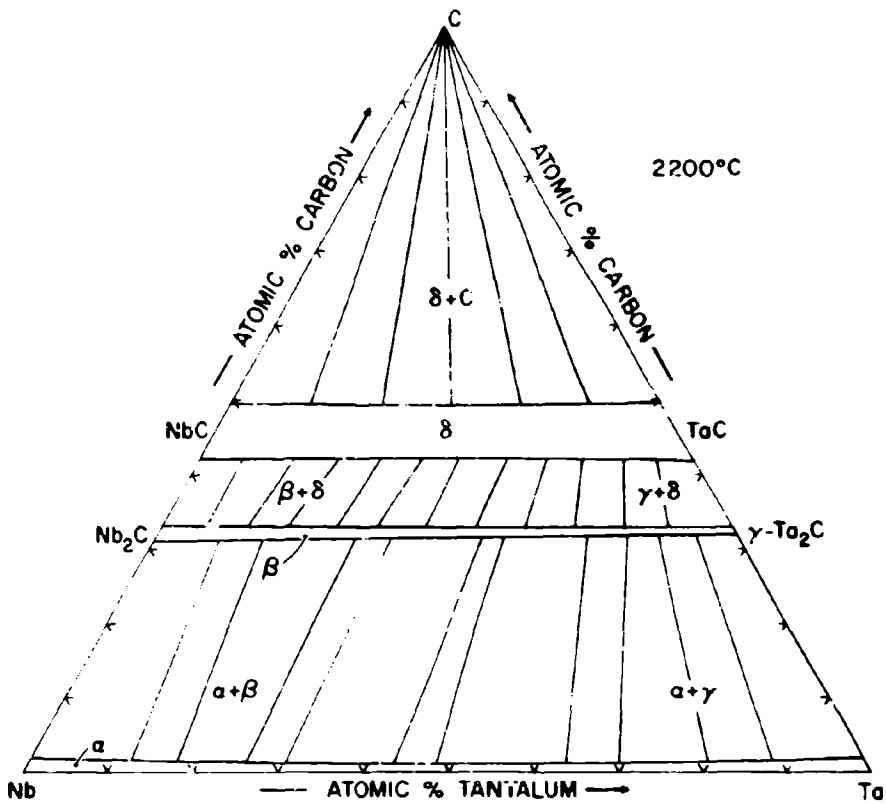

Figure III.E.11.7. Isothermal Section of the Nb-Ta-C System at 2200°C

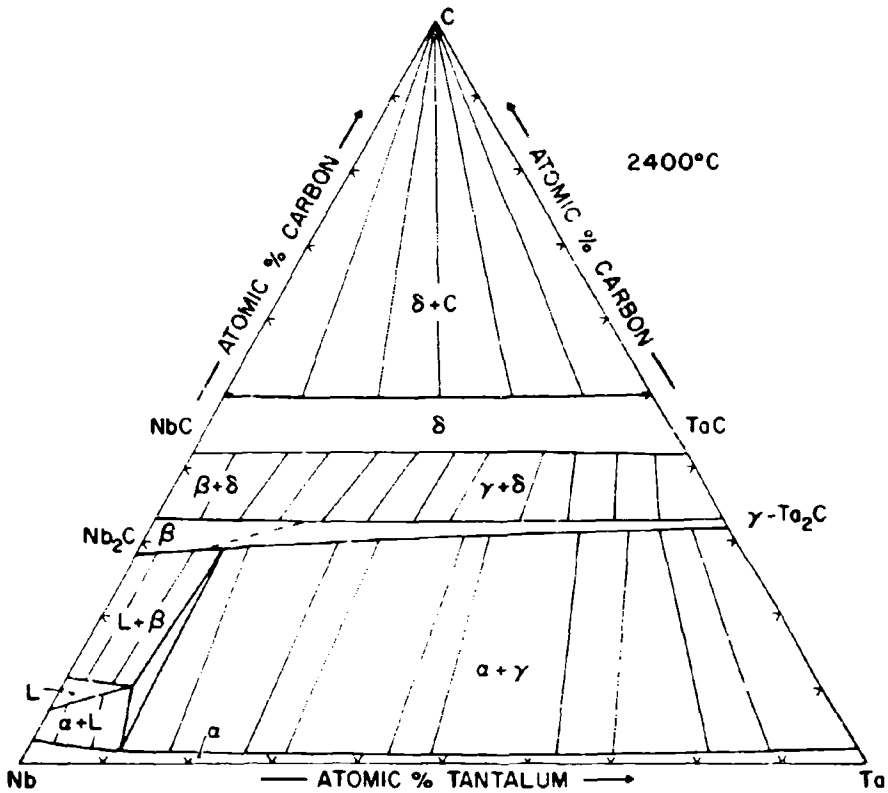

Figure III.E.11.8. Isothermal Section of the Nb-Ta-C System at 2400° C

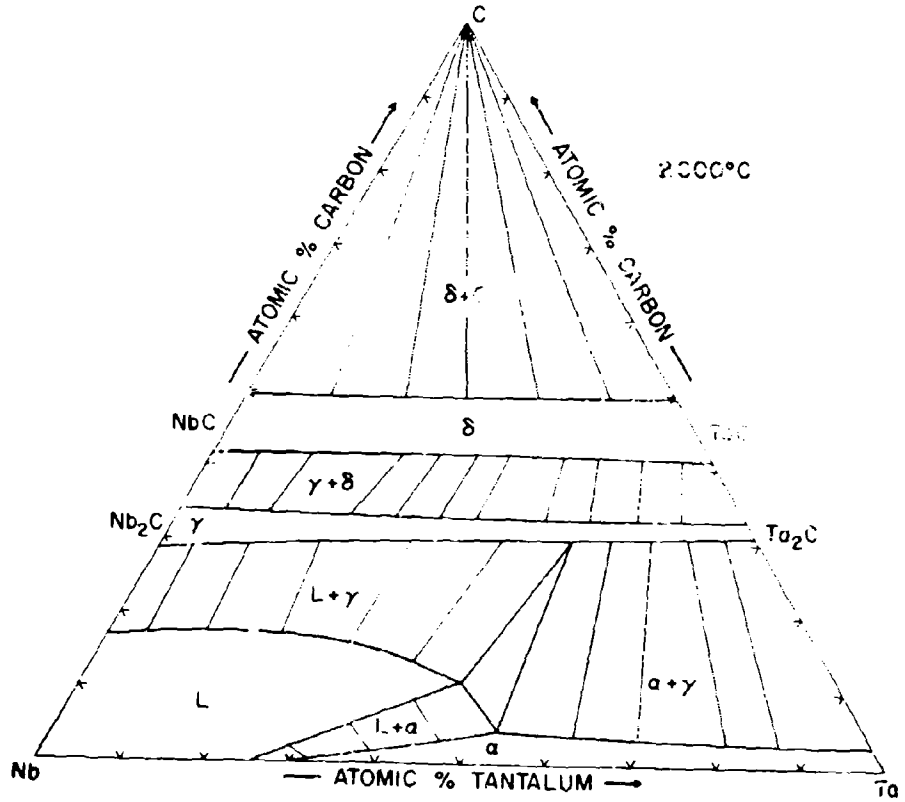

Figure III.E.11.9. Isothermal Section of the Nb-Ta-C System at 2600°C

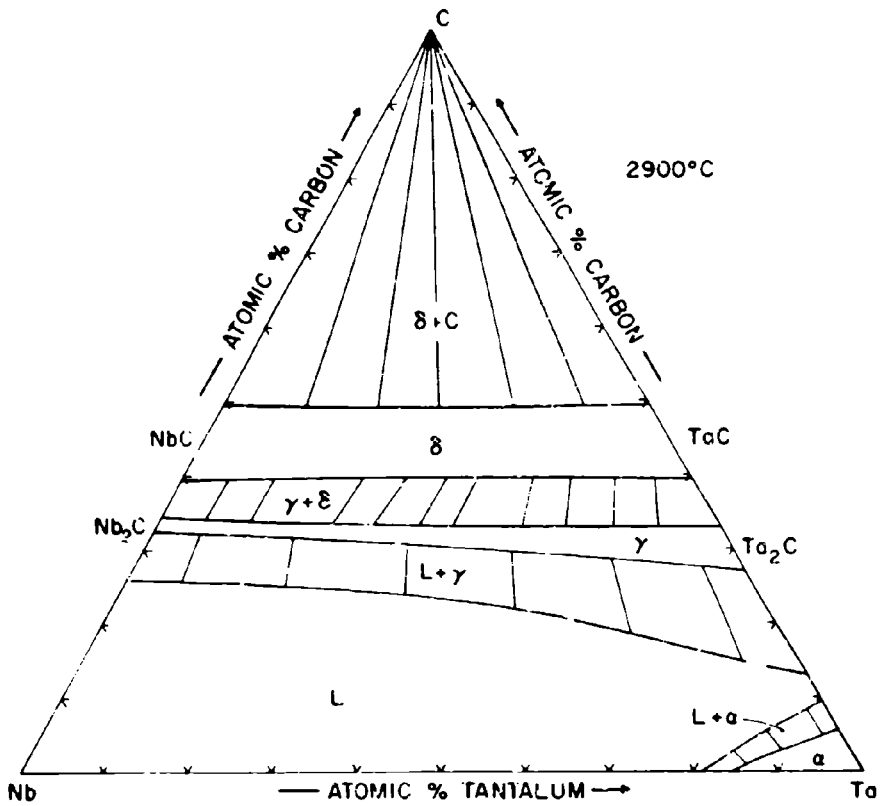

Figure III.E.11.10. Isothermal Section of the Nb-Ta-C System at 2900°C

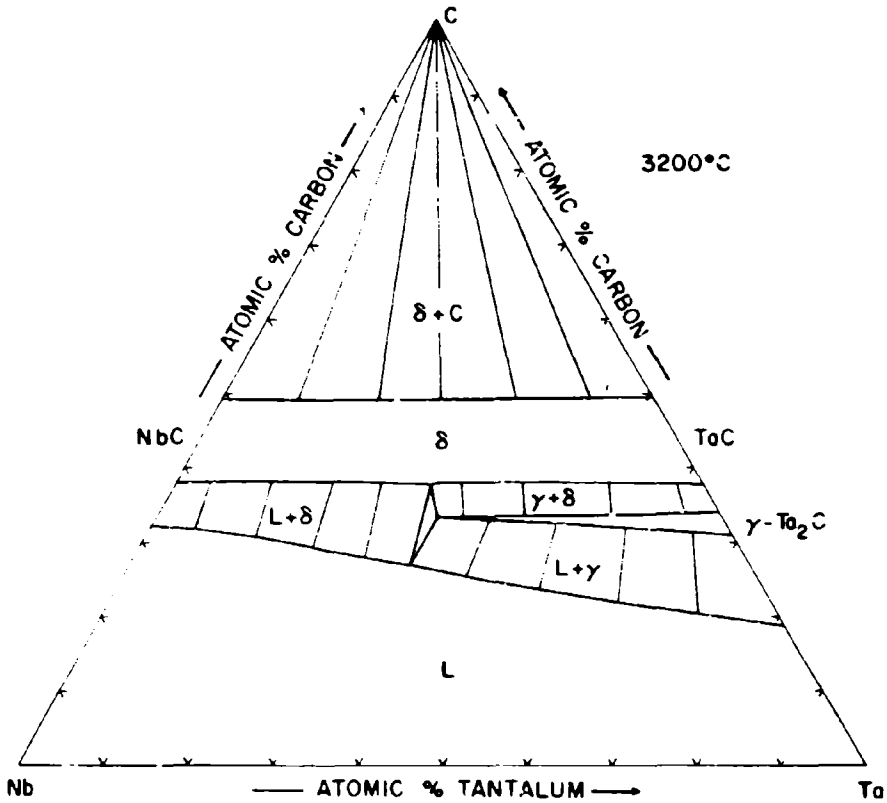

Figure III.E.11.11. Isothermal Section of the Nb-Ta-C System at 3200° C

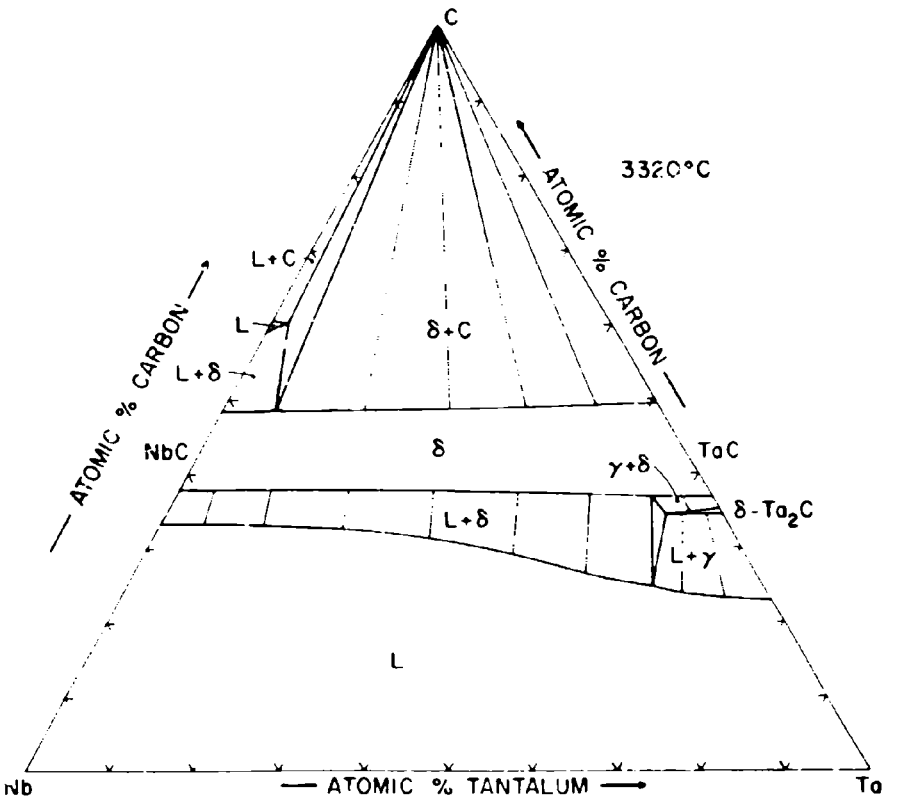

Figure III.E.11.12. Isothermal Section of the Nb-Ta-C System at 3320°C

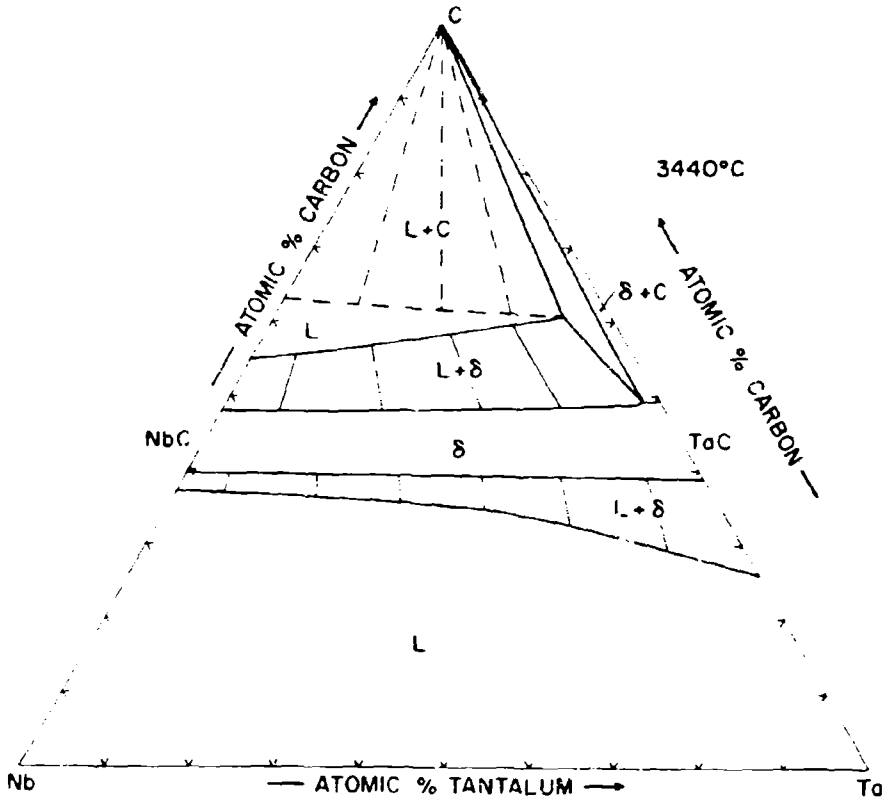

Figure III.E.11.13. Isothermal Section of the Nb-Ta-C System at 3440° C

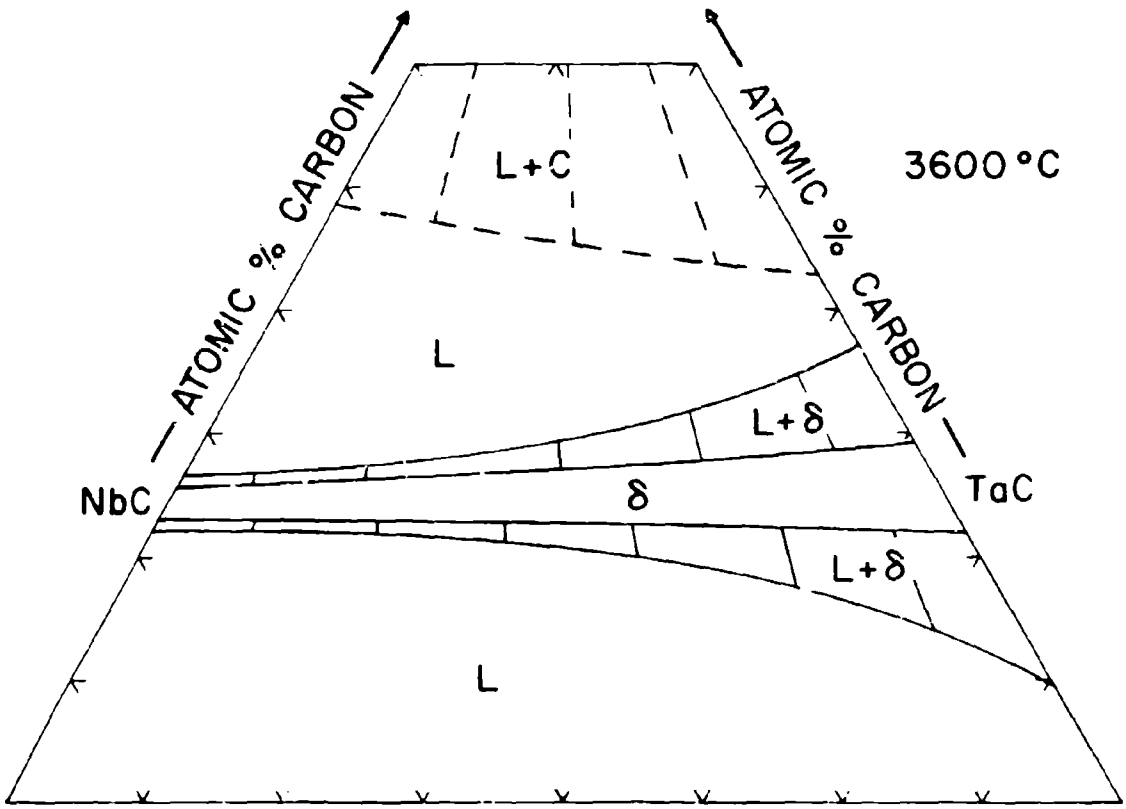

Figure III.E.11.14. Isothermal Section of the Nb-Ta-C System at 3600° C

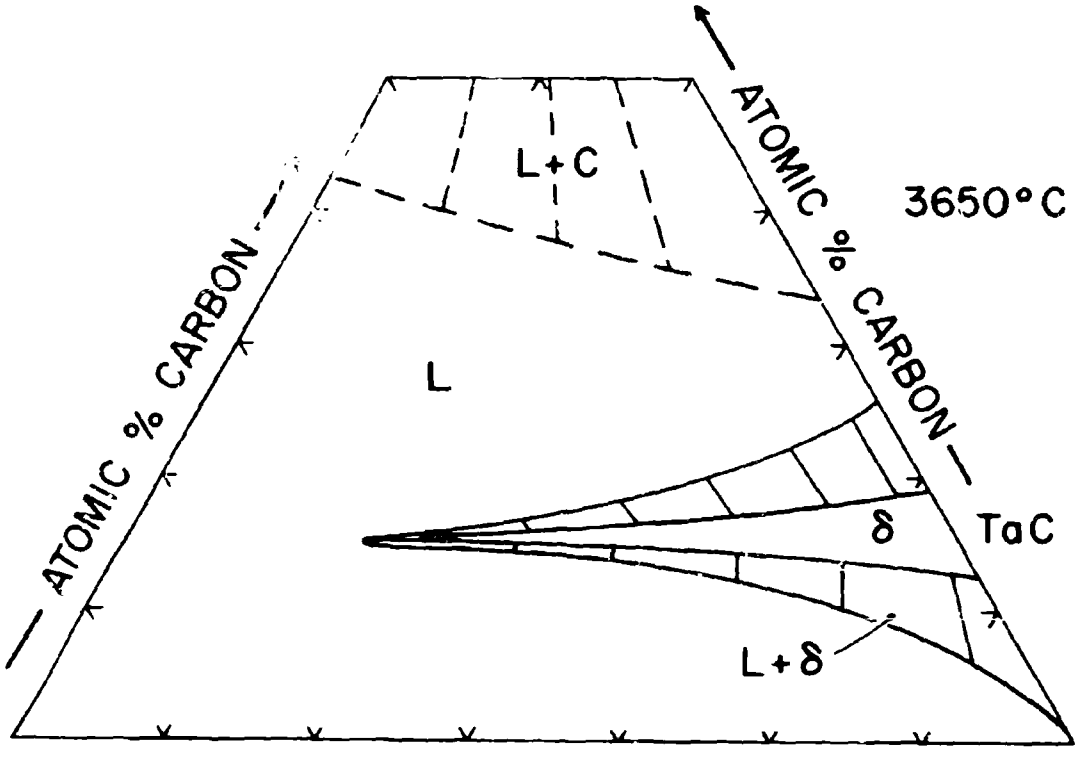

Figure III.E.11.15. Isothermal Section of the Nb-Ta-C System at 3650°C

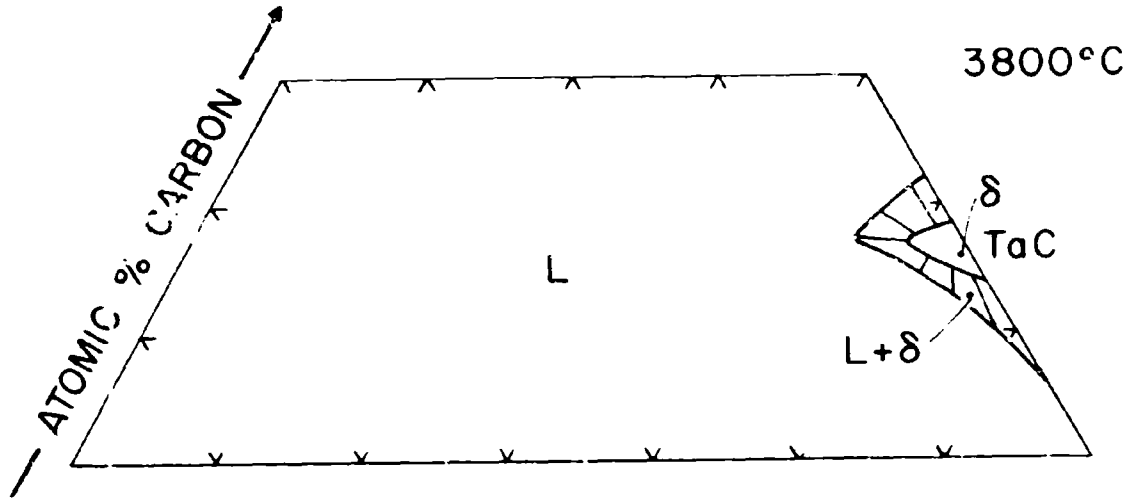

Figure III.E.11.16. Partial Isotherm of the Nb-Ta-C System at 3800°C

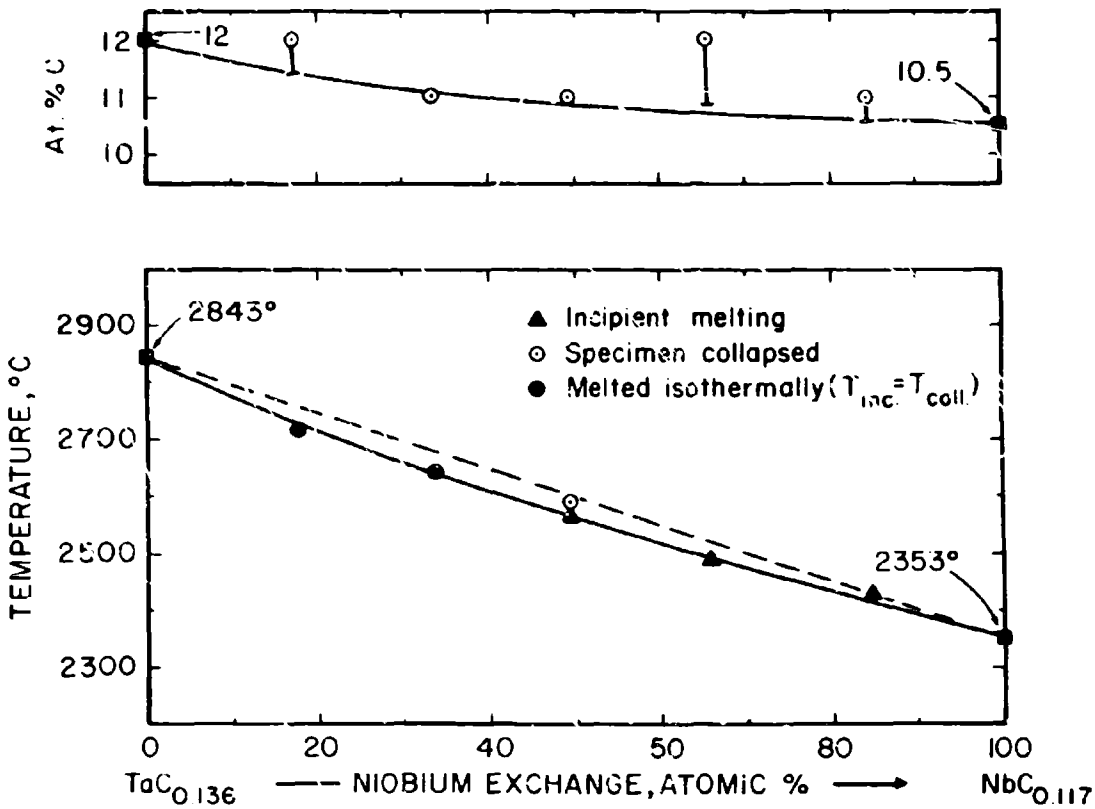

Figure III.E.11.17. Experimental Melting Temperatures and Location of the Metal + Subcarbide Eutectic Trough

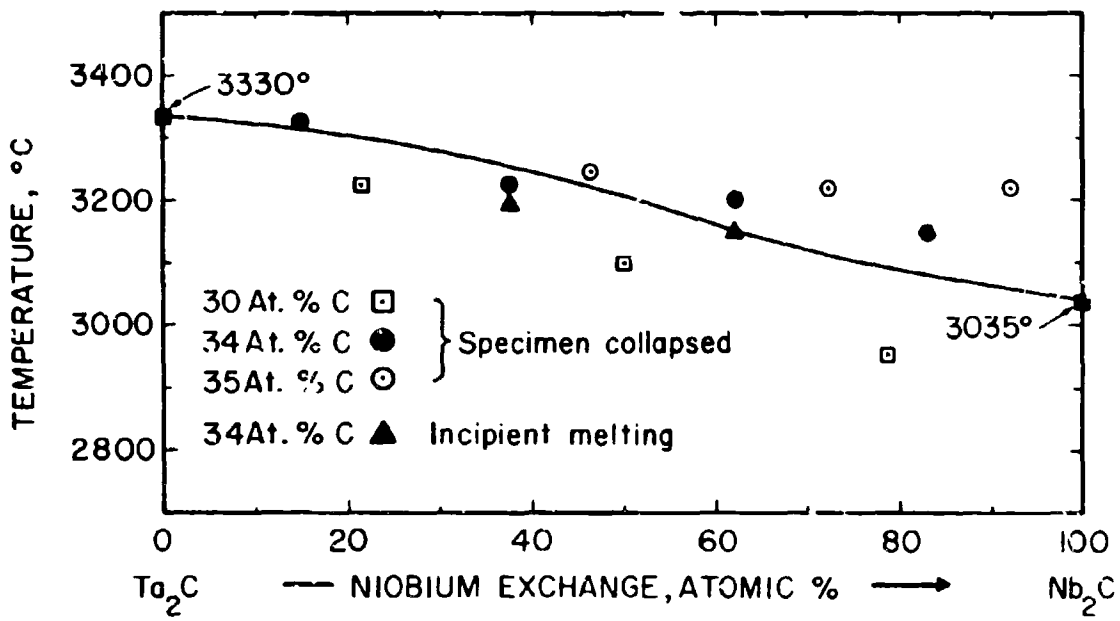

Figure III.E.11.18. Experimental Solidus Temperatures of the Subcarbide Solid Solution

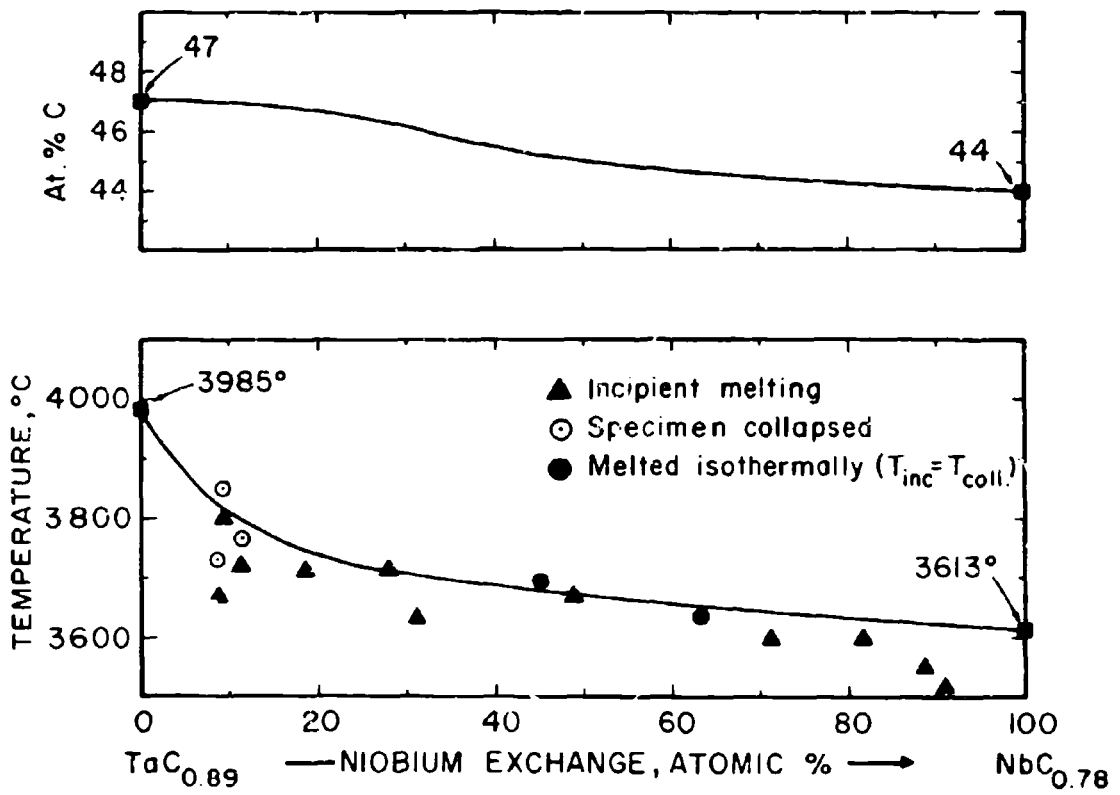

Figure III.E.11.19. Experimental Solidus Temperatures for the Monocarbide (B1) Solution

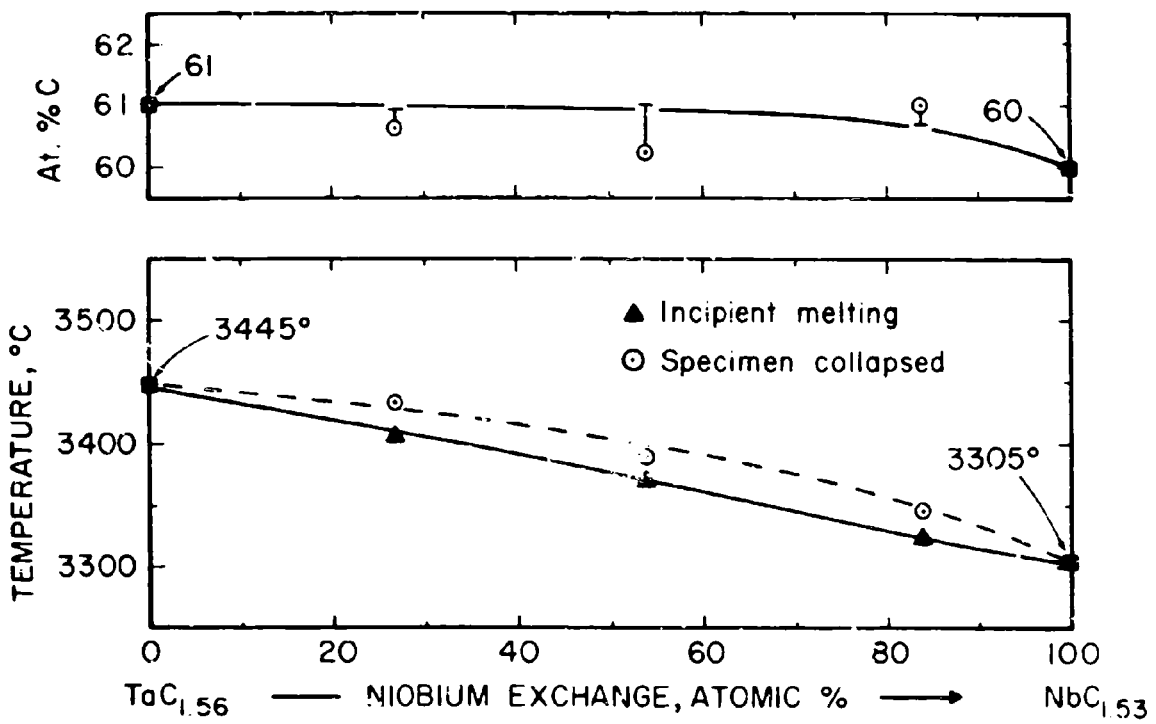

Figure III.E.11.20. Observed Melting in Metal + Monocarbide Alloys and Microscopically Estimated Location of the Eutectic Trough

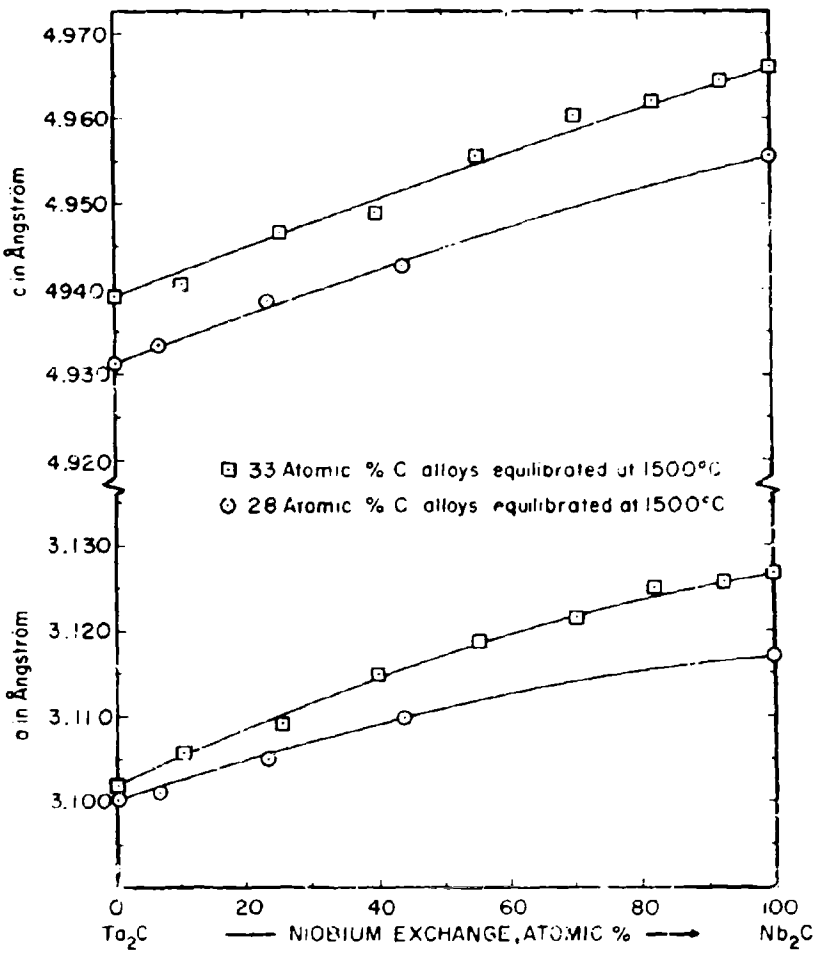

Figure III.E.11.21. Lattice Parameters of the $(Nb,Ta)_2C$ Solid Solution at 28 and 33 At.% C

(Indexing according to the L'3-type)

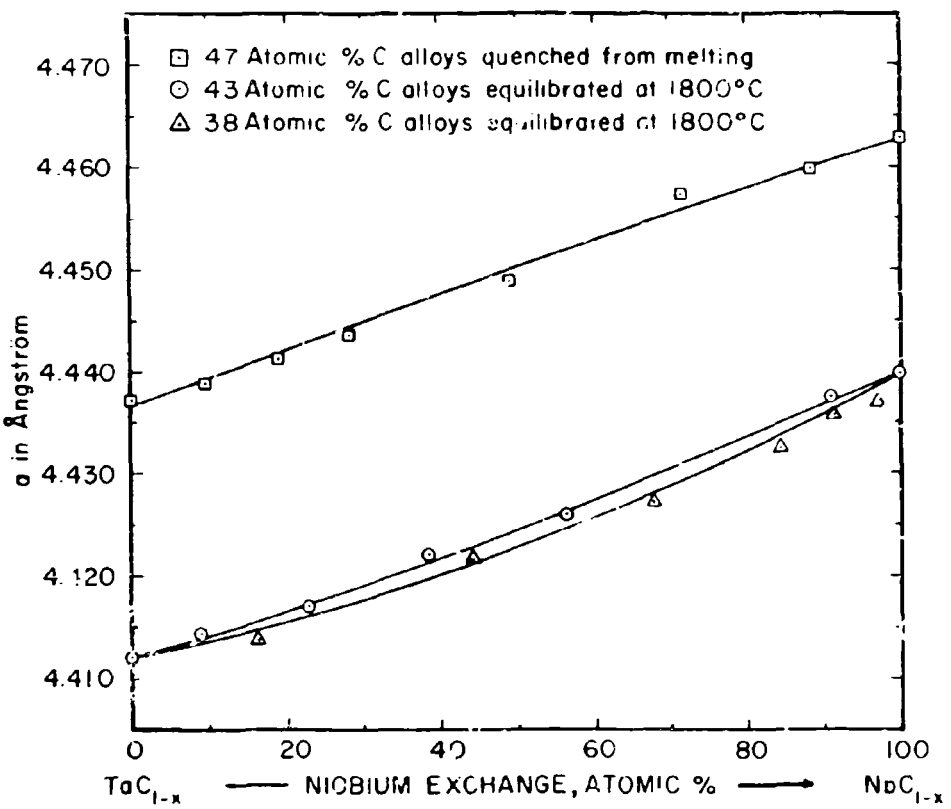

Figure III.E.11.22. Lattice Parameters of the Monocarbide (B1) Solid Solution in Carbon-Deficient Alloys

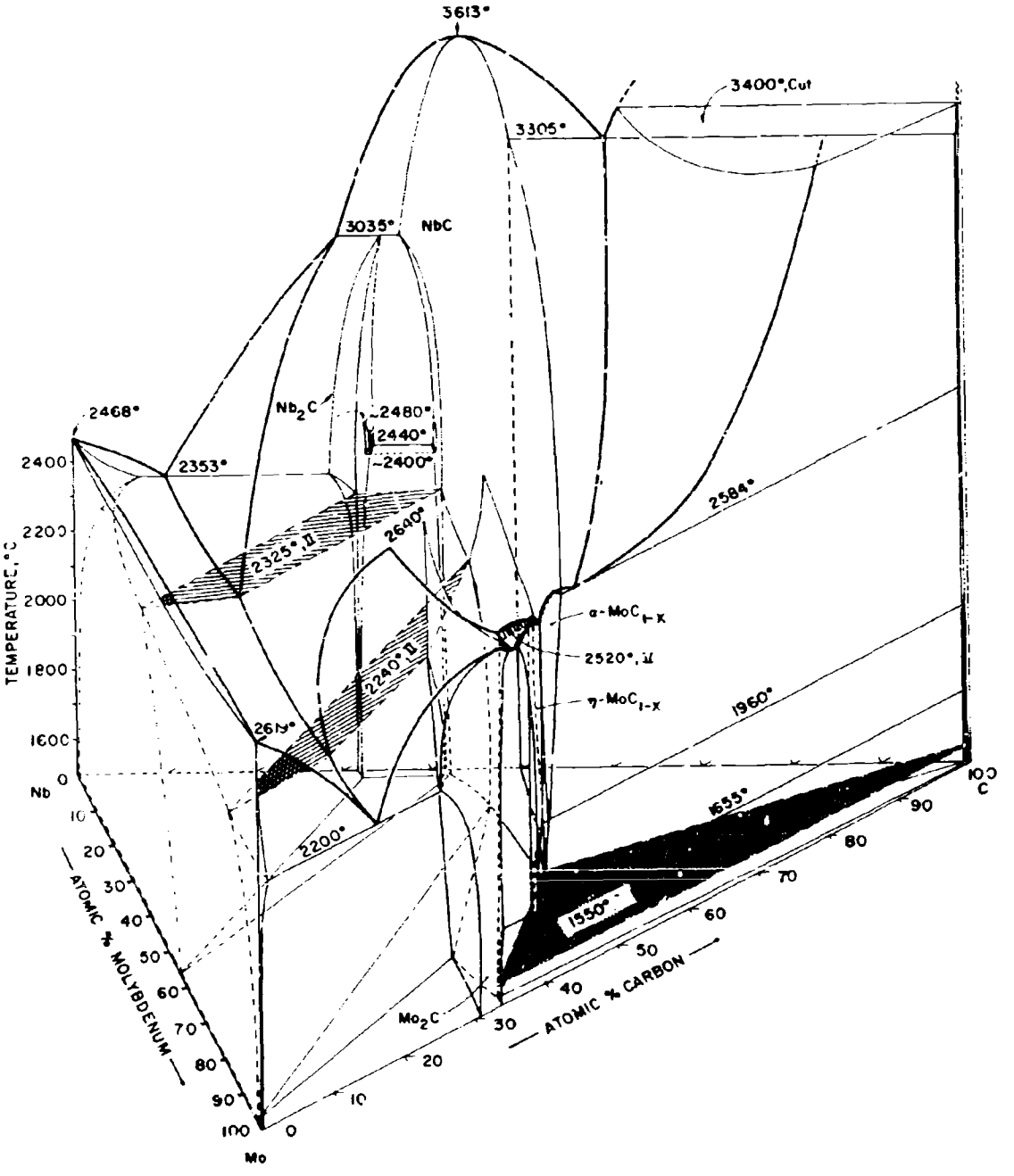

Figure III.E.12.1: Isometric View of the Nb-Mo-C System.

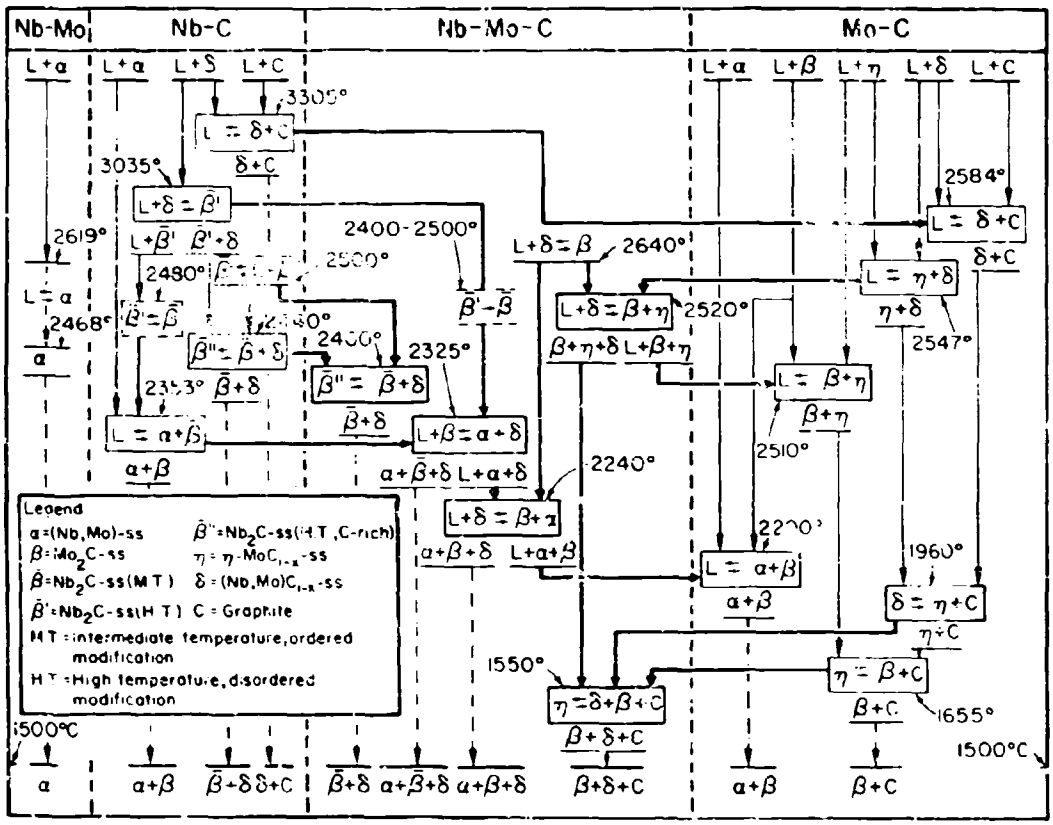

Figure III.E.12.2. Reaction Diagram for Nb-Mo-C Alloys

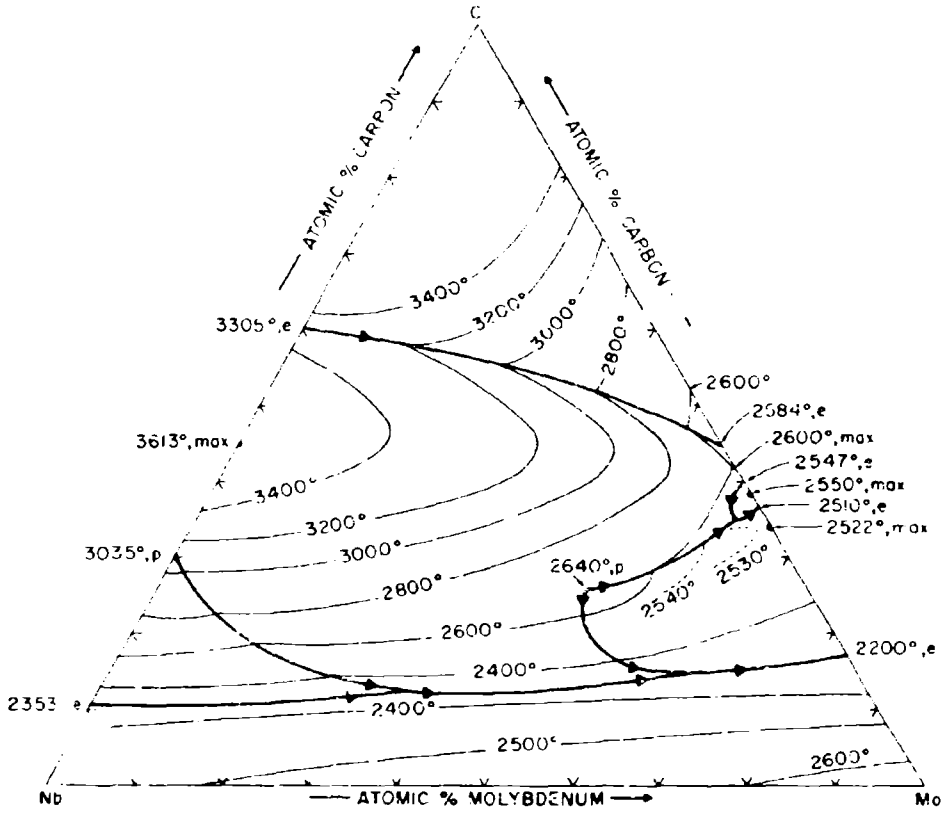

Figure III.E.12.3. Liquidus Projections in the Nb-Mo-C System

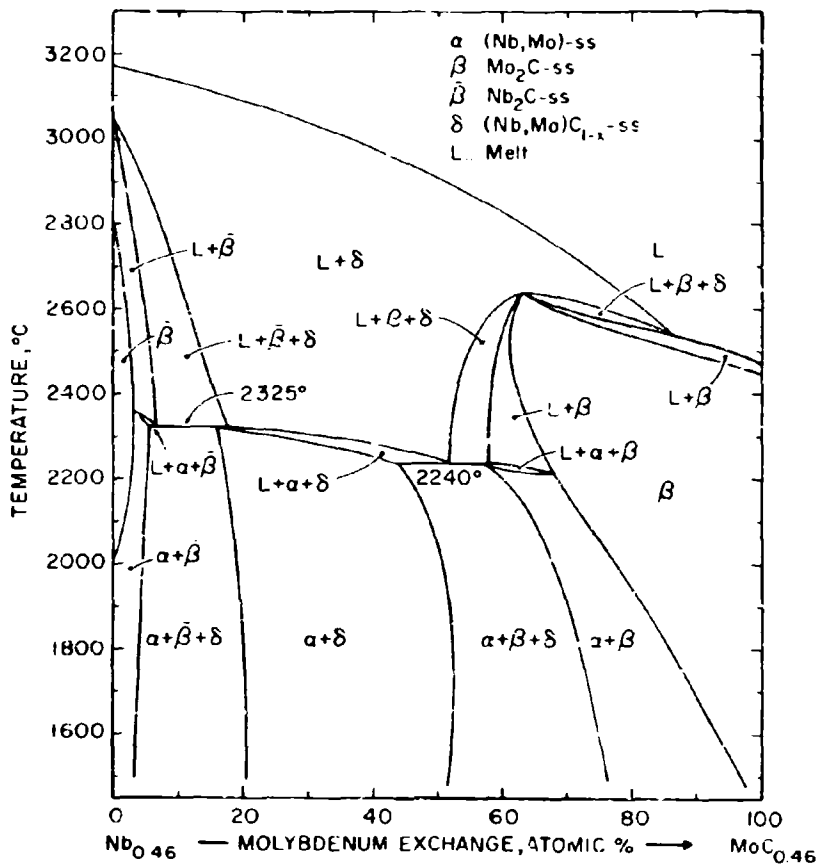

Figure III.E.12.4. Isopleth at $NbC_{0.46}$-$MoC_{0.46}$

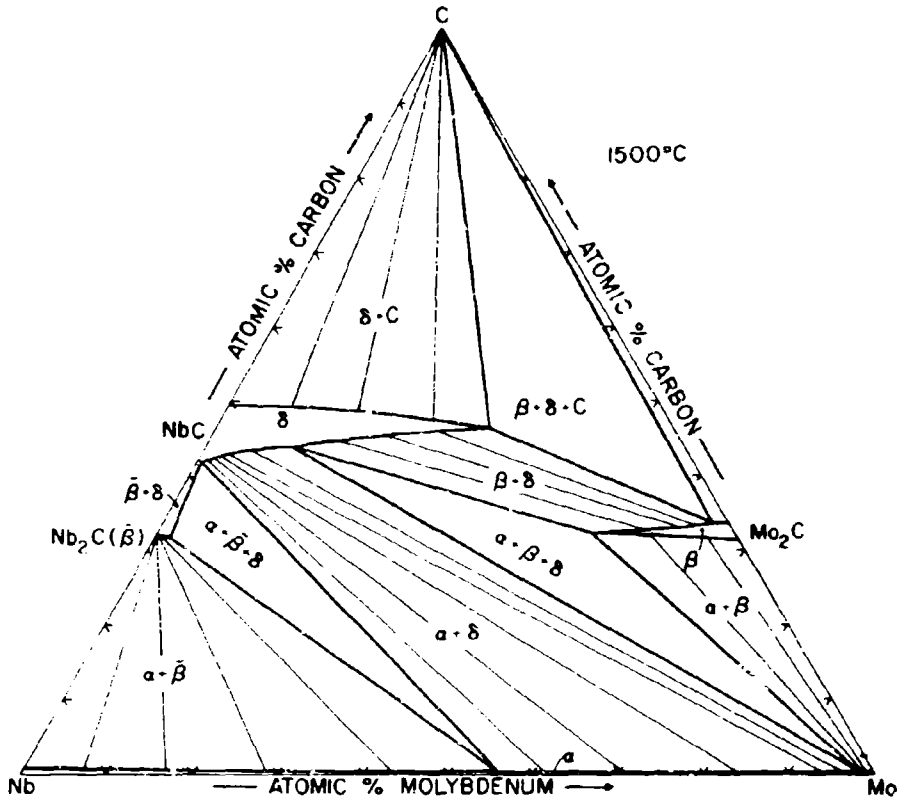

Figure III.E.12.5: Isothermal Section of the Nb-Mo-C System at 1500°C.

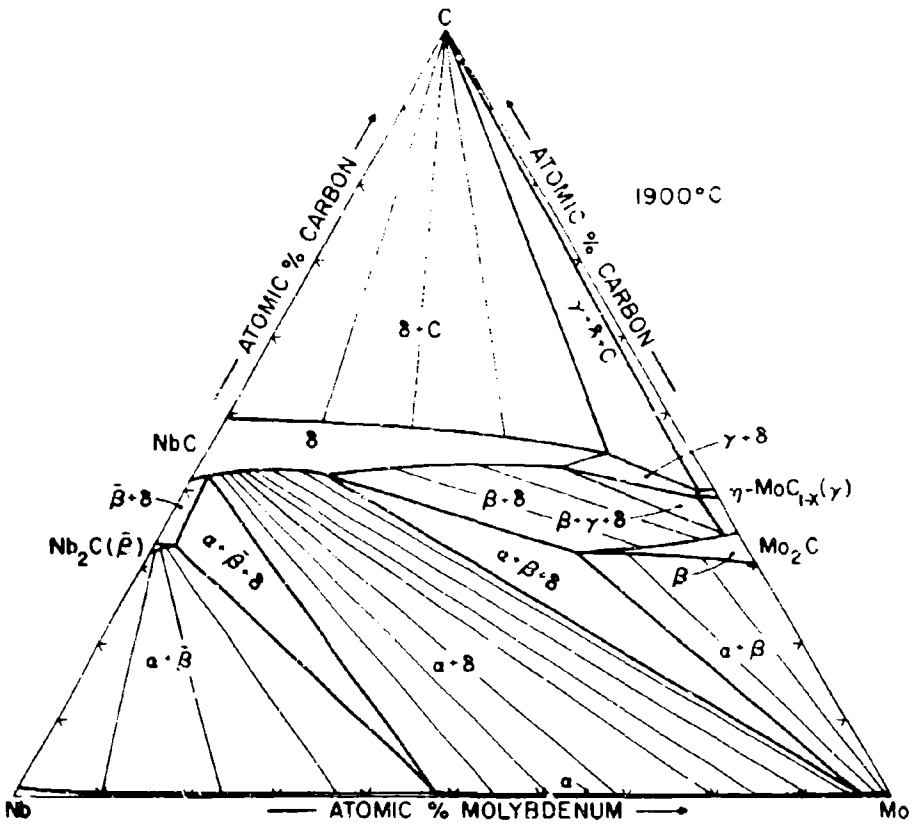

Figure III.E.12.6: Isothermal Section of the Nb-Mo-C System at 1900°C.

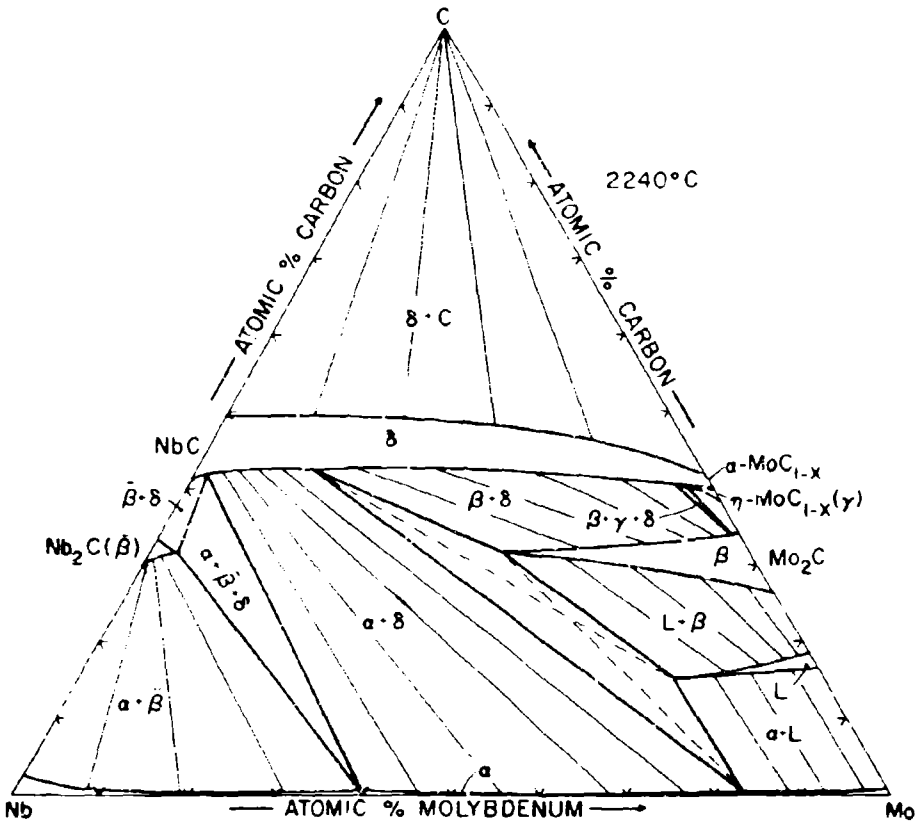

Figure III.E.12.7: Isothermal Section of the Nb-Mo-C System at 2240°C.

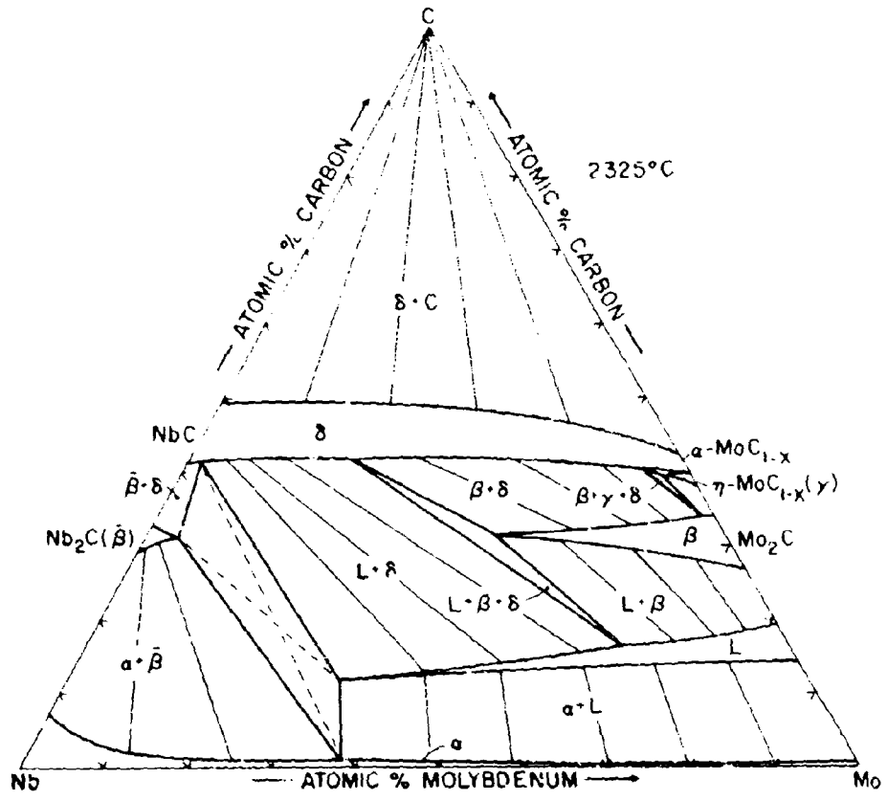

Figure III. E. 12. 8: Isothermal Section of the Nb-Mo-C System at 2325°C.

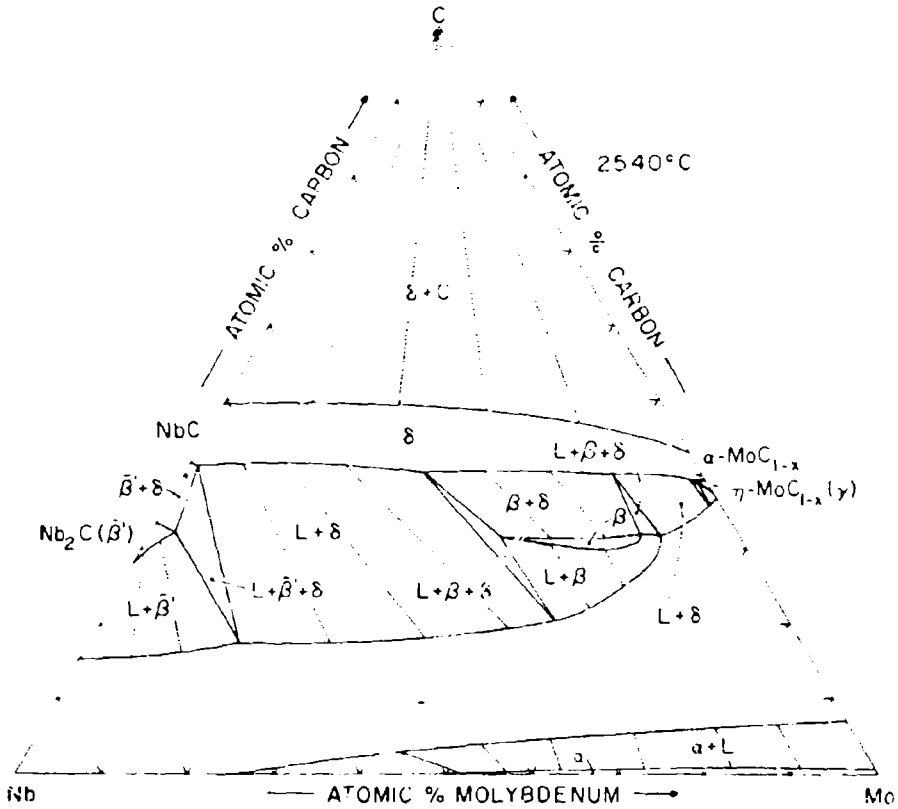

Figure III.E.12.9. Isothermal Section of the Nb-Mo-C System at 2540°C

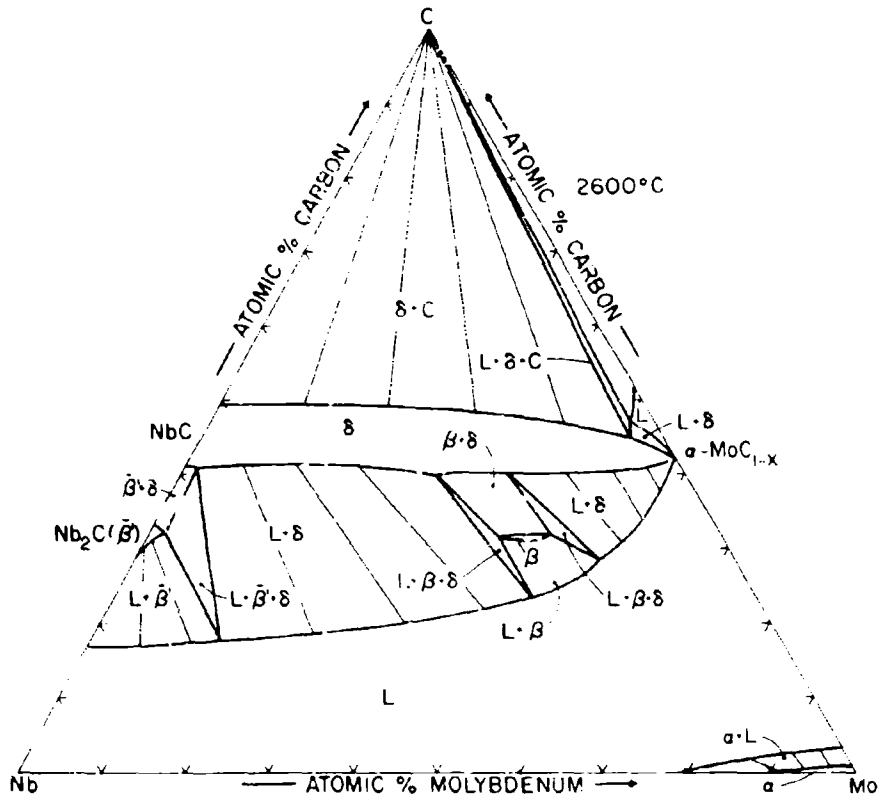

Figure III.E.12.10: Isothermal Section of the Nb-Mo-C System at 2600°C.

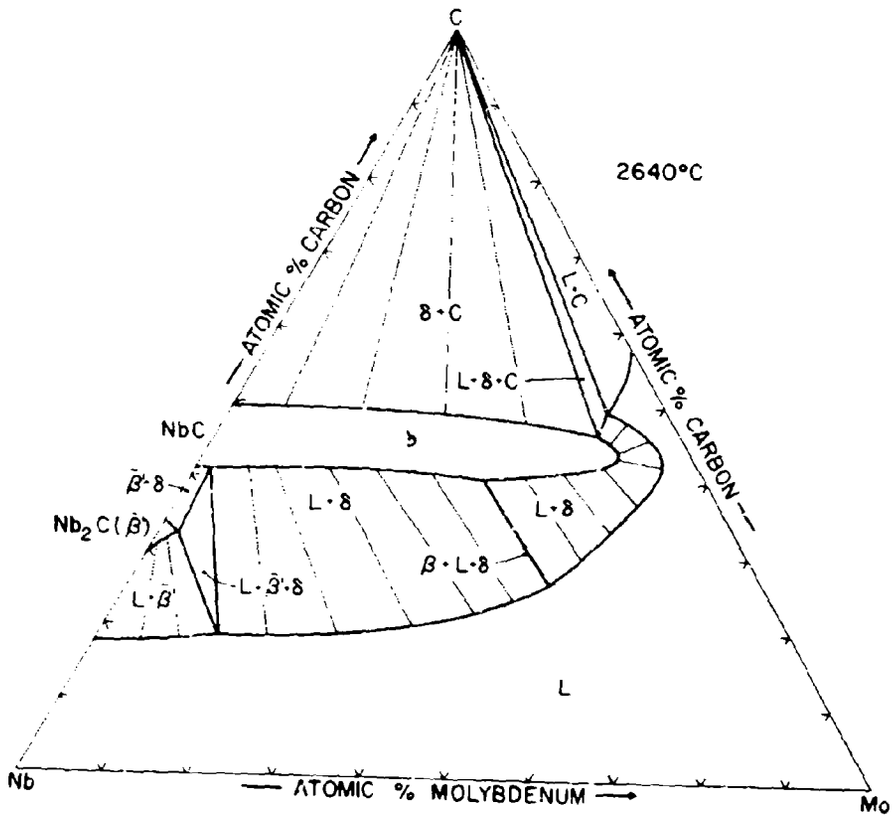

Figure III.E.12.11: Isothermal Section of the Nb-Mo-C System at 2640°C.

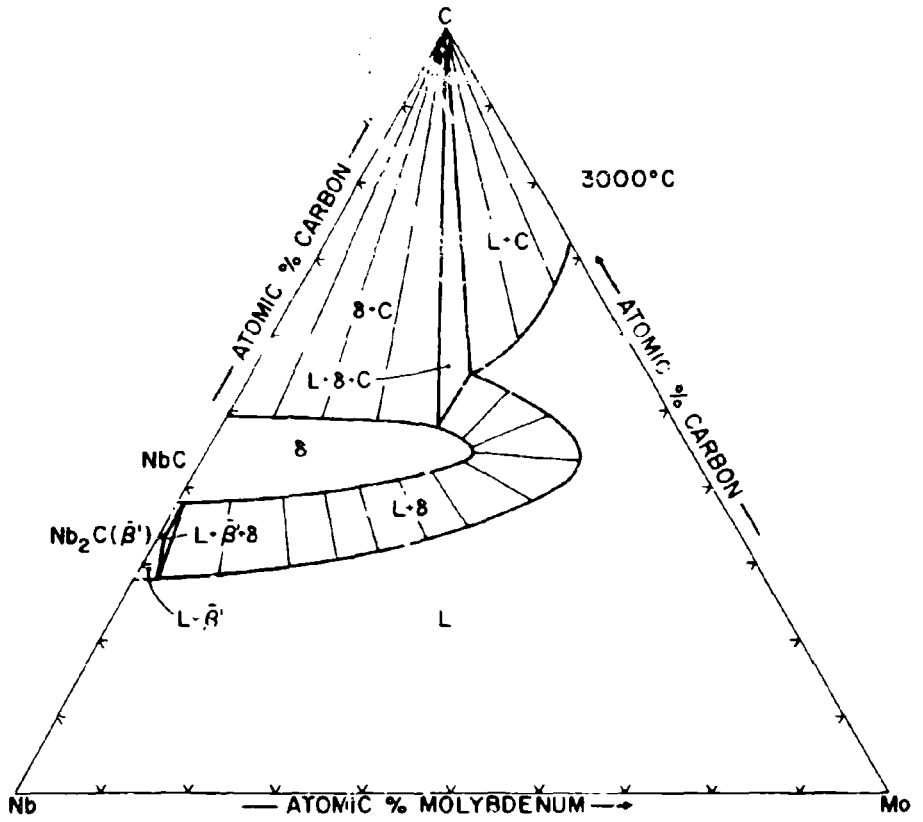

Figure III.E.12.12: Isothermal Section of the Nb-Mo-C System at 3000°C.

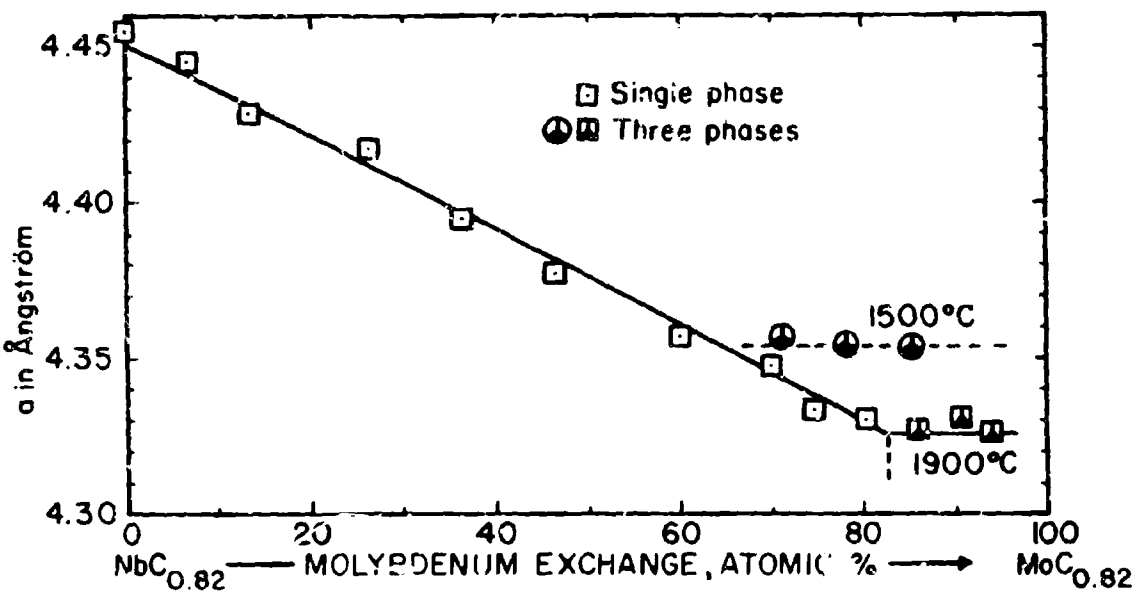

Figure III. E. 12. 13: Lattice Parameters of the Cubic Monocarbide Solid Solution Along the Section $NbC_{0.82}$-$MoC_{0.82}$, and Phase Boundary Values at 1500°C and 1900°C.

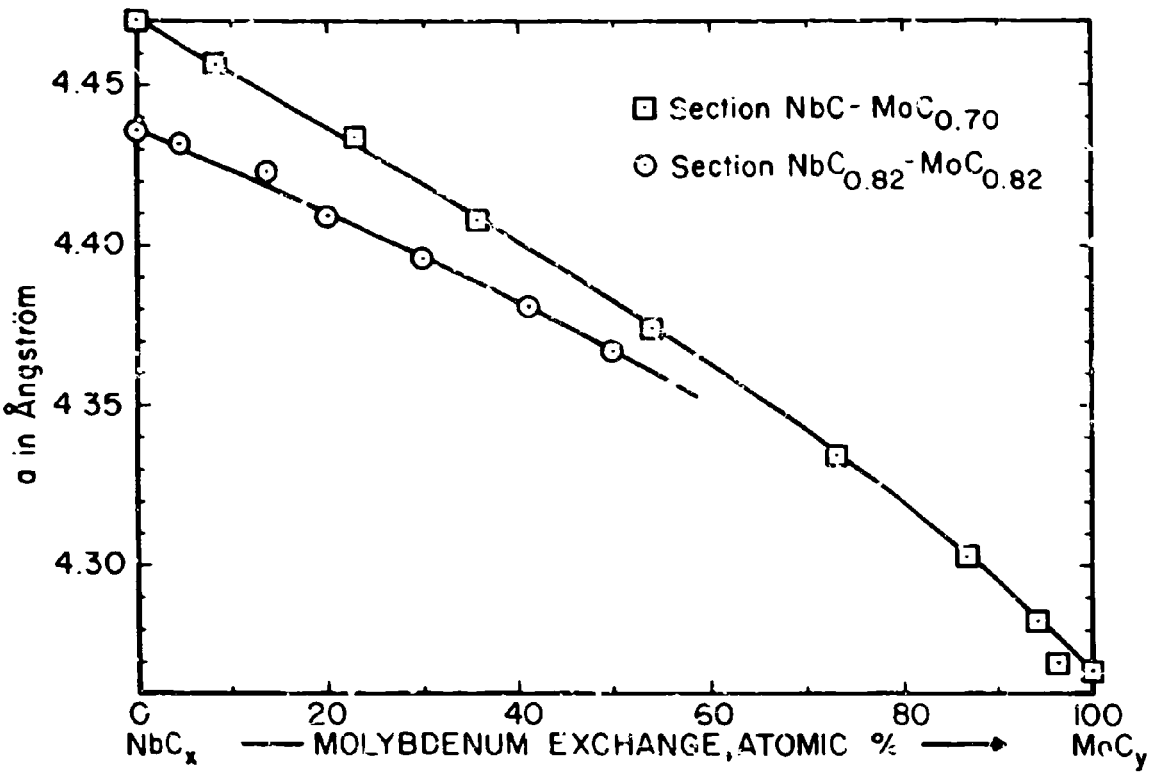

Figure III.E.12.14: Lattice Parameters of Monocarbide Alloys. Alloys Rapidly Cooled from 2200°C.

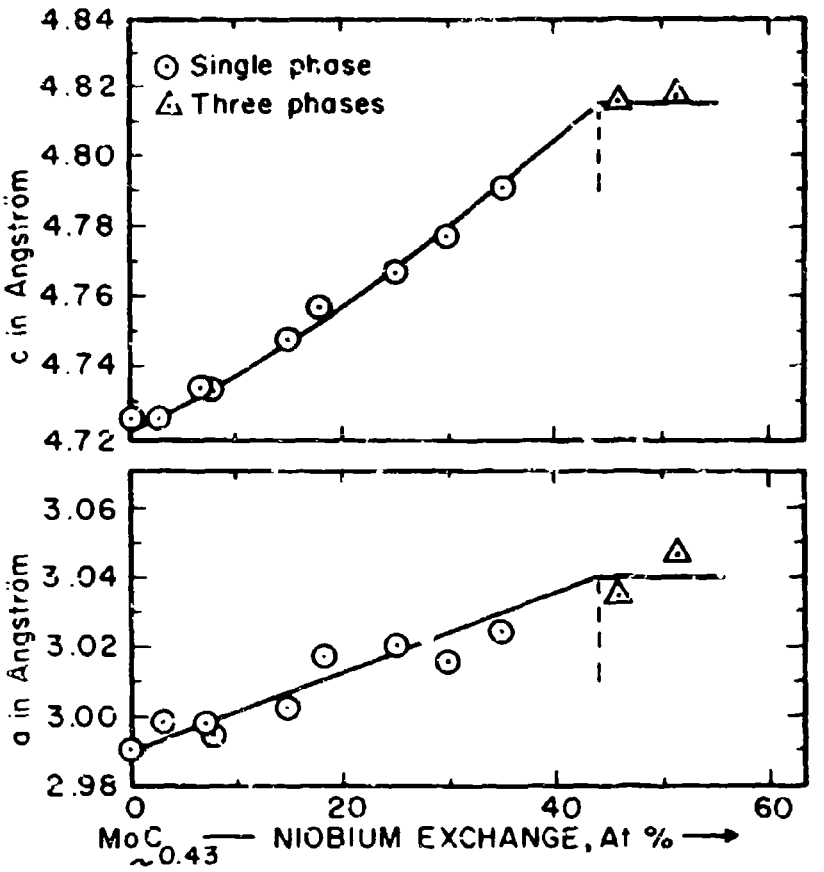

Figure III.E.12.15: Lattice Parameters of the Mo_2C Solid Solution. Alloys Rapidly Cooled from 2200°C. Parameters are Based on Indexing According to the L'3-Type.

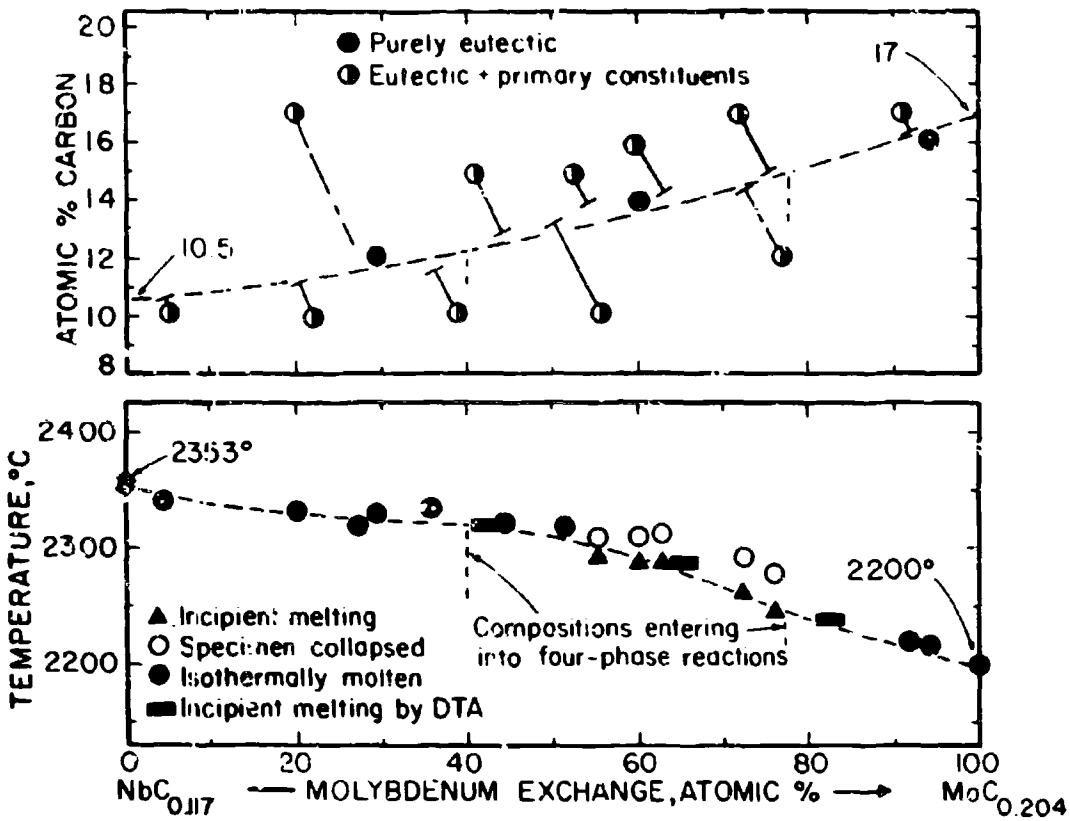

Figure III.E.12.16: Temperatures (Bottom) and Location (Top) of the Metal-Rich Eutectic Trough in the Nb-Mo-C System.

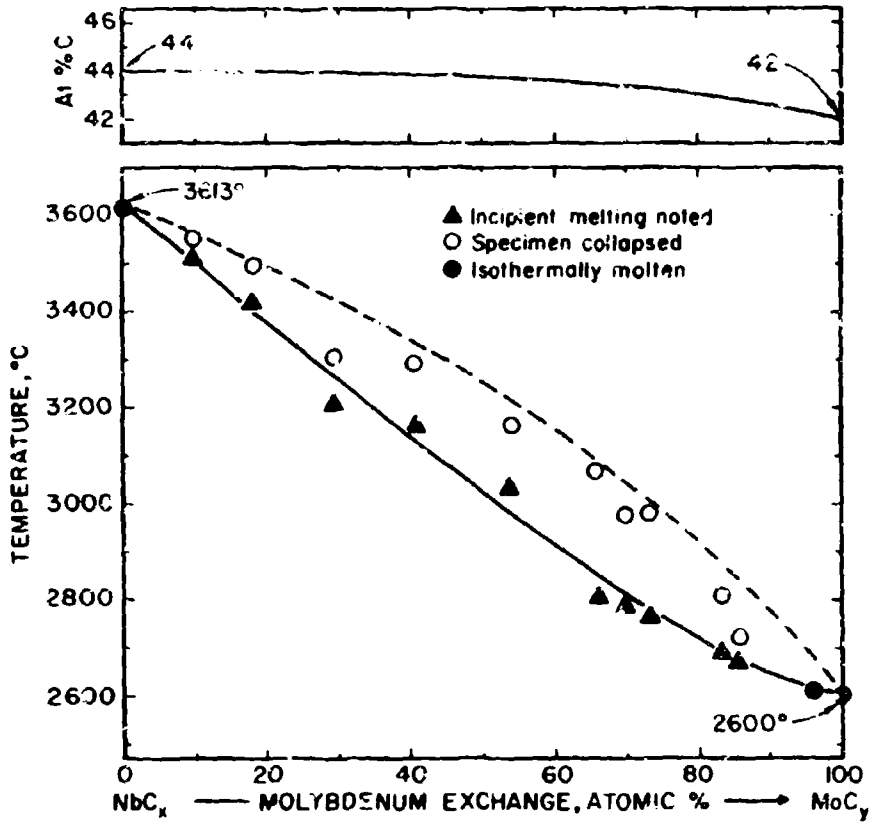

Figure III.E.12.17: Maximum Solidus Temperatures of the Cubic Monocarbide Phase.

Top: Concentration Line of the Maximum Solidus.

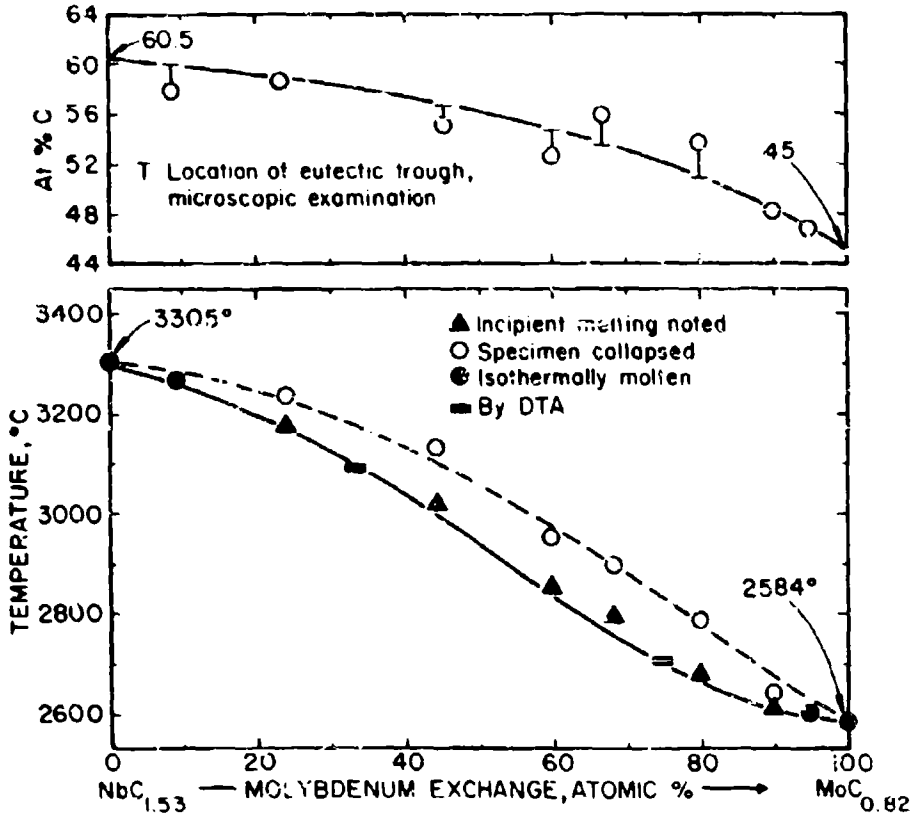

Figure III.E.12.18: Experimental Melting Temperatures (Bottom) and Location of the Monocarbide + Graphite Eutectic Trough in the Nb-Mo-C System.

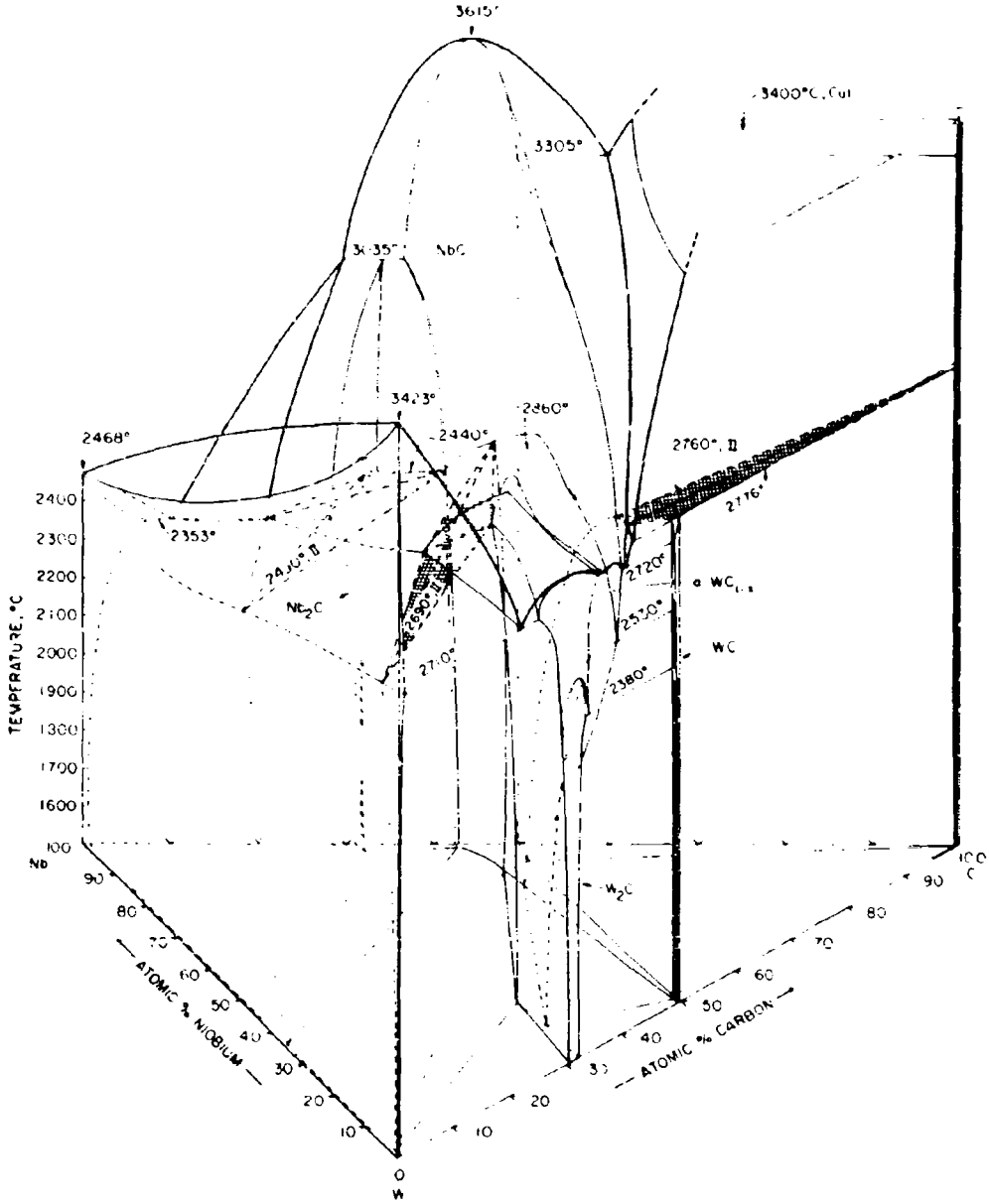

Figure III.E.13.1: Isometric View of the Phase Diagram Nb-W-C.

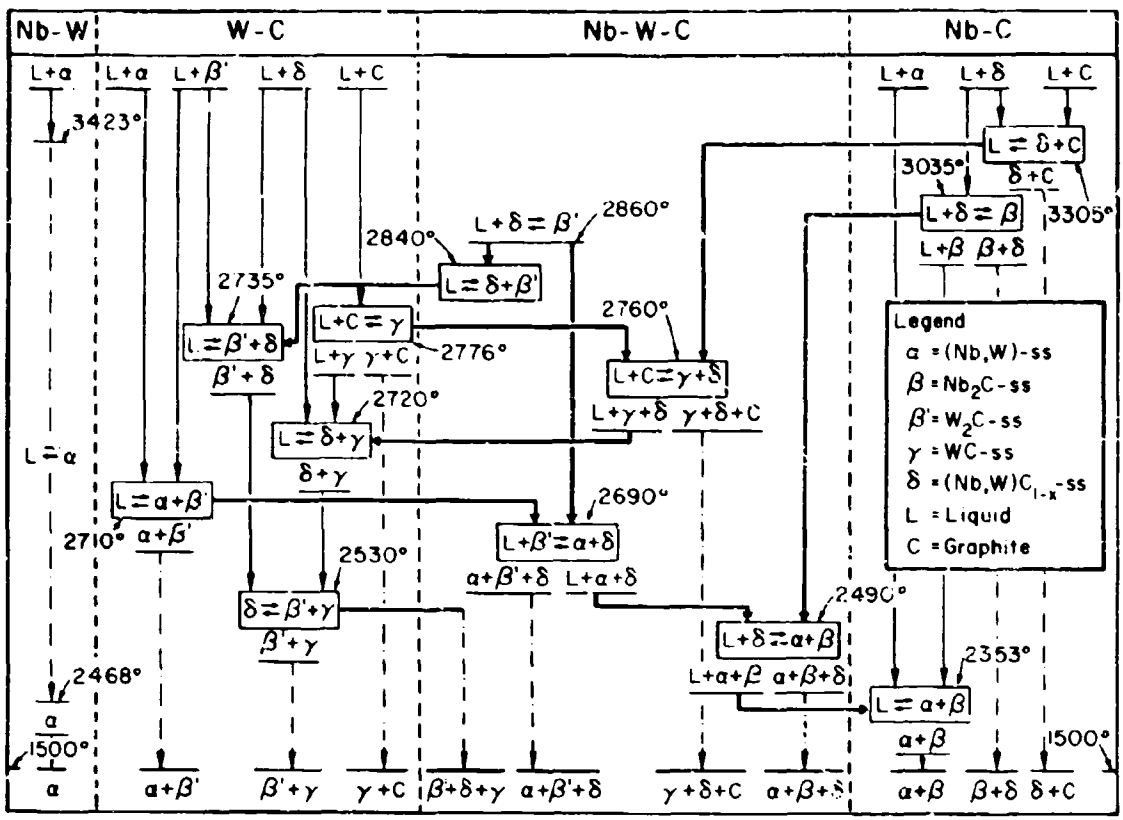

Figure III.E.13.2: Reaction Diagram for Nb-W-C Alloys.

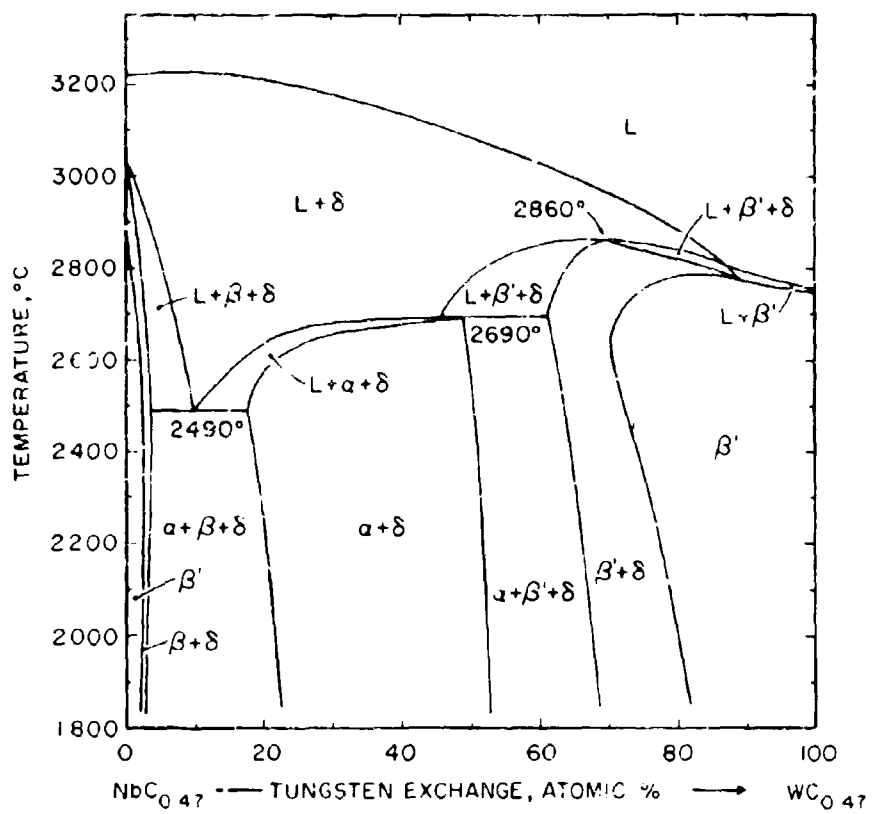

Figure III.E.13.3: Isopleth at $NbC_{0.47}$-$WC_{0.47}$.

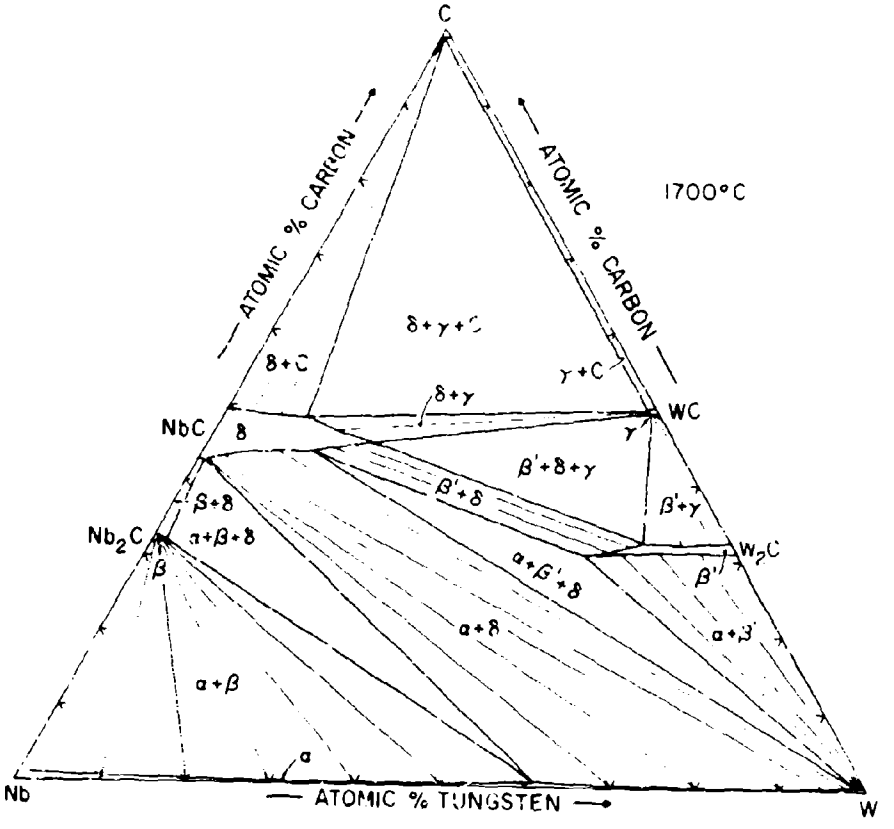

Figure III. E. 13.4: Isothermal Section of the Nb-W-C System at 1700°C.

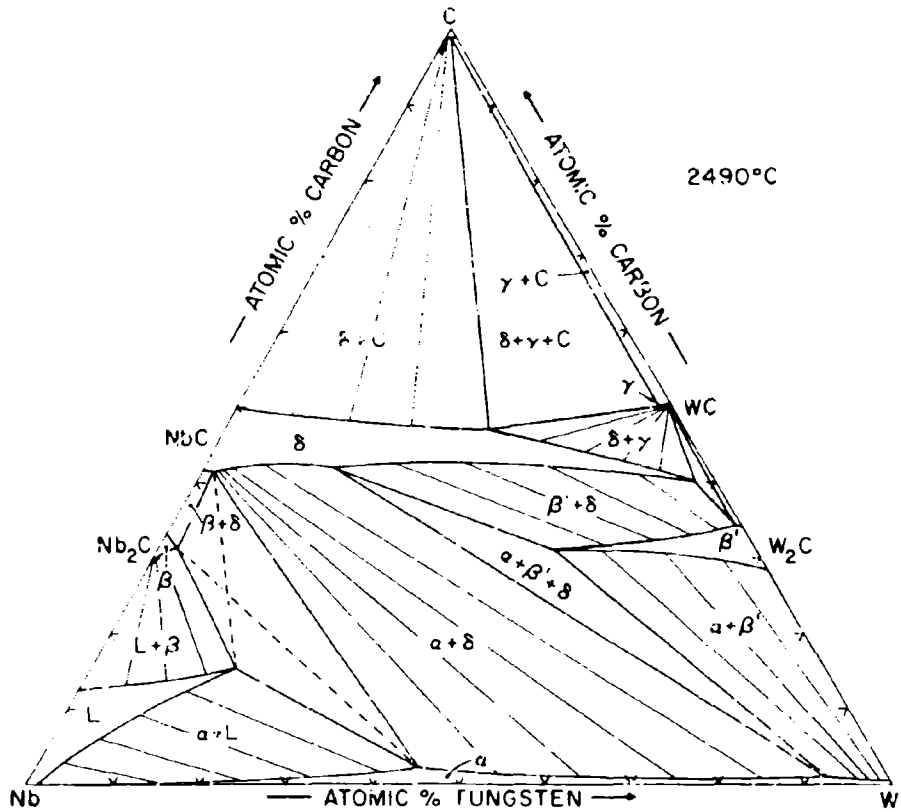

Figure III.E.13.5: Isothermal Section of the Nb-W-C System at 2490°C.

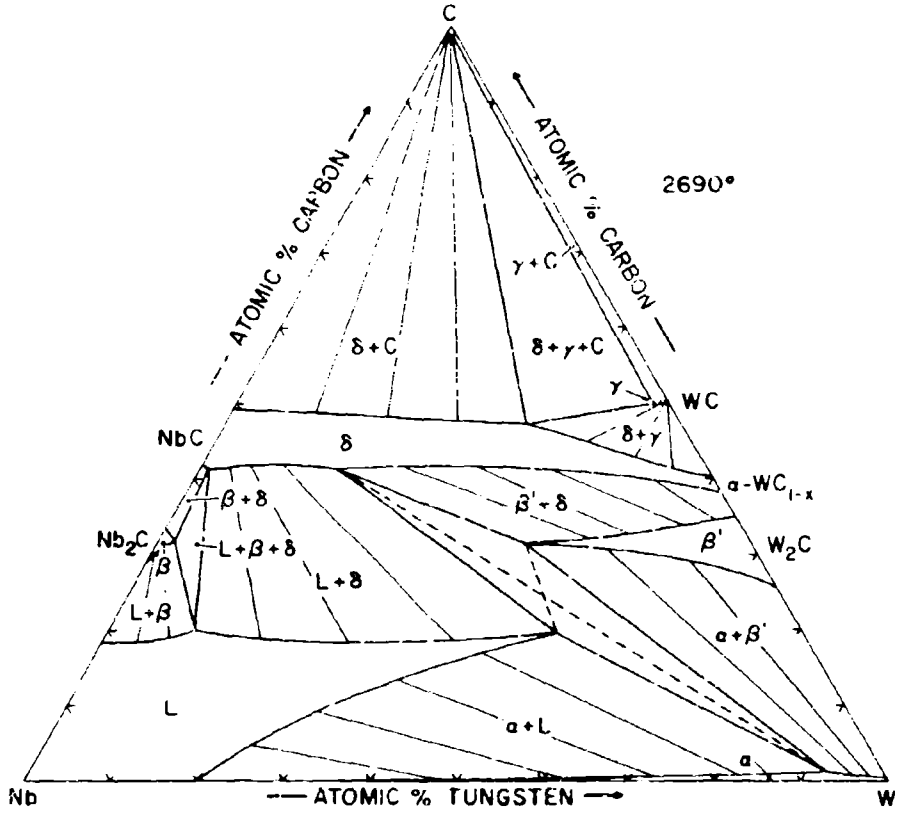

Figure III.E.13.6: Isothermal Section of the Nb-W-C System at 2690°C.

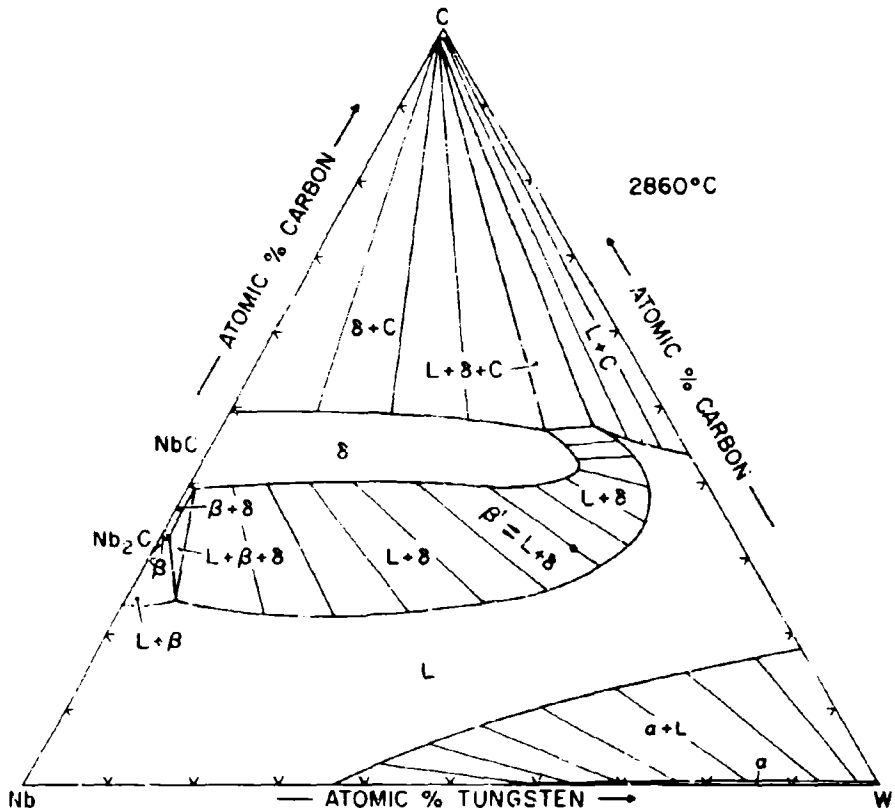

Figure III. E. 13. 7: Isothermal Section of the Nb-W-C System at 2860°C.

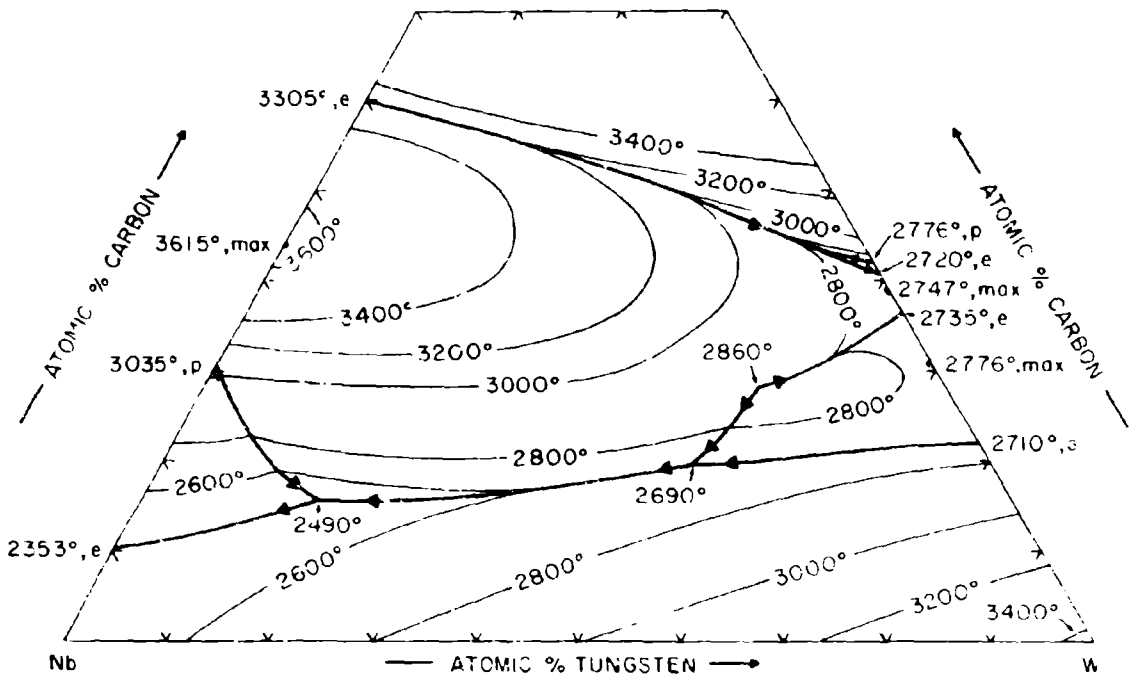

Figure III.E.13.8: Liquidus Projections in the Nb-W-C System.

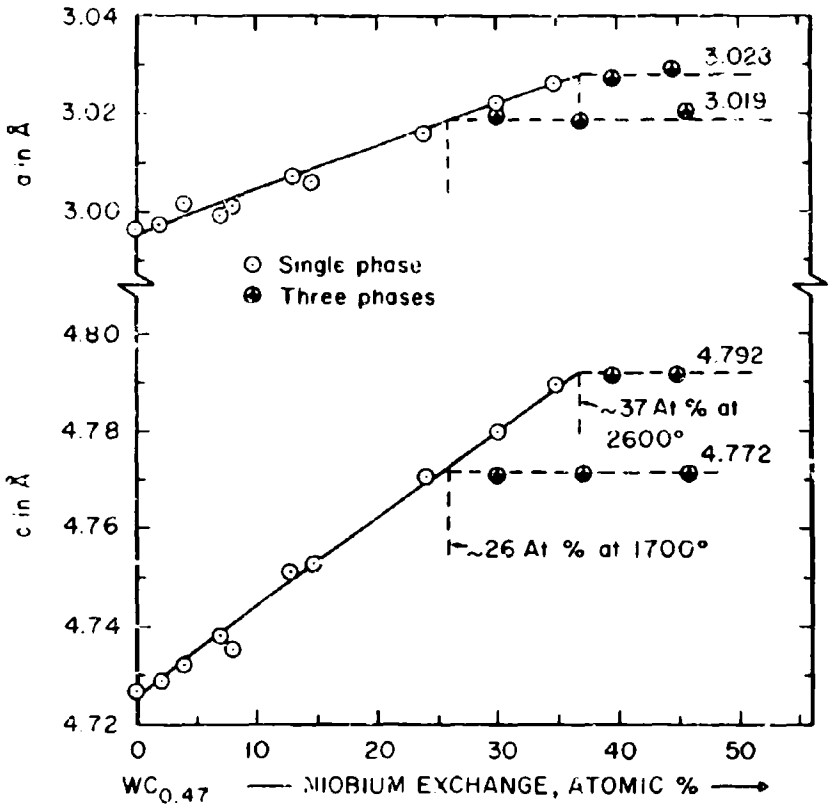

Figure III.E.13.9: Lattice Parameters of the Tungsten-Rich Subcarbide Solid Solution. Indexing of the Subcarbide Phase According to the L'3-Type.

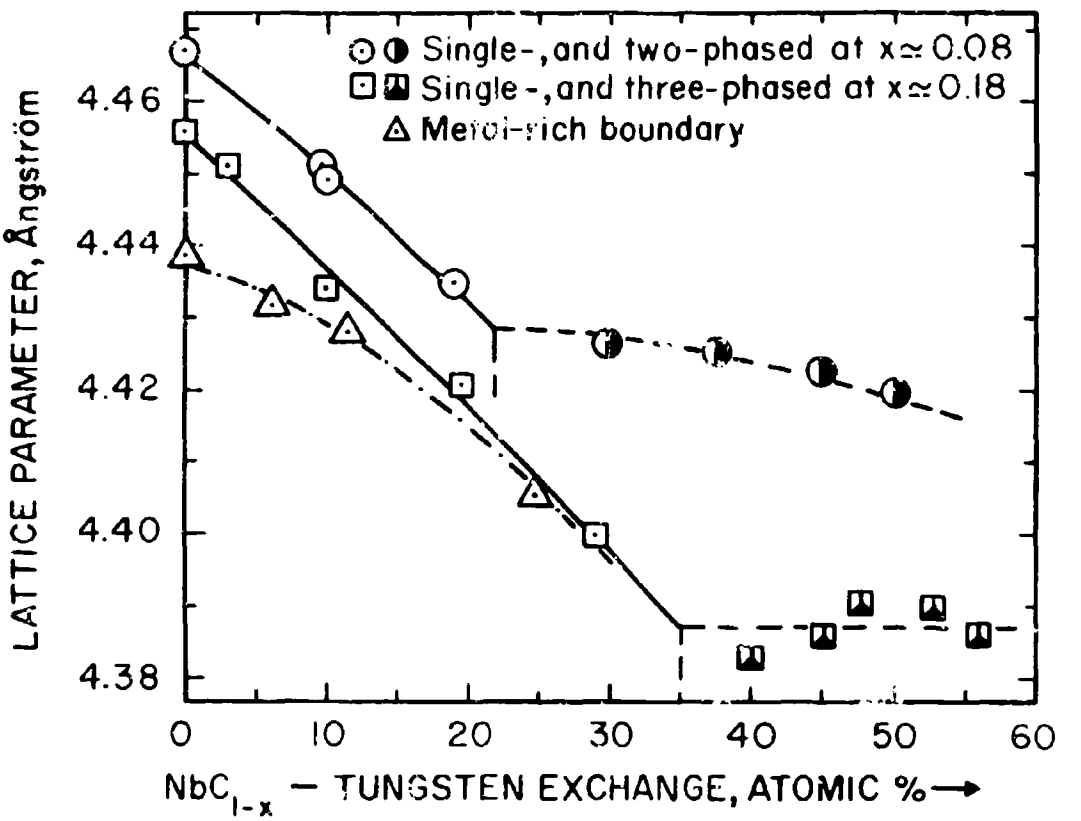

Figure III.E.13.10: Lattice Parameters of the Cubic Monocarbide Phase in 1700°C - Equilibrated Alloys.

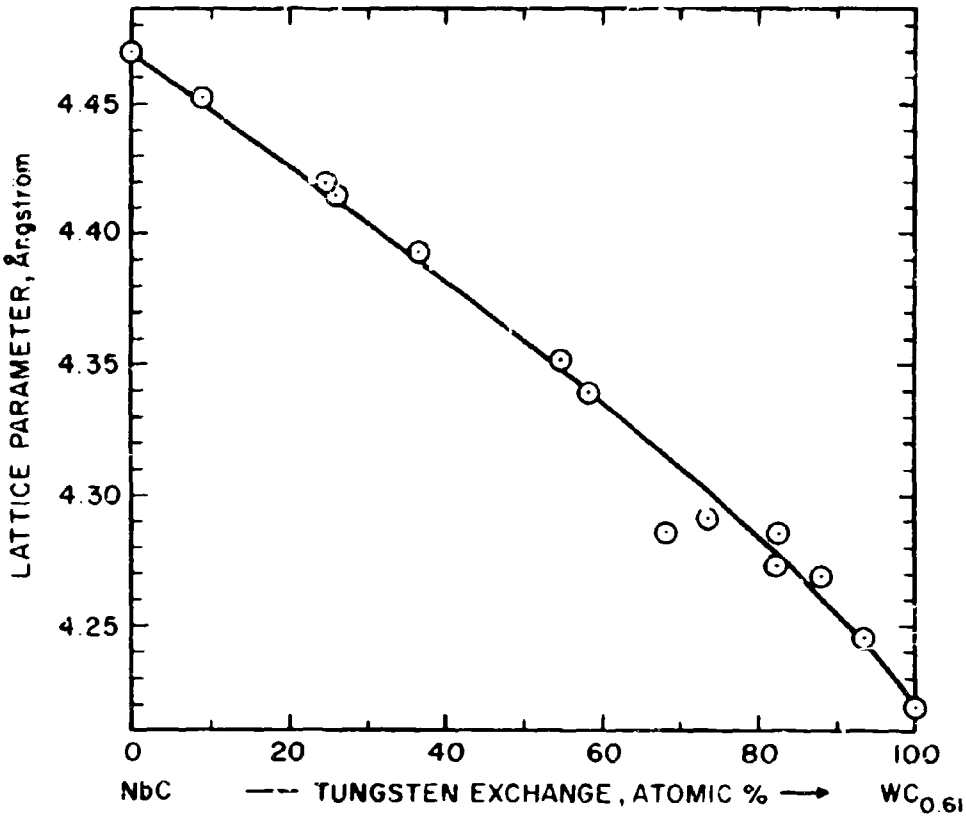

Figure III.E.13.11. Lattice Parameters of the Cubic Monocarbide Phase Along the Section NbC-$WC_{0.61}$. Alloys Containing more than 70 At.% W Tin-Quenched from T > 2500° C

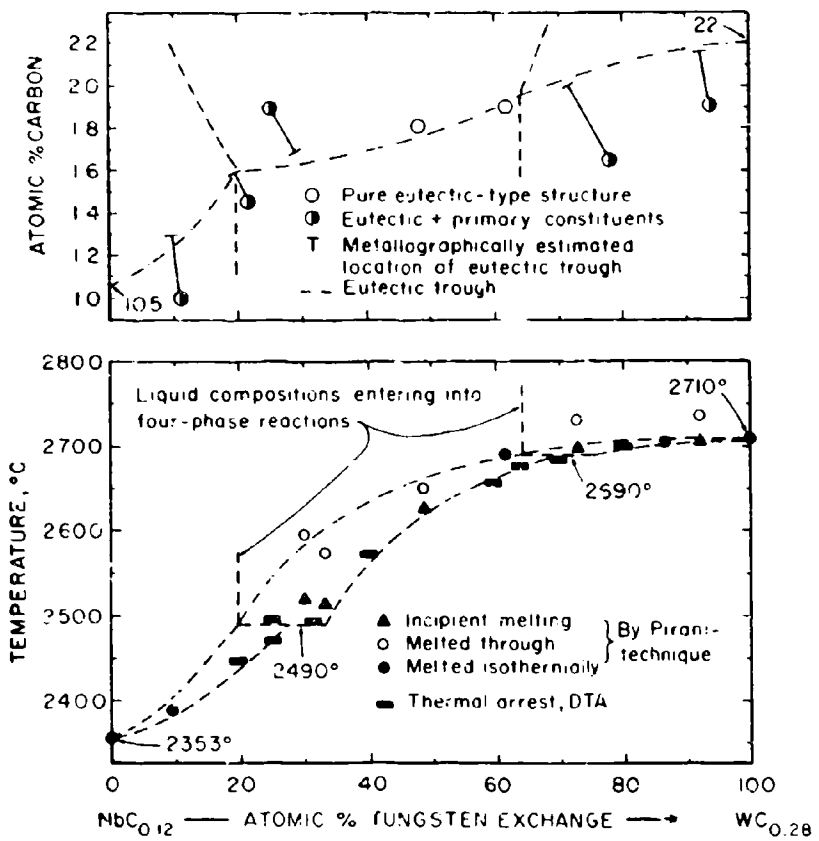

Figure III.E.13.12: Melting Along the Metal-Rich Eutectic Trough in the Nb-W-C System.

Top: Metallographically Determined Location of the Eutectic Trough.

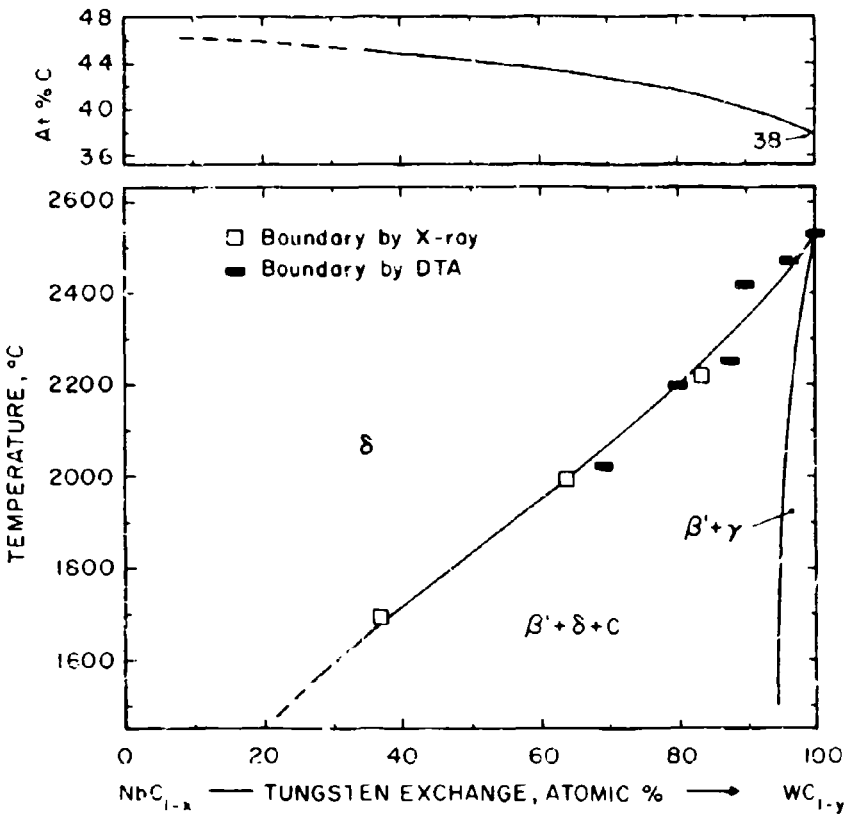

Figure III.E.13.13: Maximum Tungsten Exchange in Niobium Monocarbide as a Function of Temperature.

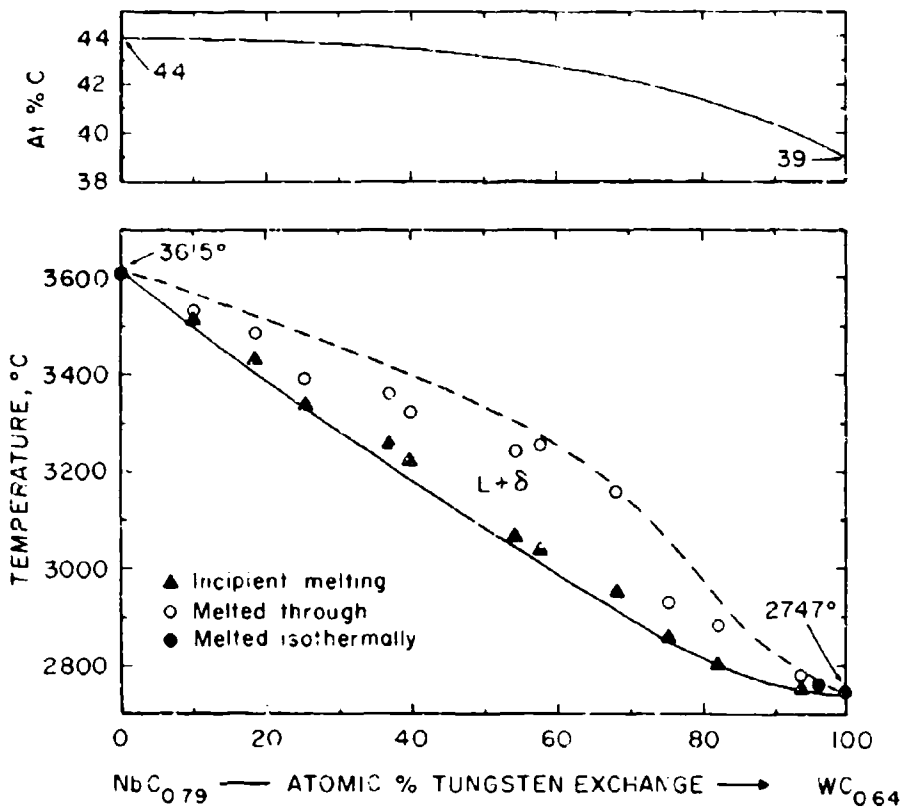

Figure III.E.13.14: Maximum Solidus Temperatures of the Monocarbide Solid Solution in the Nb-W-C System.

Top: Composition Line of the Maximum Solidus

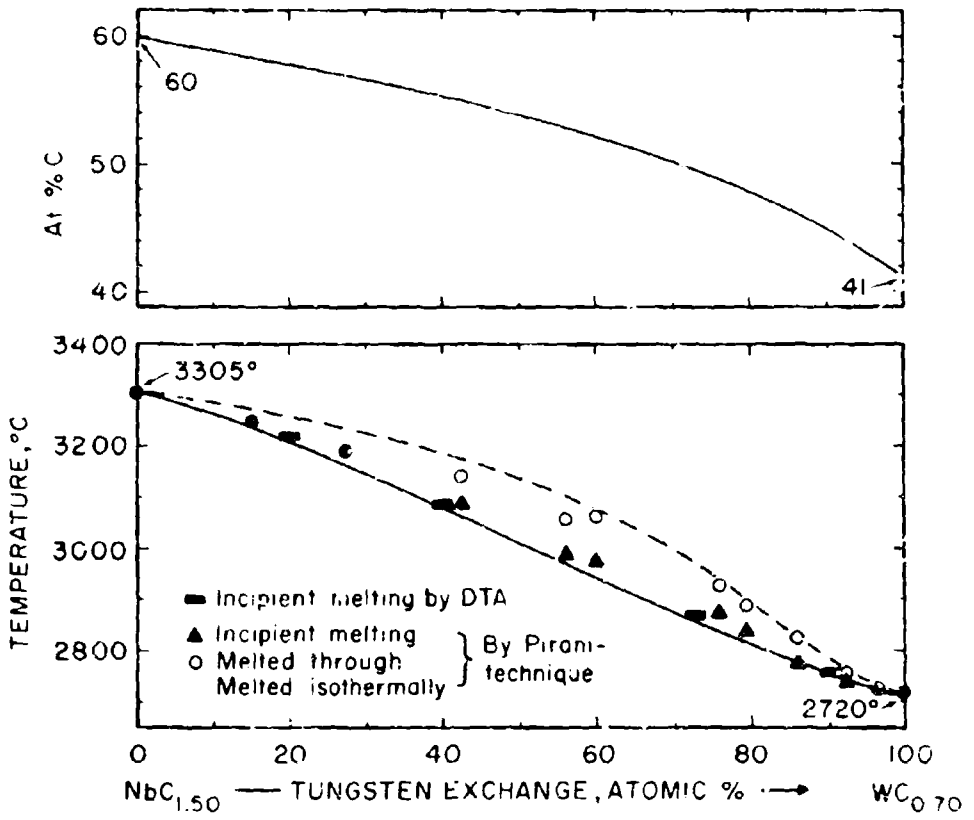

Figure III.E.13.15: Melting Along the $(Nb_2W)C_{1-x}$ + C Eutectic Trough.

Top: Metallographically Estimated Location of Eutectic Trough.

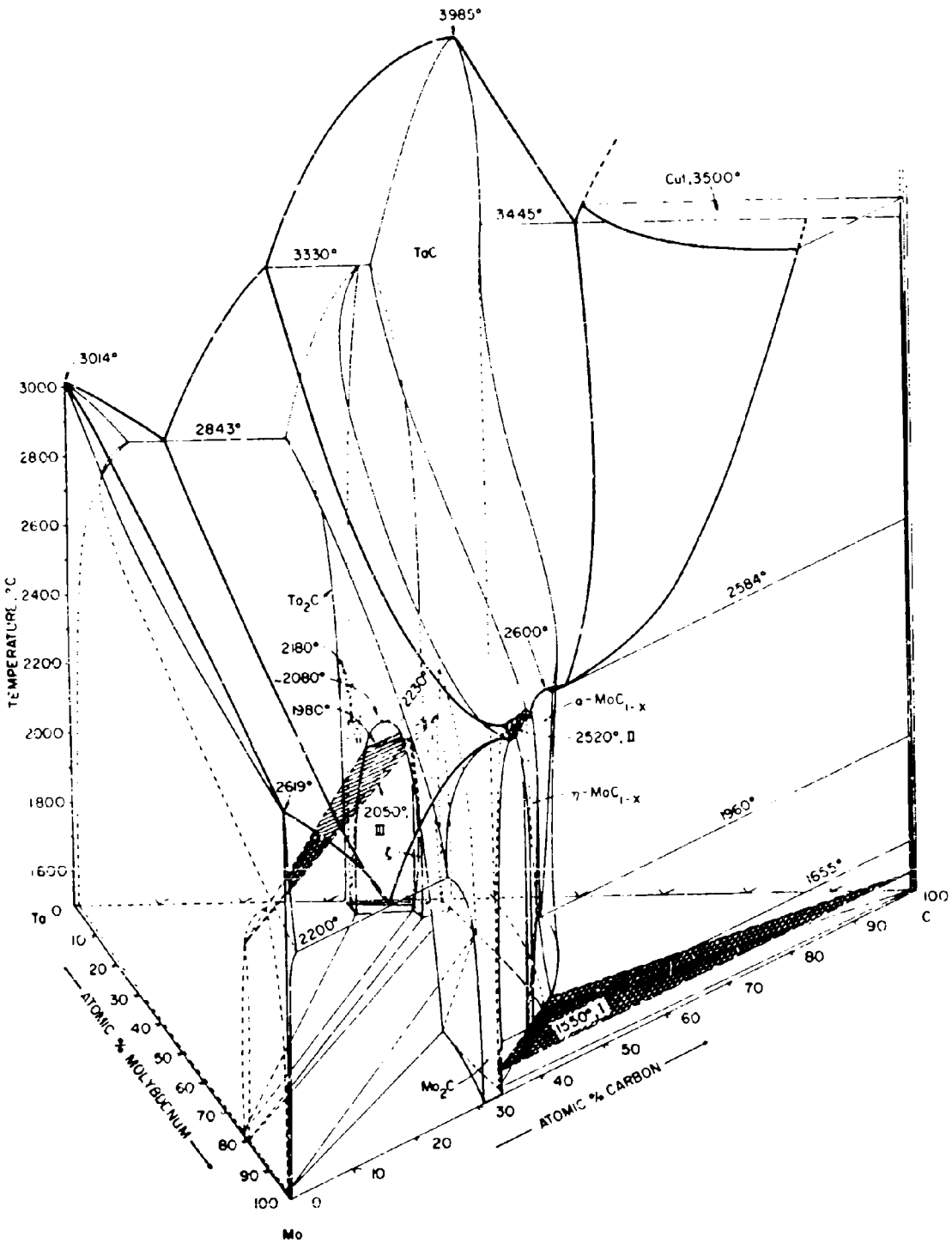

Figure III.E.14.1: Isometric View of the Ta-Mo-C System.

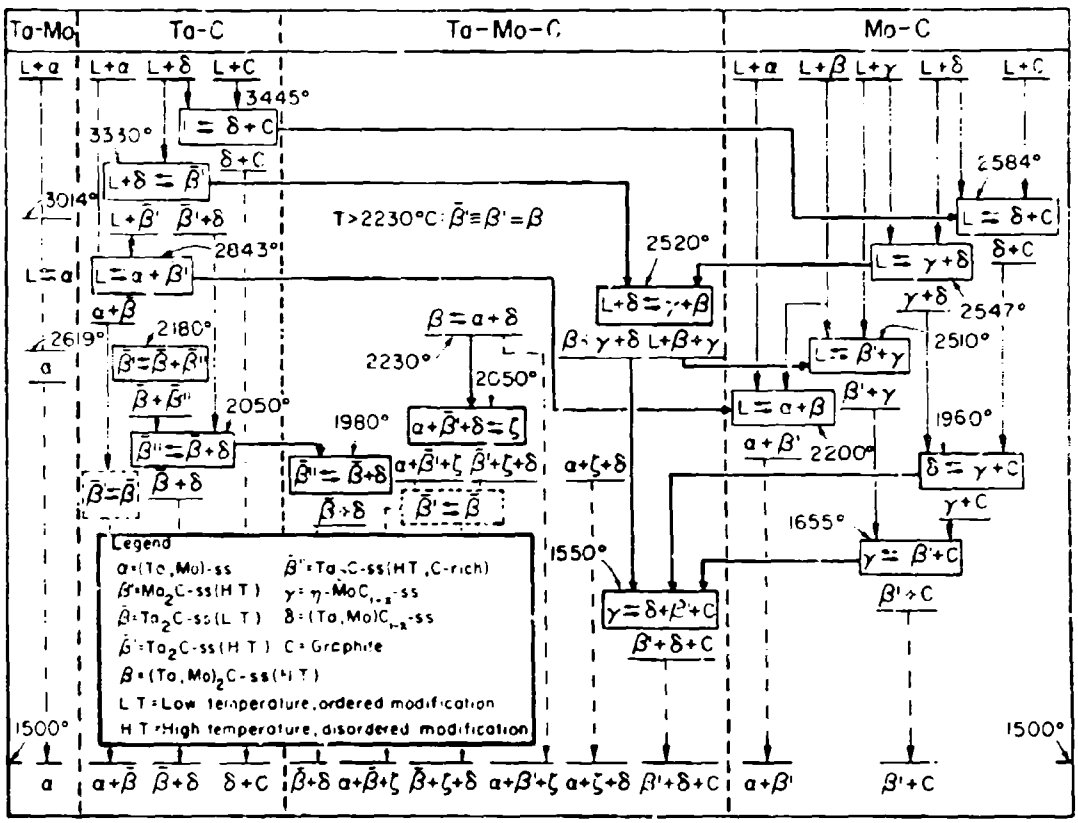

Figure III. E. 14. 2: Reaction Diagram for Ta-Mo-C Alloys.

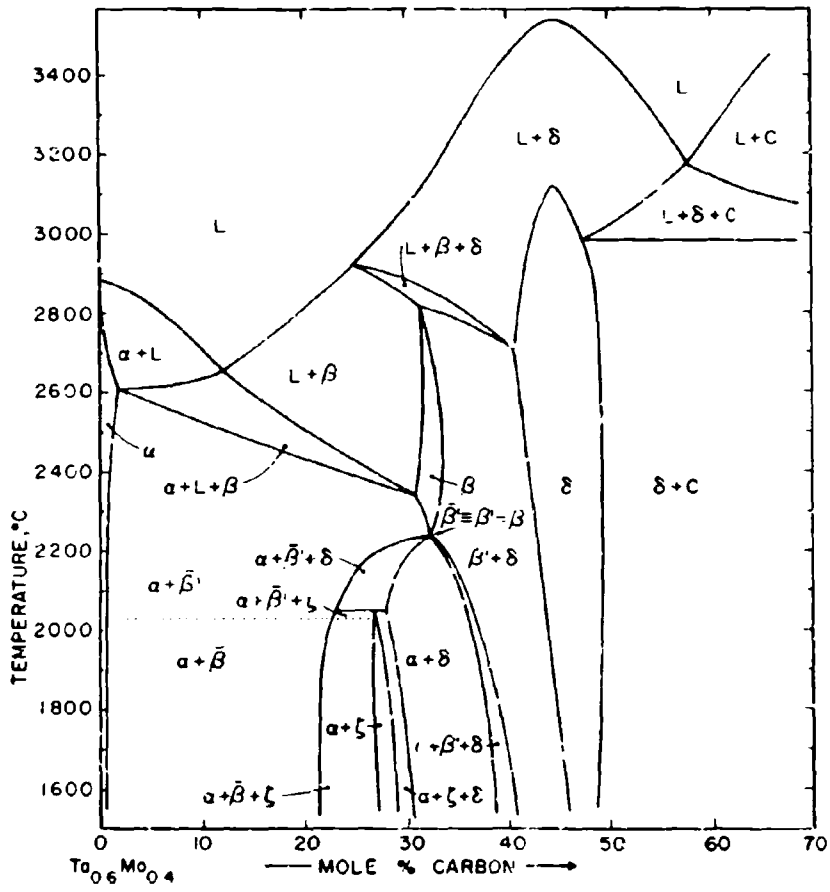

Figure III.E.14.3: Ta-Mo-C: Isopleth at $Ta_{0.6}Mo_{0.4}$-C

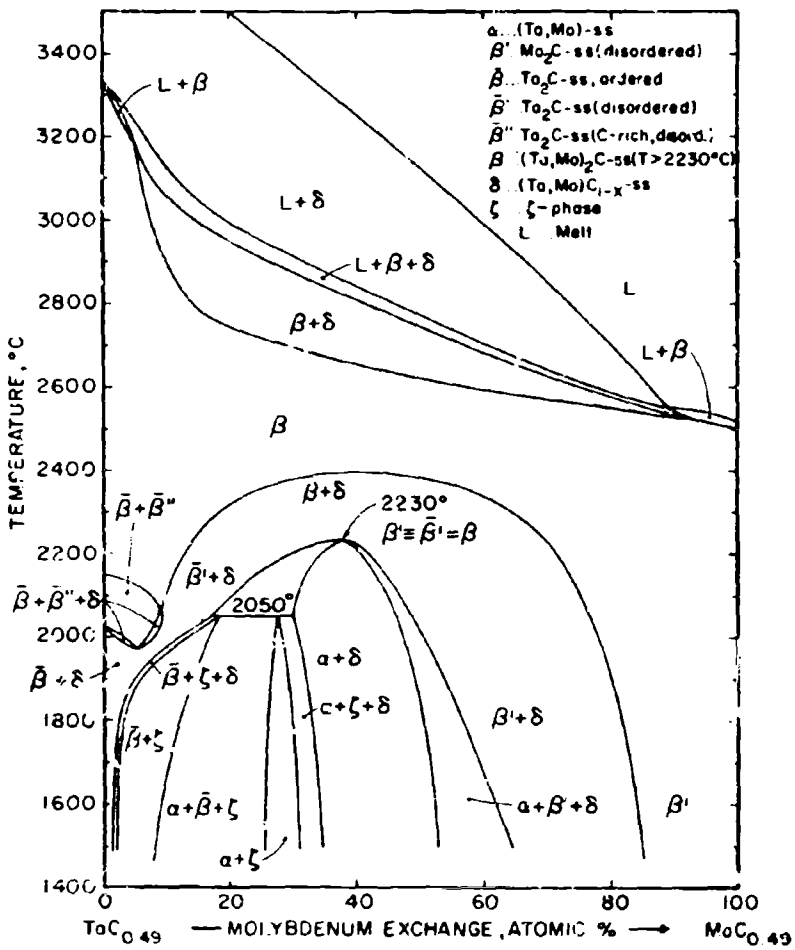

Figure III.E.14.4. Ta-Mo-C: Isopleth at $TaC_{0.49}$-$MoC_{0.49}$

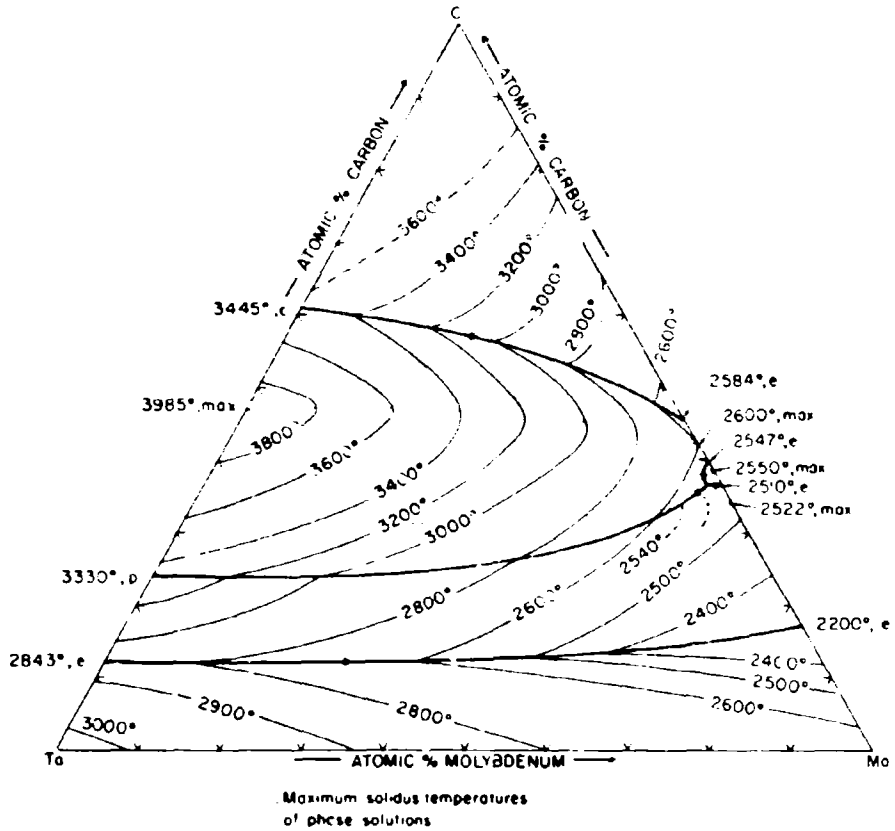

Figure III.E.14.5: Liquidus Projections in the Ta-Mo-C System.

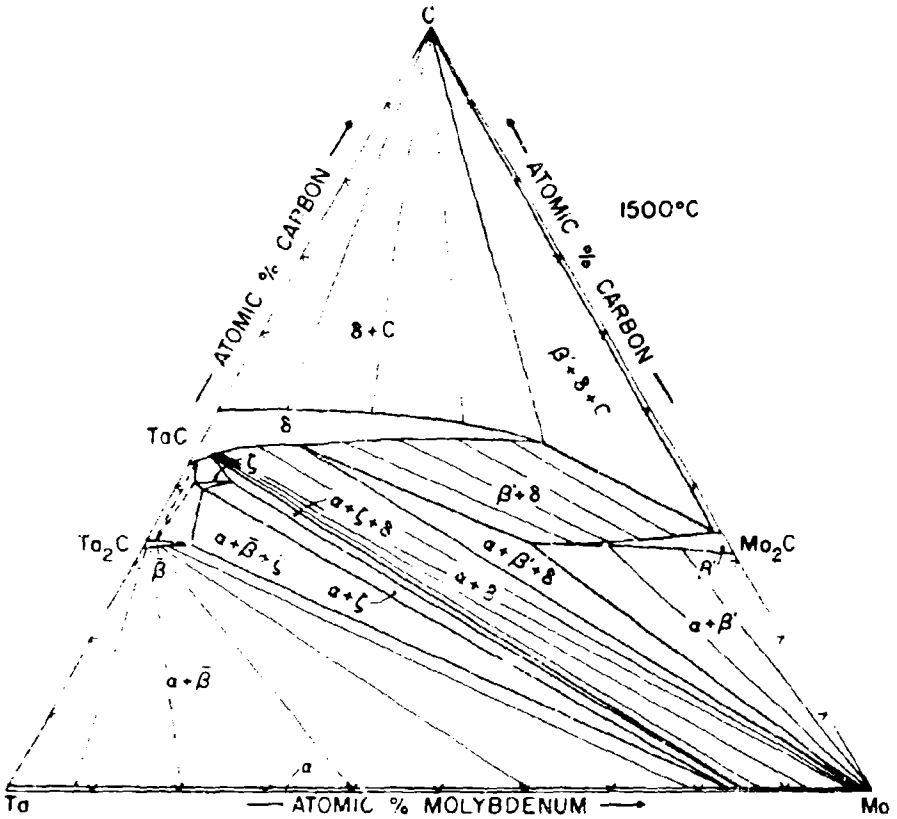

Figure III. E. 14. 6: Isothermal Section of the Ta-Mo-C System at 1500°C.

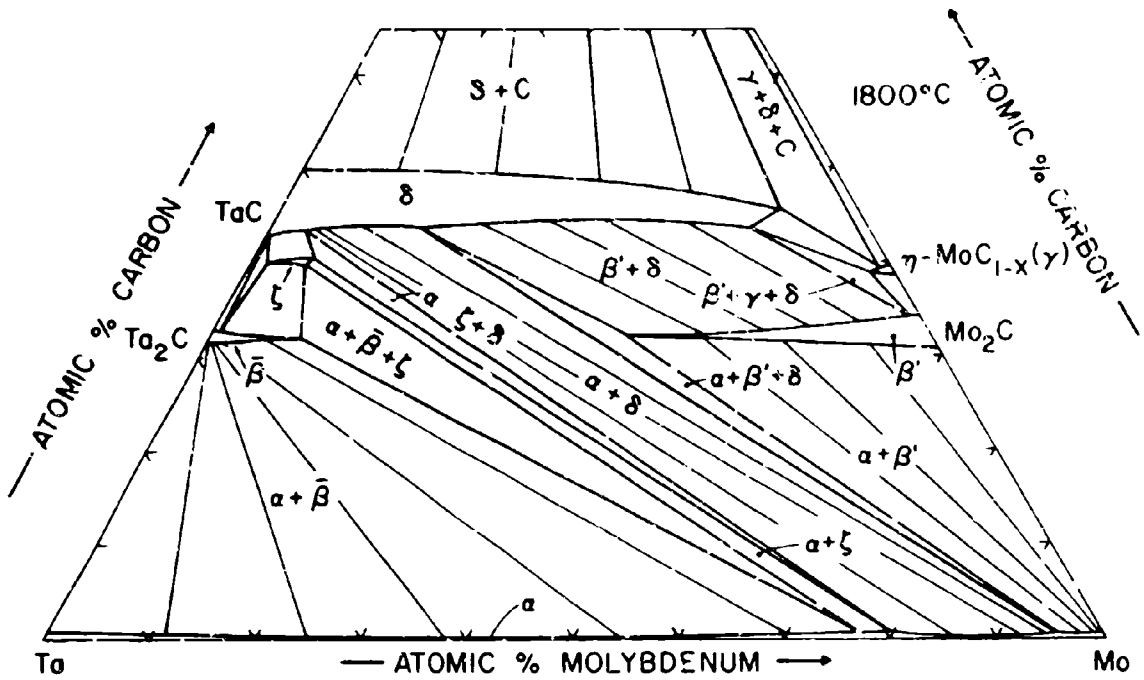

Figure III. E. 14. 7: Isothermal Section of the Ta-Mo-C System at 1800°C.

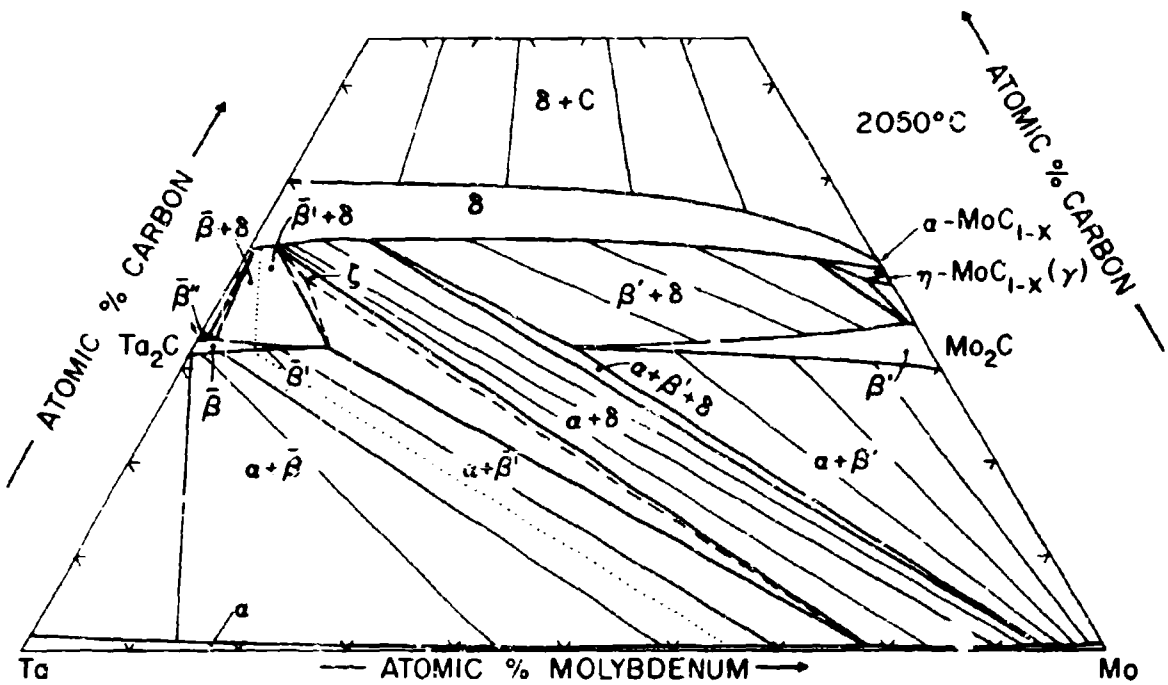

Figure III.E.14.8: Isothermal Section of the Ta-Mo-C System at 2050°C.

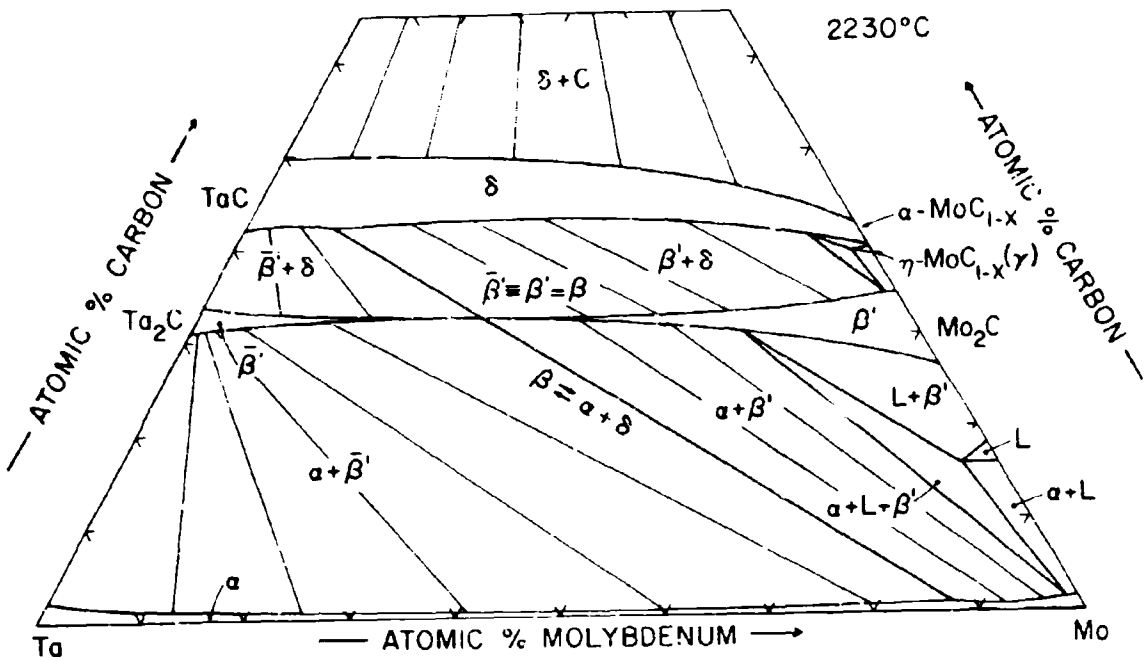

Figure III.E.14.9: Isothermal Section of the Ta-Mo-C System at 2230°C.

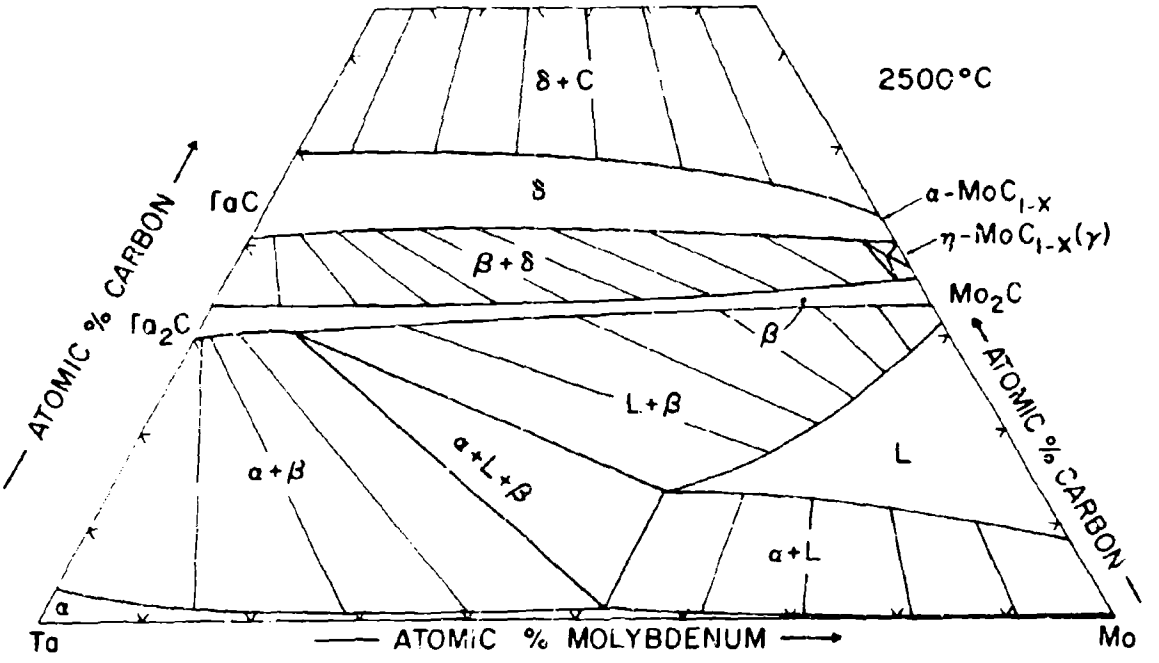

Figure III.E.14.10: Isothermal Section of the Ta-Mo-C System at 2500°C.

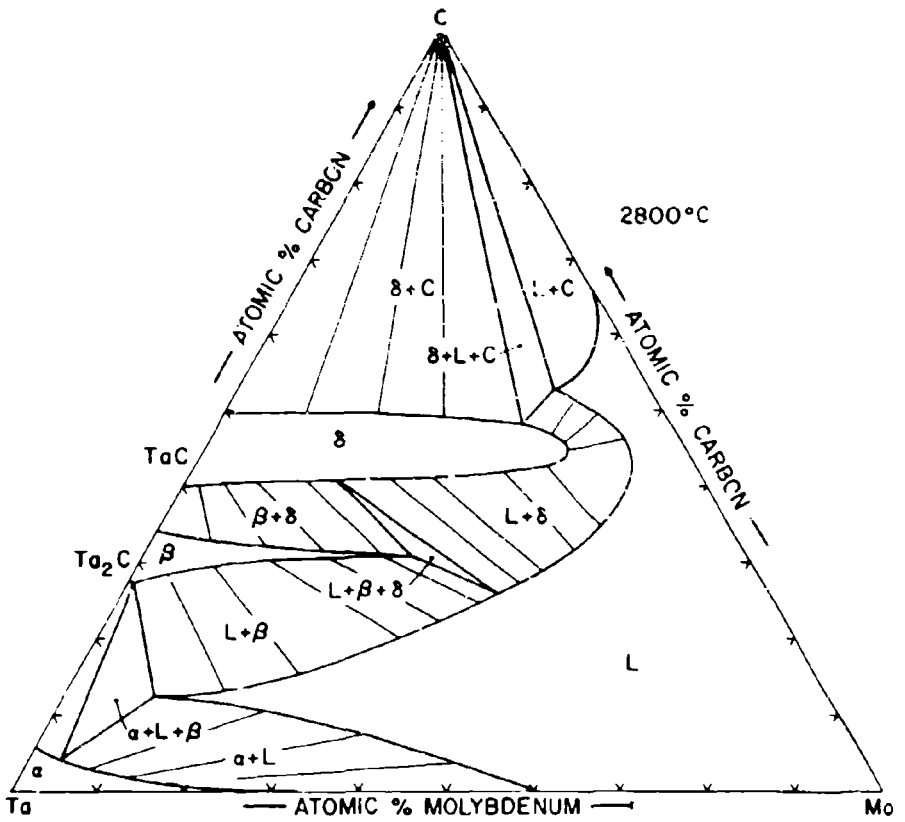

Figure III.E.14.11: Isothermal Section of the Ta-Mo-C System at 2800°C.

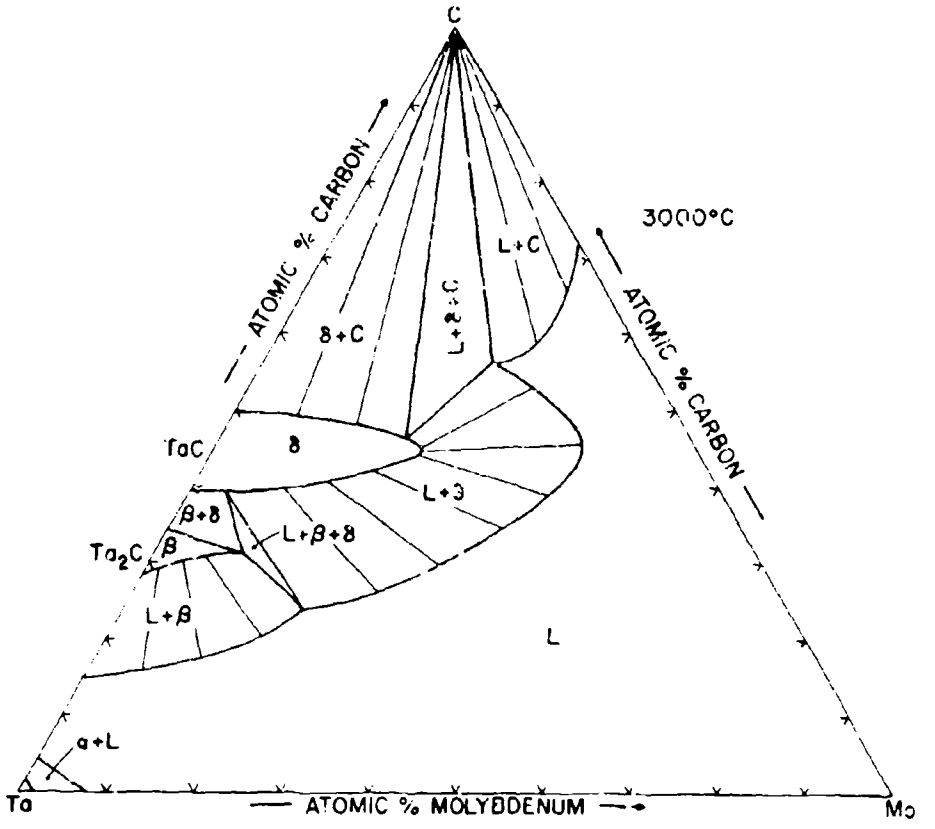

Figure III.E.14.12: Isothermal Section of the Ta-Mo-C System at 3000°C.

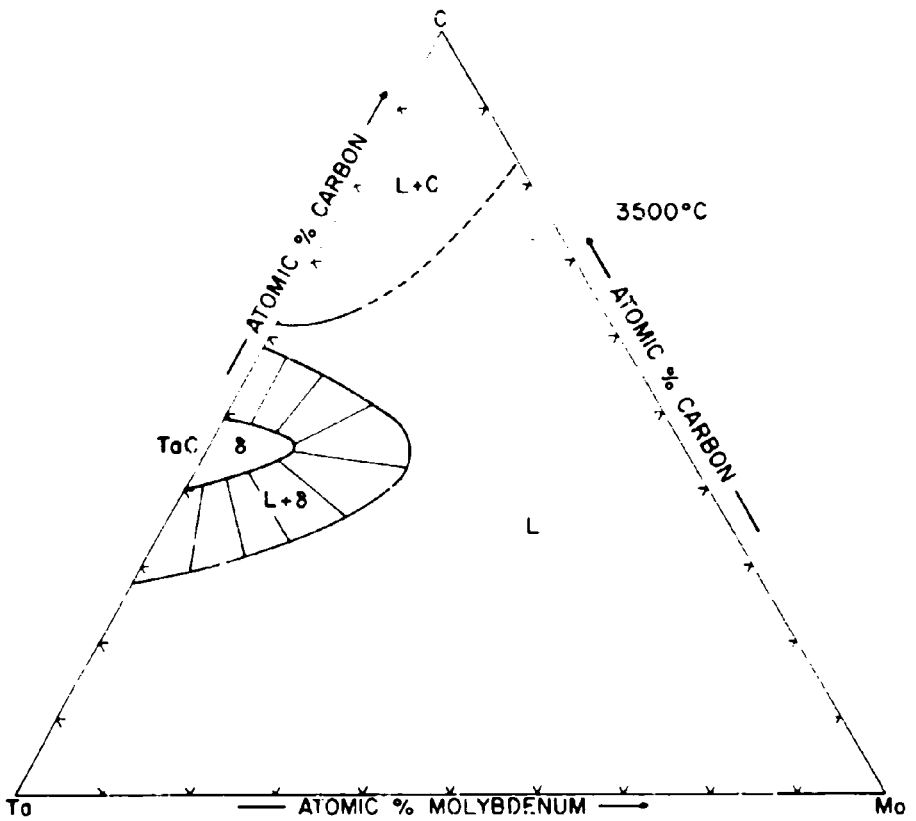

Figure III.E.14.13: Isothermal Section of the Ta-Mo-C System at 3500°C.

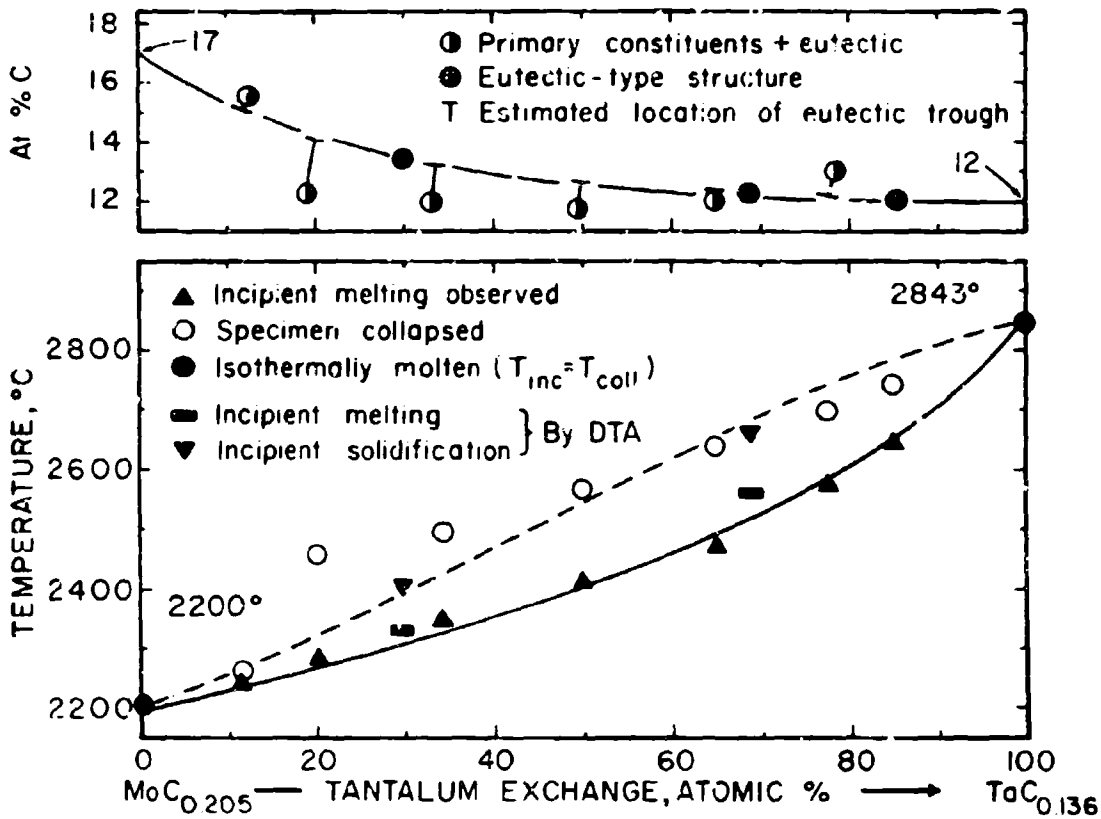

Figure III.E.14.14: Temperatures (Bottom) and Location (Top) of the Eutectic Trough Between the Metal and the Subcarbide Solid Solution in the Ta-Mo-C System.

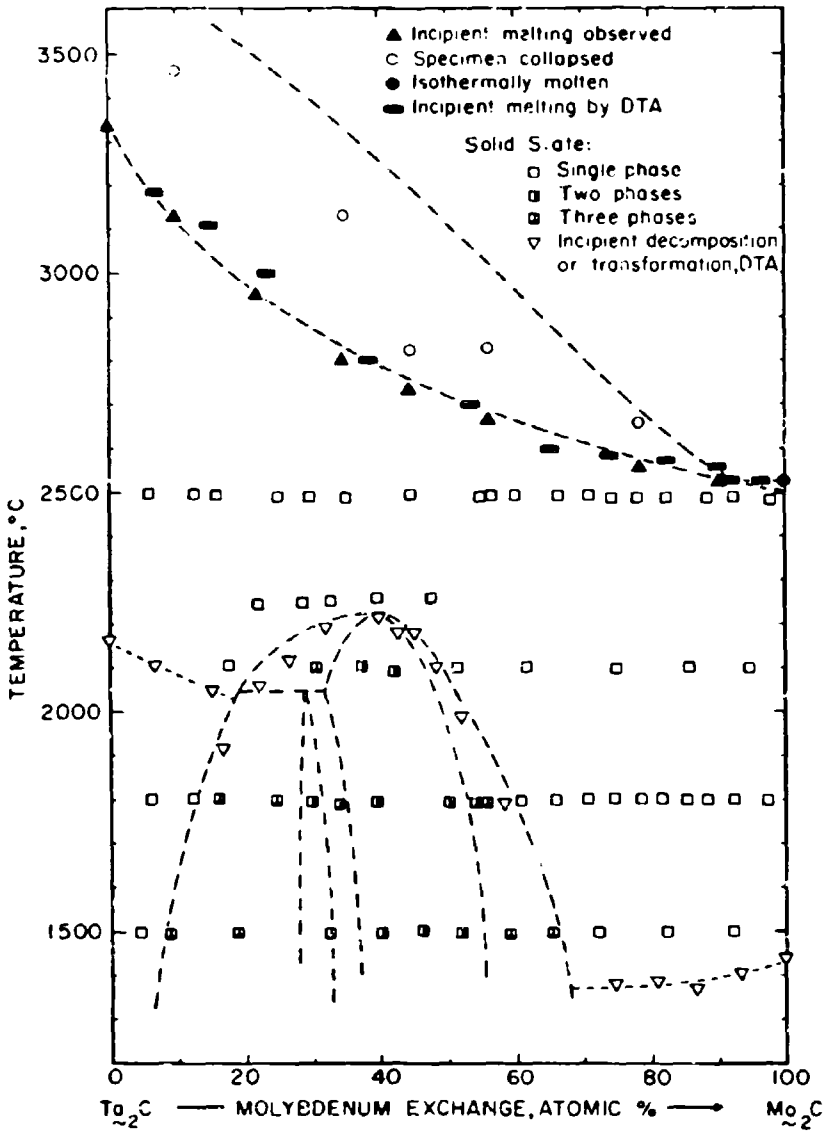

Figure III. E. 14. 15: Melting Temperatures and Qualitative Phase Evaluation of Alloys Located at the Concentration Section Ta_2C-Mo_2C.

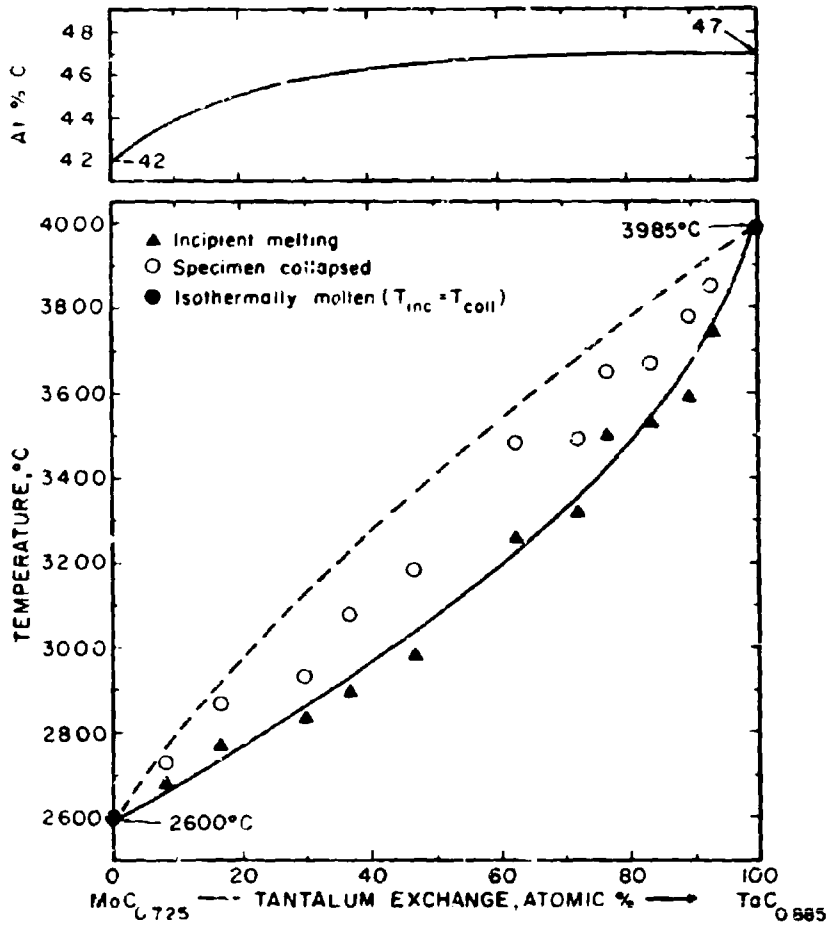

Figure III. E. 14. 16: Maximum Solidus Temperatures of the Cubic Monocarbide Phase in the Ta-Mo-C System.

Top: Composition Line of the Maximum Solidus.

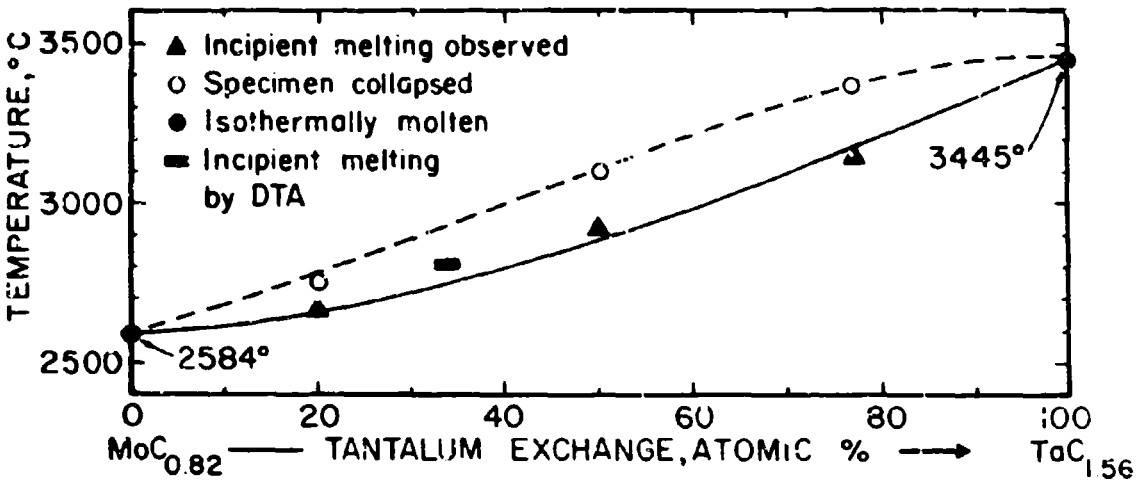

Figure III.E.14.17: Melting Along the Monocarbide + Graphite Eutectic Trough in the Ta-Mo-C System.

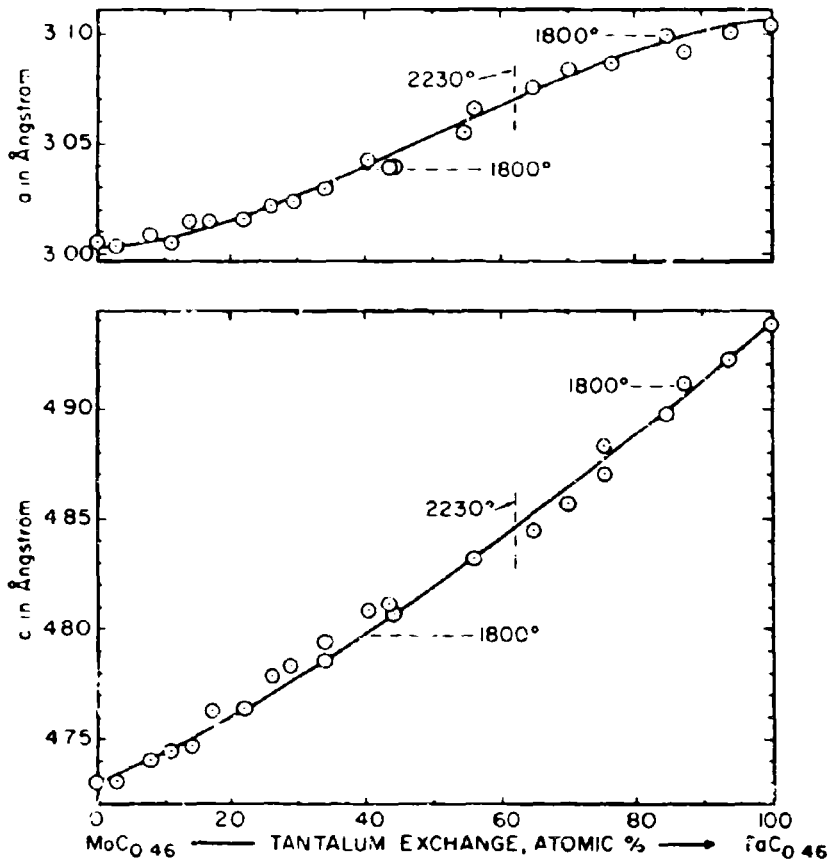

Figure III.E.14.18: Lattice Parameters of the $(Ta, Mo)_2C$ Solid Solution. Alloys Rapidly Cooled from 2500°C. Parameters are Based on Indexing According to the L'3-Type.

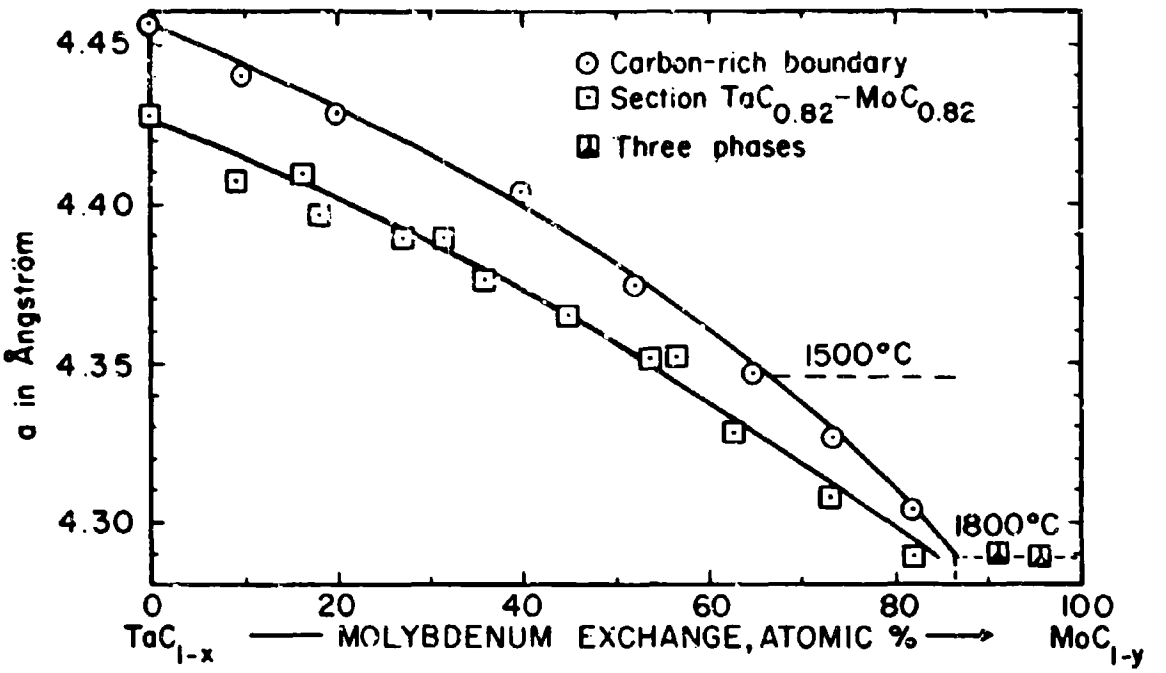

Figure III.E.14.19: Lattice Parameters of Monocarbide, $(Ta, Mo)C_{1-x}$, Alloys.

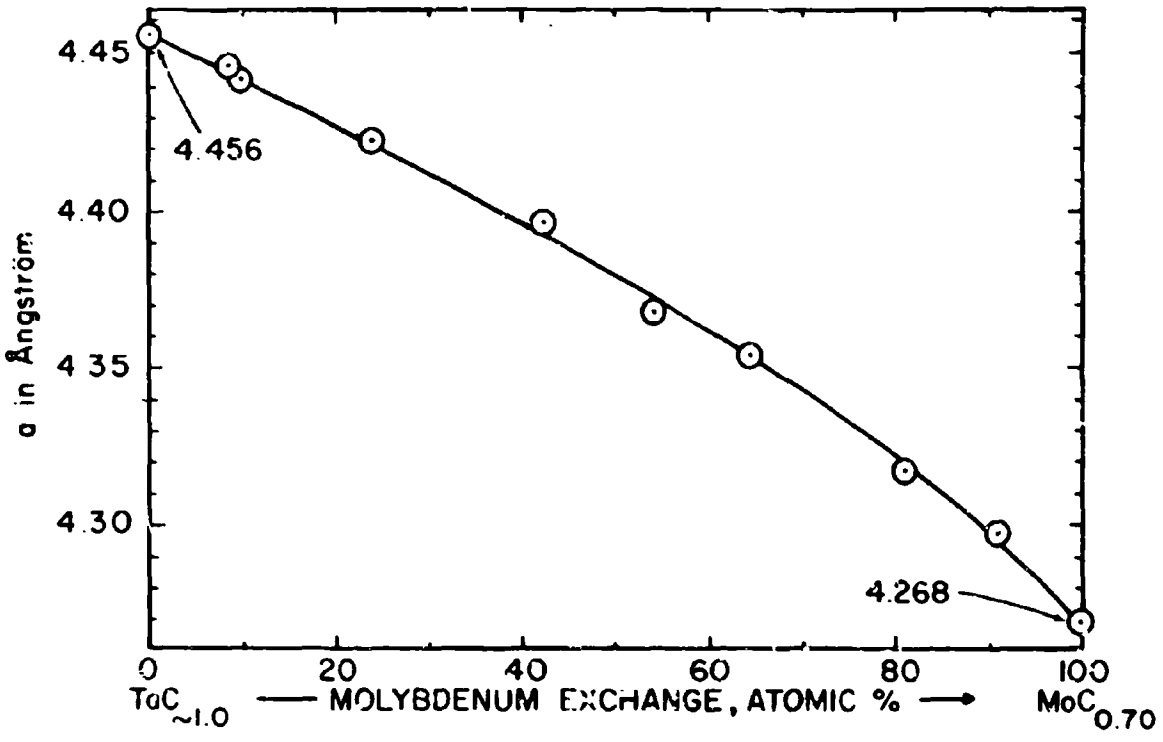

Figure III.E.14.20: Ta-Mo-C: Lattice Parameters of the Cubic Monocarbide Phase Along the Section TaC-$MoC_{0.70}$. Alloys Quenched from 2500° C.

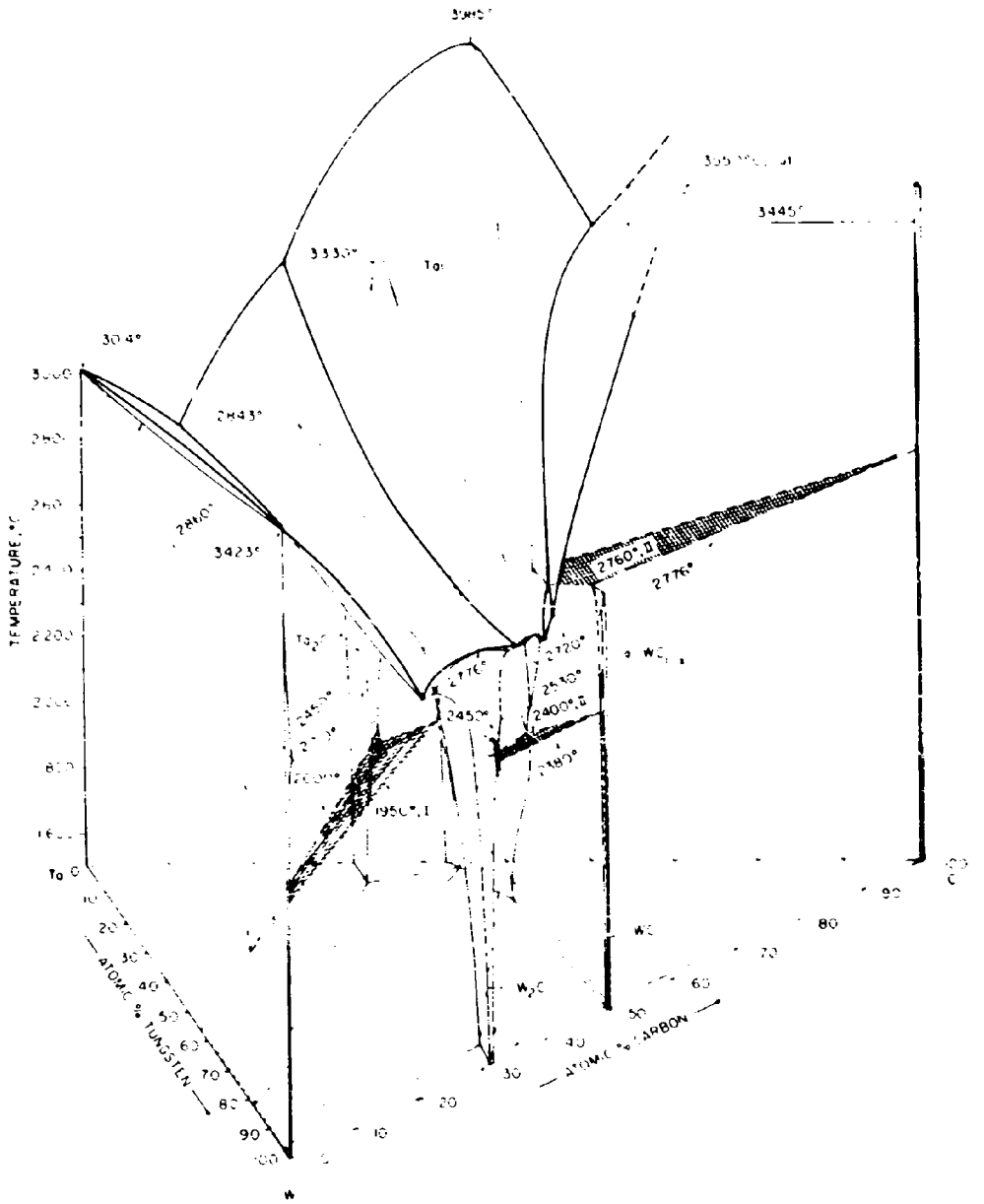

Figure III.E.15.1. Isometric View of the Ta-W-C System

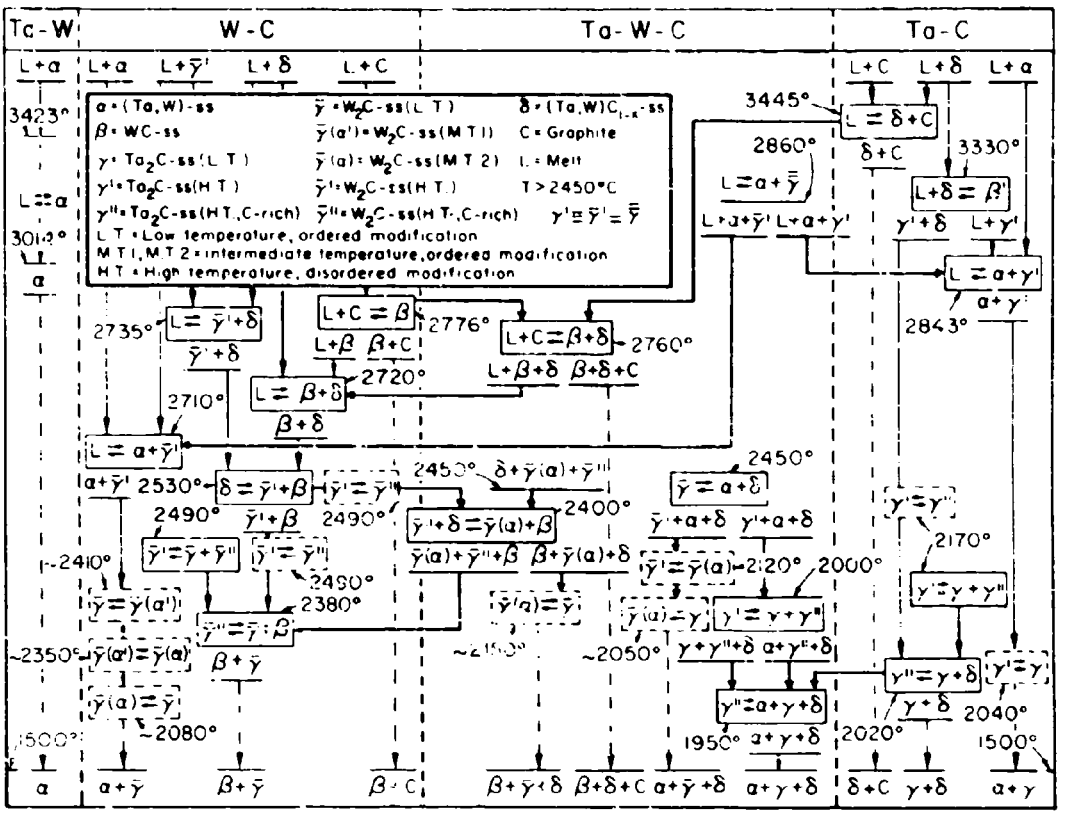

Figure III.E.15.2. Reaction Diagram for the Ta-W-C System

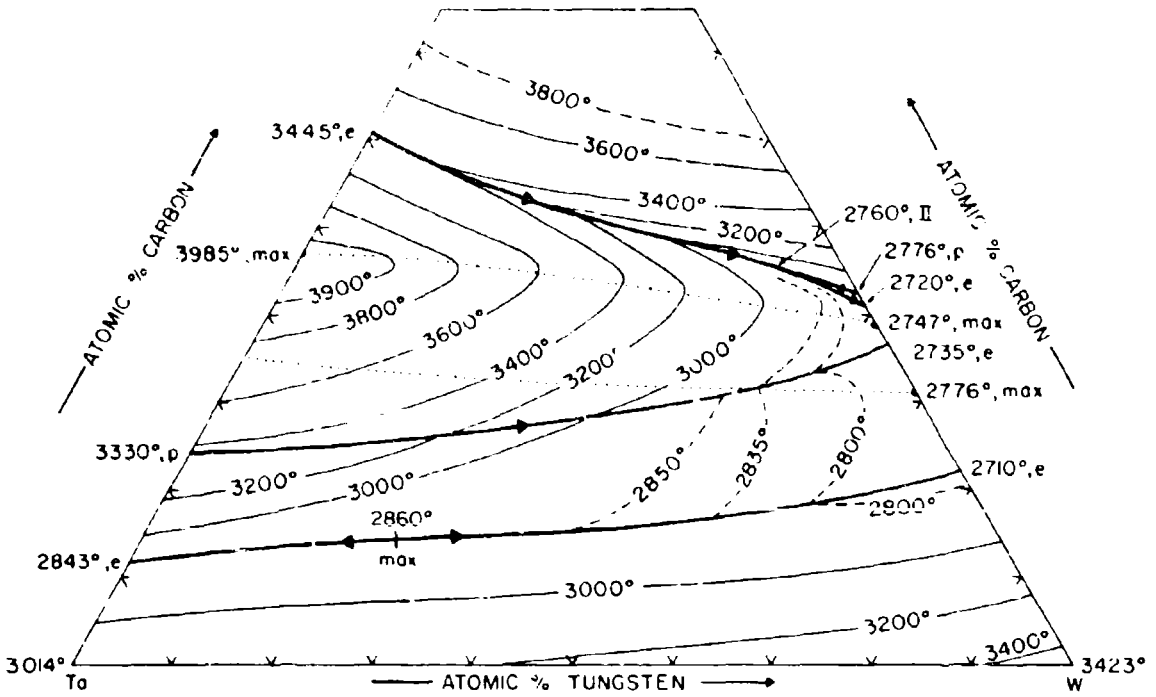

Figure III.E.15.3. Liquidus Projections in the Ta-W-C System

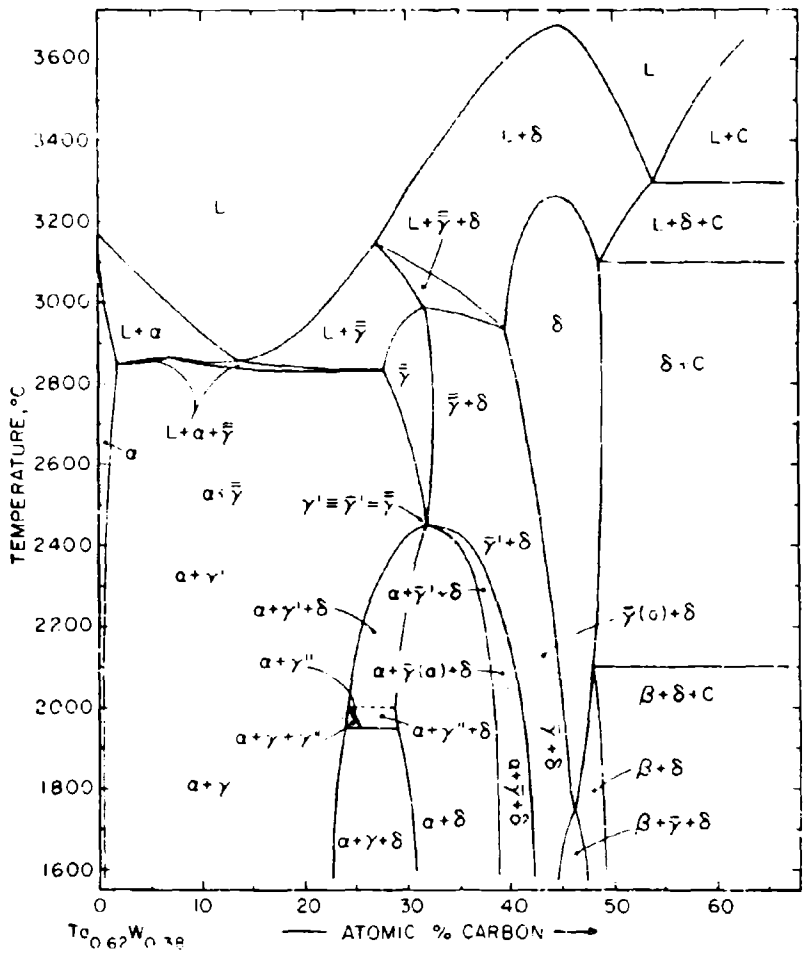

Figure III.E.15.4. Isopleth $Ta_{0.62}W_{0.38}$-C

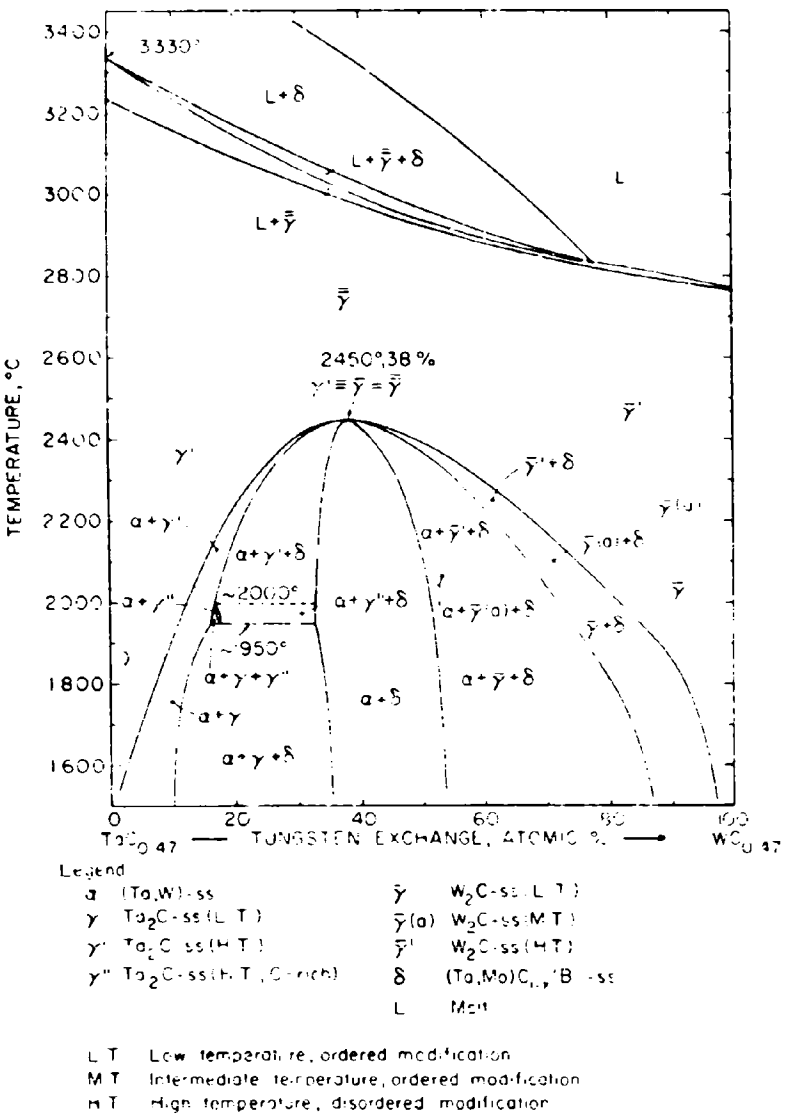

Figure III.E.15.5. Isopleth at 32 At.% C

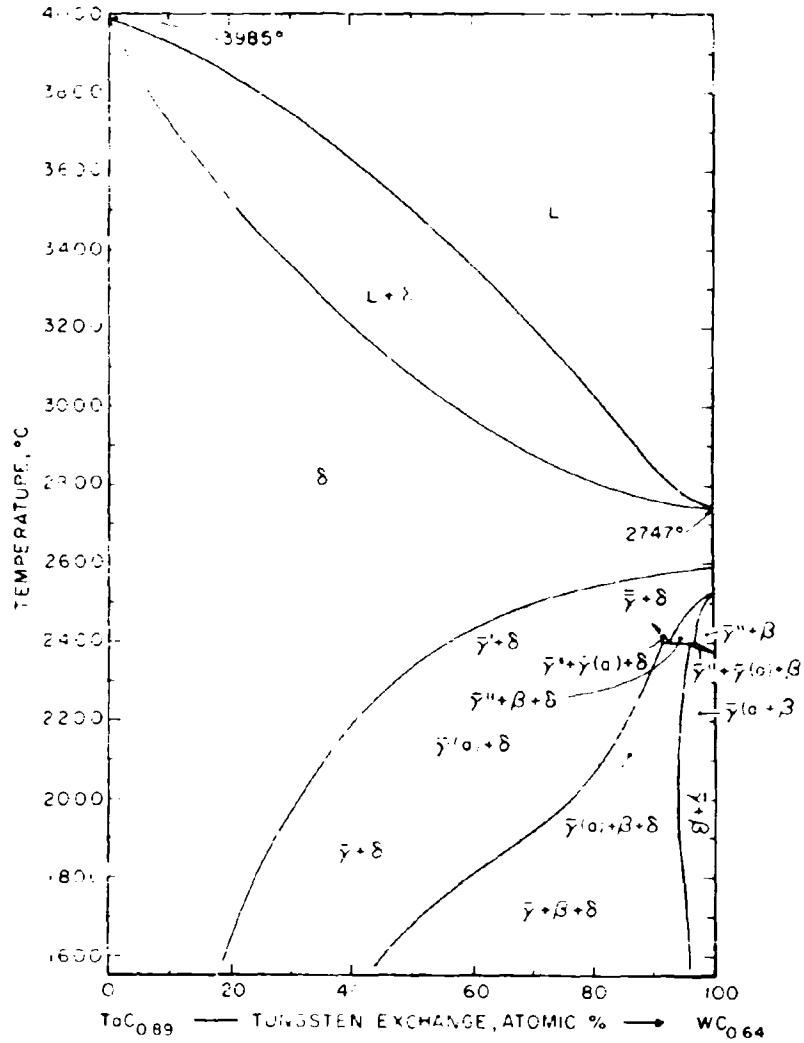

Figure III.E.15.6. Isopleth $TaC_{0.89}$-$WC_{0.64}$

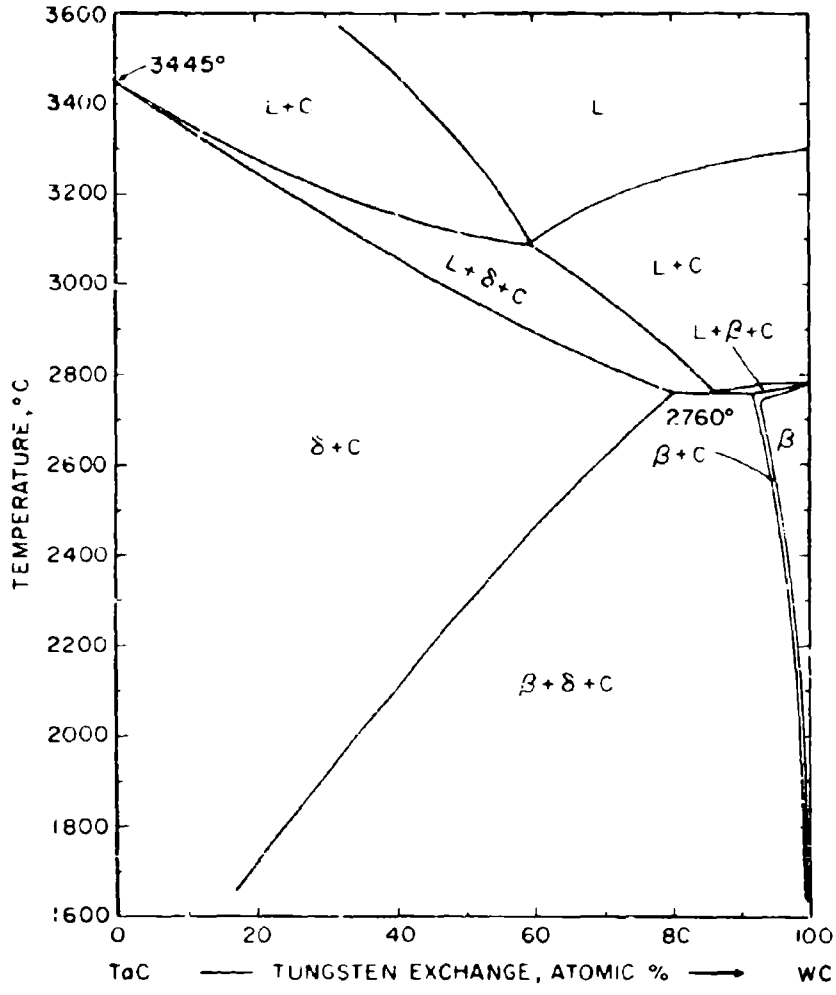

Figure III.E.15.7. Isopleth TaC-WC

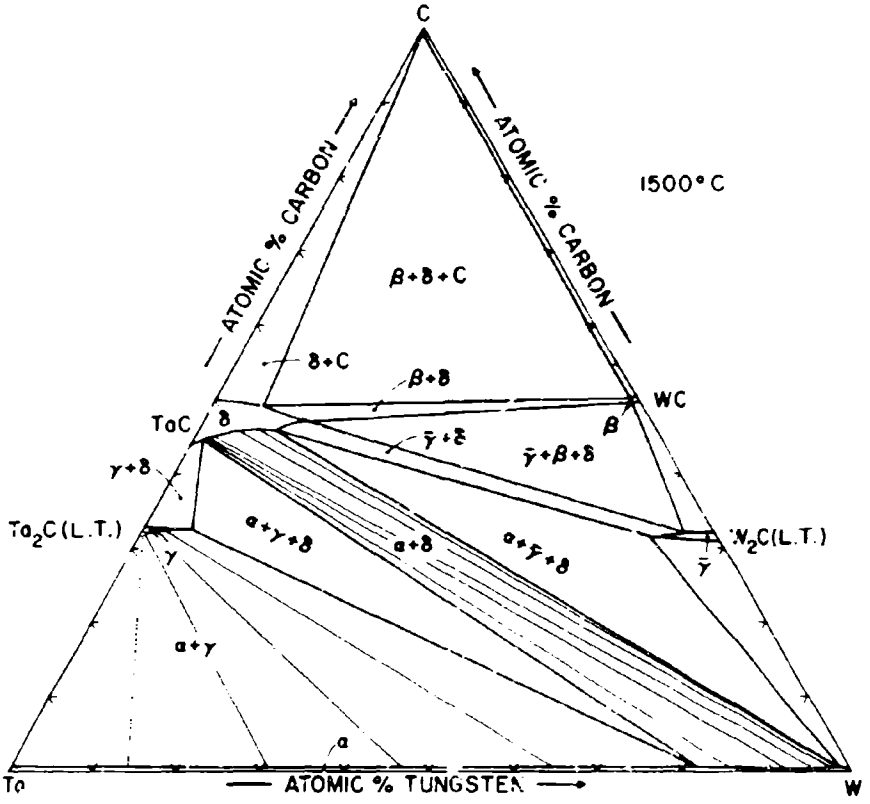

Figure III.E.15.8. Isothermal Section of the Ta-W-C System at 1500° C

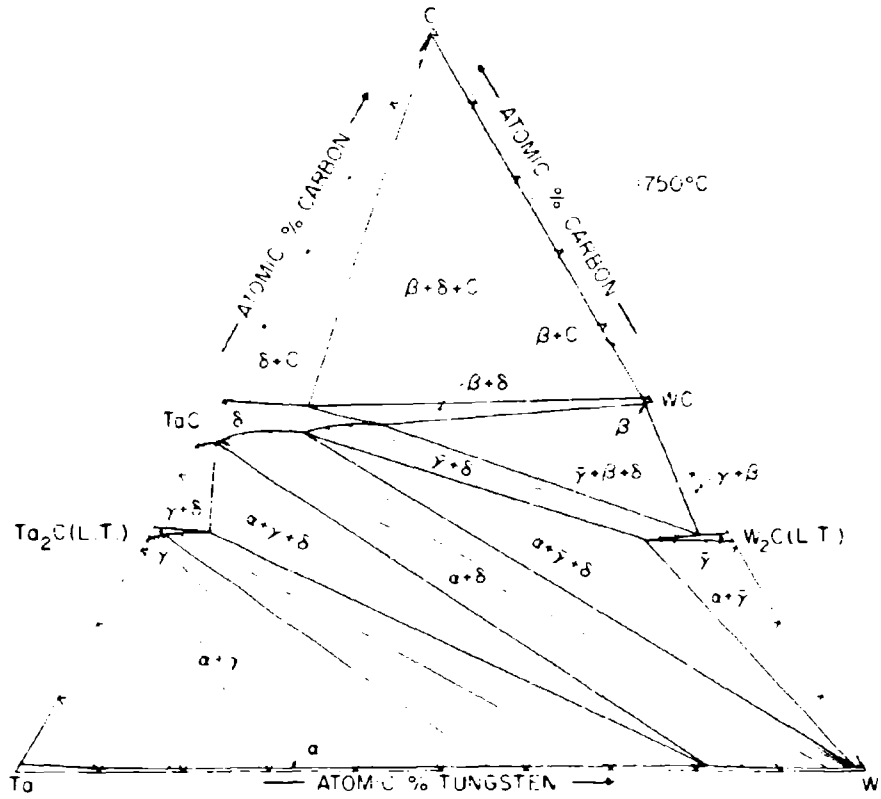

Figure III.E.15.9. Isothermal Section of the Ta-W-C System at 1750°C

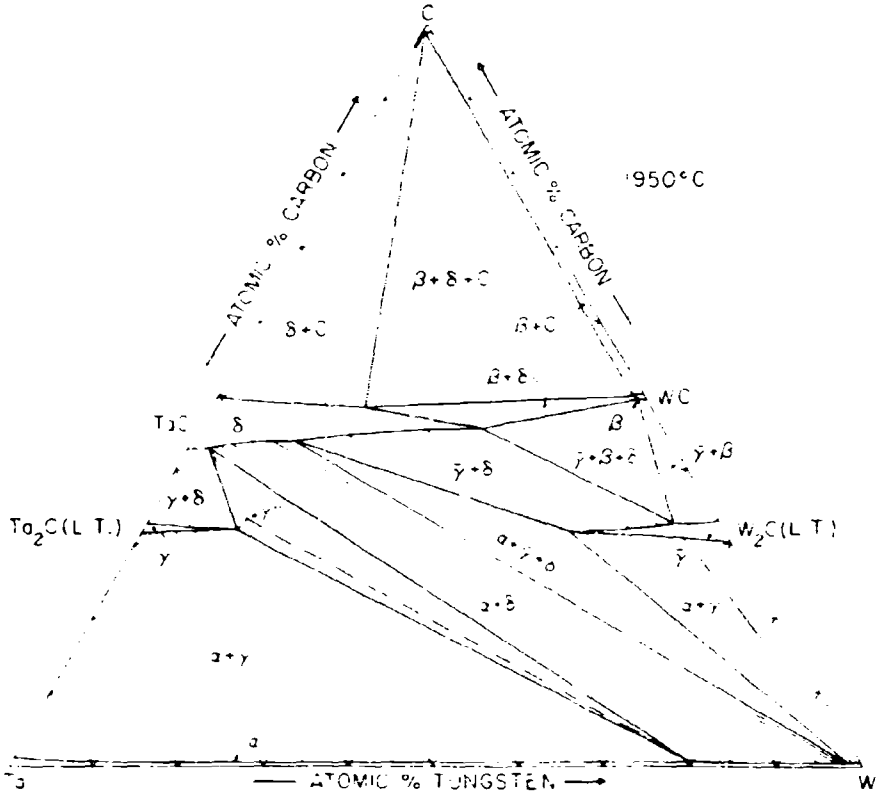

Figure III.E.15.10. Isothermal Section of the Ta-W-C System at 1950°C

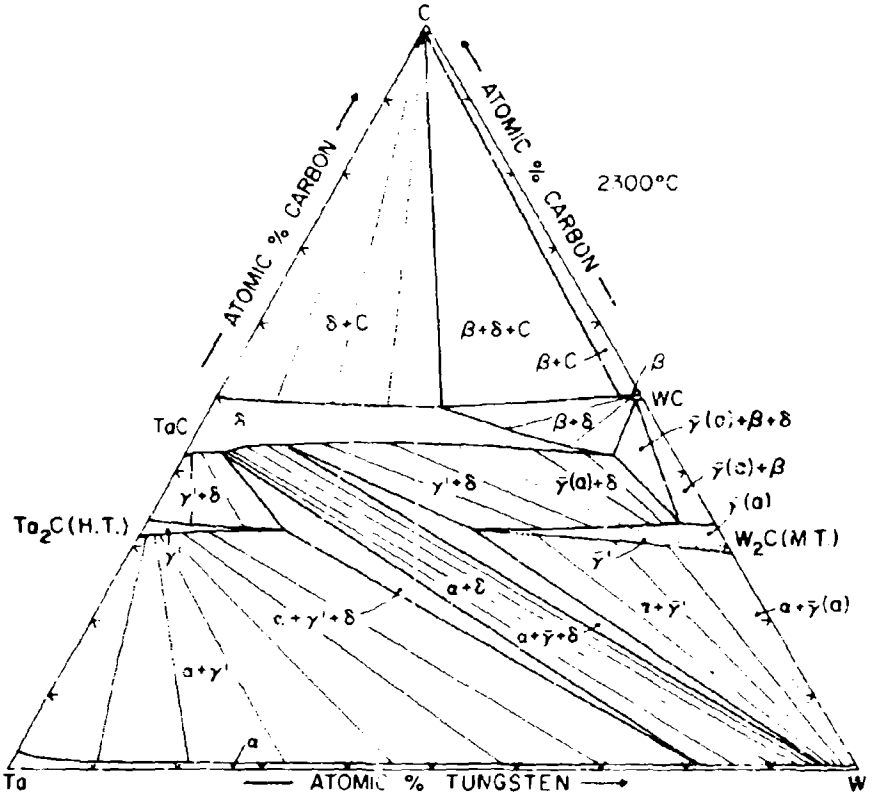

Figure III.E.15.11. Isothermal Section of the Ta-W-C System at 2300°C

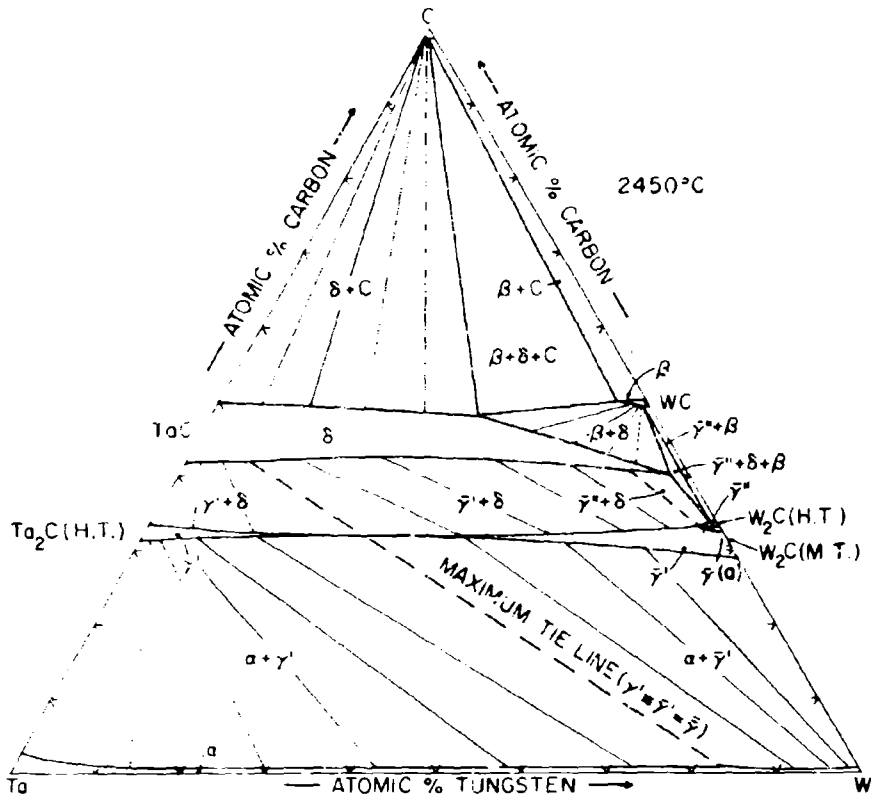

Figure III.E.15.12. Isothermal Section of the Ta-W-C System at 2450° C

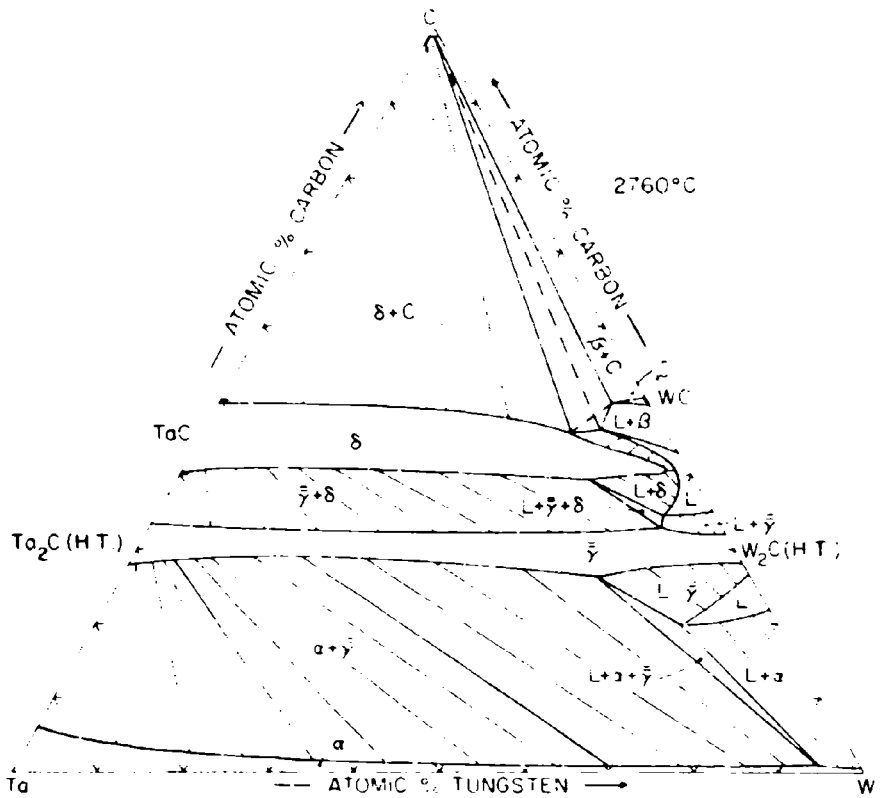

Figure III.E.15.13. Isothermal Section of the Ta-W-C System at 2760° C

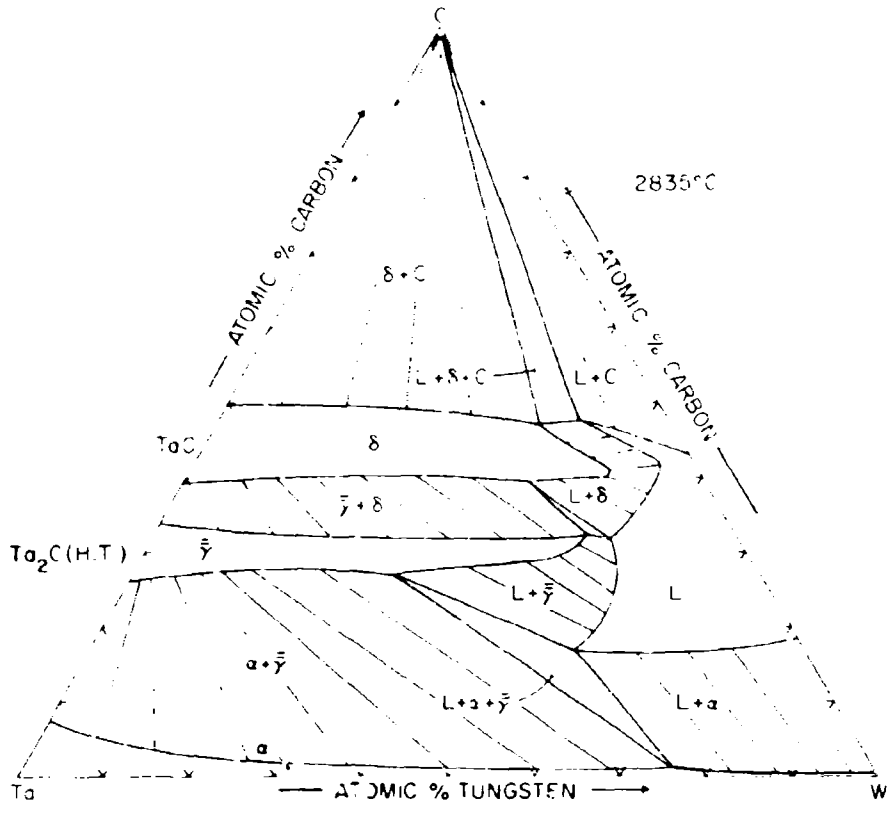

Figure III.E.15.14. Isothermal Section of the Ta-W-C System at 2835° C

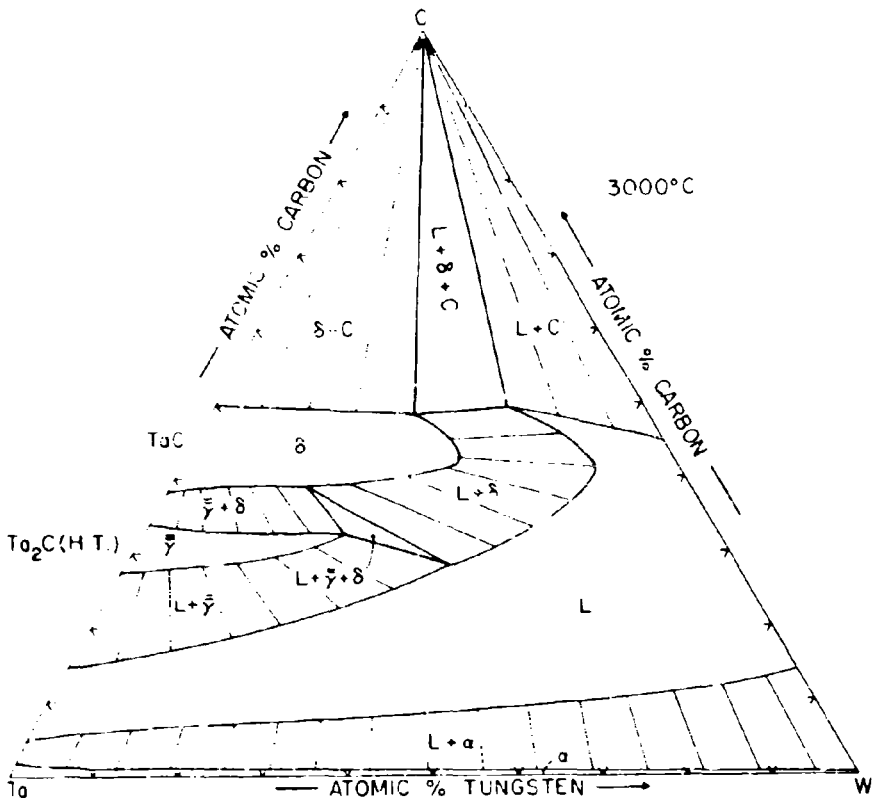

Figure III.E.15.15. Isothermal Section of the Ta-W-C System at 3000°C

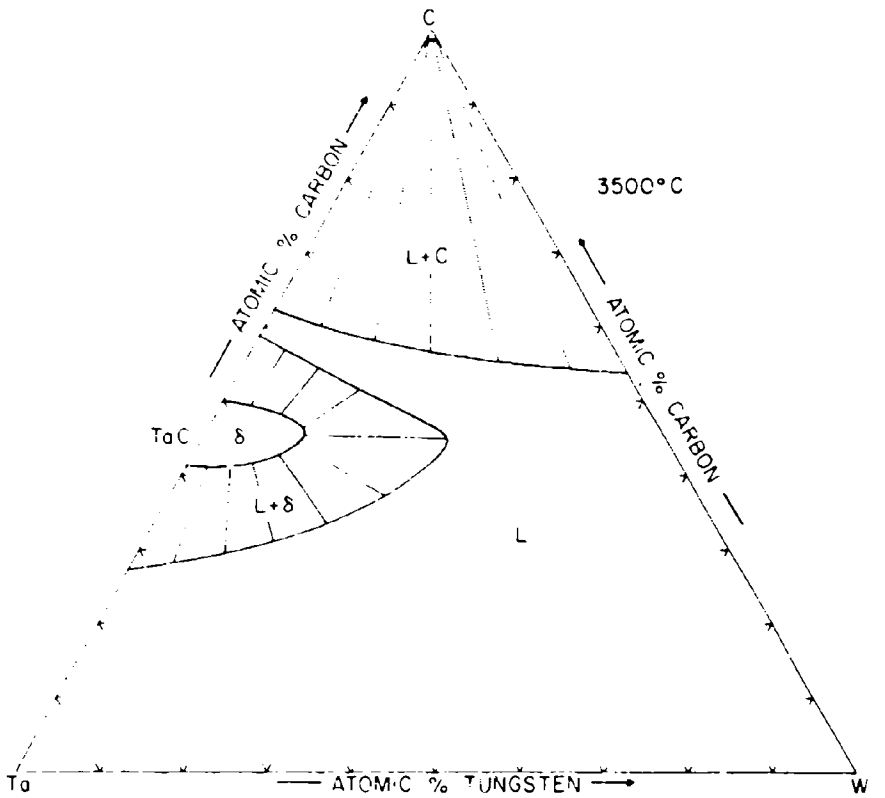

Figure III.E.15.16. Isothermal Section of the Ta-W-C System at 3500°C

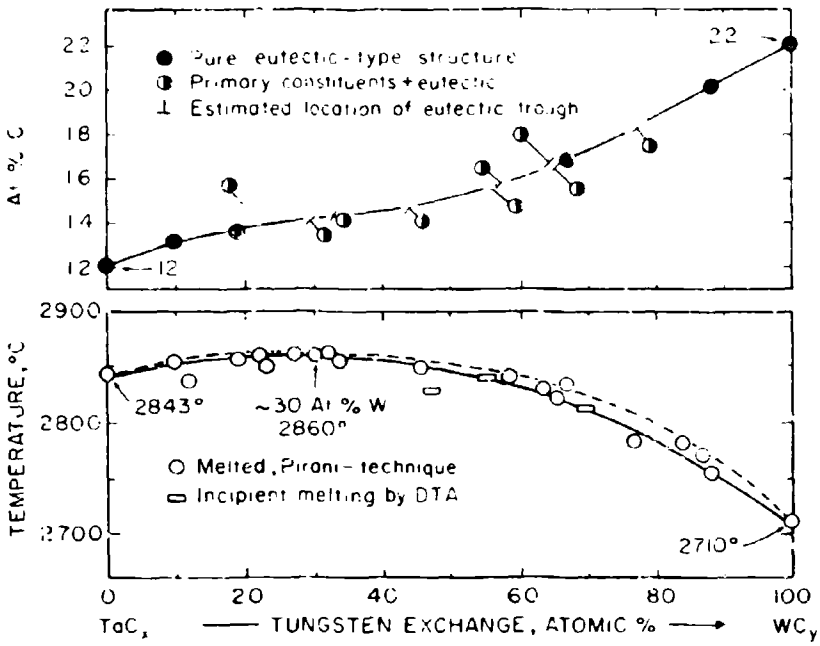

Figure III.E.15.17. Observed Melting in Alloys Located Along the Metal + Subcarbide Eutectic Trough.

Top: Microscopically Estimated Location of Eutectic Trough

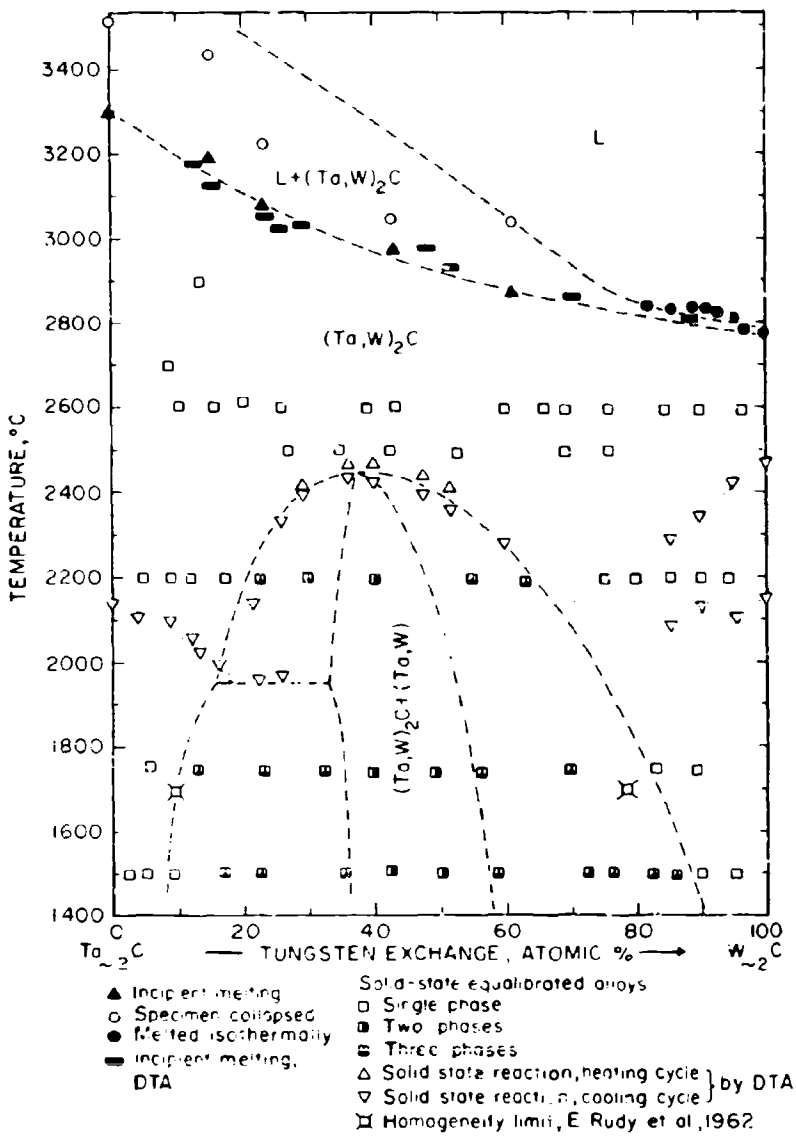

Figure III.E.15.18. Melting, Solid State Reactions, and Qualitative Phase Evaluation of Solid State-Equilibrated Alloys Located Along the Section Ta_2C-W_2C.

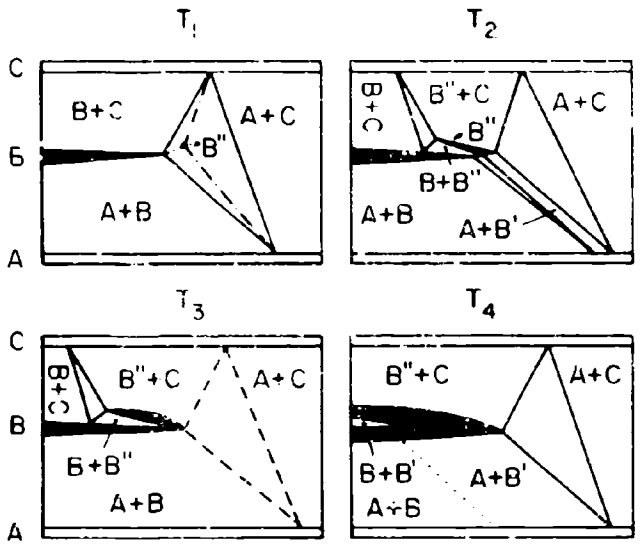

A (Ta,W)-ss

B Ta_2C-ss

C $(Ta,W)C_{1-x}$(B1)-ss

B Ta_2C-ss,ordered (C-poor)

B' Ta_2C-ss, disordered (C-poor)

B" Ta_2C-ss,disordered (C-rich)

$T_1 < T_2 < T_3 < T_4$

T_1 Class I (eutectoid) 4-phase reaction

T_2 Slightly above T_1

T_3 Limiting three-phase equilibrium

T_4 Slightly above T_3

Figure III.E.15.19. Diagrammatic Illustration of the Order-Disorder Transition of the Subcarbide Phase in the Ta-W-C Ternary

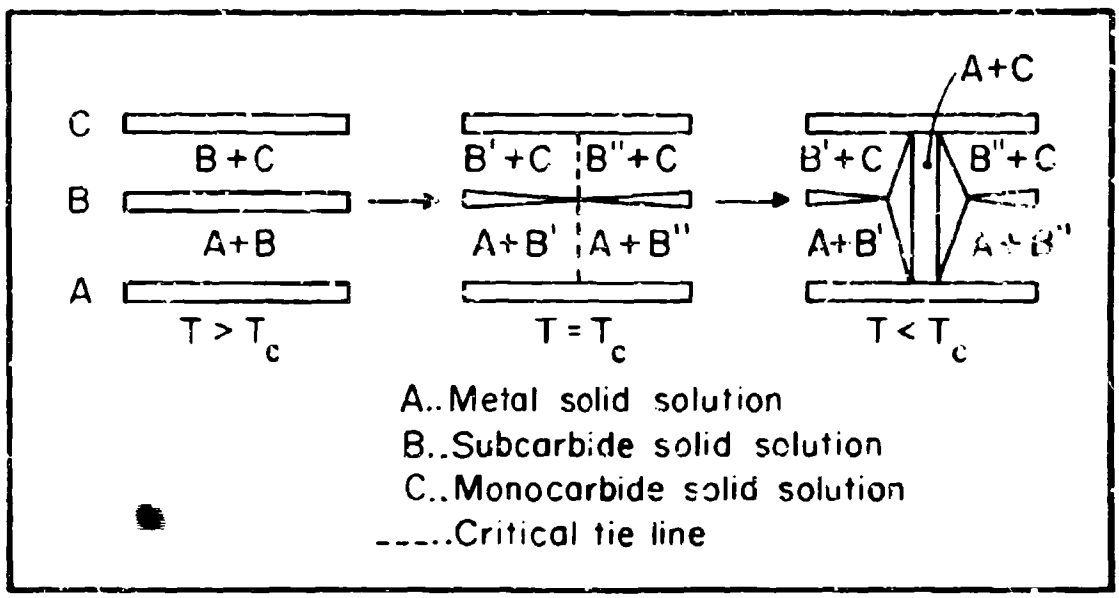

Figure III.E.15.20. Diagrammatic Illustration of the Disproportionation of the $(Ta,W)_2C$ Solid Solution Towards Lower Temperatures

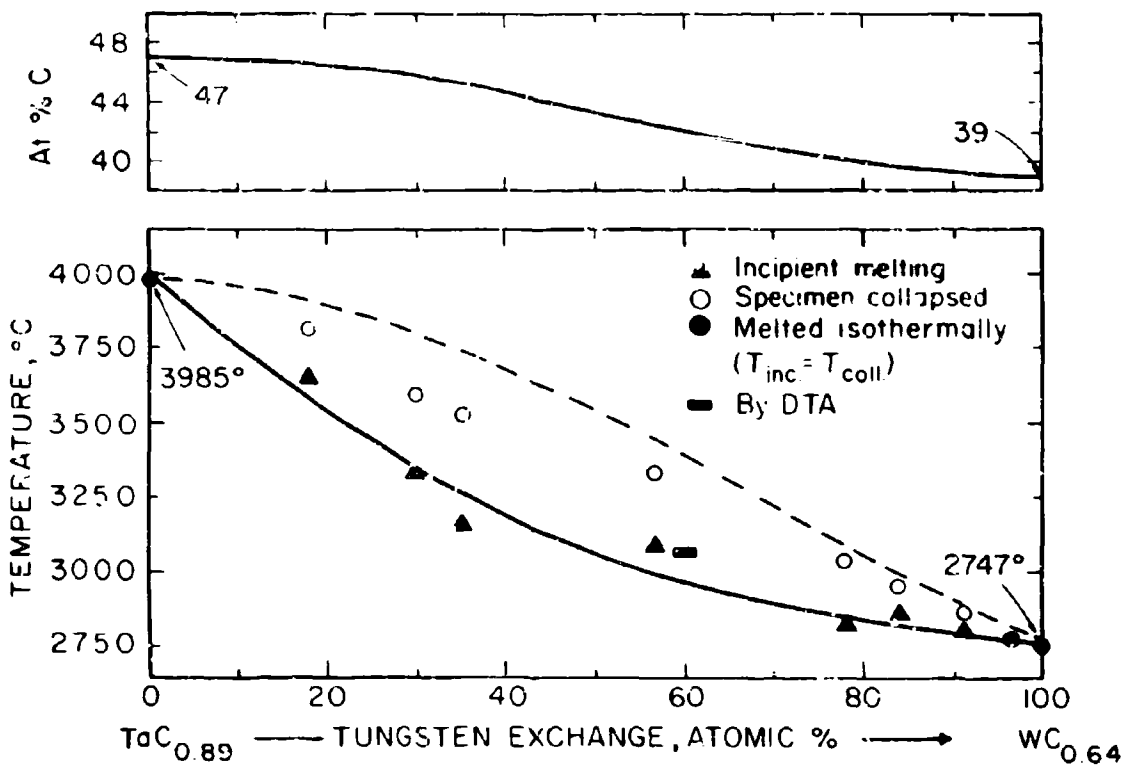

Figure III.E.15.21. Maximum Solidus Temperatures of the Monocarbide (B1) Solid Solution.

Top: Maximum Solidus Composition Line

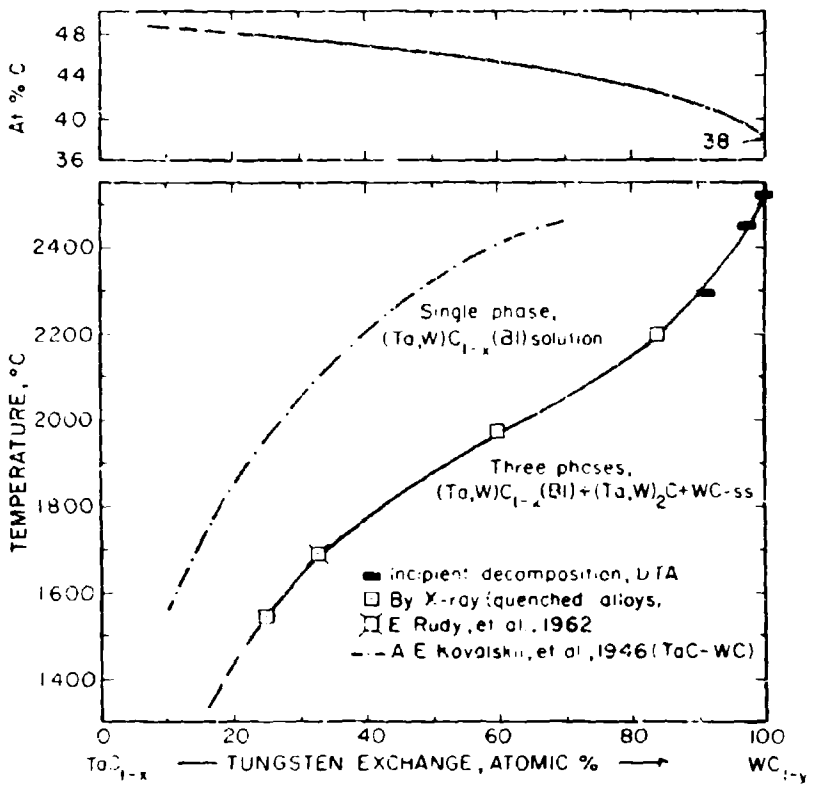

Figure III.E.15.22. Maximum Tungsten Exchange in the Cubic Monocarbide Phase.

Broken Line: Metal Exchange of the Three-Phase Vertex $\beta+\delta+C$ at the Monocarbide (δ)

Top: Composition Line of the Vertex of the Three-Phase Equilibrium $\beta+\gamma+\delta$ at the δ-Phase.

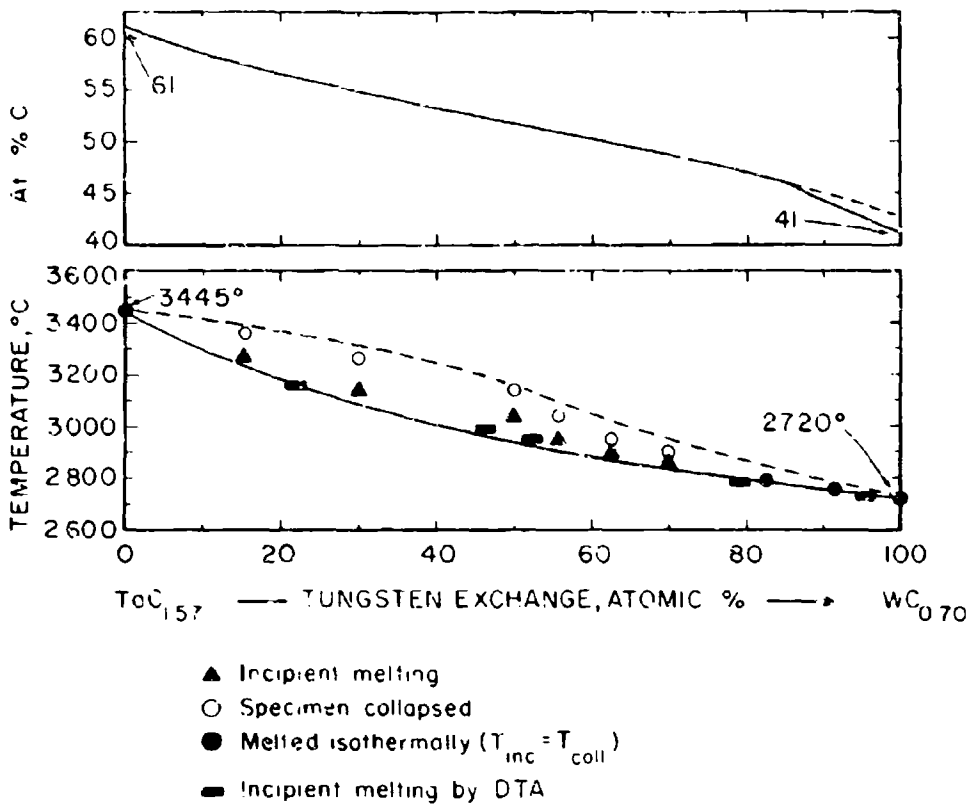

Figure III.E.15.23. Melting Along the Eutectic Troughs in the Carbon-Rich Regions of the Ta-W-C System

F. PARTIAL, QUATERNARY METAL-CARBON SYSTEMS

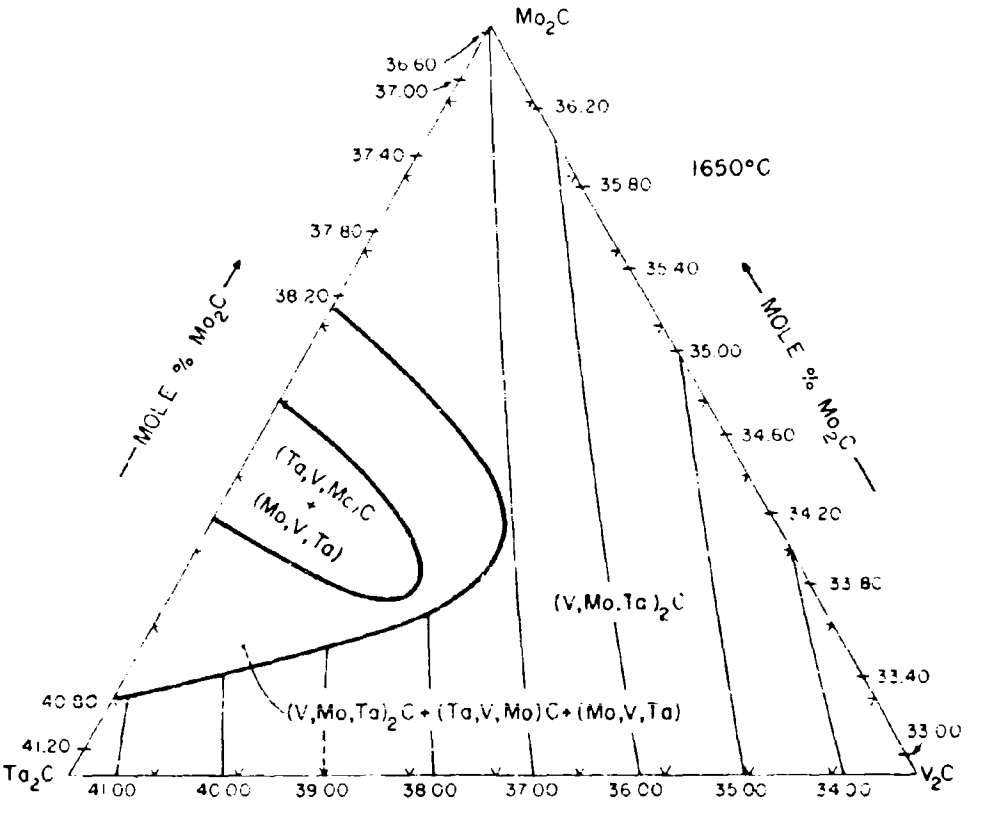

Figure III.F.1.1 Section Ta_2C-V_2C-Mo_2C at 1650°C

(Figures at Boundaries Refer to the Unit Cell Volumes of Subcarbide Solutions)

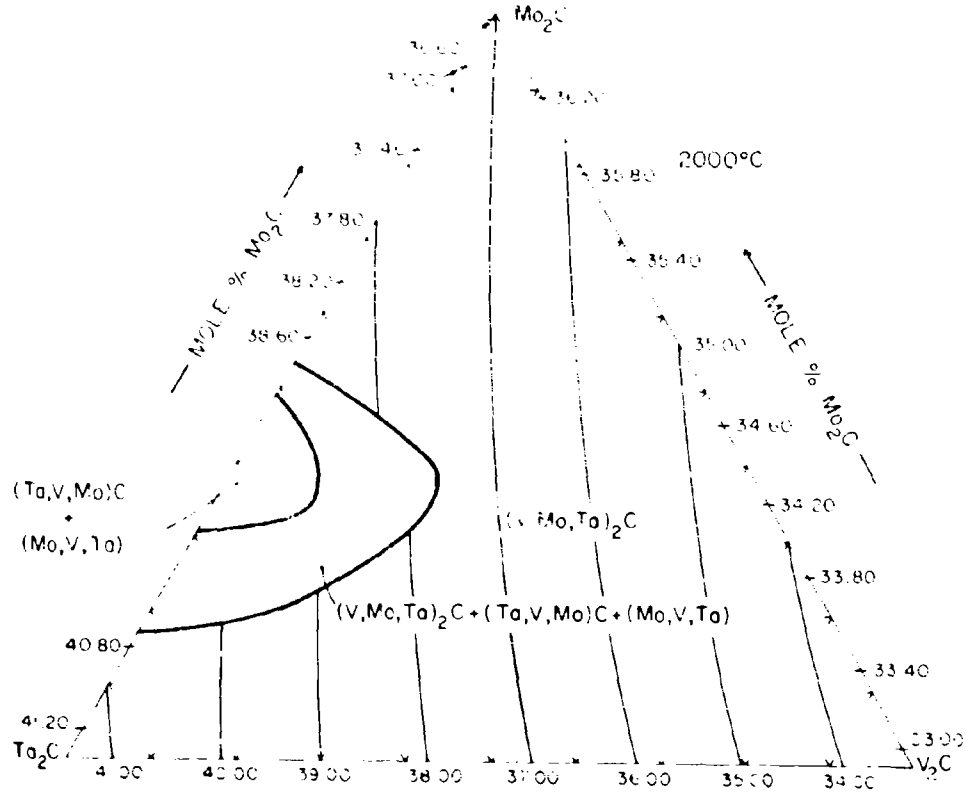

Figure III.F.1.2. Section Ta_2C-V_2C-Mo_2C at 2000°C

(Figures at Boundaries Refer to the Unit Cell Volumes of Subcarbide Solutions)

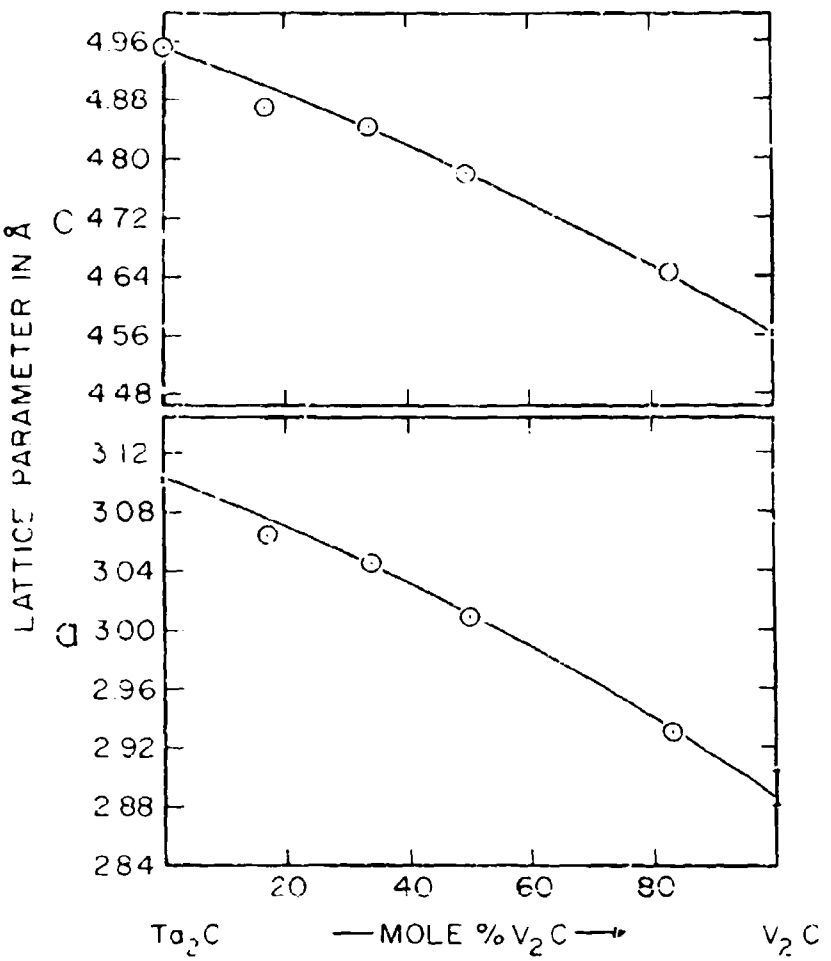

Figure III.F.1.3. Lattice Parameters of the $(Ta,V)_2C$ Solid Solution (Alloys Equilibrated at 1650° C)

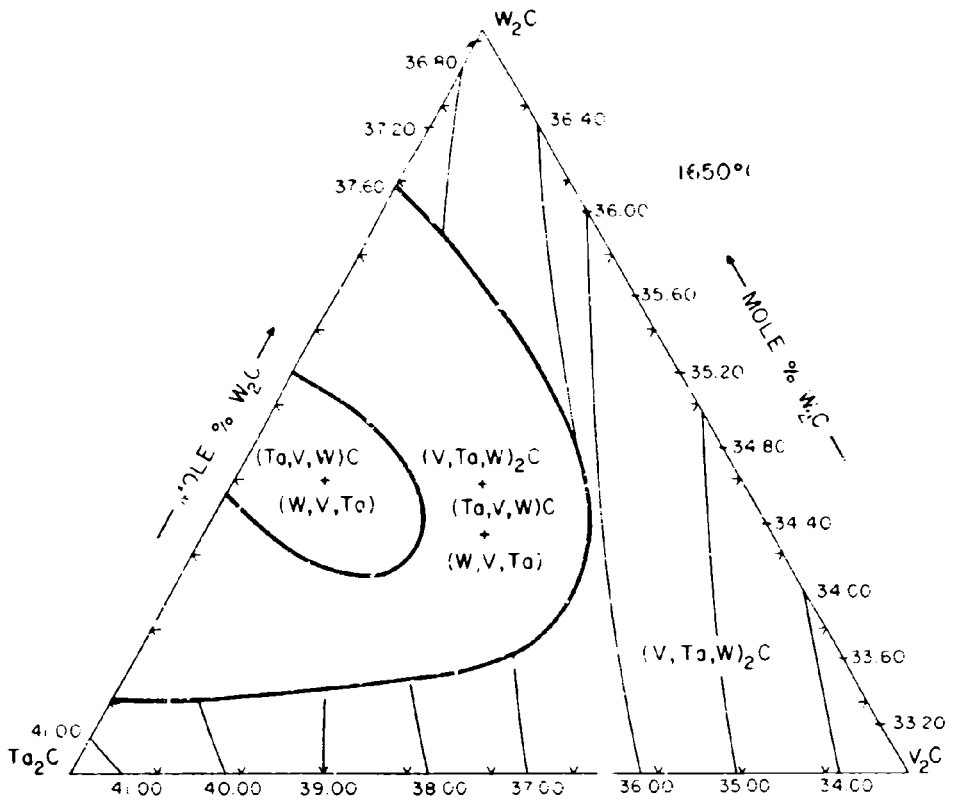

Figure III.F.2.1. Section Ta_2C-V_2C-W_2C at 1650° C

(Figures at Boundaries Refer to the Unit Cell Volumes of Subcarbide Solutions)

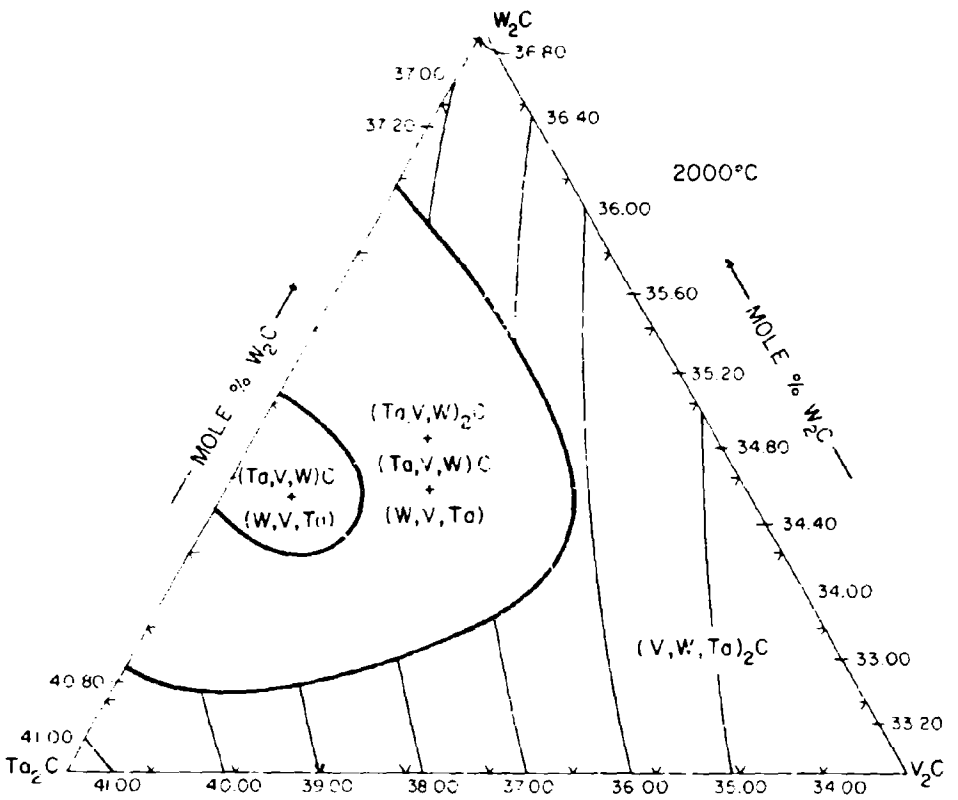

Figure III.F.2.2. Section Ta_2C-V_2C-W_2C at 2000°C

(Figures at Boundaries Refer to the Unit Cell Volumes of Subcarbide Solutions)

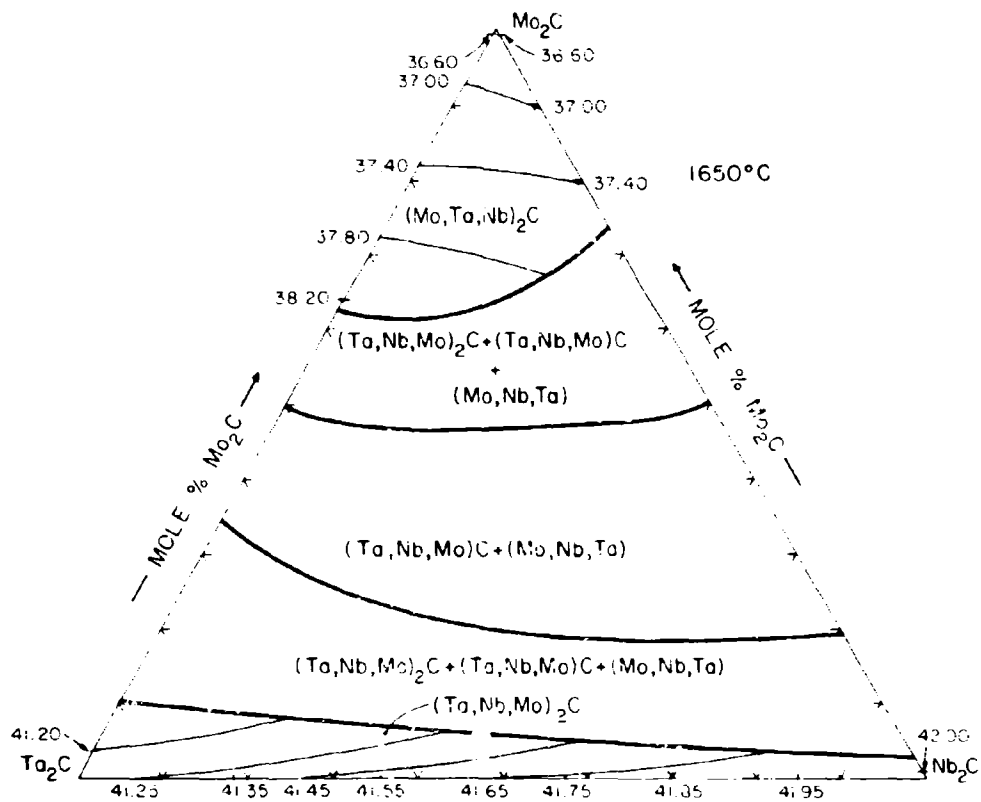

Figure III.F.3.1. Section Ta_2C-Nb_2C-Mo_2C at 1650°C

(Figures at Boundaries Refer to the Unit Cell Volumes of Subcarbide Solutions)

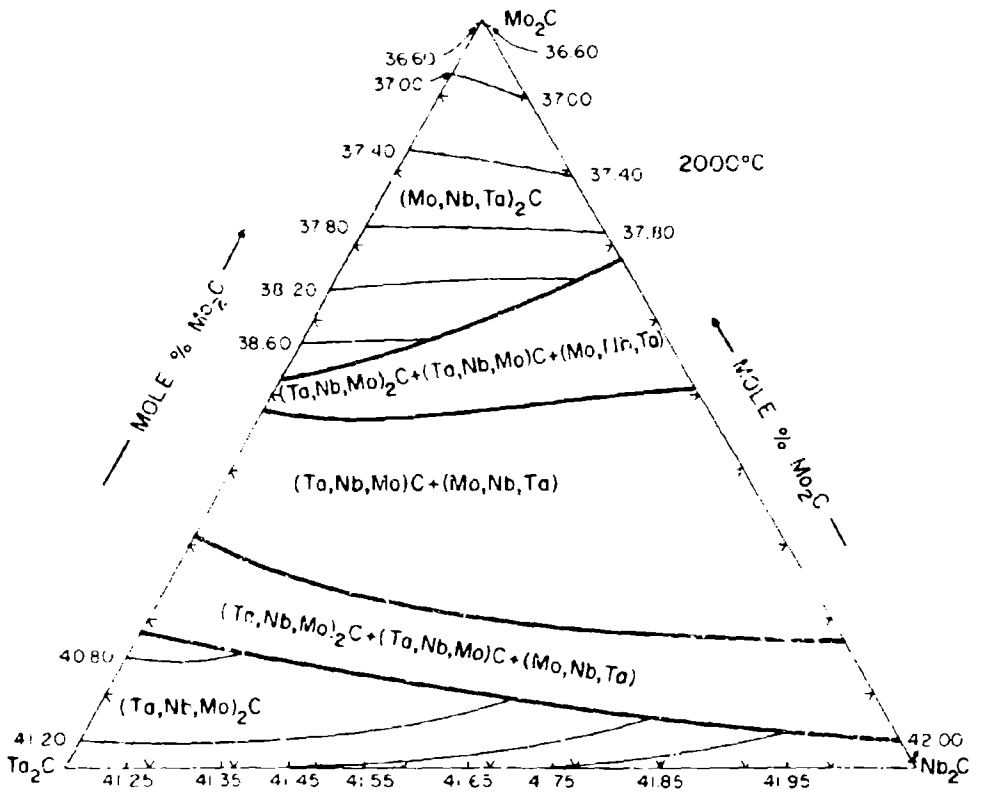

Figure III.F.3.2. Section Ta_2C-Nb_2C-Mo_2C at 2000°C

(Figures at Boundaries Refer to the Unit Cell Volumes of Subcarbide Solutions)

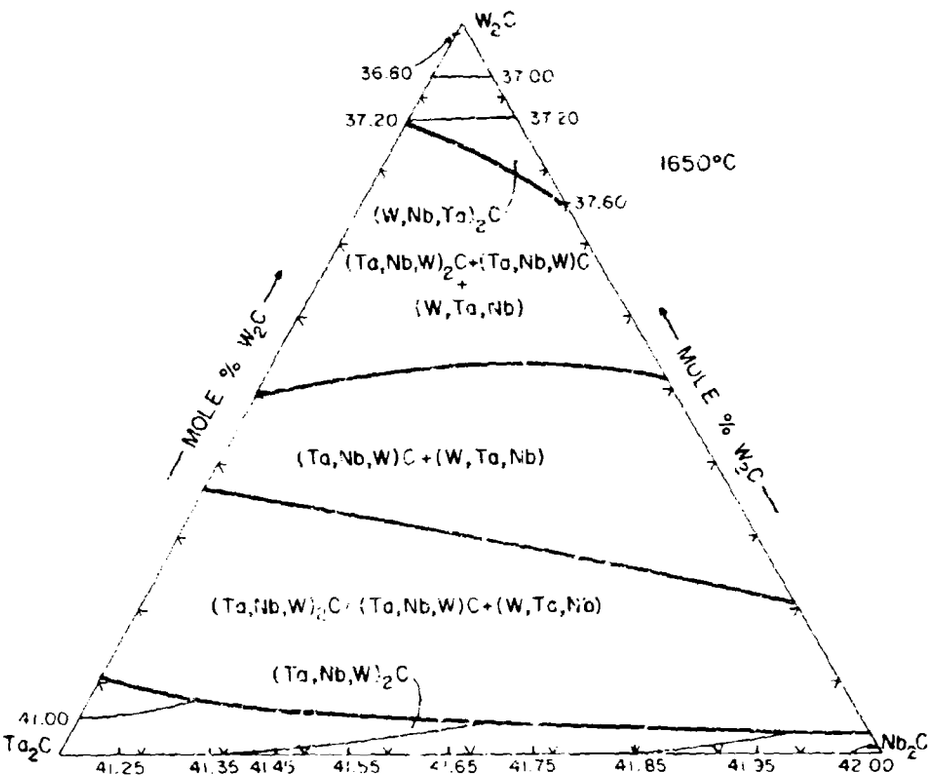

Figure III.F.4.1. Section Ta_2C-Nb_2C-W_2C at 1650° C

(Figures at Boundaries Refer to Unit Cell Volumes of Subcarbide Solutions)

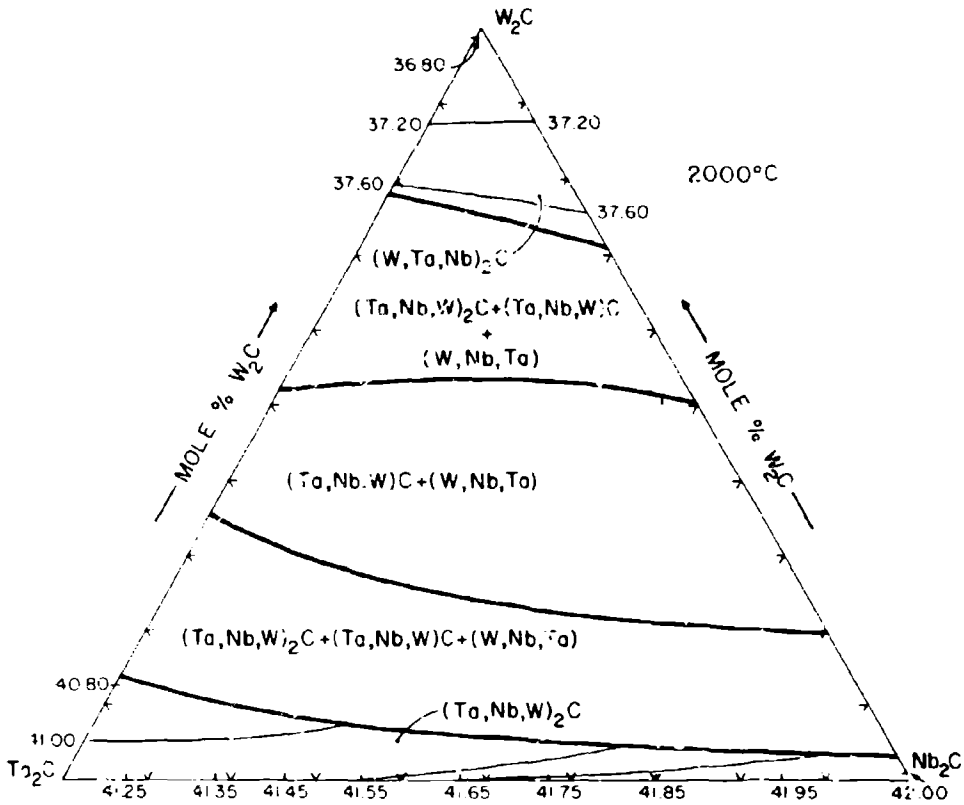

Figure III.F.4.2. Section Ta_2C-Nb_2C-W_2C at 2000°C

(Figures at Boundaries Refer to Unit Cell Volumes of Subcarbide Solutions)

G. TERNARY TRANSITION METAL-CARBON-SILICON SYSTEMS

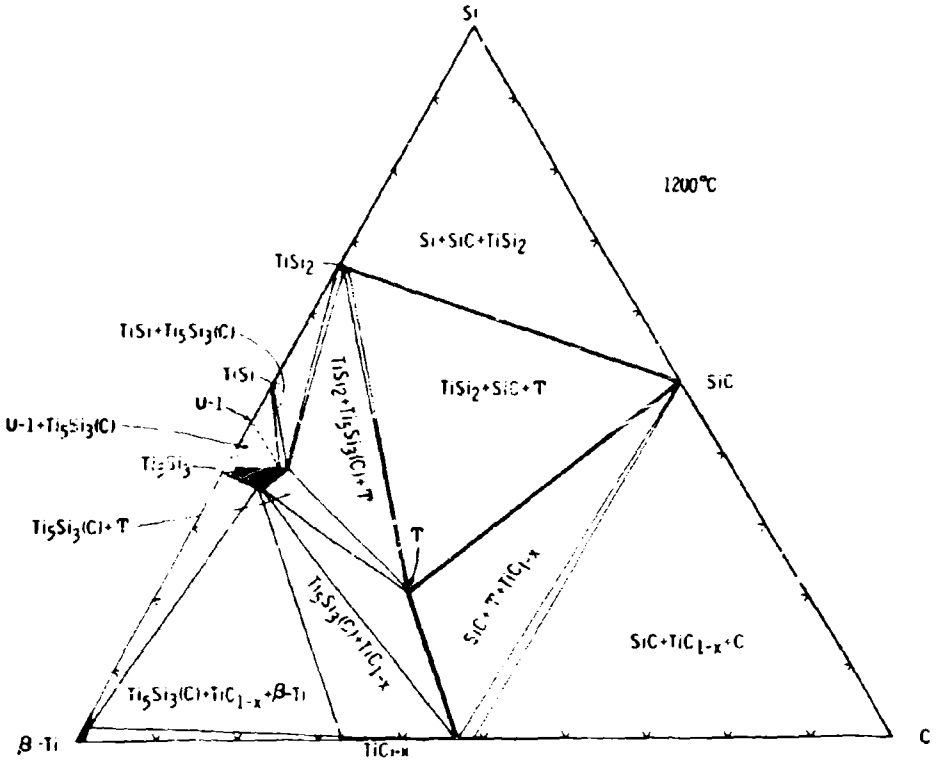

Figure III.G.1.1. Isothermal Section of the Ti-Si-C System at 1200°C

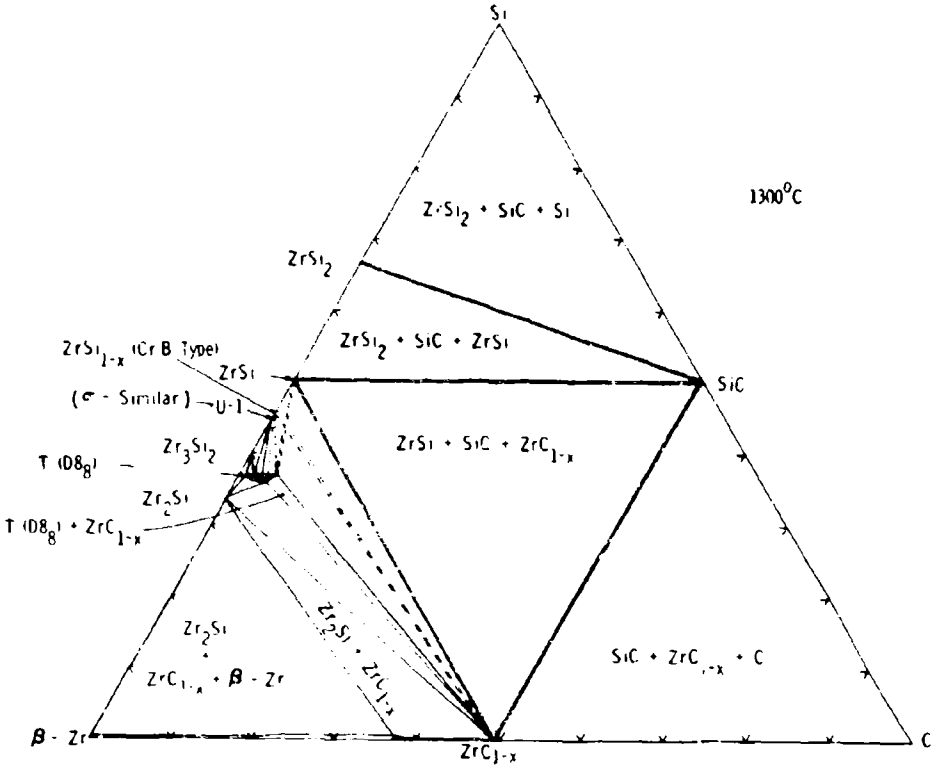

Figure III.G.2.1. Isothermal Section of the Zr-Si-C System at 1300° C

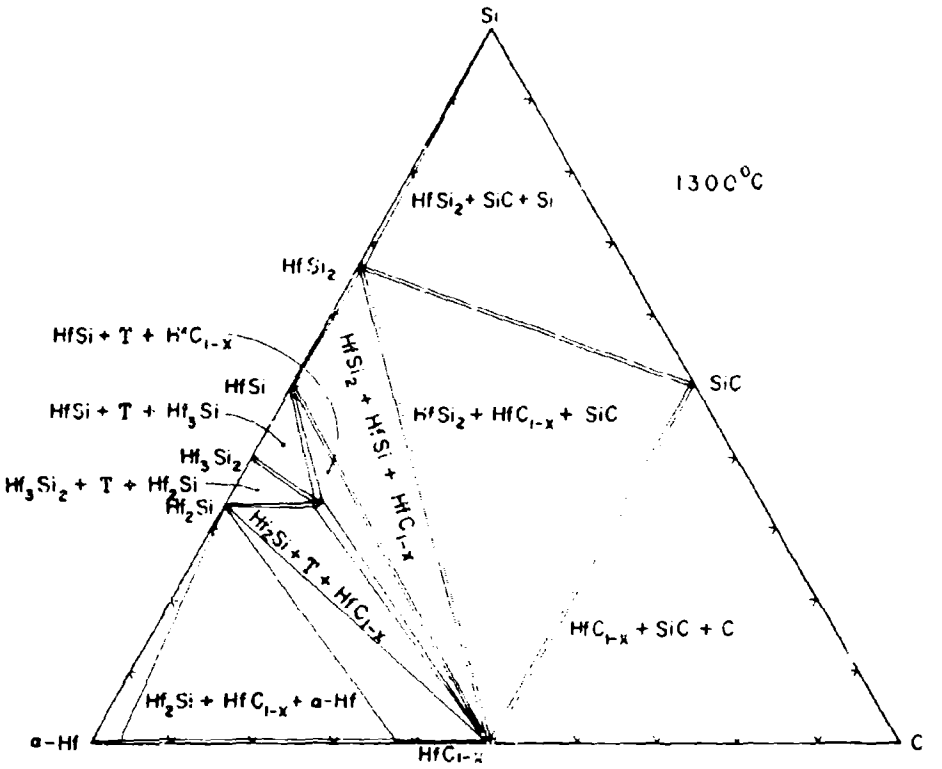

Figure III.G.3.1. Isothermal Section of the Hf-Si-C System at 1300° C

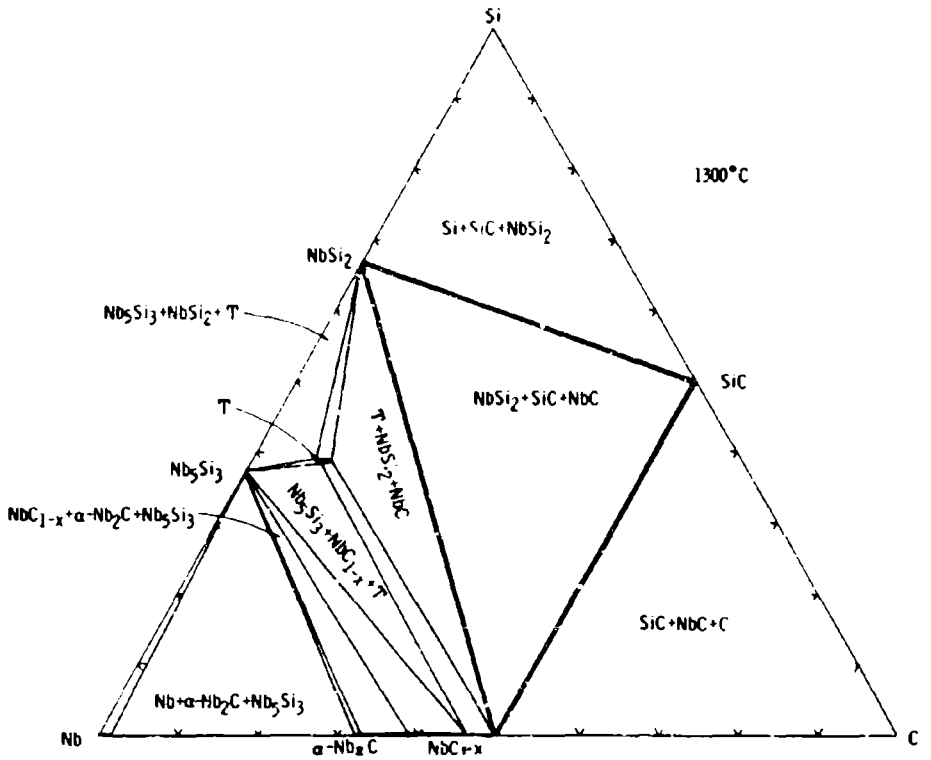

Figure III.G.4.1. Isothermal Section of the Nb-Si-C System at 1300° C

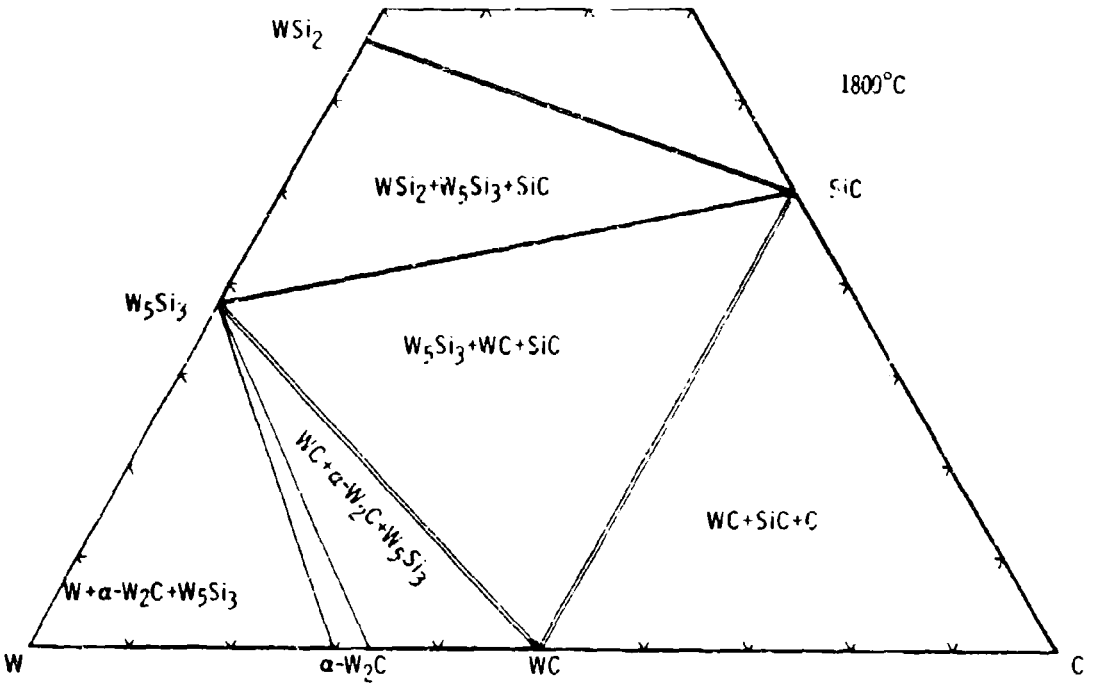

Figure III.G.5.1. Isothermal Section of the W-Si-C System at 1800° C

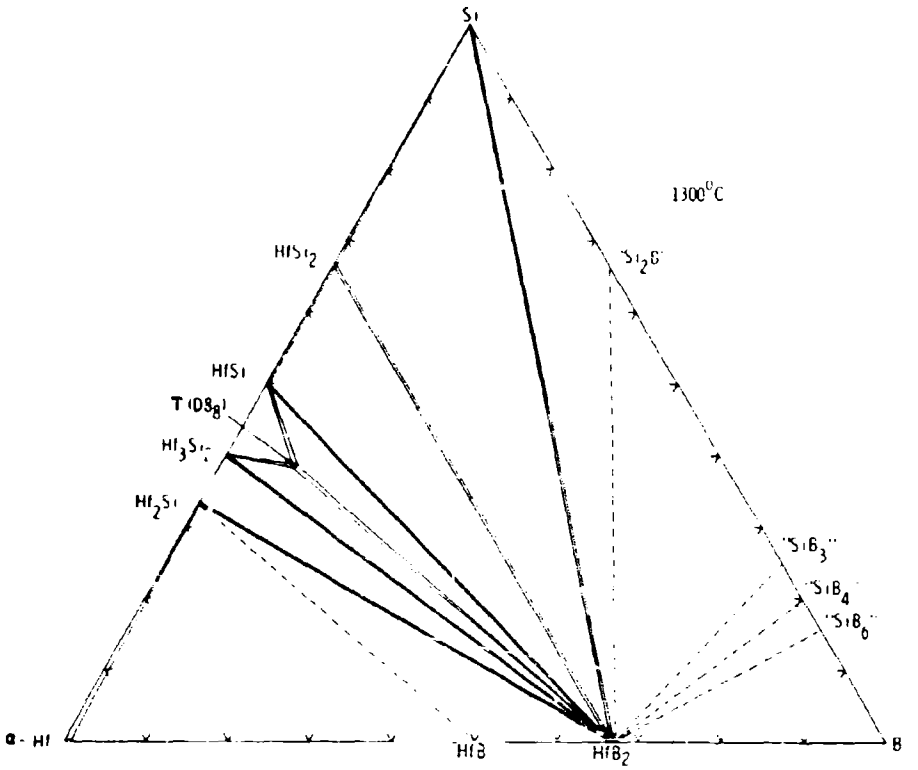

Figure III.H.1.1 Isothermal Section of the Hf-Si-B System at 1300°C

I. TERNARY TRANSITION METAL-BORON SYSTEMS

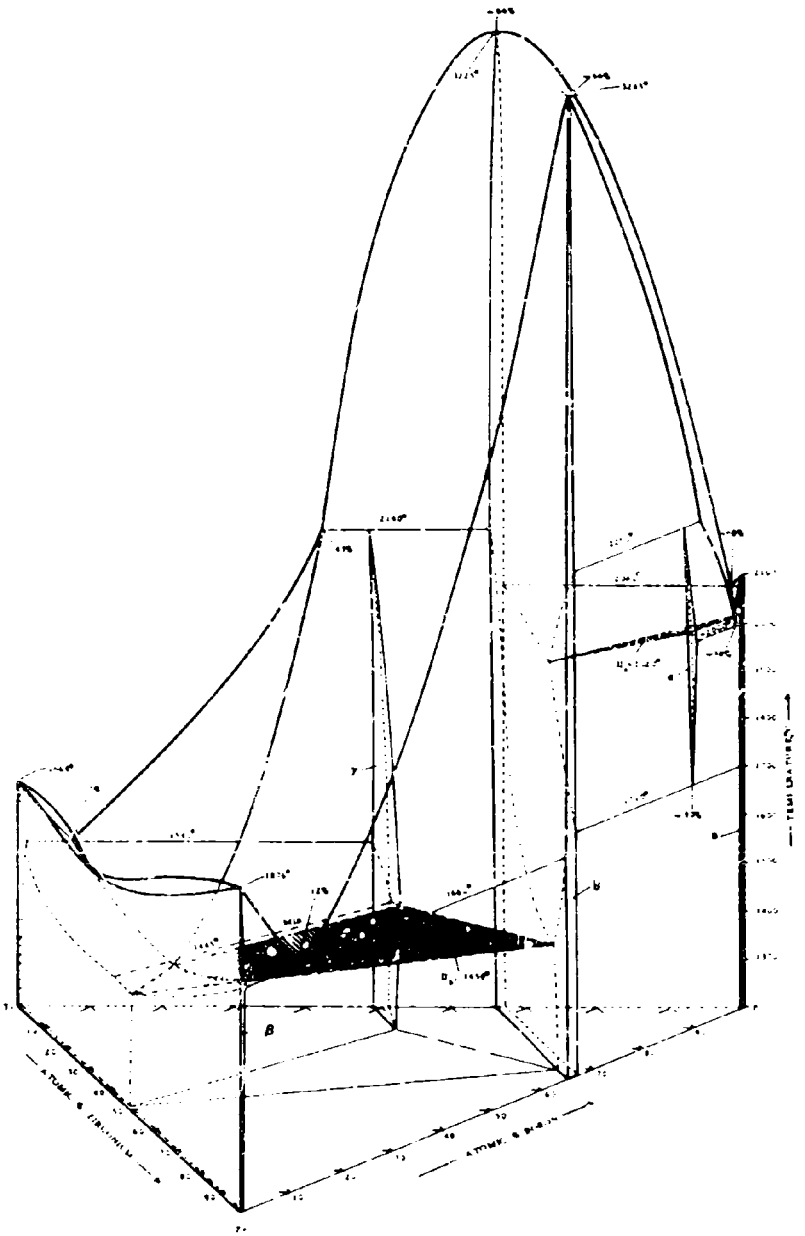

Figure III.I.1.1 Isometric View of the Ti-Zr-B System

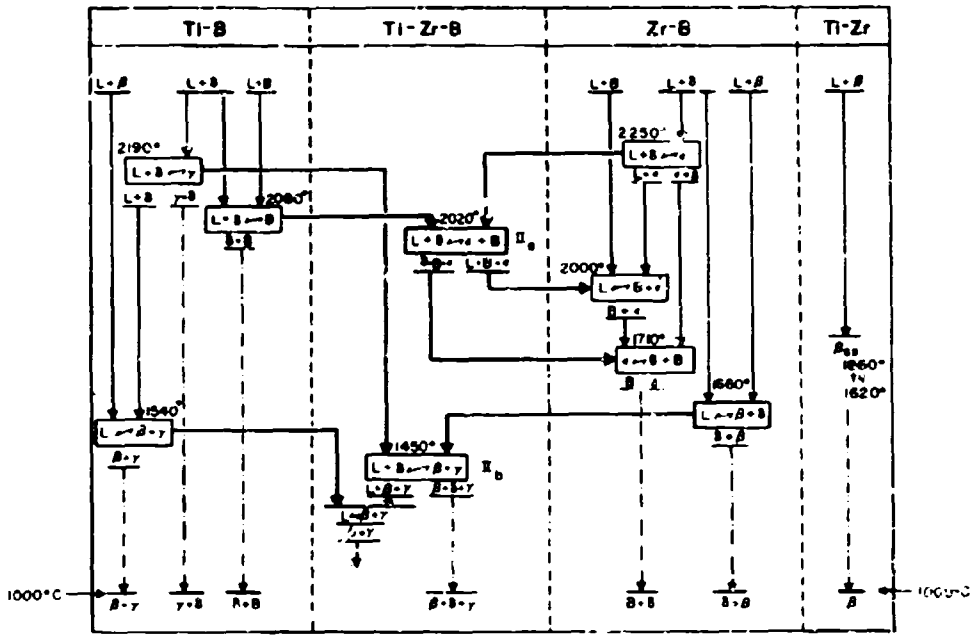

Figure III.I.1.2 Reaction Diagram for the Ti-Zr-B System

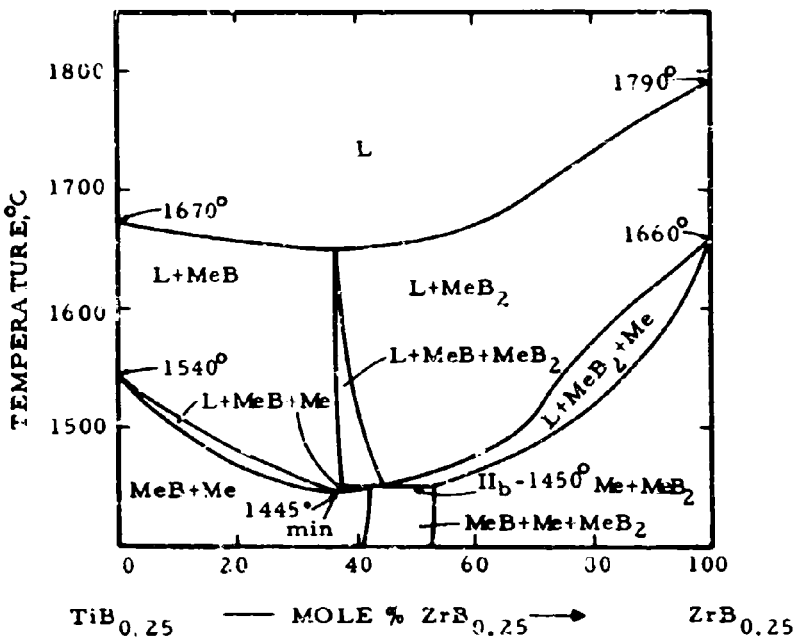

Figure III.I.1.3. Ti-Zr-B: Isopleth at 30 At.% B

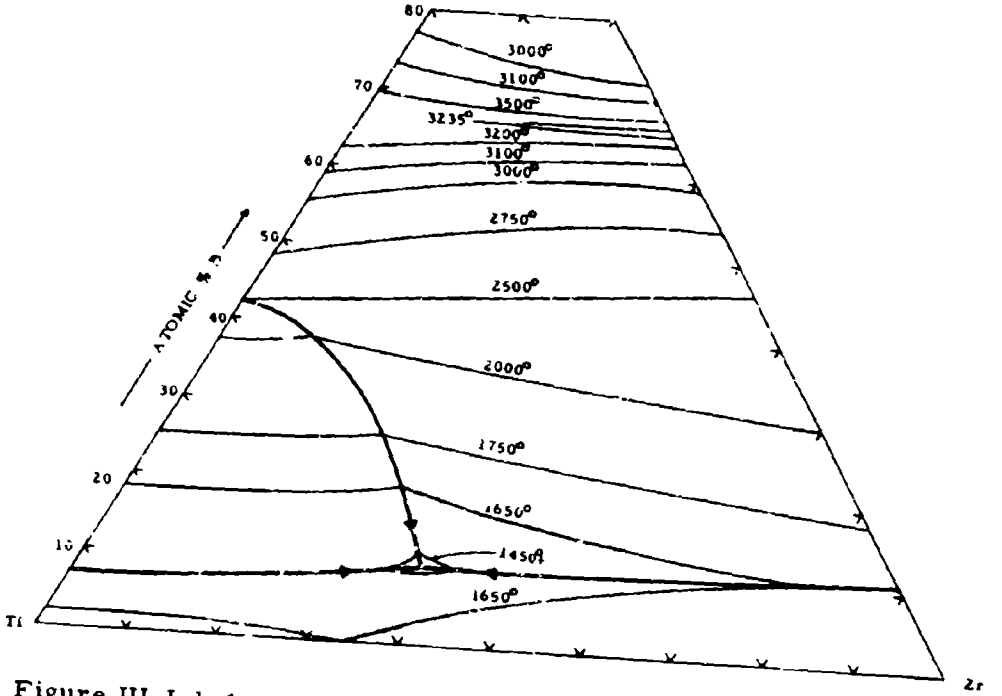

Figure III.I.1.4. Liquidus Projection in the Ti-Zr-B System

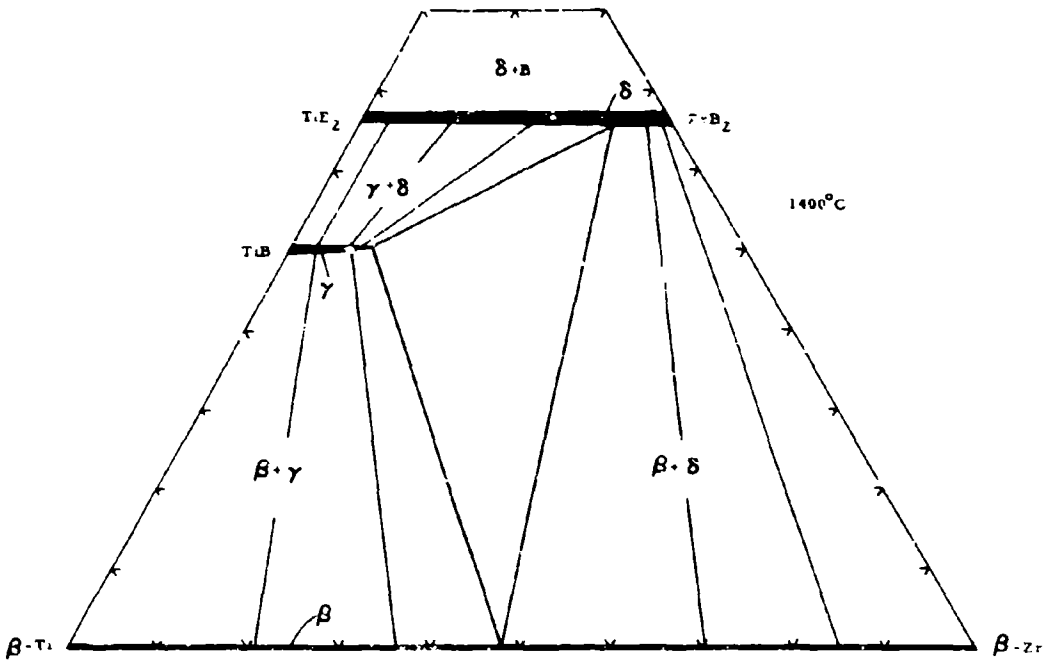

Figure III.1.1.5. Isothermal Section of the Ti-Zr-B System at 1400°C

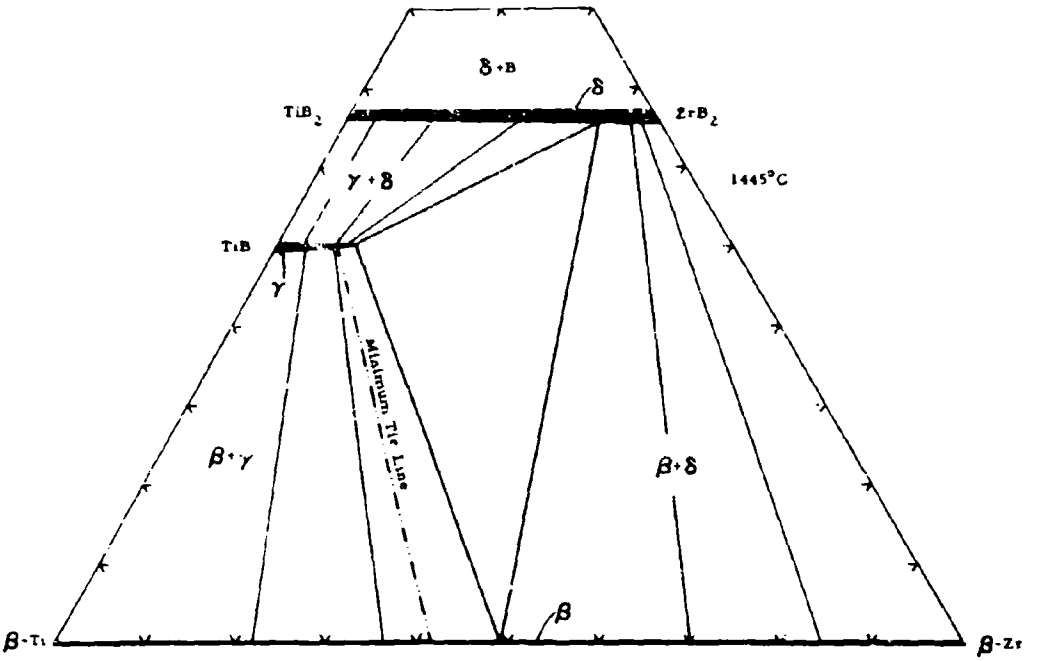

Figure III.1.1.6. Isothermal Section of the Ti-Zr-B System at 1445°C

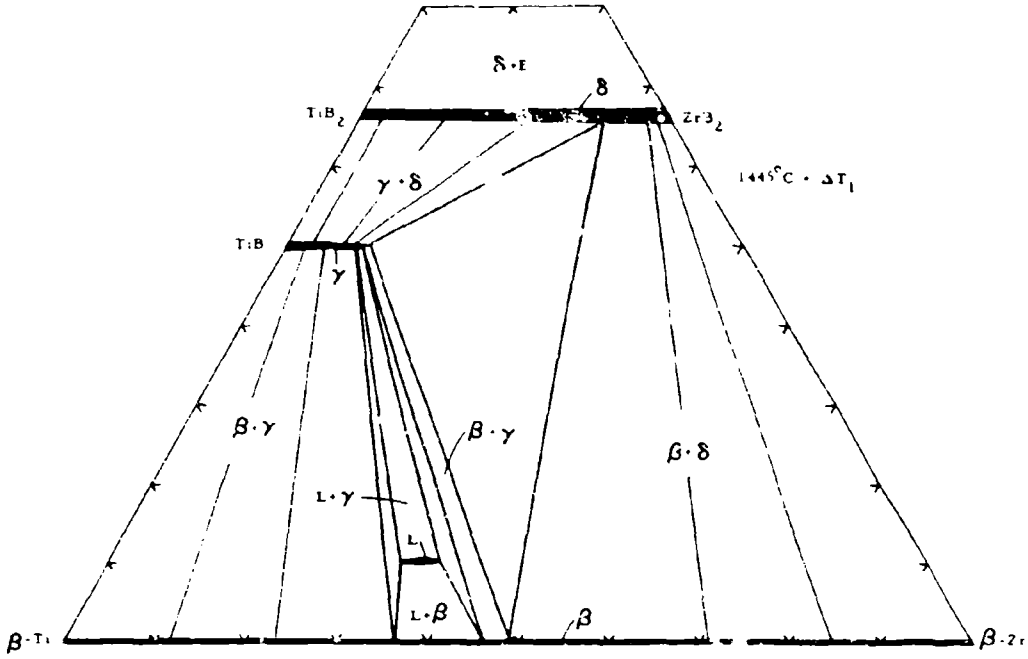

Figure III.1.1.7. Isothermal Section of the Ti-Zr-B System Slightly Above 1445°C

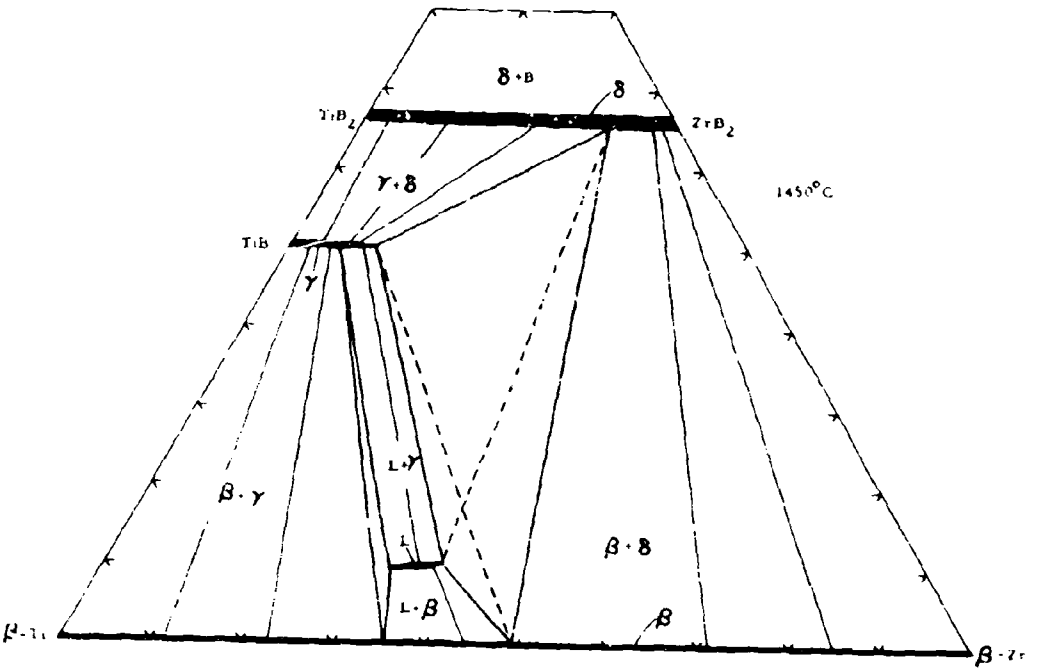

Figure III.1.1.8. Isothermal Section of the Ti-Zr-B System at 1450°C

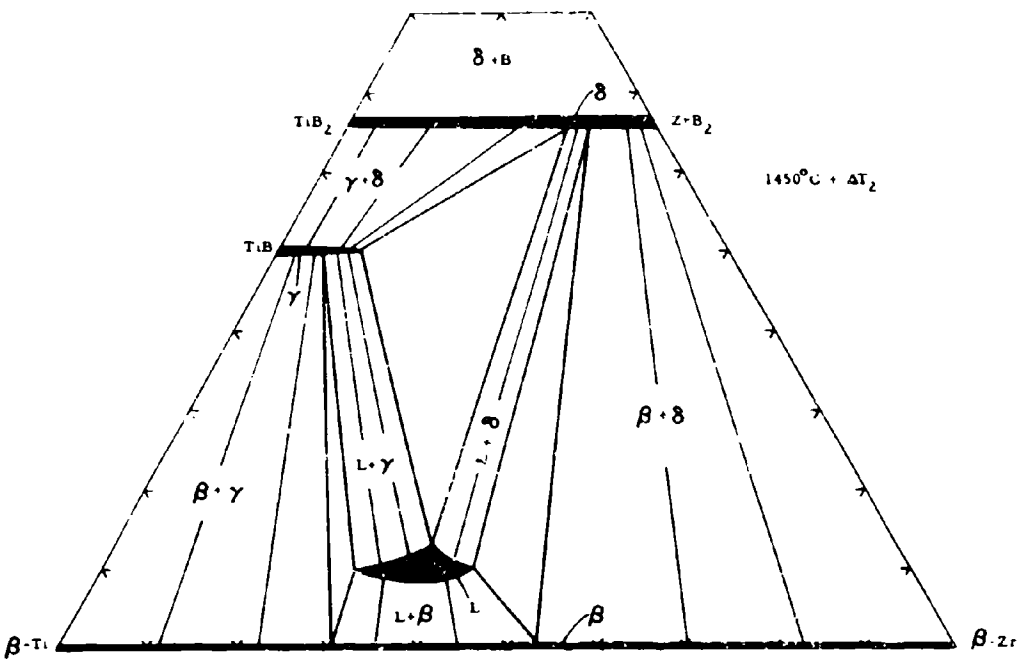

Figure III.1.1.9. Isothermal Section of the Ti-Zr-B System Slightly Above 1450° C

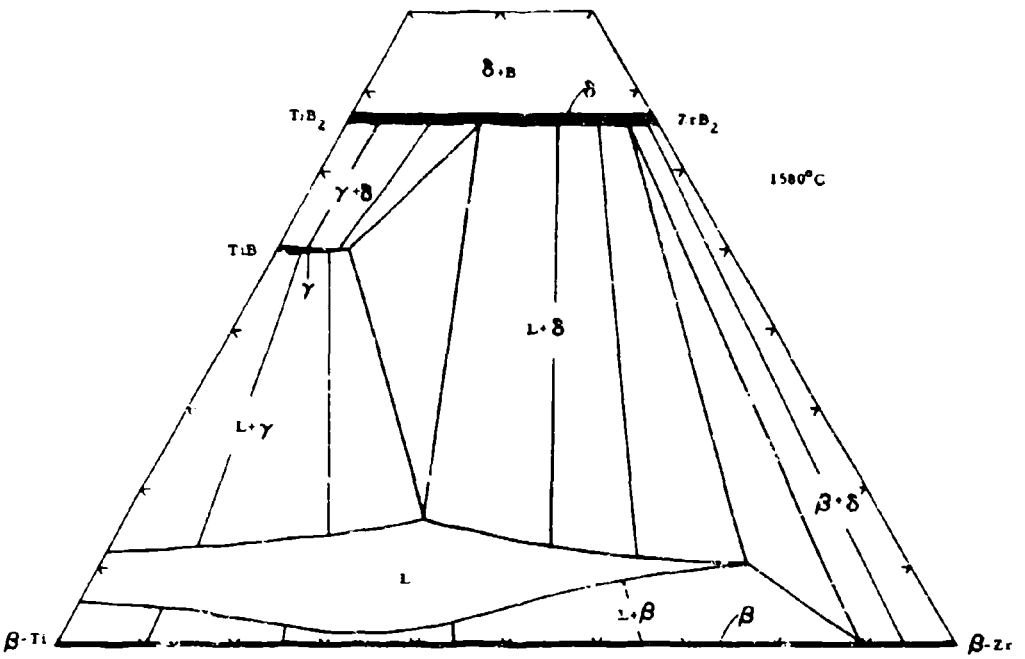

Figure III.1.1.10. Isothermal Section of the Ti-Zr-B System at 1580°C

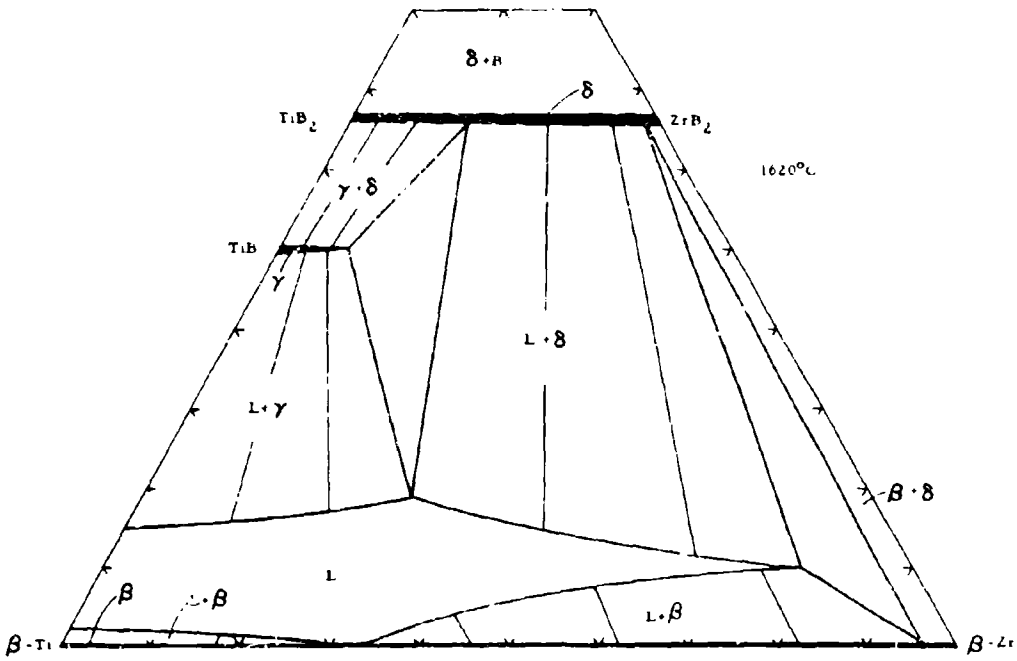

Figure III.1.1.11. Isothermal Section of the Ti-Zr-B System at 1620°C

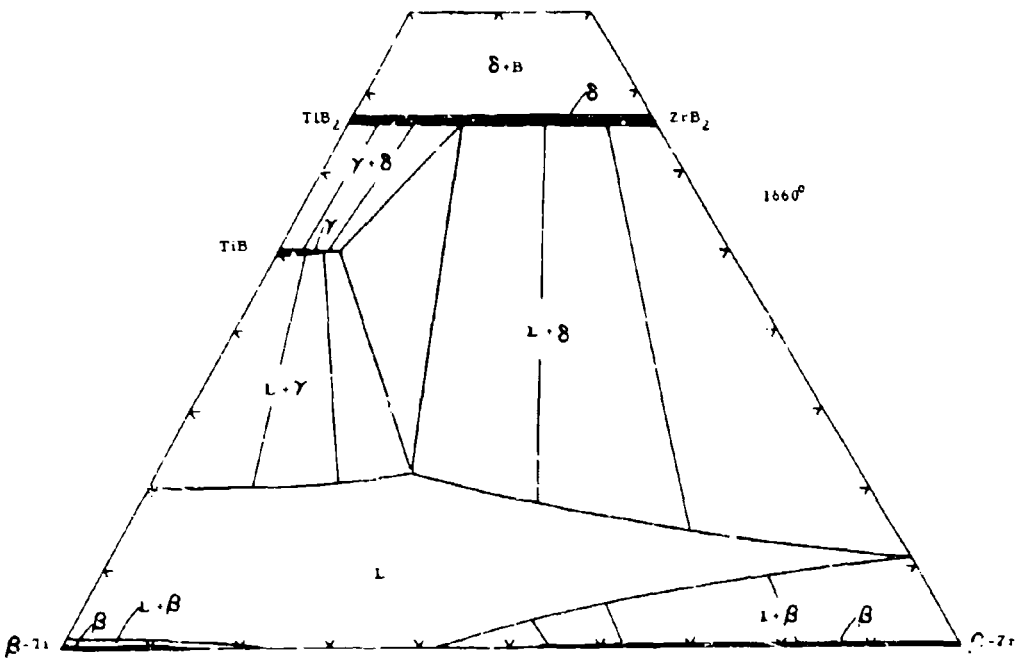

Figure III.I.1.12. Isothermal Section of the Ti-Zr-B System at 1660° C

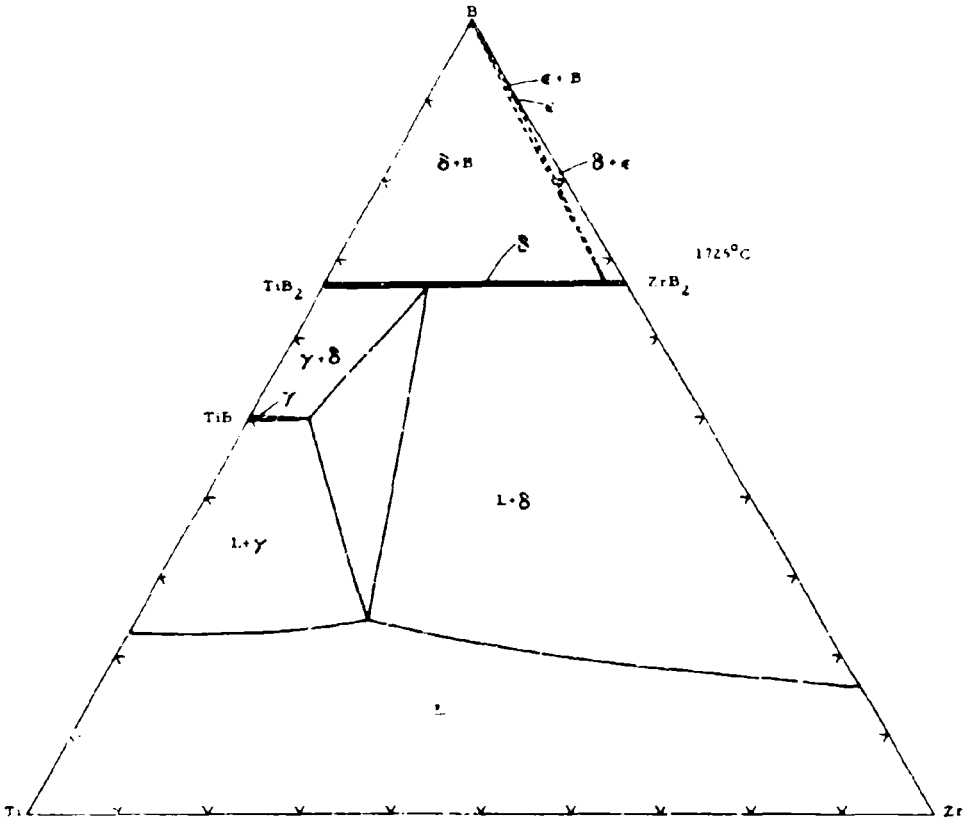

Figure III.1.1.13. Isothermal Section of the Ti-Zr-B System at 1725° C

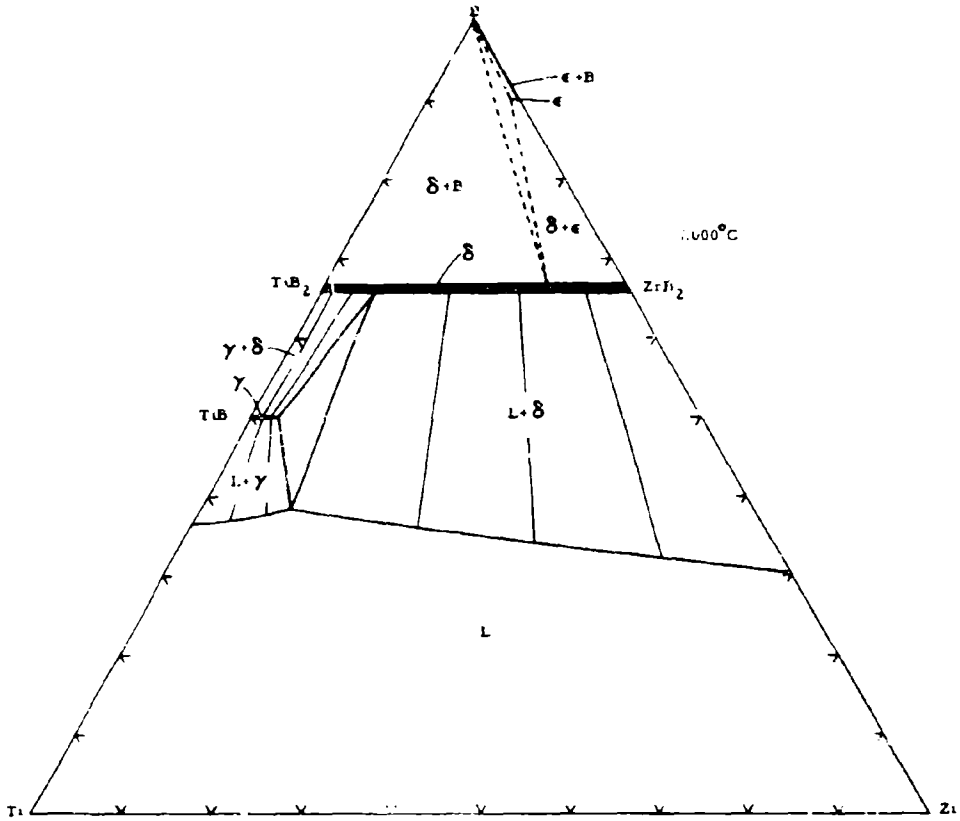

Figure III.I.1.14. Isothermal Section of the Ti-Zr-B System at 2000°C

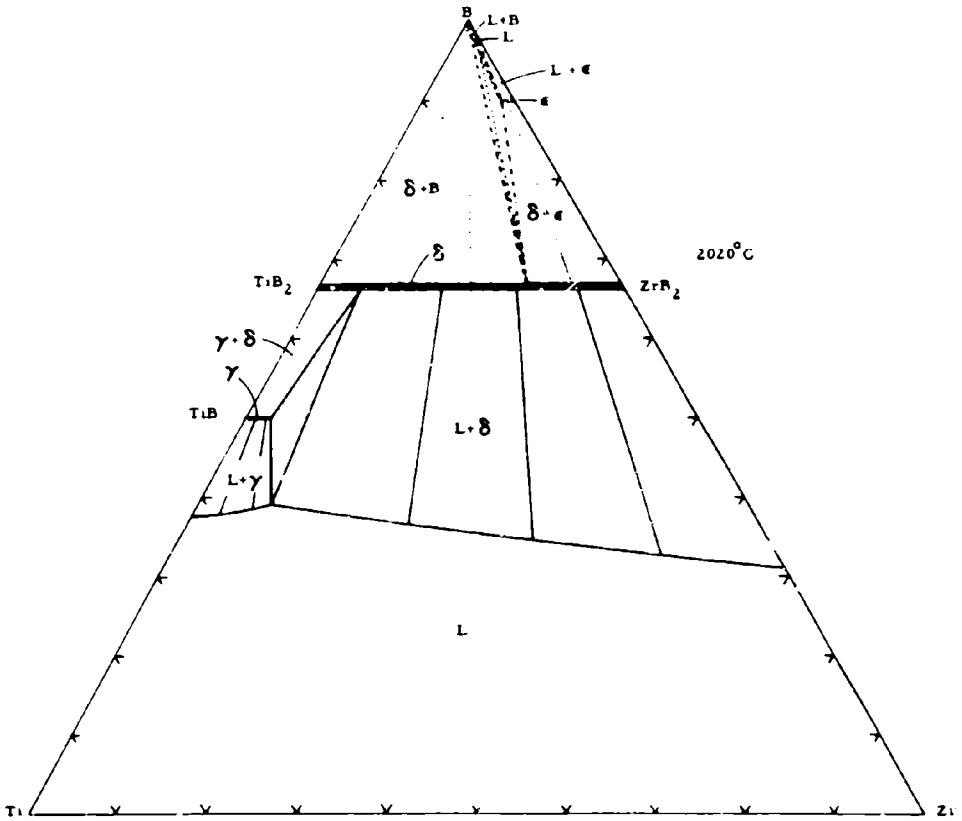

Figure III.I.1.15. Isothermal Section of the Ti-Zr-B System at 2020°C

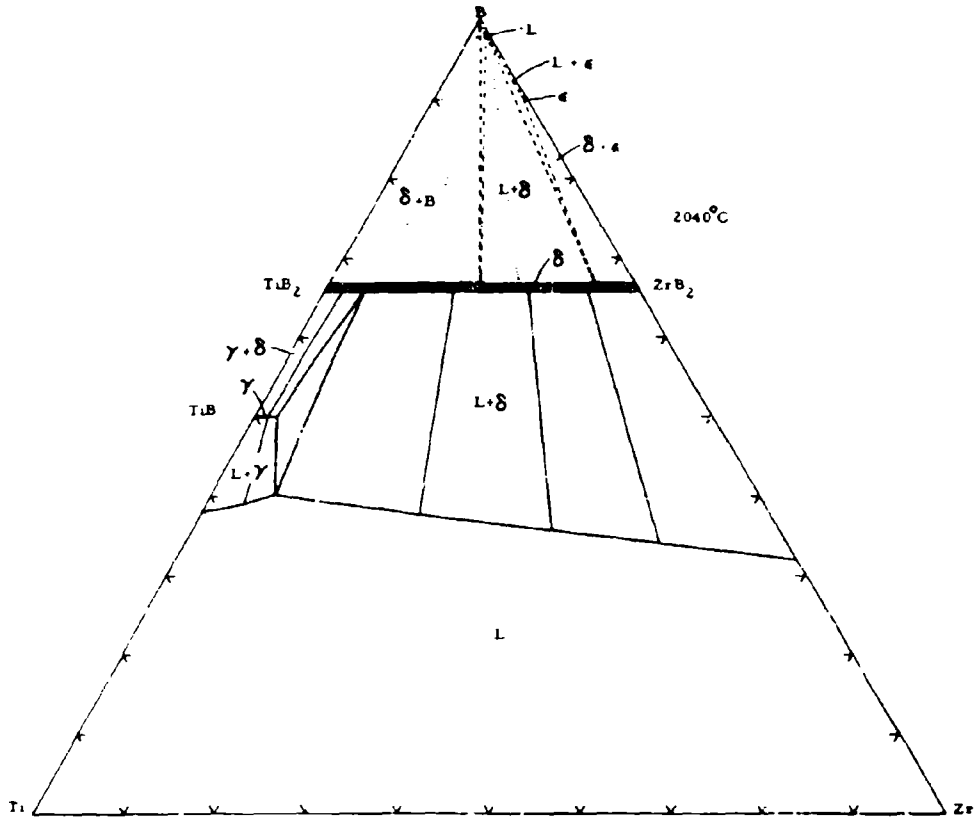

Figure III.1.1.16. Isothermal Section of the Ti-Zr-B System at 2040°C

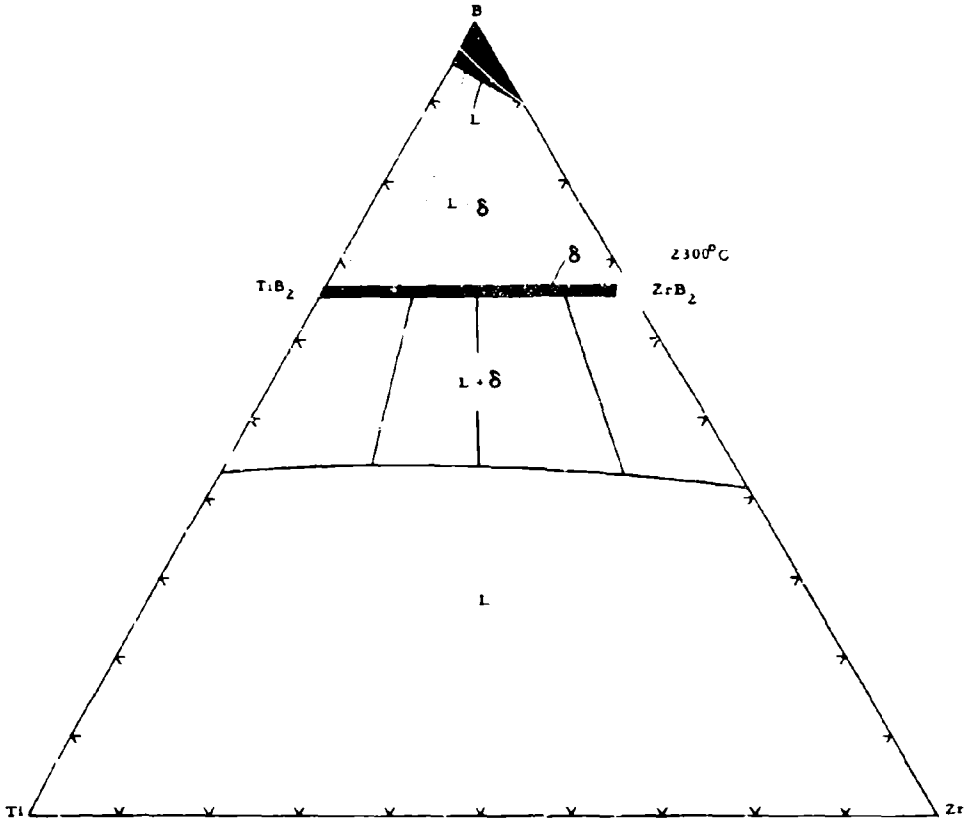

Figure III.1.1.17. Isothermal Section of the Ti-Zr-B System at 2300° C

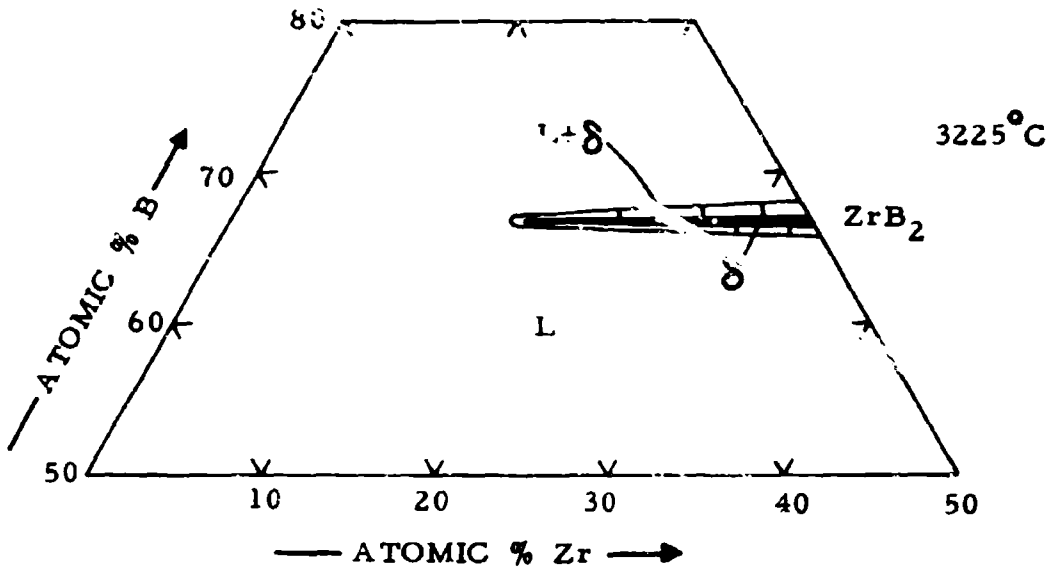

Figure III.I.1.18. Isothermal Section of the Ti-Zr-B System at 3225° C

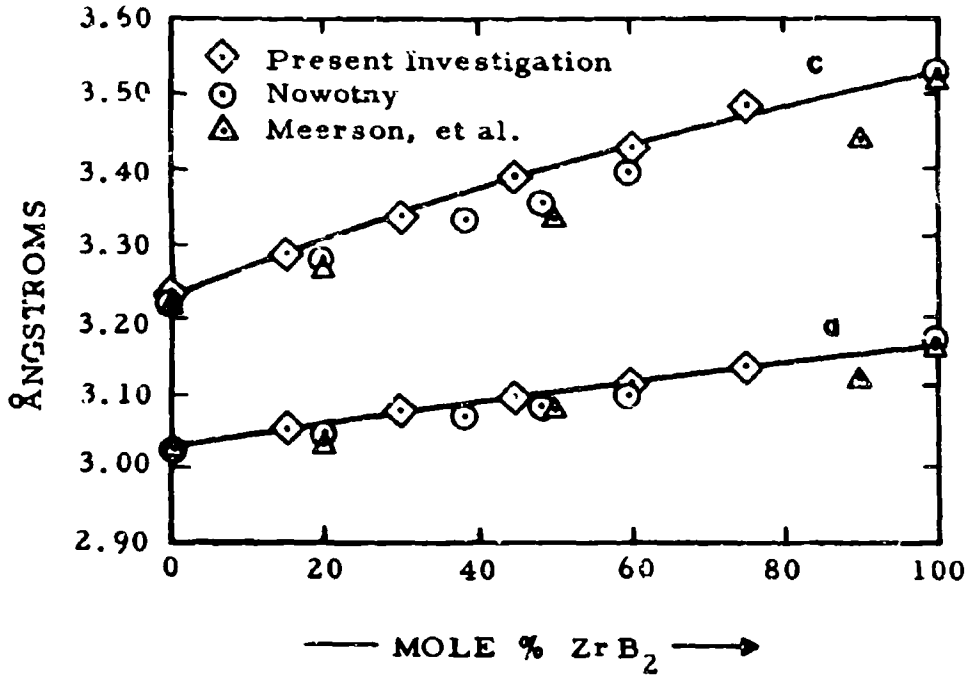

Figure III.I.1.19. Ti-Zr-B: Lattice Parameters of the Diboride Phase

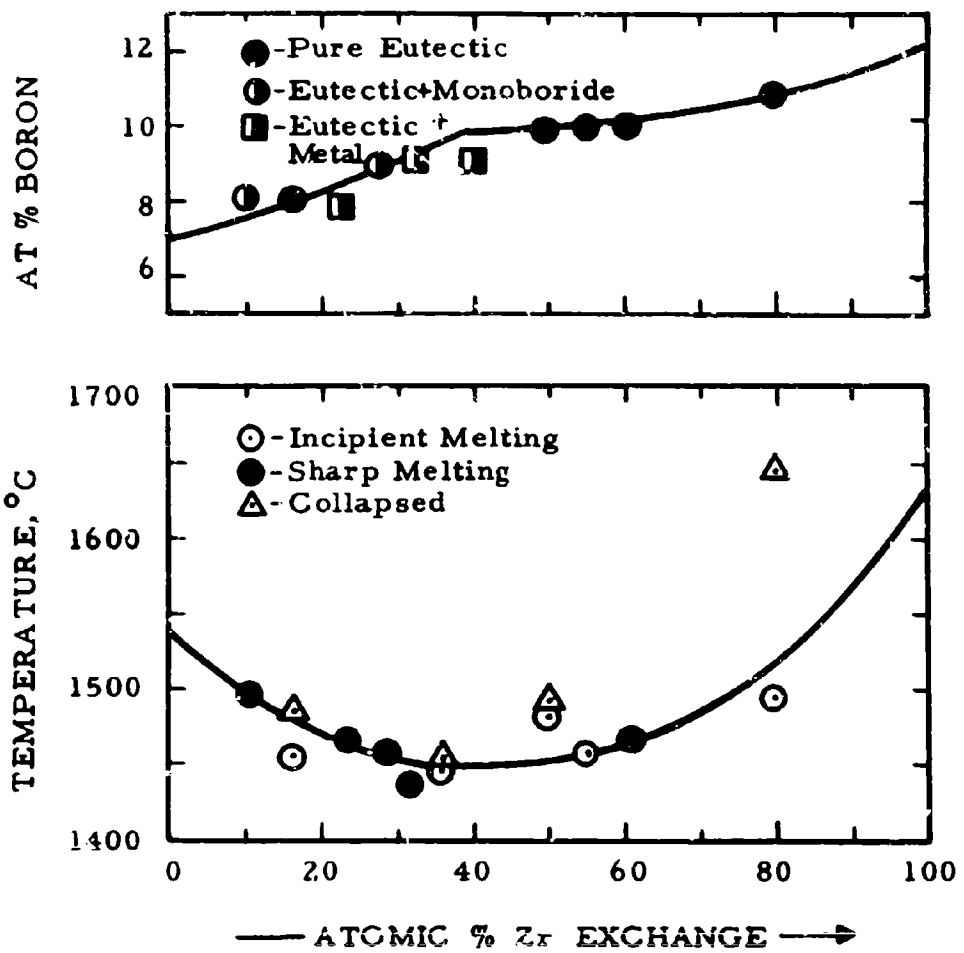

Figure III.I.1.20. Melting (Bottom) Along the Metal-Rich Eutectic Trough (Top) in the Ti-Zr-B System

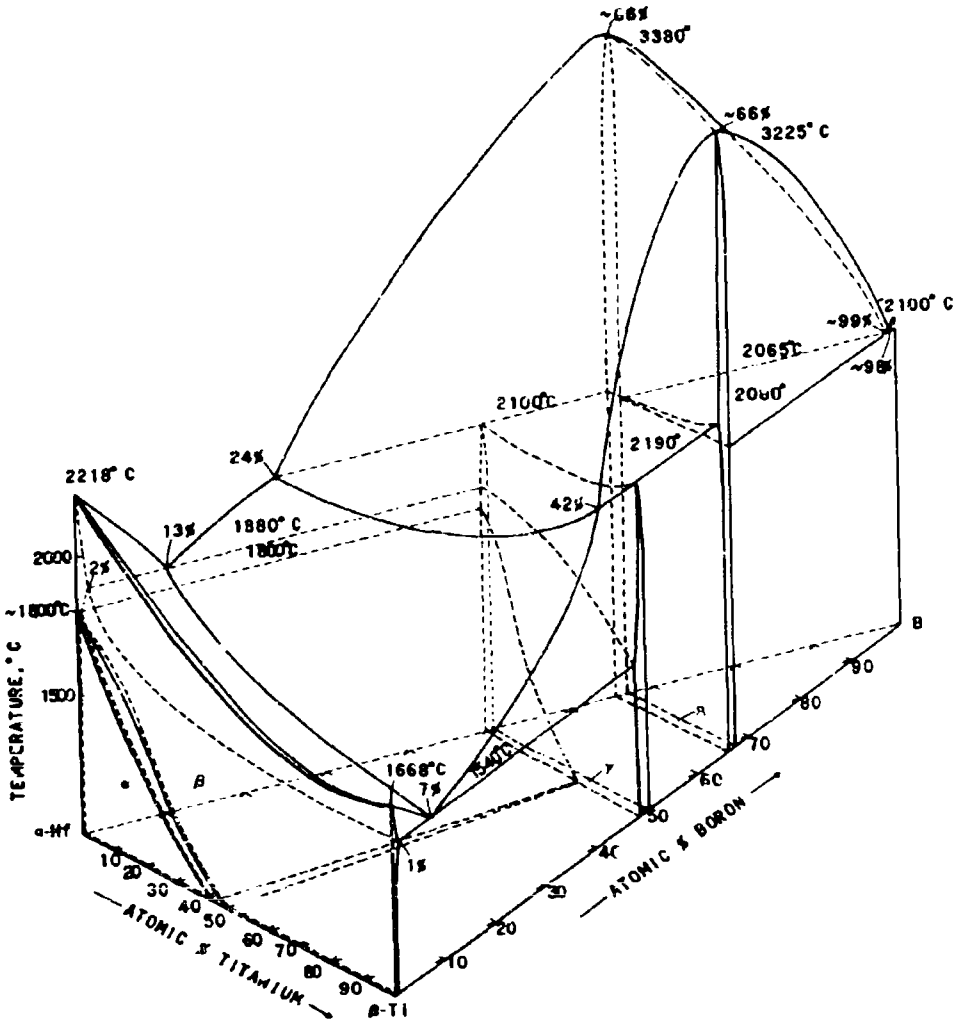

Figure III.I.2.1. Constitution Diagram of the System Ti-Hf-B

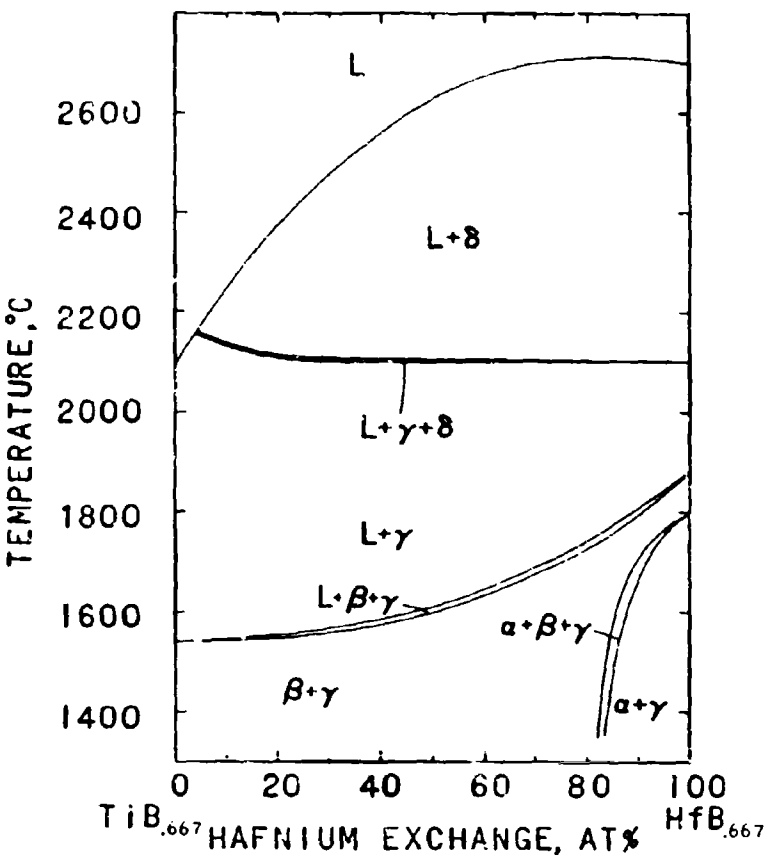

Figure III.I.2.2. Ti-Hf-B. Isopleth at 40 At.% B

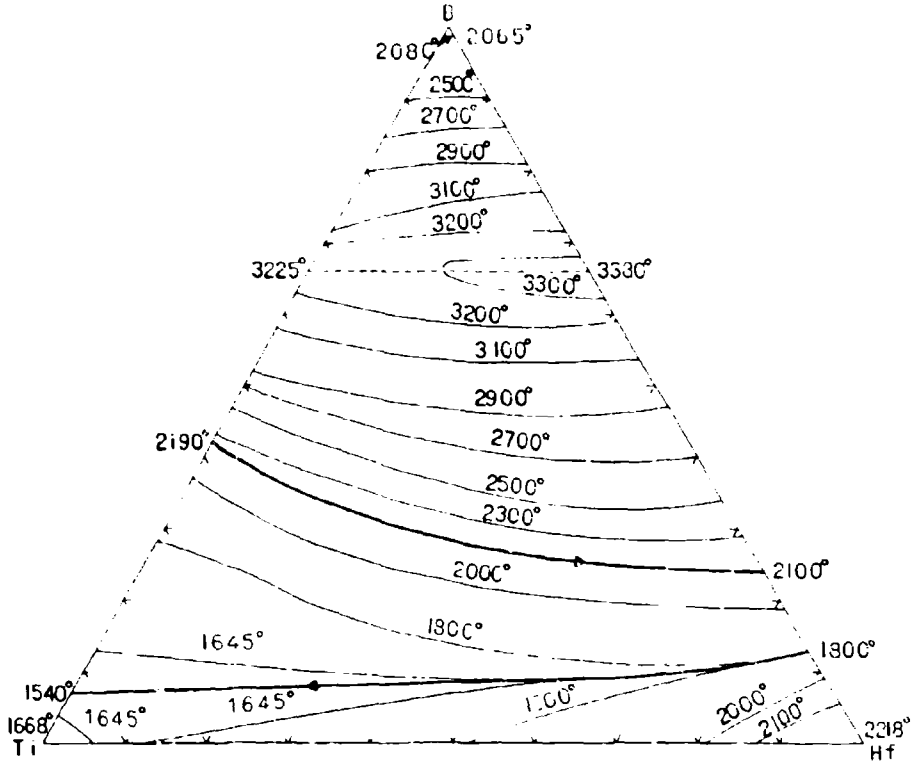

Figure III.1.2.3. Liquidus Projections in the Ti-Hf-B System

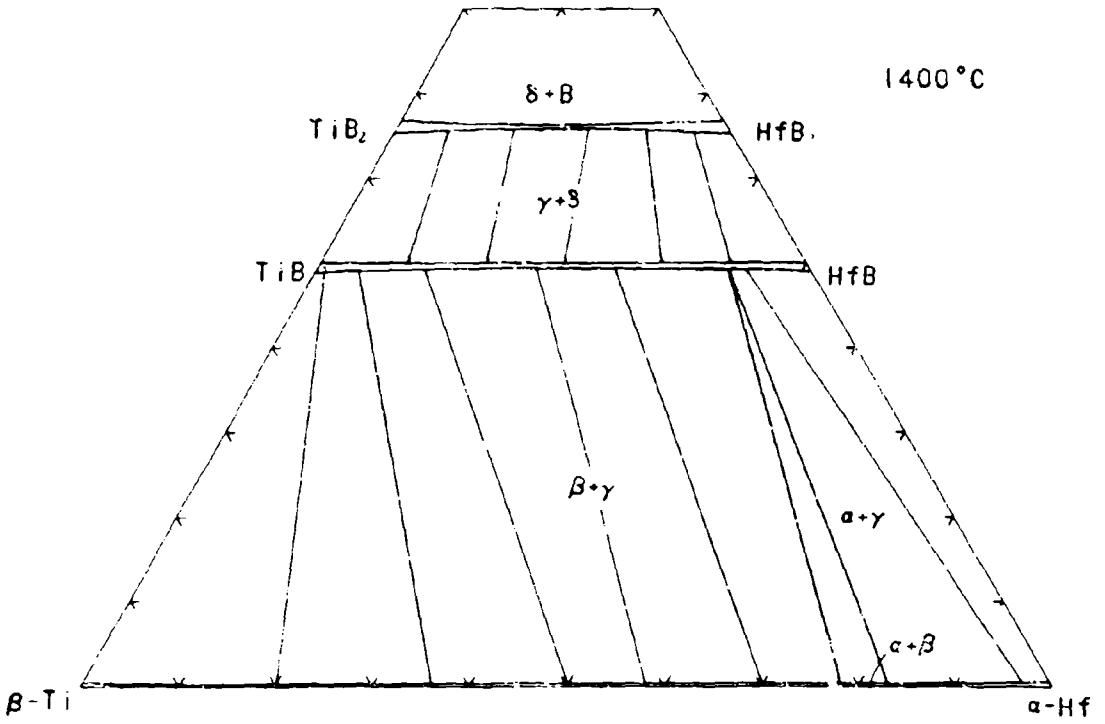

Figure III.1.2.4. Isothermal Section of the Ti-Hf-B System at 1400°C

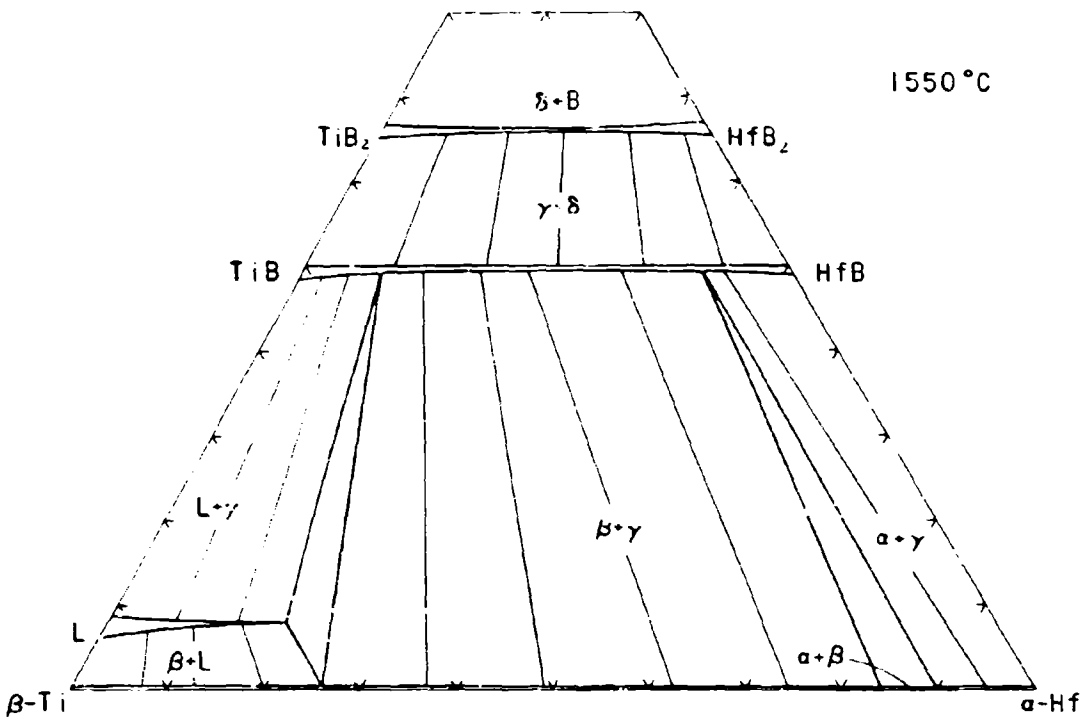

Figure III.I.2.5. Isothermal Section of the Ti-Hf-B System at 1550°C

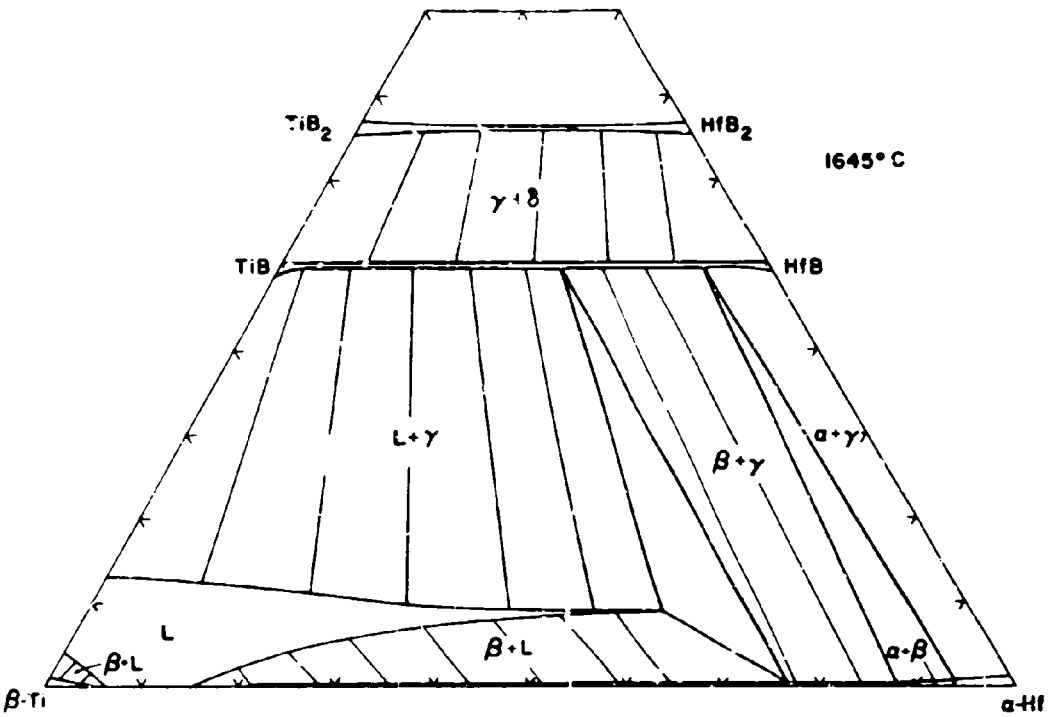

Figure III.I.2.6. Isothermal Section of the Ti-Hf-B System at 1645°C

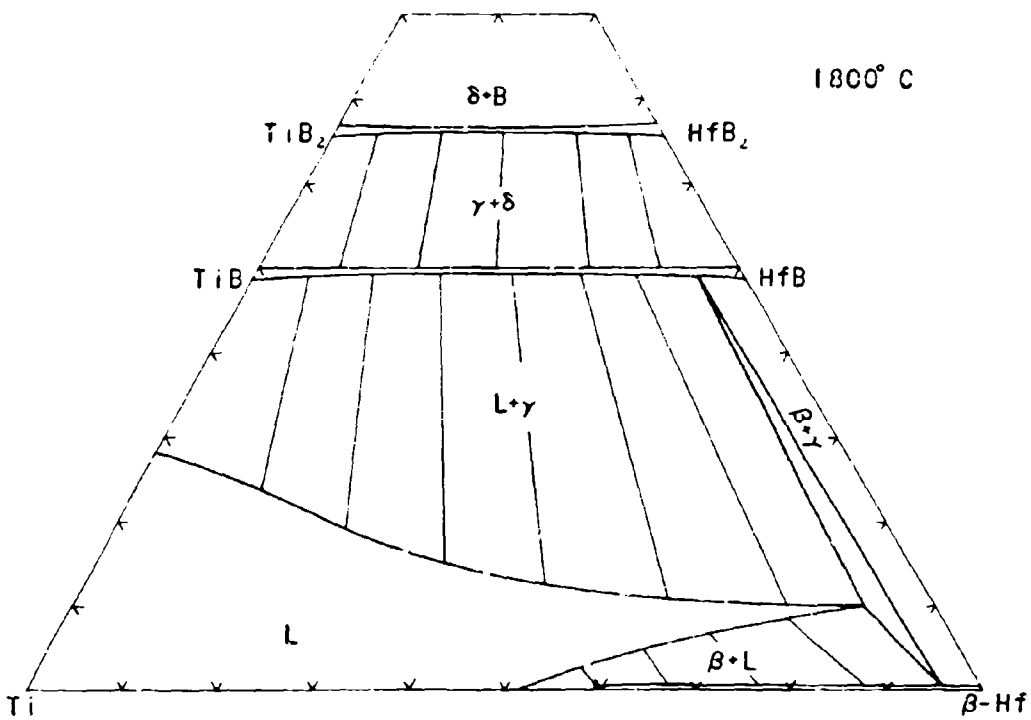

Figure III.I.2.7. Isothermal Section of the Ti-Hf-B System at 1800°C

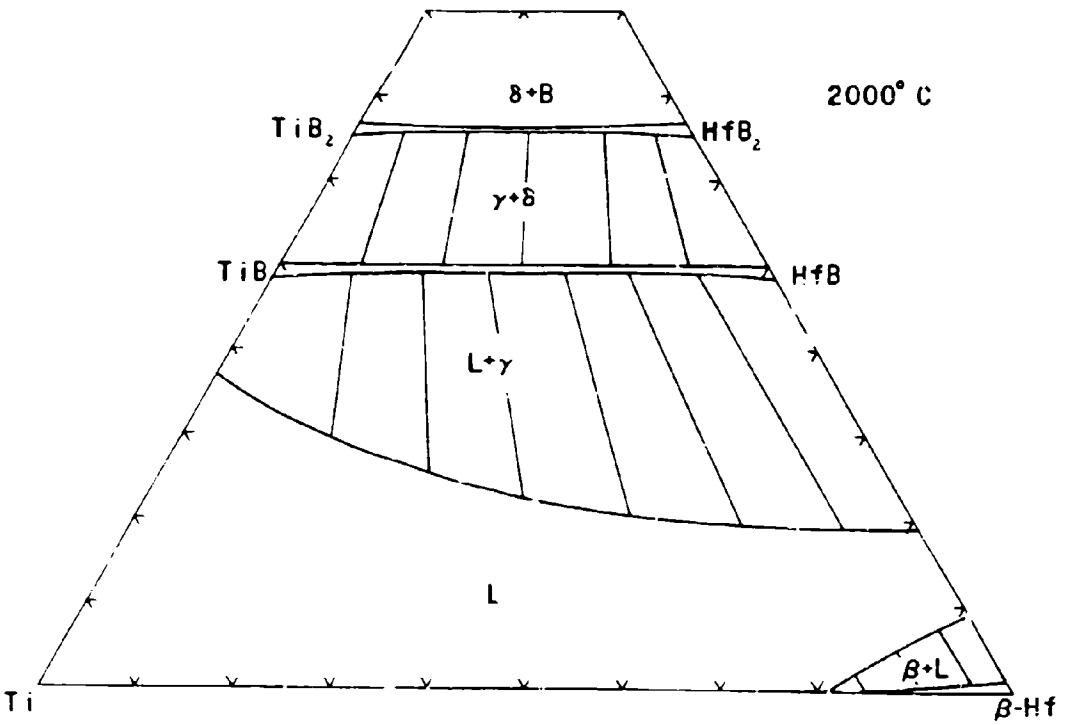

Figure III.I.2.8. Isothermal Section of the Ti-Hf-B System at 2000° C

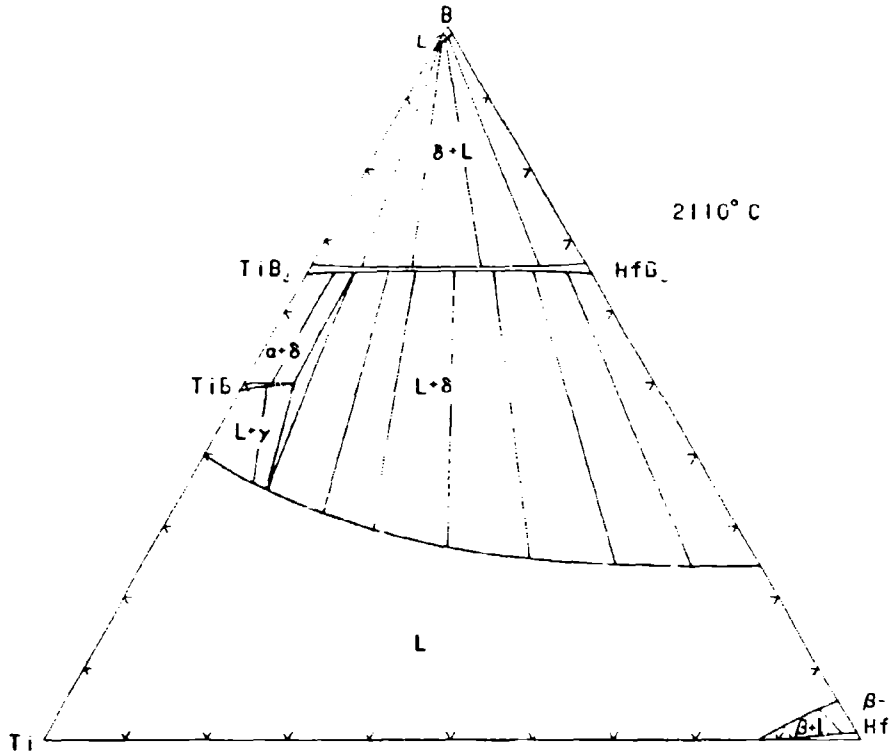

Figure III.I.2.9, Isothermal Section of the Ti-Hf-B System at 2110°C

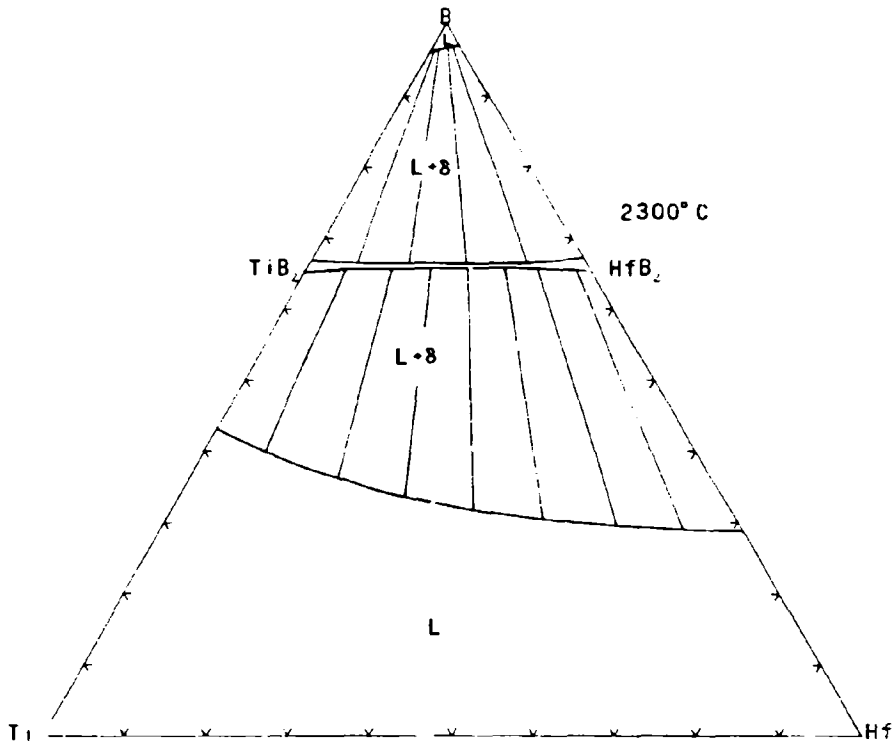

Figure III.I.2.10. Isothermal Section of the Ti-Hf-B System at 2300° C

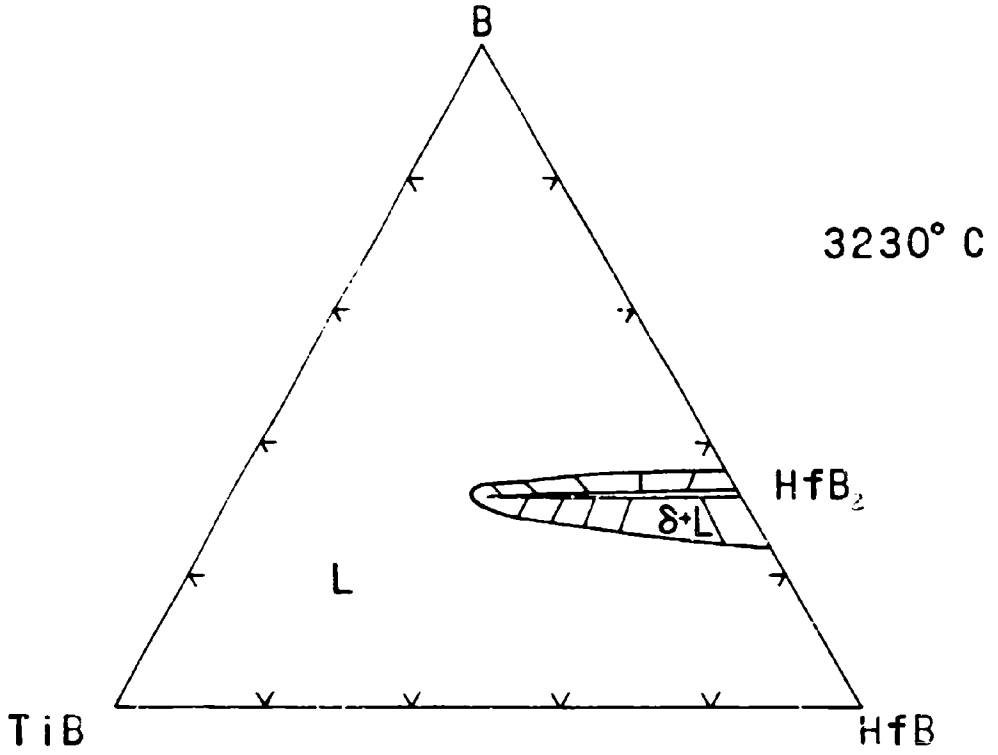

Figure III.I.2.11. Partial Isothermal Section of the Ti-Hf-B System at 3230° C

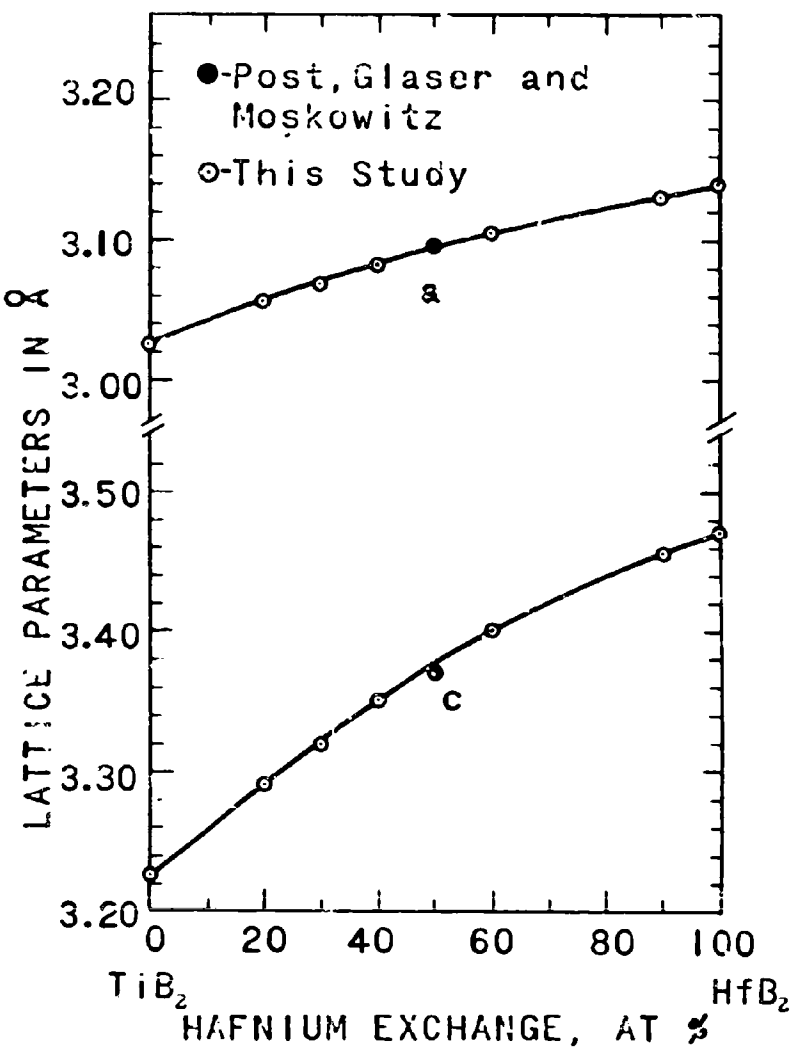

Figure III.I.2.12. Lattice Parameters of the Diboride Solid Solution

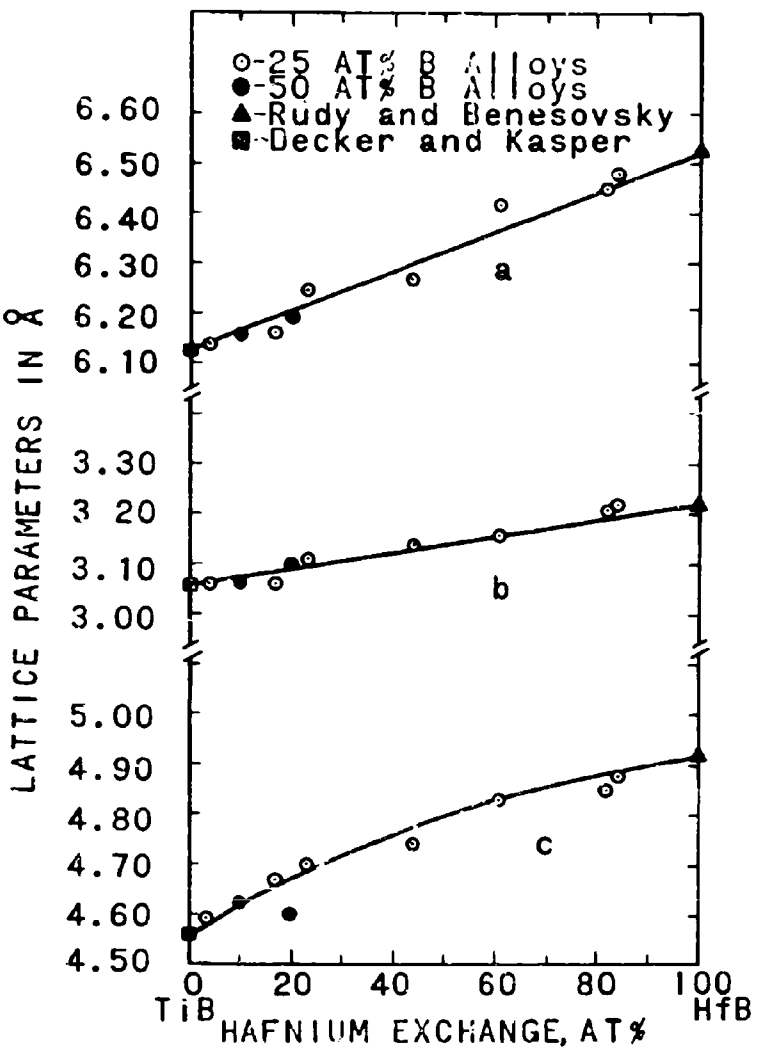

Figure III.1.2.13. Lattice Parameters of the Monoboride Solid Solution

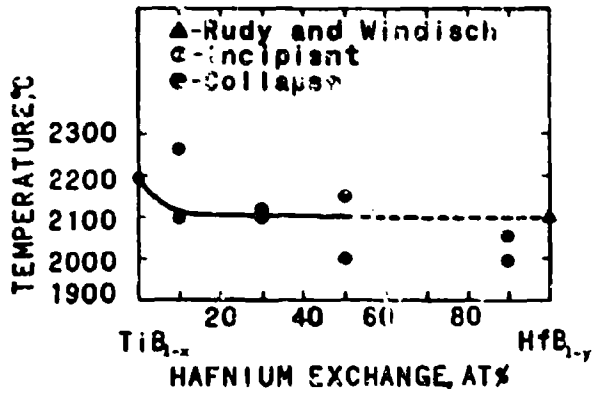

Figure III.H.2.14. Maximum Solidus Temperatures of the Solution (Ti,Hf)B. (Peritectic-Type of Melting).

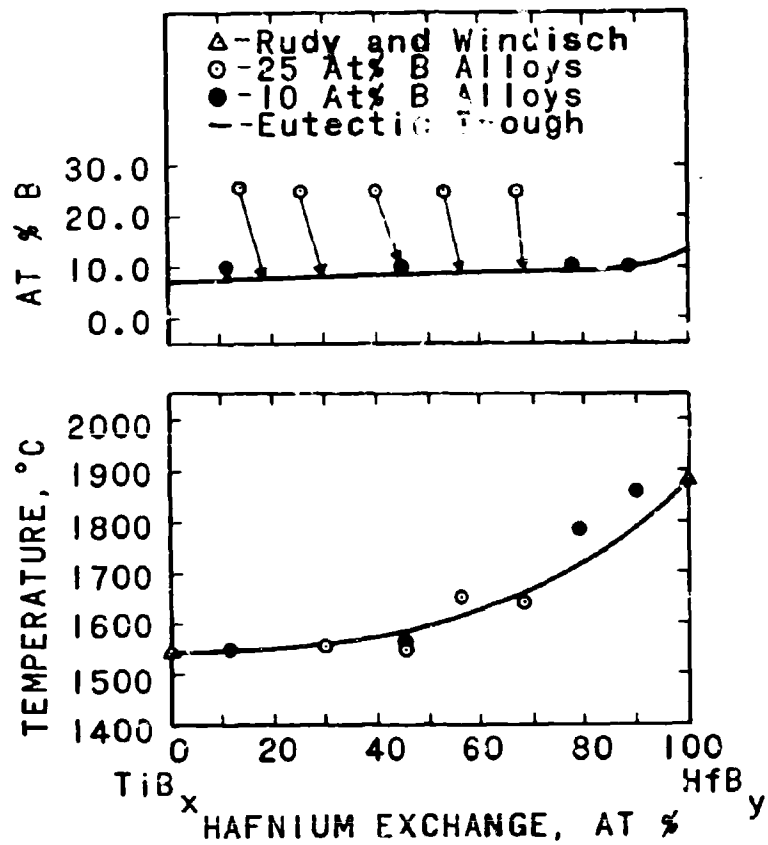

Figure III.I.2.15. Temperatures (Bottom) and Compositions (Top) for the Metal-Rich Eutectic Trough in the Ti-Hf-B System

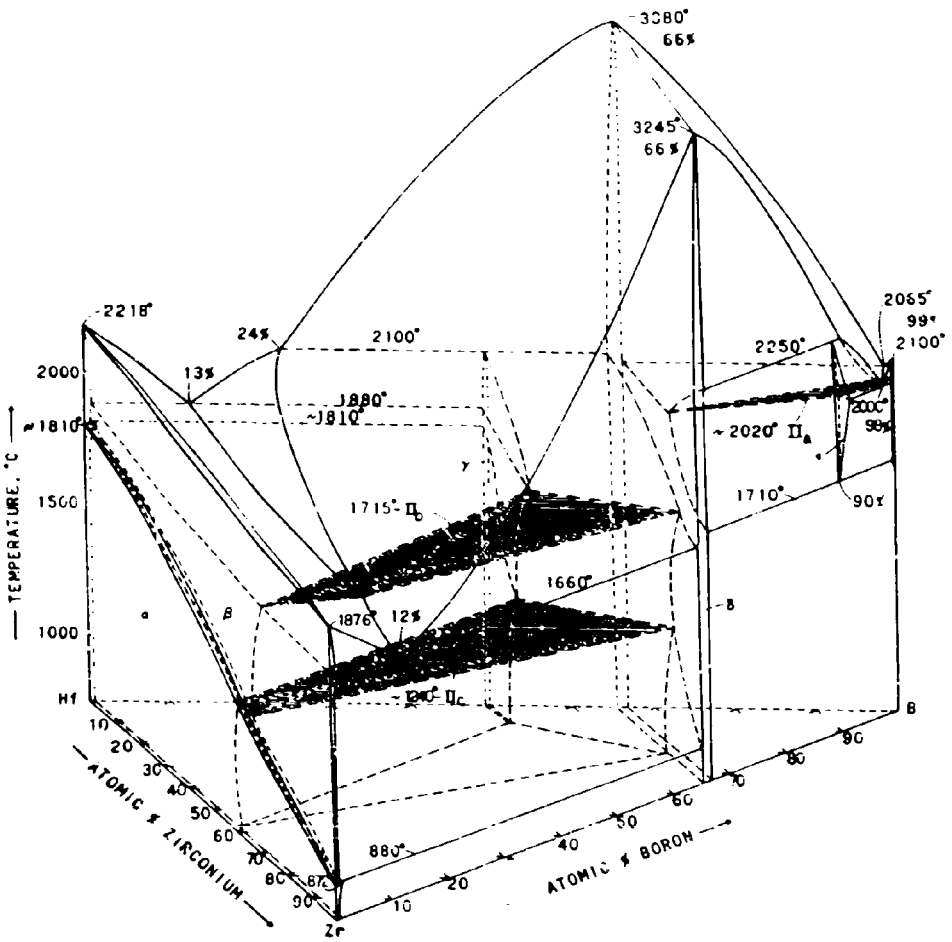

Figure III.I.3.1. Isometric View of the Zr-Hf-B System

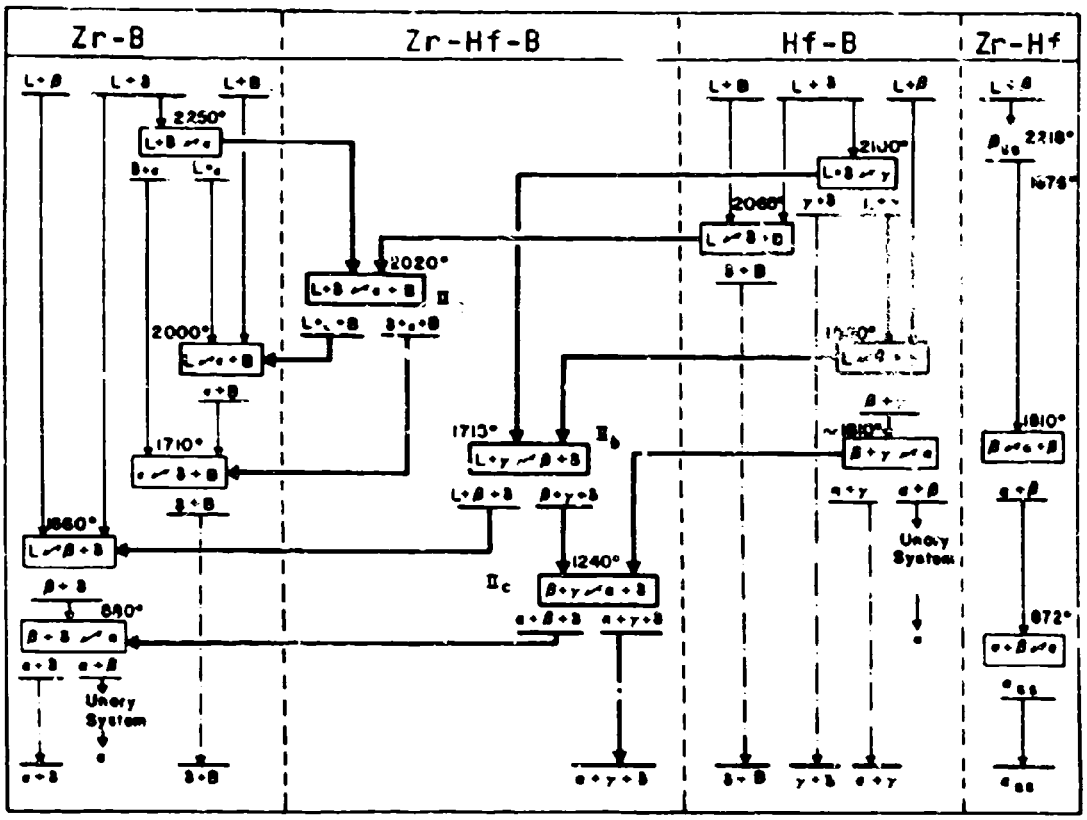

Figure III.1.3.2. Reaction Diagram for the Zr-Hf-B System

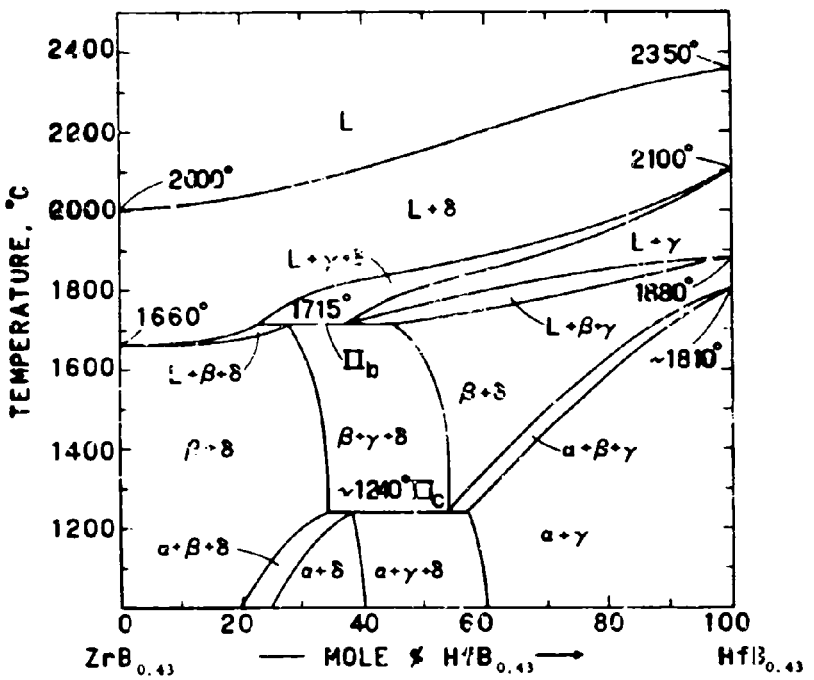

Figure III.1.3.3. Zr-Hf-B: Isopleth at 30 At.% B

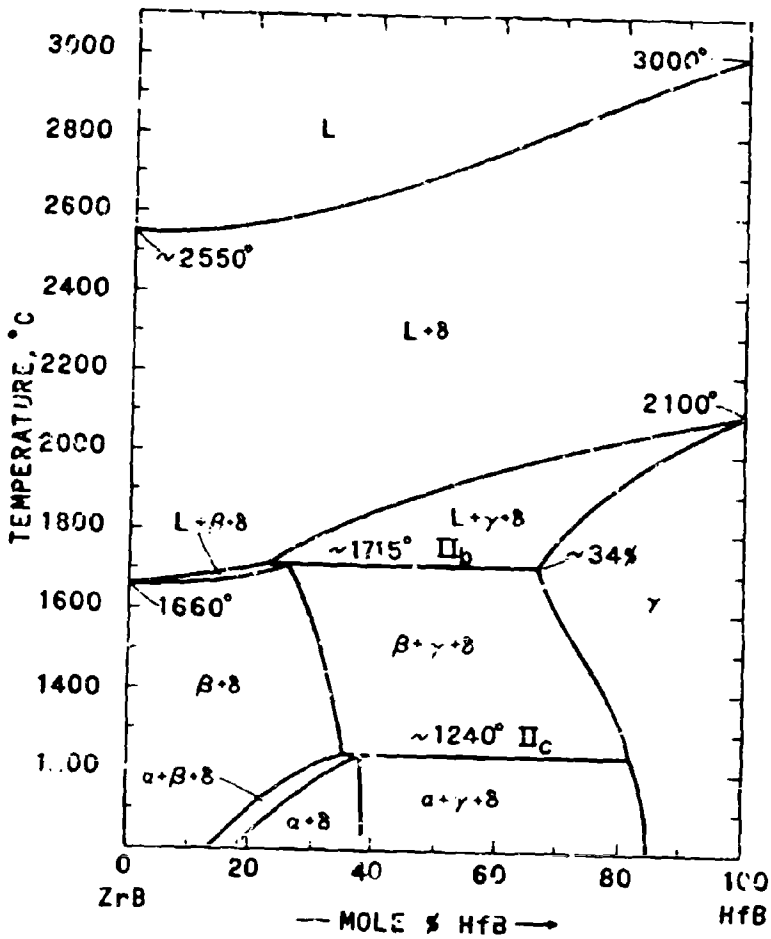

Figure III.I.3.4. Zr-Hf-B: Isopleth at 50 At.% B

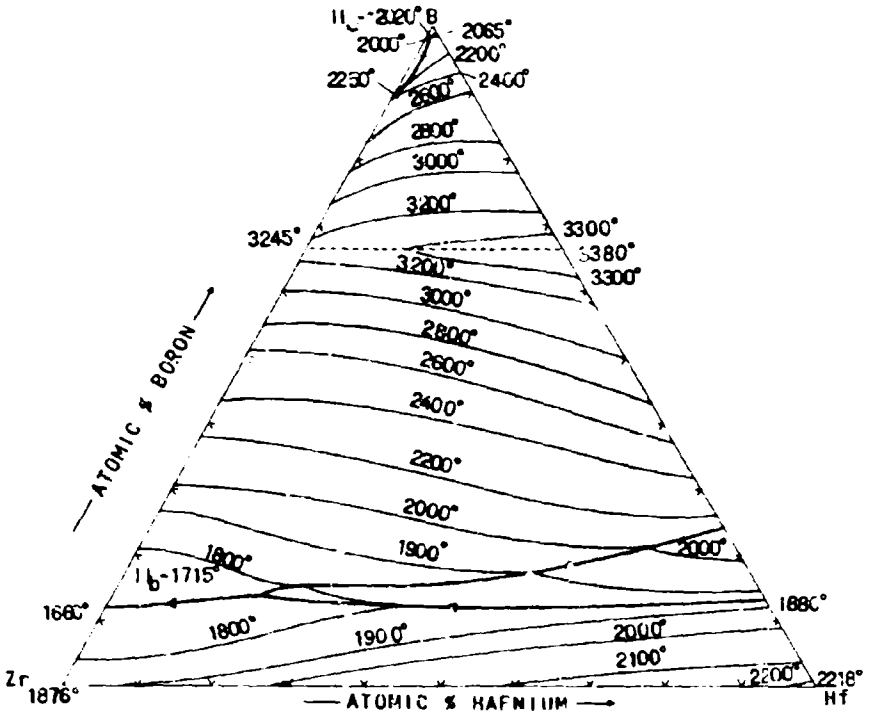

Figure III.I.3.5. Liquidus Projections in the Zr-Hf-B System.

---- Maximum Solidus Temperatures of the $(Zr,Hf)B_2$ Solid Solution

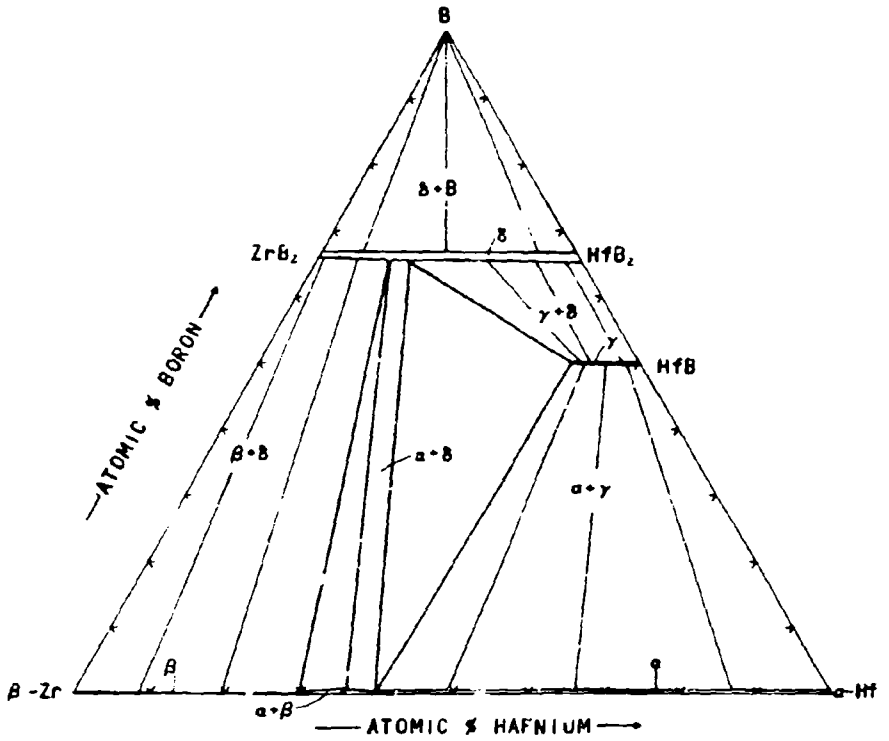

Figure III.I.3.6. Isothermal Section of the Zr-Hf-B System at 1200°C

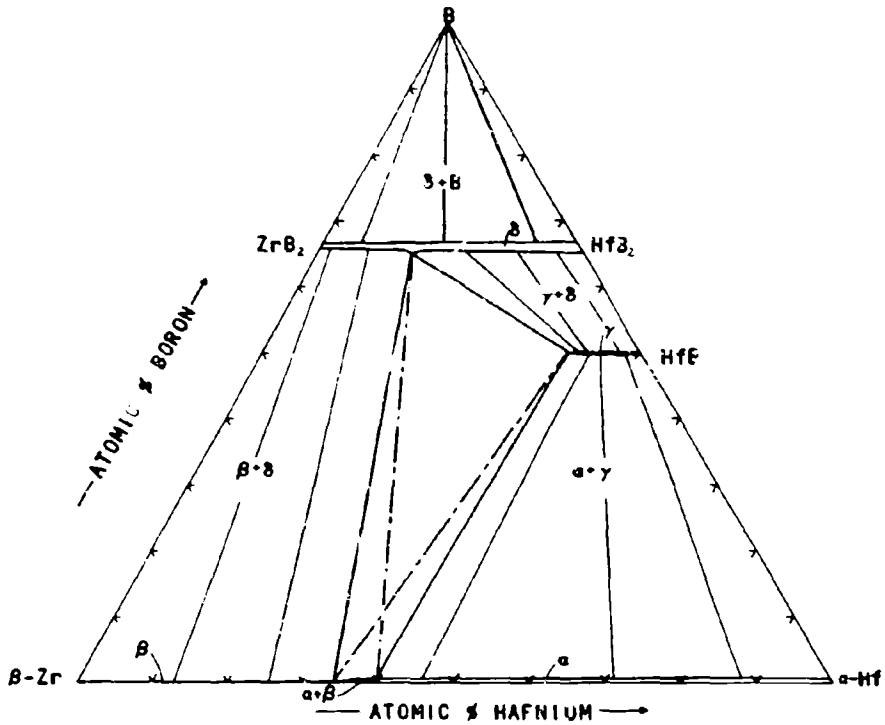

Figure III.I.3.7. Isothermal Section of the Zr-Hf-B System at 1240° C

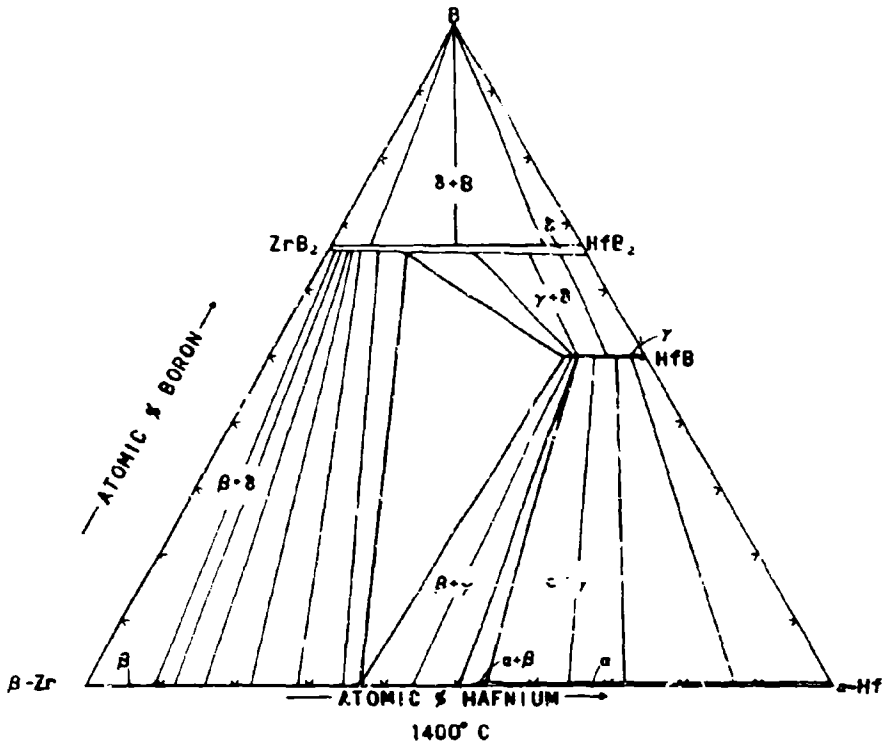

Figure III.I.3.8. Isothermal Section of the Zr-Hf-B System at 1400°C

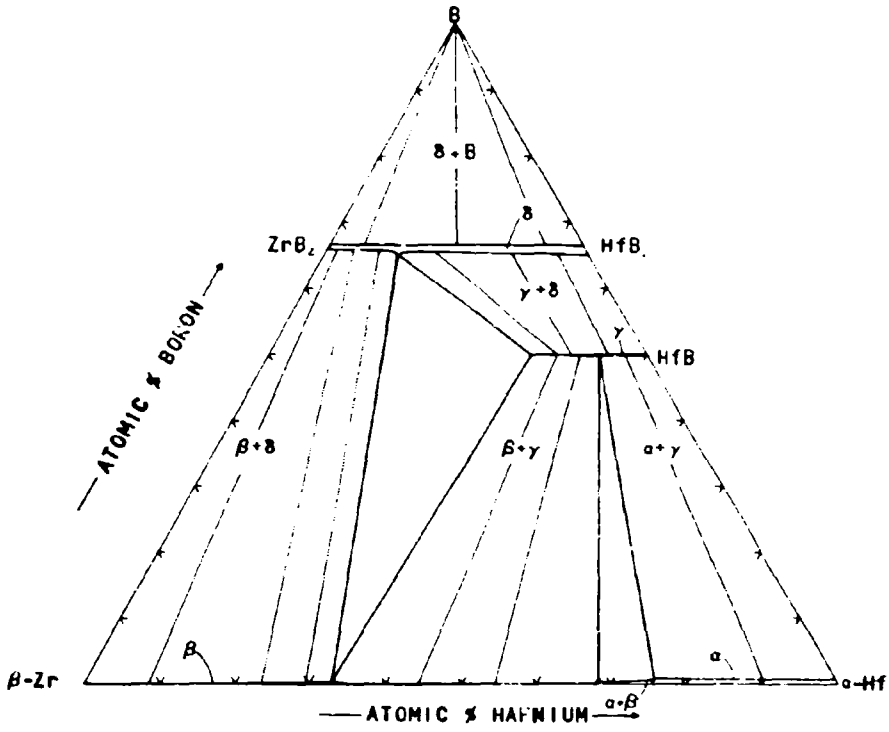

Figure III.I.3.9. Isothermal Section of the Zr-Hf-B System at 1600°C

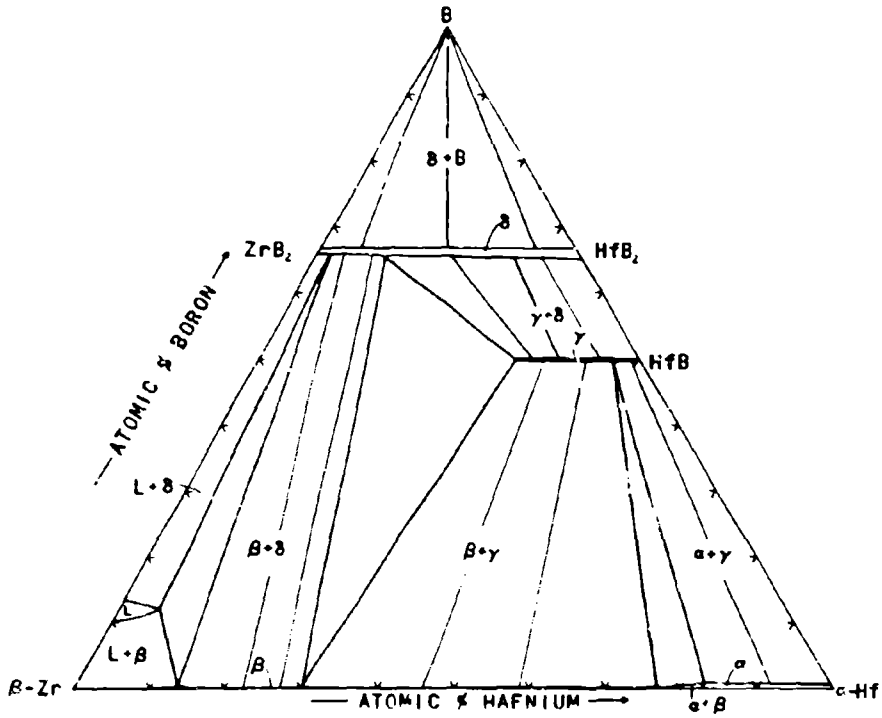

Figure III.I.3.10. Isothermal Section of the Zr-Hf-B System at 1675°C

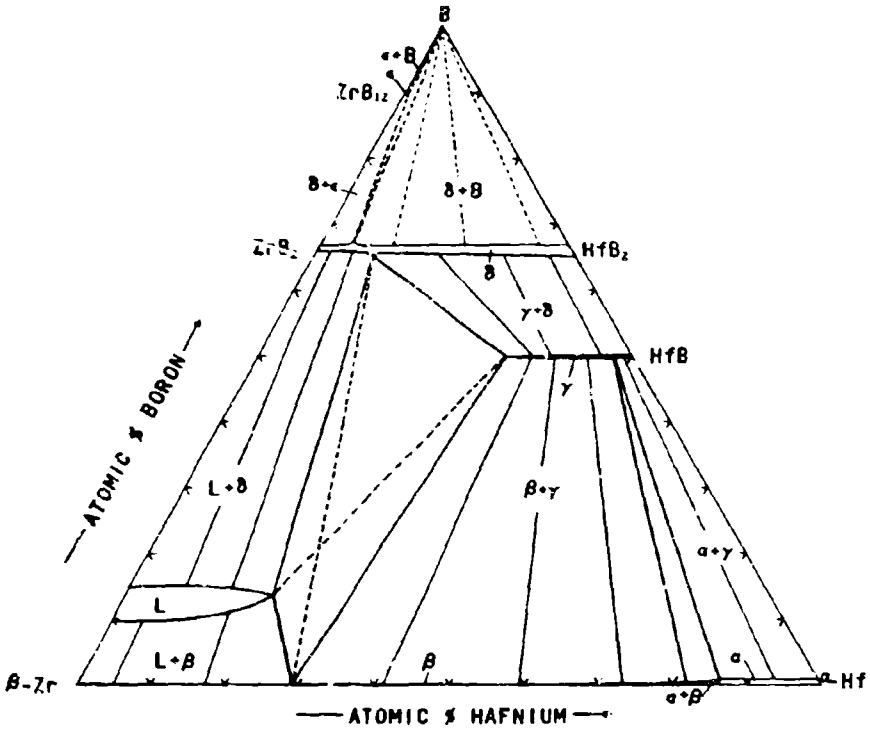

Figure III.1.3.11. Isothermal Section of the Zr-Hf-B System at 1715° C

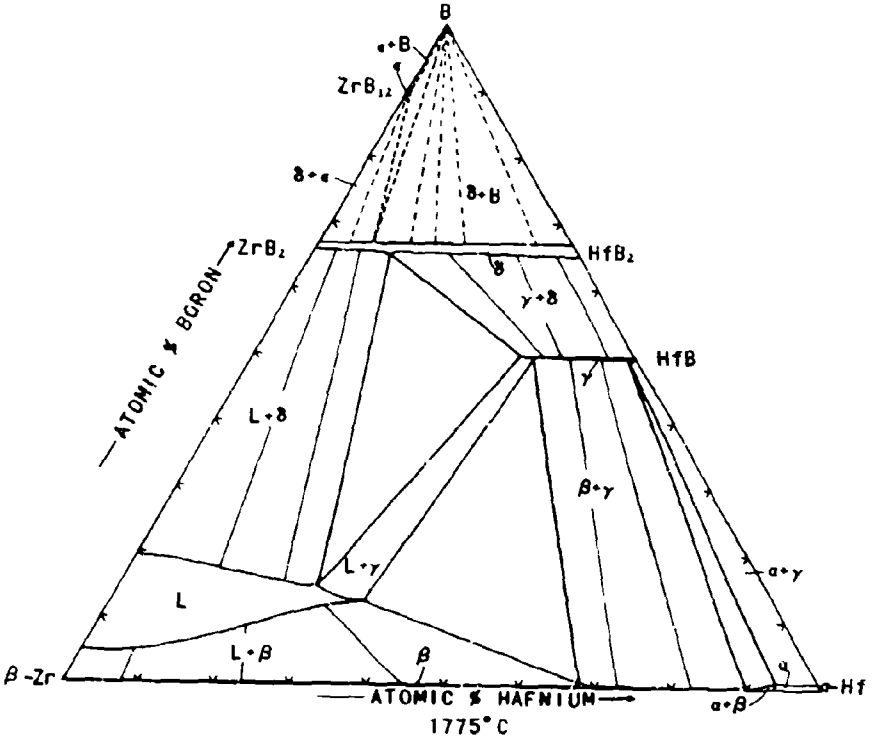

Figure III.I.3.12. Isothermal Section of the Zr-Hf-B System at 1775°C

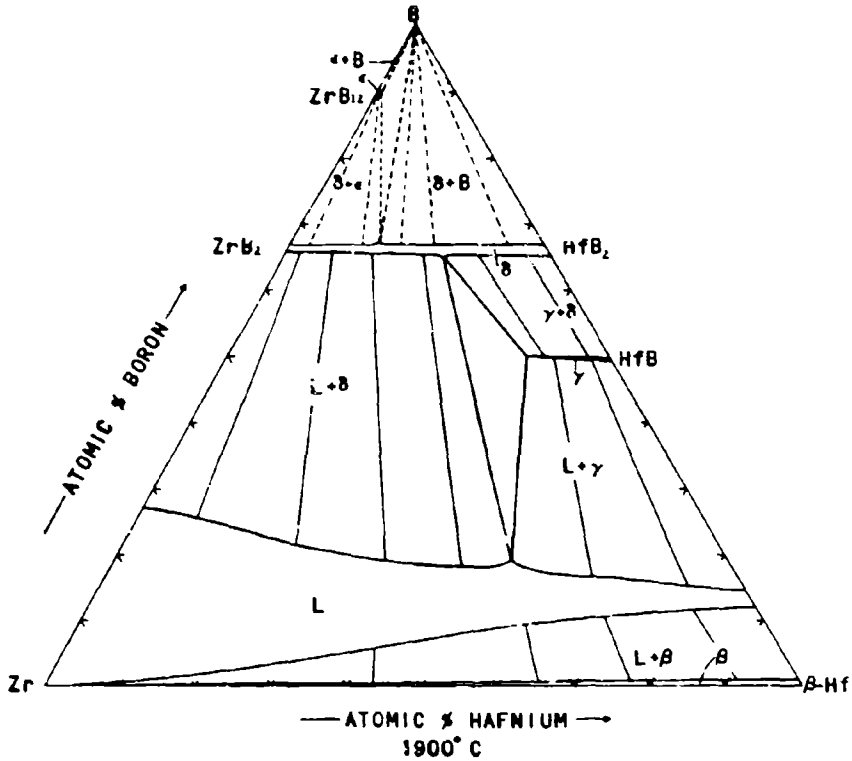

Figure III.I.3.13. Isothermal Section of the Zr-Hf-B System at 1900° C

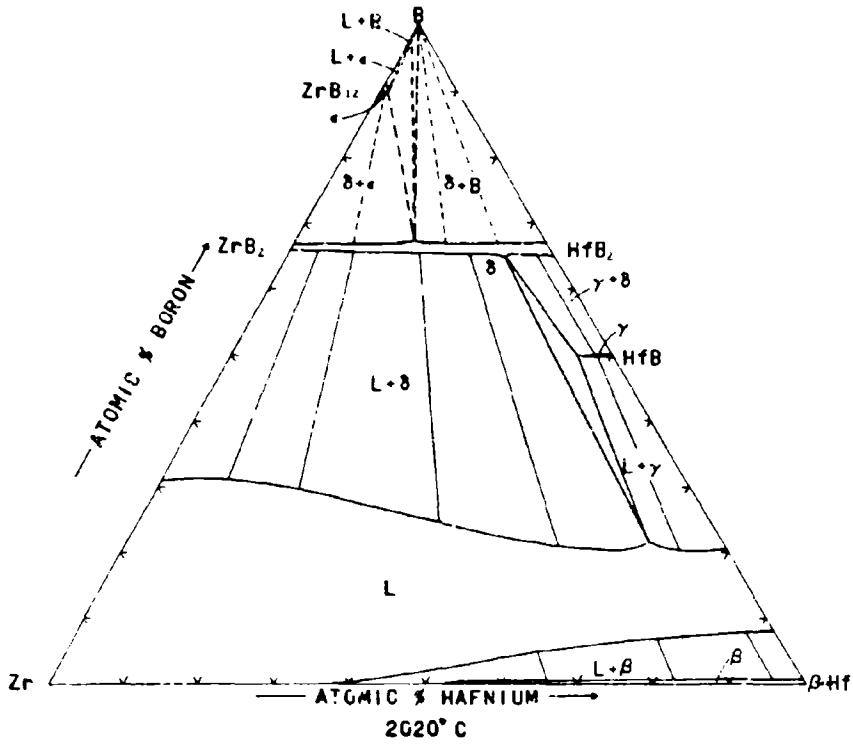

Figure III.I.3.14. Isothermal Section of the Zr-Hf-B System at 2020° C

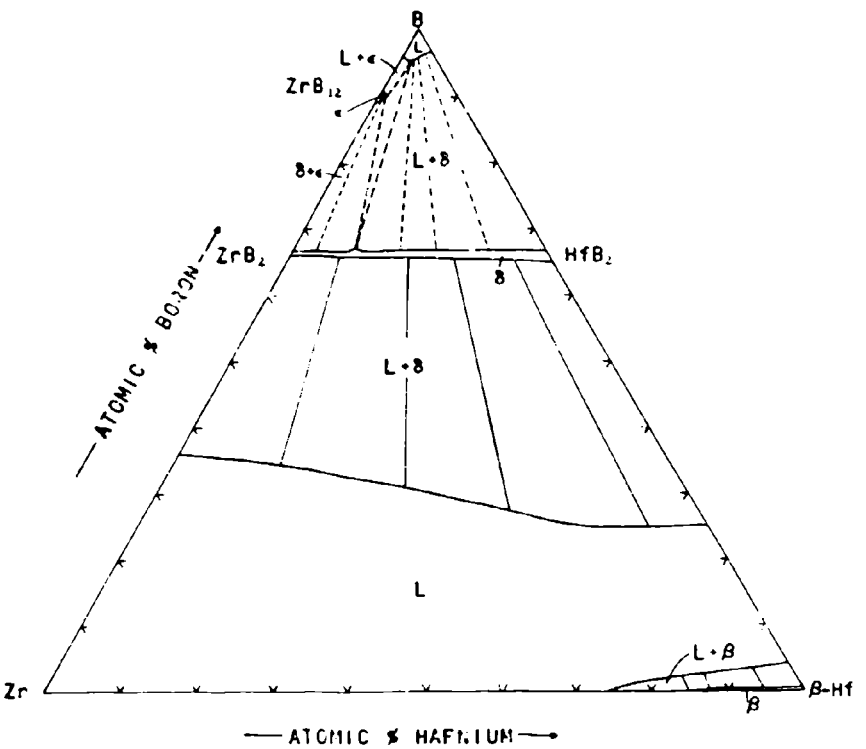

Figure III.1.3.15. Isothermal Section of the Zr-Hf-B System at 2150°C

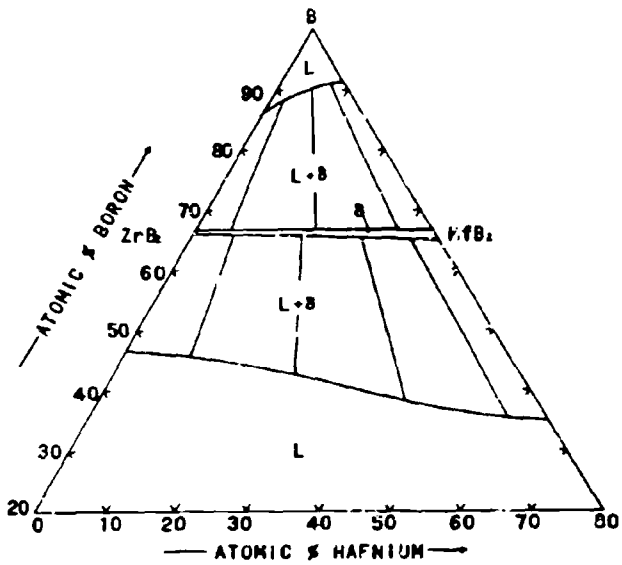

Figure III.I.3.16. Partial Isothermal Section of the Zr-Hf-B System at 2500°C

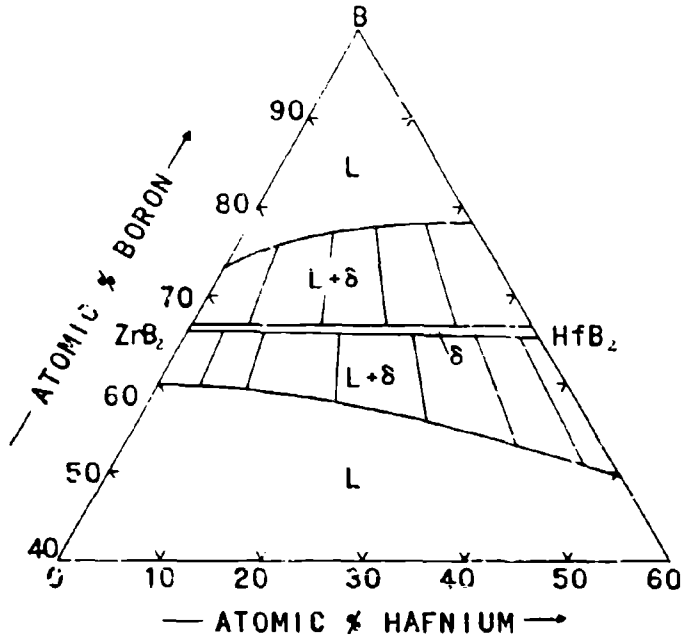

Figure III.I.3.17. Partial Isothermal Section of the Zr-Hf-B System at 3000° C

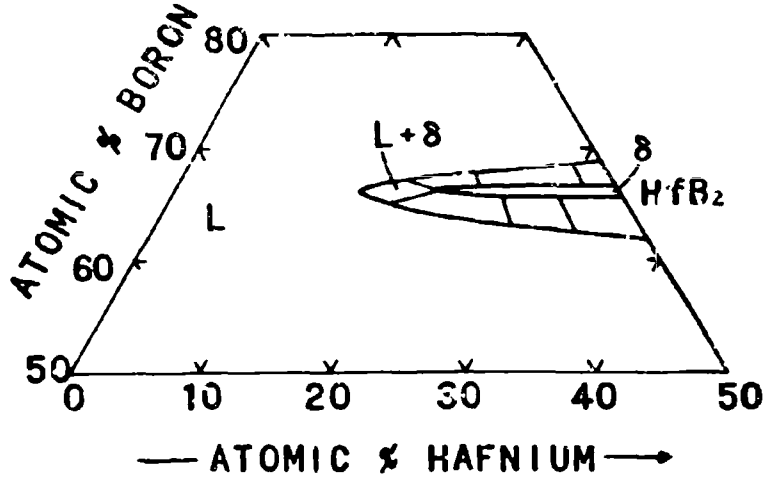

Figure III.I.3.18. Partial Isothermal Section of the Zr-Hf-B System at 3300° C

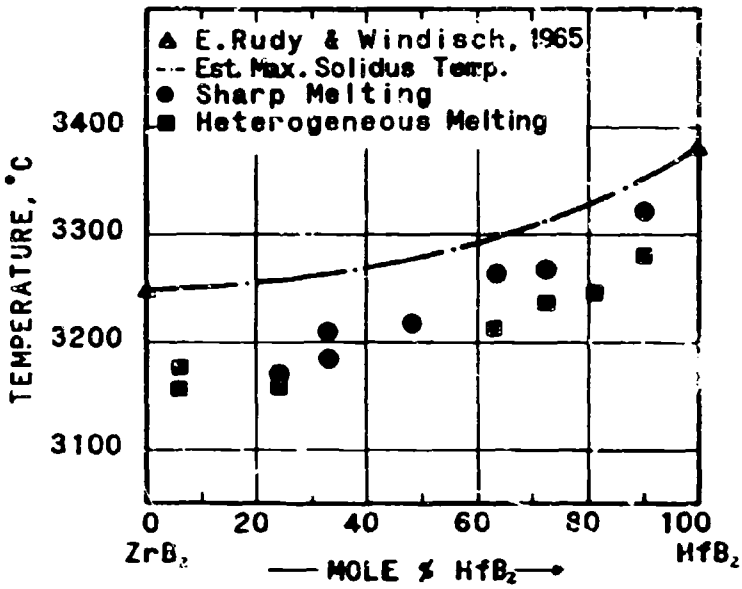

Figure III.I.3.19. Experimentally Determined Melting Temperatures of $(Zr,Hf)B_2$ Alloys and Estimated Maximum Solidus Temperatures

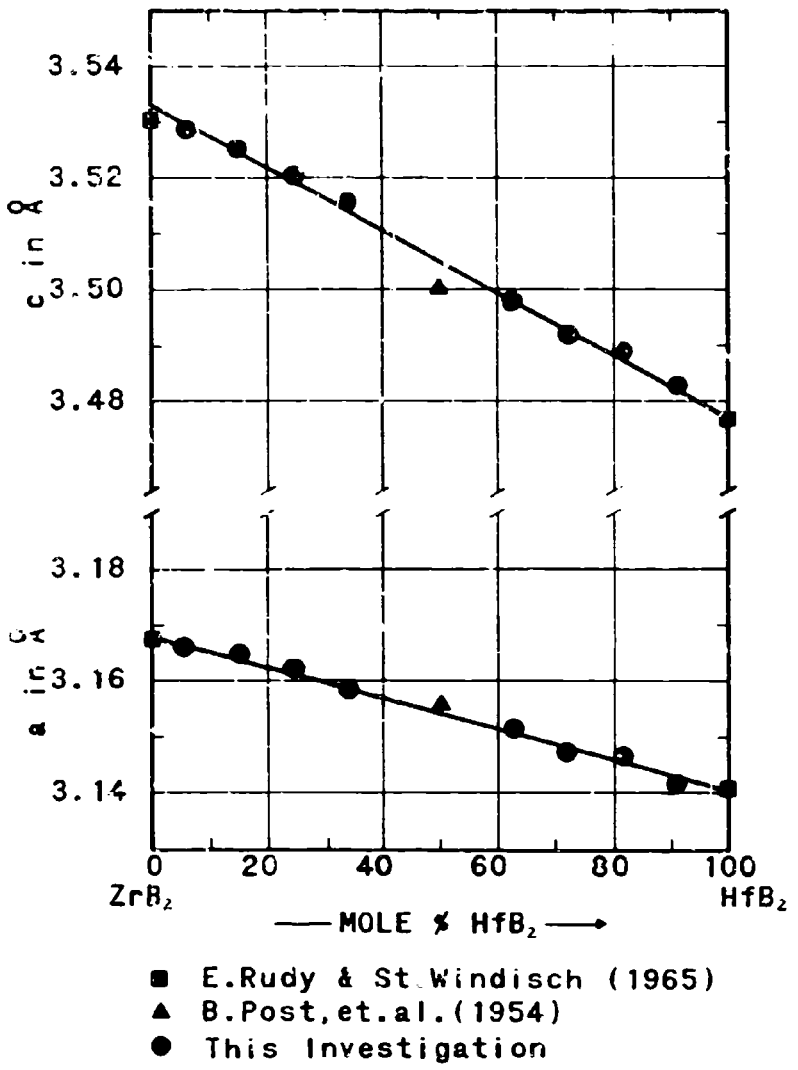

Figure III.I.3.20. Lattice Parameters of the $(Zr,Hf)B_2$ Solid Solution

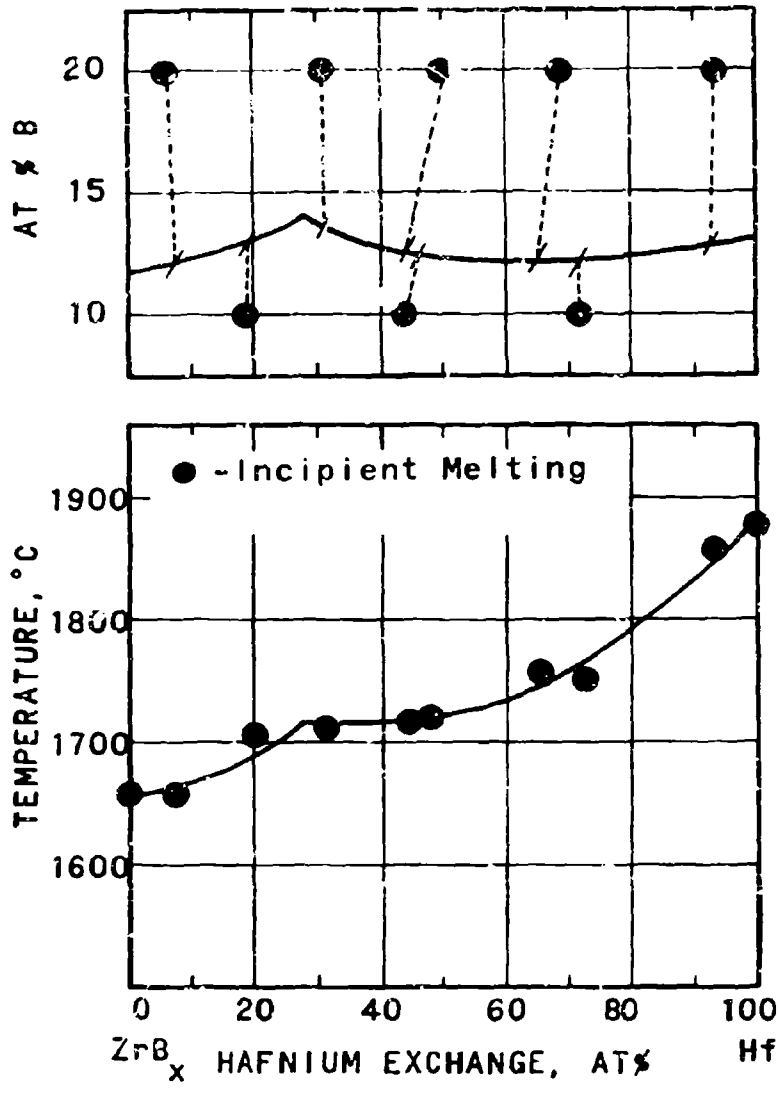

Figure III.1.3.21. Composition (Top) and Temperatures of the Metal-Rich Eutectic Trough in the Zr-Hf-B System

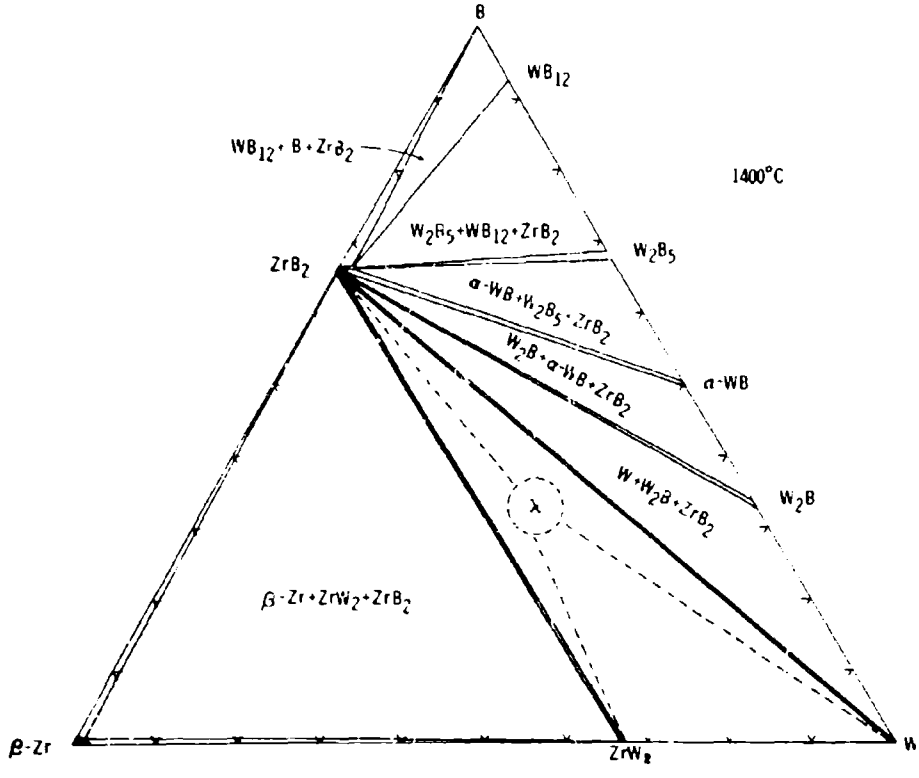

Figure III.I.4.1. Isothermal Section of the Zr-W-B System at 1400° C

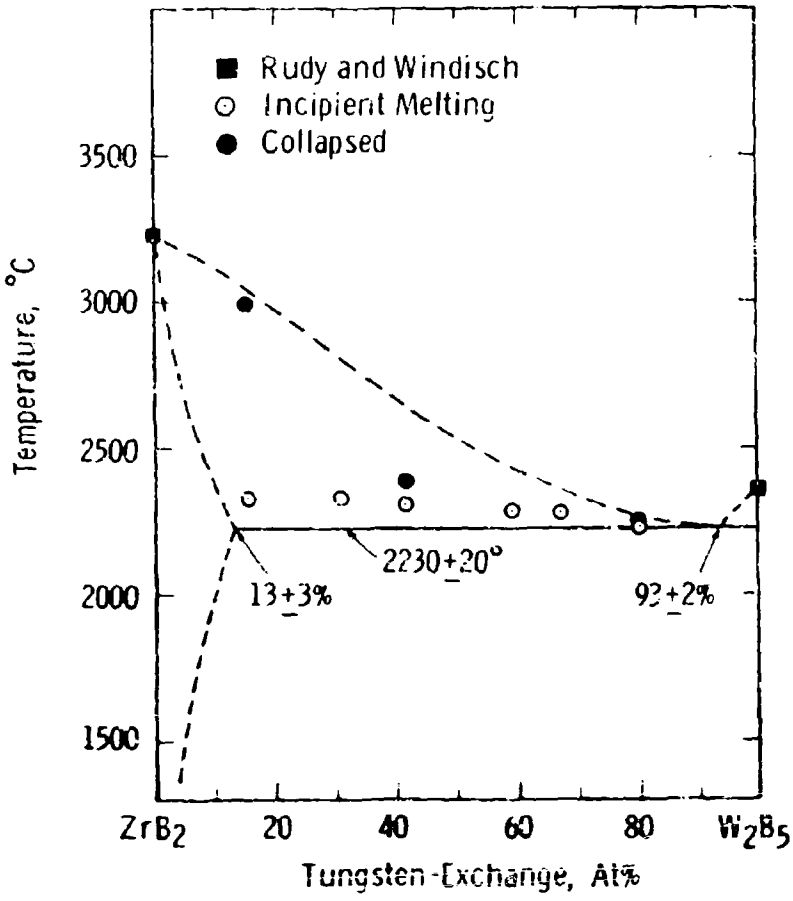

Figure III.I.4.2. Melting Along the Pseudobinary Section ZrB_2-W_2B_5

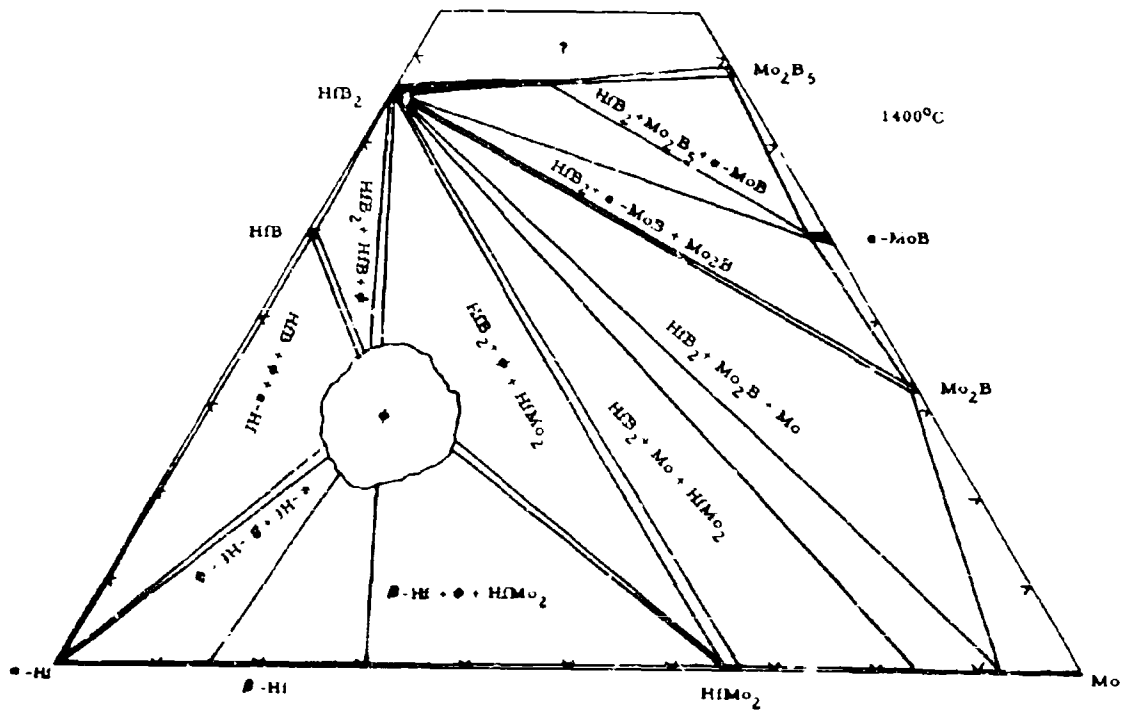

Figure III.I.5.1. Isothermal Section of the Hf-Mo-B System at 1400° C

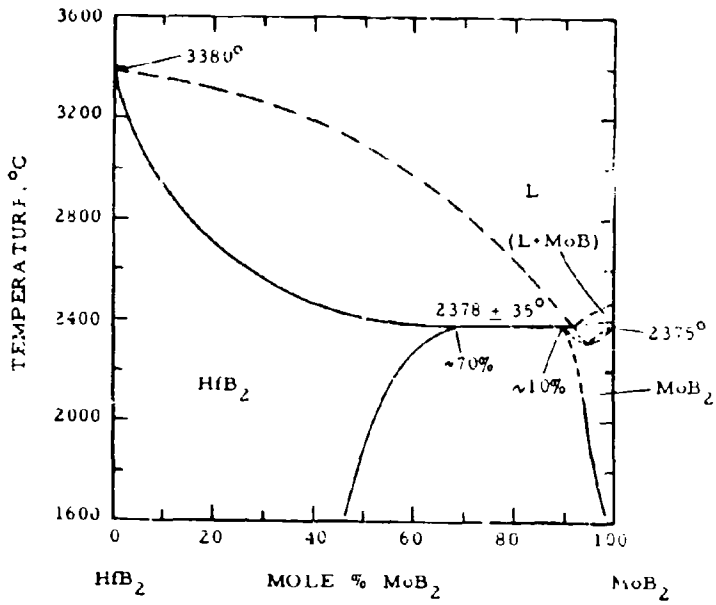

Figure III.I.5.2. HfB_2-MoB_2 Pseudobinary System

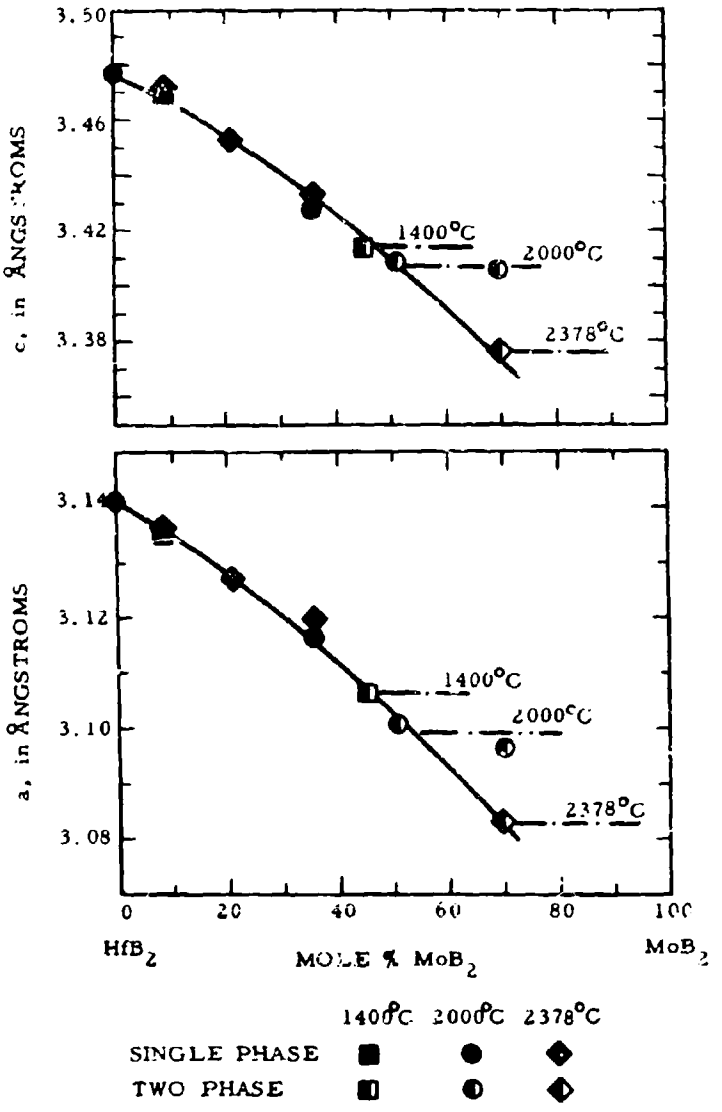

Figure III.I.5.3. Hf-Mo-B. Lattice Parameters of HfB_2-Rich Diboride Solid Solution

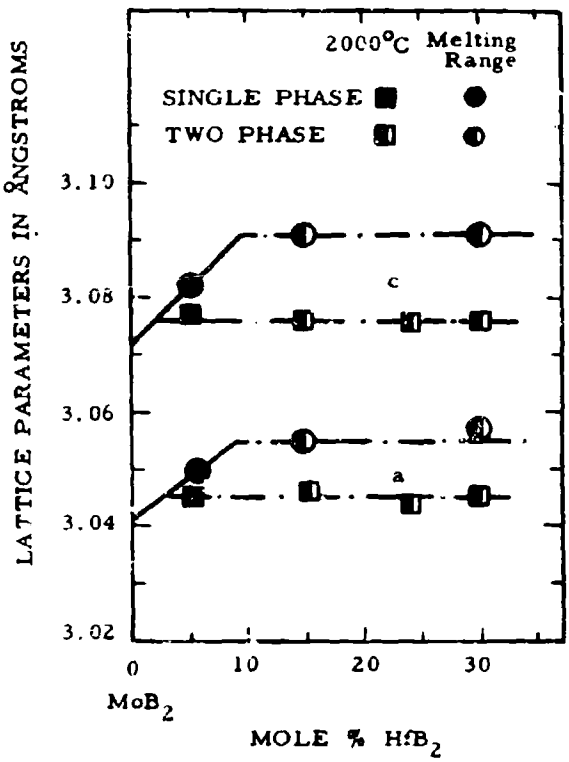

Figure III.1.5.4. Hf-Mo-B: Lattice Parameters of MoB_2-Rich Diboride Solid Solution

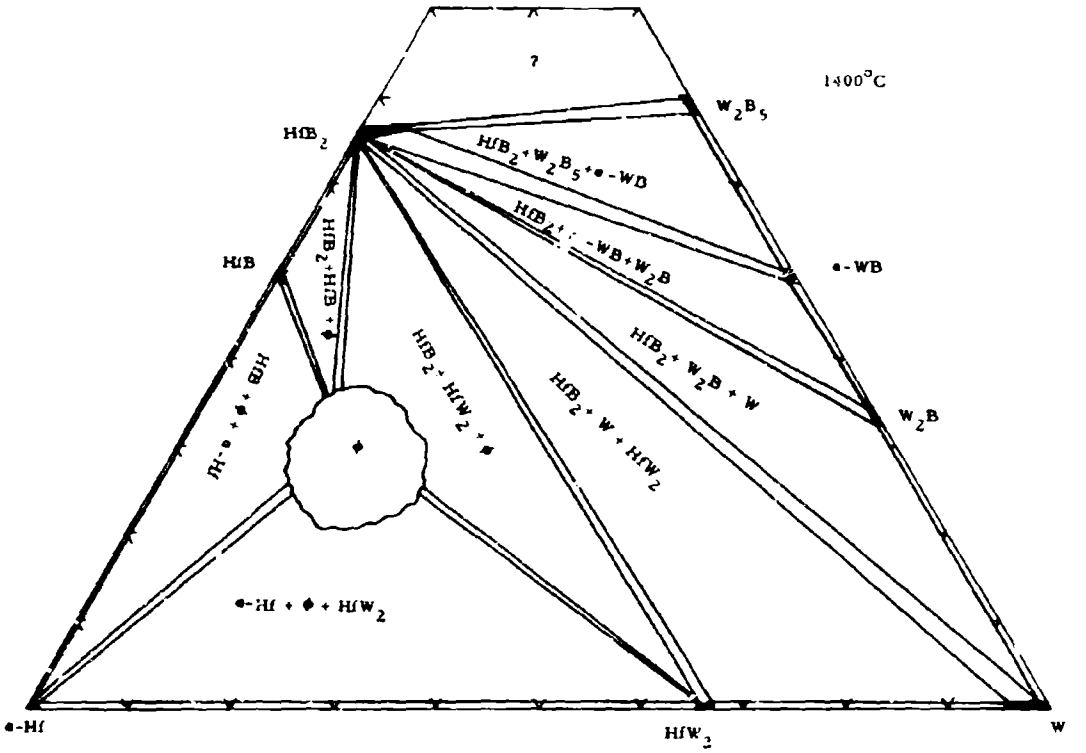

Figure III.1.6.1. Isothermal Section of the Hf-W-E System at 1400° C

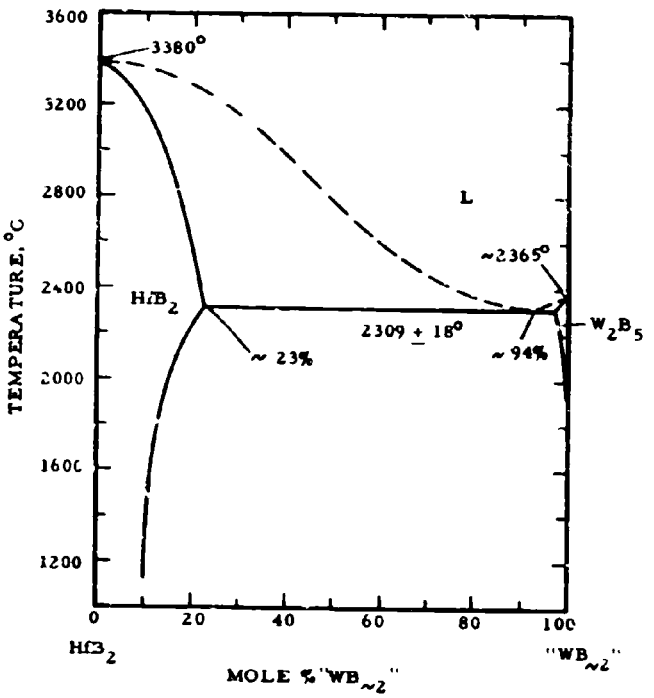

Figure III.I.6.2. HfB_2-W_2B_5 Pseudobinary Section

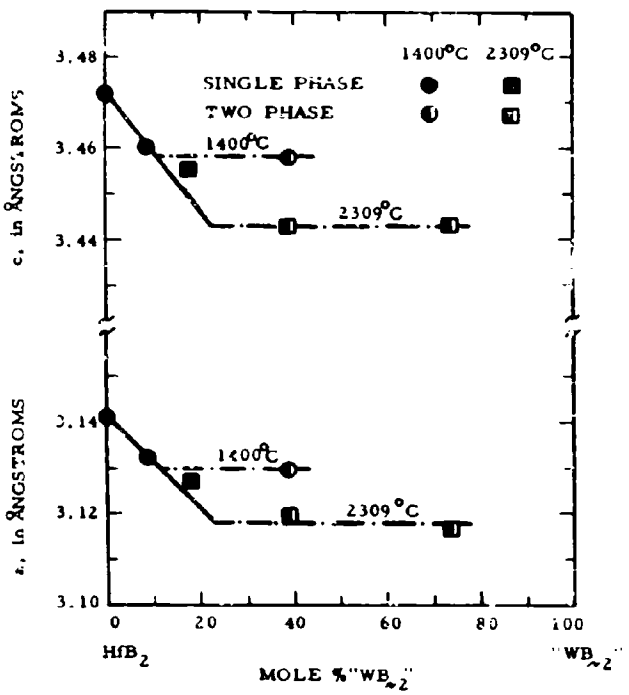

Figure III.1.6.3. Lattice Parameters of the (Hf, W)B_2 Solid Solution

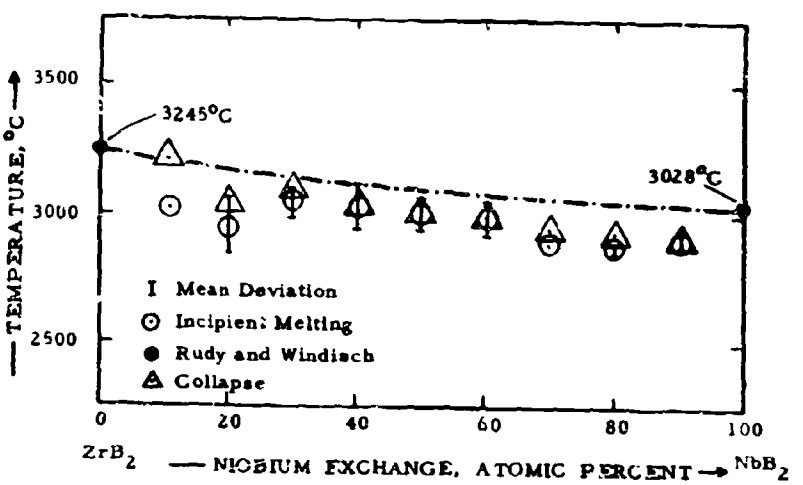

Figure III.I.7.1. Measured Solidus Temperatures for the Solution $(Zr,Nb)B_2$

— · — · — Estimated Maximum Solidus Line

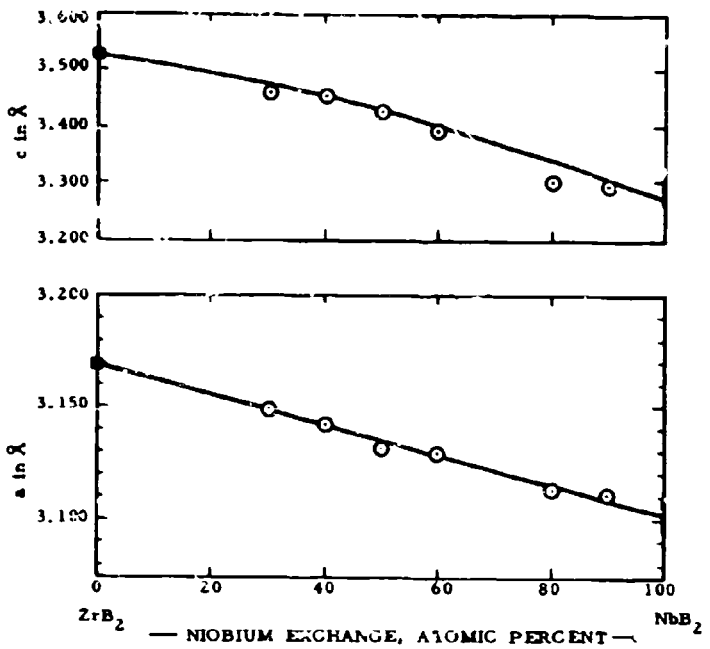

Figure III.I.7.2. Lattice Parameters of the Solid Solution $(Zr,Nb)B_2$

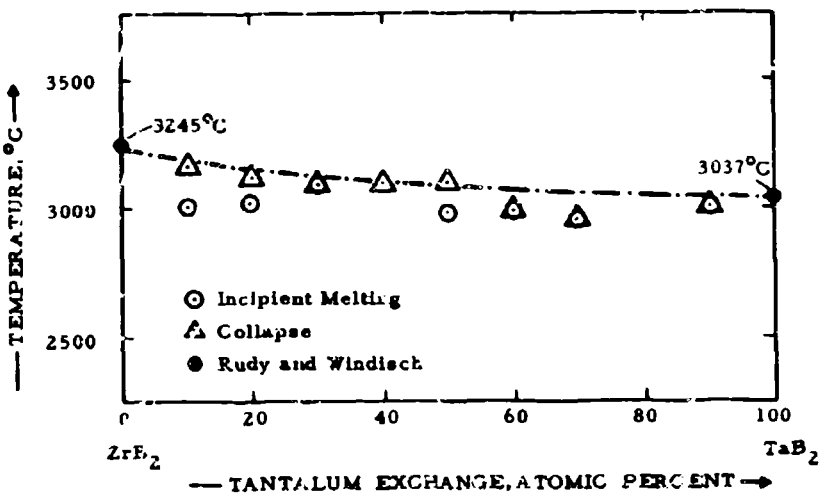

Figure III.I.8.1. Measured Solidus Temperatures of the Solid Solution $(Zr,Ta)B_2$

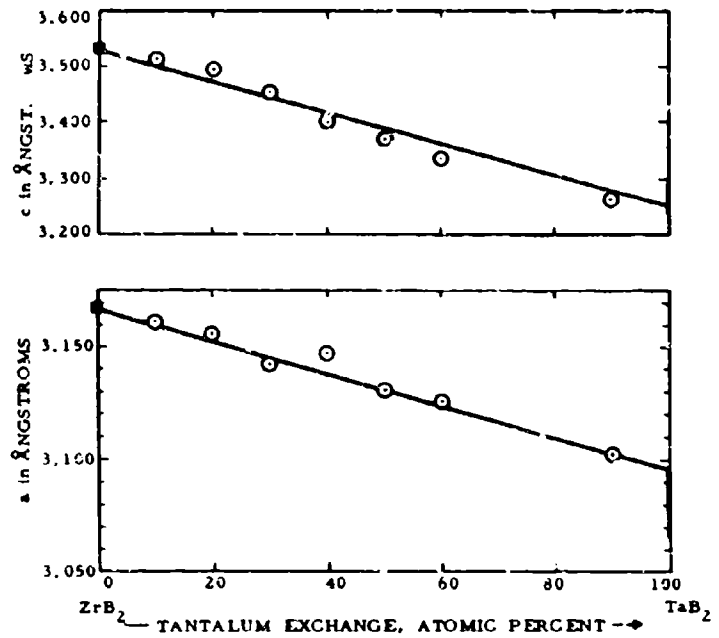

Figure III.I .8.2. Lattice Parameters of the Solid Solution $(Zr,Ta)B_2$

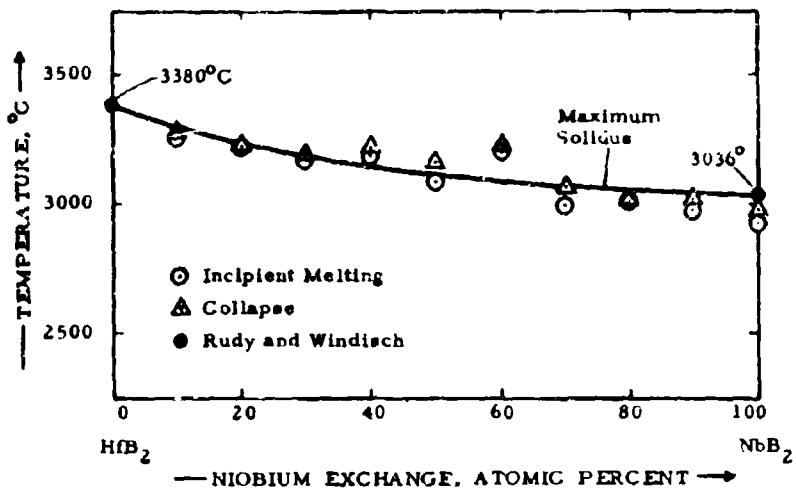

Figure III.I.9.1. Melting Temperatures of the Solid Solution $(Hf,Nb)B_2$

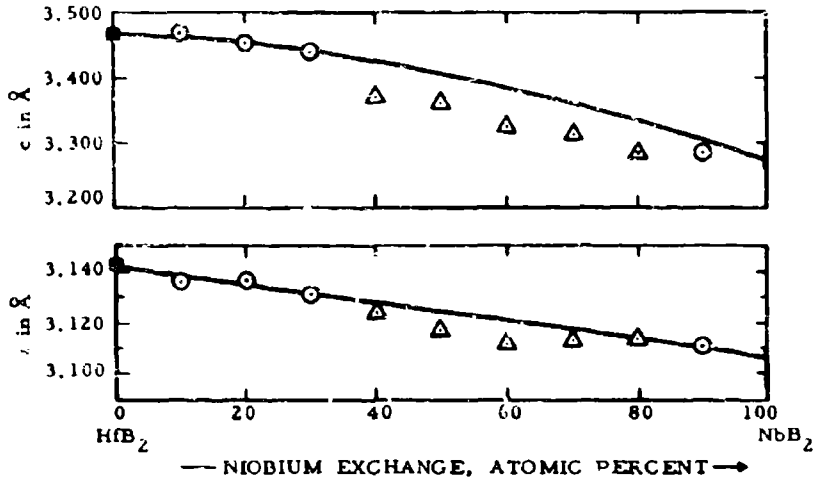

Figure III.I.9.2. Lattice Parameters of the Solid Solution $(Hf,Nb)B_2$

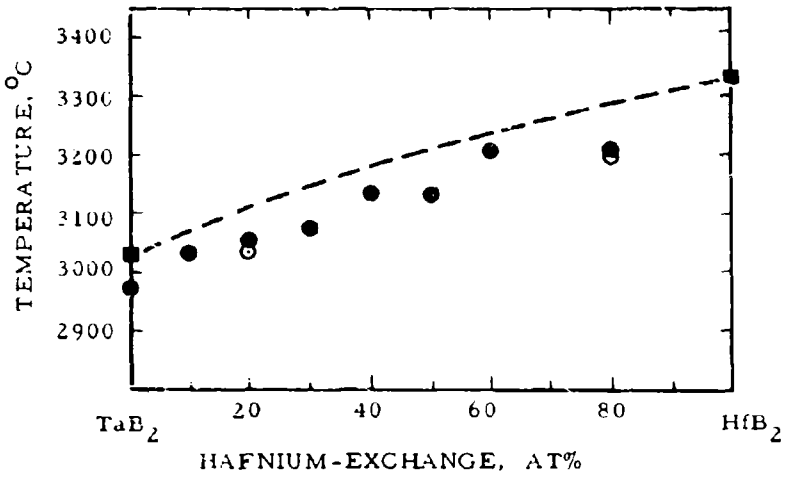

Figure III.1 .10.1. Measured Solidus Temperatures of the Solid Solution $(Ta,Hf)B_2$

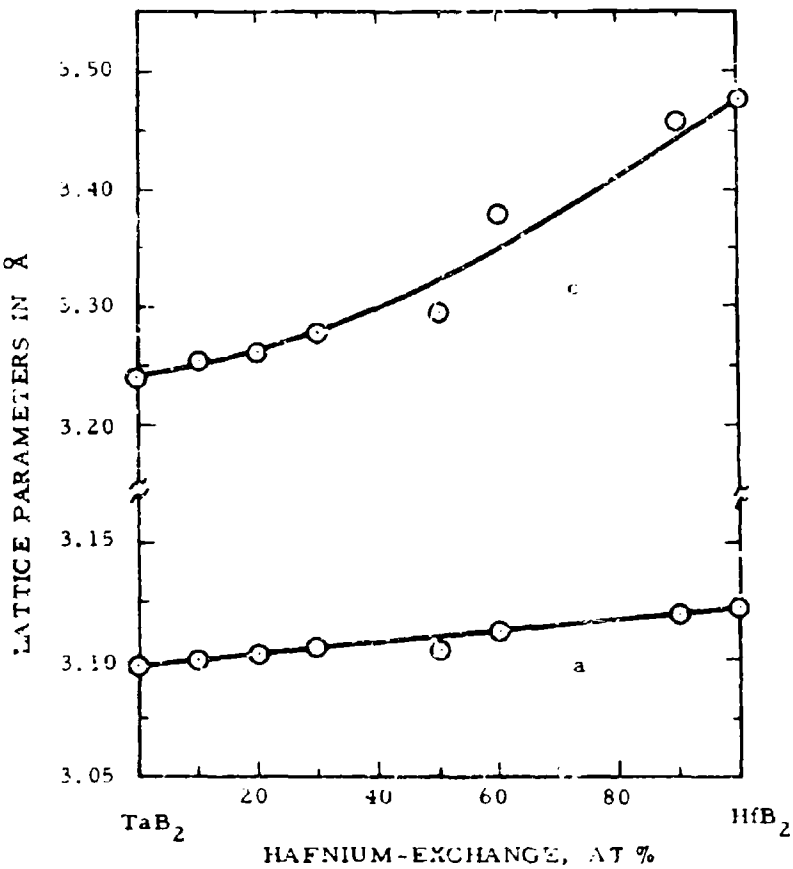

Figure III.1.10.2. Lattice Parameters of the $(Ta,Hf)B_2$ Solid Solution

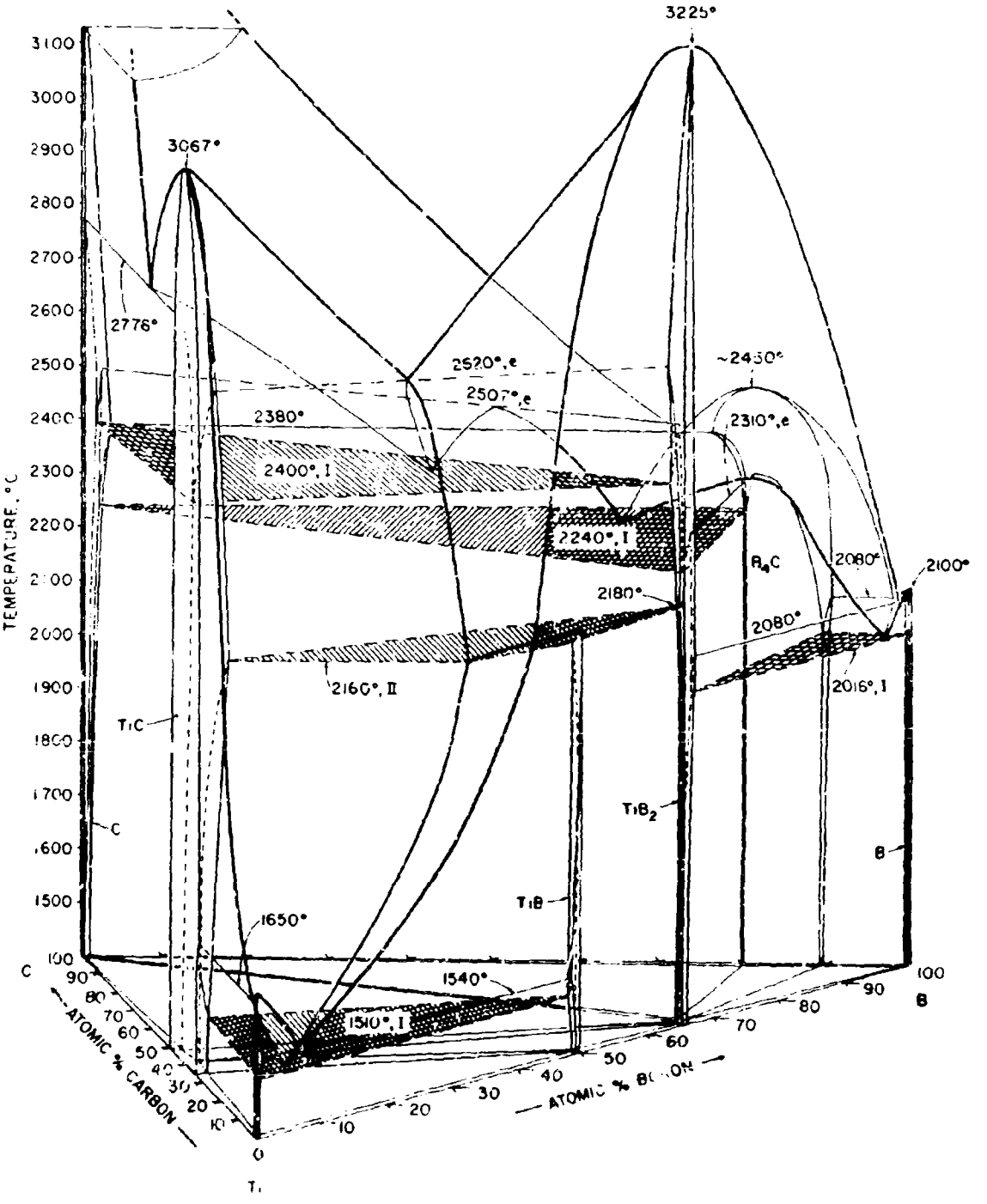

Figure III.K.1.1. Isometric View of the Ti-B-C System

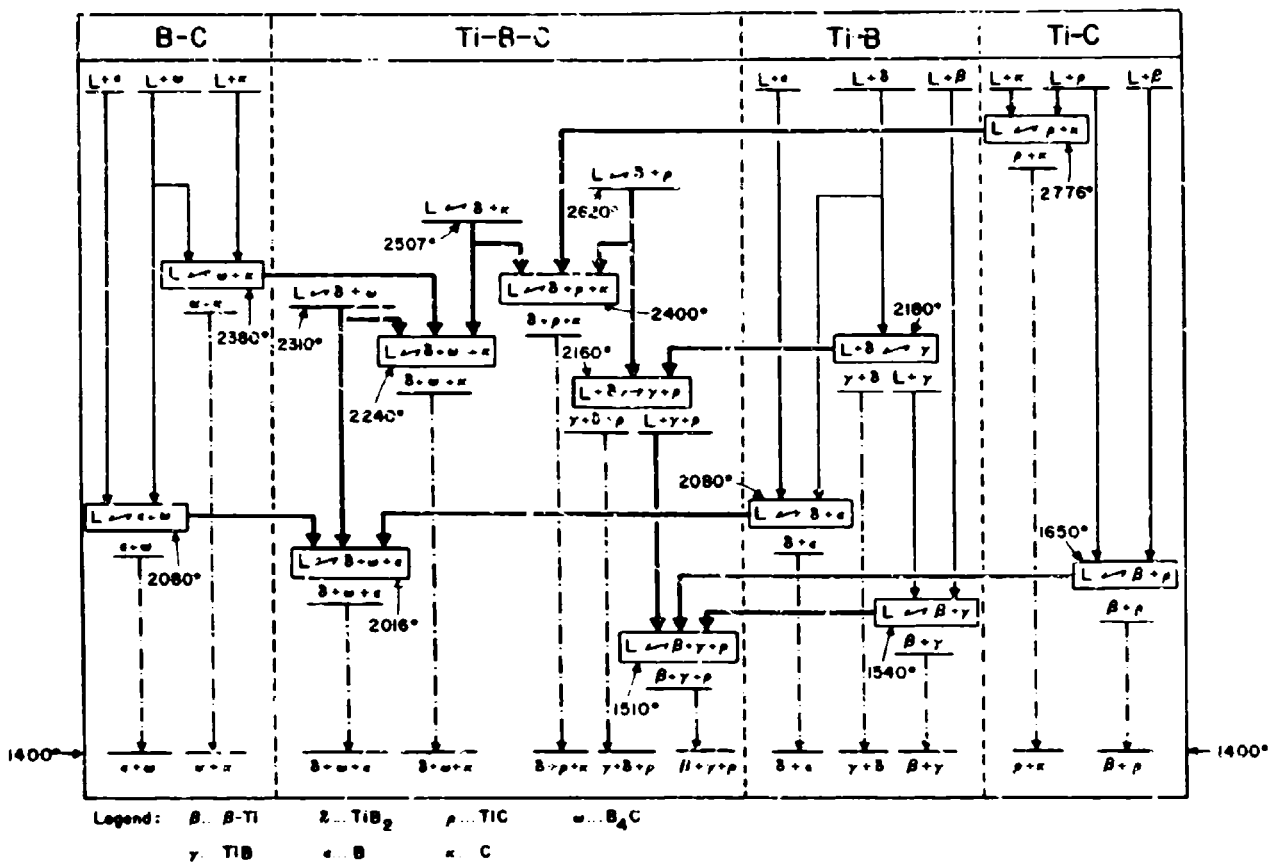

Figure III.K.1.2. Reaction Diagram for the Ti-B-C System

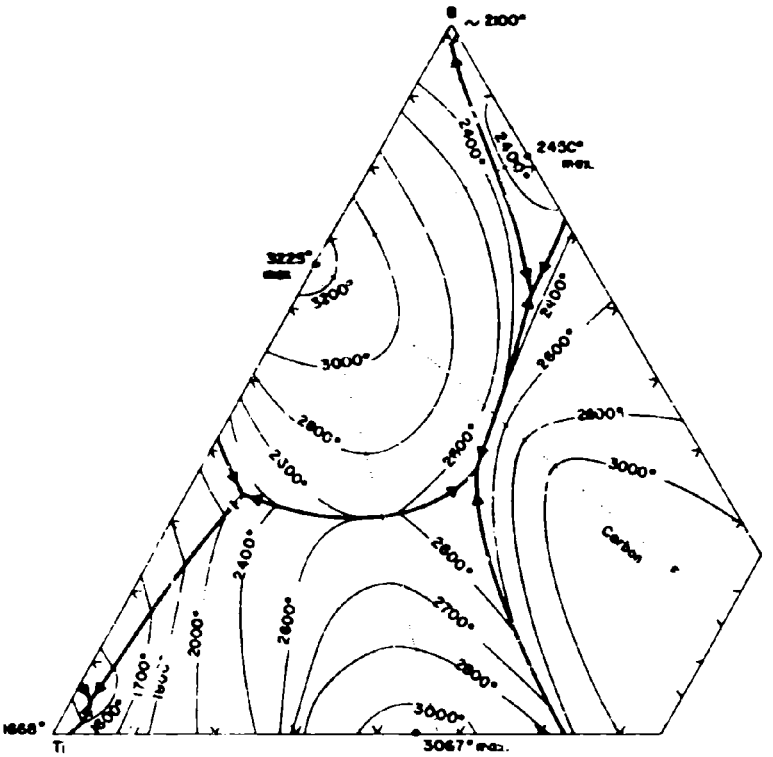

Figure III.K.1.3. Liquidus Projections for the Ti-B-C System (Approximate).

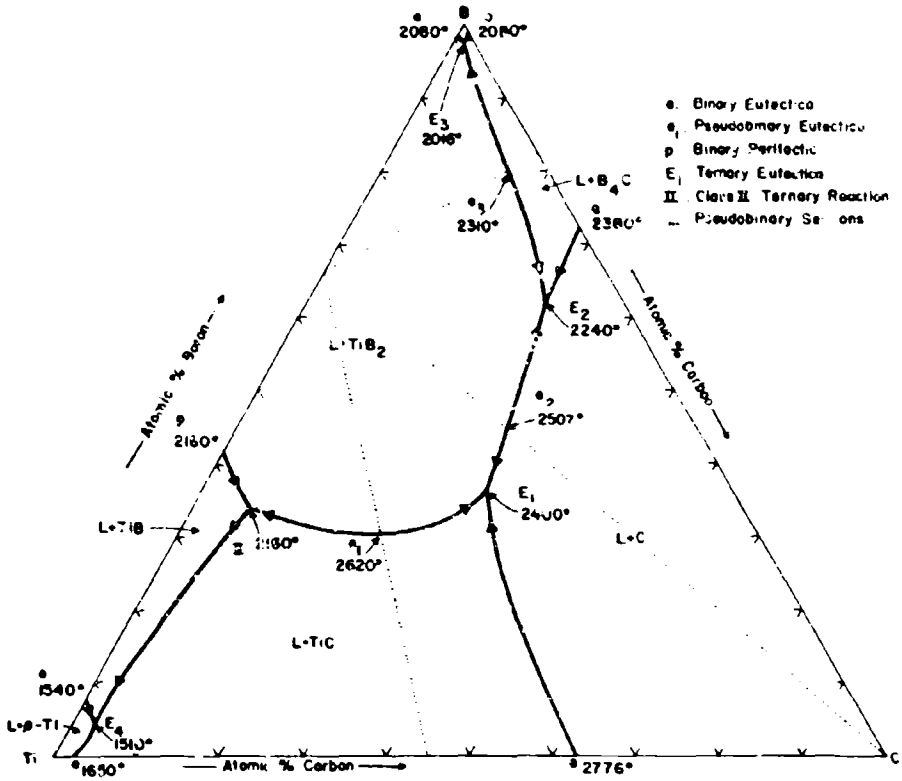

Figure III.K.1.4. Ti-B-C: Melting Troughs and Non-Variant (p = const) Equilibria Involving Liquid Phases

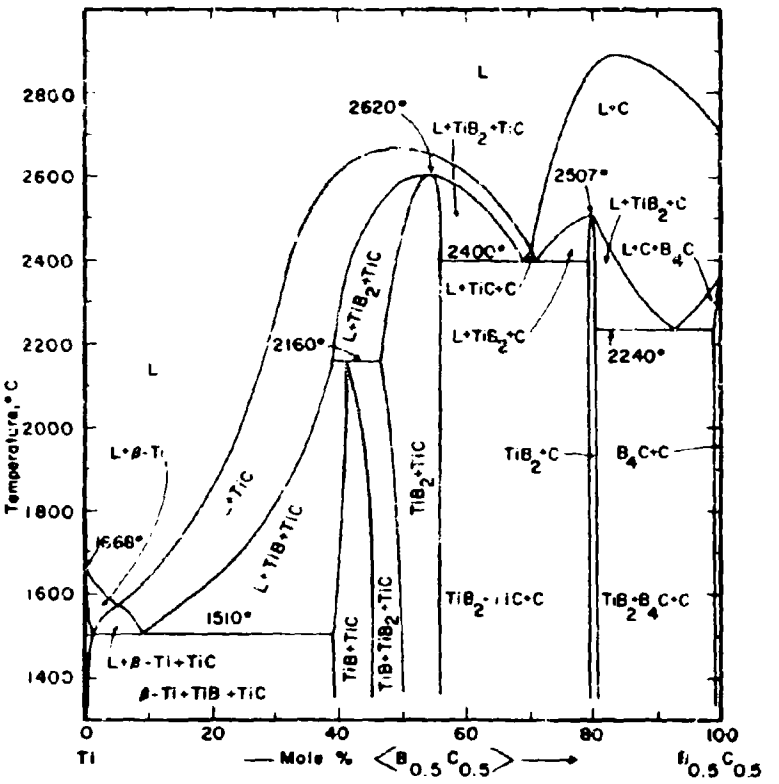

Figure III.K.1.5. Isopleth Ti-$B_{0.5}C_{0.5}$

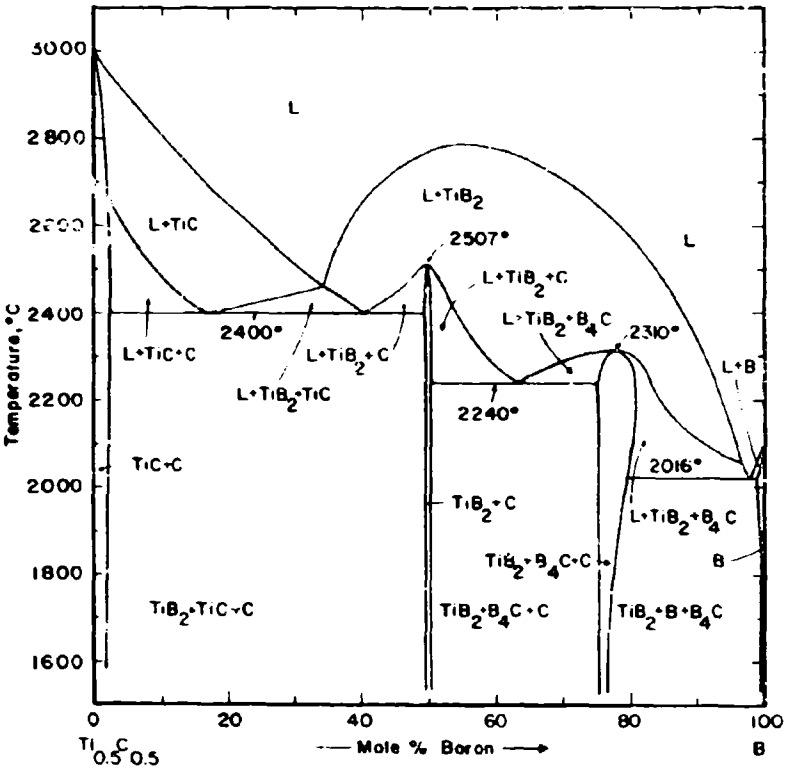

Figure III.K.1.6. Isopleth $Ti_{0.5}C_{0.5}$-B

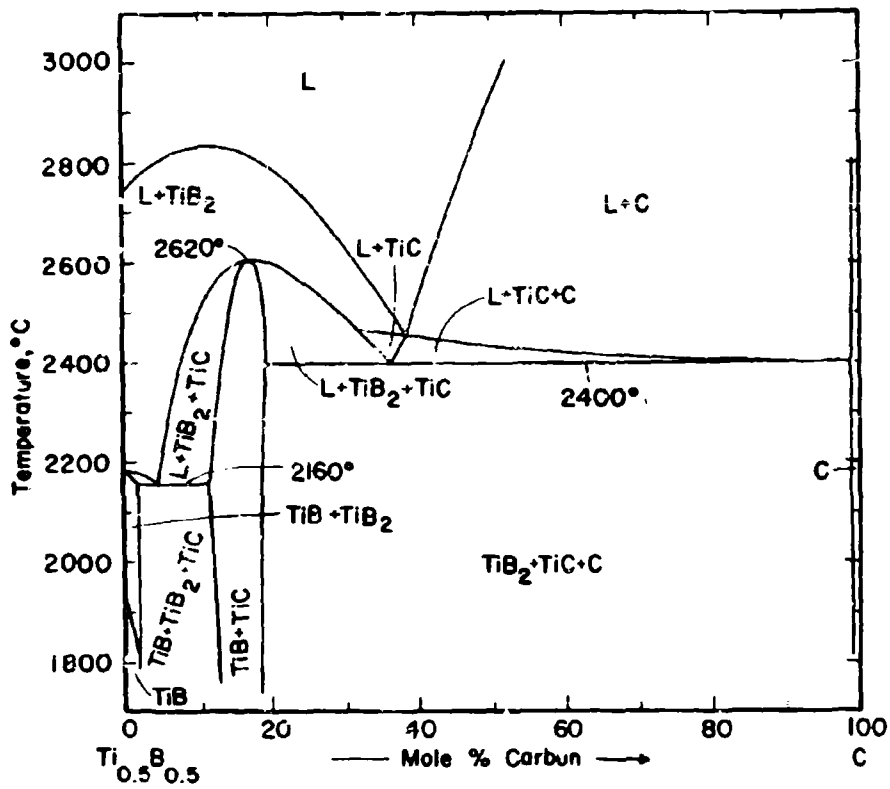

Figure III.K.1.7. Isopleth $Ti_{0.5}B_{0.5}$-C

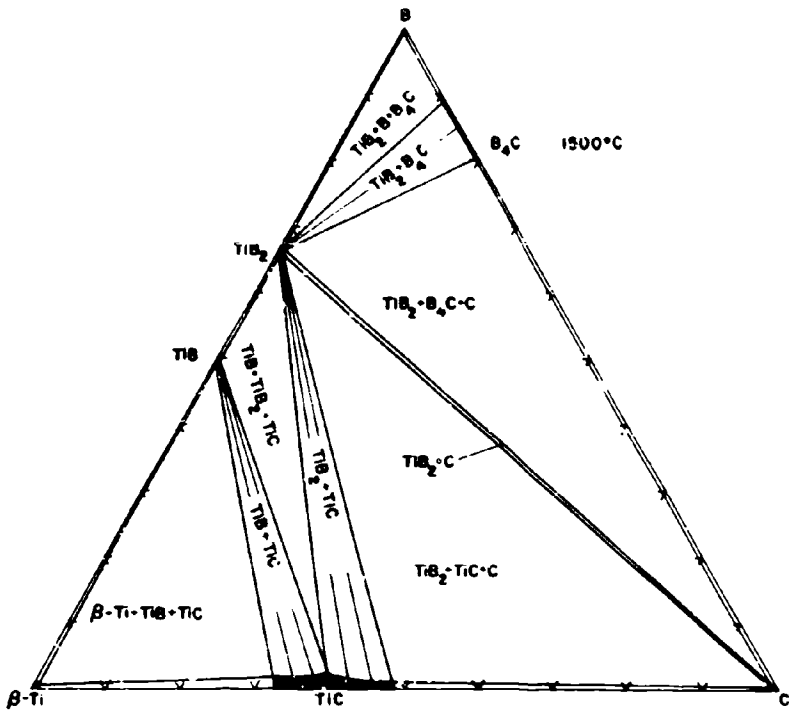

Figure III.K.1.8. Isothermal Section of the Ti-B-C System at 1500°C

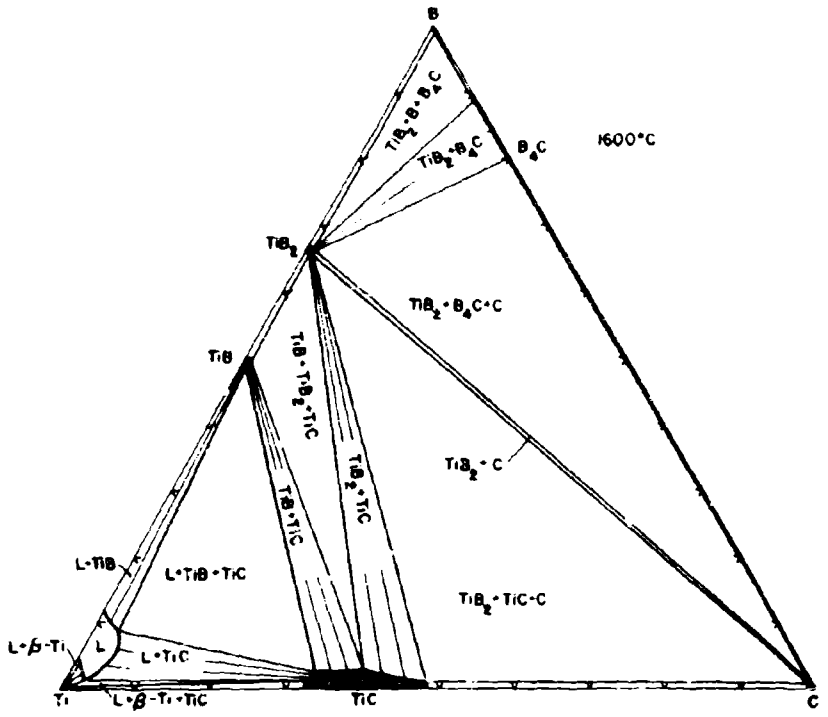

Figure III.K.1.9. Isothermal Section of the Ti-B-C System at 1600°C

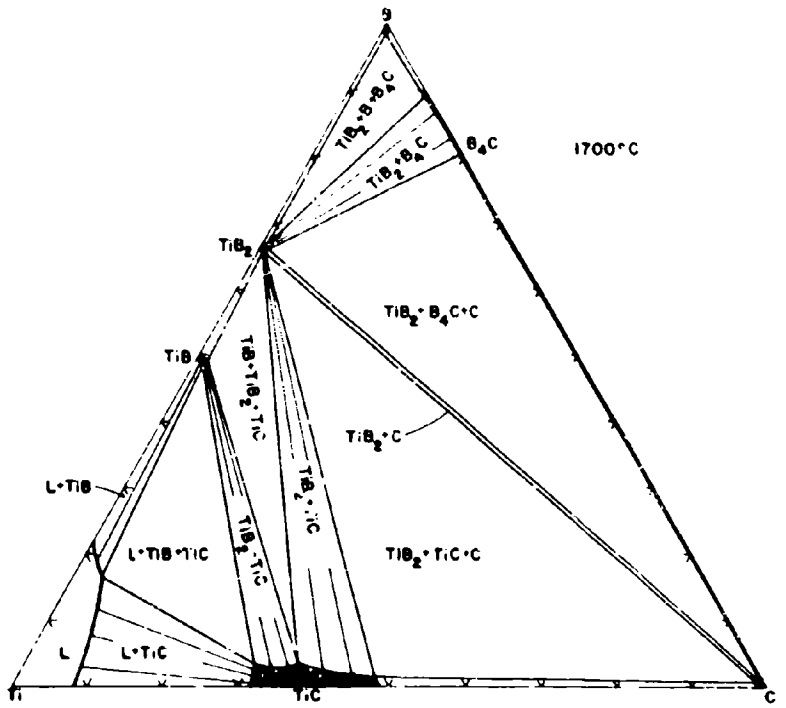

Figure III.K.1.10. Isothermal Section of the Ti-B-C System at 1700°C

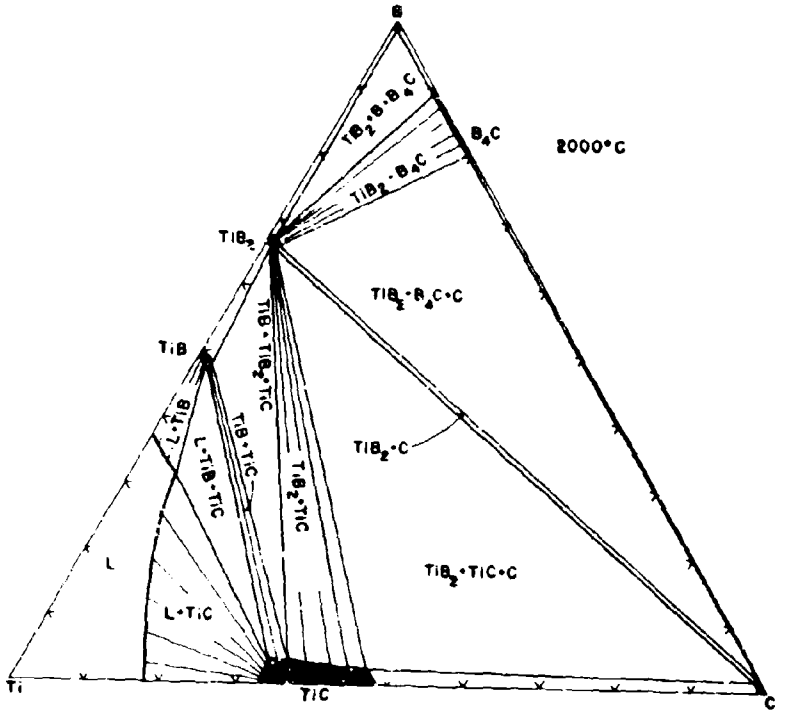

Figure III.K.1.11. Isothermal Section of the Ti-B-C System at 2000° C

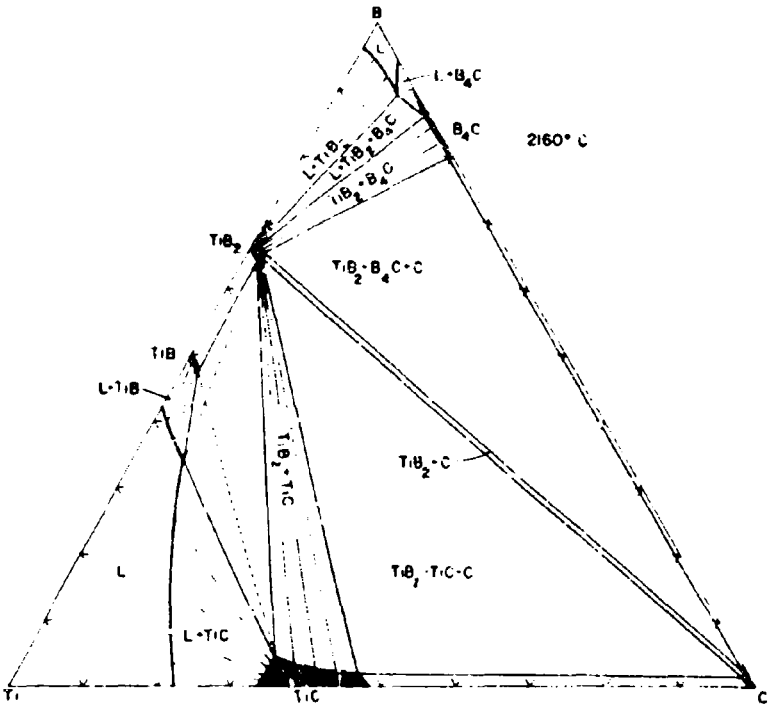

Figure III.K.1.12. Isothermal Section of the Ti-B-C System at 2160° C

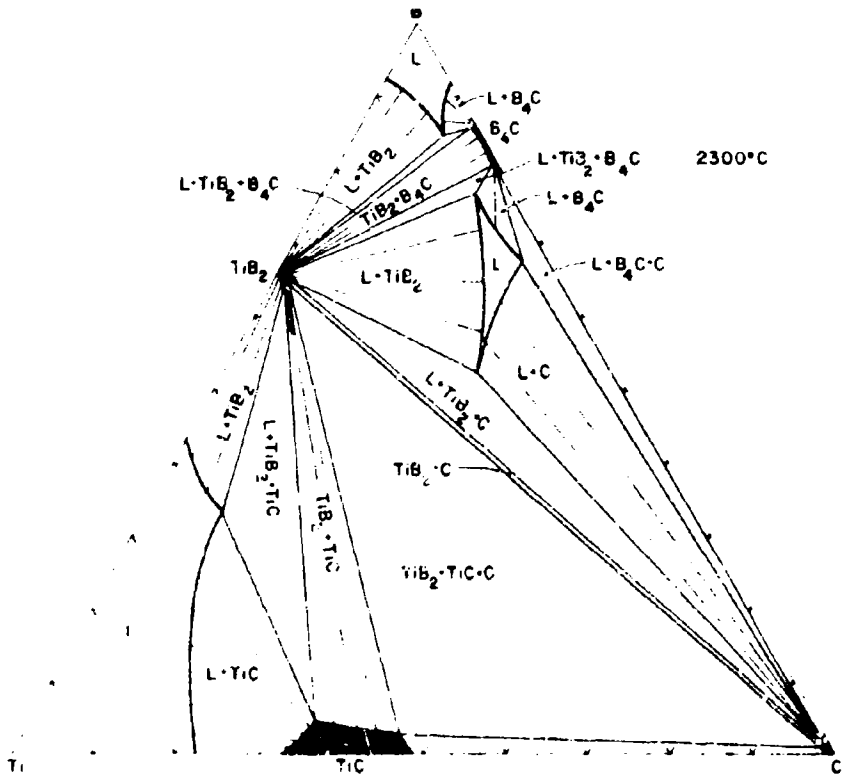

Figure III.E.1.13. Isothermal Section of the Ti-B-C System at 2300°C

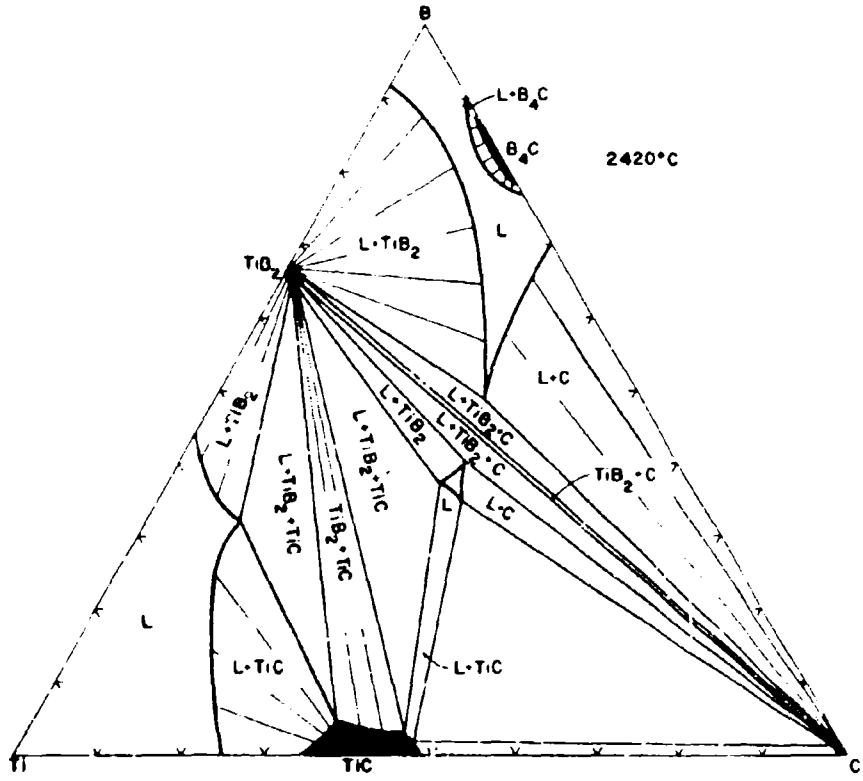

Figure III.K.1.14. Isothermal Section of the Ti-B-C System at 2420° C

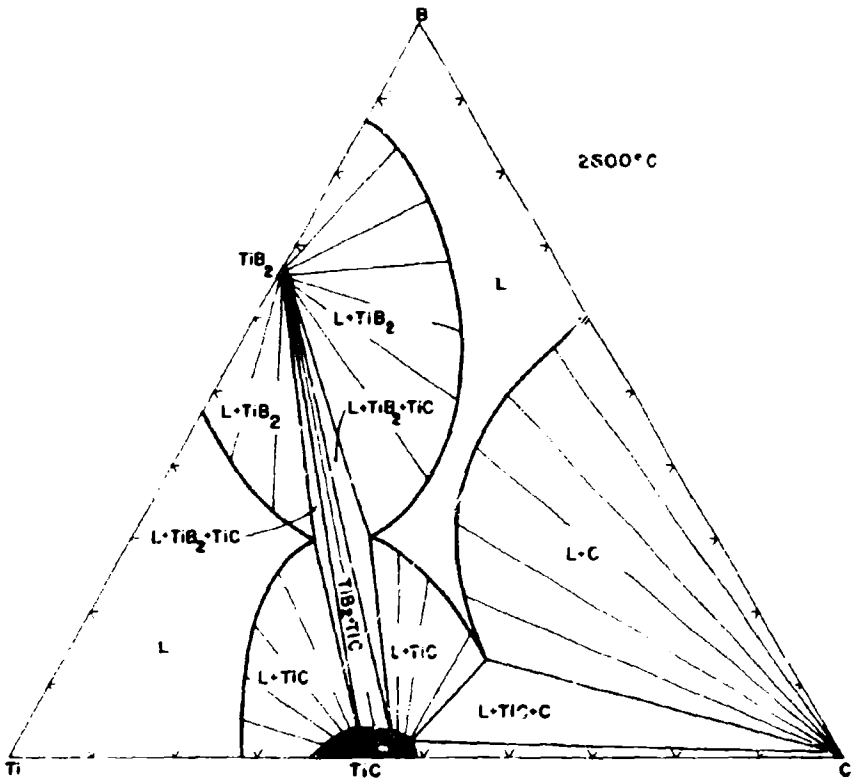

Figure III.K.1.15. Isothermal Section of the Ti-B-C System at 2600°C

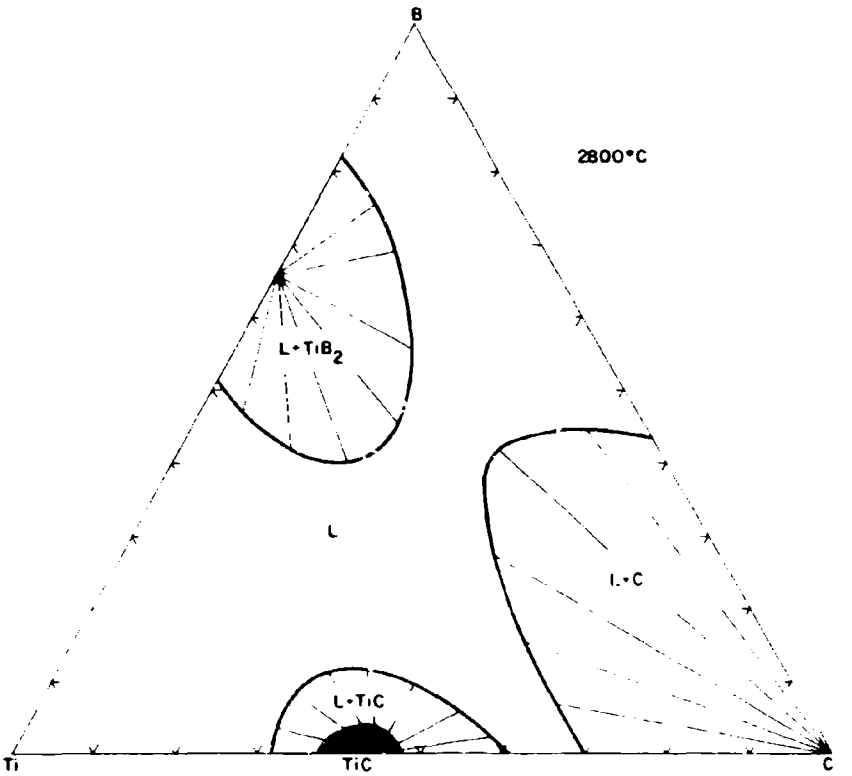

Figure III.K.1.16. Isothermal Section of the Ti-B-C System at 2800° C

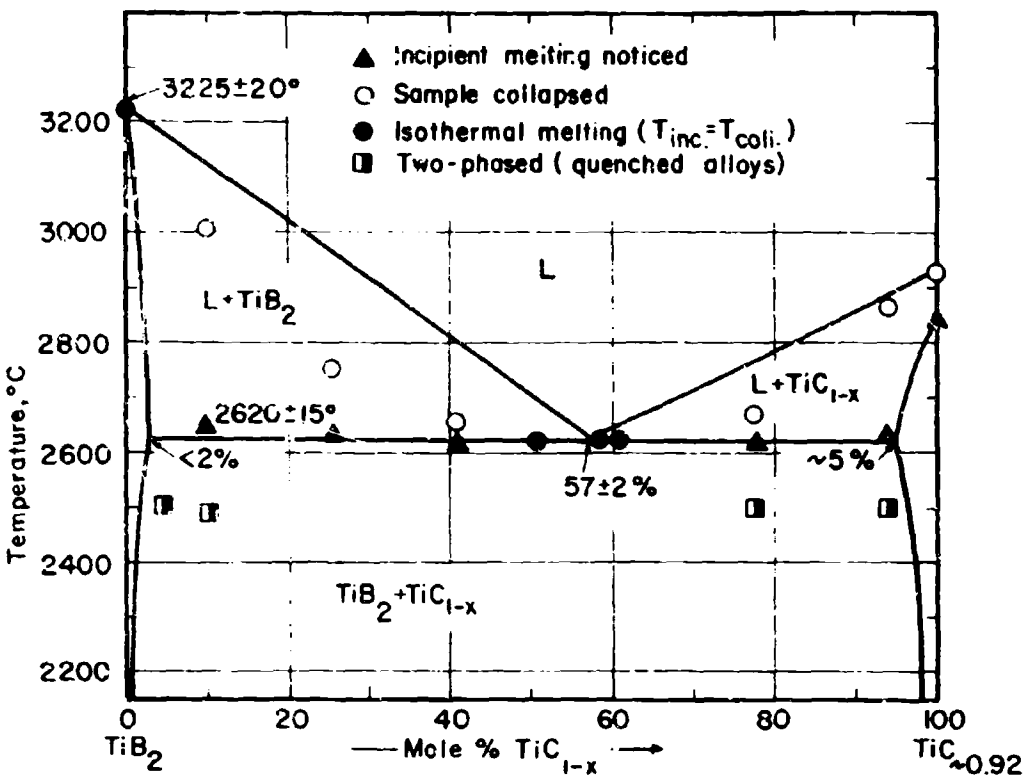

Figure III.K.1.17. Experimental Data on Alloys Located Along the Pseudobinary Section TiB_2-TiC_{1-x}

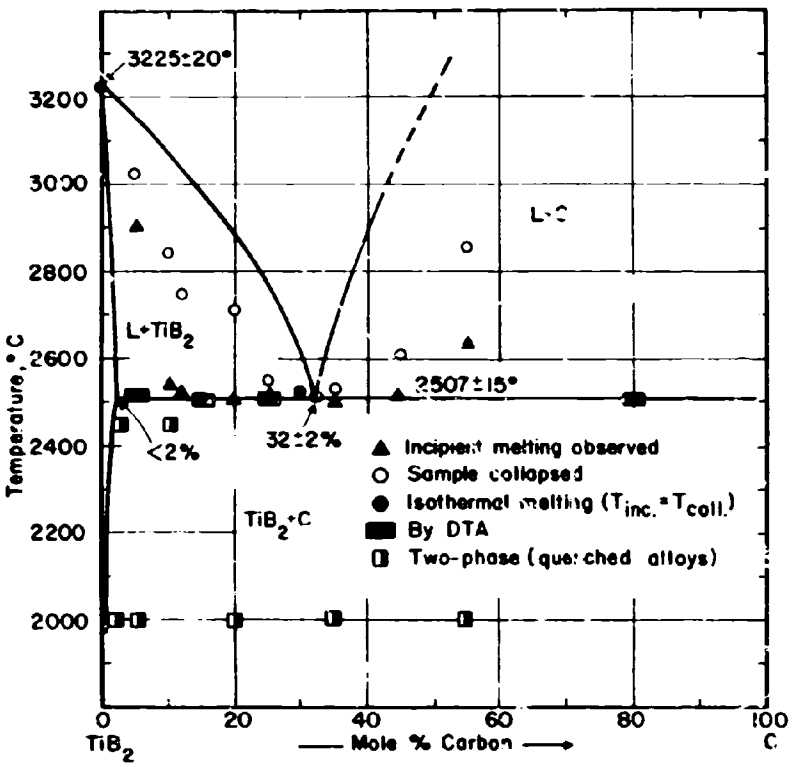

Figure III.K.1.18. Experimental Data on Alloys Located Along the Pseudobinary Section TiB_2-C

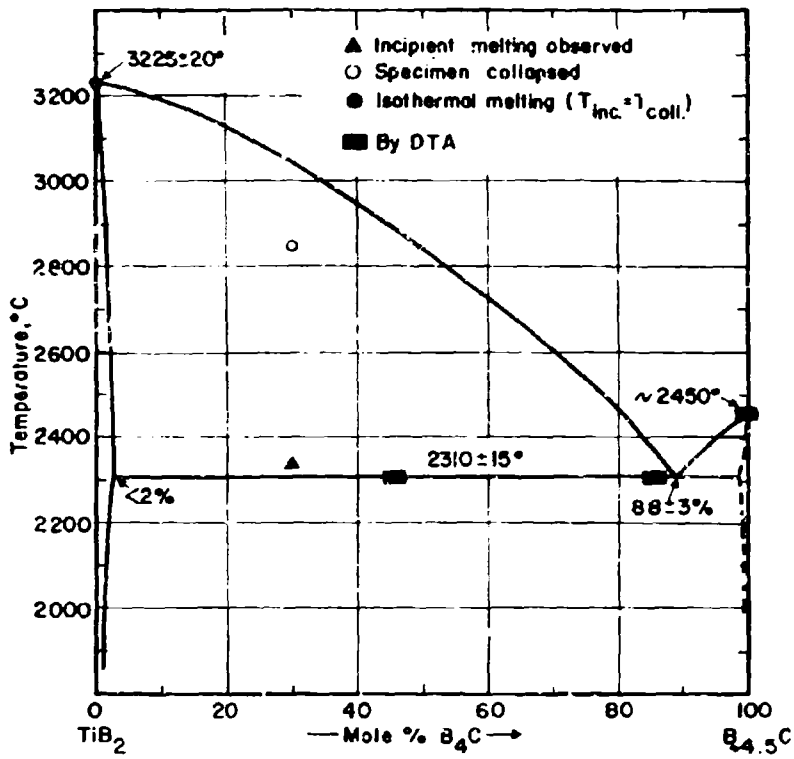

Figure III.K.1.19. Melting Along the Pseudobinary Section TiB_2-B_4C

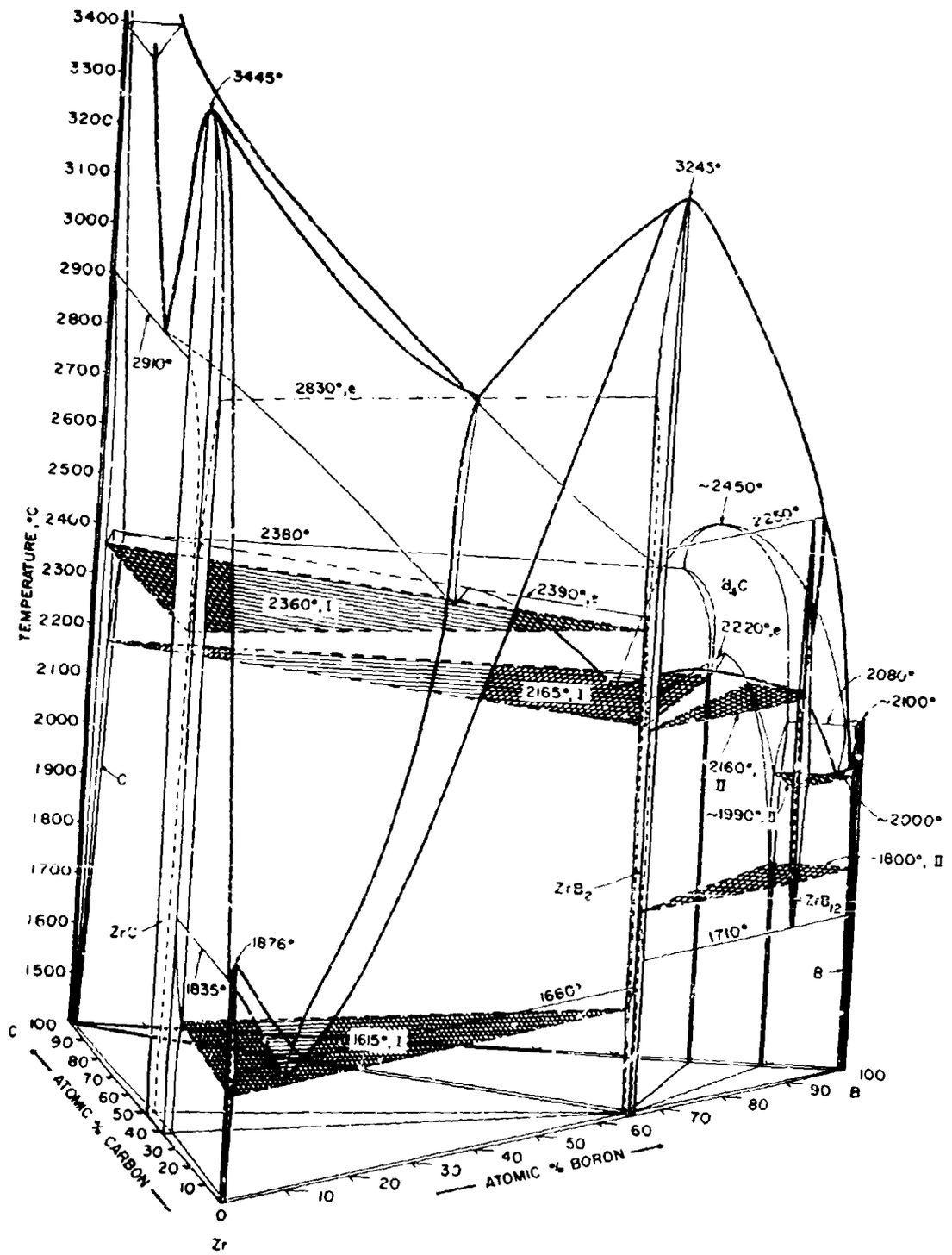

Figure III.K.2.1. Isometric View of the Zr-B-C System

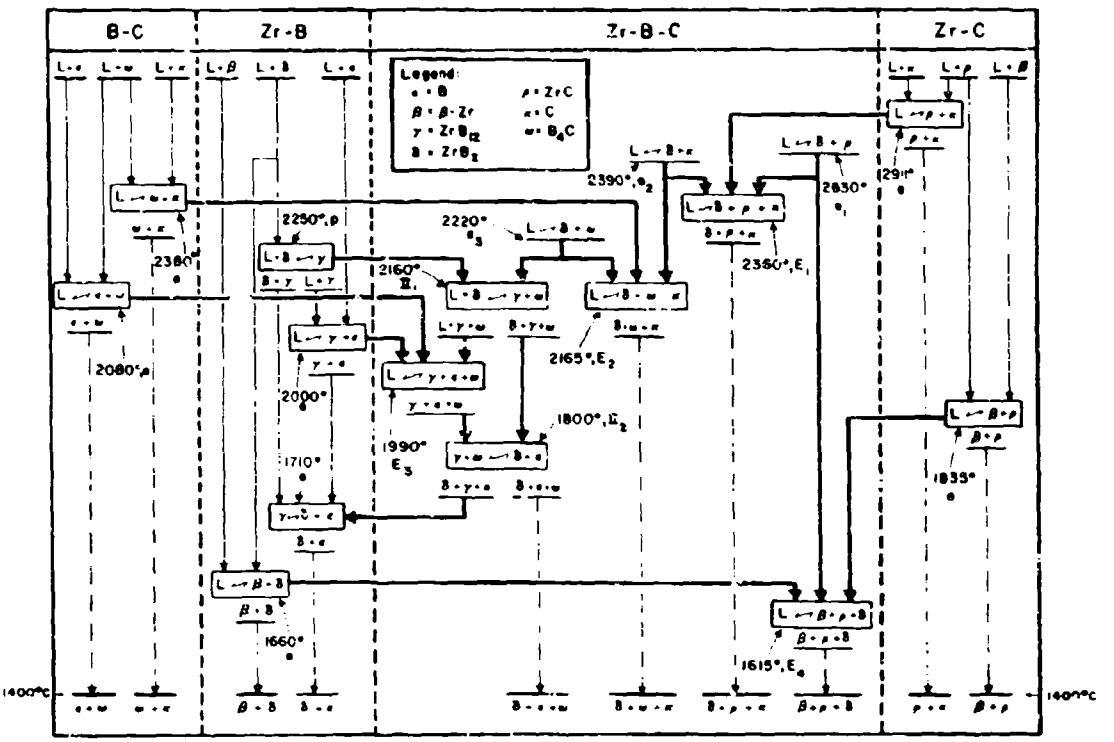

Figure III.K.2.2. Reaction Diagram for the Zr-B-C System

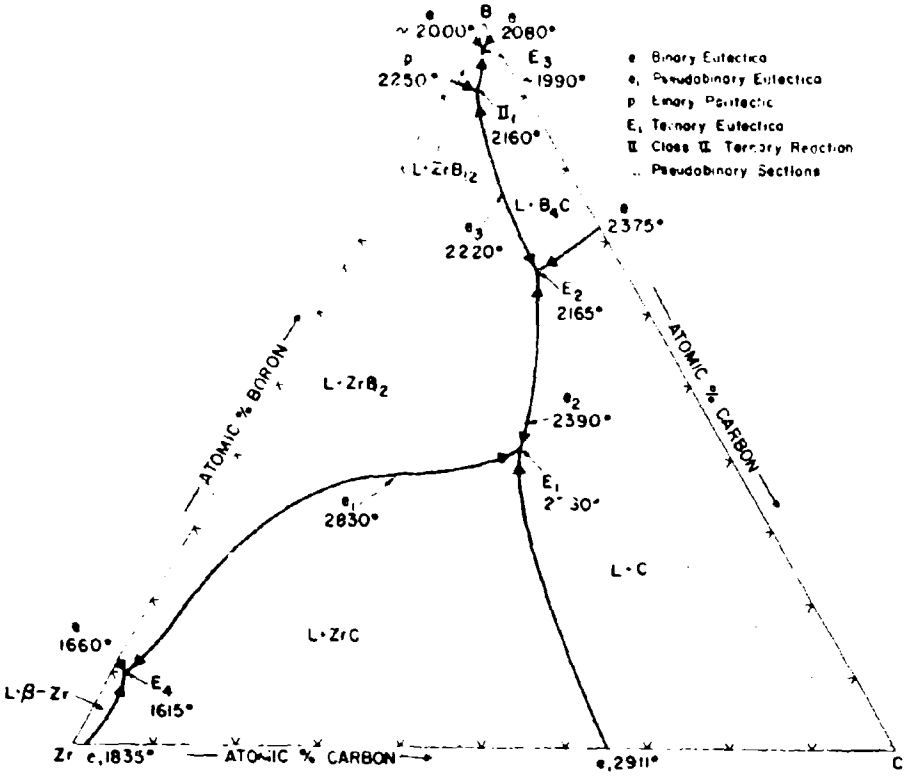

Figure III.K.2.3. Melting Troughs and Non-Variant (p = const) Equilibria Involving Liquid Phases

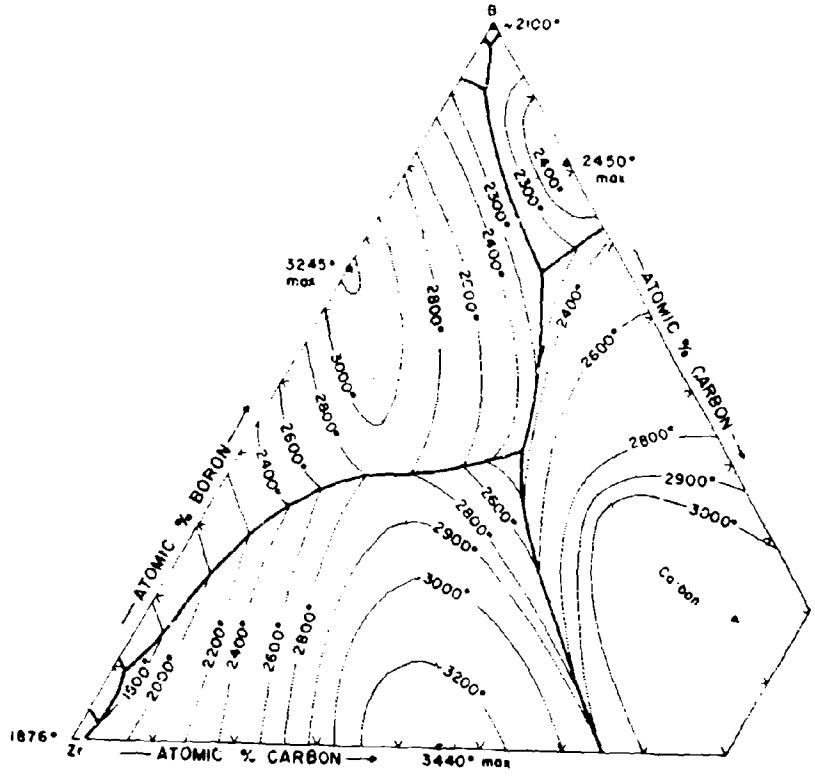

Figure III.K.2.4. Liquidus Projections for the Zr-B-C System (Approximate)

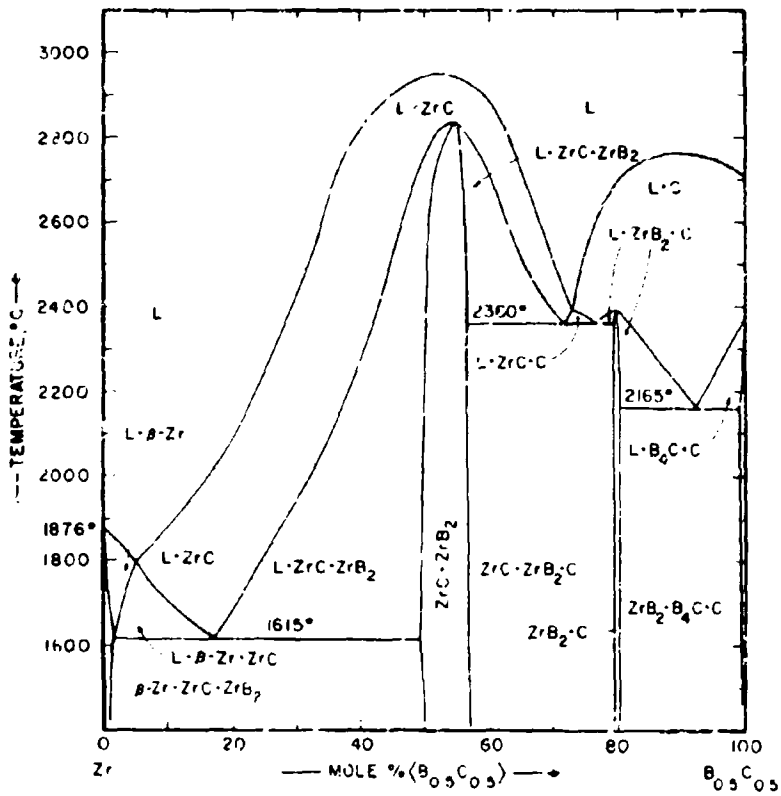

Figure III.K.2.5. Isopleth $Zr-B_{0.5}C_{0.5}$

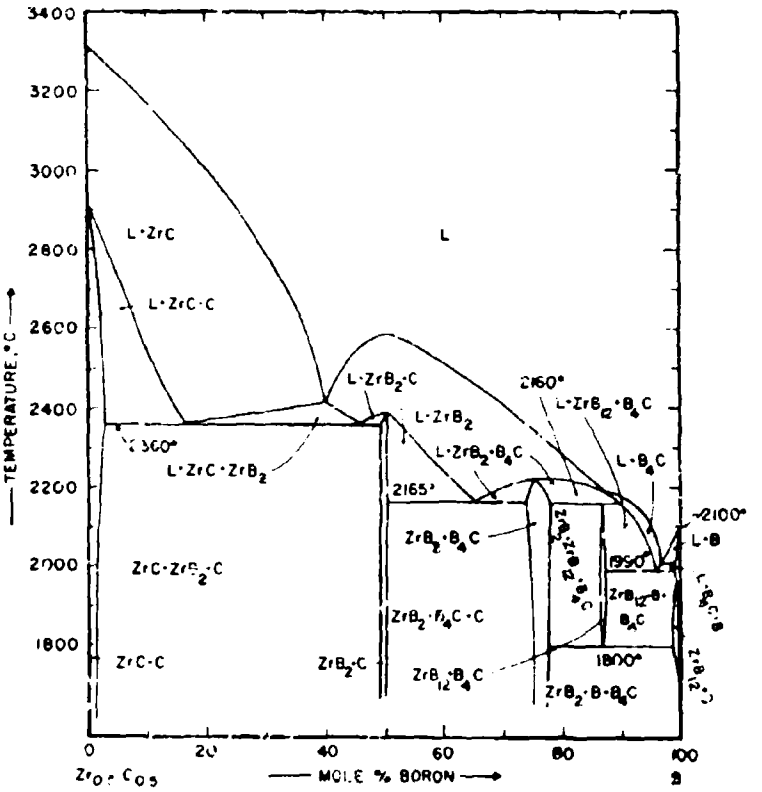

Figure III.K.2.6. Isopleth $Zr_{0.5}C_{0.5}$-B

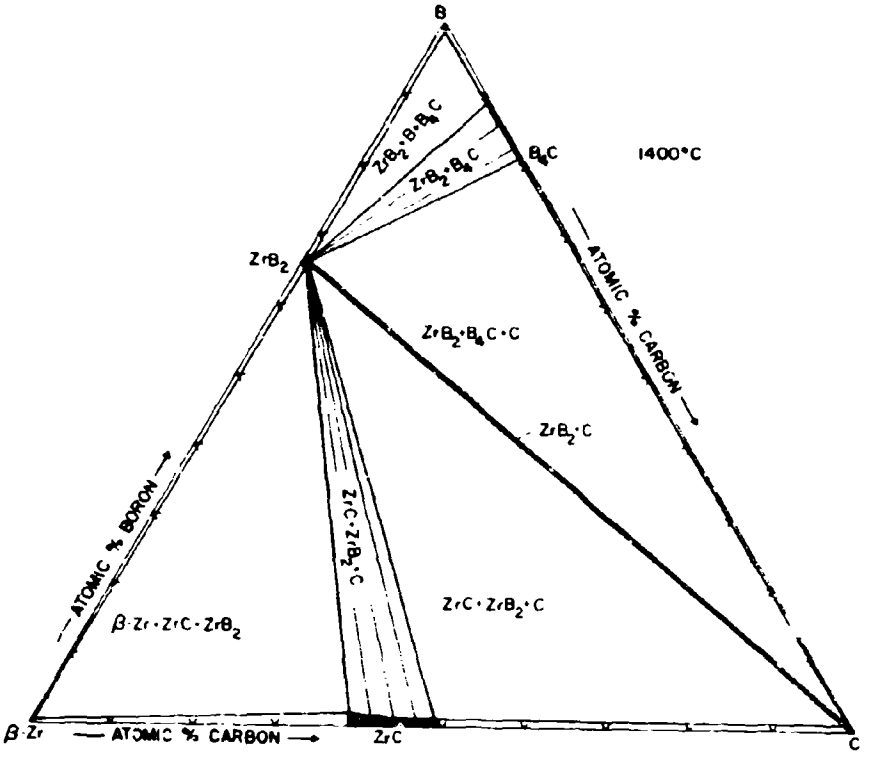

Figure III.K.2.7. Isothermal Section of the Zr-B-C System at 1400°C

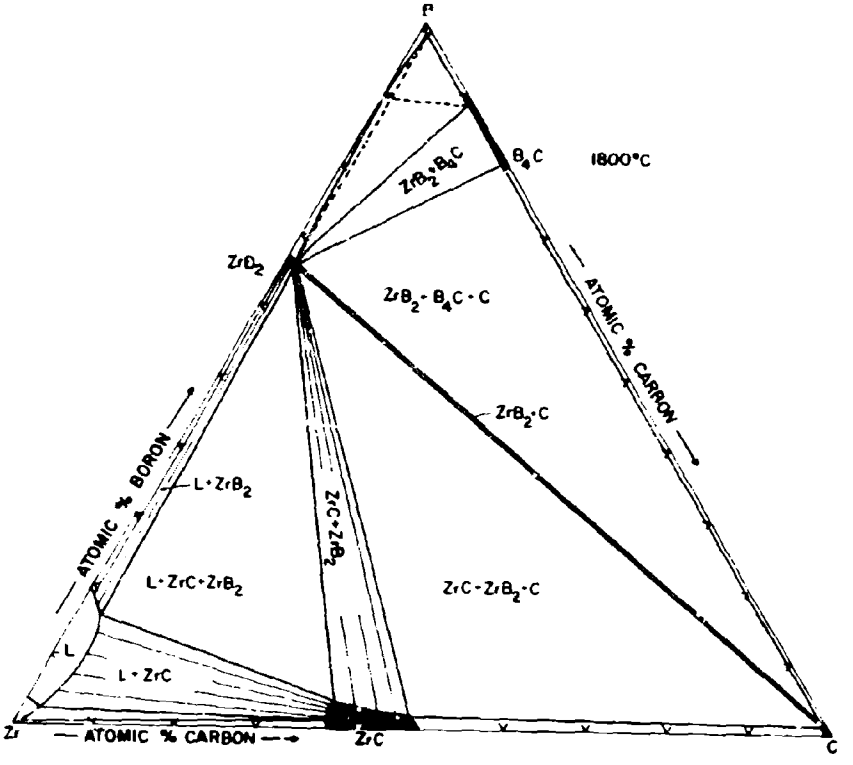

Figure III.K.2.8. Isothermal Section of the Zr-B-C System at 1800° C

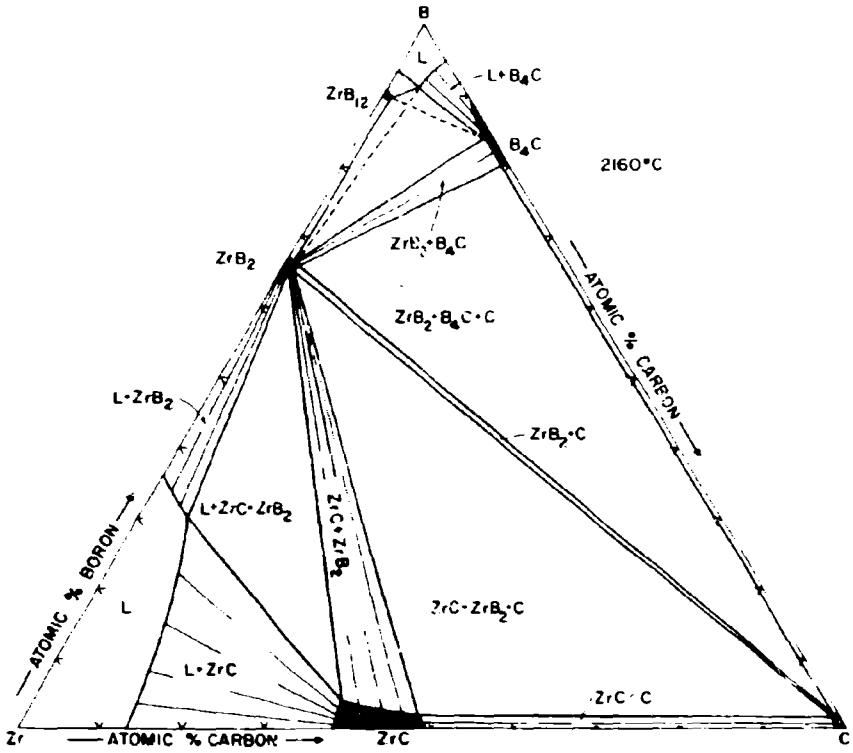

Figure III.K.2.9. Isothermal Section of the Zr-B-C System at 2160°C

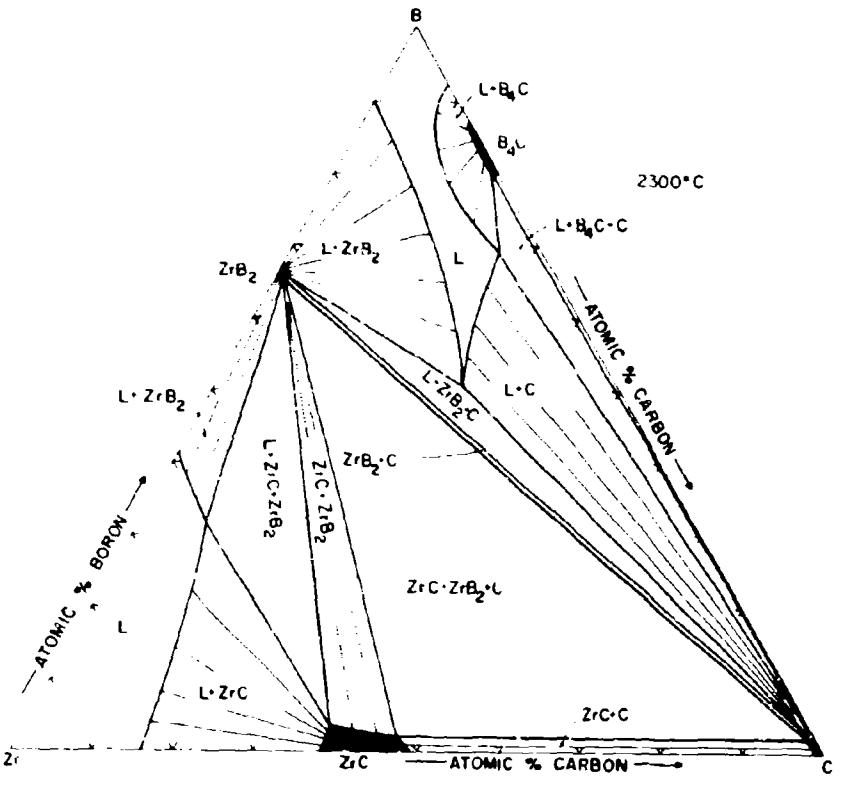

Figure III.K.2.10. Isothermal Section of the Zr-B-C System at 2300° C

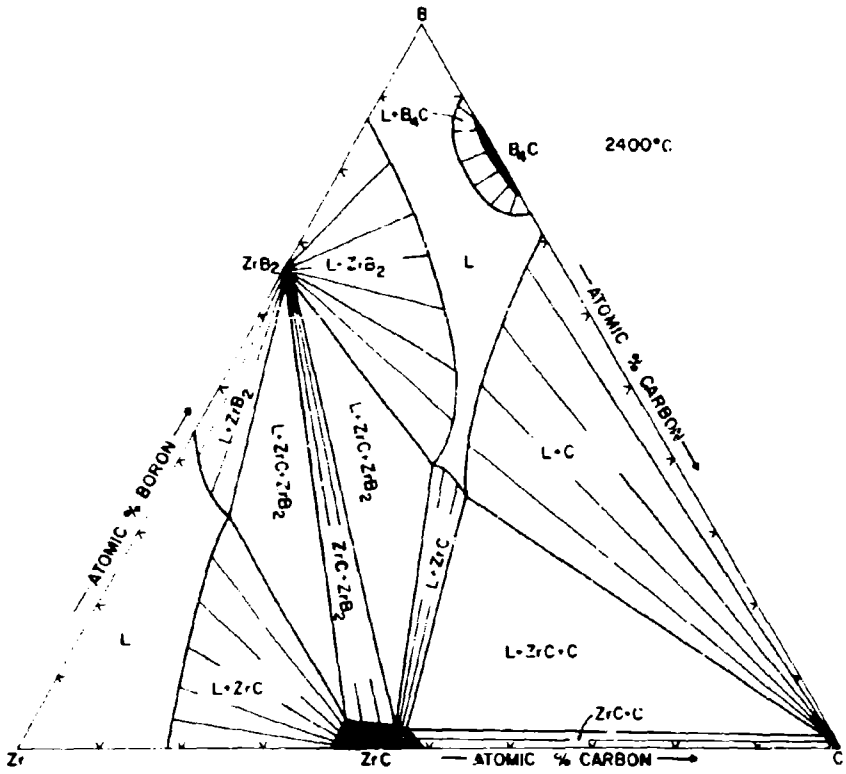

Figure III.K.2.11. Isothermal Section of the Zr-B-C System at 2400° C

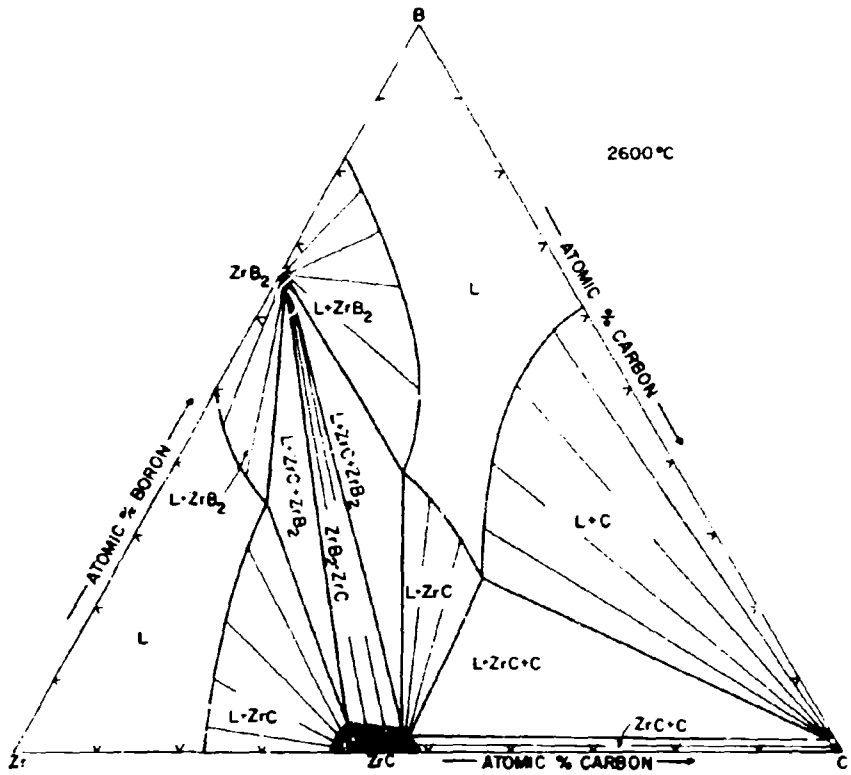

Figure III.K.2.12. Isothermal Section of the Zr-B-C System at 2600°C

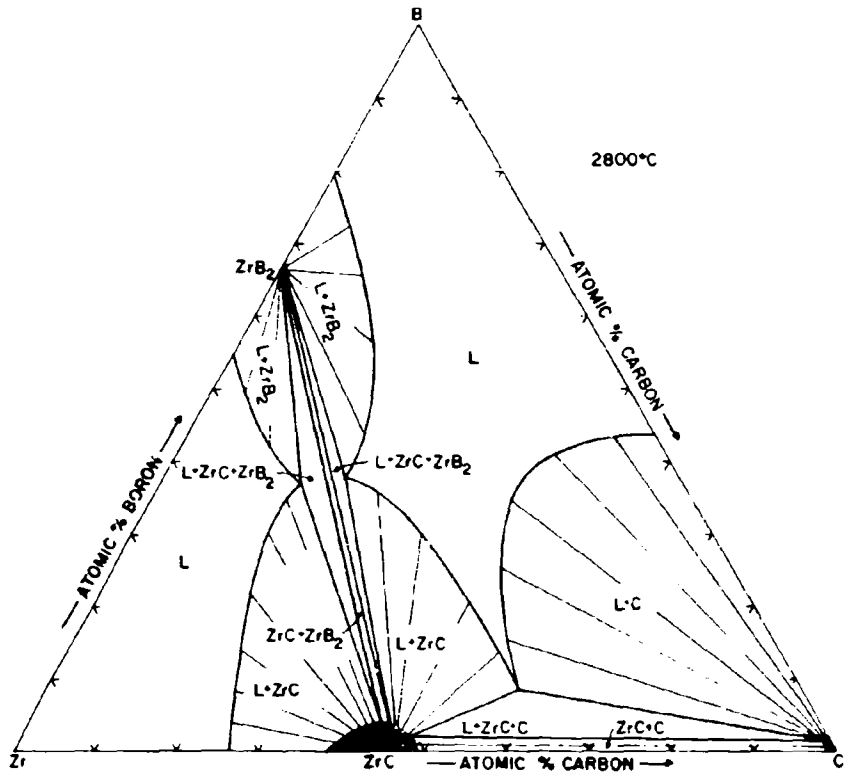

Figure III.K.2.13. Isothermal Section of the Zr-B-C System at 2800° C

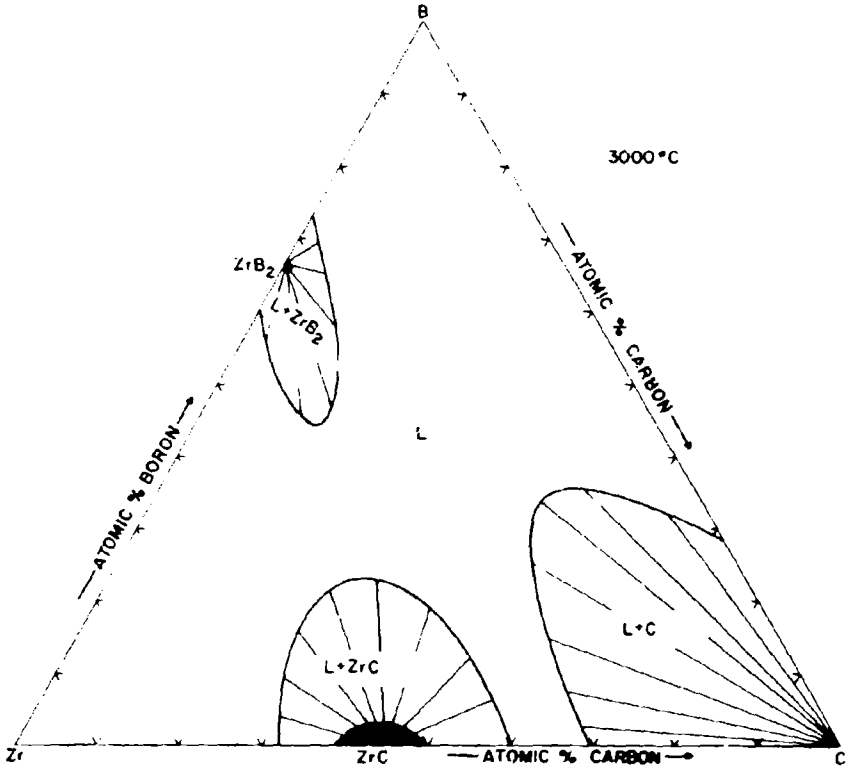

Figure III.K.2.14. Isothermal Section of the Zr-B-C System at 3000° C

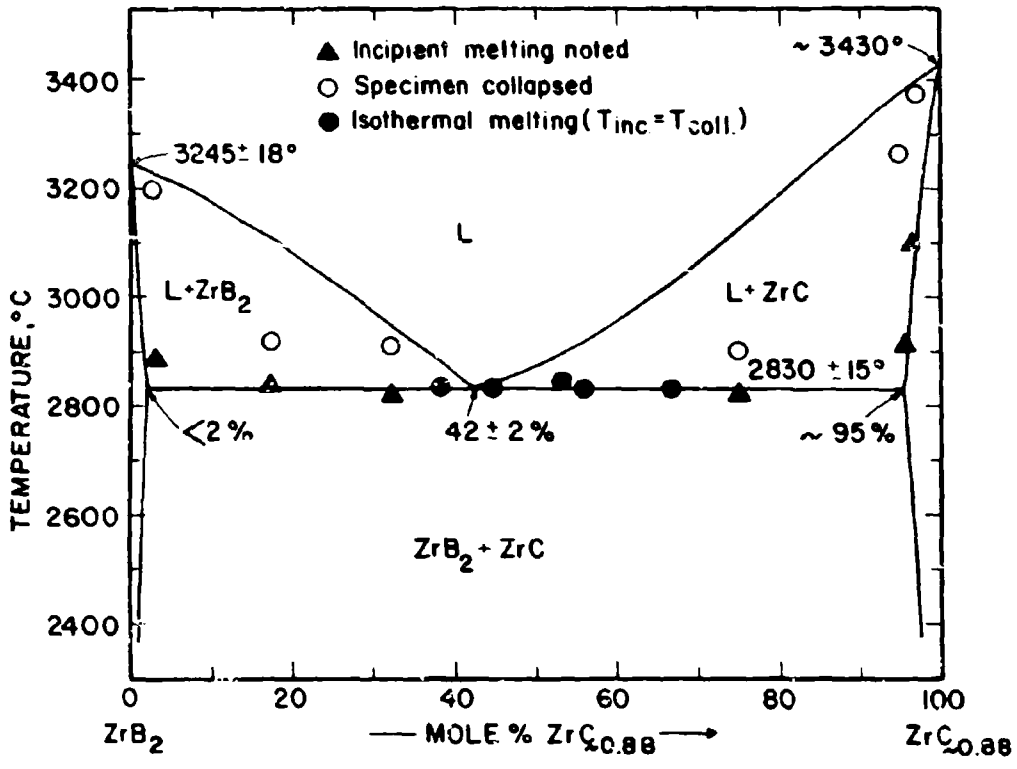

Figure III.K.2.15. Melting Along Pseudobinary Section ZrB_2 + ZrC

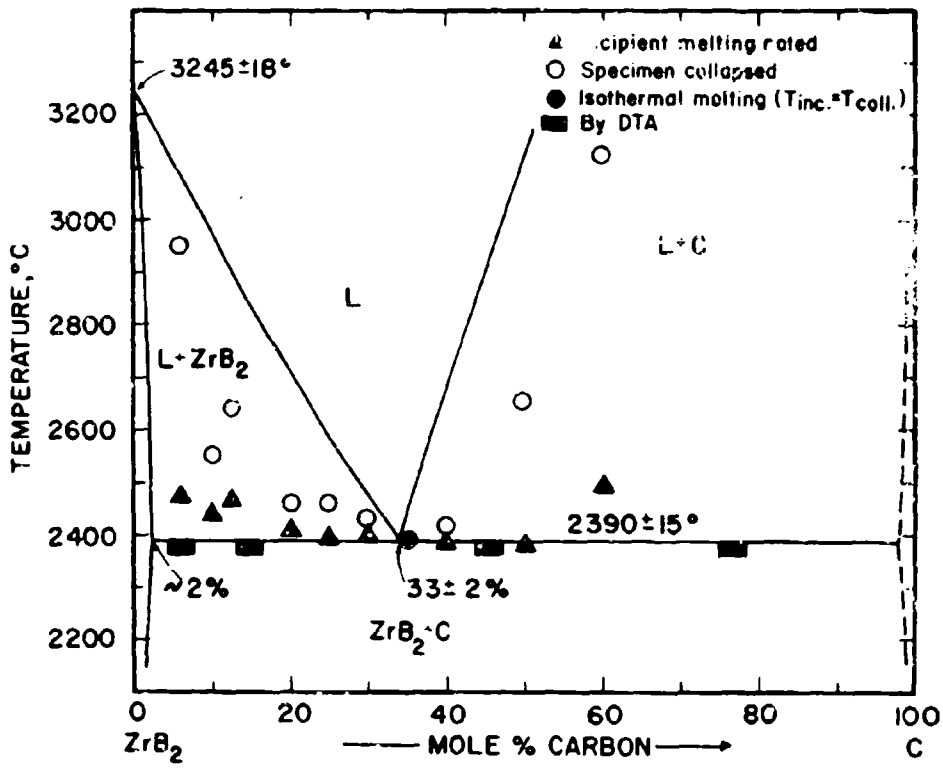

Figure III.K.2.16. Melting Along the Pseudobinary Section ZrB_2 + C

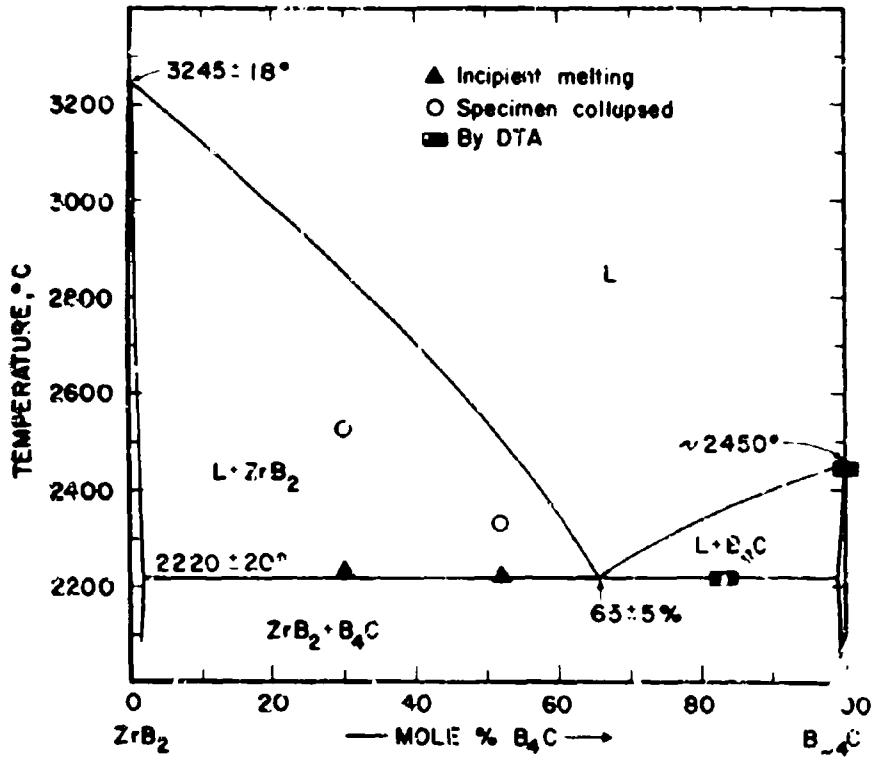

Figure III.K.2.17. Melting Along the Pseudobinary Section $ZrB_2 + B_4C$

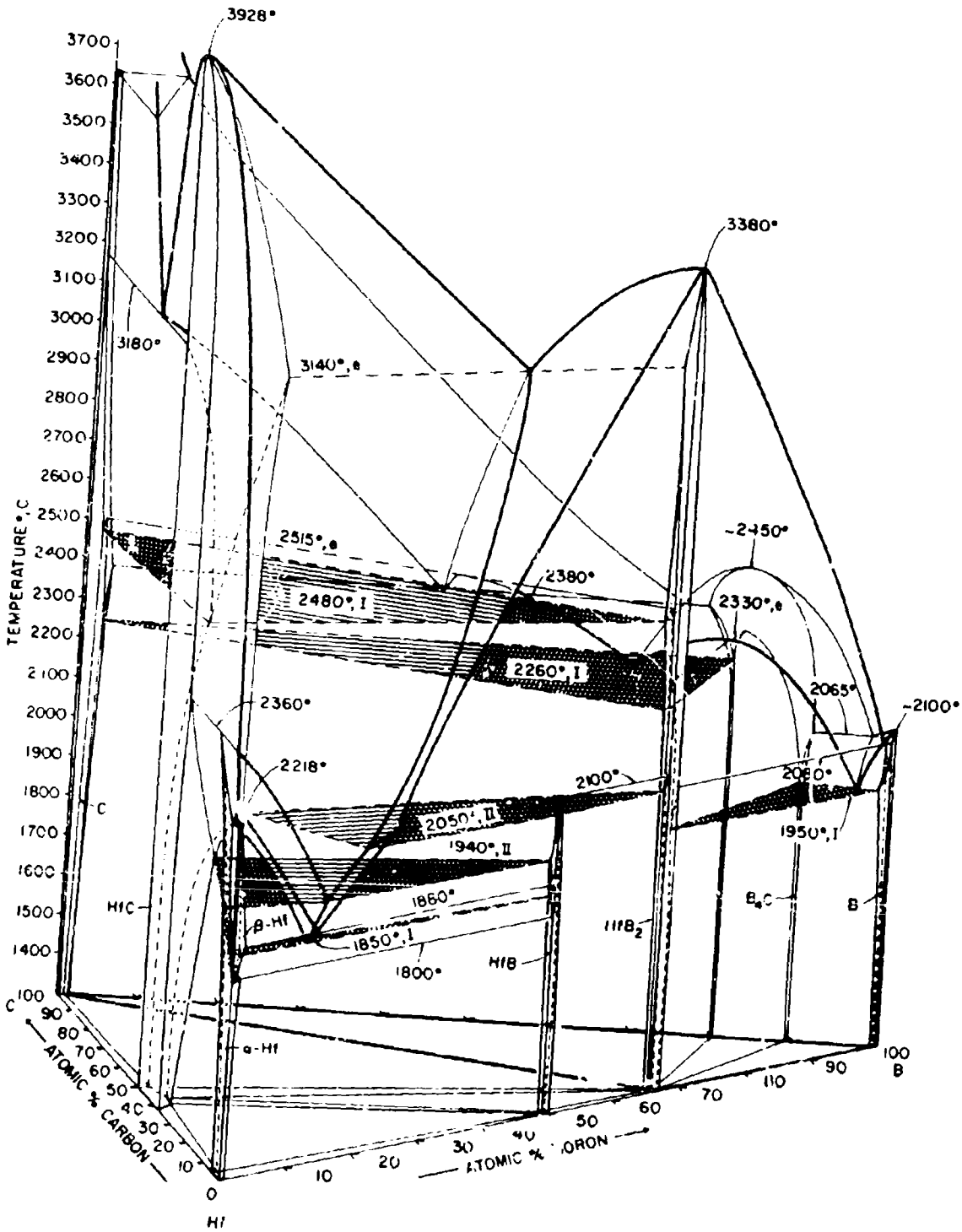

Figure III.K.3.1. Constitution Diagram of the System Hf-B-C

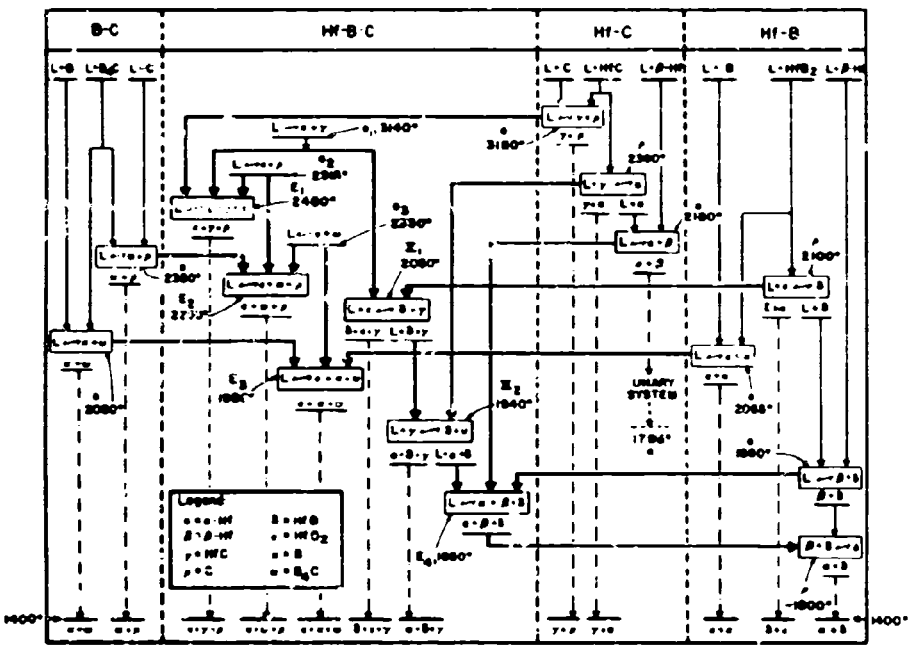

Figure III.K.3.2. Reaction Diagram for Hf-B-C Alloys

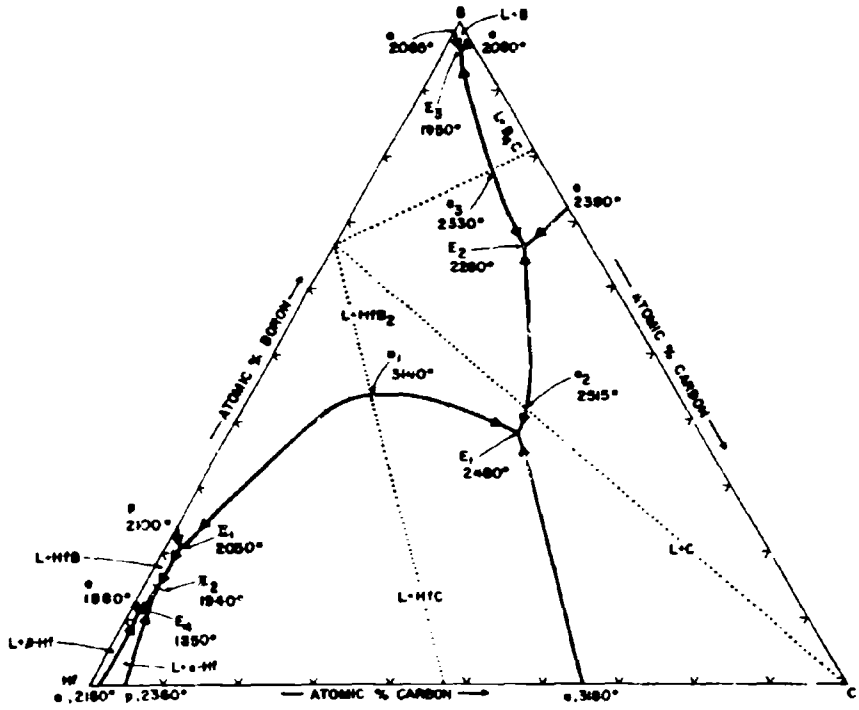

Figure III.K.3.3. Hf-B-C: Melting Troughs and Non-Variant (p = const) Equilibria Involving Liquid Phases

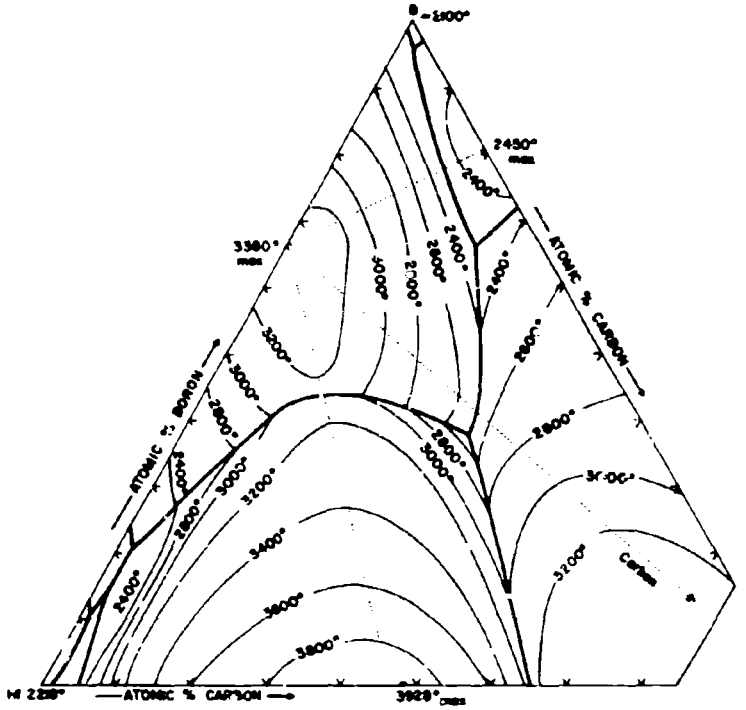

Figure III.K.3.4. Liquidus Projections in the Hf-B-C System (Approximate).

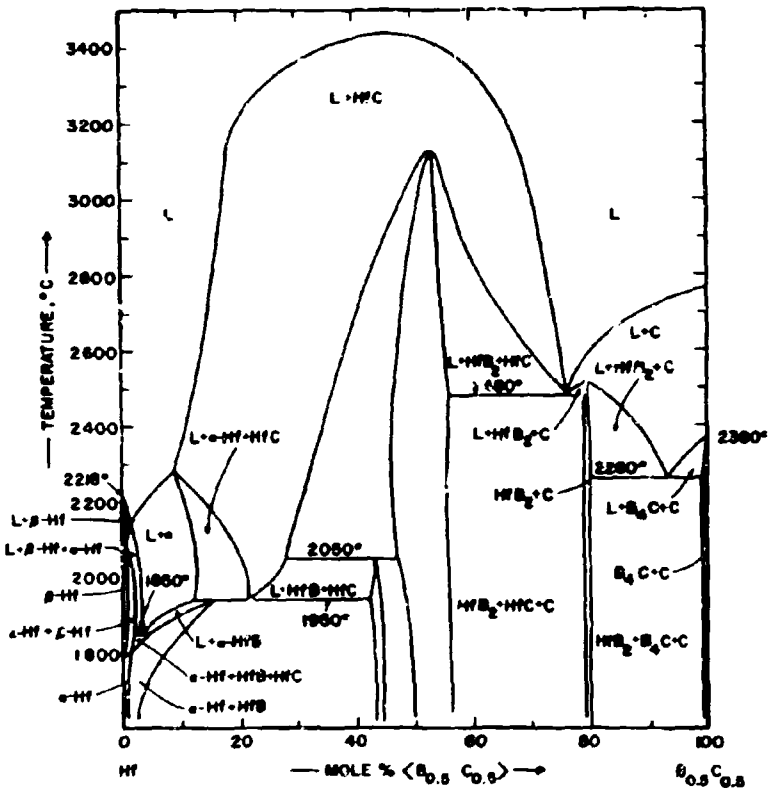

Figure III.K.3.5. Isopleth Hf-$B_{0.5}C_{0.5}$

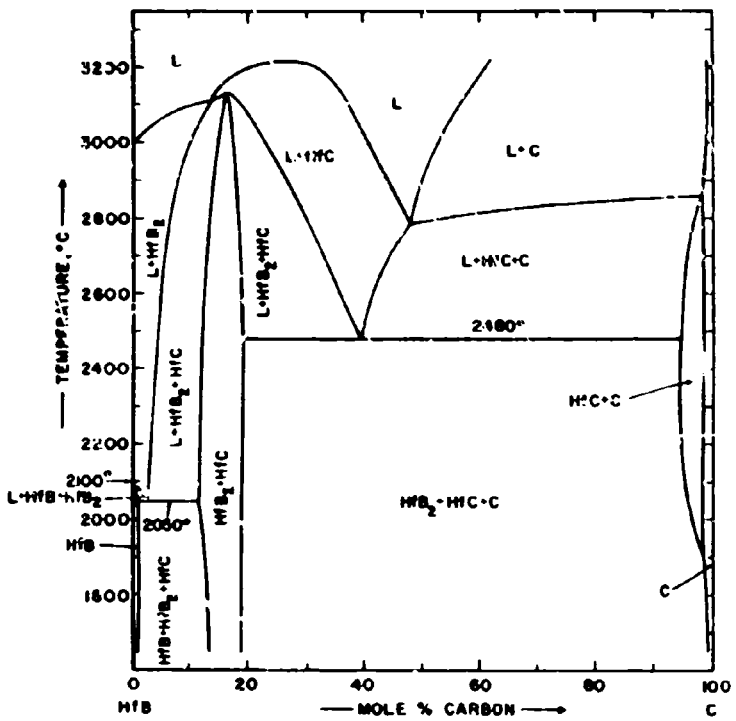

Figure III.K.3.6. Isopleth $Hf_{0.5}B_{0.5}$-C

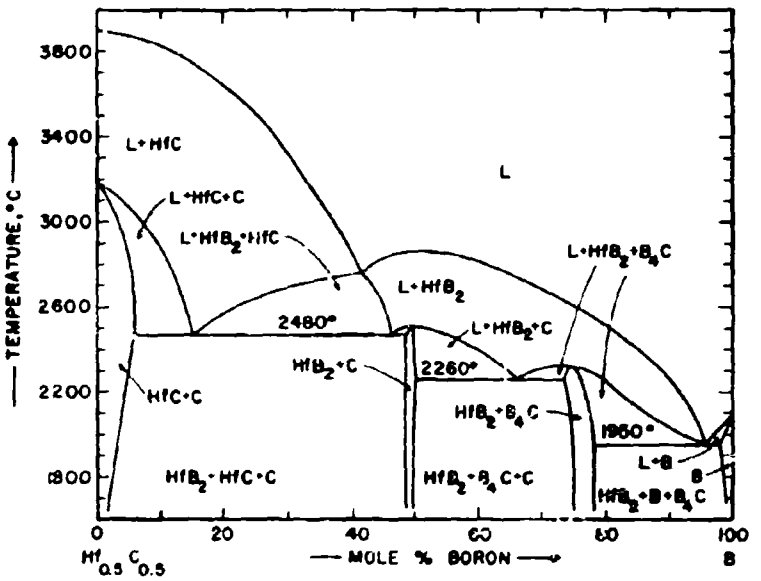

Figure III.K.3.7. Isopleth $Hf_{0.5}C_{0.5}$-B

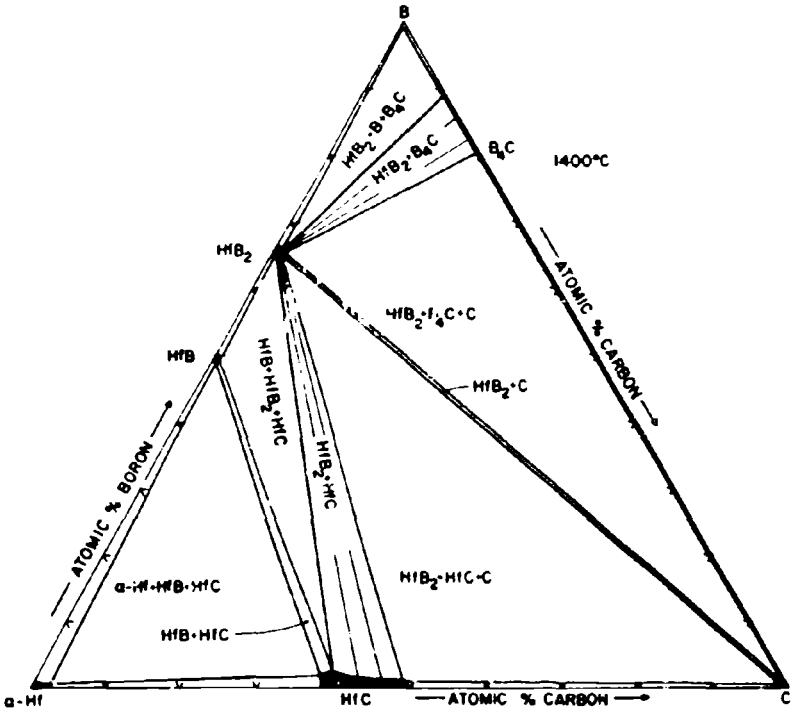

Figure III.K.3.8. Isothermal Section of the Hf-B-C System at 1400° C

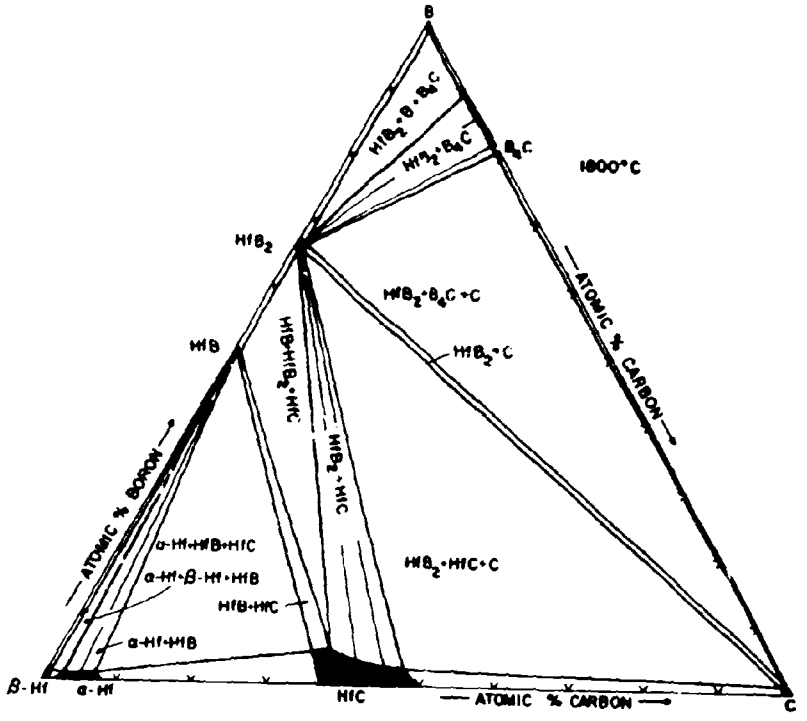

Figure III.K.3.9. Isothermal Section of the Hf-B-C System at 1800°C

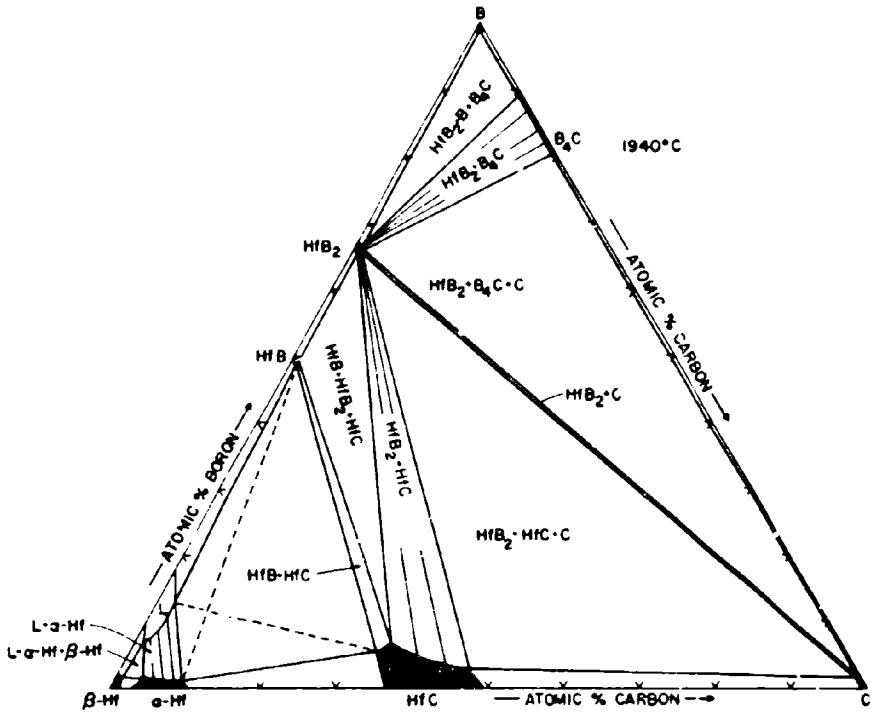

Figure III.K.3.10. Isothermal Section of the Hf-B-C System at 1940° C

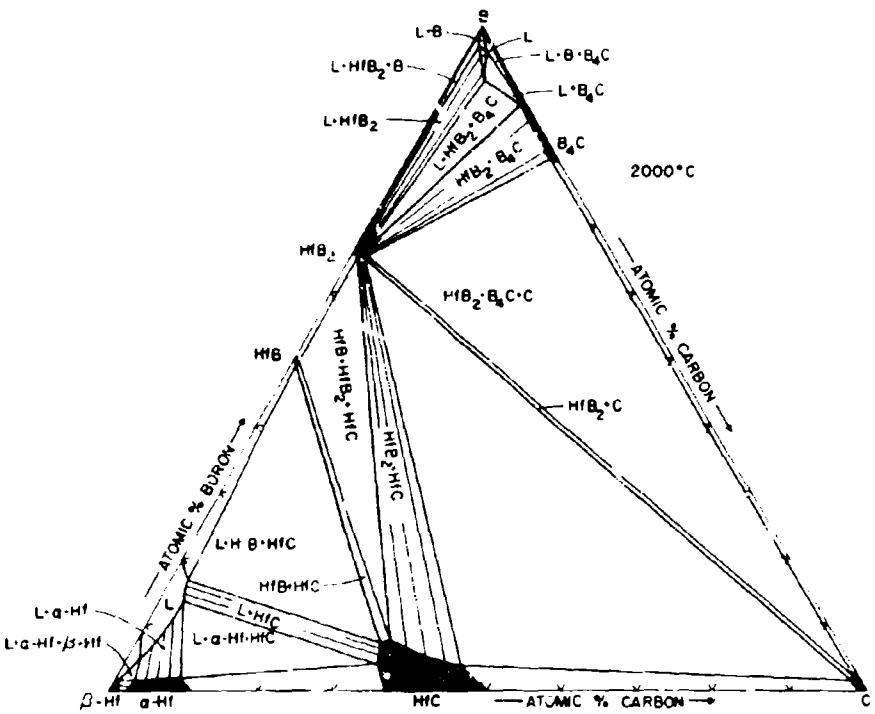

Figure III.K.3.11. Isothermal Section of the Hf-B-C System at 2000° C

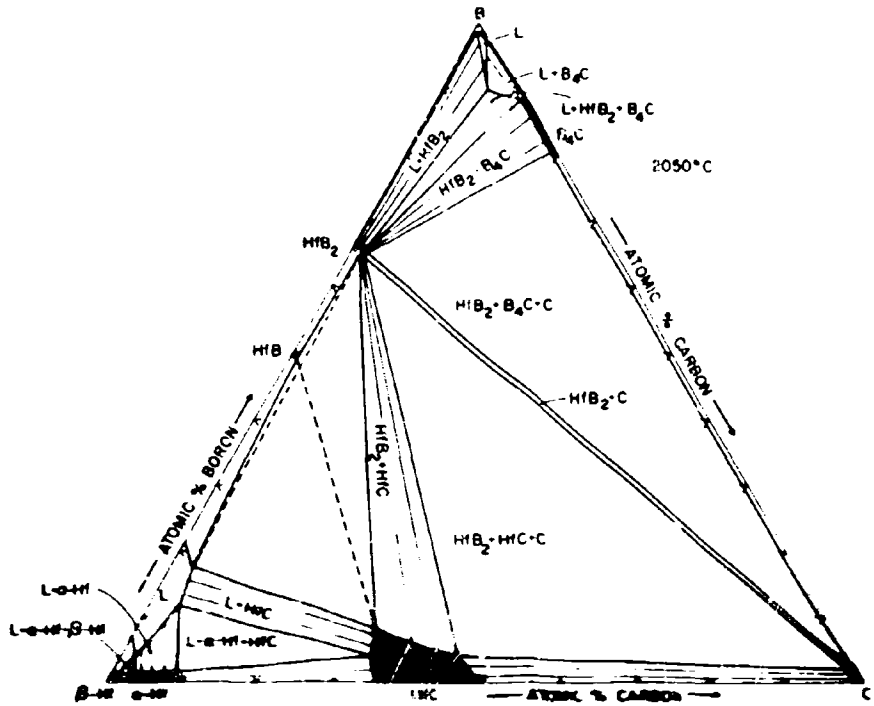

Figure III.K.3.12. Isothermal Section of the Hf-B-C System at 2050° C

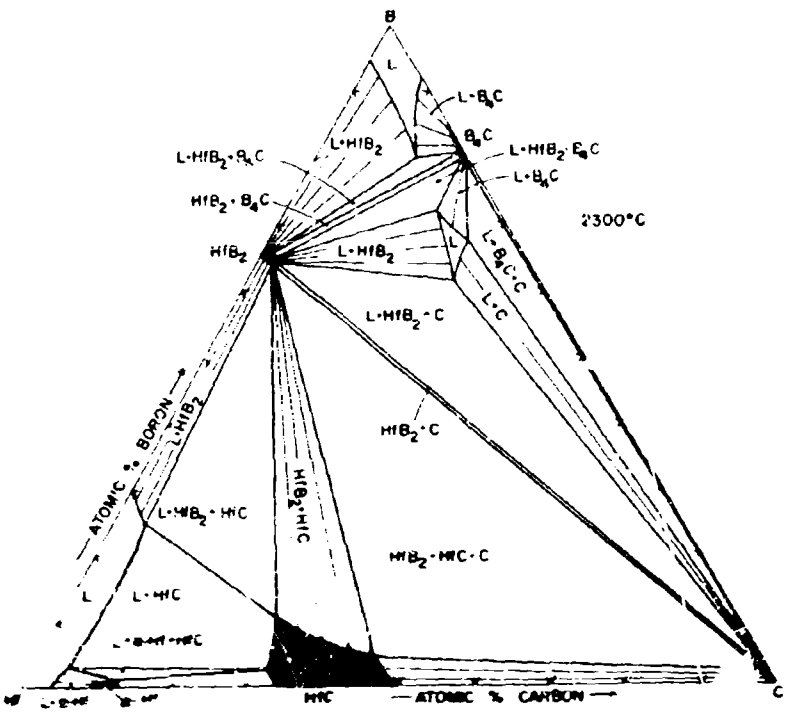

Figure III.K.5.13. Isothermal Section of the Hf-B-C System at 2300° C

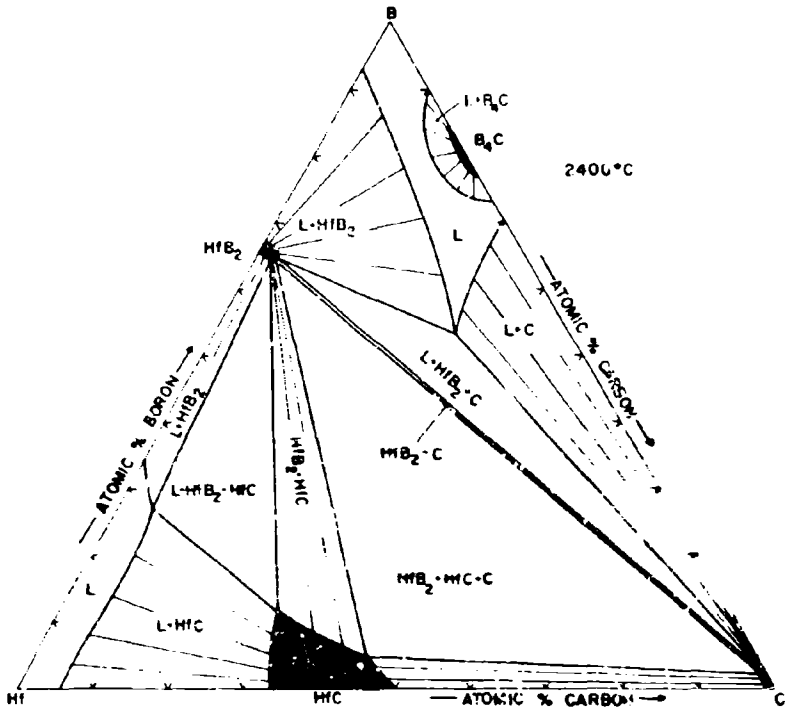

Figure III.K.3.14. Isothermal Section of the Hf-B-C System at 2400° C

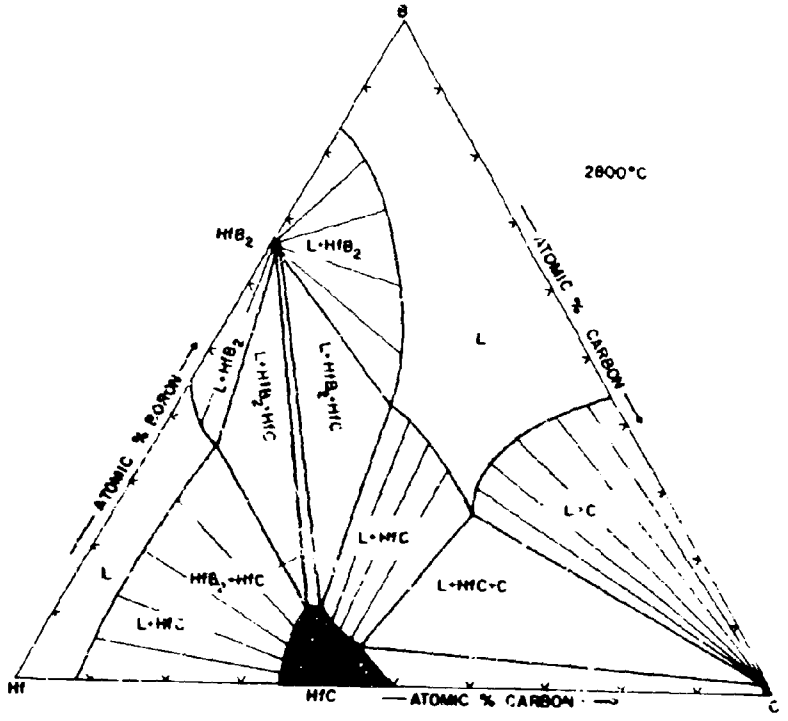

Figure III.K.3.15. Isothermal Section of the Hf-B-C System at 2800° C

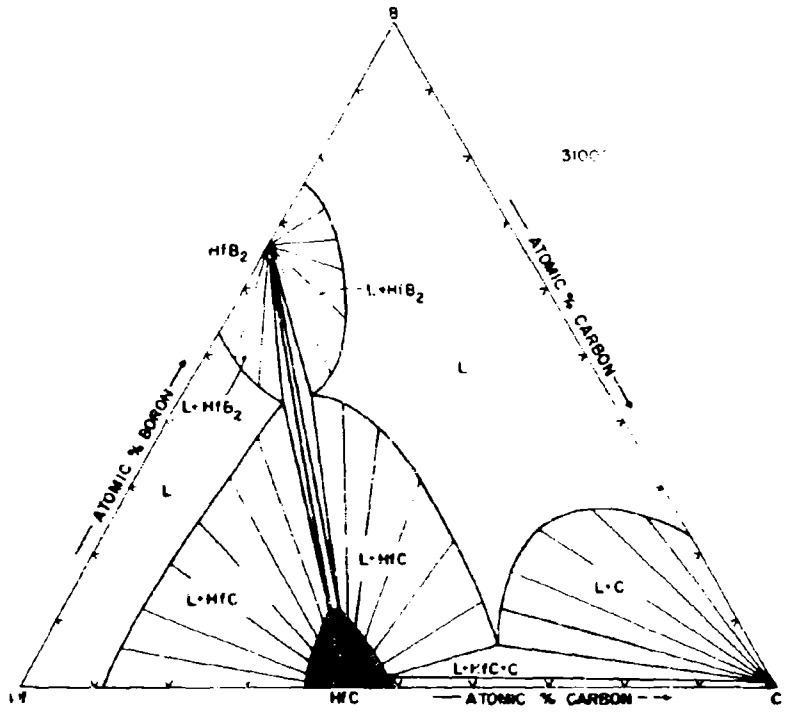

Figure III.K.3.16. Isothermal Section of the Hf-B-C System at 3100°C

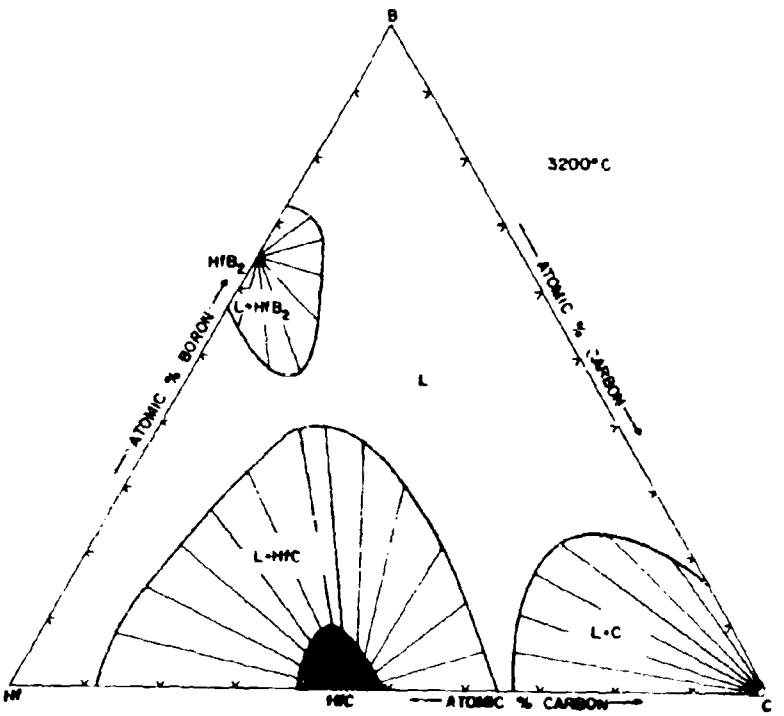

Figure III.K.3.17. Isothermal Section of the Hf-B-C System at 3200° C

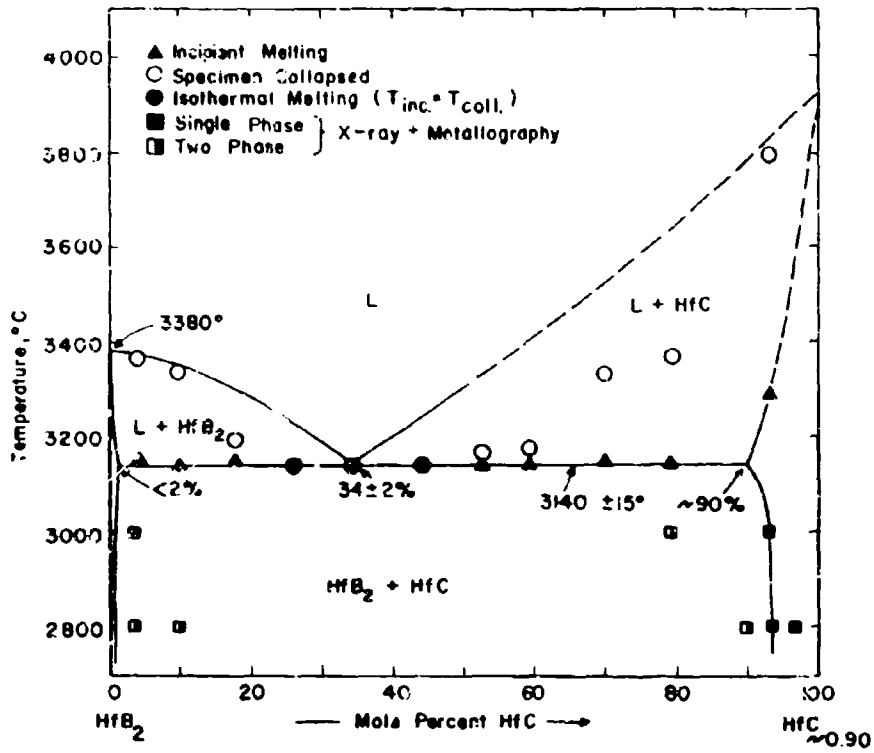

Figure III.K.3.18. Experimental Data on Alloys Located Along the Pseudobinary Section HfB_2-HfC_{1-x}

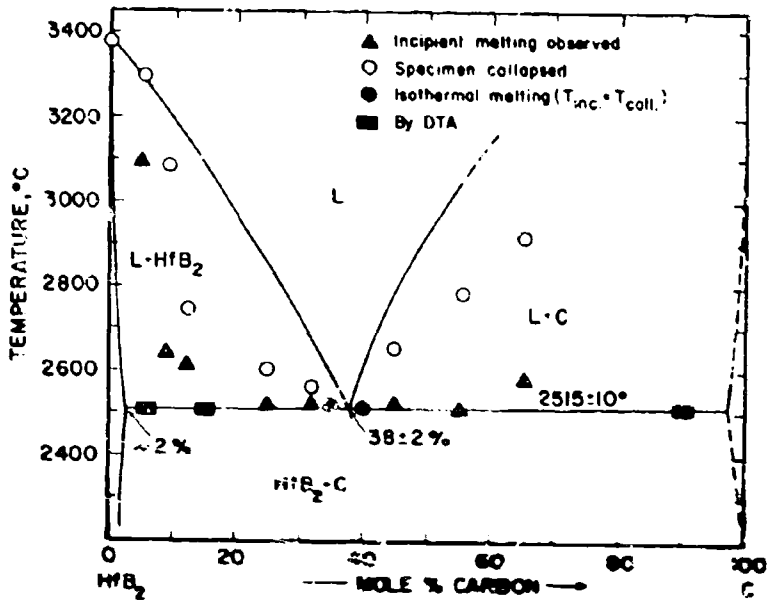

Figure III.K.3.19. Melting Along the Pseudobinary Section HfB_2-C

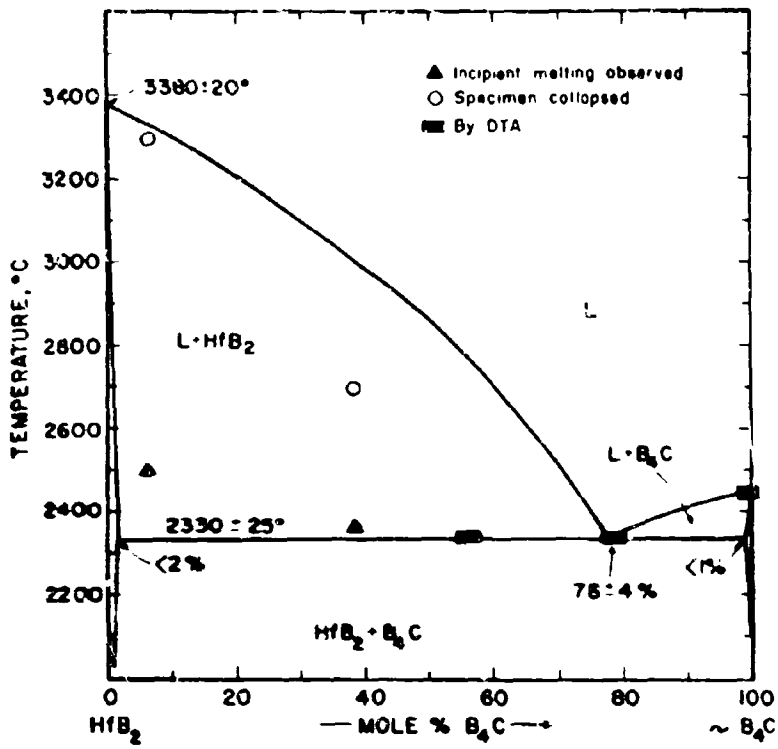

Figure III.K.3.20. Melting in Pseudobinary HfB_2 + B_4C Alloys

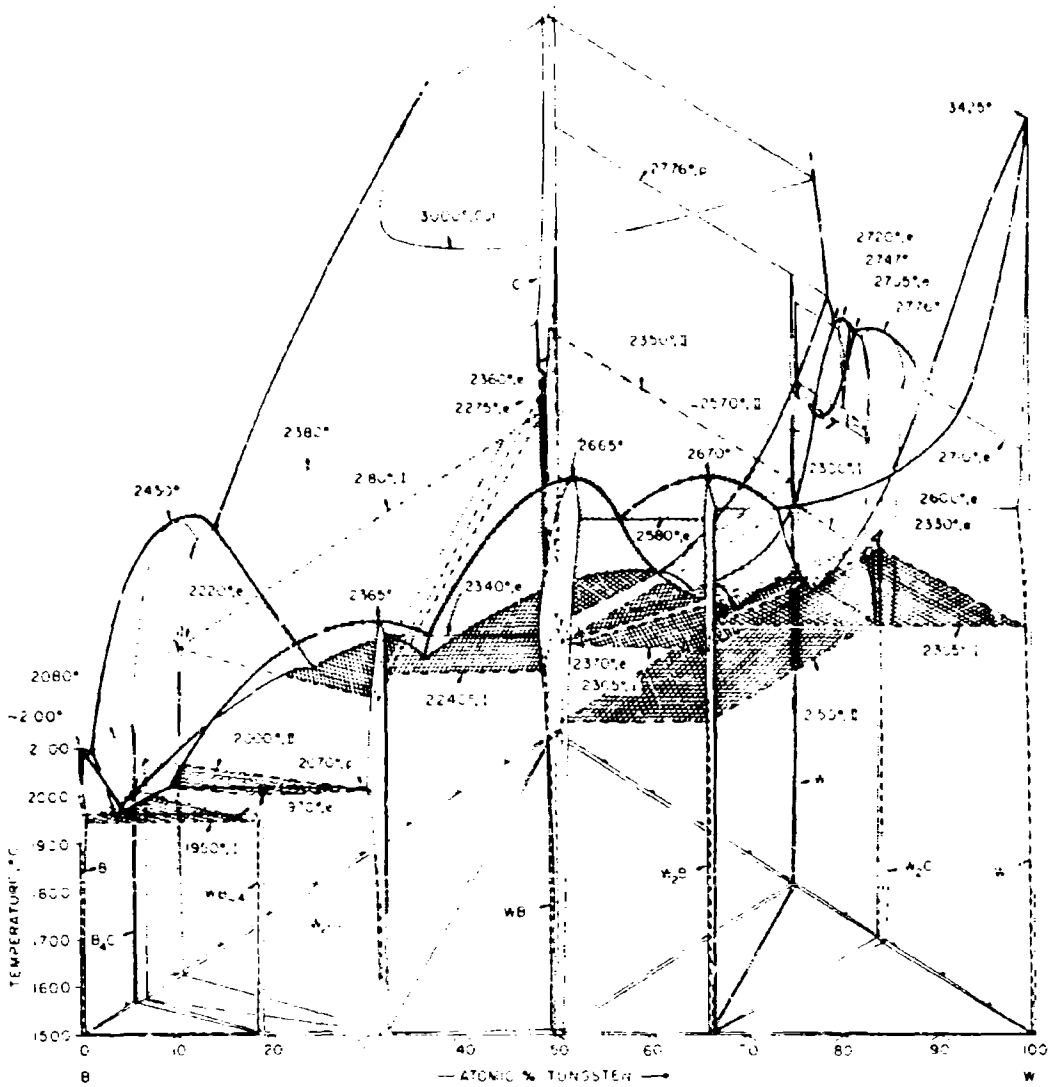

Figure III.K.4.1. Isometric View of the W-B-C System

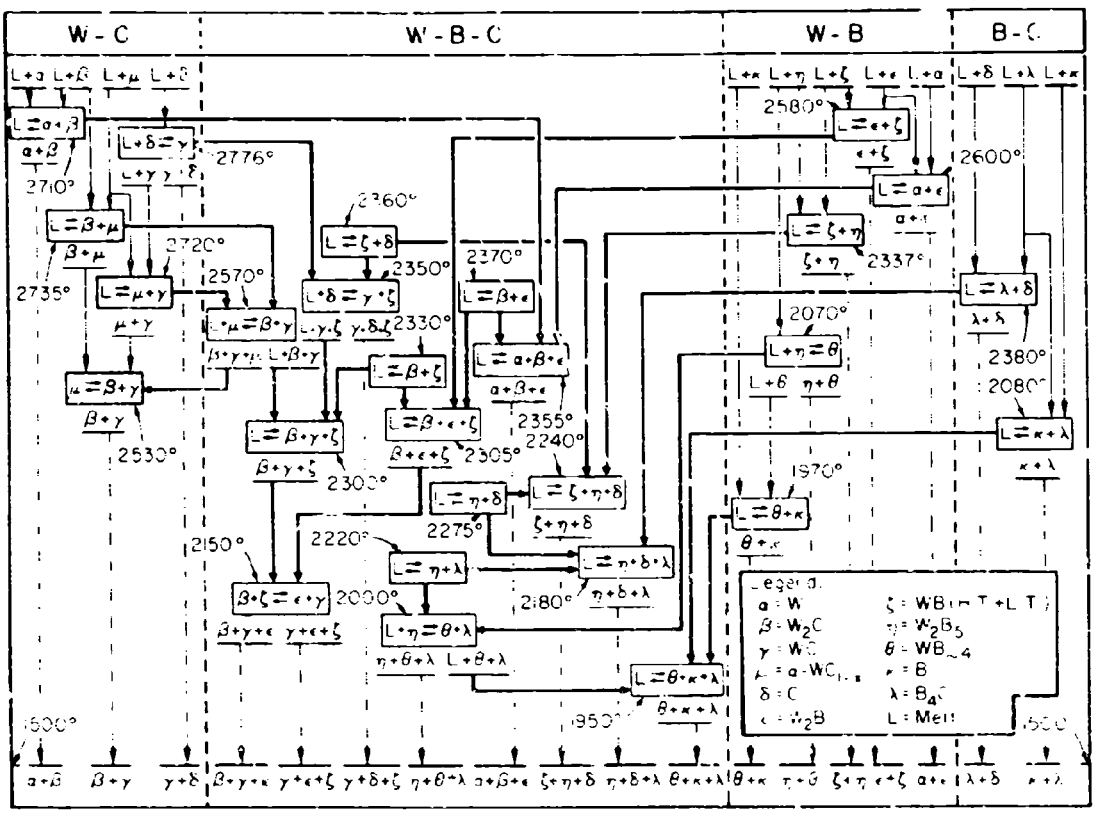

Figure III.K.4.2. Reaction Diagram for the W-B-C System

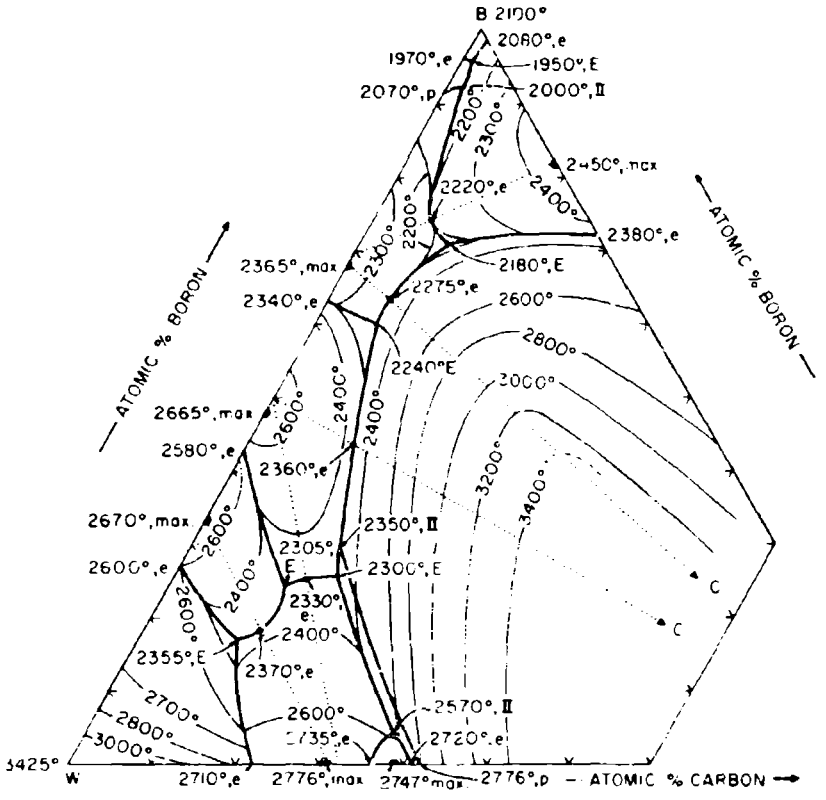

Figure III.K.4.3. Liquidus Projections in the W-B-C Systems

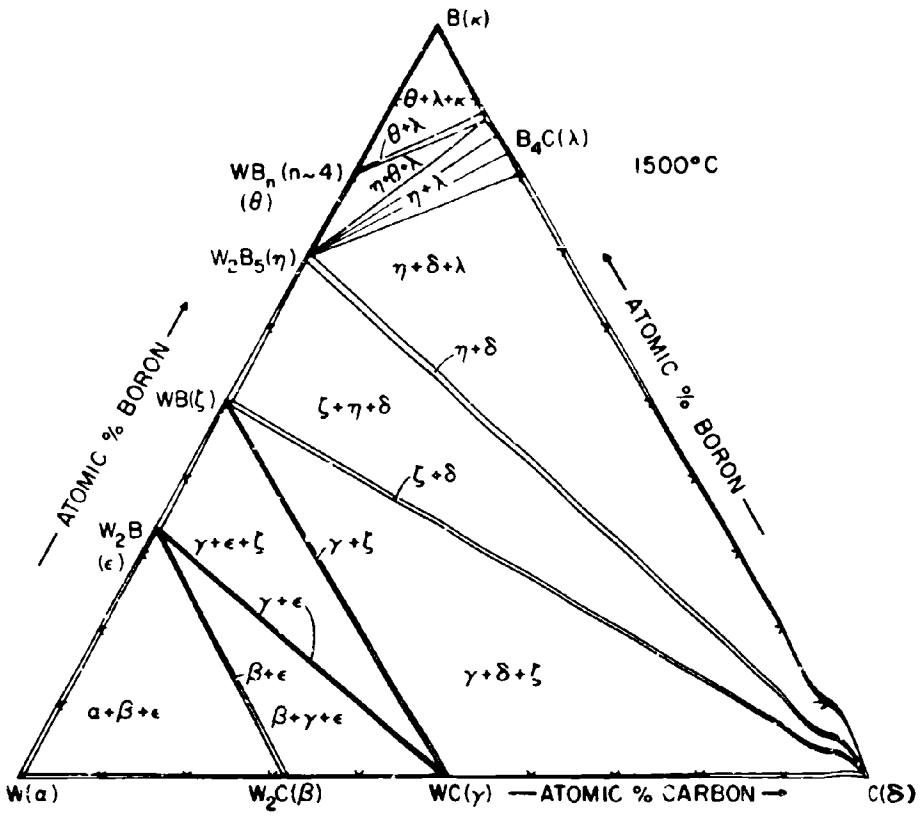

Figure III.K.4.4. Isothermal Section of the W-B-C System at 1500° C

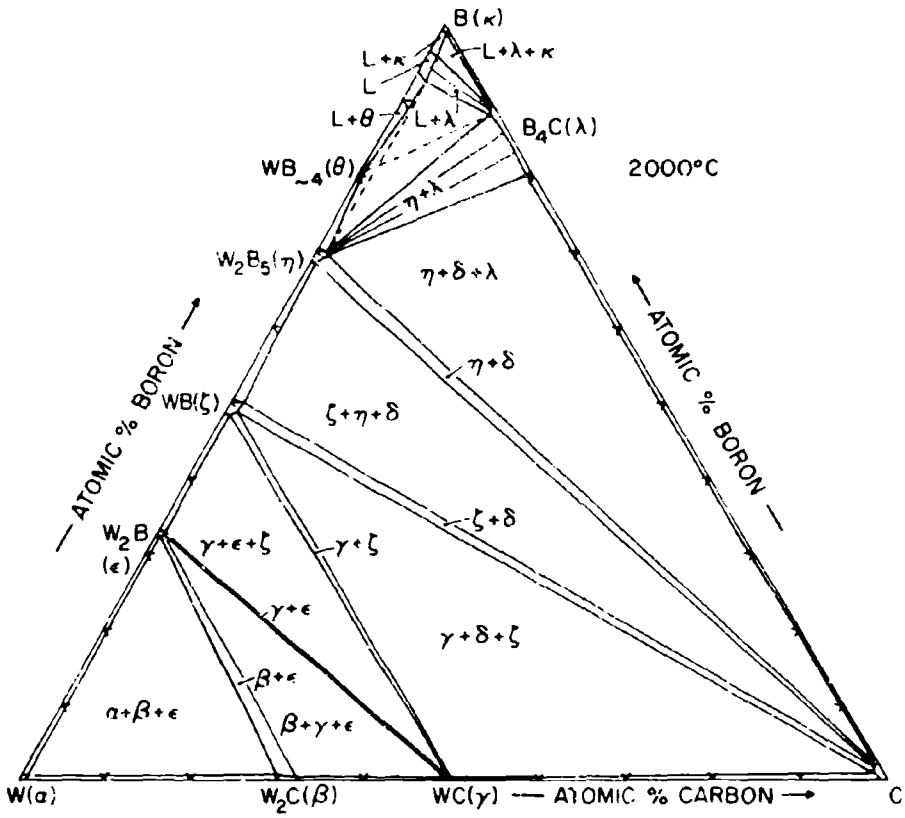

Figure III.K.4.5. Isothermal Section of the W-B-C System at 2000° C

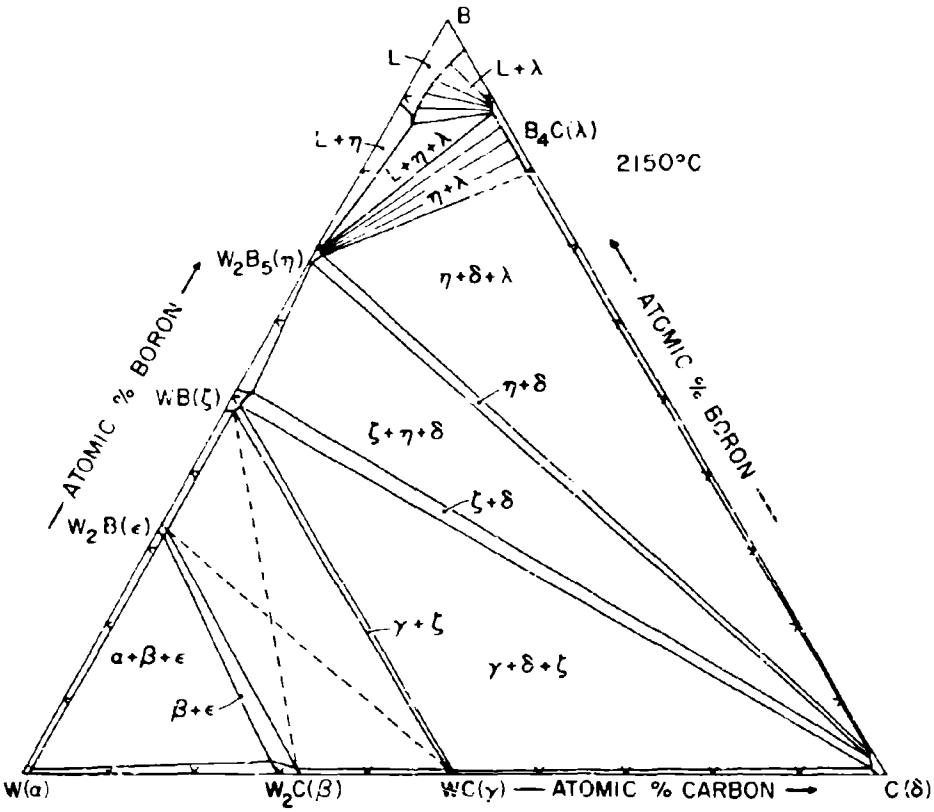

Figure III.K.4.6. Isothermal Section of the W-B-C System at 2150°C

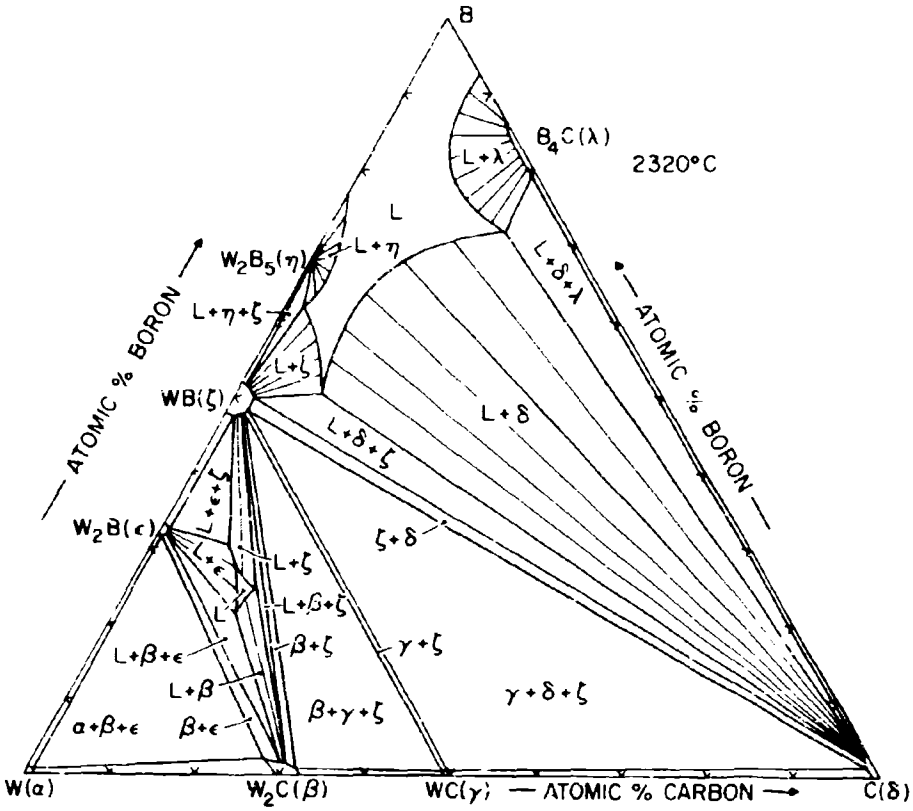

Figure III.K.4.7. Isothermal Section of the W-B-C System at 2320° C

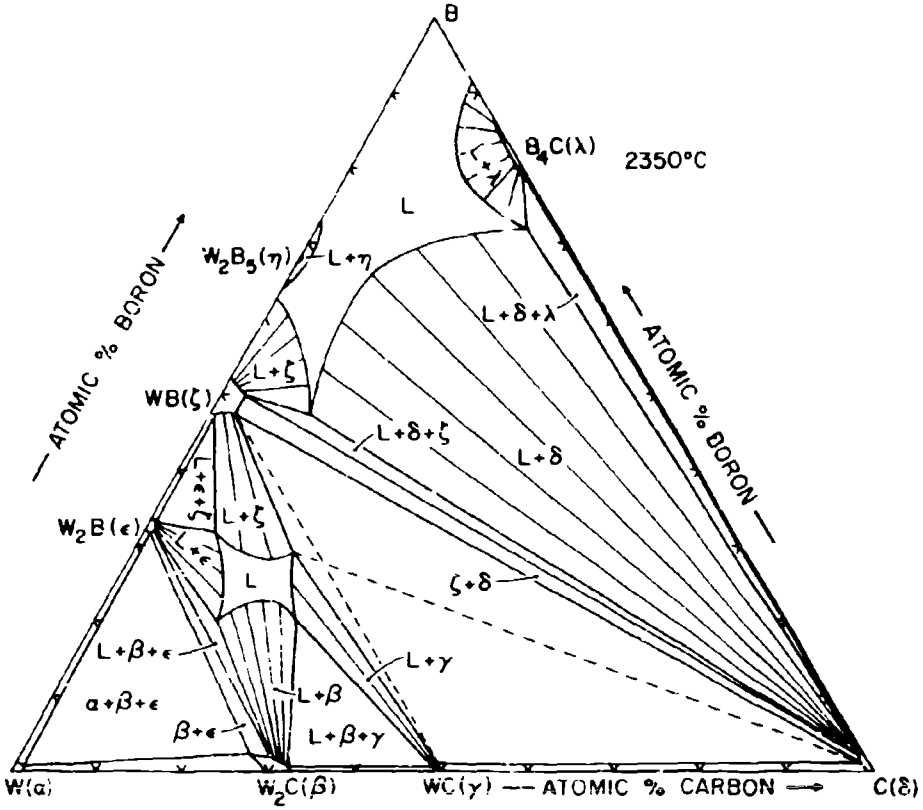

Figure III.K.4.8. Isothermal Section of the W-B-C System at 2350° C

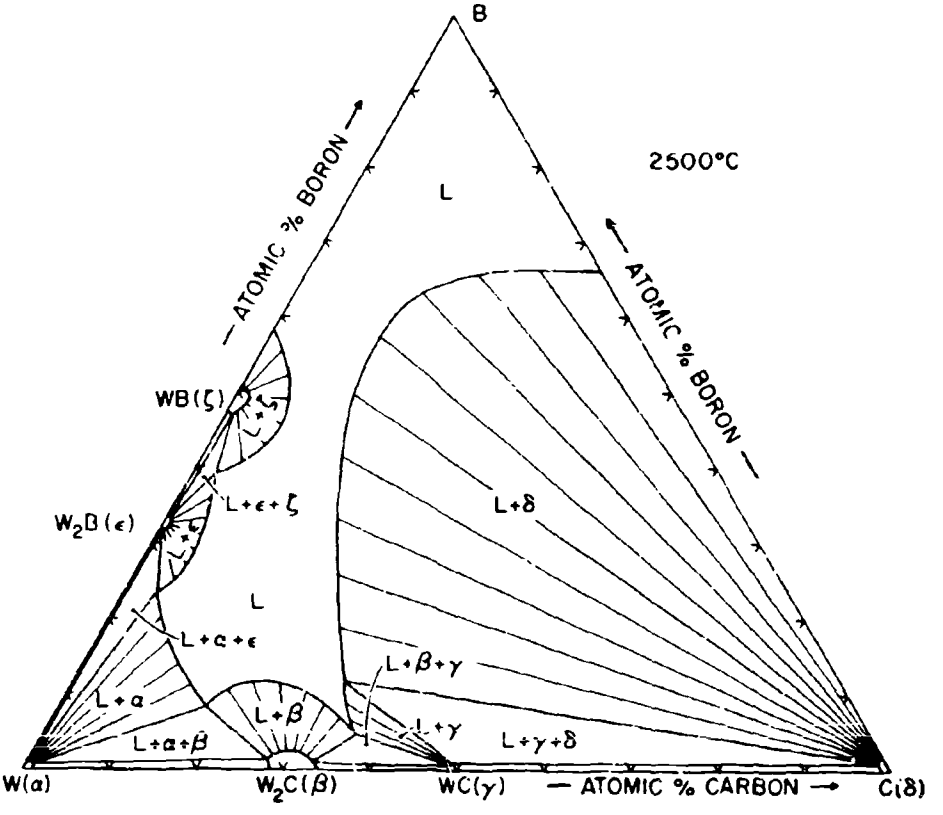

Figure III.K.4.9. Isothermal Section of the W-B-C System at 2500° C

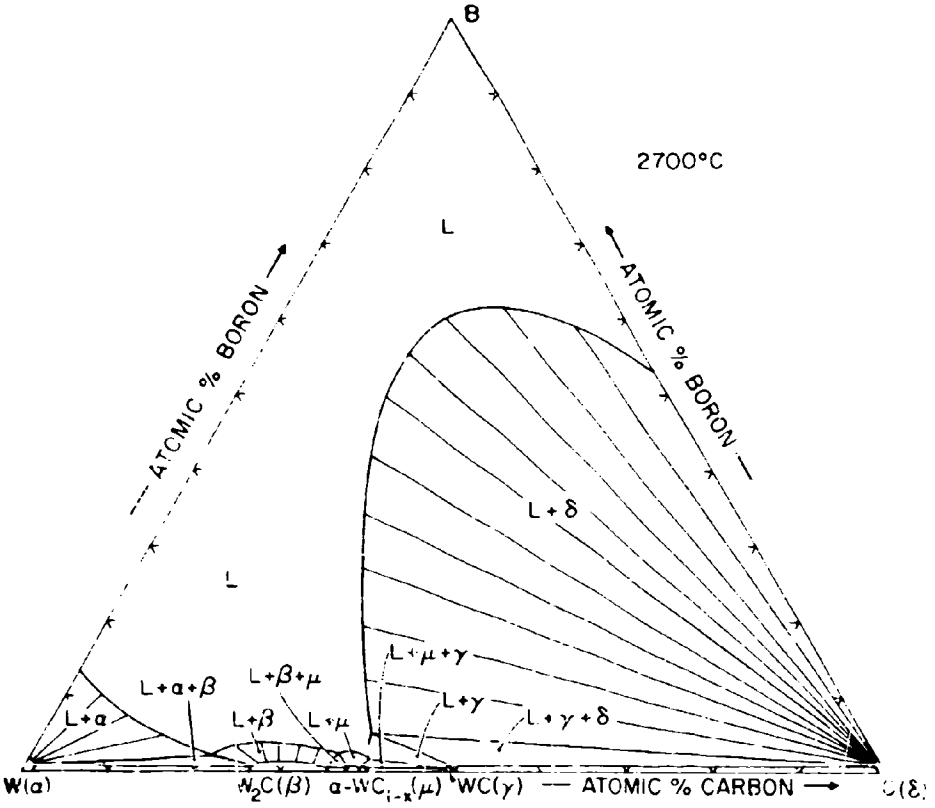

Figure III.K.4.10. Isothermal Section of the W-B-C System at 2700°C

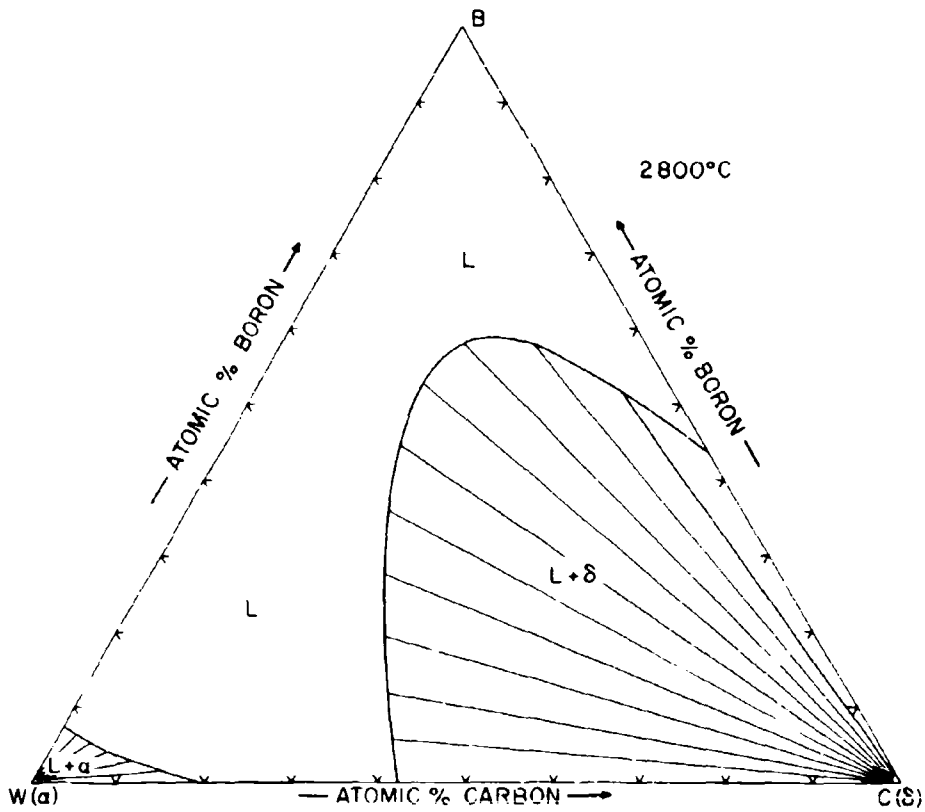

Figure III.K.4.11. Isothermal Section of the W-B-C System at 2800° C

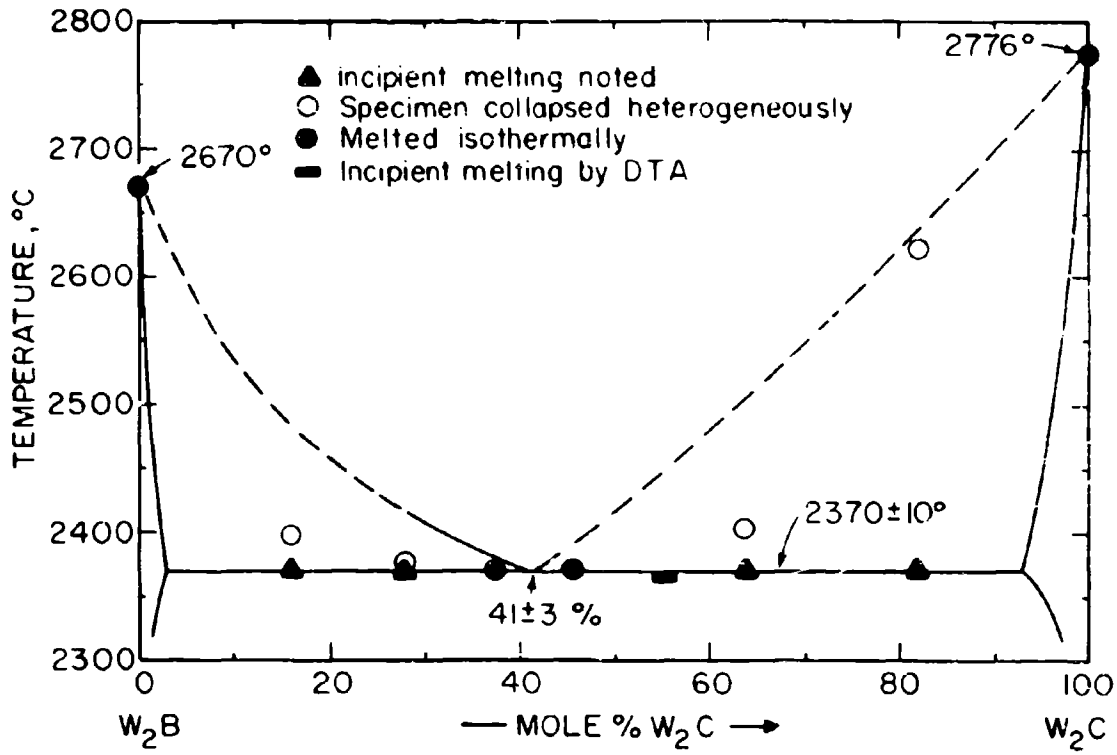

Figure III.K.4.12. Experimental Melting Temperatures at the Pseudobinary Section W_2B-W_2C

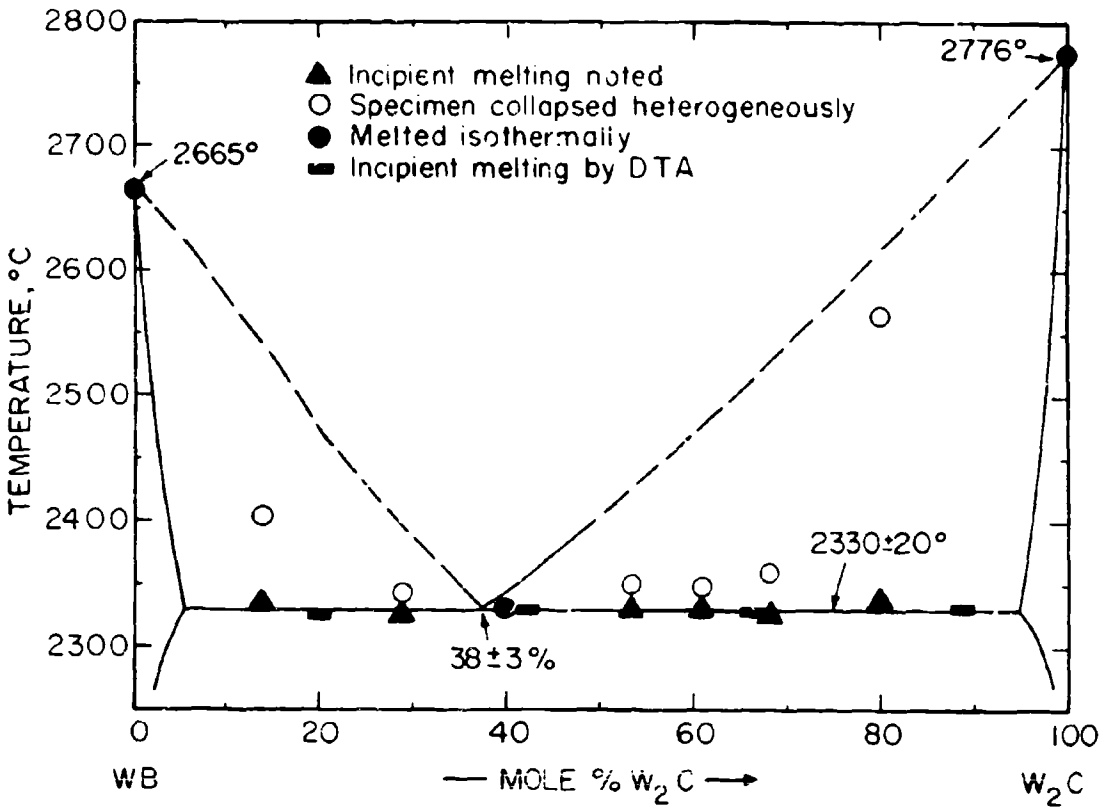

Figure III.K.4.13. Experimental Melting Temperatures at the Pseudobinary Section WB-W_2C

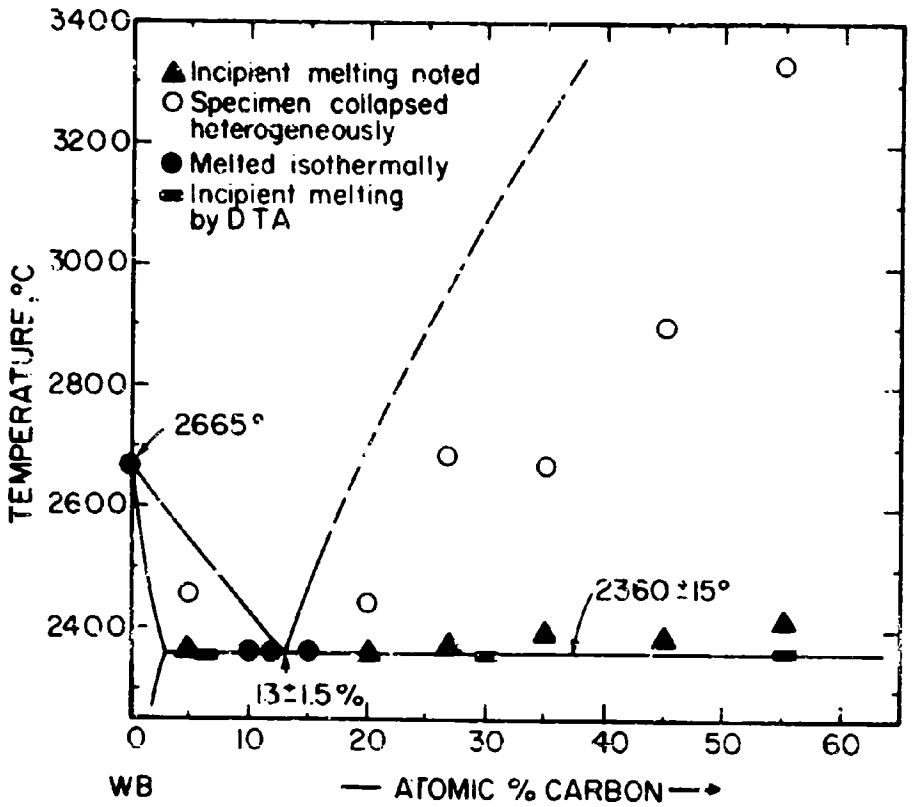

Figure III.K.4.14. Experimental Melting Temperatures at the Pseudobinary Section WB-C

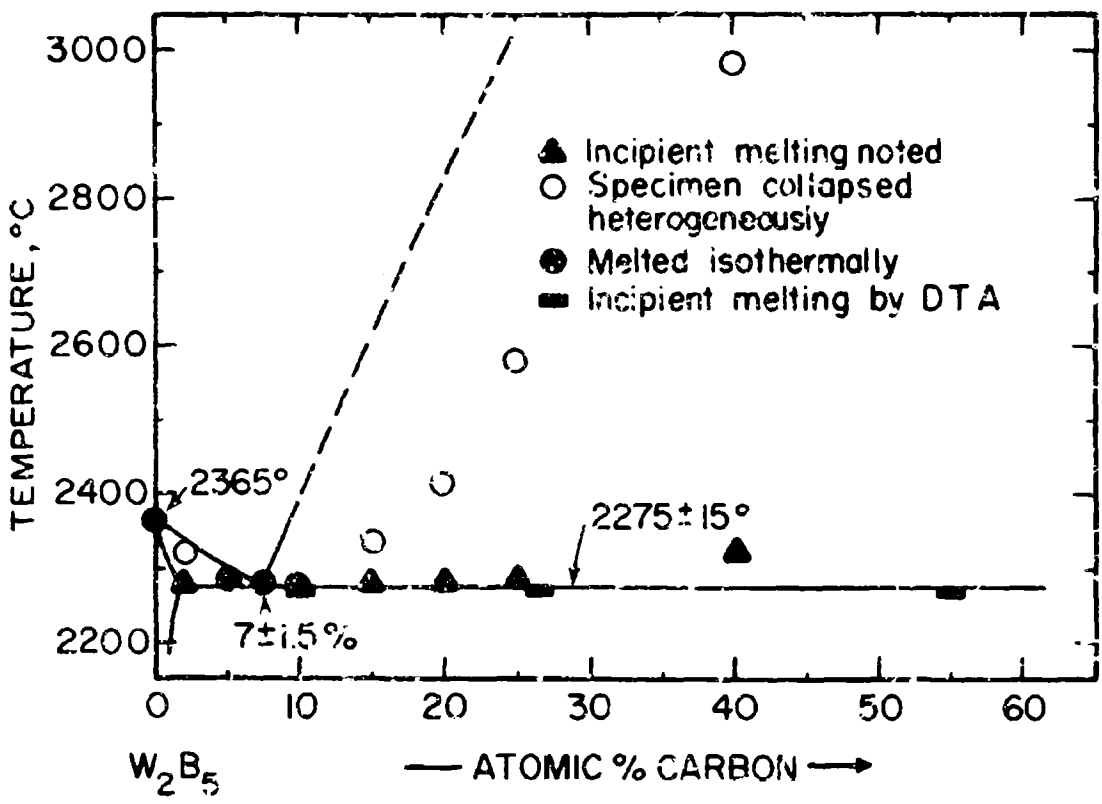

Figure III.K.4.15. Experimental Melting Temperatures at the Pseudobinary Section W_2B_5-C

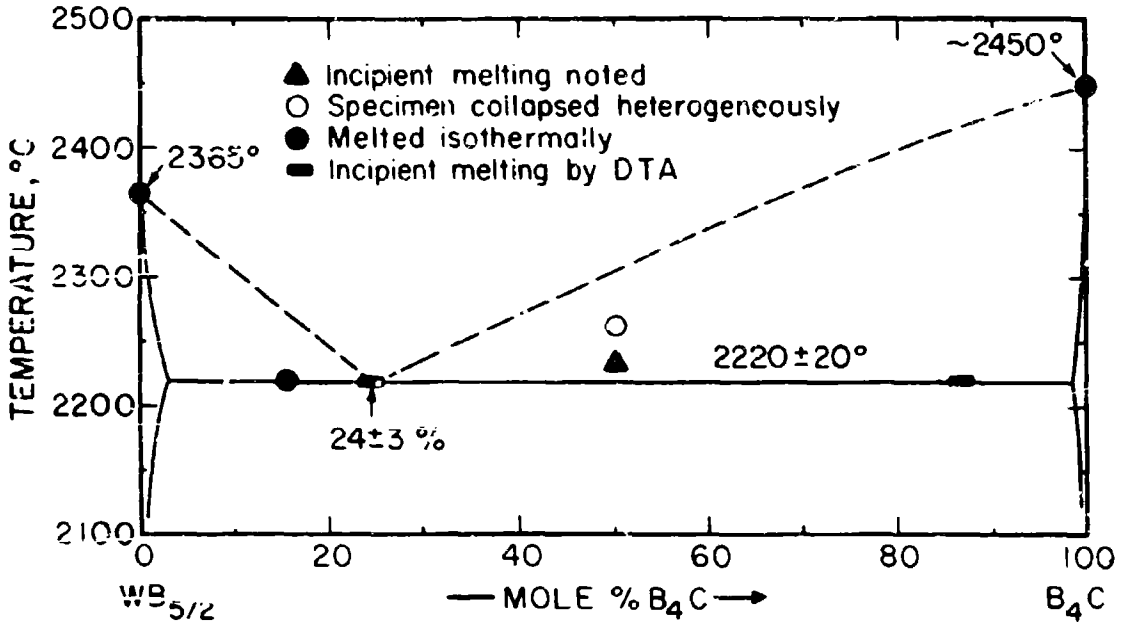

Figure III.K.4.16. Experimental Melting Temperatures at the Pseudobinary Section W_2B_5-B_4C

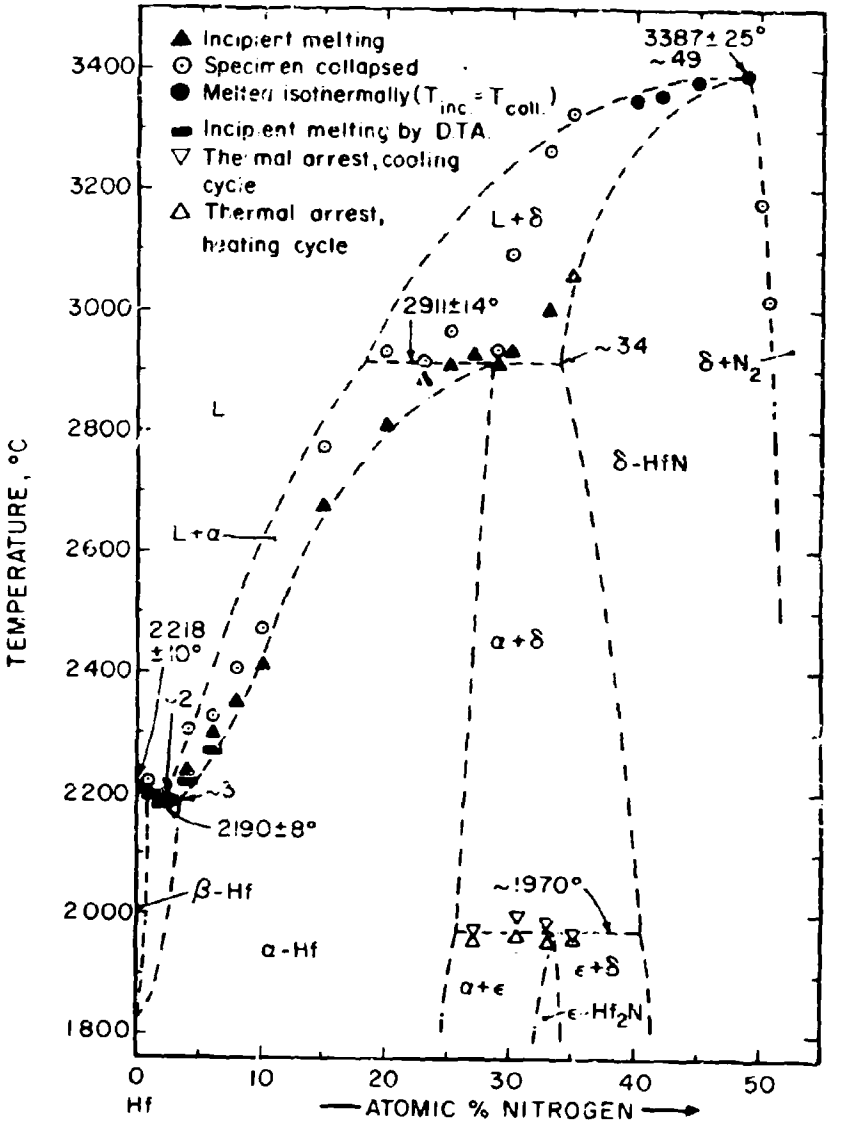

Figure III.L.1.1 The Hf-N Boundary System

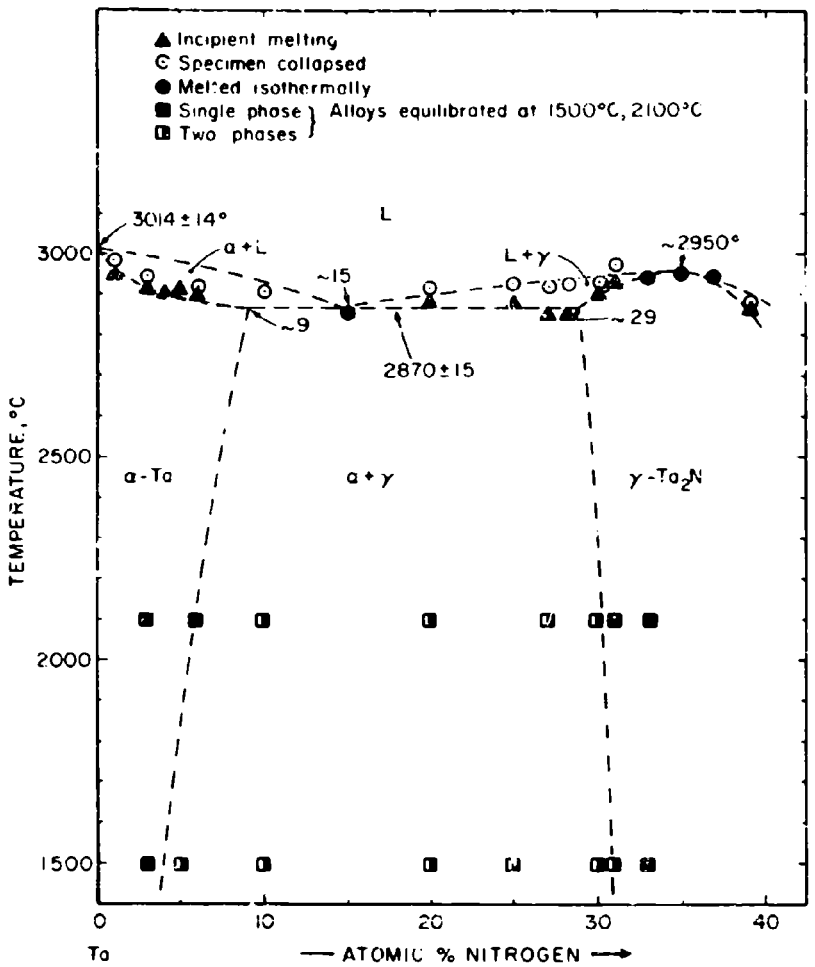

Figure III.L.1.2. The Ta-N Boundary System

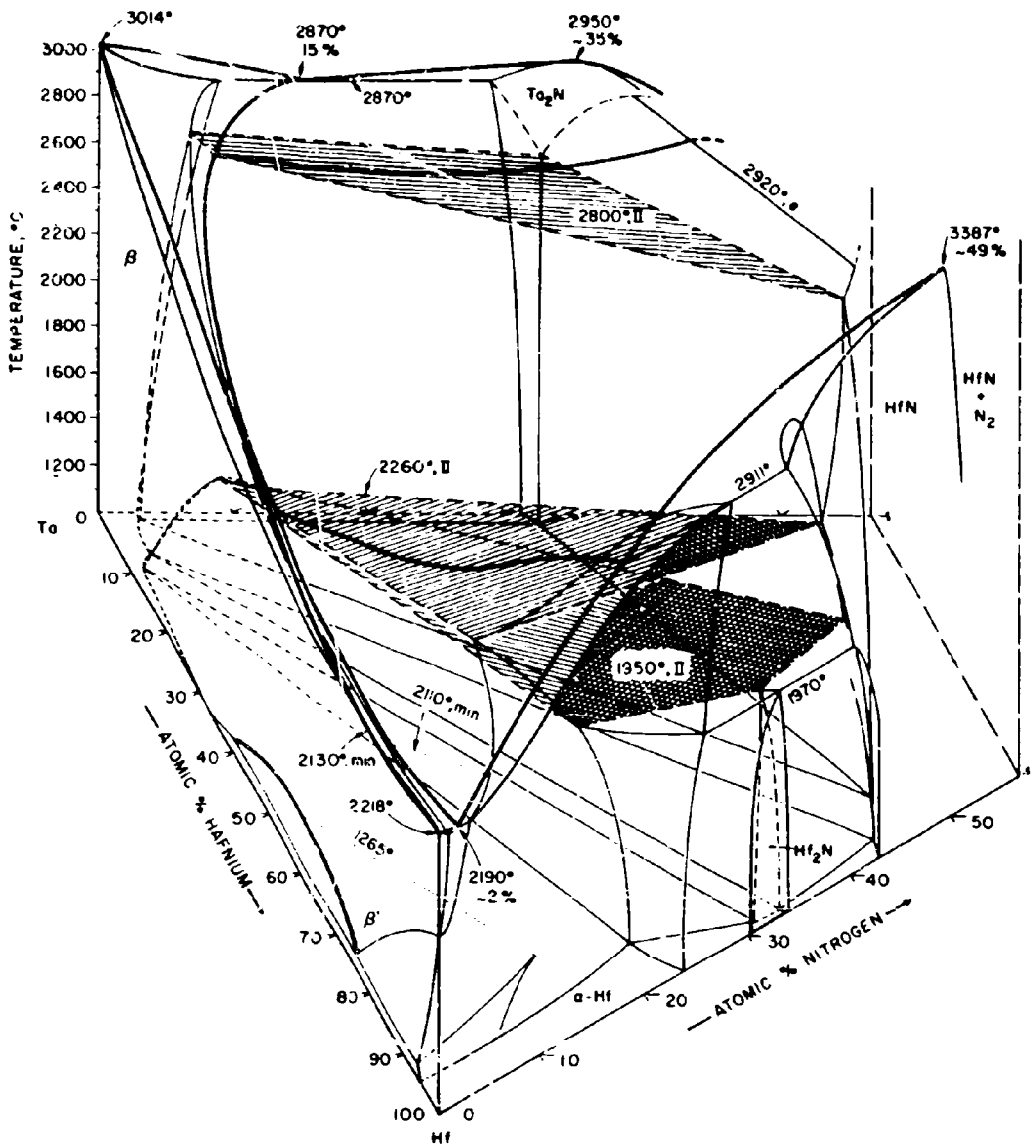

Figure III.L.1.3. Partial, Isometric View of the Hf-Ta-N System

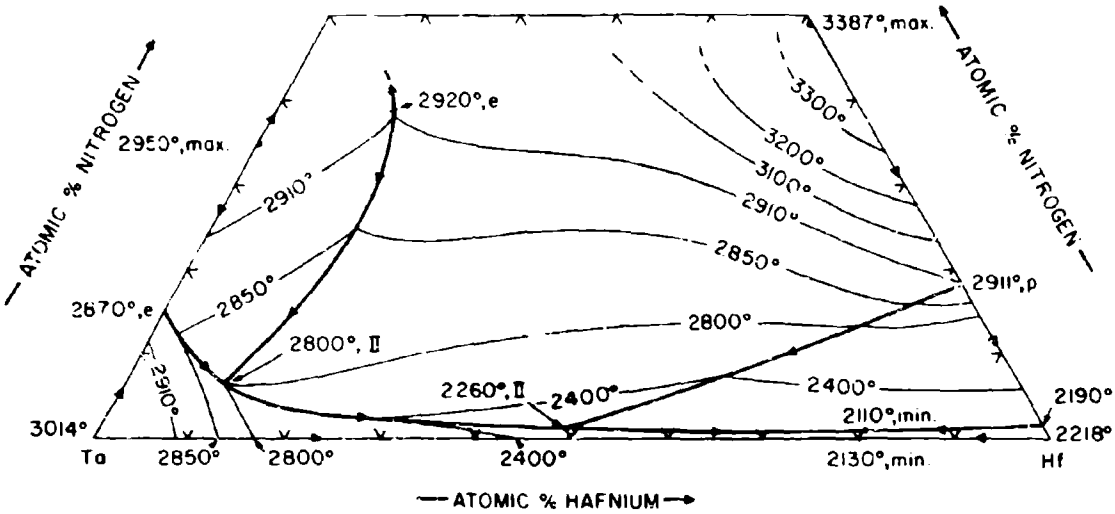

Figure III.L.1.4. Liquidus Projections in the Hf-Ta-N System

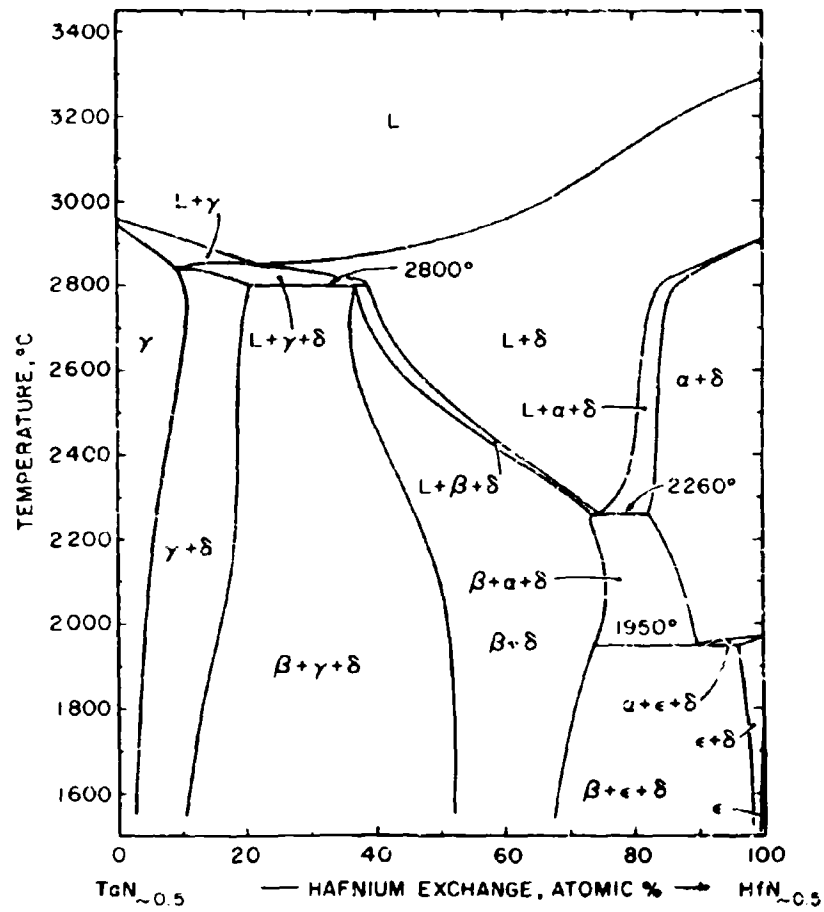

Figure III.L.1.5. Isopleth Hf_2N-Ta_2N

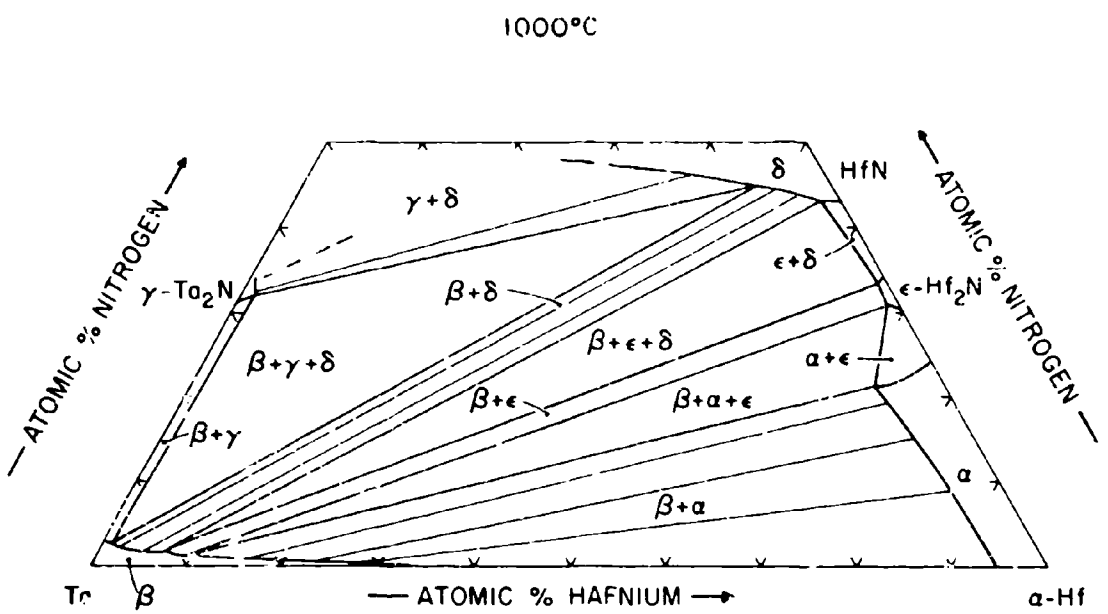

Figure III.L.1.6. Isothermal Section of the Hf-Ta-N System at 1000°C

1100°C

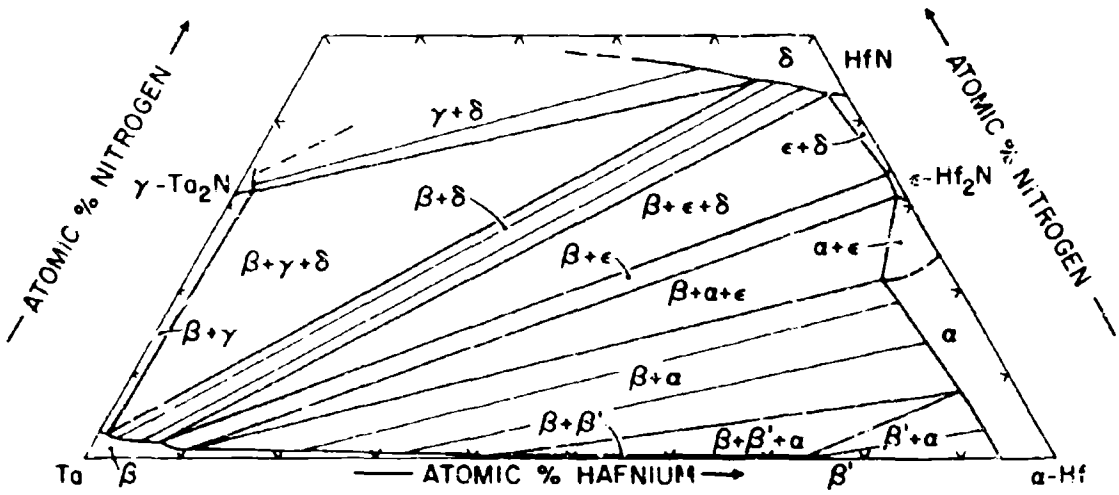

Figure III.L.1.7. Isothermal Section of the Hf-Ta-N System at 1100°C

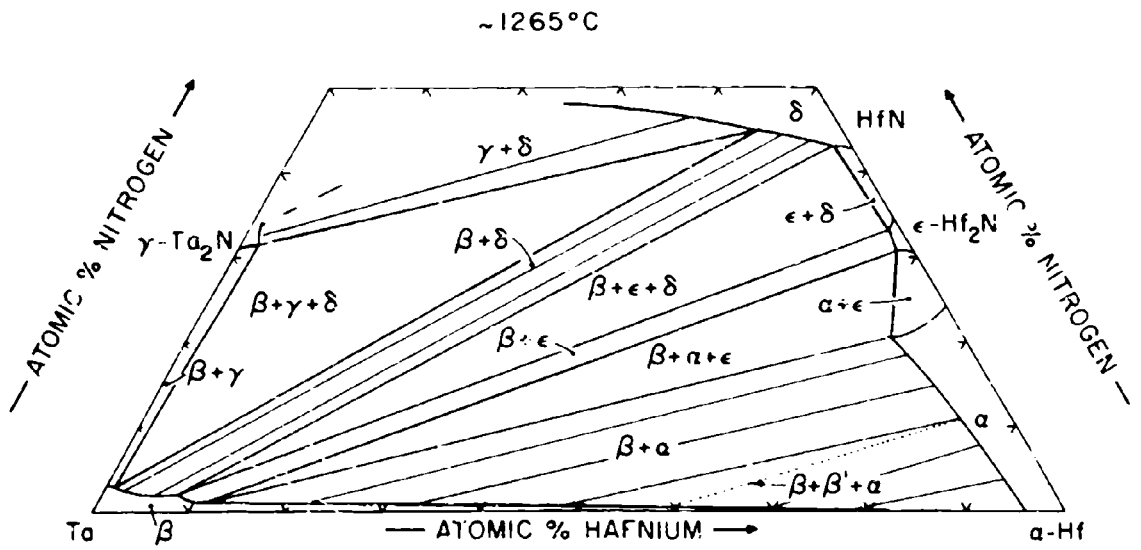

Figure III.L.1.8. Isothermal Section of tne Hf-Ta-N System at ~1265°C

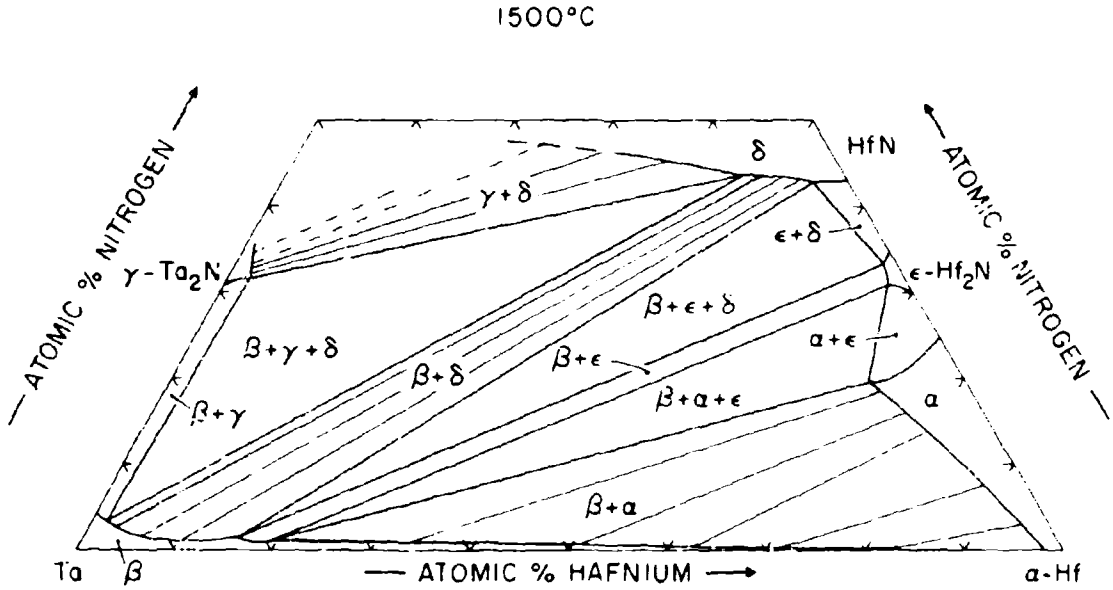

Figure III.L.1.9. Isothermal Section of the Hf-Ta-N System at 1500°C

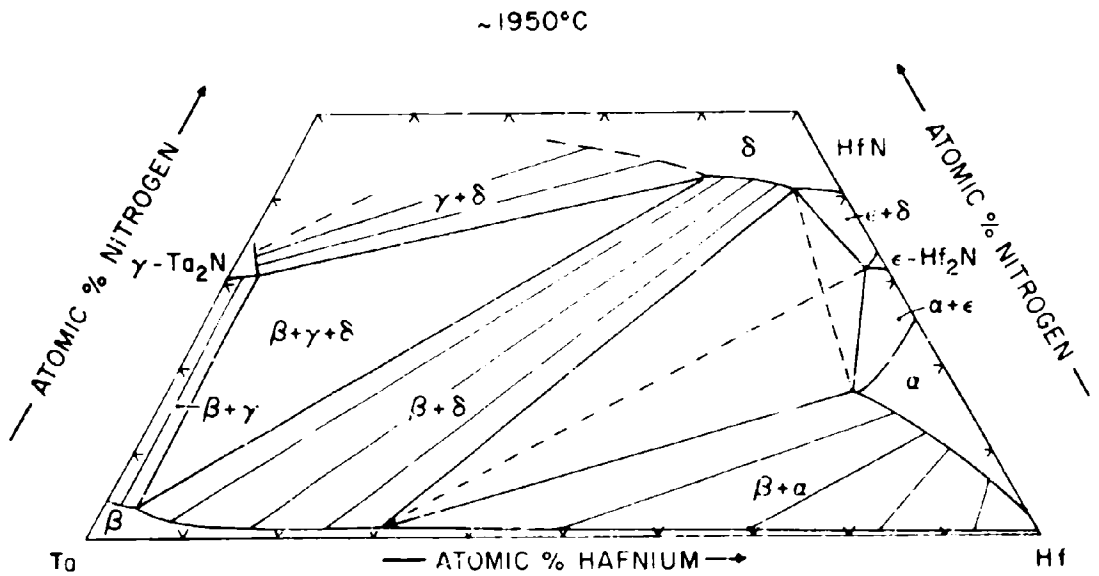

Figure III.L.1.10. Isothermal Section of the Hf-Ta-N System at 1950°C

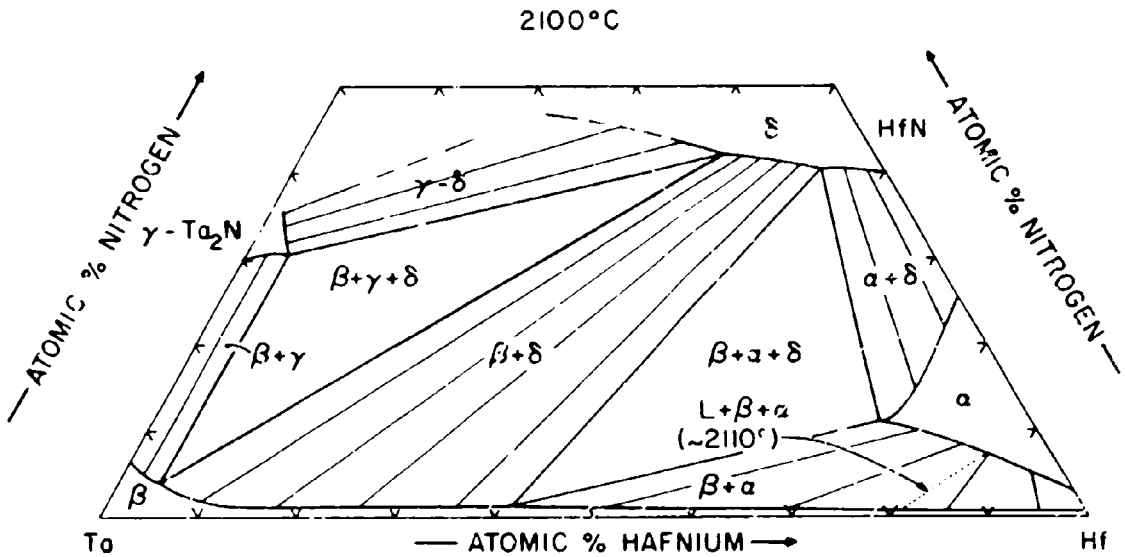

Figure III.L.1.11. Isothermal Section of the Hf-Ta-N System at 2100° C

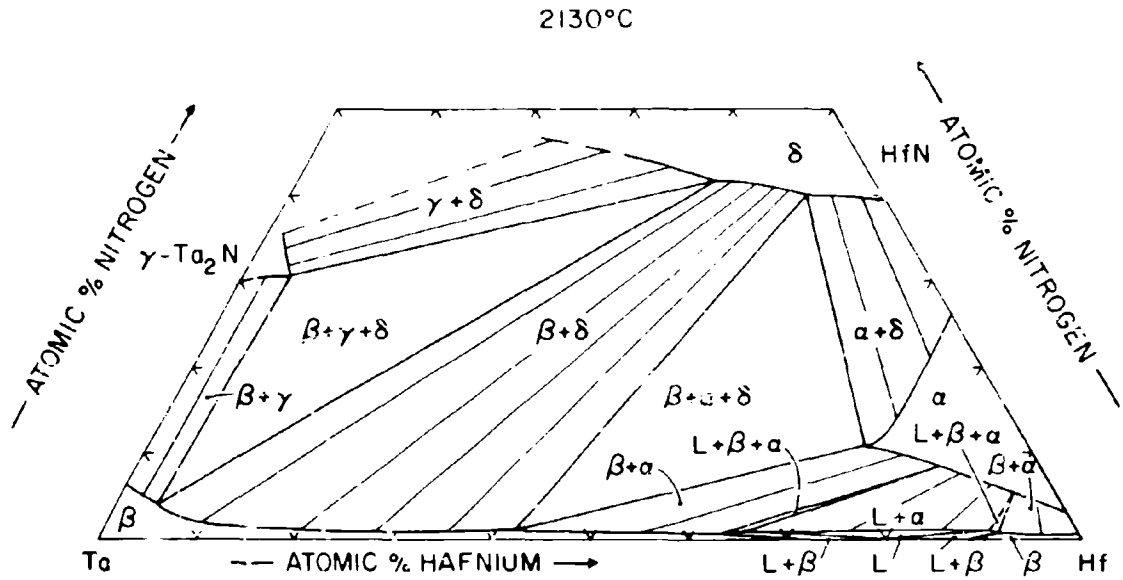

Figure III.L.1.12. Isothermal Section of the Hf-Ta-N System at 2130° C

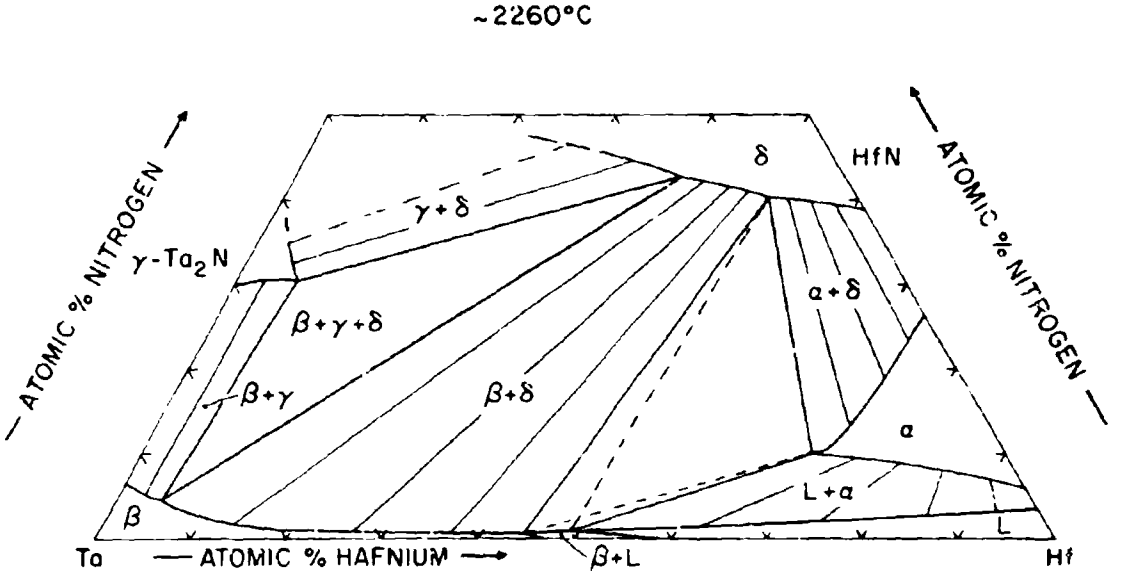

Figure III.L.1.13. Isothermal Section of the Hf-Ta-N System at 2260°C

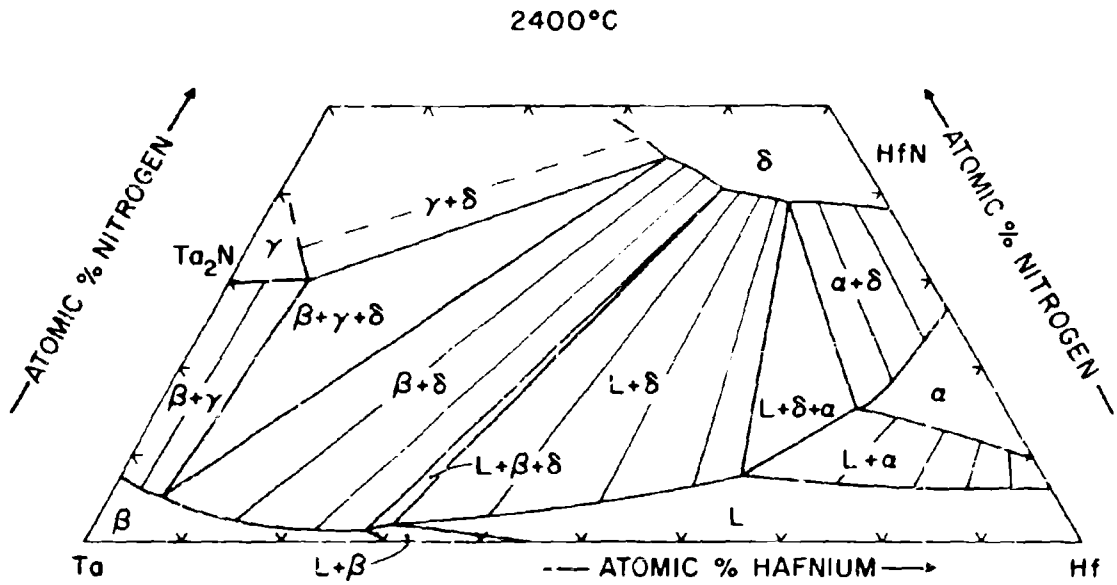

Figure III.L.1.14. Isothermal Section of the Hf-Ta-N System at 2400°C

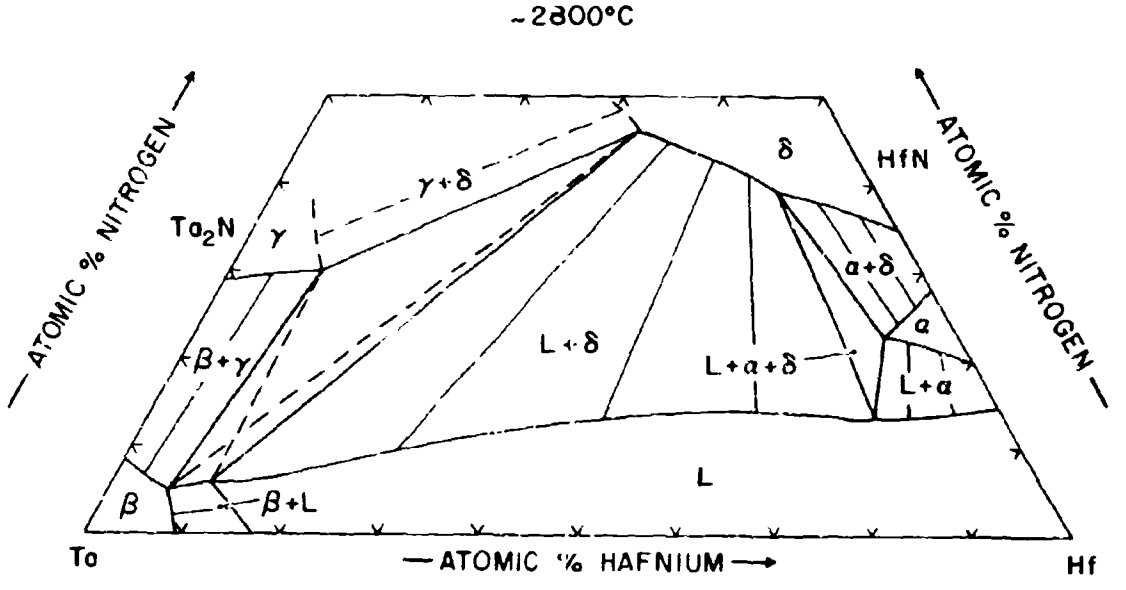

Figure III.L.1.15. Isothermal Section of the Hf-Ta-N System at 2800°C

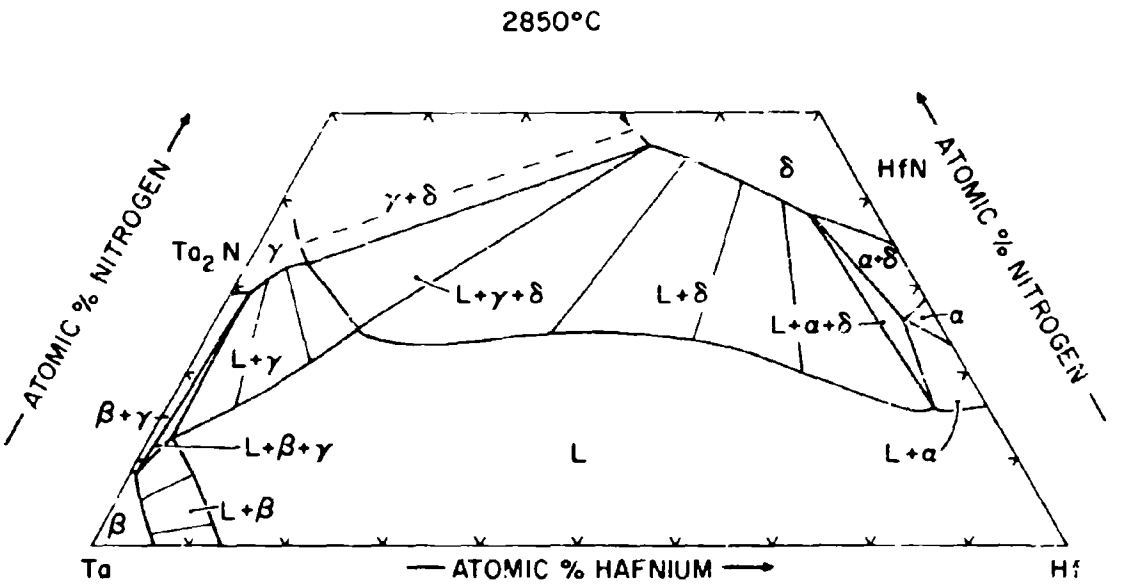

Figure III.L.1.16. Isothermal Section of the Hf-Ta-N System at 2850°C

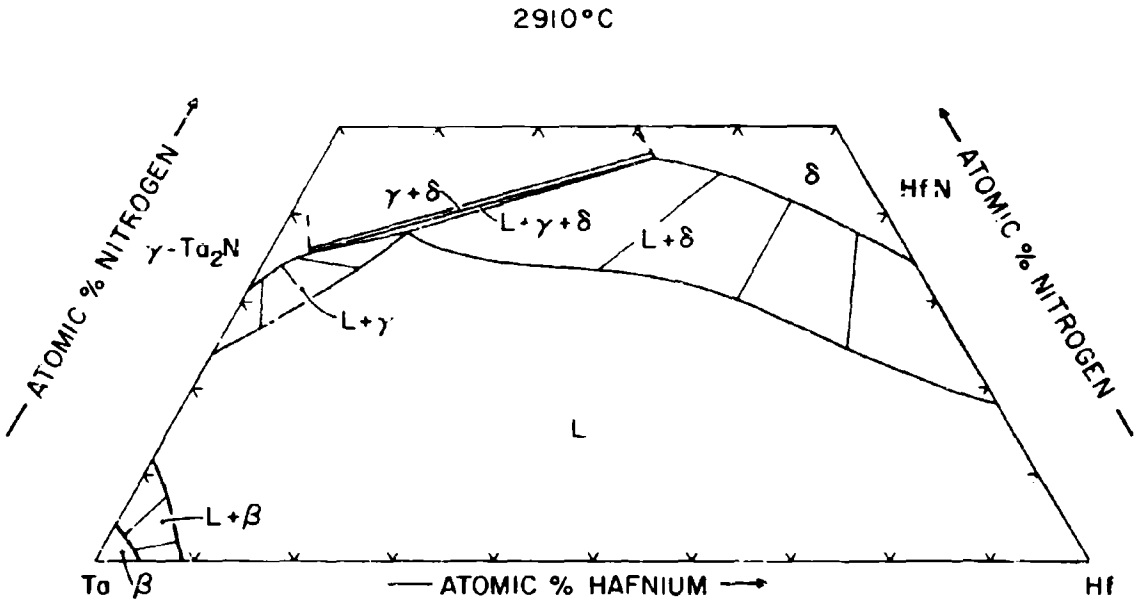

Figure III.L.1.17. Isothermal Section of the Hf-Ta-N System at ~2910° C

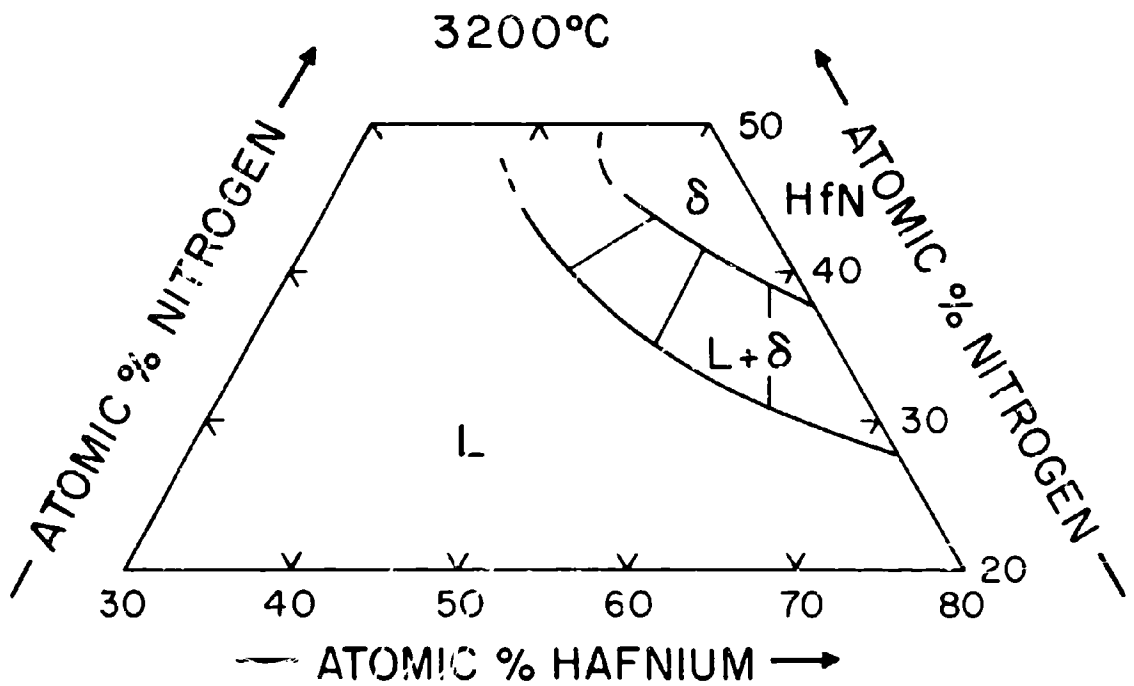

Figure III.L.1.18. Isothermal Section of the Hf-Ta-N System at 3200°C

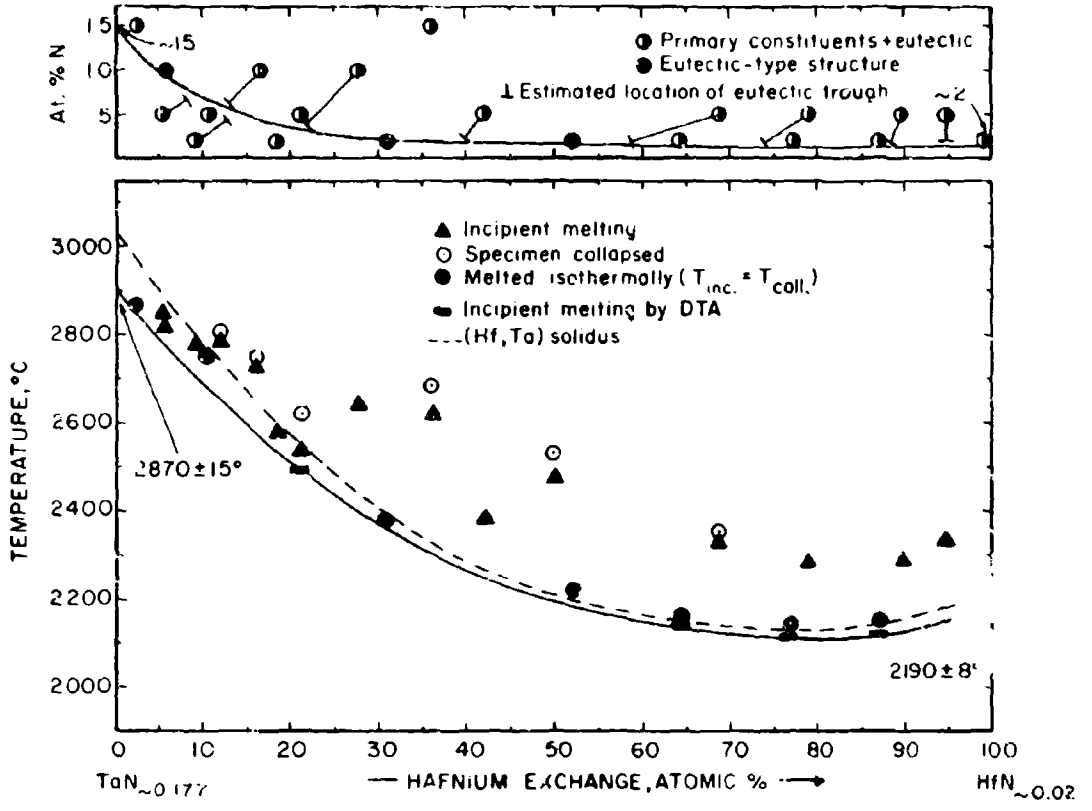

Figure III.L.1.19. Experimental Melting Temperatures at the Metal-Rich Eutectic Trough

Security Classification

DOCUMENT CONTROL DATA - R & D

(Security classification of title, body of abstract and indexing annotation must be entered when the overall report is classified)

1. ORIGINATING ACTIVITY (Corporate author) Aerojet-General Corporation Materials Research Laboratory Sacramento, California	2a. REPORT SECURITY CLASSIFICATION Unclassified 2b. GROUP N.A.

3. REPORT TITLE

Ternary Phase Equilibria in Transition Metal-Boron-Carbon-Silicon Systems

Part V. Compendium of Phase Diagram Data

4. DESCRIPTIVE NOTES (Type of report and inclusive dates)

5. AUTHOR(S) (First name, middle initial, last name)

Rudy, E.

6. REPORT DATE	7a. TOTAL NO. OF PAGES	7b. NO. OF REFS
May 1969	731	331

8a. CONTRACT OR GRANT NO.	9a. ORIGINATOR'S REPORT NUMBER(S)
AF 33(615)-1249 b. PROJECT NO. 7350 c. Task No. 735001 d.	9b. OTHER REPORT NO(S) (Any other numbers that may be assigned this report) AFML-TR-65-2, Part V.

10. DISTRIBUTION STATEMENT

Distribution of this document is unlimited. It may be released to the Clearinghouse, Department of Commerce, for sale to the General Public.

11. SUPPLEMENTARY NOTES	12. SPONSORING MILITARY ACTIVITY
	AFML (MAMC) Wright-Patterson AFB, Ohio 45433

13. ABSTRACT

This report contains a summary of the phase diagram work conducted under U.S. Air Force Contracts AF 33(615)-1249 and AF 33(615)-67-C-1513 over the time period from 1 January 1964 through April 1969. Systems studied include binary transition metal systems, binary and ternary systems of refractory transition metals with carbon, boron, silicon, and nitrogen, and selected concentration-temperature sections of higher order systems involving the same elements.

DD FORM 1 NOV 65 1473

Unclassified
Security Classification

14 KEY WORDS	LINK A		LINK B		LINK C	
	ROLE	WT	ROLE	WT	ROLE	WT
Compendium Ternary Phase Equilibria Transition Metal-Boron-Silicon-Carbon Systems						